

Technische Universität München

WACKER-Lehrstuhl für Makromolekulare Chemie

**From *Michael*-type systems to biobased lactones:
Designing novel polymer microstructures with
modified bis(phenolate)lanthanides**

Friederike Adams

Vollständiger Abdruck der von der Fakultät für Chemie der Technischen Universität München zur Erlangung des akademischen Grades eines

Doktors der Naturwissenschaften

genehmigten Dissertation.

Vorsitzender:

Prof. Dr. Lukas Hintermann

Prüfer der Dissertation:

1. Prof. Dr. Dr. h.c. Bernhard Rieger

2. apl. Prof. Dr. Wolfgang Eisenreich

3. Assoc. Prof. Dr. Ning Zhang
(nur schriftliche Beurteilung)

Hon.-Prof. Dr. Richard Fischer
(mündliche Prüfung)

Die Dissertation wurde am 27.11.2018 bei der Technischen Universität München eingereicht und durch die Fakultät für Chemie am 14.01.2019 angenommen.

“Success consists of going from failure to failure without loss of enthusiasm.”

Winston Churchill

Acknowledgement

In the first place, my special thanks go to Prof. Dr. Dr. h. c. Bernhard Rieger for the opportunity to perform my Ph.D. thesis at his chair. I really liked the topic of my dissertation.

In addition, I thank the Bavarian State Ministry of Environment and Consumer Protection for financial support within *BayBiotech* research network.

Furthermore, I especially want to thank Markus Pschenitza, Thomas Pehl, Sebastian Kernbichl, Dr. Martin Machat, Dr. Philipp Pahl, Dr. Carsten Troll, Dr. Sergei Vagin, Dr. Peter Altenbuchner, Dr. Alexander Pöthig, Dr. Tolga N.V. Karsili, Dr. Patrick Werz, Johannes Ehrmaier and Ulrike Ammari for the excellent support of my work and the performance of important measurements. At this point my great thank-you is also directed to Michael Weger, Thomas Pehl and Andreas Schaffer for the valuable discussions and proof-reading of my thesis. This made the creation of my work considerably easier.

I would also like to sincerely thank all colleagues, master students and trainees that shared a lab with me in the old building as well as in Makro Nord. Thank you for creating a cooperative atmosphere.

I further thank all Ph.D. students, Postdocs and master students at the WACKER-Chair of Macromolecular Chemistry and from my project network *BayBiotech* (especially Christian Burger and Christoph Mähler) for their good mood in the lab, during breaks and at the beer/ice cream/darts during and after work. Thank you all for helping with preparation of the manuscripts, openness to all questions and concerns, for the professional competence and the ambition with which you all have driven my work.

My parents are responsible for a significant part of the success of my work. Without the support during my Ph.D. thesis, my master's thesis, and my entire studies, I would probably never have had the opportunity to come to Munich.

Last but not least, I want to thank all those who have supported me in any other way outside the lab, for example bringing me back to a good mood after work. You are the best!

Table of content

Acknowledgement	V
List of abbreviations	XI
Publication list	XVII
1 Abstract.....	1
2 Theoretical background.....	3
2.1 The need for thermoplastic materials.....	3
2.2 Coordination-insertion polymerization.....	7
2.2.1 Ring-opening polymerization of lactones	7
2.2.2 Metal-catalyzed group-transfer polymerization.....	17
2.3 C-H bond activation.....	24
2.4 Polymers from polar monomers: Requirements and applications	27
2.4.1 Poly(3-hydroxybutyrate) as a biodegradable alternative for packaging.....	27
2.4.2 Thermoplastic elastomers from biobased copolymers	30
2.4.3 Tailor-made functional copolymers for high-tech applications	33
3 Aim of this thesis.....	37
3.1 Modulation of the metal center.....	38
3.2 Modulation of the initiator.....	38
3.3 Modulation of the ligand	40
4 Nonmetallocene lanthanides as catalysts in group-transfer polymerization	43
4.1 Bibliographic data	43
4.2 Abstract graphic (TOC).....	43
4.3 Content	44
4.4 Manuscript	45
4.5 Reprint permission of copyrighted content	56

5	Micellar block copolymers from 2-vinylpyridine and dialkyl vinylphosphonates.....	57
5.1	Bibliographic data.....	57
5.2	Abstract graphic.....	57
5.3	Content.....	58
5.4	Manuscript.....	59
5.5	Reprint permission of copyrighted content.....	64
6	Yttrium-catalyzed synthesis of bipyridine-functionalized AB-block copolymers.....	65
6.1	Bibliographic data.....	65
6.2	Abstract graphic (TOC).....	65
6.3	Content.....	66
6.4	Manuscript.....	67
6.5	Reprint permission of copyrighted content.....	75
7	Multiresponsive nanocarriers for drug delivery to cancer cells.....	77
7.1	Bibliographic data.....	77
7.2	Abstract graphic (TOC).....	77
7.3	Content.....	78
7.4	Manuscript.....	79
7.5	Reprint permission of copyrighted content.....	88
8	Group-transfer polymerization as a versatile tool for functional (co)polymers.....	89
8.1	Bibliographic data.....	89
8.2	Abstract graphic (TOC).....	89
8.3	Content.....	90
8.4	Manuscript.....	91
8.5	Reprint permission of copyrighted content.....	101
9	Tuning Material Properties of Poly(3-hydroxybutyrate): Isospecific Ring-Opening Polymerization of β -Butyrolactone.....	103

Table of content

9.1	Bibliographic data	103
9.2	Abstract graphic (TOC).....	103
9.3	Content	104
9.4	Patent application.....	109
9.5	Designation of inventor	128
10	Tuning Material Properties of Poly(3-hydroxybutyrate): Copolymerization with sustainable lactones.....	129
10.1	Bibliographic data	129
10.2	Abstract graphic (TOC).....	129
10.3	Content	130
10.4	Manuscript Draft	131
11	Summary and outlook.....	155
11.1	Group-transfer polymerization.....	155
11.2	Ring-opening polymerization.....	158
12	Zusammenfassung und Ausblick	163
12.1	Gruppentransferpolymerisation	163
12.2	Ringöffnungspolymerisation	166
13	References	171
14	Appendix	179
14.1	Supporting Information: “Toolbox of Nonmetallocene Lanthanides: Multifunctional Catalysts in Group-Transfer Polymerization”	179
14.2	Supporting Information: “Multiresponsive micellar block copolymers from 2-vinylpyridine and dialkylvinylphosphonates with a tunable lower critical solution temperature”	241
14.3	Supporting Information: “Yttrium-Catalyzed Synthesis of Bipyridine-Functionalized AB-Block Copolymers: Micellar Support for Photocatalytic Active Rhenium-Complexes”	259
14.4	Supporting Information: “Next Generation Multiresponsive Nanocarriers for Targeted Drug Delivery to Cancer Cells”	286

14.5	Supporting Information: “Process for polymerizing β -butyrolactone”	321
14.6	Supporting Information: “(Co)polymerization of (-)-Menthide and β -Butyrolactone catalyzed by Heteroaromatic Yttrium-bis(phenolates): Tuning Material Properties of Sustainable Polyesters” ..	333
15	Statutory declaration.....	363

List of abbreviations

2VP	2-vinylpyridine
4VP	4-vinylpyridine
ABS	acrylonitrile butadiene styrene
BBL	β -butyrolactone
BPL^{OR}	4-alkoxymethylene- β -propiolactone
Bdsa	bis(dimethylsilyl)amide
Btsa	bis(trimethylsilyl)amide
CL	caprolactone
CMC	critical micelle concentration
Coll	<i>sym</i> -collidine
Cp	cyclopentadienyl
CTA	chain-transfer agent
DCM	dichloromethane
DAVP	dialkyl vinylphosphonate
DEVP	diethyl vinylphosphonate
DMAA	<i>N,N</i> -dimethylacrylamide
DMVP	dimethyl vinylphosphonate
DPVP	di- <i>n</i> -propyl vinylphosphonate
DFT	density-functional theory

DLS	dynamic light scattering
DMF	<i>N,N</i> -dimethylformamide
DNA	deoxyribonucleic acid
DOX	doxorubicin
DSC	differential scanning calorimetry
EA	elemental analysis
EPR	ethylene propylene rubber
Eq.	equivalents
ESI-MS	electrospray ionization mass spectrometry
<i>et al.</i>	and others (lat.: et alii)
Gly	glycolide
GPC	gel-permeation chromatography
GTP	group-transfer polymerization
HDPE	high-density poly(ethylene)
IPOx	2- <i>iso</i> -propenyl-2-oxazoline
Iso	<i>isotactic</i>
La	lactide
LCST	lower critical solution temperature
LDPE	low-density poly(ethylene)
LLDPE	linear low-density poly(ethylene)
Ln	lanthanide
M	(-)-menthide

MBL	α -methylene- γ -butyrolactone
Me	methyl
Mebpy	6-methyl-2,2'-bipyridine
6-Me₂bpy	6,6'-dimethyl-2,2'-bipyridine
MLA	malolactone
MMA	methyl methacrylate
MMBL	methyl- α -methylene- γ -butyrolactone
MMPy	α -methylene- <i>N</i> -methylpyrrolidone
M_n	number average molar mass
M_w	mass average molar mass
nmr	nuclear magnetic resonance
P2VP	poly(2-vinylpyridine)
PA	poly(amide)
PCL	poly(ϵ -caprolactone)
PDEVP	poly(diethyl vinylphosphonate)
PDI	polydispersity index
PDMVP	poly(dimethyl vinylphosphonate)
PDPVP	poly(di- <i>n</i> -propyl vinylphosphonate)
PE	poly(ethylene)
PEG	poly(ethylene glycol)
PET	poly(ethylene terephthalate)

List of abbreviations

PHA	poly(hydroxyalkanoate)
PHB	poly(3-hydroxybutyrate)
PL	propiolactone
PLA	poly(lactide)
P_m	probability of <i>meso</i> linkages
PM	poly((-)-menthide)
PMMA	poly(methyl methacrylate)
PNIPAAm	poly(<i>N</i> -iso-propylacrylamide)
PP	poly(propylene)
ppm	parts per million
P_r	probability of <i>racemic</i> linkages
PVC	poly(vinyl chloride)
<i>Rac</i>	<i>racemic</i>
REM	rare-earth metal
RNA	ribonucleic acid
ROP	ring-opening polymerization
RT	room temperature
SAN	styrene-acrylonitrile resin
<i>Sym</i>	symmetric
<i>Syndio</i>	<i>syndiotactic</i>
TGA	thermogravimetric analysis

List of abbreviations

THF	tetrahydrofuran
TMPy	tetramethylpyrazine
TMS	trimethylsilyl
TOF	turn-over frequency
TOF*	normalized turn-over frequency
TPE	Thermoplastic elastomer
UCST	upper critical solution temperature
VL	valerolactone

Publication list

- I. Adams, F.; Altenbuchner, P. T.; Werz, P. D. L.; Rieger, B., *RSC Adv.* **2016**, 6 (82), 78750-78754.
"Multiresponsive micellar blockcopolymers from 2-vinylpyridine and dialkylvinylphosphonates with a tunable lower critical solution temperature"
- II. Adams, F.; Machat, R. M.; Altenbuchner, P.T.; Ehrmaier, J.; Pöthig, A.; Karsili, T. N. V.; Rieger, B., *Inorg. Chem.* **2017**, 56 (16), 9754-9764.
"Toolbox of Nonmetallocene Lanthanides: Multifunctional Catalysts in Group-Transfer Polymerization"
- III. Adams, F.*; Pschenitzka, M.*; Rieger, B., *ChemCatChem* **2018**, 10 (19), 4309-4316.
"Yttrium-catalyzed Synthesis of Bipyridine-functionalized AB-Block Copolymers: Micellar Support for Photocatalytic Active Rhenium-Complexes"
- IV. Adams, F.*; Pahl, P.*; Rieger, B., *Chem. Eur. J.* **2018**, 24 (3), 509-518.
"Metal-Catalyzed Group-Transfer Polymerization: A Versatile Tool for Tailor-Made Functional (Co)Polymers"
- V. Altenbuchner, P. T.*; Werz, P. D. L.*; Schöppner, P.*; Adams, F.; Kronast, A.; Schwarzenböck, C.; Pöthig, A.; Jandl, C.; Haslbeck, M.; Rieger, B., *Chem. Eur. J.* **2016**, 22 (41), 14576-84.
"Next Generation Multiresponsive Nanocarriers for Targeted Drug Delivery to Cancer Cells"

Publications beyond the scope of this thesis:

- Adams, F., *Gruppentransferpolymerisation von Michael-Monomeren*. Springer Best Masters, **2016**, ISBN: 3658135743.
- Altenbuchner, P. T.; Adams, F.; Kronast, A.; Herdtweck, E.; Pöthig, A.; Rieger, B., *Polym. Chem.* **2015**, 6 (38), 6796-6801.
"Stereospecific catalytic precision polymerization of 2-vinylpyridine via rare earth metal-mediated group-transfer polymerization with 2-methoxyethylamino-bis(phenolate)-yttrium complexes"

- Kernbichl, S*; Reiter, M.*; Adams, F.; Vagin, S.; Rieger, B., *J. Am. Chem. Soc.* **2017**, 139, 6787-6790.
“CO₂-Controlled One-Pot Synthesis of AB, ABA Block, and Statistical Terpolymers from β -Butyrolactone, Epoxides, and CO₂”
- Vagin, S. I.; Kronast, A.; Altenbuchner, P.T.; Adams, F.; Sinkel, C.; Deglmann, P.; Loos, R.; Schuffenhauer, T.; Sommer, S.; Brück, T.; Rieger, B., *Polym. Degrad. Stab.* **2017**, 143, 176-185.
“Enzymatic degradation of synthetic poly(3-hydroxybutyrates) as a tool for combinatorial microstructure determination“

*These authors contributed equally

1 Abstract

Due to their impressive diversity, the application horizon of thermoplastics is extending far beyond the use as ordinary consumer goods. They are increasingly used in a variety of industrial branches and are already an integral part of the biomedical, the construction or the electrochemical sector. The optimization of catalysts plays a significant role in modern polymer-chemistry to efficiently produce a variety of different polymeric structures. Within this thesis, modifications of well-investigated bis(phenolate)yttrium complexes is performed. These complexes are highly active in two different coordination polymerization types: Ring-opening polymerization (ROP) of lactones and group-transfer polymerization (GTP) of *Michael*-type vinyl monomers. ROP with lanthanides bearing a new ligand system is used to synthesize poly(3-hydroxybutyrate) (PHB) from *racemic* β -butyrolactone (BBL) with a, so far inaccessible, microstructure. This biodegradable PHB serves as an alternative for commonly used petroleum-based poly(propylene) for packaging industry. ROP with heteroaromatic bis(phenolate)yttrium catalysts enabled the synthesis of BAB block copolymers from BBL and (-)-menthite (M). Polymerization of (-)-menthite to poly((-)-menthite) (PM) and copolymerization with BBL was first tested with yttrium-catalysts in this thesis. The obtained *syndio*-PHB-*b*-PM-*b*-*syndio*-PHB triblock polymers show phase separation making them suitable as sustainable thermoplastic elastomers from carbon dioxide and menthol. In the second part of this work, GTP mediated by various bis(phenolate)lanthanides was first investigated in a systematic study on the influence of the metal center, ligand and initiator on the activity, initiator efficiency and stereospecificity for different monomers. Afterwards, these complexes were used for the tailor-made synthesis of functional block copolymers from 2-vinylpyridine (2VP) and dialkyl vinylphosphonates (DAVP) for high-tech applications such as drug delivery and photocatalytic reduction of carbon dioxide.

2 Theoretical background

2.1 The need for thermoplastic materials

“Polymer chemistry and physics are facing a new era, which involves simple polymers to more sophisticated macro-molecular systems. The importance of macromolecular science is expected to grow further, and developments are anticipated especially around the border with life science, physics, and the other fields of chemistry - The 21st century is shown to be the Age of Polymers.”^[1] This quote from a conference report on “Missions and Challenges of Polymer Science and Technology” shows the high significance of plastics in our daily life as commodity polymers as well as in high-tech applications as advanced polymers. Exemplary sectors for both types of polymers are packaging, agriculture, medicine, automotive, electronics or aerospace.^[2-3] The demand for an enormous variety of different polymeric materials is also reflected in the growth of the plastic market which passed the steel production by volume already in 1989.^[4] The production of polymeric materials has increased drastically from 1.5 million tons in 1950 to 335 million tons in 2016, with an annual growth rate of 4% from 2015 to 2016 (Figure 1, left). As the Asian region is responsible for 50% of the worldwide plastic production, the production of plastics in Europe (19%; 60 million tons in 2016) is relatively low.^[3, 5]

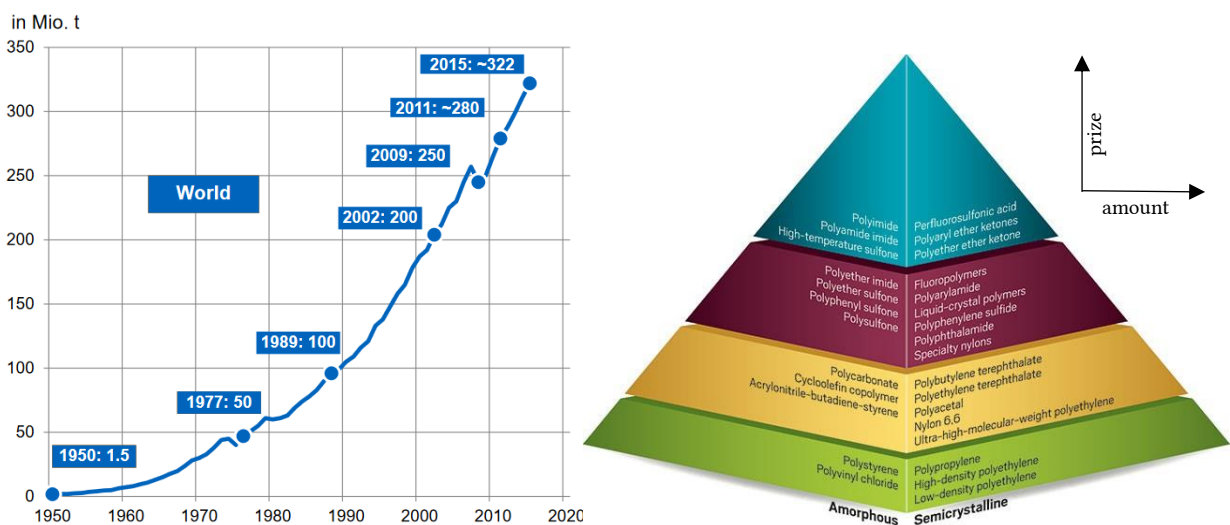


Figure 1: Left) Growth of the world plastic market from 1950 to 2015. Includes thermoplastics, poly(urethanes), thermosets, elastomers, adhesives, coatings and sealants and PP-fibres. Not included PET-, PA- and poly(acryl)-fibres.^[4] Right) Classification of some thermoplastic polymers in the categories “commodity polymers” (green), “engineering/ midrange polymers” (yellow) and “advanced polymeric materials (high-performance and ultra polymers)” (red and blue) with differentiation of amorphous and semi-crystalline properties.^[6]

The major amount of produced polymers are thermoplastics (Figure 1, right). Thermoplastics consist of linear and slightly branched chains that interact *via* non-covalent forces (e.g. *van-der-Waals* forces or hydrogen bonds). When heated, these molecular chains can be shifted against each other and the material is deformable, while it retains its shape upon cooling. A distinction is made between amorphous (softening) and *semi*-crystalline (melting) thermoplastics. Amorphous polymers consist of polymer chains that are randomly arranged which leads to an absence of a melting temperature. These polymers soften above their glass transition temperature (T_g), because the polymer chains start to move against each other.^[7] *Semi*-crystalline polymers are ordered partly (in dependence of the degree of crystallinity), hence containing crystalline and amorphous parts. Fully crystalline substances have a melting temperature (T_m) at which a structural change from the ordered state to the disordered state occurs abruptly. *Semi*-crystalline substances therefore have both, a glass-transition and a melting-temperature upon heating, whereby the glass transition temperature is below the melting temperature.^[8] Consequently, thermoplastics are easily processable by various techniques. In dependence of their crystallinity injection molding, blow/film molding, calendering, or extrusion can be performed. As a result, thermoplastics can be formed in a multitude of different shapes, which causes a wide range of applications in everyday life.^[7]

The longest known thermoplastic polymer is *Celluloid*®, which is a compound from nitrocellulose and camphor first known as *Parkesine*®, *Xylonite*® and *Ivoride*® in the 1860s, before being patented in 1869 and being registered under the trade name *Celluloid*® in 1872 from *John Wesley Hyatt*. It was developed as the replacement for natural products (horn, hair, feathers) and to primarily stop ivory poaching and trading. Afterwards, it was versatilely used for toothbrushes, automobiles, piano keys, safety glasses, eyeglass frames or photographic films in *Kodak* cameras.^[8-14] Due to the unique selling point of *Celluloid*®, the celluloid industry started to grow and was also supported by *DuPont* and *Monsanto*. But with the rise of newly developed synthetic materials which found their way into our daily life - poly(styrene) (PS) and poly(vinyl chloride) (PVC) were started to produce in 1930 and 1931 by I.G. Farben - *Celluloid*® was completely displaced from the plastic market.^[9-10] Meanwhile, poly(ethylene) (PE) is the most commonly produced commodity plastic with a percentage of 67% of the world thermoplastic production (more than 200 million tons per year) and can be produced in form of films or hollow bodies such as beverage bottles or wrapping film. The first commercial production of slightly-branched PE (low-density PE (LDPE)) started in 1939 by ICI.^[8, 10-15]

As also indicated before, thermoplastics can be subdivided into three different groups, however, this is not a chemical, but an application-related classification due to their mechanical and thermal properties and their production costs.^[16] The commodity polymers are the most commonly ones with a total

demand of 85% (230 m t.) of the world production.^[4] Polymers that can be produced from simple and petrochemical-based olefins in a large-scale are included in this category. Examples are PE (LDPE, linear low-density PE (LLDPE), high-density PE (HDPE)), poly(propylene) (PP), poly(methyl methacrylate) (PMMA), PVC or PS. As these materials are synthesized cost-efficient, they are used in low-tech applications such as packaging, household or agriculture.^[9]

Engineering or 'midrange' polymers are produced with 10% (25 Mio. t) of the worldwide demand for plastics in much lower quantities than the before mentioned commodity polymers.^[4] Efficient synthesis routes are established, but the production costs are much higher than for the commodity polymers. Therefore, these plastics are applied for engineering purposes in low-volume applications having advanced mechanical and thermal properties. Polymers with these featured properties are mostly copolymers of styrene with acrylonitrile (SAN = styrene acrylonitrile resin) or acrylonitrile with butadiene rubber (ABS = acrylonitrile butadiene styrene). In addition, different aromatic poly(esters) from terephthalic acid with different glycols (e.g. PET = poly(ethylene terephthalate)) fall under this category. Also aliphatic poly(amides) (PA) belong to these category known as *Nylon*[®] (PA 6.6 = poly(amide-6.6)) developed by *DuPont* and *Perlon*[®] (PA-6 = poly(amide-6)) introduced by IG Farben.^[9]

The last class of thermoplastics are the advanced polymers or high-performance polymers. As every single polymer in this category has mostly only one excellent specific property for one single application, they are produced on a small scale with a high prize.^[9] Due to their versatility a lot of different high-performance polymers exist to address versatile requirements such as tensile strength, thermal stability, surface properties, photo resistance, self-reinforcement, chemical inertness, reversible responsiveness to different stimuli, etc.^[2, 9, 17] The most popular family, in which poly(imides), poly(arylene ethers) and phenylethynyl-terminated oligomers are located, exhibits excellent heat stability and mechanical strength.^[2] In this thesis, also smart and functional polymers are included in the term advanced polymers. Polymers that bear special chemical groups dissimilar from their backbone making them suitable for chemical, biochemical, physical, and pharmaceutical uses are called functional polymers. If these macromolecules have functionalities that are reversible addressable *via* physical or chemical stimuli (pH, temperature, light, etc.), smart polymers are obtained. Smart and functional polymers are included in the category of advanced polymers, because they are applied in high-tech applications in which enhanced reactivity, phase separation, the transport of small substances or electric charge, the conversion of light or self-assembly is necessary. To obtain these properties, functional polymers can be synthesized as homo- or copolymers with different macromolecular architectures. Block-, graft- or 3-dimensional structures are only a few examples (Figure 2).^[18]

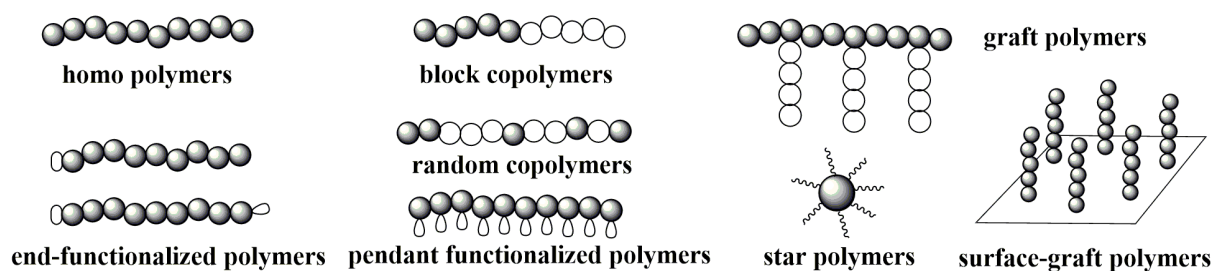


Figure 2: Different polymeric architectures from homo- and copolymers. Adapted from ref. [17] and [19].

Furthermore, tacticity of the polymers plays a crucial role when applying these materials. As the microstructure has a strong influence on the crystallinity, it determines the thermal and mechanical properties of the polymer. The distinction of microstructures and sequences in the polymer is, in most cases, quantitatively possible *via* nmr spectroscopy. Furthermore, the assignment of the signals in the nmr spectrum are individual for each polymer and are based on nmr spectra from oligomers and 2D nmr studies. In addition, physical and statistical calculations are required.^[20-21] The splitting pattern of a signal is influenced by the neighboring centers of the respective stereo center. By looking at the nearest neighboring groups, three signals, the so-called triads, arise defined as *mm* (*isotactic*), *mr / rm* (*heterotactic*), and *rr* (*syndiotactic*) (Figure 3). In case of a good resolution of the nmr spectrum, the nmr signals even split depending on the configuration of the next two neighboring stereocenters. The result is a splitting into ten different pentads. To numeralize these linkages the percentage of the respective triad/pentade in relation to the total signal can be given. A further possibility is the calculation of the possibility of *meso-* (P_m) or *racemic-* (P_r) linkages with $P_m = mm + [0.5 \times (mr+rm)]$ and $P_r = rr + [0.5 \times (mr+rm)]$.^[22] The analysis of the nmr spectra gives also conclusions about the polymerization mechanism. If the last incorporated molecule from the polymer chain influences the stereochemistry of the newly coordinating monomer, a chain end control mechanism (*Bernoulli-* or *Markov-distribution*) is apparent. If a chiral catalyst environment acts stereoregulating, the polymerization proceeds *via* an enantiomorphic site-control mechanism.^[22]

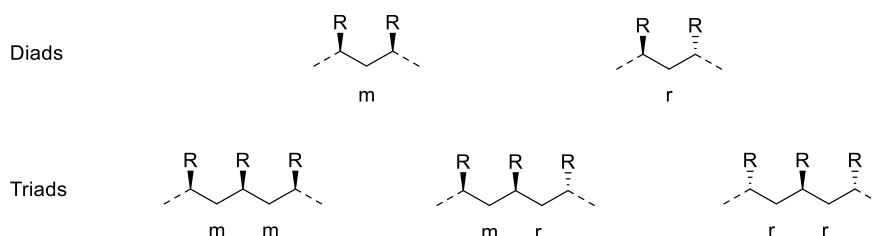


Figure 3: Stereoconfiguration in *meso-* and *racemic-*linkages.^[22]

2.2 Coordination-insertion polymerization

To produce polymers with very narrow molar mass distributions, a predictable molar mass, several functionalities and a specific tacticity coordination polymerization techniques are necessary. These methods are able to efficiently synthesize materials with specific thermal and mechanical properties. Highly efficient synthesis routes are mandatory not only for high-performance polymers, but also for commodity polymers to produce cost-efficient tons of polymeric material as potential bulk raw materials.

The coordination polymerization was developed by *Karl Ziegler* and *Giulio Natta* which shared the *Nobel* prize in chemistry in 1963. They were able to polymerize non-polar monomers (1-alkenes, cycloalkenes, dienes, alkynes) *via* coordination polymerization. In contrast to commonly used polymerization types (chain- or step-growth polymerization), they could perform these reactions with low pressure and low temperature.^[23-24] In 1953, *Karl Ziegler* developed the polymerization of ethylene at the *Max-Planck* Institute for Coal Research in Mülheim an der Ruhr with titanium catalysts (e.g. TiCl_4 in combination with aluminum alkyls or alkyl halides). Then in 1954, *Giulio Natta* used them to synthesize stereoregular polymers from propylene.^[23]

Since then, olefin polymerization with new generations of metalorganic homogeneous catalysts has grown to the largest area in polymer production. These highly active and stereoselective catalyst are used to produce diverse polyolefins such as HDPE, LLDPE, high-melting polypropylene or ethene-propene rubber (EPR).^[23]

2.2.1 Ring-opening polymerization of lactones

Besides polyolefins as commodity polymers, tailor-made polymers for more challenging and specific applications are in high demand in industry. A significant ratio of these engineering polymers is produced *via* ring-opening polymerization (ROP). Most polymers produced *via* ROP are sold as ecofriendly specialty materials, because they are biobased, biocompatible and/or biodegradable.^[25] In this field, the ROP of ϵ -caprolactam to PA-6 (*Nylon-6*, *Perlon*®) is best-known. Besides lactams, also lactones can be converted to their respective polymers *via* ROP. The most prominent examples for lactones are ϵ -caprolactone (ϵCL), *racemic* β -butyrolactone (BBL), *meso* or *racemic* lactide (LA), glycolide (Gly), δ -valerolactone (δVL) and β -propiolactone (βPL) (Figure 4).

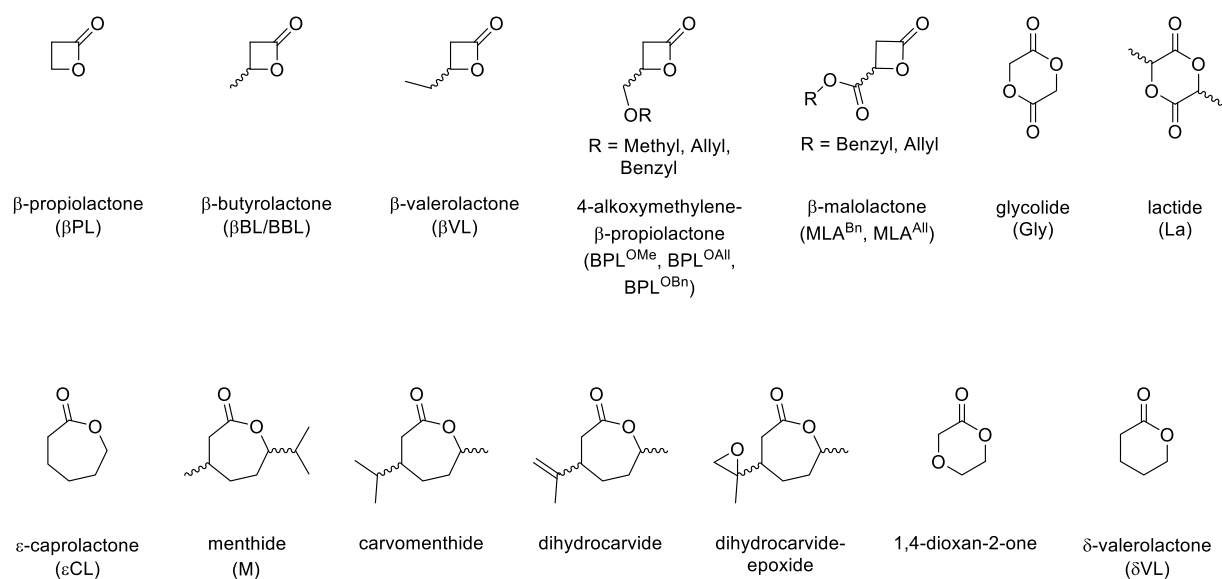


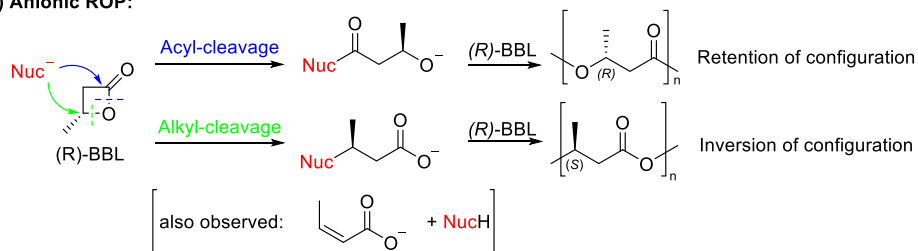
Figure 4: Selection of lactones for anionic and coordination ROP (without stereoinformation).

The resulting poly(esters) were first synthesized by polycondensation reaction, but to reach high molecular weight polymers ROP of the respective lactones is a very attractive and simple route. Using this polymerization type “tailor-made” polymers with very narrow molar mass distributions and a predictable molar mass are reachable.^[26] The number of processes reported for the ROP of lactones is extremely high. Most prominent are ROP reactions *via* anionic or coordinative polymerization techniques. The driving force is often the reduction of the ring strain of the lactone and four-, six- and seven-membered lactones can be converted easily to the respective polymers. In case of five-membered rings usually oligomers are obtained due to a fast reverse reaction.^[25]

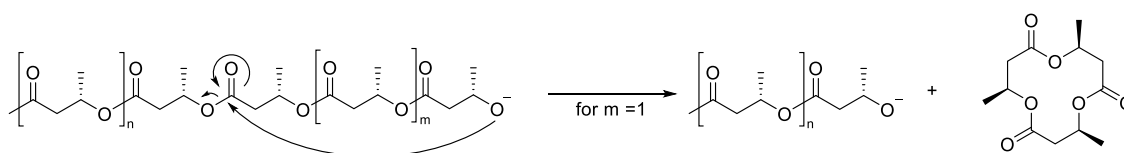
The anionic ring-opening polymerization of β -lactones can proceed by two different mechanisms. When the lactone is attacked by a negatively charged initiator (nucleophilic metal alkoxide) at the carbonyl group, an acyl-oxygen cleavage takes place, resulting in an alkoxy-terminated species. This mechanism is also observed for other lactones besides β -lactones. Solely for β -lactones, a carboxyl-terminated species is obtained if the lactone is attacked (e.g. by a carboxylate salt) at the alkyl position and thus by cleavage of the alkyl-oxygen bond. This mechanism is preferred for β -lactones. Both mechanisms are shown in Scheme 1.1 with (R)- β -butyrolactone ((R)-BBL) as monomer.^[25, 27-29] In case of the acyl-bond cleavage, a retention of configuration of the stereocenter is obtained. During alkyl-bond cleavage, the configuration of the stereocenter is inverted.^[30] Till now, different contrary opinions were raised for the exact mechanisms of the attack of different nucleophilic initiators to β -lactones.^[25, 28, 31] If there are no protic species involved in the polymerization, it is a living-type

polymerization, because termination reactions do not take place. One major disadvantage of ROP are transesterification reactions, as the alkoxide species of the growing chain and the initiator can react with all ester functions, in detail not only with the one of the lactone, but also with all other ester groups incorporated in the polymer chain (Scheme 1.2). Therefore, cyclic oligomers, a loss in molecular-weight and a broadening of the molar mass distribution occur. The use of a more sterically hindered and less nucleophilic initiator can provoke an attack at the more reactive lactone ester function than at the polymeric ester functions, which leads to a higher selectivity. The second disadvantage is the inability to obtain high molecular-weight poly(3-hydroxybutyrate) (PHB) from *rac*-BBL, because of several side reactions (Scheme 1).

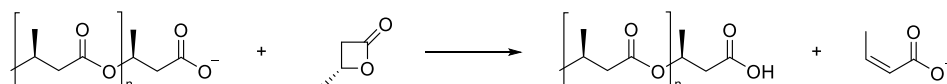
1) Anionic ROP:



2) Transesterification reactions:



3) Transfer to monomer during polymerization with β -lactones:



Scheme 1: Anionic ROP of (R)-BBL (1) and possible side-reactions of β -lactones during this polymerization technique (2+3).^[27]

As PHB is one of the most common members of the class of poly(hydroxyalkanoates) (PHA), efficient polymerization starting from BBL is a major goal. To overcome these disadvantages, a good control of the polymerization is needed and can be reached by using alkoxide-based metals as initiators. This opened the field of coordinative ring-opening polymerization.^[25, 32] One of the first examples of anionic living-type coordination-insertion polymerization was reported by *Teyssié et al.* in 1976 by use of bimetallic $\text{Al}_2/\text{Zn(II)}$ and $\text{Al}_2/\text{Co(II)}$ μ -oxo alkoxides with ϵCL , βPL , and δVL (Figure 5). No transfer or terminations reactions were observed, shown by a linear relationship between conversion and molar masses and narrow polydispersities. Mechanistic studies showed, that the monomer is inserted into the

aluminum-oxygen bond *via* acyl-oxygen cleavage during polymerization (Scheme 2).^[33-34] Furthermore, *Proctor, Billingham* and *Smith* were able to polymerize *racemic* BBL, which is much more difficult to convert with these systems, but the reaction was extremely slow, not perfectly living-type in its mechanism and only 45% were converted after 14 days at 40 °C. In addition, *atactic* PHB was obtained.^[32]

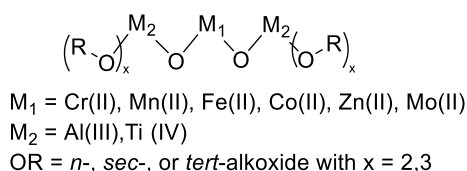
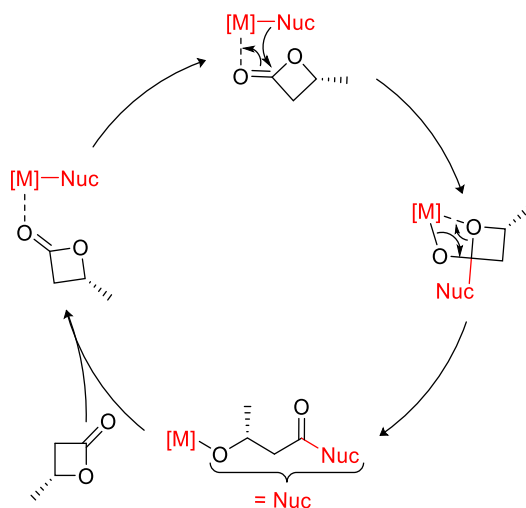


Figure 5: First efficient bimetallic μ -oxo alkoxides for controlled coordinative ROP.^[33]

Since then, an enormous number of catalysts were reported in literature that initiate ROP of lactones, but especially lanthanide complexes showed high activity while maintaining good control over the polymerization. First examples were published in 1992 by *McLain* and *Drysdale*, who showed that lanthanide-*iso*-propoxides (Ln = Y, Er, Dm, Dy, La), which occur as oxo-alkoxide cluster, are able to polymerize ϵ CL in a controlled and fast reaction.^[25] *Evans* and *Katsumata* showed the activity of samarium(II) as metal center in $(\text{C}_5\text{Me}_5)_2\text{Sm}(\text{thf})_x$ metallocenes for polymerization of ϵ CL.^[35] The monomer and catalyst scope was broadened by *Yasuda* and coworkers, who used lanthanide-alkyls ($\text{SmMe}(\text{C}_5\text{Me}_5)_2(\text{thf})$, $[\text{SmH}(\text{C}_5\text{Me}_5)_2]_2$) for the living-type polymerization of ϵ CL and δ VL and lanthanide-alkoxides ($\text{SmOEt}(\text{C}_5\text{Me}_5)_2(\text{OEt}_2)$, $[\text{YOMe}(\text{C}_5\text{H}_5)_2]_2$, $\text{YOMe}(\text{C}_5\text{Me}_5)_2(\text{thf})$) for these two monomers and β PL.^[36] Afterwards, also more simple yttrium, neodymium and lanthanum *iso*-propoxides (e.g. by *in situ* reaction of *iso*-propanol with $\text{Y}[\text{N}(\text{SiMe}_3)_2]_3$, $\text{Nd}[\text{N}(\text{SiMe}_3)_2]_3$ or yttrium/lanthanum tris(2,6-*tert*-butylphenolate)s) were used for the controlled polymerization of L-lactide, *meso*-lactide, ϵ CL, δ -hexalactone and δ VL.^[37-42] Mechanistic studies with $\text{La}(\text{O}^i\text{Pr})_3$ showed, that the polymerization proceeds in a typical anionic coordination manner *via* acyl-oxygen cleavage similar to the first aluminum μ -oxo alkoxides (Scheme 2). In the course of these publications, BBL was also mentioned as monomer, but the polymerization remained less controllable due to side- and termination-reactions.^[42] Solely, *Spassky et al.* performed partly living-type and fast reactions with *rac*-BBL using yttrium 2-methoxyethoxide, verified by narrow polydispersities and the possibility to perform copolymerizations with L-lactide.^[43] This group was also able to isospecifically polymerize *rac*-BBL with organometallic species (ZnEt_2 , CdMe_2 , AlEt_3) and chiral (*R*)-3,3-dimethylbutane-1,2-diol *via* acyl-oxygen cleavage of the monomer (Figure 6, left). Zinc and aluminum complexes converted the (*R*)-BBL, whereas cadmium species incorporated the (*S*)-monomer. In course of these polymerizations, zinc was identified as the most active metal-center. It was shown, that the catalyst possesses different active sites

leading to crystalline polymer of only moderate enantiomeric enrichment and amorphous polymer that has to be separated by precipitation.^[44] Similar observations were made by polymerization of *rac*-BBL with aluminoxane-catalysts.^[45-47]

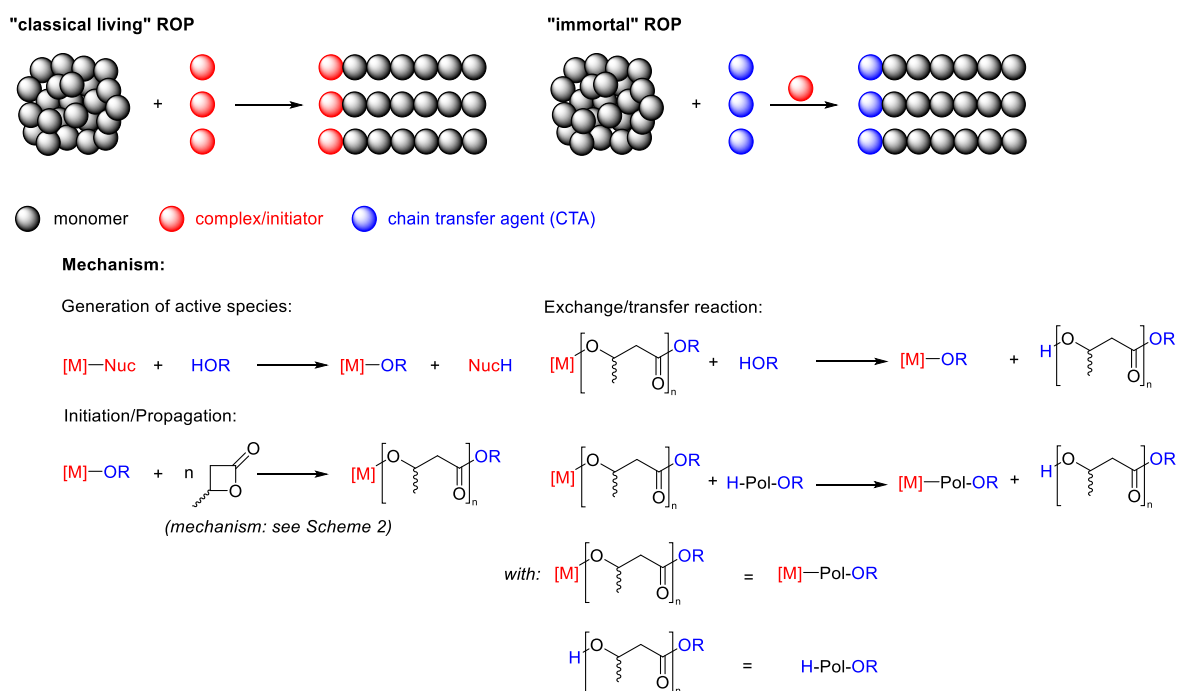


Nuc = nucleophilic initiating group: OR, NR₂, alkyl, etc.

[M] = oxophilic metal center with ligands: [Ln], [Zn], [Al], etc.

Scheme 2: Reaction mechanism for anionic coordinative ROP with nucleophiles based on metals.

The first highly active zinc-based catalysts were reported by *Hillmyer* and *Tolman* and by *Coates et al.* *Hillmyer* and *Tolman* investigated dizinc- or zinc-alkoxides and zinc-bis(phenolates) for ϵ CL, (-)-menthlide and lactide polymerization, but not for BBL as monomer.^[48-51] *Coates et al.* used zinc-single-site β -diiminates for lactide, *rac*-BBL and *rac*- β VL polymerization (Figure 6, middle).^[30, 52] Coordination-insertion polymerizations were performed in a living-manner with up to 2000 equivalents of monomer under mild conditions, resulting in narrow distributed polymer; but in case of BBL only *atactic* PHB was obtained.^[30] Similar β -diiminato-complexes with bis(trimethylsilyl)amide (btsa = N(SiMe₃)₂) as initiator and up to 10 eq. of alcohol, which act *in situ* as chain transfer agent (CTA), were published by *Carpentier et al.* It was the first example of a successful immortal polymerization of a β -lactone.^[53] Whereas during living polymerization protic compounds such as alcohols can instantaneously quench the propagation, immortal polymerization is “resistant” against these protic substances. The number of polymer chains is higher than the amount of initiator molecules, because the protic compounds serve as chain transfer agents. After formation of the active species by replacing the nucleophilic initiator of the catalyst with the CTA, very rapid chain transfer/exchange reactions take place that are faster than the propagation reaction generating a polymer with narrow molar mass distributions (Scheme 3).^[54-55]



Scheme 3: Distinction between "living" and "immortal" polymerization and mechanism for "immortal" ROP. Adapted from ref. [56].

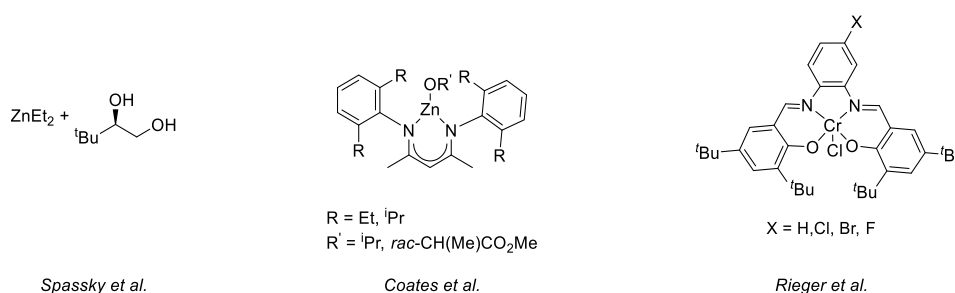
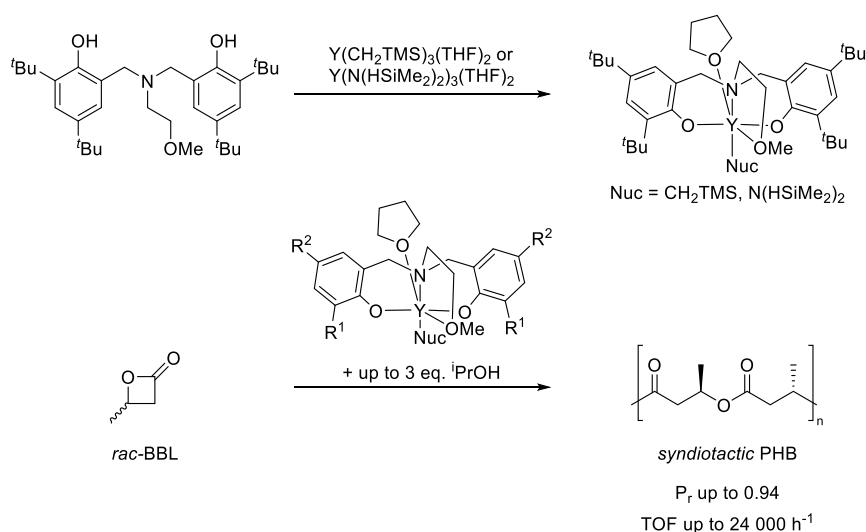


Figure 6: Transition-metal complexes for polymerization of *rac*-BBL.^[30]

Recently, *Rieger* and coworkers published electron-deficient β -diiminato-zinc-ethyl complexes that bear trifluoromethane-groups in the ligand backbone, enabling increased activities due to a higher *Lewis*-acidity of the resulting complexes.^[57] The same group described chromium(III)-salphen complexes for polymerization of *rac*-BBL to *isotactic*-enriched PHB (P_m up to 66%) as a blend with *syndiotactic* and *atactic* proportions and a high molecular mass, but also leading to a very broad polydispersity and a low isotacticity (Figure 6, right). A slow heterogeneous catalytic process and an occurrence of a simultaneous *iso*- and *syndio*-enrichment in this polymerization technique was assumed with different chromium-species in a bimetallic or even multimetallic mechanism.^[58-60]

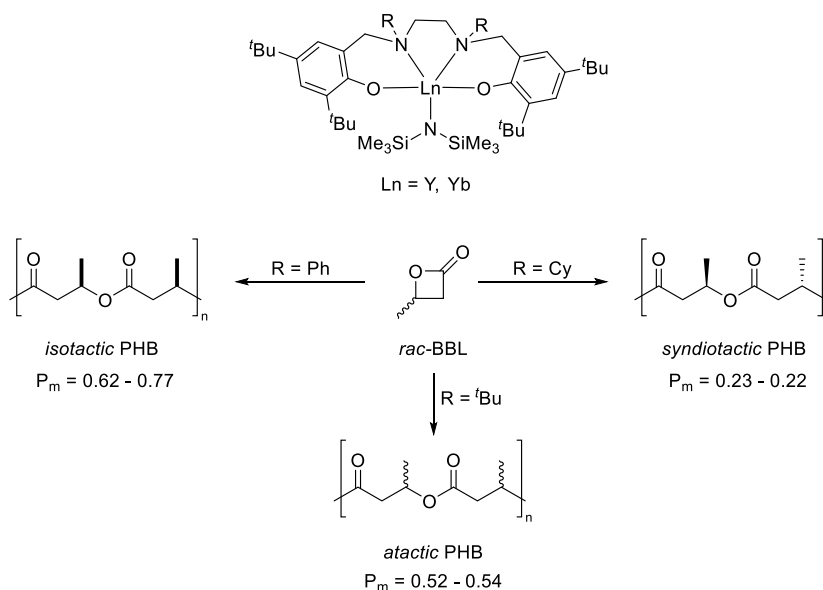
The first *syndiotactic* PHB was obtained in a living-type polymerization reaction with various tin-complexes (e.g. Bu_3SnOMe , distannoxanes).^[61-64] However, only very slow polymerization led to low *syndiotactic* dyads in the polymer. The mechanical properties of these *syndiotactically* enriched polymers are insufficient to use them as engineering plastics.^[27] Therefore, further extensive research on lanthanides was carried out as previous studies showed the high potential of these metal centers, to perform controllable and especially stereospecific reactions of *racemic* BBL. *Carpentier* and coworkers did not only investigate zinc-complexes, but they also synthesized aminoalkoxy-bis(phenolate)yttrium complexes. The first complexes were bis(dimethylsilyl)amide ($\text{bdsa} = \text{N}(\text{HSiMe}_2)_2$) and bis(trimethylsilyl)methyl (CH_2TMS) yttrium-complexes with a *tert*-butyl substituted aminomethoxy-bis(phenolate) ligand ($[\text{ONOO}]^{\text{tBu}}$), which only differ in their nucleophilic initiator, and were first tested in methyl methacrylate polymerization.^[65] These complexes were synthesized by the reaction of an yttrium precursor ($[\text{Y}(\text{Nuc})_3(\text{thf})_2]$; $\text{Nuc} = \text{CH}_2\text{TMS}, \text{N}(\text{HSiMe}_2)_2$) with one equivalent of the protonated ligand (H_2L ; $\text{L} = [\text{ONOO}]^{\text{tBu}}$). Crystallographic analysis revealed that in both complexes one thf molecule serves as a coordinating ligand, therefore the yttrium atom is six-fold coordinated and the complex forms a distorted octahedron (Scheme 4).^[65] Afterwards, these complexes and an analogue lanthanum-complex were tested in ROP of lactide and showed very high activity.^[66] In addition, further ligands with more sterically demanding substituents (e.g. adamantyl, CMe_2Ph) and neodymium as metal center were successfully tested in this polymerization. Furthermore, *in situ* replacement of the initiator with 1-50 equivalents of 2-propanol was performed. Very efficient initiators for the synthesis of *heterotactic* poly(lactide) from *rac*-lactide were observed in “classical-living” or “immortal” ROP with controlled molar weights and very narrow molar weight distributions. The sterically demanding ligands played an important role in achieving high heteroselectivity in this chain-end controlled polymerization.^[67-68] All these symmetrical aminoalkoxy-bis(phenolate) ligands $[\text{ONOO}]^{\text{R}}$ are synthesized by a *Mannich* reaction with the corresponding substituted phenol, formaldehyde, and the respective amine.^[69] This dianionic ligands are superior to others as they can stabilize the highly oxophilic and electrophilic metal center in presence of large amounts of alcohol.^[56] The monomer scope was broadened, when this group published the syndiospecific BBL polymerization with these complexes (Scheme 4). Especially, the *in situ* generated *iso*-propoxide complex with a $\text{CMe}_2\text{Phenyl}$ or a *tert*-butyl aminomethoxy-bis(phenolate) ligand were highly active (TOF up to 24000 h^{-1}) with generating low polydispersities, even if 2000 eq. of *rac*-BBL are used, and *syndiotactic* PHB with a tacticity of up to 94%. A chain-end mechanism according to the *Bernoulli*-model was calculated for this polymerization type.^[70-71] Immortal ROP with *rac*-BBL was only slightly possible with up to 3 equivalents of *iso*-propanol leading to polymer chains with narrow polydispersities, a use of more than 5 eq. of alcohol was not possible and led to a drastic decrease in activity.^[56, 68]



Scheme 4: Synthesis of $[\text{ONOO}]^{\text{tBu}}\text{Y}(\text{Nuc})(\text{thf})$ complexes ($\text{Nuc} = \text{CH}_2\text{TMS}$ or $\text{N}(\text{HSiMe}_2)_2$) and their use in syndiospecific ROP of *rac*-BBL.^[65, 70]

Over time, a multitude of different initiators^[72-75], ligand substituents,^[76-77] rare-earth metals,^[73-75, 77-81] chain transfer agents^[68] and side arms/backbones^[73-75, 77-78, 80-83] were introduced to the bis(phenolate) catalysts.^[84] None of these complexes could reach the performance of the original complexes in BBL polymerization regarding stereospecificity or activity. Solely, a CPh_3 -substituted aminoalkoxy-bis(phenolate)yttrium complex produced PHB with similar *syndiotactic* proportions to the $\text{CMe}_2\text{Phenyl}$ -substituted one.^[71] Rieger *et al.* investigated in detail the influence of different metal centers on the activity and stereoselectivity of *tert*-butyl-substituted bis(phenolate) complexes with a *bdsa* initiator analogue to complex $[\text{ONOO}]^{\text{tBu}}\text{Y}(\text{bdsa})(\text{thf})$ in BBL polymerization and substantiated their results with DFT-calculations. Kinetic measurements showed a monometallic coordination–insertion mechanism of the catalysts. They obtained an increase of activity and stereoselectivity with decrease in metal-radius ($\text{Sm} < \text{Tb} < \text{Y} < \text{Lu}$). The highest turnover frequency (TOF) of 6900 h^{-1} for an amido-complex and P_r of 88% was obtained for the $\text{Lu}[\text{ONOO}]^{\text{tBu}}(\text{bdsa})(\text{thf})$ complex. Remarkably, they could not reproduce the high activity of the yttrium-complex with an amide initiator and the low polydispersity of the resulting *syndio*-PHB reported before by Carpentier *et al.*^[79] DFT-calculations were used to determine the energetic differences between *iso*- and *syndio*-propagation, because none of the bis(phenolate) complexes produced *iso*-enriched PHB until then. A strong influence of the ligand on the propagation mechanism was calculated. In case of the preferred *syndio*-propagation, steric repulsion between the ligand's substituents and the methyl-group of BBL is decisive for this mechanism as it is lower than for *iso*-propagation.^[79]

Very recently, Yao *et al.* reported on the use of novel diamine-bis(phenolate)ytterbium and yttrium catalysts that produce *isotactic* and *syndiotactic* PHB in dependence of the substituents bound to the nitrogen-atoms of the ligand backbone (Scheme 5). If phenyl groups are used *isotactic* to *isotactic*-enriched PHB is obtained with $P_m = 0.66$ (yttrium) to $P_m = 0.77$ (ytterbium). Cyclohexyl and *tert*-butyl groups led to *syndiotactic* PHB ($P_m = 0.23 - 0.22$) and *atactic* PHB ($P_m = 0.52 - 0.54$), respectively.^[85]

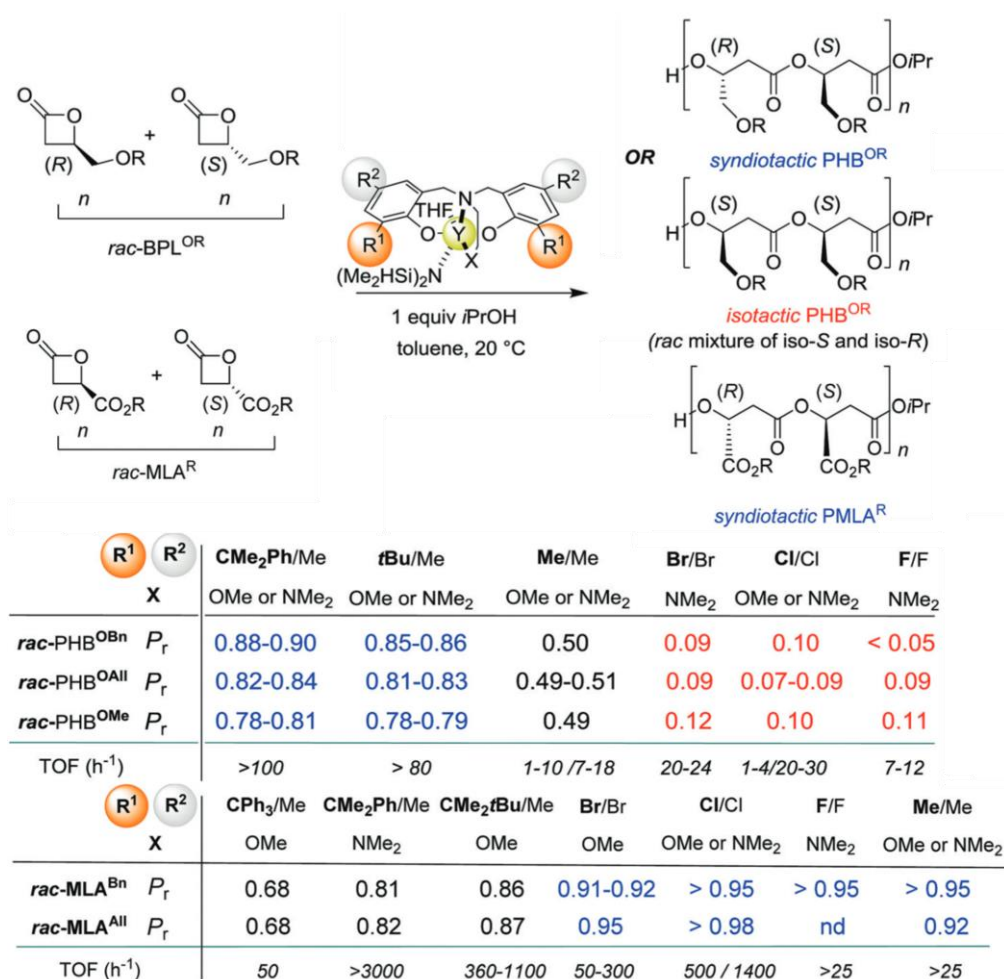


Scheme 5: Stereospecific switchable polymerization of *rac*-BBL with rare-earth metal bis(phenolate)amide complexes with different substituents at the nitrogen of the ligand structure.^[85]

Furthermore, other ligand structures were introduced to these complexes. Salalen-,^[86] phenoxy-thioether-^[87], salen-like fluoros dialkoxy-diimino-^[88], mixed fluoros alkoxy/phenoxy-diimino-^[89] enediamido-^[90], phenoxy-amidinate-^[84] bis(guanidinate)-^[91], and bis(amide)^[92]-complexes all showed a good control in “living” or “immortal” ROP of lactide or BBL. But overall, they could not reach the reactivity or selectivity of the bis(phenolate) complexes.

To obtain *isotactic* poly(ester) similar to PHB, different β -lactones with more bulky substituents were tested in ROP with bis(phenolates). The first stereoselective controlled ROP of functionalized *racemic* β -lactones (4-alkoxymethylene- β -propiolactones (BPL^{OR}) and β -malolactones (MLA^R) was reported by Carpentier *et al.* The highly active bis(phenolate)ytterbium catalysts with the general structure [(ONOO)^RY(bdsa)(thf)] bearing different substituted ligands and one equivalent of *iso*-propanol were used (Scheme 6).^[93] A simple change of the sterical crowding or the electronic properties of the ligand had a drastic influence on the resulting microstructure of the polymer in case of all *racemic* BPL^{OR} (R = methyl, allyl or benzyl) monomers. Chloro-substituents promote highly isoselective

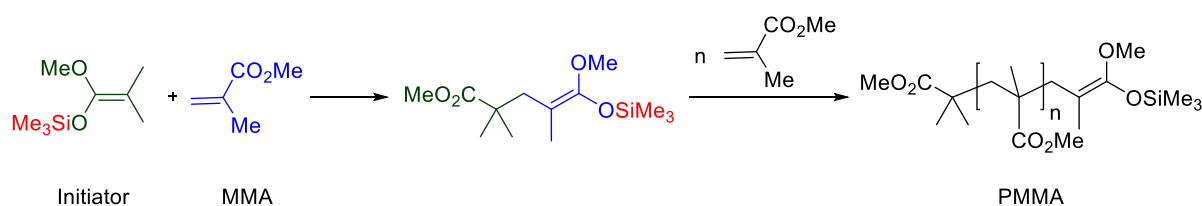
polymerization, bulky-substituents led to *syndio*-propagation. DFT calculations show that Cl-H interactions between the ligand and a proton of the methylene-proton of the side group of the growing polymer chain play a significant role in an *iso*-propagation of BPL^{OR} as they lower the energetic barrier.^[93] Same effect was shown by using bromo- and fluoro-substituents.^[94] Interestingly, using *racemic* β -malolactones MLA^R (R = allyl or benzyl) instead as monomers each catalyst produced *syndiotactic* polymers with various degrees of *syndiotactic* diads (chloro/fluoro/methyl-substituents: P_r up to > 0.95). This is again in accordance with DFT calculations, because the exocyclic methylene group of BPL is exchanged against a carbonyl-group in MLA which disables Cl-H interactions in the propagation step.^[95]



Scheme 6: Polymerization of *rac*-BPL^{OR} and *rac*-MLA^R with [ONOO]^{RY}(N(SiHMe₂)₂)(thf) and one equivalent of *iso*-propanol. Adapted from [93-95].

2.2.2 Metal-catalyzed group-transfer polymerization of polar vinyl monomers

The controlled living polymerization of α,β -unsaturated esters, ketones and nitriles, such as methyl acrylates, dimethylacrylamides or acrylonitriles has been studied by *Sogah* and *Webster* in the early 1980s.^[96] For the initiation of this polymerization type, which proceeds *via* an anionic-catalyzed conjugate addition, ketene silyl acetals were used.^[96-97] The mechanism of this polymerization is exemplified by reaction of methyl methacrylate (MMA) with dimethylketene-methyl-trimethylsilyl acetal shown in Scheme 7. In the early stages, it was stated, that the trimethylsilyl-group (red) in each polymerization step is transferred to the new monomer to form a new silyl end. Because of this transfer of the silyl end, the name "group-transfer polymerization" (GTP) has emerged.^[96, 98] The possibility of carrying out living-type addition polymerizations has opened a new field in polymerization catalysis.^[98] At a later date, criticism of this mechanism was made, and considerations were expressed that there occurs no group-transfer of the trimethylsilyl group in chain growth and only a group-transfer between the two chain ends can take place (poly-1-4-addition *via* an ester-enolate-anion intermediate), nevertheless the name of the polymerization has been preserved.^[98-100]



Scheme 7: Group-transfer polymerization of MMA with organosilicon initiators according to *Sogah* and *Webster*.^[96]

Since these first studies on GTP, various catalytic systems were investigated in this, until now less popular, polymerization type. In case of metal-catalyzed GTP all systems have a similar polymerization mechanism in common, which is basically a poly-1,4-*Michael*-addition. The initiation occurs *via* the attack of a nucleophile at the 4-position of the first monomer. The propagation proceeds through the repeated attack of the enolate-species of the monomer to a new monomer unit in its current 1,4-unsaturated form. A new enolate-species is formed, coordinated to the metal center, which again attacks a monomer. Therefore, α,β -unsaturated carbonyl compounds and nearly all types of *Michael*-type acceptor systems are suitable so far for this special case of an anionic polymerization type.^[101-104] The enormous scope of available monomers is depicted in Figure 7. Beneficial for GTP in comparison to classical anionic polymerization is the stabilization of the chain-end enabling highly controlled reactions at room and elevated temperature in which side reactions are prohibited.^[100-102]

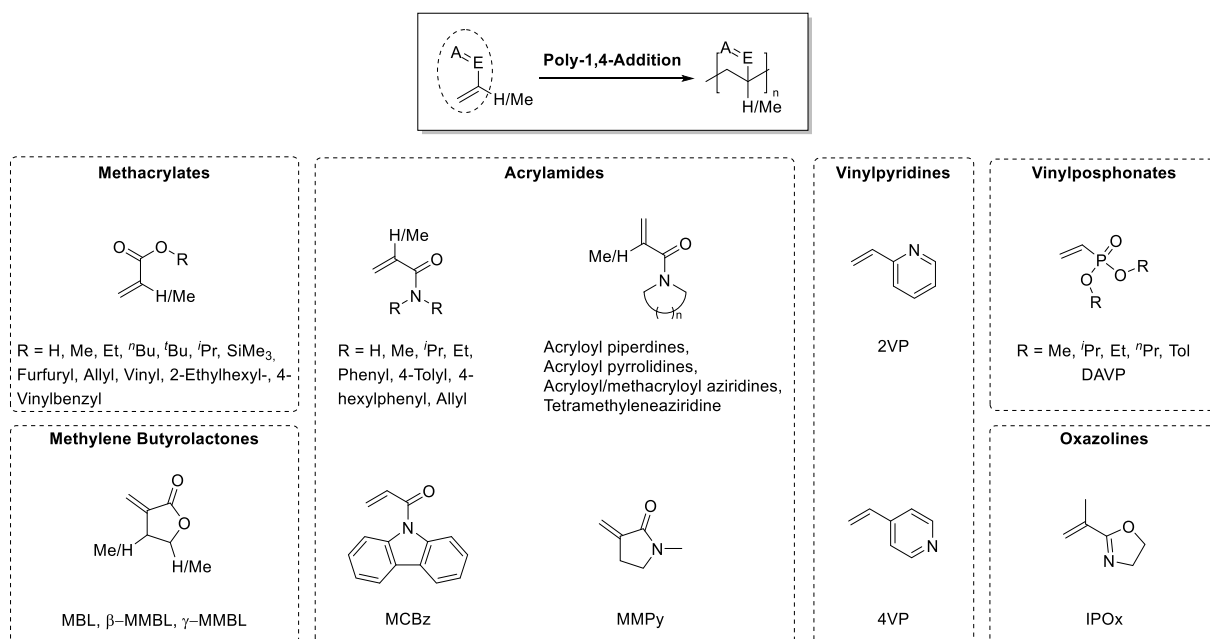
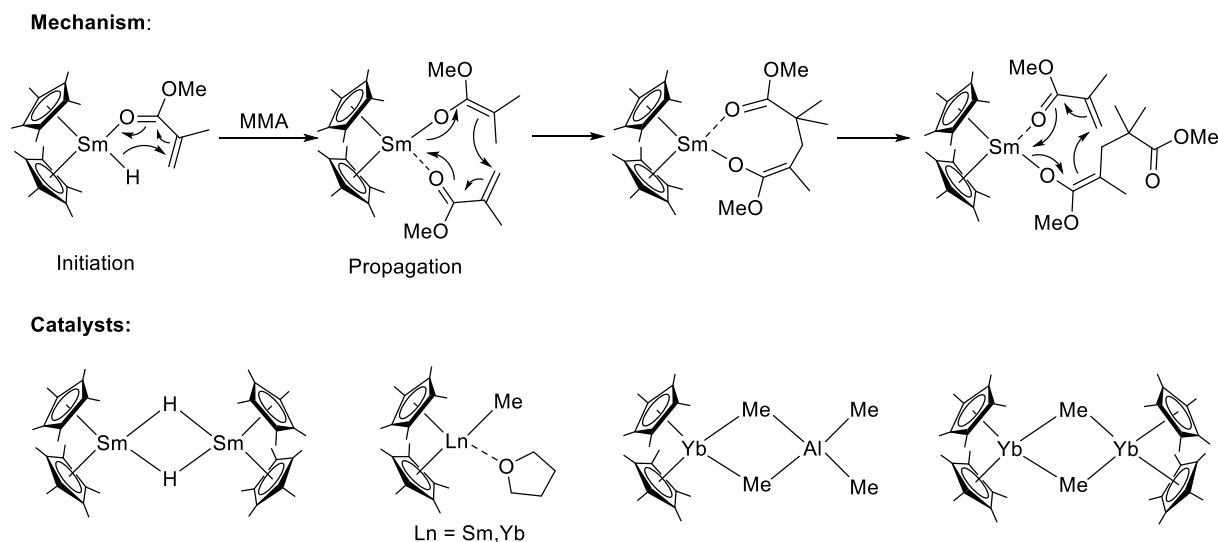


Figure 7: Scope of *Michael*-type monomers suitable for metal-catalyzed GTP. Adapted from ref. [17].

Studies on transition-metal-catalyzed polymerization of methyl methacrylate were first carried out in 1992 by two independent research groups, after researching samarium-mediated CH and CO activation with complexes of this type between 1985 and 1988.^[105-106] Yasuda *et al.* synthesized high molecular weight, *syndiotactic* poly(methyl methacrylate) (P_r up to 95%) with very low polydispersities ($D < 1.05$) *via* living-type GTP catalyzed by organolanthanide(III) complexes such as $[(Cp^*)_2SmH]_2$ (Scheme 8). These catalysts were active at temperatures between -95 and 40 °C. The isolation and crystallographic analysis of a 2:1 adduct of MMA and $[(Cp^*)_2SmH]_2$ showed that one of the two MMA molecules is present as an enolate and the other in its keto form. This is coordinated *via* the carbonyl group to the metal center. A monometallic, 8-membered, cyclic transition state according to Yasuda *et al.* arises in the propagation step (Scheme 8).^[107] The intramolecular repulsion of two methyl-groups of the MMA monomers involved in the propagation step was supposed to be crucial for the *syndio*-propagation of the polymerization.^[105] Even if *iso*-butylmagnesium and 4-vinylmagnesium, which had previously been used to polymerize methyl methacrylate, are also able to produce *syndiotactic* polymer, very low temperatures were necessary and the polymer was isolated in low yields and with small molecular weights.^[107] In addition, introduction of chiral ligand moieties (e.g. *neo*-menthyl) to the organolanthanide complexes could change the syndiospecificity of similar catalysts with different metal centers (La, Y, Sm, Lu) into an isotacticity. The *isotactic* ratio of the polymer was the highest when low polymerization temperatures (-35 °C) were used. At room temperature the stereoregularity was lower and polydispersities were extremely high ($D \leq 7.9$).^[108]



Scheme 8: Initiation and propagation mechanism for MMA polymerization according to *Yasuda et al.* and scope of used catalysts.^[107]

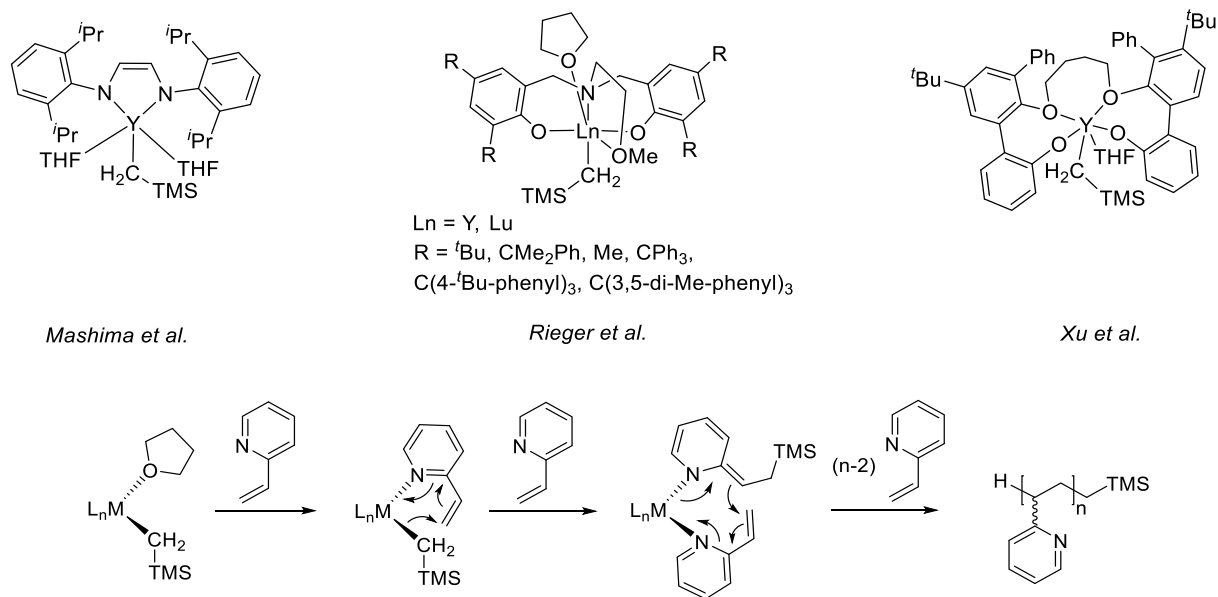
The second group investigated at the same time another special class of well-investigated catalysts for GTP which are zirconocene complexes. *Collins* and *Ward* examined the polymerization of MMA in the presence of a cationic and a neutral zirconocene as a two-component system ($[\text{Cp}_2\text{ZrMe}(\text{thf})][\text{BPh}_4]$) and $(\text{Cp}_2\text{ZrMe}_2)$.^[109-110] It has been shown that the polymerization proceeds *via* a chain-end control and with low polydispersities ($D = 1.2 - 1.4$) of the resulting *syndiotactic* poly(methyl methacrylate).^[109] Related studies performed by these two groups show that the propagation mechanism is not similar to that proposed for the organolanthanides investigated by *Yasuda et al.* as the propagation step includes a bimetallic intermediate.^[110] Isospecific MMA polymerization *via* enantiomeric-site control was enabled through introduction of chiral moieties to these catalyst.^[110] Further studies uncovered the relationship between the ligand-structure and the microstructure of obtained PMMA if similar single component cationic zirconocenes were used. While MMA polymerization with $[\text{Me}_2\text{CCpIndZrMe}(\text{thf})][\text{BPh}_4]$ was highly isospecific at room temperature, using symmetric $[\text{Me}_2\text{CCp}_2\text{ZrMe}(\text{thf})][\text{BPh}_4]$ led to *syndiotactic* PMMA at low temperatures.^[111-112] The scope of available monomers for zirconocene-mediated GTP was broadened when in 2004 *Mariott* and *Chen* used highly active chiral *ansa*-metallocenium enolate cations ($\text{rac}-(\text{C}_2\text{H}_4(\text{Ind})_2)\text{Zr}(\text{thf})[\text{OC}(\text{O}^i\text{Pr})=\text{CMe}_2][\text{MeB}(\text{C}_6\text{F}_5)_3]$) first for isoselective polymerization of *N,N*-dimethylacrylamide (DMAA) and MMA and afterwards for various acrylamides, methacrylates and renewable methylene butyrolactones in a living, monometallic and intramolecular coordinative conjugate-addition mechanism.^[113-118]

As sustainability is an emerging topic in the field of macromolecular chemistry, the exchange of petroleum-based monomers is an essential task in creating new synthetic polymers. Since 2010, *Chen et al.* have investigated the polymerization catalysis of renewable methylene butyrolactones *via* GTP mechanism. The naturally occurring α -methylene- γ -butyrolactone (MBL), the plant biomass-derived γ -methyl- α -methylene- γ -butyrolactone (γ MMBL) and β -methyl- α -methylene- γ -butyrolactone (β MMBL) were polymerized with different samarocenes, nonmetallocene lanthanides, alane-based *Lewis*-Pairs and zirconocene-catalysts. The obtained polymers show enhanced thermal properties pointed out by high glass transition and decomposition temperatures (T_g up to 227 °C) which are much higher than for *atactic* PMMA.^[117, 119-120]

Regarding the scope of *Michael*-monomers used, diverse methacrylates and acrylamides were investigated almost exclusively. Monomers such as vinylphosphonates which show high biocompatibility and water-solubility were not considered and were instead synthesized *via* free-radical or anionic methods. However, radical polymerization of dialkyl vinylphosphonates resulted only in the preparation of oligomers with low molecular weights without quantitative conversion. In addition, side-products are formed by intramolecular hydrogen transfer from the alkyl side chain to the polymer backbone. This transfer generates radicals in the side chains, to which new monomers add. These P-O-C bonds are more unstable and easier to cleave leading to low molecular weight polymer.^[121] The anionic polymerization of vinyl phosphonates is also possible, as *Gopalkrishnan et al.* proved in 1988. This method was applied in 2008, when *Parvole* and *Jannasch* polymerized diethyl vinylphosphonate (DEVP) with an anionic method using *n*-butyllithium and 1,1-diphenylethylene as a co-initiator onto polysulfones. The co-initiator reduces the nucleophilicity of the initiator to prevent nucleophilic attack at the phosphorus atom and the deprotonation of the acidic proton in α -position to the phosphorus. Nevertheless, anionic polymerization of vinyl phosphonates gave only polymers with a broad molecular weight distribution and a maximum molecular weight of 100 kg/mol.^[121] In 2010, *Rieger et al.* investigated these dialkyl vinylphosphonates (DAVPs) as monomers in lanthanocene-catalyzed polymerization. Over the years, they used lanthanocenes with the general form Cp_2LnX ($X = Cp, Me, CH_2SiMe_3, Ln = Gd-Lu$). Because of the structural and electronic similarity of DAVPs to MMA, the group-transfer polymerization of vinyl phosphonates also shows a living character which results in low polydispersity and high molecular weights.^[121-124] The first studies on Cp_2YbCl and Cp_2YbMe already showed good activity of this catalysts in GTP of diethyl vinylphosphonate, but were outperformed by simple Cp_3Ln ($Ln = Lu, Yb, Tm, Er, Ho, Dy$) complexes which produced well controlled polymers with exceptional high activity ($TOF^* > 265000\ h^{-1}$; $TOF^* =$ adjusted TOF by the initiator efficiency).^[122-123] In further studies, a *Yasuda*-type mechanism was confirmed.^[125] The group of *Rieger* also tested the group-

transfer polymerization for other monomers such as 2-*iso*-propenyl-2-oxazoline (IPOx), DMAA, and 2-vinylpyridine (2VP) with these lanthanocenes. Here again, all polymerizations showed a living character indicated by low polydispersity and an exact control of molecular weights.^[19, 126] Besides MMA, lanthanocenes were not yet considered for stereospecific polymerization and, in addition, showed insufficient polymerization activity for 2VP and IPOx. As a consequence, investigations in organometallic chemistry are also concerning the development of new mono- and polydentate ligands in the rare-earth metal-mediated group-transfer polymerization, which go beyond the previously studied cyclopentadienyl system.^[126-127]

In 2003, *Carpentier et al.* investigated the activity of bis(phenolate)yttrium complexes with two different initiators for the polymerization of MMA (see chapter 2.2.1 for characterization and synthesis).^[65] *Rieger et al.* utilized similar 2-aminoalkoxy-bis(phenolate) catalysts with the general form (ONOO)^RY(CH₂TMS)(thf) (R = ^tBu, CMe₂Ph) for the polymerization of 2VP, DMAA, DEVP and IPOx under mild conditions with moderate to high activities (Scheme 9). Regarding 2VP polymerization, these complexes showed at this time the highest activity (TOF = 1110 h⁻¹) with an exceptional high initiator efficiency of 0.99, which means that 99% of the complex molecules are active in polymerization. In addition, very low molar mass distributions (*D* = 1.01 – 1.07) of poly(2-vinylpyridine) (P2VP) were observed. ESI-MS studies with oligomeric 2-vinylpyridine demonstrated that the reaction is initiated by an attack of the nucleophilic CH₂TMS-group to the first monomer in a 6-electron process. *In situ* IR monitoring of the polymerization confirmed a monometallic *Yasuda*-type polymerization mechanism. In addition, kinetic measurements were performed which showed opposing trends for metallocenes and nonmetallocenes regarding the impact of the metal radius and the monomer-type on the activation energy.^[128] In 2011, *Mashima et al.* showed that polymerization of 2VP is also possible with an endiamido-yttrium catalyst (Scheme 9). The obtained polymers showed only low molecular weights, but *Mashima* stated that this P2VP is nearly perfectly *isotactic* ([*mmmm*] = 95%).^[129] Criticism of these results was expressed as the tacticity-determining nmr spectra were recorded in a different solvent (CDCl₃), as would have been necessary for the pentade splitting and calculation of [*mmmm*] (CD₃OD). Spectra in CDCl₃ show different chemical shifts, intensities and coupling constants.^[130]



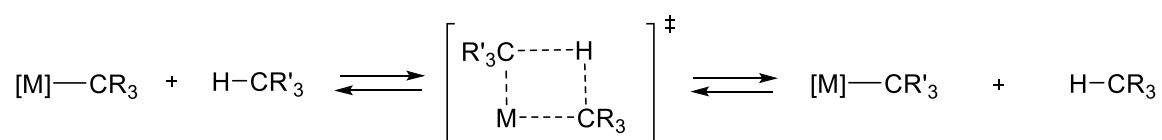
Scheme 9: Nonmetallocene lanthanides that are active in GTP of 2VP and the assumed polymerization mechanism of 2VP.^[128-129, 131]

Until 1960, 2-vinylpyridine was exclusively produced *via* radical methods and *atactic* polymer was obtained. Afterwards, *Natta et al.* developed an anionic method in which organometallic compounds, such as magnesium, beryllium or aluminum amides were used. The polymerization is initiated by insertion of the monomer into a polarized metal-carbon or metal-nitrogen bond.^[132-133] In the reaction of 2VP with magnesium amides of the general form X-Mg-NR₁R₂ (R₁, R₂ = alkyl groups) at 45 °C crystalline and *isotactic* P2VP was obtained. This high tacticity is explained due to a favored arrangement of two monomer units in the polymer by coordination of the magnesium in *gauche*-position.^[134] Polymerizations with lithium- or sodium-containing organic compounds at -78 °C lead to only *isotactic* oligomers, but *atactic*, amorphous P2VP due to a lower coordination ability of the 2-vinylpyridine to alkali metals. Studies on molecular weights and conversions showed that these polymerization do not follow a living-type reaction mechanism.^[132] Since 1980, *Soum* and *Fontanille* investigated the living anionic polymerization of 2VP with organomagnesium compounds in nonpolar solvents to achieve a stereospecific polymerization. To avoid side reaction by attack of the nucleophile at the pyridine ring, they used organometallic compounds which are reduced in their reactivity. Benzylpicolyl-magnesium was used to induce tacticity through unsymmetrical active sites *via* coordination of the nitrogen atoms of the last two monomeric units in the polymer chain to the magnesium. Isotacticities of up to 93% could be achieved by *Markov* chain-end control.^[135-136] Recently, three different other approaches towards highly isospecific 2VP polymerization with lanthanide-complexes were established by the groups of *Xu* and *Rieger*.^[130-131, 137-138] Newly developed

C_1 -symmetric bis(phenolate)yttrium catalyst investigated by *Rieger et al.* show a dependence of the steric demand of the *ortho*-position at the phenolate rings on the isotacticity of the resulting P2VP. *Isotacticities* up to $P_m = 92\%$ could be reached with a bis(phenolate) catalyst bearing a tris(3,5-dimethylphenyl)methyl-group in *ortho*-position of one phenolate-ring. Mechanistic investigations *via* proton-nmr studies revealed an enantiomorphic site-control as the tacticity-determining mechanism.^[130, 137] The group of *Xu* developed yttrium bis(phenolate)ether catalysts in which the stereospecificity of the complex depends on the number of carbon-atoms in the backbone of the ligand. Poly(2-vinylpyridine) with highly isotactic ($P_m = 0.97$) and high-molecular weight characteristics was obtained (Scheme 9).^[131] A simpler approach by this group with lutetium-complexes with the general form $[\text{Lu}(\text{CH}_2\text{TMS})_3(\text{X})_2]$ ($\text{X} = \text{pyridine, thf}$), which were only used as precursor complexes so far, produced perfectly *isotactic* P2VP with $[\text{mmmm}] = 99\%$. Despite the high activity of these catalysts, the absence of regulating ancillary ligands led to a rise of the polydispersities of the polymers ($\mathcal{D} = 1.22 - 2.34$).^[138]

2.3 C-H bond activation

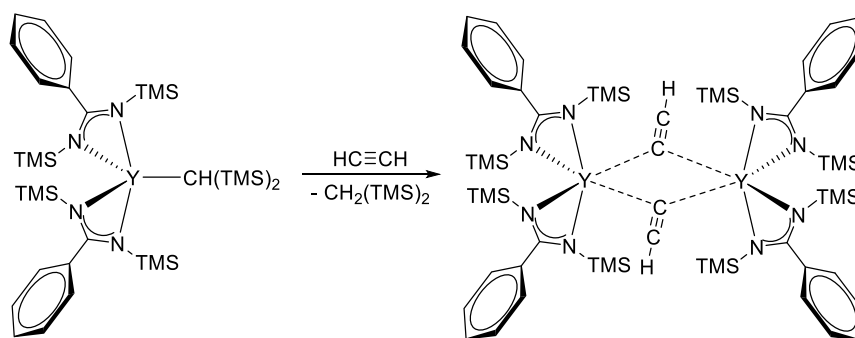
Lanthanide-complexes can undergo σ -bond metathesis in a $[2\sigma+2\sigma]$ cycloaddition (Scheme 10). This type of C-H bond activation of trivalent lanthanides is one of the most effective methods in metalorganic chemistry for the cleavage of C-H bonds. These are, with a bond energy between 90 - 100 kJ/mol and a low acidity and basicity, one of the most unreactive and difficult bonds to cleave. As trivalent lanthanides and d^0 -transition metals do not possess any electrons for oxidative addition- and reductive elimination-reactions, σ -bond metathesis is the only way to introduce new molecules to these complexes *via* C-H bond activation.^[139-142]



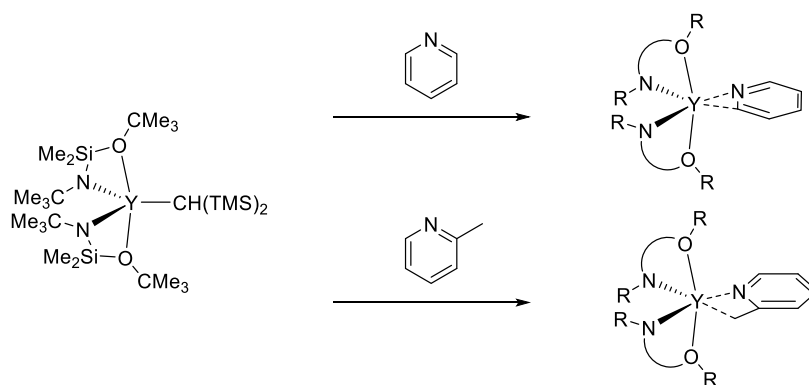
Scheme 10: C-H bond activation by d^0 transition-metal complexes and trivalent lanthanides through σ -bond metathesis.^[22]

This C-H activation was first demonstrated by *Watson* in 1983 with ^{13}C -labeled methane and $(\text{Cp}^*)_2\text{LuCH}_3$ and by activation of benzene, pyridine, and phosphorylidene with cyclopentadienyl-lanthanide-methyl complexes. These were the first examples of the activation of an sp^3 -hybridized C-H bond in methane which is known to be unfavorable to undergo σ -bond metathesis.^[143-145] Over the last 30 years, many catalysts have been developed that are able to activate C-H bonds selectively under mild conditions. However, this field of research is still basic and is only rarely used in application.

Since 1993, *Teuben et al.* have been investigating the reactivity of nonmetallocene yttrium catalysts bearing two chelating N,N' -bis(trimethylsilyl)benzamidinato ligands towards C-H bond activation of ethyne. A dimer with two newly formed $\text{Y}-\mu\text{-C}$ bonds is generated, as shown in Scheme 11.^[146] The group also investigated the C-H bond activation of heteroaromatic substances such as pyridine or α -picolyl derivatives. A bis(N,O -bis(*tert*-butyl)alkoxy(dimethylsilyl)amido)yttrium complex was reacted with pyridine, methyl-pyridine, and ethyl-pyridine to form the respective bis(alkoxysilylamido)yttrium-pyridyl and -picolyl complexes (Scheme 12). In case of reaction with 2-picoline and ethyl-pyridine C-H bond activation occurred solely at the sp^3 -alkyl group. Crystallographic analysis of the pyridine-activated complex show that the pyridyl ligand coordinates *via* a $\eta^3\text{-(C,C,N)}$ -*aza*-allylic motif.^[147]

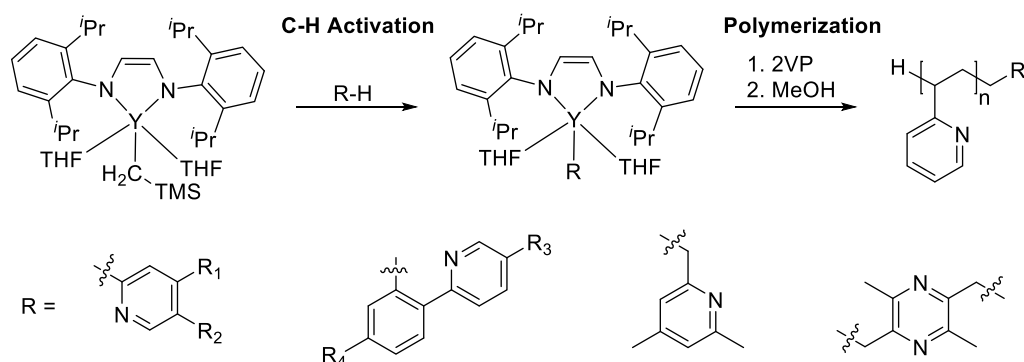


Scheme 11: Synthesis of dimeric bis(*N,N'*-bis(trimethylsilyl)benzamidinato) yttrium ethynyl complex via σ -bond metathesis.^[146, 148]



Scheme 12: Synthesis of bis(alkoxysilylamido)yttrium-pyridyl-complexes.^[147]

Afterwards, *Mashima* and coworkers investigated the possibility of terminal functionalization of P2VP by C-H bond activation of a variety of alkynes and heteroaromatic compounds such as 2,4,6-trimethylpyridine (*sym*-collidine), 1-trimethylsilyl-1-propyne, or 2,3,5,6-tetramethylpyrazine (TMPy) with yttrium-en-diamido complexes.^[129, 149] The catalysts with the novel pyridyl initiators were prepared *in situ* by σ -bond metathesis and studied in the polymerization of 2-vinylpyridine (Scheme 13).^[129] The group further investigated more complex and multistep C-H bond activation with similar yttrium-en-diamido-complexes and different heteroaromatics (e.g. 2-trimethylsilylpyridine, benzo[h]quinolone). They obtained a pyridyl-yttrium-mediated 2,2'-bipyridyl formation via unique $\text{C}(\text{sp}^2)\text{-C}(\text{sp}^2)$ coupling of 2-phenylpyridine.^[150] Polymerization studies of these complexes were not performed.



Scheme 13: Polymerization of 2-vinylpyridine with C-H bond activated pyridyl-yttrium-en-diamido complexes.^[129]

Mechanistic studies on lanthanocenes with strongly basic alkylinitiators, performed by *Rieger* and coworkers, showed that DEVP polymerization with these initiators are slow due to possible side reactions. Deprotonation of the acidic α -CH occurs and initiation *via* nucleophilic attack of the initiator to the first monomer does not take place. New and more efficient initiators can be introduced *via* C-H bond activation by σ -bond metathesis. C-H bond activation of heteroaromatic compounds with rare-earth cyclopentadienyl systems were successfully performed. The reaction of $\text{Cp}_2\text{Y}(\text{CH}_2\text{TMS})(\text{thf})$ with one equivalent of *sym*-collidine led to the formation of $\text{Cp}_2\text{Y}(\text{CH}_2(\text{C}_5\text{H}_2\text{Me}_2\text{N}))$. C-H activation with the analogous lutetium catalyst was also successful but the reaction is less active. An increase in initiator efficiency for DEVP polymerization was observed.^[151] Recently, three-fold C-H bond activation of 1,3,5-tris(3,5-dimethyl-4-pyridinyl)benzene with $\text{Cp}_2\text{YCH}_2\text{TMS}(\text{thf})$ gave a trinuclear catalyst. This catalyst allowed the fast synthesis of star-shaped polymeric structures. Visualization of these star-polymers was achieved by transformation of poly(2-*iso*-propenyl-2-oxazoline) into P(IPOx-g-EtOx)-copolymers with subsequent analysis *via* AFM. Based on these findings a detailed study on the initiator efficiency of multinuclear complexes was conducted.^[152]

2.4 Polymers from polar monomers: Requirements and applications

2.4.1 Poly(3-hydroxybutyrate) as a biodegradable alternative for packaging

The use of thermoplastic polymers, such as poly(ethylene), poly(ethylene terephthalate) or poly(vinyl chloride), in households, automotive or the health care industry is nowadays self-evident.^[153] The growing limitation of raw materials rises to the challenge of having an economical handling of fossil resources. Therefore, the substitution of petrochemical-based plastics with polymers that are based on renewable resources is imperative. Carbon dioxide, terpenes, carbohydrates or vegetable oils can serve as sustainable monomers.^[154-156] In addition, recycling of polymers is often not possible or too cumbersome and expensive. As a result, they are stored on landfills or are burned, since they cannot be degraded in environment. Polymers that can be decomposed by microorganisms are an effective way to overcome these problems.^[153] Polyesters built up the fourth largest group of natural biomacromolecules, following the three major groups nucleic acids, proteins and polysaccharides.^[157] This class provides us with important polymers such as PET.^[157] In addition, poly(hydroxyalkanoates) are a well-known class of poly(esters), in which poly(3-hydroxybutyrate) is one of the most commonly used PHA. It was first discovered in 1925 by *Lemoigne* by extraction of PHB from *Bacillus megaterium*.^[158] When it is synthesized naturally *via* microorganisms, it serves as an intracellular carbon and energy storage compound in the cell cytoplasm and occurs in its strictly (R)-*isotactic* form. It is biodegradable as many depolymerase enzymes can cleave the ester bonds to generate hydroxybutyrate without generation of toxic decomposition products.^[159-163] Because of its high crystallinity and thermoplastic properties (*Young's* modulus, tensile strength), and thus its very similar properties to oil-based polymers (*isotactic* PP, PET, *Nylon-6,6*®), it is considered as a conceivable alternative for applications of these polymers (Table 1).^[158]

Table 1: Comparison of thermal and mechanical properties of natural PHB with conventionally used thermoplastic polymers.^[158]

Polymer	Melting Temp. [°C]	Glass transition Temp. [°C]	<i>Young's</i> modulus [GPa]	Tensile strength [MPa]	Strain [%]	Density [g/cm ³]
Natural PHB	175-180	-4	3.5-4.0	40	3.0-8.0	1.25
<i>Isotactic</i> PP	170-176	-10	1.0-1.7	29.3-38.6	500-900	0.90
PET	250-265	75	2.2-2.9	56-70	100-7300	1.35
<i>Nylon-6,6</i> ®	265	80	2.8	83	60	1.14

In addition, PHB has similar UV-resistance and oxygen barrier properties as *isotactic* PP making it very suitable as packaging material.^[158] However, the application is limited because of its low thermostability (melting point near to decomposition temperature) and high crystallinity which makes it brittle (very low strain elongation) and hard to process.^[27, 158] These drawbacks provoked an increasing research in the synthesis of PHB with various microstructures (Figure 8). Besides natural PHB, that occurs in its strictly (R)-*isotactic* form, ring-opening polymerization of different enantiomeric mixtures of β -butyrolactone can be used to obtain other microstructures of PHB. Either the use of solely (R)- or (S)-enantiomer can lead to *isotactic* polymer. If a *racemic* mixture of these two enantiomers is used three different microstructures are conceivable: *isotactic*, *atactic* or *syndiotactic*.

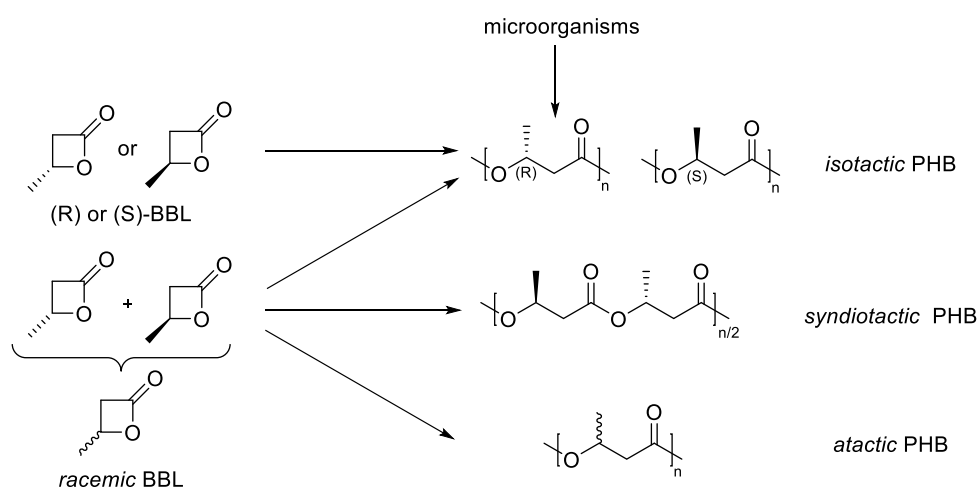


Figure 8: Possible stereoconfigurations of PHB after ROP of β -butyrolactone and production of exclusively (R)-PHB from microorganisms.

To replace *isotactic* PP with PHB, it is necessary to lower the melting temperature and increase the strain. In addition, the biodegradability must be sustained. To obtain these properties the crystallinity has to be reduced, but the configuration of the stereocenters have to be predominantly in (R) configuration. In the last years, it was shown, that the microstructure indeed has a significant influence on the thermal and mechanical properties (Table 2).^[158] Doi and coworkers performed a systematic study on the thermal and mechanical properties and the enzymatic degradation of *isotactic* PHB with decreasing percentage of *meso*-linkages. These polymers were synthesized with a specific ratio of (R)- and (S)-butyrolactone or (R)- and *rac*-BBL *via* ring-opening polymerization using ZnEt_2 or a distannoxane catalyst (see 2.2.1). Variable *isotactic* PHB ($[i] = 0.46 - 1.0$; $[i]$ = *isotactic* diad fraction; also called *meso*-diad) and *syndiotactic* PHB ($[i] = 0.30$) with molar masses ranging from 15-145 kg/mol were obtained.^[164-165] It was shown, that the melting point decreases with decreasing *isotactic* diads,

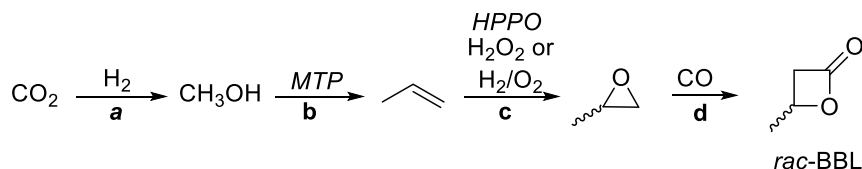
until disappearance of the melting point when *atactic* PHB is analyzed. Therefore, *atactic* PHB is oily and cannot be used as packaging material. When decreasing the *isotacticity* of the polymers, the *Young's* modulus and the tensile strength decreases, but the sample becomes more flexible and soft indicated by the strong increase in the elongation at break from 5 to 740% (Table 2, left). Enzymatic degradation experiments of these polymer samples were conducted with a PHB depolymerase from *Pseudomonas pickettii* in a potassium phosphate buffer. The amount of released hydroxybutyrate during enzymatic degradation against time was measured *via* absorbance-measurements of the reaction solution. Surprisingly, the rates for enzymatic degradation were higher for the synthetic *isotactic* PHB ($[i] = 0.68 - 0.94$) than for the strictly (R)-*isotactic* natural PHB ($[i] = 1.0$). The fastest degradation (seven times faster than for natural PHB) was observed for a polymer sample with $[i] = 0.76$. *Doi* and coworker suggested, that chains in the amorphous state are faster degraded than the ones in the crystalline state. Therefore, a decrease in crystallinity as observed for samples with lower tacticity increases the enzymatic degradation rate. However, *atactic* and *syndiotactic* PHB showed nearly no degradation (Table 2, right).^[164]

Table 2: Comparison of thermal and mechanical properties and enzymatic degradation of PHB with different tacticities.^[164]

<i>Isotactic diad</i> [i]	Melting Temp. [°C]	Glass-transition Temp. [°C]	<i>Young's</i> modulus [GPa]	Tensile strength [MPa]	Elongation at break [%]
1.00	177	5	1.5	38	5
0.84	132	6	1.9	15	7
0.76	107	6	0.3	11	10
0.68	92	5	0.09	11	740
0.30	62	6	0.02	13	1020

As mentioned before, a potential chemical synthesis route for PHB with this desired *isotacticity* ($P_m = 0.65 - 0.80$) might be the ring-opening polymerization of *racemic* β -butyrolactone. As BBL can be produced from carbon dioxide, it is an interesting monomer for sustainable PHB production (Scheme 14).^[166-172] Although nearly all conceivable PHB microstructures can now be synthesized by the ROP pathway, the stereoselective and efficient synthesis of (R)-PHB and (R)-*isotactically* enriched PHB ($P_m \geq 0.65$) from *racemic* BBL has been unsuccessful, despite intensive research in this field over a long period of time (see chapter 2.2.1).^[58, 70, 79, 173-176] Although, it would be possible to prepare *isotactic*

PHB by using enantiomerically pure β -butyrolactone, i.e. either only the (R)-enantiomer or the (S)-enantiomer, this option is not feasible as the separation of enantiomers is very time and cost consuming.



Scheme 14: Synthesis of *rac*-BBL: a) Catalytic hydrogenative conversion of carbon dioxide to methanol^[166]; b) Methanol-to-propylene(MTP)-process^[177]; c) Epoxidation of propylene (e.g. HPPO-process)^[167-170]; d) Ring expansion of propylene oxide^[171-172]

2.4.2 Thermoplastic elastomers from biobased copolymers

Beyond carbon dioxide, various natural products can be used for the preparation of biobased polymers. An important class among these are terpenes. They are characterized by the fact that their carbon skeleton consists of isoprene (C_5 -units) (Figure 9).^[178]

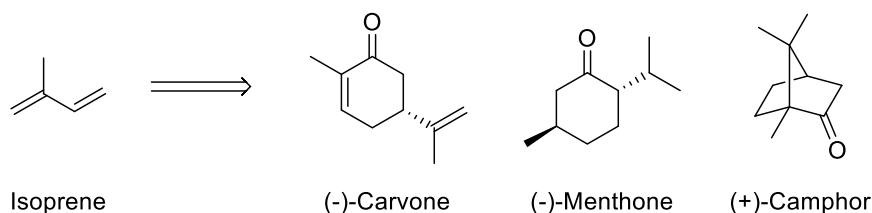
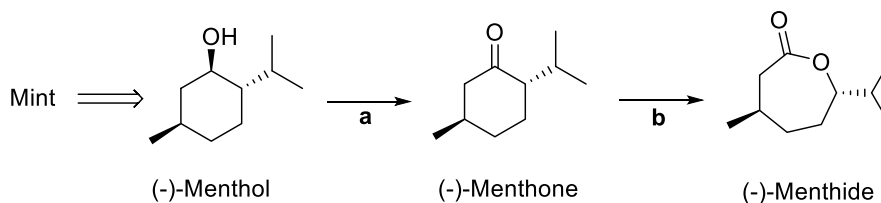


Figure 9: Cyclic terpenes (-)-menthone, (-)-carvone or (+)-camphor derived from skeletal structure isoprene.

The naturally occurring, cyclic representatives such as (-)-menthone or (-)-carvone can be converted to the corresponding lactones, which can be used as monomers for ROP.^[51, 179-181] (-)-Menthide is synthesized from the cyclic monoterpene (-)-menthol. (-)-Menthol can be obtained from the oils of plants named *Mentha Arvensis* and is produced annually in the scale of thousands of tons and is used in the pharmaceutical, fragrance and food industry (Scheme 15).^[51, 182]



Scheme 15: Synthesis of (-)-menthide: a) Oxidation of (-)-menthol^[183]; b) Baeyer-Villiger-oxidation^[51, 184]

After *Hall* and *Schneider* in 1958 performed polymerization of (-)-menthite for the first time using sodium, in 2005, the groups of *Tolman* and *Hillmyer* used zinc-alkoxides to polymerize menthite.^[51, 185-186] The reactions occurred in a controlled fashion and poly((-)-menthite) (PM) with molar masses up to 91 kg/mol with narrow to slightly broader molar mass distributions ($\mathcal{D} = 1.1 - 1.6$) were obtained. With higher catalyst loading and thus a higher molar mass of the polymer the polydispersity decreased.^[51] Since then, poly((-)-menthite) has been the subject in recent research, particularly in ABA triblock copolymers for the production of thermoplastic elastomers.^[187-188] Thermoplastic elastomers (TPE) are a special class among thermoplastics. They combine the properties of elastomers and thermoplastics, as they have the elasticity of elastomers, but can also be deformed at elevated temperatures like thermoplastics. In general, the molecular chains are not covalently linked within thermoplastic elastomers in contrast to elastomers. The use of block copolymers can lead to a phase separation of the two components in the block copolymer which causes a multiphase morphology. One phase is then the “soft” elastomer (amorphous, low T_g) while the other one is “hard” (high T_g or T_m) segment which prevents the diffusion and ensures that the material returns to its original shape (Figure 10). The most-established TPE copolymer is a styrene-butadiene-styrene-BAB block copolymer (SBS). The styrene parts are located only at the end of the polymer chains and therefore hold the chains together as they have a high T_g . The polybutadiene-part is the mid-block and has a rubber-like behavior due to its low glass-transition temperature.^[189]

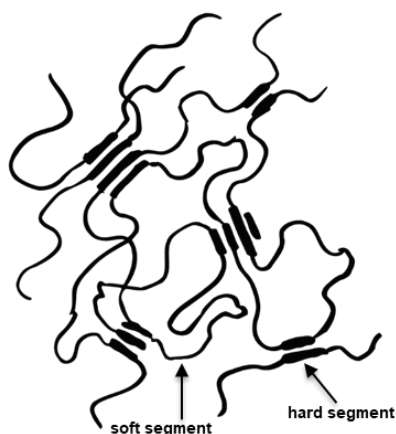
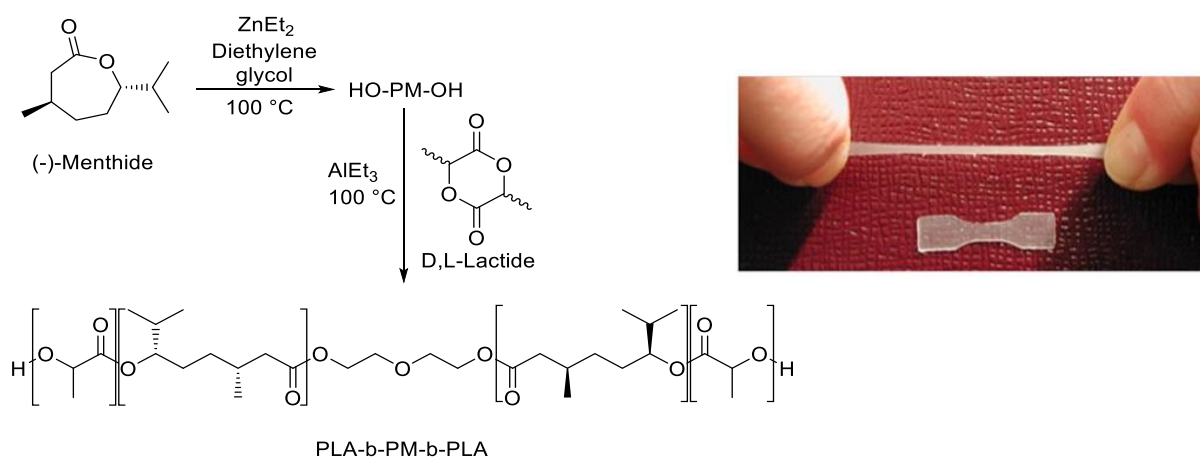


Figure 10: General structure of a BAB block copolymer consisting of a *semicrystalline*/hard and an amorphous/soft segment. Adapted from ref. [190].

Hillmyer and *Tolman* synthesized an α,ω -functionalized poly((-)-menthite) *via* ring-opening polymerization of (-)-menthite with diethylene glycol and diethyl zinc as the catalyst. Quenching with water afforded the dihydroxy-terminated poly((-)-menthite). The reaction of this telechelic polymer

with triethylaluminum formed the corresponding aluminum alkoxide macroinitiator for the controlled polymerization of lactide to yield renewable and sustainable PLA-b-PM-b-PLA triblock copolymer (Scheme 16). The molar mass and composition of the triblock polymer could easily be adjusted by the monomer-to-initiator ratio. Microphase separation in these copolymers was confirmed by small-angle X-ray scattering (SAXS) and differential scanning calorimetry (DSC). These BAB block copolymer form TPEs with soft PM and hard PLA segments and showed varying compositions and morphologies. Tensile measurements verified elongations and elastomeric properties of the PLA-b-PM-b-PLA TPEs.^[191] The groups also synthesized triblock polymers with different types of poly(lactide). Either amorphous poly(D,L-lactide) or *semicrystalline*, enantiopure poly(L-lactide) or poly(D-lactide) end segments were used. The *Young's* moduli and ultimate tensile strengths of the *semicrystalline* copolymers were up to three-times higher, than for their amorphous analogs.^[192]



Scheme 16: Synthesis of PLA-b-PM-b-PLA triblock polymers as renewable thermoplastic elastomers. Adapted from ref. [191] and [193].

Over the years, *Tolman* and *Hillmyer* developed a method using $\text{Sn}(\text{Oct})_2$ to obtain PLA-b-PM-b-PLA in a one-pot reaction *via* sequential ring-opening polymerization.^[184] In addition, poly(lactide) was substituted by Tulipalin A (α -methylene- γ -butyrolactone (MBL)), a natural substance found in the common tulip *Tulipa gesneriana L.*, resulting in fully renewable PMBL-b-PM-b-PMBL triblock polymers. Phase-separation was elucidated with DSC, AFM, and SAXS analysis. Tensile measurements showed high elongation and elastic recovery properties making these materials suitable candidates for high-performance and engineering thermoplastic elastomer materials.^[194] As a result, cyclic terpenes offer the possibility to produce versatile (co)polymers from renewable raw materials.^[51, 179-180, 195]

2.4.3 Tailor-made functional copolymers for high-tech applications

Besides ring-opening polymerization, group-transfer polymerization is a very efficient method to produce functional (co)polymers. Already in the 1970s, *DuPont* produced AB block copolymers of methyl methacrylate *via* group-transfer polymerization, which were used as dispersing agents for paints.^[100] Because of the living character of this polymerization type, it is possible to prepare block copolymers of all *Michael*-type monomers among another. Therefore, this polymerization type is also predestinated for the synthesis of other types of polymeric architectures e.g. star- and graft-copolymers (*vide supra*, Figure 2). Due to the enormous scope of accessible monomers, a multitude of combinations are possible by using monomers with different functional groups (Figure 7).^[19, 101] In metal-catalyzed GTP, the first block must be the monomer with lowest coordination strength to the metal center. To determine the relative coordination strength statistical copolymerization were conducted revealing an order of DAVP > (R)MAA > (R)MA > IPOx > 2VP (R = any substituent).^[115, 126] *Via* sequential addition of the next monomer(s) after the previous one is consumed entirely, AB-, ABC-, and multiblock-copolymers are easily available. *Rieger et al.* studied the preparation of block copolymers of 2VP and IPOx with other monomers. 2VP and IPOx can only be polymerized as the first block because of the lowest coordination strength to the metal center. Block copolymers with all other *Michael*-monomers (DEVP, DMAA, IPOx, MMA) as the second block were synthesized.^[126, 196] If monomers of the same class are used, block copolymers and random copolymers can be produced (Figure 11). Block copolymers are accessible by sequential addition, as described above.^[118, 197] Random copolymers are prepared by pre-additional mixing of monomers of the same kind followed by addition to the catalyst solution.^[198]

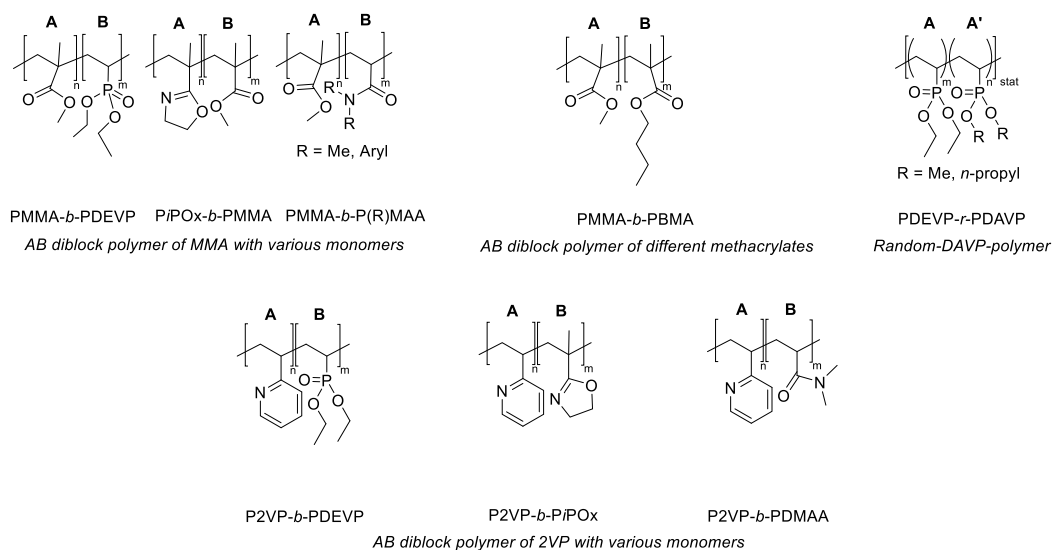


Figure 11: Examples of random and block copolymers synthesized *via* GTP.^[113, 115, 118, 128, 198]

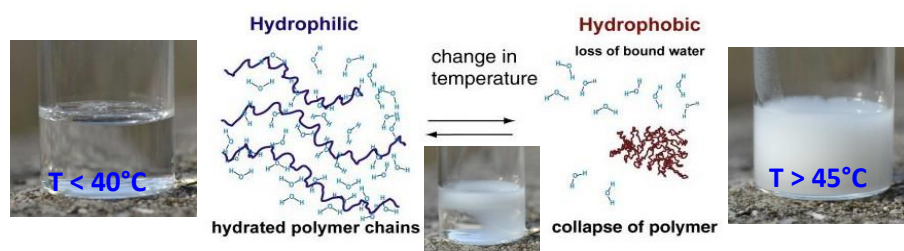
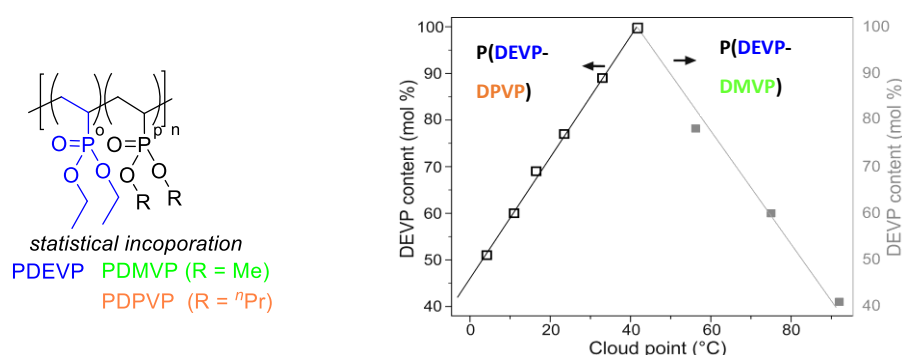
DEVP Homopolymer:

DEVP-DAVP statistical copolymer:


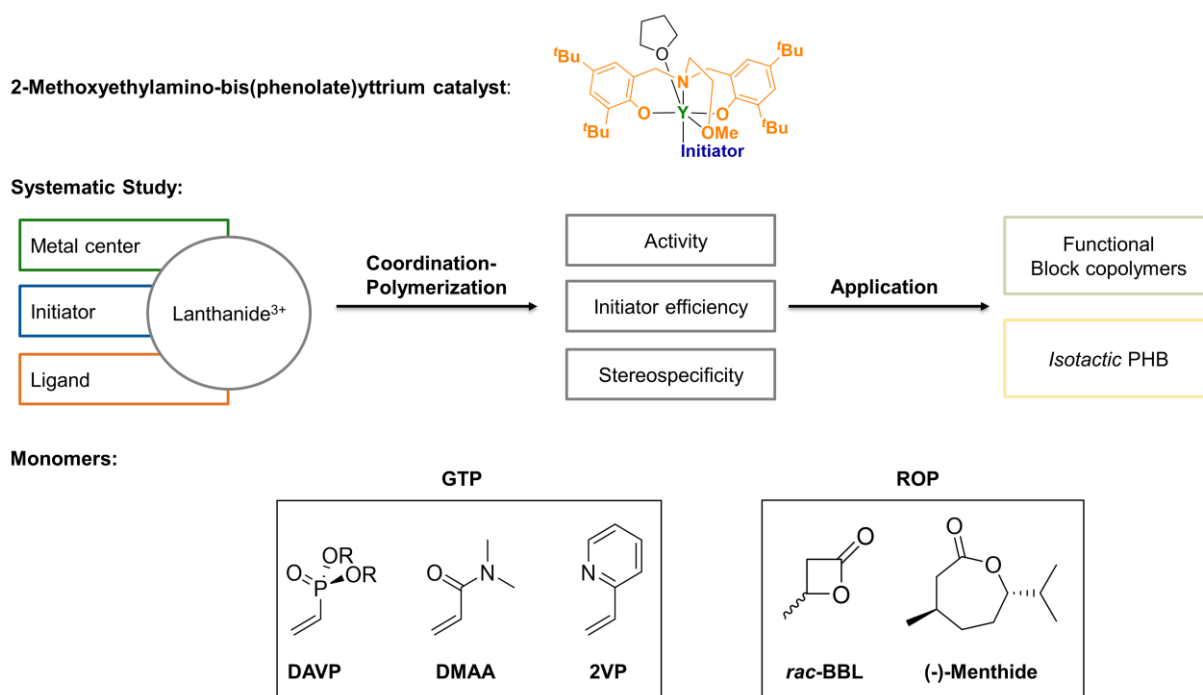
Figure 12: Lower critical solution temperature of DEVP homopolymer and shift of LCST in statistical copolymers of DEVP with different DAVPs. Adapted from. [123, 198-199].

As polymers with reversible and controllable stimuli-responsive properties are in high demand for medical applications, *Rieger et al.* performed studies on random copolymers of different hydrophilic dialkyl vinylphosphonates *via* REM-GTP.^[198] As poly(vinylphosphonates) show a differing solubility behavior depending on the nature of the ester side chain, different substituted vinylphosphonates were tested. Not only the side chain, but also the temperature plays a significant role in the solubility of a polymer in a solvent. Is a single (homogeneously mixed) phase only soluble above a certain temperature, the polymer possesses an upper critical solution temperature (UCST). The segregation below this temperature is an enthalpy driven process. If a solution is only thermodynamic stable below a critical temperature this temperature is called lower critical solution temperature (LCST). This temperature characterizes the maximum temperature at which the polymer can be dissolved. The precipitation that occurs at this temperature is in contrast to the UCST an entropically induced act.^[189] While hydrophilic poly(dimethyl vinylphosphonate) (PDMVP) is soluble in water, more hydrophobic poly(di-*iso*-propyl vinylphosphonate) shows high solubility in many organic solvents. As a result, poly(diethyl vinylphosphonate) (PDEVP) lays between these two extremes with an amphiphilic

behavior. Therefore, DEVP exhibits a LCST following a coil-globule transition mechanism (collapse of the macromolecule) which is near to the physiological range (Figure 12). The so far unreported LCST of PDEVP in water has been evaluated and a strong dependence on both, concentration and molecular weight of the polymer, was observed which lays between 40 – 46 °C.^[123] Afterwards, *Rieger* and coworkers showed that statistical copolymers of DEVP with DMVP and DPVP (di-n-propyl vinylphosphonate) exhibit a tunable LCST between 5 and 92 °C (Figure 12). The cloud points correlate linear with the content of hydrophilic/hydrophobic comonomer. These copolymers exhibit a sharp and reversible phase transition and only minor environmental effects on the cloud points such as concentration and additives were observed. As a result, these LCST-polymers are promising candidates for biomedical applications.^[198]

3 Aim of this thesis

Tripodal dianionic diamino- or aminoalkoxy-bis(phenolate) ligands ($[\text{ONXO}]^{\text{R1,R2}}$ with $\text{X} = \text{NR}_2, \text{OR}$) are a privileged class of ligands which attracted much interest in combination with group 3 and group 4 metals for generating highly efficient polymerization catalysts. When using yttrium as metal center, these complexes are highly active catalysts in two different coordination polymerization types: Ring-opening polymerization of lactones and group-transfer polymerization of *Michael*-type vinyl monomers (chapter 2.2). Within this thesis, modifications of the $[\text{ONOO}]^{\text{tBu}}\text{Y}(\text{CH}_2\text{TMS})(\text{thf})$ (TMS = trimethylsilyl) complex are performed to enable the synthesis of functional block copolymers and to synthesize polymers with so far inaccessible microstructures. These modifications include the exchange of the metal center, the initiator and the ligand (Scheme 17). Supplementary, the newly synthesized complexes were intensively studied in ROP and GTP of various monomers to provide insights into their activity, initiator efficiency and stereospecificity in these two polymerization types. Regarding ROP, *racemic* β -butyrolactone and (-)-menthide were chosen as monomers as both can be synthesized from renewable resources. GTP was performed with different functional monomers to enable a distinction between electron-donating (2VP) and non electron-donating monomers (DEVP, DMAA).



Scheme 17: Overview of the aim of this thesis: Modifications of a bis(phenolate)yttrium complex, systematic study of GTP and ROP and synthesis of functional block copolymers and *isotactic* PHB.

3.1 Modulation of the metal center

Changes in the metal center from yttrium to lutetium should be performed regarding the influence of the ionic radius on the polymerization. Because the 4f-electrons have no contribution to the binding valence orbitals, lutetium is an isoelectronic equivalent to yttrium, but with an increased *Lewis*-acidity. Similar bis(dimethylsilyl)amide catalysts $[(\text{ONOO})^{\text{tBu}}\text{Ln}(\text{bdsa})(\text{thf})]$ ($\text{Ln} = \text{Sm}, \text{Tb}, \text{Y}, \text{and Lu}$) have already been synthesized for mechanistic investigations of the ring-opening polymerization of β -butyrolactone and showed an increasing catalytic activity with decreasing ionic radius ($\text{Y} < \text{Lu}$). In this thesis, analogue CH_2TMS -complexes should be synthesized and investigated in group-transfer polymerization of the before mentioned monomers regarding the influence of the metal center on the activity, initiator efficiency and stereospecificity of the complexes (Figure 13).

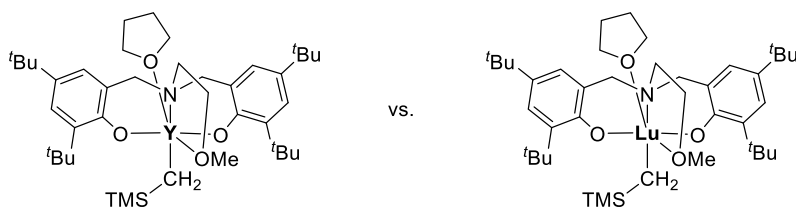
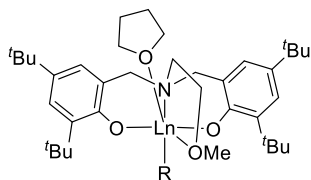


Figure 13: Bis(phenolate)yttrium and lutetium complexes with the structure $[(\text{ONOO})^{\text{tBu}}\text{Ln}(\text{CH}_2\text{TMS})(\text{thf})]$ ($\text{Ln} = \text{Y}$ and Lu).

3.2 Modulation of the initiator

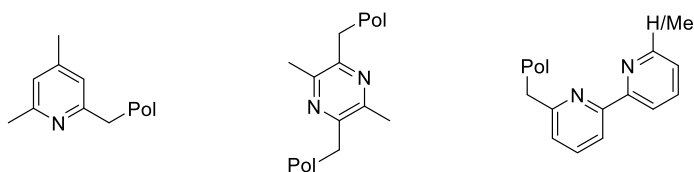
Our attention was also directed towards C-H bond activation of heteroaromatic compounds as σ -bond metathesis of alkylanthanide complexes has previously been reported as a versatile tool towards end-group functionalized polymers. Heteroaromatic electron-donating initiators (*sym*-collidine, 6-methyl-bipyridine (6-Mebpy) and 2,3,5,6-tetramethylpyrazine) should be introduced to improve the initiator efficiency and to perform a comparison with the highly basic alkylinitiators (Figure 14).

General catalyst structures:



R = C-H bond activated heteroaromatic compound

End-group-functionalized (co)polymers:



Pol = polymer

Figure 14: C-H bond activation of *sym*-collidine, 6-methyl-bipyridine and 2,3,5,6-tetramethylpyrazine with bis(phenolate) complexes and subsequent polymerization.

The use of rare-earth metal-mediated group-transfer polymerization allows not only precise molecular weights and narrow molecular weight distributions, but also the synthesis of block copolymers in a living-type mechanism *via* simple sequential addition of different monomers. In this thesis, C-H bond activation *via* σ -bond metathesis should also be performed to develop a new type of block copolymer-structure *via* GTP. As hydrophilic DEVP shows thermoresponsive behavior and hydrophobic 2VP shows a pH-dependent solubility, AB, and BAB block copolymers (A = 2VP; B = DEVP) should be synthesized, to obtain multiresponsive copolymers that self-assemble to micelles (Figure 15). A potential shift of the LCST of these polymers should be studied *via* statistical incorporation of dialkyl vinylphosphonates with variable hydrophilicity into the PDEVP-block. For the synthesis of BAB block copolymers, which are in detail B-A-X-A-B-systems (X = initiator), the bifunctional TMPy initiator and for the AB-polymers the catalyst with a CH_2TMS initiator must be tested. Both copolymer systems can be tested as drug delivery systems. In addition, our aim is to synthesize 2VP-DEVP-block copolymers with bipyridine (bpy) as end-groups. This aim can be achieved through C-H bond activation of α -methylated bipyridines to obtain a bpy-functionalized yttrium-catalyst. After polymerization, these bipyridines can serve as end-groups in the block copolymers and may enable metal complexation by the reaction of bpy-block copolymers with $[\text{Re}(\text{CO})_5\text{Cl}]$, providing a $[\text{Re}(\text{CO})_3(\text{bpy})\text{Cl}]$ motif as the end-group. If successful complexation is obtained, micellization experiments and reactions regarding the rhenium-mediated photocatalytic reduction of CO_2 to CO can be performed.

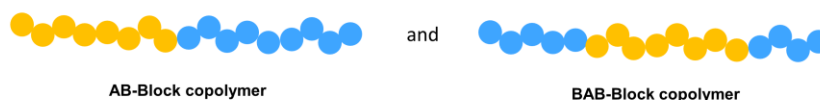
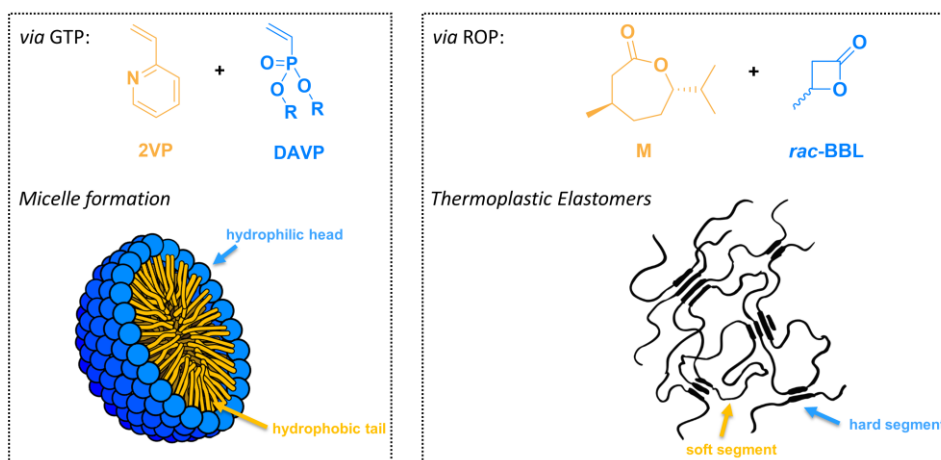
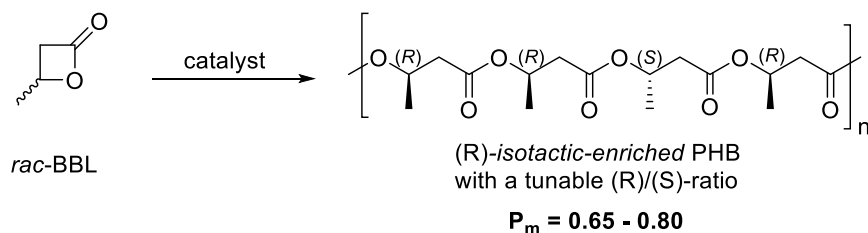
Target blockcopolymer structures:**Applications:**

Figure 15: Synthesis of AB and BAB block copolymers *via* GTP and ROP for micelle formation and for the synthesis of thermoplastic elastomers.

The polymerization of (-)-menthide has not been tested with lanthanoid complexes so far, which should be investigated in this thesis. In addition, heteroaromatic initiators are not yet known for initiating ROP. Therefore, we, herein, want to test these complexes as catalysts for BBL and (-)-menthide polymerization. Under tension, highly *syndiotactic* or *isotactic* PHB fractures at very low strains, and is therefore unsuitable for use in numerous applications where elasticity is necessary.^[158] As a result, there is no need for *syndio* PHB even though there are a multitude of efficient synthesis routes established (see chapter 2.2.1). Modulation of the stress-strain properties can be reached by incorporation of PHB into block copolymers, however, block copolymers of PHB remain rare in literature and copolymers with crystalline *syndiotactic* PHB are not accessible or published so far. To obtain thermoplastic elastomers, BAB block copolymers are necessary in which a “hard” *semi* crystalline B-segment (high T_g) is combined with a “soft” amorphous A-segment (low T_g) (chapter 2.4.2). To obtain thermoplastic elastomers, the aim is to develop AB and BAB block copolymers, in which the “hard” semicrystalline PHB-segment (A) is combined with “soft” amorphous poly((-)-menthide) (B) (Figure 15). For the synthesis of BAB block copolymers, the bifunctional tetramethylpyrazine initiator and for the AB-polymers the catalyst with a bis(dimethylsilyl)amide initiator should be used.

3.3 Modulation of the ligand

Studies by various groups were concentrating on the ROP of β -butyrolactone, a low-cost feedstock derived from CO_2 , for the synthesis of PHB. As mentioned before, they were only able to produce *atactic* or *syndiotactic* PHB, which is not biodegradable. Just recently, but after the start of this thesis, solely one route towards *isotactic* PHB ($P_m = 0.22 - 0.77$) was published by Yao *et al.* The aim is therefore to produce a less, but still (R)-*isotactic* form of PHB ($P_m = 0.65 - 0.80$) from *racemic* β -butyrolactone as this microstructure preserves its biodegradability and has, in addition, a lower melting-point and is less brittle (see 2.4.1; Scheme 18).



Scheme 18: *Isotactic-enriched* to *isotactic* (R)-PHB as the target structure for stereoselective ROP of *rac*-BBL.

In search for more active and stereoselective catalysts for isoselective ring-opening polymerization of *racemic* BBL, our attention was directed to chiral rare-earth metal complexes. The introduction of a chiral ligand should be realized by using the versatile chiral agent 1,1'-binaphthol. The utilization of binaphthol in lanthanide complexes for asymmetric reactions was first published by *Shibasaki et al.* in 1992 for an enantioselective nitro-aldol reaction.^[200] Just a few binaphthol-derivatives were since then investigated in lanthanide chemistry, but in most of the cases the structures could not be synthesized, were complicated or could never be characterized by crystallographic methods.^[201]

The exchange of the bis(phenolate) ligand with a binol-box ligand, which is used in the *Ohta* group for the lanthanide-catalyzed asymmetric 1,3-dipolar cycloaddition and which is based on a combination of the chiral substance binaphthol (binol) and the versatile ligand PyBox, will be investigated in this thesis (Figure 16).^[202] Complexation with a yttrium precursor should then lead to the desired complex structure analogue to the bis(phenolate) complexes. This is to be tested in the ring-opening polymerization of *racemic* BBL. The aim is to investigate the activity of the complex as well as the microstructure of the resulting polymer and its thermal and mechanical properties. An isoselective ROP, whereby only the (R)-isomer of BBL is incorporated into the polymer chain and the (S)-butyrolactone remains predominantly in solution is desired (Scheme 18). Only a small proportion of (S)-stereo defects should be incorporated to optimize the mechanical properties.

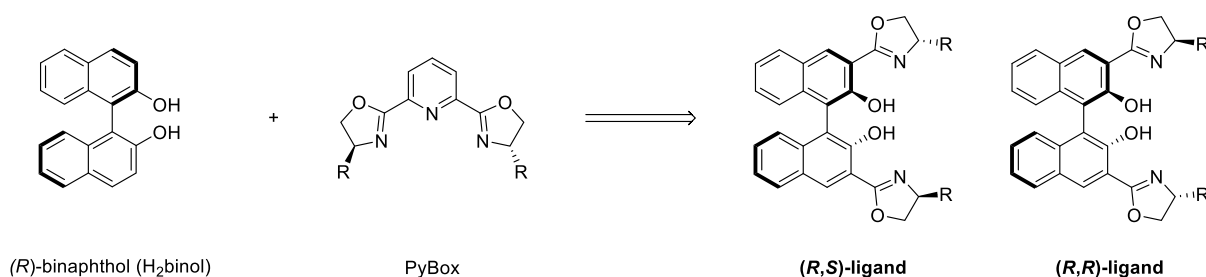


Figure 16: Chiral binol-box ligand derived from binaphthol and PyBox for the synthesis of a chiral lanthanide-complex.

4 Nonmetallocene lanthanides as catalysts in group-transfer polymerization

4.1 Bibliographic data

Title: “Toolbox of Nonmetallocene Lanthanides: Multifunctional Catalysts in Group-Transfer Polymerization”

Status: Full paper, Publication Date (Web): August 10, 2017

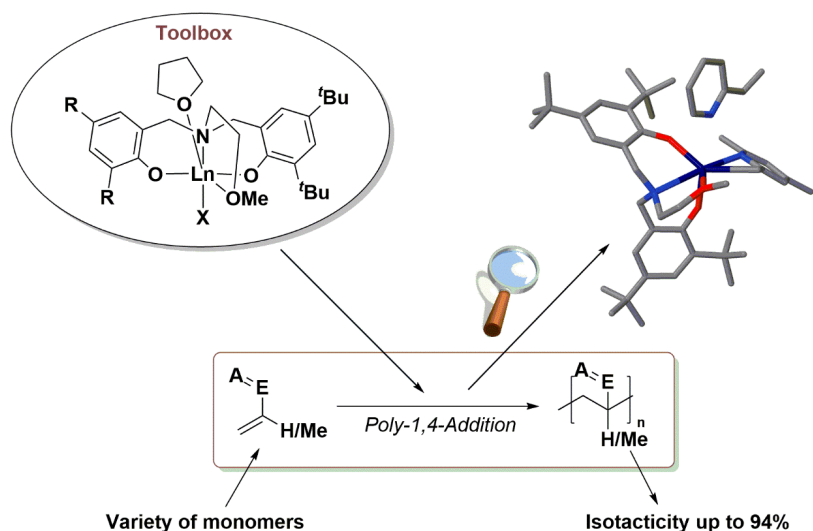
Journal: *Inorganic Chemistry*, 2017, 56, 9754-9764

Publisher: American Chemical Society

DOI: 10.1021/acs.inorgchem.7b01261

Authors: Friederike Adams, Martin R. Machat, Peter T. Altenbuchner, Johannes Ehrmaier, Alexander Pöthig, Tolga N. V. Karsili, and Bernhard Rieger¹

4.2 Abstract graphic (TOC)



¹ F. Adams planned and executed all experiments and wrote the manuscript. M. Machat and P. T. Altenbuchner helped by preparing the manuscript. M. Machat also helped with high-temperature nmr-measurements. P. T. Altenbuchner planned some synthesis routes concerning the C-H bond activation. A. Pöthig conducted the SC-XRD-measurement and processed the crystallographic data. J. Ehrmaier and T. N. V. Karsili performed DFT-calculations. All work was supervised by B. Rieger.

4.3 Content

Sectors such as health care or mobility are keen to develop new high performance and functional polymers. To create such materials, a high precision synthesis of these macromolecules is essential. Rare earth metal-mediated group-transfer polymerization (REM-GTP) was a so far underestimated method for the efficient and accurate synthesis of a variety of functional polymers. In the last years, our group reported on homo- and copolymerization of several types of polar vinyl monomers with metallocene and nonmetallocene catalysts. In this manuscript, a fundamental study of isostructural 2-methoxyethylamino-bis(phenolate)lanthanide complexes is performed to combine the experimental findings of REM-GTP with in-depth quantum chemical calculations on the initiation process of this polymerization. This study offers deeper insight into the ongoing initiation and reaction mechanism and the electronic properties of the catalysts. This analysis covers the differentiation of electron-donating and non-donating vinyl monomers, the impact of the ionic radii of the metal centers (yttrium and lutetium) and the contrast of two initiators (highly nucleophilic alkylinitiators vs. electron-donating heteroaromatics). The investigation includes the effect of these parameters on the activity, initiator efficiency and tacticity of the obtained polymers and discloses the possibility to generate a toolbox of different catalysts, in which each individual one is favored for a particular monomer or stereoselectivity. A higher acidity of lutetium led to an improved activity in 2-vinylpyridine polymerization (highest declared turn over frequency), while C–H bond activation *via* σ -bond metathesis with a pyridine-based substrate was shown to be a versatile tool towards efficient initiators. These boosted initiator efficiencies enabled a highly isoselective polymerization, because low-temperature polymerizations were enabled. In this publication, we established REM-GTP with bis(phenolate)lanthanides as a multifunctional method for the efficient synthesis of new, high-performance and high-precision polymers with variable tacticity, controllable molecular weights and narrow molar mass distributions.

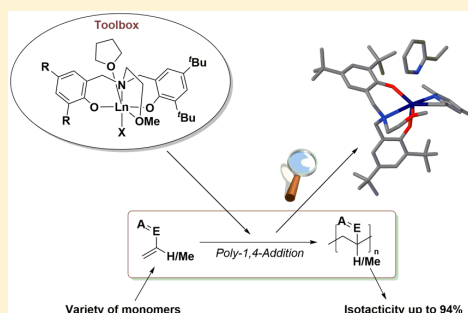
4.4 Manuscript

Toolbox of Nonmetallocene Lanthanides: Multifunctional Catalysts in Group-Transfer Polymerization

Friederike Adams,^{†,‡} Martin R. Machat,^{†,‡} Peter T. Altenbuchner,^{†,‡} Johannes Ehrmaier,[§] Alexander Pöthig,^{‡,§} Tolga N. V. Karsili,[§] and Bernhard Rieger^{*,†,‡,§}[†]WACKER-Lehrstuhl für Makromolekulare Chemie, [§]Chair of Theoretical Chemistry, and [‡]Department Chemie & Catalysis Research Center, Technische Universität München, 85748 Garching bei München, Germany

Supporting Information

ABSTRACT: Herein, we present a fundamental study of isostructural 2-methoxyethylamino-bis(phenolate)-lanthanide complexes $[(\text{ONOO})^{\text{R}}\text{M}(\text{X})(\text{THF})]$ ($\text{M} = \text{Lu}, \text{Y}$; $\text{R} = \text{tBu}, \text{CMe}_2\text{Ph}$, $\text{X} = \text{CH}_2\text{TMS}$, collidine; $\text{THF} = \text{tetrahydrofuran}$; $\text{TMS} = \text{trimethylsilyl}$) for rare-earth metal-mediated group-transfer polymerization (GTP). This analysis includes the differentiation of electron-donating and non-donating vinyl monomers and two metal centers with regard to the ionic radius (yttrium and lutetium). In addition, highly nucleophilic alkyl initiators are compared with electron-donating heteroaromatic initiators. Our examinations include the impact of these parameters on the activity, initiator efficiency, and tacticity of the obtained polymers. Density functional theory calculations and proposed catalyst structure determinations via X-ray analysis support these investigations. This facilitates the selection of the best metal and initiator combination to address efficient and stereospecific polymerization of a broad range of Michael monomers. $[(\text{ONOO})^{\text{tBu}}\text{Lu}(\text{X})(\text{THF})]$ shows the highest activity of 2220 h^{-1} (normalized turnover frequency) for the polymerization of 2-vinylpyridine due to the higher Lewis-acidity of lutetium. Through $\text{C}(\text{sp}^3)\text{-H}$ bond activation, catalysts with higher initiator efficiency in N,N' -dimethylacrylamide (DMAA) and diethylvinylphosphonate polymerization were synthesized. Remarkably, $[(\text{ONOO})^{\text{tBu}}\text{Y}(\text{collidine})(\text{THF})]$ was capable of stereospecifically polymerizing DMAA to highly isotactic poly(DMAA) ($P_m = 0.94$). Overall, the kinetics studies reveal a living-type GTP mechanism for all of the tested catalysts, enabling precise molecular-weight predeterminations with narrow molecular weight distributions ($\mathcal{D} \leq 1.06$).



INTRODUCTION

One of the core challenges in polymer synthesis is the creation of highly complex and well-defined structures from simple molecules. To synthesize polymers for high-tech applications, it is necessary to accurately influence the mechanical and thermal properties via changes in the microstructure or molecular weight. Therefore, the availability of catalysts for the precise synthesis of these polymers is an essential requirement. The living character and high activity of rare-earth metal-mediated group-transfer polymerization (REM-GTP) are two advantages of this polymerization method. Beyond that, molecular weights are precisely controllable, and narrow molecular weight distributions are observed. Currently, different types of Michael-type polar vinyl monomers have been homopolymerized and copolymerized via REM-GTP (Figure 1).^{1–8} The possibility of using different phosphorus and nitrogen-containing polar vinyl monomers leads to different functionalities, which enables access to various fields for application.^{1,9–12}

REM-GTP with a symmetric 2-aminoalkoxy-bis(phenolate)-yttrium trimethylsilylmethyl complex (**1a**) is one of the first examples of a nonmetallocene system. This catalyst showed

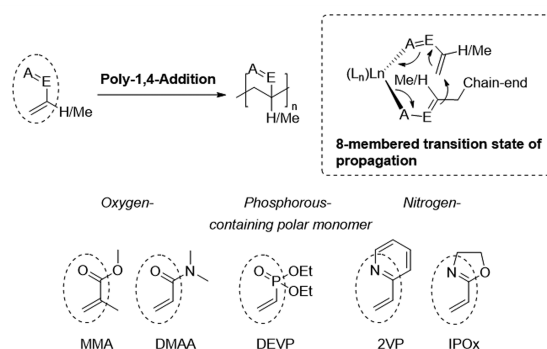


Figure 1. REM-GTP of Michael-type oxygen-, phosphorus-, and nitrogen-containing vinyl monomers.

good activities for various monomers without inducing tacticity.^{13,14} Recently, two different approaches toward highly

Received: May 19, 2017

Published: August 10, 2017

stereospecific polymerization of prochiral 2-vinylpyridine (2VP) with nonmetallocene lanthanides have been established by the groups of Rieger and Lu.^{6,15,16} As lanthanocenes show insufficient polymerization activity and stereospecificity for various monomers, the scope of bis(phenolate)lanthanide complexes is further broadened by this contribution.^{11,13} A systematic study on the activity, initiator efficiency, and stereospecificity (with reference to three different parameters) is presented herein. The experimental investigations are substantiated with detailed density functional theory (DFT) calculations and proposed catalyst structure determinations via X-ray analysis. For the first parameter, a distinction was made between electron-donating and nonelectron-donating monomers. For the second parameter, changes in the metal center (from yttrium to lutetium) were performed with regard to the influence of the ionic radius on the polymerization. The last parameter was generated by the introduction of a new heteroaromatic electron-donating initiator. This initiator was then compared with highly basic alkyl initiators. Two different types of initiators were investigated, as different initiation mechanisms can occur. Strongly basic alkyl initiators can be inefficient if they favor deprotonation of an acidic α -CH and do not initiate polymerization via nucleophilic attack (see Figure 2).^{13,17} To eliminate side reactions and the slow deprotonation-mediated initiation, heteroaromatic initiators can be used instead.

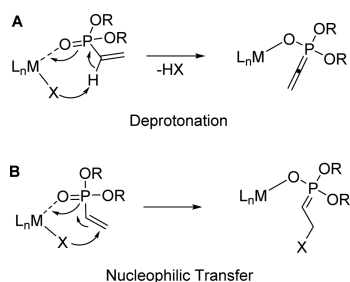


Figure 2. Initiation pathways for REM-GTP of DAVP via deprotonation (A) or nucleophilic transfer (B).

To introduce these heteroaromatic initiators, C–H bond activation can be utilized.^{12,18–26} Lanthanide complexes are able to activate compounds such as 2,4,6-trimethylpyridine (*sym*-collidine) via σ -bond metathesis. This type of C–H bond activation is a common way to access C–H bond cleavage, because oxidative addition and reductive elimination reactions

are not possible with trivalent lanthanides. This σ -bond metathesis was first shown by Watson et al. in 1983 via the activation of isotopically labeled methane, benzene, and pyridine with a cyclopentadienyl-lutetium-methyl complex.^{27,28}

RESULTS AND DISCUSSION

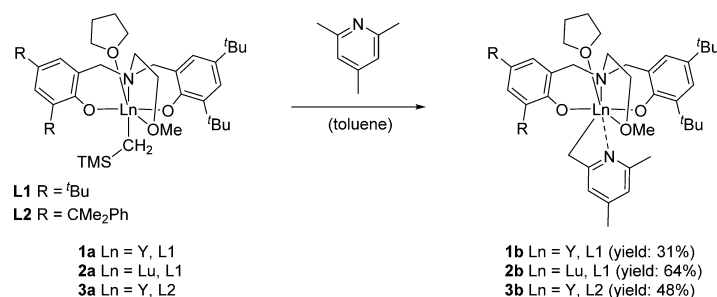
Synthesis and Characterization of Alkylanthanide Complexes. The symmetrically substituted 2-methoxyethylamino-bis(phenolate) ligand (**L1**) was synthesized via a modified Mannich reaction of 2,3-di-*tert*-butylphenol with 2-methoxyethylamine in a formaldehyde solution.²⁹ The asymmetric ligand (**L2**) was only accessible through a multistep reaction. The final nucleophilic substitution reaction of the cumyl-substituted 2-methoxyethylaminophenolate with the *tert*-butyl-substituted phenol-methylenebromide led to the desired ligand in moderate yield (see Supporting Information).¹⁵

For the synthesis of $(\text{ONOO})^{\text{Ln}}(\text{CH}_2\text{TMS})(\text{THF})$ (**1a–3a**) ($\text{Ln} = \text{Y, Lu}$; TMS = trimethylsilyl; THF = tetrahydrofuran) complexes, 1 equiv of the respective ligand was reacted with 1 equiv of the precursor, $\text{Ln}(\text{CH}_2\text{TMS})_3(\text{THF})_3$, in a mixture of toluene/pentane at 0 °C and stirred overnight at room temperature (Supporting Information). As yttrium complexes **1a** and **3a** were isolated in moderate yields (43 to 47%), lutetium analogue **2a** was synthesized in good yields of up to 75%. The monomeric structure of every complex was verified via ¹H NMR spectroscopy.^{15,30}

C–H Bond Activation. Initially, we tested the reactivity of complexes **1a–3a** toward *sym*-collidine (Scheme 1). Time-resolved ¹H NMR experiments of the reaction were performed at room and elevated temperatures (60 and 80 °C, respectively) to investigate the tendency to activate *sym*-collidine. These experiments revealed strongly varying ambitions for the catalysts to undergo C–H bond activation (Figure 2 and Supporting Information, Figures S1–S3).

For all complexes, only very slow activation was observed at room temperature. Increased temperatures led to significant changes in the reactivity, and catalyst **1a** was transformed to complex **1b** in the presence of 1 equiv of 2,4,6-trimethylpyridine within 4 h at 60 °C (see Figure 3). ¹H NMR examinations revealed that after the addition of *sym*-collidine (Figure 3, spectrum 2: 6.77, 2.47, and 2.24 ppm), the signals for the CH₂TMS initiator of complex **1a** decreased (comparison with spectrum 1). The concurrent increase of the tetramethylsilane signal (SiMe₄: 0 ppm) indicated the ongoing metathesis reaction. In the same manner, two new signals arose in the aromatic region, representing the binding of collidine. Two signals in the aliphatic region show the two new methyl groups (spectrum 4). The reaction was straightforward, and no side

Scheme 1. C–H Bond Activation of Catalysts **1a–3a** with *sym*-Collidine in Toluene to Obtain Complexes **1b–3b**



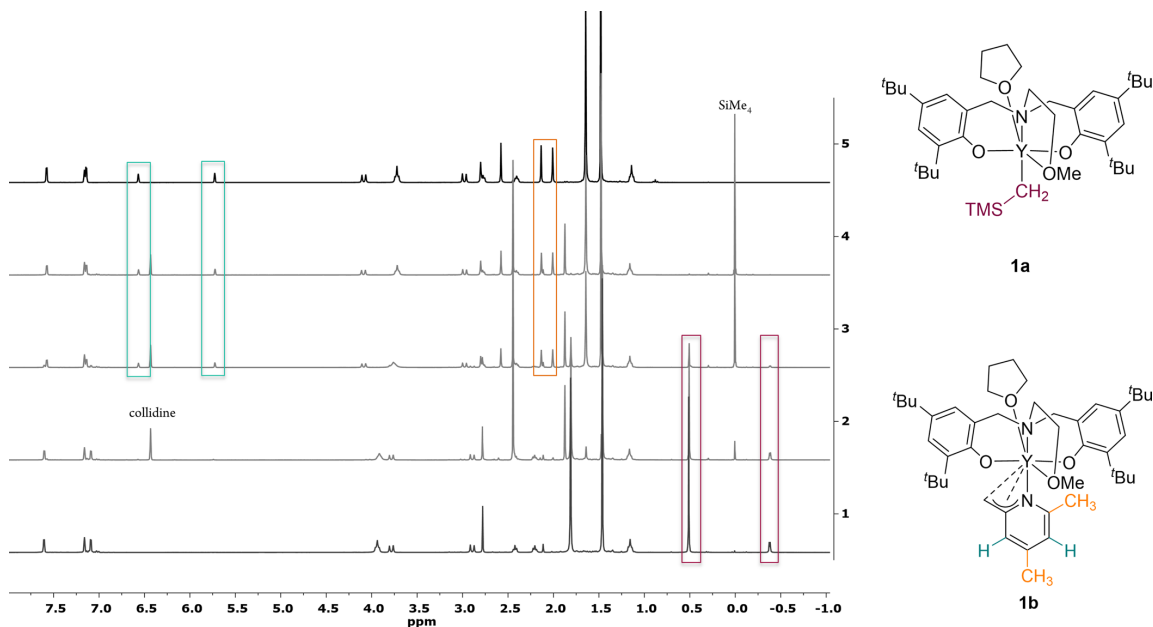


Figure 3. ^1H NMR kinetic experiments for the C–H bond activation of *sym*-collidine with complex **1a** in C_6D_6 . (1) Complex **1a**. (2) Immediately after addition of *sym*-collidine. (3) 40 min; 60 °C. (4) 4 h; 60 °C. (5) Complex **1b**.

reactions occurred, which enabled us to scale up the catalyst synthesis of **1b** in toluene. Purification was performed via recrystallization from pentane at -30 °C (spectrum 5). The interaction between the metal center and the initiator via an activated CH_2 group was verified by ^1H - and ^{13}C NMR spectroscopy. 2J -Coupling ($J = 2.9$ Hz) of the CH_2 signal at 2.80 ppm in the ^1H NMR spectrum (spin = 1/2, leading to a splitting as a doublet) and a splitting of the carbon atom at 52.5 ppm ($^1J = 6.0$ Hz) in the ^{13}C NMR spectra underscored the successful C–H bond activation.

Compound **2a** was more reluctant in its reactivity toward *sym*-collidine; nevertheless, quantitative C–H bond activation could be achieved after 9 d at 80 °C. As the 4f electrons have no contribution to the binding valence orbitals, lutetium can be seen as an isoelectronic equivalent to yttrium. Therefore, the σ -bond metathesis was investigated to determine the influence of the effective ionic radius. Lutetium is more Lewis-acidic/electrophilic owing to its higher effective nuclear charge, leading to a stronger binding of the nucleophilic CH_2TMS initiator.³¹ This led to a prolonged reaction time for C–H bond activation. These observations and suggestions were in accordance with hard-soft acid-base (HSAB) theory. Complex **2b** was isolated in good yields via recrystallization in pentane. No formation of side products was observed during the activation with compound **1a** and **2a**, which highlighted the remarkable stability of the catalysts. Only complex **3a** slowly decomposed at elevated temperatures. Hence, complex **3b** was generated through the reaction of **3a** with *sym*-collidine at room temperature over 6 d in moderate yield. In all reactions, the Lu complexes were generated in higher yields than the Y analogues due to the higher insolubility in pentane. For all C–H bond-activated compounds, recrystallization in pentane afforded the desired complexes with the general structure $(\text{ONOO})^{\text{tBu,R}}\text{Ln}((4,6\text{-dimethylpyridin-2-yl)methyl})(\text{THF})$

(**1b–3b**) (Scheme 1). All C–H bond-activated compounds were characterized via NMR spectroscopy and elemental analysis. In the case of complex **1b**, X-ray diffraction analysis was used to analyze the proposed complex structure.

Structure Analysis. Crystals of complex **1b** were grown through recrystallization from pentane at -30 °C. Against all expectations, and in contrast to the NMR spectra, the complex crystallized as two independent molecules without tetrahydrofuran as a coordinating solvent (see Figure S4, Supporting Information). As a consequence, the yttrium is coordinated in a sevenfold manner and not in the generally favored octahedral coordination sphere. Nevertheless, the 2-methoxy-bis(phenolate) ligand coordinated in the same way as in complex **1a**.³² The solid-state structure of one independent molecule of complex **1b** is shown in Figure 4. The three Y–O bonds are equatorial, whereas the nitrogen is ordered axial to the yttrium center. Owing to the missing tetrahydrofuran, which coordinates equatorial to the yttrium in **1a**, the bond angles between the yttrium and the oxygen atoms differ in these two compounds and are larger in **1b**. Fundamental for the performed C–H bond activation is the coordination of the (4,6-dimethylpyridine-2-yl)-methyl initiator to the metal center. The Y–N bond is shorter than the Y– C_α bond; thus, the initiator is primarily coordinated via the Y–N moiety.

The C–C bond lengths in the aromatic ring were all similar and lay between double- and single-bond lengths (1.362[1.364] to 1.423[1.424] Å; Figure 4), as might be expected for aromatic systems (bond lengths for the second independent molecule are given in parentheses). Remarkably, the $\text{C}(\text{sp}^3)\text{–H}$ activated methyl–methyl bond ($\text{C}_{34,\alpha}\text{–C}_{35,\text{ipso}}$) had a reduced length of 1.400[1.399] Å. Consequently, double-bond character was predominant, and the activated methyl group was conjugated in the aromatic system. One C–C bond of the heteroaromatic system (1.423[1.424] Å, Figure 4, $\text{C}_{35,\text{ipso}}\text{–C}_{36,\text{ortho}}$) was even

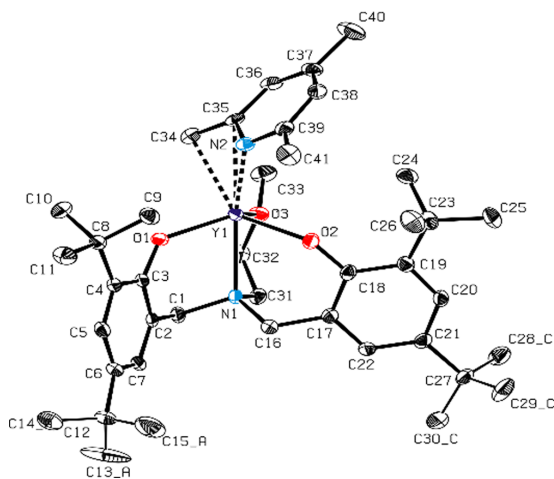


Figure 4. ORTEP-style representation of **1b**. Hydrogen atoms and the second independent molecule are omitted for clarity. Ellipsoids with 50% probability. Selected bond lengths (Å) and angles (deg): Y(1)–O(1), 2.1130(15); Y(1)–O(2), 2.1318(16); Y(1)–O(3), 2.3641(16); Y(1)–N(1), 2.5385(19); Y(1)–N(2), 2.3950(19); Y(1)–C(34), 2.608(2); Y(1)–C(35), 2.740(2); N(2)–C(35), 1.386(3); N(2)–C(39), 1.361(3); C(34)–C(35), 1.400(4); C(35)–C(36), 1.423(3); C(36)–C(37), 1.362(4); C(37)–C(38), 1.413(4); C(38)–C(39), 1.366(3); C(39)–C(41), 1.493(3); C(37)–C(40), 1.508(4); O(1)–Y(1)–O(2), 119.74(6); O(1)–Y(1)–O(3), 123.02(6); O(2)–Y(1)–O(3), 99.09(6); N(1)–Y(1)–N(2), 167.93(6); O(1)–Y(1)–C(34), 91.17(7); N(2)–Y(1)–C(34), 55.94(7).

slightly longer than the activated methyl group, indicating the high charge delocalization of the latter group. The tilt of the phenyl ring was calculated with the help of the C_{α} –Y– C_{ipso} angle. The value of 80.12° and a relatively short Y– C_{ipso} bond (2.740[2.715] Å) indicated binding of the collidine occurred via an allylic motif. From these findings, the η^3 -(C,C,N)-aza-allylic binding to the yttrium center was evident. This coordination type is an intermediate between an η^2 -alkyl-amine and an η^1 -amido-olefin coordination, as Teuben and co-workers investigated in bis(alkoxysilylamido)-yttrium-pyridyl complexes.²⁰ The two other methyl groups possessed single-bond character with bond lengths of 1.493[1.496] and 1.508[1.502] Å; therefore, they were not integrated into the conjugated system.

As the deprotonated collidine species can be seen as a benzyl-type ligand, **1b** was compared to the literature-known complex $[Y(\text{CH}_2\text{Ph})_3(\text{THF})_3]$ with respect to the charge

delocalization and allylic binding motif (see Figure S5 and Table S3, Supporting Information). Whereas the benzyl ligand in $[Y(\text{CH}_2\text{Ph})_3(\text{THF})_3]$ was primary bond via the Y– C_{α} , the collidine ligand in **1b** is coordinated via Y–N binding. The longer Ln– C_{α} bond of **1b** and the shorter C_{α} – C_{ipso} bond (higher double bond character) indicated a more pronounced multihapto binding due to the higher charge delocalization (see Table 1). The η^3 -allylic binding in **1b** was also confirmed by the higher phenyl tilt (80.12° vs 117.17°) and the shorter Ln– C_{ipso} bond. The same parameters can be used to compare the collidine structures regarding the impact of the metal size. As we were not able to isolate crystals of **2b**, we used DFT calculations instead. Harder et al. stated that within benzyl-lanthanide(III) complexes, some parameters do not vary significantly along the lanthanide series.³³ Nevertheless, we compared the DFT-calculated structures fully aware that only slight trends might be observed. Overall, these calculations predicted a higher end-on coordination in place of a side-on coordination, as found in the solid-state structure of **1b** (see Table 1). Less allylic bindings were calculated for both metals, as indicated by the longer Ln– C_{ipso} bonds and the broader C_{ipso} – C_{α} –Ln angles. Within these calculations, the same trends as in the series of different benzyl lanthanides were observed.^{33–35} Because of the higher Lewis acidity of lutetium, a higher charge localization is provoked. The C_{α} – C_{ipso} bond elongates on account of weaker charge delocalization. As lutetium polarizes the negative charge more than yttrium, the allylic binding motif becomes weaker. As a result, the Ln– C_{ipso} bond was longer, and the C_{ipso} – C_{α} –Ln angle was broader. The less distinct multihapto binding with decreasing ion size is also shown by the Ln– C_{α} bond shortening.

Group-Transfer Polymerization. The isolated catalysts (**1a–3b**) were employed in the GTP of vinyl monomers diethylvinylphosphonate (DEVF), *N,N'*-dimethylacrylamide (DMAA), and 2VP to evaluate the general activities, initiator efficiencies, and the microstructures of the isolated polymers. Poly-2-vinylpyridine (P2VP) is a polymer for high-performance applications due to its pH-dependent solubility. Several examples of block copolymers containing hydrophobic 2VP are known in the literature where micelle formation occurs due to their amphiphilic character.^{36–43} Therefore, our attention was directed to enhancements in 2VP polymerization. First, the initiation mechanisms of the C–H bond-activated complexes were elucidated by end-group analysis of oligomeric 2VP. This was produced by reacting catalyst **1b** with 10 equiv of 2VP and monitoring the reaction via NMR spectroscopy. Electrospray ionization mass spectrometry (ESI-MS) analysis of the

Table 1. REM-GTP Polymerization Results of Catalyst **1a–3b** of 2VP^a

entry	[cat]	time [min]	conversion [%]	$M_{n,\text{calc}}$ (1×10^4) [g/mol] ^b	$M_{n,\text{exp}}$ (1×10^4) [g/mol]	\bar{D}^c	I^d	TOF* ^e [h ⁻¹]	P_m^f
1 ¹³	1a	90	99	2.1	2.3	1.01	0.99	1110	0.55
2	2a	130	99	2.3	7.4	1.06	0.30	1750	0.56
3 ¹⁵	3a	120	99	2.2	3.9	1.00	0.71	440	0.57
4	1b	60	99	2.0	4.1	1.01	0.42	1080	0.54
5	2b	45	99	2.0	4.9	1.06	0.43	2220	0.54
6	3b	180	99	2.0	4.7	1.06	0.42	470	0.56

^aReactions performed with [2VP] = 2.7 mmol, [2VP]/[Cat] = 200/1, at 25 °C in 2 mL of solvent, conversions determined by ¹H NMR spectroscopy and $M_{n,\text{exp}}$ determined by GPC-MALS. ^b $M_{n,\text{calc}}$ from $M_{n,\text{calc}} = M \times (([M]/[Cat]) \times \text{conversion})$. ^cPolydispersity calculated from $M_{w,\text{exp}}/M_{n,\text{exp}}$ as determined by GPC-MALS. ^d $I = M_{n,\text{calc}}/M_{n,\text{exp}}$ at the end of the reaction. ^eTOF* = TOF/*I*; normalized TOF for the active metal centers. ^f P_m is the probability of meso linkages between monomer units and was determined by ¹³C NMR spectroscopy of the quaternary carbon atom (Supporting Information).^{15,44}

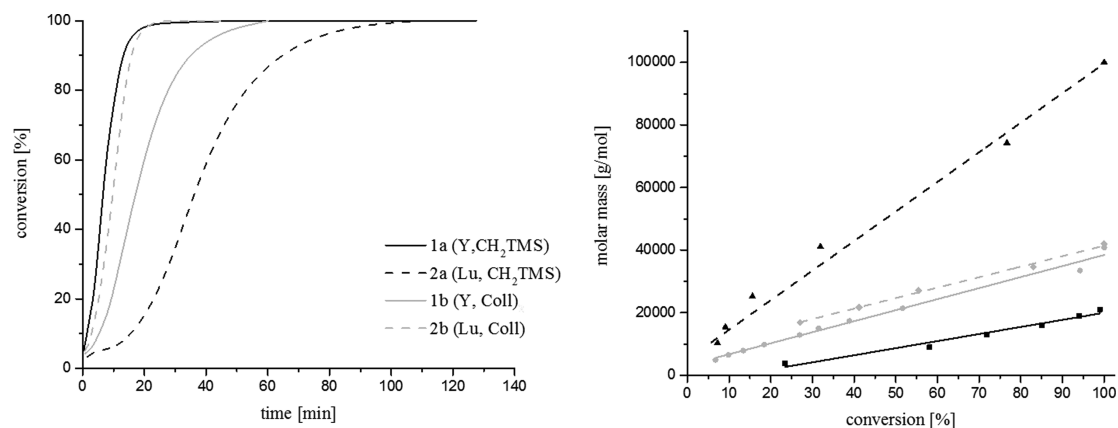


Figure 5. (left) Catalytic activity of catalysts **1a/b** and **2a/b** (Y = line; Lu = dashed; CH₂TMS = black; *sym*-collidine (coll) = gray; catalyst: 135 μ mol, 2VP: 27 mmol, toluene: 20 mL, $T = 25$ °C) measured via the aliquot method. (right) Linear growth of the absolute molecular weight (M_n) (determined by GPC-MALS) as a function of monomer conversion (gravimetrically determined).

respective oligomers showed signals corresponding to $n \times M_{2VP} + M_{\text{collidine}}$ with either H⁺ or Na⁺ as the charge carrier (Supporting Information, Figure S6). The initiating groups were clearly visible in the ESI-MS; a nucleophilic transfer reaction of the initiator via monomer insertion into a Y–C bond is apparent (Figure 2). The evidence of a nucleophilic transfer reaction for the initiation of 2VP polymerization with **1a** has already been reported in a previous study.¹³ On the basis of the observed mechanism, these findings were further elucidated via DFT calculations (*vide infra*).

To determine conversions and kinetic parameters of the polymerization, aliquots were taken at regular time intervals during polymerization. The conversion was gravimetrically calculated. Absolute molecular masses and mass distributions were measured by gel-permeation chromatography multiangle light scattering (GPC-MALS). The polymerization of 2VP with all 2-methoxyethylamino-bis(phenolate) catalysts proceed in a living fashion, as indicated by the narrow polydispersities ($1.00 \leq \bar{D} \leq 1.06$) and good agreement between the experimentally determined and theoretically expected M_n values (Table 1). The plots of conversion against the absolute molecular mass reveal a linear relationship between M_n and conversion, underlining the living fashion of the polymerization (Figure 5 and Supporting Information, Figures S9, S10, S12, and S13). If the conversion is plotted against time, the polymerizations can be compared with regard to the activity of the different catalysts. Catalysts **1a** and **3a** were tested in the GTP of 2VP in a previous contribution from our group, and we had already shown that the increased steric demand of the bis(phenolate) ligand led to a decrease in catalyst activity and initiator efficiency (Table 1, Entries 1 and 3). In both cases, only atactic P2VP was obtained.¹⁵ As expected, changing the initiator to *sym*-collidine did not impact the normalized turnover frequencies (TOF*), since the activity is solely influenced by the metal center and the ligand, which are both involved in the propagation mechanism (Table 1, Entries 4 and 6).

The introduction of the collidine initiator led to a decrease in initiator efficiency of the complexes from 99% (**1a**)/71% (**3a**) to 42% (**1b**/3b); therefore, no improvement was found for the yttrium-based bis(phenolate)-mediated 2VP polymerization. Remarkably, the change of the metal center to lutetium increased the catalytic activity; complexes **2a** and **2b** were the

most active catalysts (TOF* = 1750–2220 h⁻¹) in the polymerization of 2VP while maintaining accurate control over the molecular masses ($\bar{D} = 1.06$). Owing to the higher Lewis-acidity of lutetium, the stronger polarization of the coordinating monomer in the propagation mechanism may be decisive for the higher activity. The stronger binding of the CH₂TMS initiator in compound **2a** (*vide supra*) was reflected in the initiator efficiency, which was lower in comparison to the respective yttrium compounds. In contrast to the yttrium complexes, the change in initiator from **2a** to **2b** was a suitable approach for improving the initiator efficiency and led to an increase of ~45%. As the tacticity of P2VP is influenced by an enantiomorphic site control mechanism, the change of metal has no effect on the tacticity.¹⁵

Recently, we reported on nontoxic phosphorus-containing poly(dialkylvinylphosphonate)s (DAVPs) in combination with P2VP as advanced micellar systems for drug-release applications.^{26,45} On the basis of these results, our study also included the detailed investigation of DEVP polymerization (alkyl chain = ethyl) with the above-mentioned catalysts. Complexes **1a–3a**, with an alkyl initiator, all showed relatively low initiator efficiency in the polymerization of DEVP (Supporting Information, Table S4). In the case of DEVP, basic alkyl initiators are inefficient due to deprotonation of the acidic α -CH of the first monomer (see Figure 2). Especially, complex **2a** demonstrates a low initiator efficiency, leading to a time-shifted and slower initiation, resulting in an increase of the molecular mass distribution ($\bar{D} = 1.48–1.50$). Initiation via the collidine initiator led to an increase in efficiency up to 80%. The polydispersity ($\bar{D} = 1.03–1.14$) of the polymers was improved as slow initiation via deprotonation was eliminated. In contrast to 2VP polymerization, the two metal species showed similar tendencies when the initiator was changed. In addition, the activity and initiator efficiency of the lutetium species seemed to be lower than for the yttrium catalysts.

Poly(DMAA) (PDMAA) is of special interest regarding the application as stimuli-responsive materials (micelles, hydrogels, and nanocomposites).^{46–51} The polymerization of DMAA was investigated with regard to catalyst activity and the microstructure of PDMAA. Because of the exothermic nature of the polymerization, the reaction was performed at low temperatures (–78, –50, and –20 °C). When refrigerated monomer

Table 2. REM-GTP Polymerization Results of Catalyst 1a–3a and 1b for DMAA^a

entry	[cat]	T_{Add} [°C] ^b	T_{Polym} [°C] ^c	conversion [%]	$M_{n,\text{calc}}$ ^e (1×10^4) [g/mol]	$M_{n,\text{exp}}$ (1×10^4) [g/mol]	\bar{D}	f^f	P_m^g
1	1a	-78	-50	99	1.9	18.4	1.42	0.10	0.91
2	1a	-50	-50	99	2.1	24.4	1.49	0.09	0.91
3	1a	-20	-20	99	1.9	8.5	1.66	0.22	0.89
4	1a	0	0	99	2.0	4.3	2.12	0.47	0.83
5	2a	-78	-20	99	2.1	57.7	1.17	0.04	0.56
6 ^d	2a	-78	-20	94	1.9	48.3	1.34	0.04	0.56
7	2a	-15	-15	99	2.0	18.8	1.69	0.11	
8	2a	0	0	99	2.0	7.5	2.22	0.26	
9	3a	-78	-50	99	2.3	15.1	1.30	0.15	0.90
10	1b	-78	-78	99	2.0	6.6	1.06	0.30	0.94

^aReactions performed with [DMAA] = 2.15 mmol (-35 °C), [DMAA]/[Cat] = 200/1, in 4.5 g of dichloromethane, conversions determined by ¹H NMR spectroscopy, and $M_{n,\text{exp}}$ determined by GPC-MALS. Several attempts to polymerize DMAA with catalysts 2a and 3a failed. ^bTemperature of the reaction mixture at addition of monomer. ^cEstimated temperature when polymerization occurred; observed through the increase in viscosity and end of stirring. ^dQuenching after 3 min; first time for the nonquantitative conversion of the slowest catalyst. ^e $M_{n,\text{calc}}$ from $M_{n,\text{calc}} = M \times (([\text{DMAA}]/[\text{cat}]) \times \text{conversion})$. ^f $f = M_{n,\text{calc}}/M_{n,\text{exp}}$ at the end of the reaction. ^g P_m is the probability of *meso*-linkages between monomer units and was determined by high-temperature ¹H NMR spectroscopy in DMSO-*d*₆ at 140 °C.

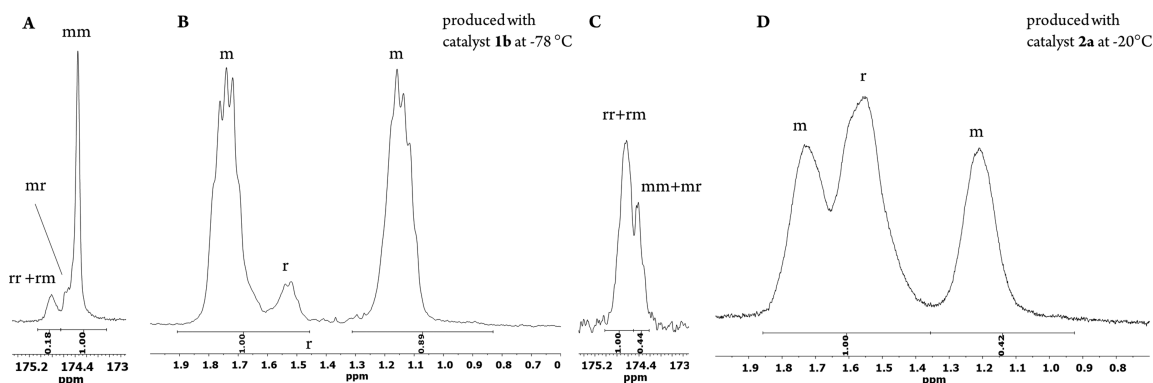


Figure 6. (A) Carbonyl region of the ¹³C NMR spectra (126 MHz, CDCl₃, 25 °C) of PDMAA prepared with catalyst 1b. (B) Backbone methylene signal in the ¹H NMR spectra (300 MHz, deuterated dimethyl sulfoxide (DMSO-*d*₆), 140 °C) of PDMAA prepared with catalyst 1b.⁵² (C) Carbonyl region of the ¹³C NMR spectra (126 MHz, CDCl₃, 25 °C) of PDMAA prepared with catalyst 2a. (D) Backbone methylene signal in the ¹H NMR spectra (300 MHz, DMSO-*d*₆, 140 °C) of PDMAA prepared with catalyst 2a.⁵²

was added to the reaction mixture at a certain temperature, and no polymerization initiation was observed, the mixture was slowly warmed. The end of polymerization was apparent through the increased viscosity and the immediate end of stirring. Kinetic measurements were not possible. At 0 °C the reaction was not controllable. The alkyl-yttrium complexes 1a and 3a showed no activity at -78 °C; warming to -50 °C led to an immediate reaction but with low initiator efficiencies (Table 2, entries 1 and 9). Because of a delayed and spontaneous reaction, as well as the rapidly rising viscosity of the reaction mixture, the molecular mass distributions were higher than expected for a living-type polymerization mechanism ($\bar{D} \leq 1.49$). Reactions were also performed at higher temperatures to investigate the influence of temperature on initiator efficiency and tacticity. These polymerizations indeed demonstrated a higher initiator efficiency, as more catalytic centers were active at higher temperatures; however, a higher molecular mass distribution, up to 2.22 (Table 2, entries 3, 4, 7, and 8), was found. Polymerizations that were gradually warmed from -78 °C, in comparison with those performed directly at elevated temperatures, showed similar results, which attests the reproducibility of the results (Table 2, entries 1 and 2). The stronger binding of the alkyl initiator to electrophilic

lutetium (complex 2a) was expressed by a very low initiator efficiency, since the polymerization did not start until warming to -20 °C. As a consequence, it was possible to quench the polymerization before quantitative conversion. A conversion of 94% in 3 min for complex 2a showed the high activity of this catalyst and all of the other tested catalysts. In comparison to previous studies on coordinative-DMAA polymerization, these bis(phenolate)lanthanides were highly active.^{52–54} We searched for initiators that were also active at -78 °C to overcome the problem of high molecular mass distributions and the low initiator efficiency for the yttrium complexes. The introduction of *sym*-collidine led to an improvement for DMAA polymerization (Table 2, entry 10) since the initiator efficiency was improved, facilitating a polymerization at -78 °C. Because of this fact, a very low polydispersity of 1.06 was observed, demonstrating the high suitability of complex 1b for the polymerization of DMAA.

The polymerization of DMAA was also studied in regard to the resulting microstructures. Figure 6 depicts the carbonyl region of the ¹³C NMR spectra and the backbone methylene signal in the high-temperature (HT) ¹H NMR spectra of PDMAA prepared with catalysts 1b and 2a. Assignment of the *m*- and *r*-dyad of the methylene proton was performed

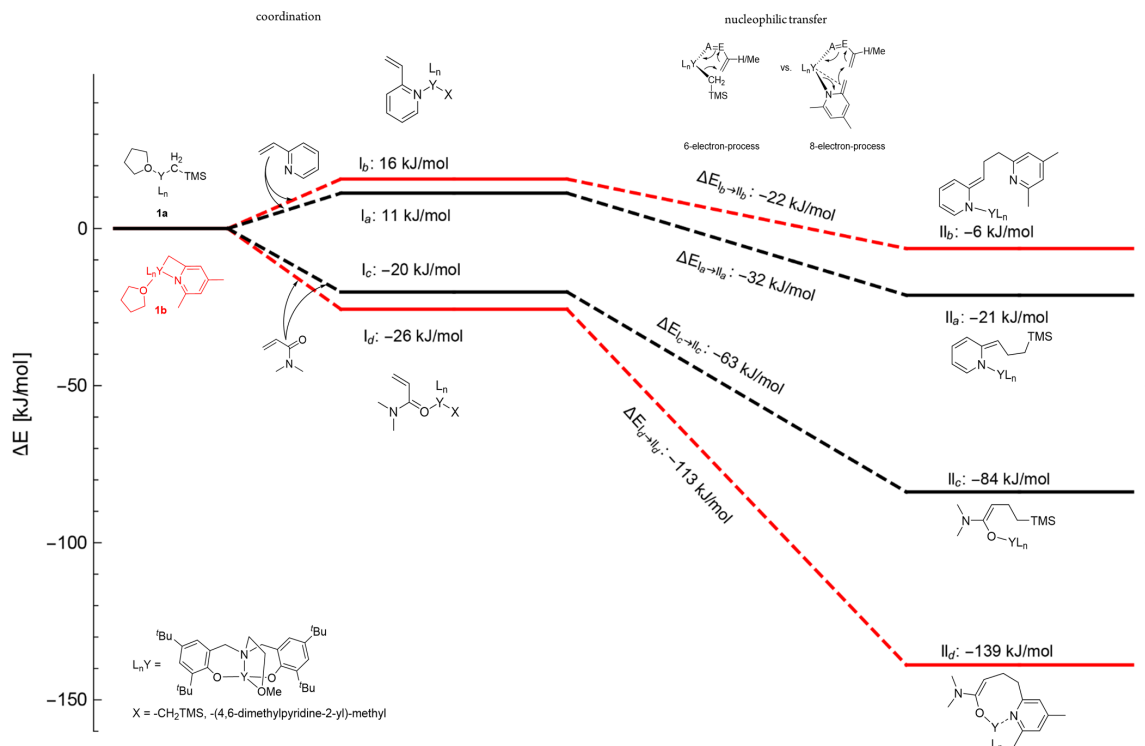


Figure 7. Reaction path for the initiation process: catalyst **1a** (black) and **1b** (red) with 2VP and DMAA.

analogously to the method of Kakuchi et al. For the triad distribution of the carbonyl signal, assignment was performed analogously to the method of San Román et al.^{52,55} For DMAA, higher initiator efficiencies were found for the heteroaromatic compound **1b**; therefore, polymerization was possible at -78 °C. This was reflected by the increasing percentage for *meso*-linkages in the polymer. Catalyst **1b** produced PDMAA with the highest isotacticity ($P_m = 0.94$). This value was determined as the proportion of *m*-dyad in the methylene region of the ^1H NMR spectrum. Complexes **1a** and **3a**, which were active at -50 °C, both produced PDMAA with slightly lower isotacticity ($P_m = 0.91$ and 0.90 , respectively). The slight increase in steric demand of ligand **L2** in **3a** did not affect the tacticity. On account of this, it was obvious that the lutetium complex (**2a**), which was only active at -20 °C, would produce PDMAA with a lower tacticity. Figure 6 shows that only atactic polymer was obtained. To analyze if this decrease in tacticity was only caused by the increase in temperature, polymerizations with **1a** were performed at -20 and 0 °C. The temperature rise led, in fact, to a decrease in isotacticity, but the catalyst still produced isotactic PDMAA ($P_m = 0.89$). Remarkably, not only the temperature but also the metal center has an impact on the tacticity. Because of these findings, different mechanisms for determining the stereoselectivity were expected for polymerizations with 2VP (enantiomorphic site control) and DMAA (chain-end control).

Radical and anionic polymerizations are only able to produce PDMAA with moderate isotacticity ($[\text{mm}] = 54\text{--}81$). Chiral *ansa*-zirconocenium catalysts, developed by Chen et al., exclusively produce isotactic PDMAA; however, the applic-

ability of those systems on the additional vinyl monomers, beyond acrylamides, was not investigated.^{53,54} In comparison, catalyst **1b** is a suitable generalist for DMAA polymerizations. This catalyst combines high activity and increased initiator efficiency with a low polydispersity and high polymer isotacticity.

Density Functional Theory Calculations on the Initiation Process. DFT calculations at the B3LYP level of theory, coupled with the LANL2DZ basis set, were used to uncover the mechanistic proceedings during the initiation process of GTP with 2VP (electron-donating monomer) and DMAA (nonelectron-donating monomer). These calculations were performed to assess the feasibility of the initiation reaction for the two different initiators (alkyl initiator (**1a**) vs collidine (**1b**)). Gas-phase geometry optimization of **1a**, **1b**, DMAA, and 2VP gave the starting-point geometries for the ensuing reaction path (Figure 7) and reference energies. Then, the monomers were chelated to the isolated complexes (THF served as the exchange molecule) as the first step of initiation, resulting in structures $\text{I}_a\text{--I}_d$.¹³ The chelated structures were optimized again to obtain the respective coordination energies. Finally, the products $\text{II}_a\text{--II}_d$ generated via a nucleophilic transfer reaction were calculated to gain insights into the relative energies of the product with respect to the reactants and the isolated systems. The electronic energies associated with the reaction path are depicted in Figure 7 and refer to the minimum-energy geometry of the isolated monomers and catalysts. The stepwise profiles of the initiation process reaction sequence for DMAA and 2VP are depicted in black for catalyst **1a** and red for catalyst **1b**. It is evident for DMAA that initiation with either

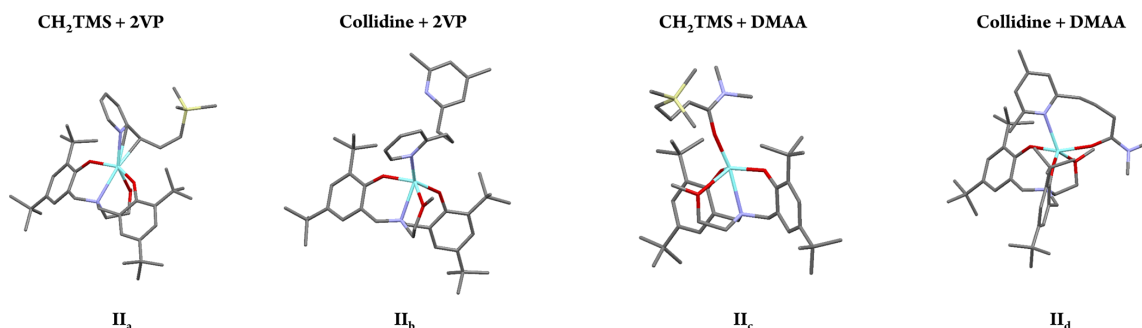


Figure 8. Optimized structures II_{a-d} after nucleophilic attack of the initiator to the monomer (light blue = yttrium; red = oxygen; purple = nitrogen; yellow = silicon; gray = carbon).

catalyst leads to a net favorable driving force for nucleophilic transfer ($\text{II}_c = -84$ kJ/mol; $\text{II}_d = -139$ kJ/mol) confirming our experimental observations. Both catalysts were able to initiate the polymerization, and cooling was necessary to avoid thermal desorption and to ensure isothermal conditions. Whereas both catalysts show a thermodynamically favored process, the calculations indicate that the initial coordination step, as well as the nucleophilic transfer reaction, are energetically more preferred using collidine as an initiator (catalyst **1b**). This was manifested in lower-energy products I_d and II_d . These computations were in good agreement with the experimental findings. The experiments of DMAA with catalyst **1a** could be performed at -50 °C, whereas the reactions with catalyst **1b** had to be cooled to -78 °C for a controlled reaction due to the significantly stronger exothermic nature of the reaction.

Attempts at raising the temperatures led to the evaporation of the solvent, as the heat dissipation was not sufficient. Polymerizations with 2VP were conducted at room temperature, since the reaction was less exothermic. Again, this was supported by the calculations, which indicated a slightly endothermic process, which was associated with the coordination step ($\text{I}_a = +11$ kJ/mol; $\text{I}_b = +16$ kJ/mol). Consequently, reactions at -78 °C were not successful.¹³ The calculated energy differences between the initiation of 2VP with **1a** and **1b** show only small differences. Contrary to DMAA initiation, **1a** seems to be slightly energetically favored for initiating 2VP polymerization ($\text{II}_a = -21$ kJ/mol; $\text{II}_b = -6$ kJ/mol). Again, this is in accordance with the experimental results, in which **1a** shows a higher initiator efficiency. We were able to calculate two transition states for initiation with complexes **1a** and **1b** ($\text{I}_b \rightarrow \text{II}_b$ and $\text{I}_c \rightarrow \text{II}_c$). In both cases, the transition states were ~ 1 eV above the reactant energy levels ($\text{I}_b \rightarrow \text{II}_b = 1.2$ eV; $\text{I}_c \rightarrow \text{II}_c = 0.9$ eV). Given the stabilization gained by the initial monomer coordination (barrierless, since this represents a long-range attraction) and the zero-point energy, the energy barrier is not expected to hinder the reactivity as also confirmed by the experiment. Attempts in optimizing all other transition states along the nucleophilic transfer path proved challenging and were limited by convergence problems as well as high computational costs.

As the experimental finding shows a less-efficient initiation in 2VP polymerization with collidine than with the alkyl initiator, we were interested in the electronic and steric properties of the optimized geometries (I_{a-d} and II_{a-d}). By comparing structures II_a and II_b (after nucleophilic transfer of the respective initiator to 2VP) it seemed that the collidine moiety of II_b was

completely detached from the metal center (Figure 8). As known, 2VP is a strong electron donor, and when used in tandem with an electron-donating molecule like the pyridine moiety in **1b**, an overload of electron density to the metal center is provoked. This overload in electron density weakens the binding energy of the collidine moiety, which explains the detachment from yttrium in the optimized geometry. The geometry I_b of the initial coordination step already confirmed dissociation of one electron-donating molecule (Figure 9).

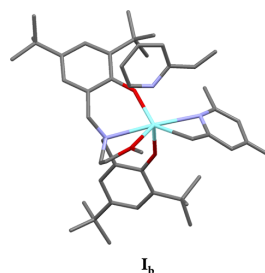


Figure 9. Geometry of I_b (light blue = yttrium; red = oxygen; purple = nitrogen; gray = carbon).

Because of the coordination of the electron-donating collidine initiator, coordination of the 2VP via the nitrogen atom is disfavored. This led to the detachment of the monomer from yttrium. It appears that high electron density/charge localization on the nucleophilic carbon atom of the initiator (predominant in alkyl initiators) is essential for nucleophilic attack of barely coordinated 2VP. The combination of an electron-donating nitrogen atom and reduced electron density on the activated CH_2 group of collidine (due to charge delocalization) was not sufficient for efficient nucleophilic transfer to 2VP. These assumptions were in accordance with the experimental findings, as initiation with collidine was less efficient than initiation via an alkyl species.

We were interested in the initiator efficiencies of **1a** and **1b** in IPOx polymerization (Supporting Information, Table S5) to verify our examinations on the validity for all nitrogen-coordinating Michael monomers. The results underline our postulation, as they were very similar to 2VP polymerization results. High initiator efficiency was observed for alkyl initiators ($I = 0.93$), whereas less-efficient initiation was predominant with the heteroaromatic collidine initiator ($I = 0.47$).

Table 3. Comparison and Advantages of the Best Suitable Catalysts According to the Respective Monomer

monomer		metal center		initiator		advantage of catalyst
N-coordinating	O-coordinating	Y	Lu	CH ₂ TMS	collidine	
2VP		+		+		high initiator efficiency
	DEVP	+	+	+	+	high activity
	DMAA	+	+ ^a		+	improved initiator efficiencies
						improved <i>D</i>
						high activity
						high isotacticity of PDMAA
						improved <i>D</i>

^a2b shows just a slightly broader *D* and initiator efficiency in comparison to 1b.

To show that the opposite trend is evident in DMAA polymerization, the isolated structures II_b and II_c were compared (see Figure 8). An eight-membered cycloaddition-type nucleophilic transfer reaction of I_d involving the CH₂ substituent of collidine leads to the formation of an aliphatic chain (II_d). The N–Y bond was not completely cleaved after the addition process, since the pyridine moiety remained coordinated to the metal center. In comparison, the CH₂TMS moiety of structure II_c shows a complete detachment from the Y atom and is solely bound via the oxygen atom of DMAA. This can be understood by considering that the CH₂TMS moiety in 1a is a poor electron donor when compared with the pyridine moiety of 1b and, thus, has weaker binding energy. In addition, DMAA itself has electron-withdrawing character, and electron density overload is not caused by initiation with electron-donating collidine. The coordination of DMAA simultaneously with the attached electron-donating collidine does not provoke an electron overload at the metal center, neither in I_d nor in II_d. Therefore, the calculation results underline our experimental findings and enable a comparison between the different initiators, metal centers, and monomers during the initiation process.

CONCLUSION

In this study, REM-GTP with isostructural 2-aminoalkoxybis-(phenolate)yttrium and lutetium complexes 1a–3b was examined. This study showed moderate-to-exceptionally high catalyst activities with various polar monomers. Kinetic studies in 2VP polymerization revealed that all of the tested catalyst systems followed a living-type mechanism, allowing precise molecular weight control with very narrow molecular-weight distributions. A heteroaromatic molecule was efficiently introduced as an initiator via C–H bond activation. Altogether, these structure variations made it possible to tune the activity, initiator efficiency, and the resulting microstructures of 2VP, DEVP, and DMAA polymerization. Lutetium catalysts [(ONOO)^{tBu}Lu(X)(THF)] (2a/2b), with a higher effective nuclear charge, demonstrated the highest activity for GTP of 2VP. Bis(phenolate)yttrium complexes with heteroaromatic initiators showed decreased efficiency in polymerization with electron-donating monomers (2VP and IPOx), because electron density overload was provoked at the yttrium center. Computational studies underline that the coordination of nitrogen-donating monomers (containing a free electron pair) is hindered with yttrium catalysts when an electron-donating initiator is used. Since all of the other monomers were nonelectron-donating systems, the change of initiator via C–H bond activation with 2,4,6-collidine led to an enhancement in initiator efficiency. Deprotonation of the acidic α -CH is avoided with heteroaromatic initiators, which, until now, was solely

assumed for DEVP polymerization while neglecting the electronic effects. For DMAA polymerization, yttrium catalyst 1b was highly active, and the resulting polymer microstructure exhibited high isotacticity ($P_m = 94\%$) while maintaining a narrow molecular mass distribution. In summary, this study facilitates the selection of the ideal initiator and metal combination for obtaining the most efficient and stereospecific polymerization system for a broad range of polar vinyl monomers. Table 3 summarizes the most suitable catalysts for each monomer type studied.

ASSOCIATED CONTENT

Supporting Information

The Supporting Information is available free of charge on the ACS Publications website at DOI: 10.1021/acs.inorgchem.7b01261.

Experimental section, further analytic data, DFT calculations, X-ray data (CCDC 1547971), and polymer characteristics (PDF)

Accession Codes

CCDC 1547971 contains the supplementary crystallographic data for this paper. These data can be obtained free of charge via www.ccdc.cam.ac.uk/data_request/cif, or by emailing data_request@ccdc.cam.ac.uk, or by contacting The Cambridge Crystallographic Data Centre, 12 Union Road, Cambridge CB2 1EZ, UK; fax: +44 1223 336033.

AUTHOR INFORMATION

Corresponding Author

*E-mail: rieger@tum.de.

ORCID

Alexander Pöthig: 0000-0003-4663-3949

Bernhard Rieger: 0000-0002-0023-884X

Author Contributions

The manuscript was written through contribution of all authors. All authors have given approval to the final version of the manuscript.

Notes

The authors declare no competing financial interest.

ACKNOWLEDGMENTS

F.A. thanks the Bavarian State Ministry of Environment and Consumer Protection for financial support within BayBiotech research network. J.E. acknowledges support by the International Max Planck Research School of Advanced Photon Science. We thank T. Helbich, S. Vagin, A. Kronast, and B. Soller for the valuable discussions. The authors thank D. Mayer and B. Rehl for proofreading of the manuscript.

REFERENCES

- (1) Soller, B. S.; Salzinger, S.; Rieger, B. Rare Earth Metal-Mediated Precision Polymerization of Vinylphosphonates and Conjugated Nitrogen-Containing Vinyl Monomers. *Chem. Rev.* **2016**, *116* (4), 1993–2022.
- (2) Soller, B. S.; Zhang, N.; Rieger, B. Catalytic Precision Polymerization: Rare Earth Metal-Mediated Synthesis of Homopolymers, Block Copolymers, and Polymer Brushes. *Macromol. Chem. Phys.* **2014**, *215* (20), 1946–1962.
- (3) Chen, E. Y. X. Coordination Polymerization of Polar Vinyl Monomers by Single-Site Metal Catalysts. *Chem. Rev.* **2009**, *109* (11), 5157–5214.
- (4) Yasuda, H.; Furo, M.; Yamamoto, H.; Nakamura, A.; Miyake, S.; Kibino, N. New Approach to Block Copolymerizations of Ethylene with Alkyl Methacrylates and Lactones by Unique Catalysis with Organolanthanide Complexes. *Macromolecules* **1992**, *25* (19), 5115–5116.
- (5) Ihara, E.; Morimoto, M.; Yasuda, H. Living Polymerizations and Copolymerizations of Alkyl Acrylates by the Unique Catalysis of Rare Earth Metal Complexes. *Macromolecules* **1995**, *28* (23), 7886–7892.
- (6) Xu, T.-Q.; Yang, G.-W.; Lu, X.-B. Highly Isotactic and High-Molecular-Weight Poly(2-Vinylpyridine) by Coordination Polymerization with Yttrium Bis(Phenolate) Ether Catalysts. *ACS Catal.* **2016**, *6* (8), 4907–4913.
- (7) Yasuda, H.; Yamamoto, H.; Yokota, K.; Miyake, S.; Nakamura, A. Synthesis of Monodispersed High Molecular Weight Polymers and Isolation of an Organolanthanide(III) Intermediate Coordinated by a Penultimate Poly(MMA) Unit. *J. Am. Chem. Soc.* **1992**, *114* (12), 4908–4910.
- (8) Collins, S.; Ward, D. G. Group-Transfer Polymerization Using Cationic Zirconocene Compounds. *J. Am. Chem. Soc.* **1992**, *114* (13), 5460–5462.
- (9) Seemann, U. B.; Dengler, J. E.; Rieger, B. High-Molecular-Weight Poly(Vinylphosphonate)s by Single-Component Living Polymerization Initiated by Rare Earth Metal Complexes. *Angew. Chem., Int. Ed.* **2010**, *49* (20), 3489–3491.
- (10) Salzinger, S.; Seemann, U. B.; Plikhta, A.; Rieger, B. Poly(Vinylphosphonate)s Synthesized by Trivalent Cyclopentadienyl Lanthanide-Induced Group Transfer Polymerization. *Macromolecules* **2011**, *44* (15), 5920–5927.
- (11) Zhang, N.; Salzinger, S.; Soller, B. S.; Rieger, B. Rare Earth Metal-Mediated Group-Transfer Polymerization: From Defined Polymer Microstructures to High-Precision Nano-Scaled Objects. *J. Am. Chem. Soc.* **2013**, *135* (24), 8810–8813.
- (12) Kaneko, H.; Nagae, H.; Tsurugi, H.; Mashima, K. End-Functionalized Polymerization of 2-Vinylpyridine through Initial C-H Bond Activation of N-Heteroaromatics and Internal Alkynes by Yttrium Ene-Diamido Complexes. *J. Am. Chem. Soc.* **2011**, *133* (49), 19626–19629.
- (13) Altenbuchner, P. T.; Soller, B. S.; Kissling, S.; Bachmann, T.; Kronast, A.; Vagin, S. I.; Rieger, B. Versatile 2-Methoxyethylaminobis(Phenolate)Yttrium Catalysts: Catalytic Precision Polymerization of Polar Monomers via Rare Earth Metal-Mediated Group Transfer Polymerization. *Macromolecules* **2014**, *47* (22), 7742–7749.
- (14) Carpentier, J. F. Rare-Earth Complexes Supported by Tripodal Tetradentate Bis(Phenolate) Ligands: A Privileged Class of Catalysts for Ring-Opening Polymerization of Cyclic Esters. *Organometallics* **2015**, *34* (17), 4175–4189.
- (15) Altenbuchner, P. T.; Adams, F.; Kronast, A.; Herdtweck, E.; Pöthig, A.; Rieger, B. Stereospecific Catalytic Precision Polymerization of 2-Vinylpyridine via Rare Earth Metal-Mediated Group Transfer Polymerization with 2-Methoxyethylamino-Bis(Phenolate)-Yttrium Complexes. *Polym. Chem.* **2015**, *6* (38), 6796–6801.
- (16) Kronast, A.; Reiter, D.; Altenbuchner, P. T.; Vagin, S. I.; Rieger, B. 2-Methoxyethylamino-Bis(Phenolate)Yttrium Catalysts for the Synthesis of Highly Isotactic Poly(2-Vinylpyridine) by Rare-Earth Metal-Mediated Group Transfer Polymerization. *Macromolecules* **2016**, *49* (17), 6260–6267.
- (17) Salzinger, S.; Soller, B. S.; Plikhta, A.; Seemann, U. B.; Herdtweck, E.; Rieger, B. Mechanistic Studies on Initiation and Propagation of Rare Earth Metal-Mediated Group Transfer Polymerization of Vinylphosphonates. *J. Am. Chem. Soc.* **2013**, *135* (35), 13030–13040.
- (18) Duchateau, R.; van Wee, C. T.; Meetsma, A.; Teuben, J. H. Bis(Trimethylsilyl)Benzamidinate: A Promising Spectator Ligand in Organoyttrium Chemistry. Synthesis and Reactivity of {[C6h5c(Nsime3)2]2y-Mu-R}2 (R = H, C.Tplbond.Ch) and X-Ray Structure of {[C6h5c(Nsime3)2]2y-Mu-C.Tplbond.Ch}2. *J. Am. Chem. Soc.* **1993**, *115* (11), 4931–4932.
- (19) Duchateau, R.; van Wee, C. T.; Teuben, J. H. Insertion and C-H Bond Activation of Unsaturated Substrates by Bis(Benzamidinato)-Yttrium Alkyl, [Phc(Nsime3)2]2yr (R = Ch2ph-Thf, Ch(Sime3)2), and Hydrido, {[Phc(Nsime3)2]2y(M-H)}2, Compounds. *Organometallics* **1996**, *15* (9), 2291–2302.
- (20) Duchateau, R.; Brussee, E. A. C.; Meetsma, A.; Teuben, J. H. Synthesis and Reactivity of Bis(Alkoxyisylamido)Yttrium H2-Pyridyl and H2-A-Picolyl Compounds. *Organometallics* **1997**, *16* (25), 5506–5516.
- (21) Ihara, E.; Koyama, K.; Yasuda, H.; Kanehisa, N.; Kai, Y. Catalytic Activity of Allyl-, Azaallyl- and Diaza-Pentadienylanthanide Complexes for Polymerization of Methyl Methacrylate. *J. Organomet. Chem.* **1999**, *574* (1), 40–49.
- (22) Labinger, J. A.; Bercaw, J. E. Understanding and Exploiting C-H Bond Activation. *Nature* **2002**, *417* (6888), 507–514.
- (23) Rad'kov, V.; Dorcet, V.; Carpentier, J.-F.; Trifonov, A.; Kirillov, E. Alkylttrium Complexes of Amidine-Amidopyridinate Ligands. Intramolecular C(Sp3)-H Activation and Reactivity Studies. *Organometallics* **2013**, *32* (5), 1517–1527.
- (24) Shibata, Y.; Nagae, H.; Sumiya, S.; Roachat, R.; Tsurugi, H.; Mashima, K. 2,2[Prime or Minute]-Bipyridyl Formation from 2-Arylpyridines through Bimetallic Dityttrium Intermediate. *Chem. Sci.* **2015**, *6* (10), 5394–5399.
- (25) Soller, B. S.; Salzinger, S.; Jandl, C.; Pothig, A.; Rieger, B. C-H Bond Activation by Sigma-Bond Metathesis as a Versatile Route toward Highly Efficient Initiators for the Catalytic Precision Polymerization of Polar Monomers. *Organometallics* **2015**, *34* (11), 2703–2706.
- (26) Altenbuchner, P. T.; Werz, P. D.; Schöppner, P.; Adams, F.; Kronast, A.; Schwarzenböck, C.; Pöthig, A.; Jandl, C.; Haslbeck, M.; Rieger, B. Next Generation Multiresponsive Nanocarriers for Targeted Drug Delivery to Cancer Cells. *Chem. - Eur. J.* **2016**, *22* (41), 14576–84.
- (27) Watson, P. L. Facile C-H Activation by Lutetium-Methyl and Lutetium-Hydride Complexes. *J. Chem. Soc., Chem. Commun.* **1983**, No. 6, 276–277.
- (28) Watson, P. L. Methane Exchange Reactions of Lanthanide and Early-Transition-Metal Methyl Complexes. *J. Am. Chem. Soc.* **1983**, *105* (21), 6491–6493.
- (29) Tshuva, E. Y.; Groysman, S.; Goldberg, I.; Kol, M.; Goldschmidt, Z. [Onxo]-Type Amine Bis(Phenolate) Zirconium and Hafnium Complexes as Extremely Active 1-Hexene Polymerization Catalysts. *Organometallics* **2002**, *21* (4), 662–670.
- (30) Bouyahyi, M.; Ajellal, N.; Kirillov, E.; Thomas, C. M.; Carpentier, J.-F. Exploring Electronic Versus Steric Effects in Stereoselective Ring-Opening Polymerization of Lactide and B-Butyrolactone with Amino-Alkoxy-Bis(Phenolate)-Yttrium Complexes. *Chem. - Eur. J.* **2011**, *17* (6), 1872–1883.
- (31) Arndt, S.; Okuda, J. Cationic Alkyl Complexes of the Rare-Earth Metals: Synthesis, Structure, and Reactivity. *Adv. Synth. Catal.* **2005**, *347* (2–3), 339–354.
- (32) Cai, C.-X.; Toupet, L.; Lehmann, C. W.; Carpentier, J.-F. Synthesis, Structure and Reactivity of New Yttrium Bis(Dimethylsilyl)-Amido and Bis(Trimethylsilyl)Methyl Complexes of a Tetradentate Bis(Phenoxide) Ligand. *J. Organomet. Chem.* **2003**, *683* (1), 131–136.
- (33) Harder, S.; Ruspici, C.; Bhriani, N. N.; Berkemann, F.; Schürmann, M. Benzyl Complexes of Lanthanide (II) and Lanthanide

- (iii) Metals: Trends and Comparisons. *Zeitschrift für Naturforschung B* **2008**, *63* (3), 267–274.
- (34) Ge, S.; Meetsma, A.; Hessen, B. Scandium, Yttrium, and Lanthanum Benzyl and Alkynyl Complexes with the N-(2-Pyrrolidin-1-Ylethyl)-1, 4-Diazepan-6-Amido Ligand: Synthesis, Characterization, and Z-Selective Catalytic Linear Dimerization of Phenylacetylenes. *Organometallics* **2009**, *28* (3), 719–726.
- (35) Behrle, A. C.; Schmidt, J. A. Synthesis and Reactivity of Homoleptic A-Metalated N, N-Dimethylbenzylamine Rare-Earth-Metal Complexes. *Organometallics* **2011**, *30* (15), 3915–3918.
- (36) Martin, T. J.; Procházka, K.; Munk, P.; Webber, S. E. Ph-Dependent Micellization of Poly(2-Vinylpyridine)-Block-Poly(Ethylene Oxide). *Macromolecules* **1996**, *29* (18), 6071–6073.
- (37) Atanase, L. I.; Riess, G. Micellization of Ph-Stimulable Poly(2-Vinylpyridine)-B-Poly(Ethylene Oxide) Copolymers and Their Complexation with Anionic Surfactants. *J. Colloid Interface Sci.* **2013**, *395*, 190–197.
- (38) Kang, N.-G.; Kang, B.-G.; Koh, H.-D.; Changez, M.; Lee, J.-S. Block Copolymers Containing Pyridine Moieties: Precise Synthesis and Applications. *React. Funct. Polym.* **2009**, *69* (7), 470–479.
- (39) Kumar, S.; Changez, M.; Murthy, C. N.; Yamago, S.; Lee, J.-S. Synthesis of Well-Defined Amphiphilic Block Copolymers by Organotellurium-Mediated Living Radical Polymerization (Terp). *Macromol. Rapid Commun.* **2011**, *32* (19), 1576–1582.
- (40) Klinger, D.; Wang, C. X.; Connal, L. A.; Audus, D. J.; Jang, S. G.; Kraemer, S.; Killips, K. L.; Fredrickson, G. H.; Kramer, E. J.; Hawker, C. J. A Facile Synthesis of Dynamic, Shape-Changing Polymer Particles. *Angew. Chem., Int. Ed.* **2014**, *53* (27), 7018–7022.
- (41) Talingting, M. R.; Munk, P.; Webber, S. E.; Tuzar, Z. Onion-Type Micelles from Polystyrene-Block-Poly(2-Vinylpyridine) and Poly(2-Vinylpyridine)-Block-Poly(Ethylene Oxide). *Macromolecules* **1999**, *32* (5), 1593–1601.
- (42) Changez, M.; Kang, N.-G.; Kim, D. W.; Lee, J.-S. Hollow Flower Micelles from a Diblock Copolymer. *Nanoscale* **2013**, *5* (23), 11554–11560.
- (43) Borchert, U.; Lipprandt, U.; Bilanz, M.; Kimpfler, A.; Rank, A.; Peschka-Stüss, R.; Schubert, R.; Lindner, P.; Förster, S. Ph-Induced Release from P2vp-Peo Block Copolymer Vesicles. *Langmuir* **2006**, *22* (13), 5843–5847.
- (44) Brigodiot, M.; Cheradame, H.; Fontanille, M.; Vairon, J. P. Microstructure of Poly(2-Vinylpyridine): Correlation between ¹³C and In.M.R. Determinations. *Polymer* **1976**, *17* (3), 254–256.
- (45) Adams, F.; Altenbuchner, P. T.; Werz, P. D. L.; Rieger, B. Multiresponsive Micellar Block Copolymers from 2-Vinylpyridine and Dialkylvinylphosphonates with a Tunable Lower Critical Solution Temperature. *RSC Adv.* **2016**, *6* (82), 78750–78754.
- (46) Mariott, W. R.; Chen, E. Y. X. Stereochemically Controlled Pmma-Exfoliated Silicate Nanocomposites Using Intergallery-Anchored Metalloccenium Cations. *J. Am. Chem. Soc.* **2003**, *125* (51), 15726–15727.
- (47) Aoki, T.; Kawashima, M.; Katono, H.; Sanui, K.; Ogata, N.; Okano, T.; Sakurai, Y. Temperature-Responsive Interpenetrating Polymer Networks Constructed with Poly(Acrylic Acid) and Poly(N,N-Dimethylacrylamide). *Macromolecules* **1994**, *27* (4), 947–952.
- (48) Barker, I. C.; Cowie, J. M. G.; Huckerby, T. N.; Shaw, D. A.; Soutar, I.; Swanson, L. Studies of the “Smart” Thermoresponsive Behavior of Copolymers of N-Isopropylacrylamide and N,N-Dimethylacrylamide in Dilute Aqueous Solution. *Macromolecules* **2003**, *36* (20), 7765–7770.
- (49) Jayachandran, K. N.; Takacs-Cox, A.; Brooks, D. E. Synthesis and Characterization of Polymer Brushes of Poly(N,N-Dimethylacrylamide) from Polystyrene Latex by Aqueous Atom Transfer Radical Polymerization. *Macromolecules* **2002**, *35* (11), 4247–4257.
- (50) Mueller, K. F. Thermotropic Aqueous Gels and Solutions of N,N-Dimethylacrylamide-Acrylate Copolymers. *Polymer* **1992**, *33* (16), 3470–3476.
- (51) Bekiari, V.; Sotiropoulou, M.; Bokias, G.; Lianos, P. Use of Poly(N,N-Dimethylacrylamide-Co-Sodium Acrylate) Hydrogel to Extract Cationic Dyes and Metals from Water. *Colloids Surf., A* **2008**, *312* (2–3), 214–218.
- (52) Fuchise, K.; Sakai, R.; Satoh, T.; Sato, S.-i.; Narumi, A.; Kawaguchi, S.; Kakuchi, T. Group Transfer Polymerization Of N,N-Dimethylacrylamide Using Nobel Efficient System Consisting of Dialkylamino Silyl Enol Ether as an Initiator and Strong Brønsted Acid as an Organocatalyst. *Macromolecules* **2010**, *43* (13), 5589–5594.
- (53) Mariott, W. R.; Chen, E. Y. X. Stereospecific, Coordination Polymerization of Acrylamides by Chiral Ansa-Metalloccenium Alkyl and Ester Enolate Cations. *Macromolecules* **2004**, *37* (13), 4741–4743.
- (54) Mariott, W. R.; Chen, E. Y. X. Mechanism and Scope of Stereospecific, Coordinative-Anionic Polymerization of Acrylamides by Chiral Zirconocenium Ester and Amide Enolates. *Macromolecules* **2005**, *38* (16), 6822–6832.
- (55) Bulai, A.; Jimeno, M. L.; Alencar de Queiroz, A.-A.; Gallardo, A.; San Román, J. ¹H And ¹³C Nuclear Magnetic Resonance Studies on the Stereochemical Configuration of Bis(N,N-Dimethyl-2,4-Dimethylglutarylamine) and Poly(N,N-Dimethylacrylamide). *Macromolecules* **1996**, *29* (9), 3240–3246.

4.5 Reprint permission of copyrighted content



RightsLink®

Home

Create Account

Help



ACS Publications
Most Trusted. Most Cited. Most Read.

Title: Toolbox of Nonmetallocene Lanthanides: Multifunctional Catalysts in Group-Transfer Polymerization
Author: Friederike Adams, Martin R. Machat, Peter T. Altenbuchner, et al
Publication: Inorganic Chemistry
Publisher: American Chemical Society
Date: Aug 1, 2017
Copyright © 2017, American Chemical Society

LOGIN

If you're a **copyright.com user**, you can login to RightsLink using your copyright.com credentials. Already a **RightsLink user** or want to [learn more?](#)

PERMISSION/LICENSE IS GRANTED FOR YOUR ORDER AT NO CHARGE

This type of permission/license, instead of the standard Terms & Conditions, is sent to you because no fee is being charged for your order. Please note the following:

- Permission is granted for your request in both print and electronic formats, and translations.
- If figures and/or tables were requested, they may be adapted or used in part.
- Please print this page for your records and send a copy of it to your publisher/graduate school.
- Appropriate credit for the requested material should be given as follows: "Reprinted (adapted) with permission from (COMPLETE REFERENCE CITATION). Copyright (YEAR) American Chemical Society." Insert appropriate information in place of the capitalized words.
- One-time permission is granted only for the use specified in your request. No additional uses are granted (such as derivative works or other editions). For any other uses, please submit a new request.

BACK

CLOSE WINDOW

Copyright © 2018 [Copyright Clearance Center, Inc.](#) All Rights Reserved. [Privacy statement.](#) [Terms and Conditions.](#) Comments? We would like to hear from you. E-mail us at customercare@copyright.com

5 Micellar block copolymers from 2-vinylpyridine and dialkyl vinylphosphonates

5.1 Bibliographic data

Title: “Multiresponsive micellar block copolymers from 2-vinylpyridine and dialkylvinylphosphonates with a tunable lower critical solution temperature”

Status: Communication, Accepted manuscript: August 10, 2016

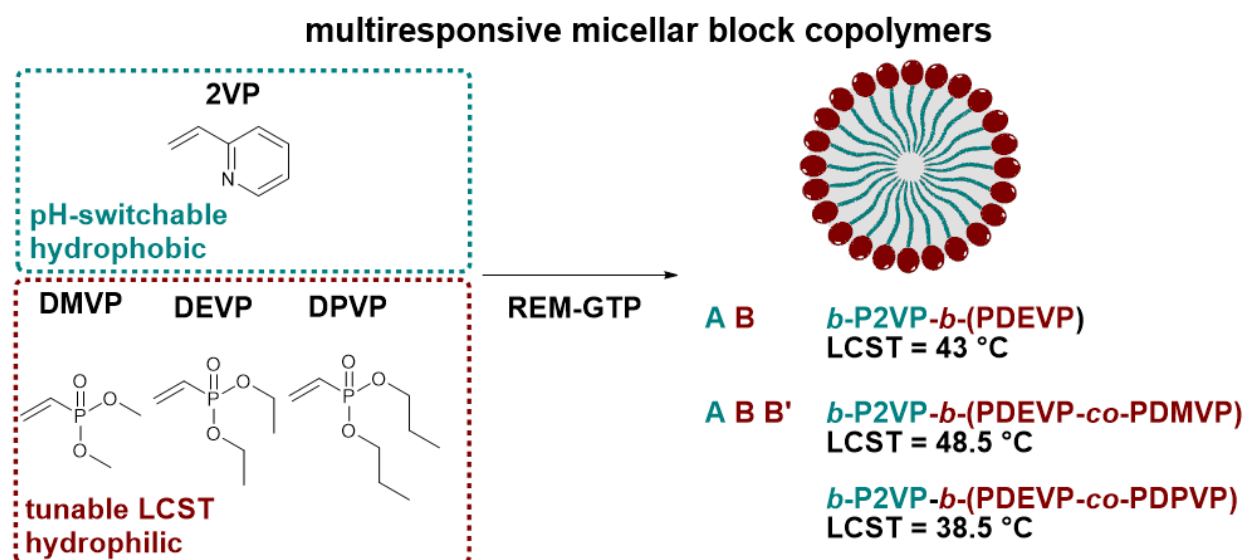
Journal: *RSC Advances*, 2016, 6, 78750-78754

Publisher: Royal Society of Chemistry

DOI: 10.1039/c6ra17160e

Authors: Friederike Adams, Peter T. Altenbuchner, Patrick D. L. Werz, and Bernhard Rieger²

5.2 Abstract graphic



² F. Adams wrote the manuscript and conducted experiments. P. T. Altenbuchner and P. D. L. Werz performed experiments. All work was supervised by B. Rieger.

5.3 Content

Polymers with reversible and controllable thermoresponsive properties are in high demand. However, the intensely studied poly(*N*-iso-propylacrylamide) (PNIPAAm) or poly(ethylene glycol) (PEG) systems all have significant disadvantages, e.g. long response time, lack of functionality, or loss of their functions in biological fluids. Thus, there is need for alternatives to broaden the choice of biocompatible, multi-stimuli-responsive polymers. The use of rare-earth metal-mediated group-transfer polymerization (REM-GTP) allows not only precise molecular weights and narrow molecular weight distributions, but also the synthesis of block copolymers by using different kind of monomers. In the last years, our group developed highly active catalysts for the homo- and copolymerization of polar vinyl monomers such as 2-vinylpyridine, diethyl vinylphosphonate and *N,N*-dimethylacrylamide. The accessibility of phosphorus- and nitrogen-containing monomers in REM-GTP, especially, dialkyl vinylphosphonates with their thermoresponsive behavior and 2-vinylpyridine with its pH-dependent solubility can be used to synthesize novel multi-responsive advanced micelles. In addition, the suitability of phosphorous containing polymers for medical applications is well known, because of their water solubility and non-toxicity. Within this publication REM-GTP is used to produce AB block copolymers from 2VP and DEVP with narrow molecular weight distributions and precise molecular weights controlled by the monomer feed. The synthesized tailor made, multi-responsive and biocompatible block copolymers self-assemble to novel micelle structures above their critical micelle concentration and exhibit a tunable lower critical solution temperature and a pH-dependent solubility. To use the LCST for release in the human body, the LCST must be tuned to the physiologically relevant temperature range. In our study we show, that only the vinylphosphonate block has influence on the thermoresponsive behavior and can selectively be utilized to shift the LCST through incorporation of small amounts of dimethyl vinylphosphonate and di-*n*-propyl vinylphosphonate. The possibility to diversify the micelle structure *via* monomer feed, to generate desired properties, opens a new field for the application of amphiphilic micelles.

5.4 Manuscript

RSC Advances



COMMUNICATION

View Article Online
View Journal | View IssueCite this: *RSC Adv.*, 2016, 6, 78750Received 4th July 2016
Accepted 10th August 2016

DOI: 10.1039/c6ra17160e

www.rsc.org/advances

Multiresponsive micellar block copolymers from 2-vinylpyridine and dialkylvinylphosphonates with a tunable lower critical solution temperature†

F. Adams, P. T. Altenbuchner,* P. D. L. Werz and B. Rieger*

AB and ABB' block copolymers were synthesized with a 2-methoxyethylamino-bis(phenolate) yttrium catalyst. 2-Vinylpyridine and diethylvinylphosphonate were chosen to obtain amphiphilic block copolymers. The obtained tailor made, so far unexplored and multi-responsive polymers self-assemble to form micelles and show a pH-sensitivity and a LCST. To tune the LCST other dialkylvinylphosphonates were incorporated leading to a shift of the LCST.

The availability of catalysts for precise and efficient synthesis of polymers with controllable molecular weights and narrow molar mass distributions is the basic requirement to establish high-performance polymers for diverse applications. Such plastics are simply available *via* rare earth metal-mediated group transfer polymerisation (REM-GTP). The living character of GTP and the high activity of rare earth metals in this polymerisation type allows not only precise molecular-weights and narrow molecular-weight distributions, but also the synthesis of block copolymers, thus leading to plenty of possible combinations by using different kinds of monomers. In the last years, our group developed highly active metallocene catalysts for REM-GTP and reported on the application of non metallocene-catalysts for the homo- and copolymerization of polar vinyl monomers.^{1–12} We reported on the homo- and copolymerization of 2-vinylpyridine (2VP) and diethylvinylphosphonate (DEVP) among others with 2-methoxyethylamino-bis(phenolate)-yttrium catalysts and showed high initiator efficiencies for the polymerization of 2-vinylpyridine and a living-type polymerization mechanism.^{12,13} The accessibility of phosphorus and nitrogen-containing monomers in REM-GTP, especially, dialkylvinylphosphonates with their thermoresponsive behaviour and 2-vinylpyridine with

its pH-dependent solubility opens a new field of high performance polymers.^{1,14,15} In addition, micelles from AB-polymeric material in general show high loading capacity of hydrophobic substances, a lower dissociation rate and also unique disposition characteristics making them highly suitable systems for drug delivery.¹⁶ Therefore, these polar vinyl monomers should be investigated in combination for the first time in matters of their applicability in drug targeting, since many pathological processes provoke an increase in temperature or a pH-value decrease. Within this publication, complex 1 is employed as a highly active catalyst for the generation of AB block copolymers from 2VP and DEVP to evaluate the influence of chain length and composition on stability, thermoresponsive behaviour and micellation. Furthermore, we investigate the synthesis of amphiphilic ABB' block copolymer structures from 2-vinylpyridine and dialkylvinylphosphonates (DEVP, dimethylvinylphosphonate (DMVP) and di-*n*-propylvinylphosphonate (DPVP)) to obtain amphiphilic block copolymers with an accurately and easily tunable lower critical solution temperature within an expanded temperature range (Fig. 1).

The synthesis of AB and ABB' block copolymers required the sequential addition of the monomers 2VP (A) and DAVP (B =

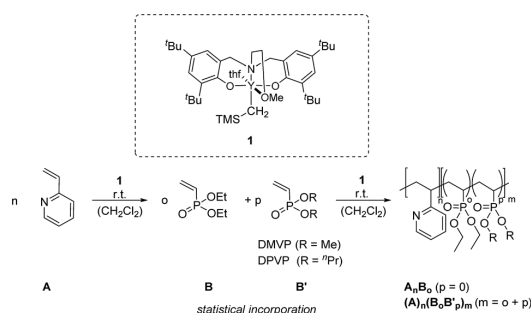


Fig. 1 Sequential REM-GTP of 2VP and DAVP (DEVP, DMVP, DPVP) with catalyst 1 at room temperature to obtain AB and ABB' polymers.

WACKER-Lehrstuhl für Makromolekulare Chemie, Technische Universität München, Lichtenbergstraße 4, 85747 Garching bei München, Germany. E-mail: rieger@tum.de; Web: <http://www.makro.ch.tum.de>; Fax: +49-89-289-13562; Tel: +49-89-289-13570
† Electronic supplementary information (ESI) available. See DOI: 10.1039/c6ra17160e



DEVP, B' = DMVP and DPVP) on the basis of their intrinsic coordination strength to each other (DAVP > 2VP).¹⁴

After dissolving the calculated amount of catalyst in dichloromethane, the respective equivalents of 2VP were added in one portion. The polymerization is quantitative after a short period of time (90 min) at room temperature. Before addition of monomer B (and B') an aliquot sample is taken from the solution and quenched by the addition of CD₃OD (calculation of conversion of 2-vinylpyridine *via* ¹H-NMR and for GPC analysis). The advantage of GTP compared to other polymerization types is the synthesis of homopolymer with an exact adjustable mass and a very low polydispersity. The monomer addition for the vinylphosphonates (BB'-random-copolymer) is achieved through simple pre-addition mixing of DEVP and DMVP/DPVP and subsequent addition to the reaction mixture making GTP a suitable method for generating blockcopolymers effortlessly. The desired block copolymers were isolated through precipitation from *n*-pentane. All polymer samples show atactic microstructures, monomodal distributions and very narrow molecular weight distributions ($D < 1.15$) (Table 1). As a benefit, no fraction of P2VP-homopolymer is observed in the blockcopolymer as found for anionic polymerization when performing blockcopolymerizations with P2VP.¹⁷ In addition, no homopolymer of PDAVP is formed due to an initiator efficiency of 99% for catalyst 1 for the 2VP polymerization avoiding unreacted catalyst in the reaction mixture.¹² This advantage is of great interest for drug delivery systems leading to unimodal blockcopolymers all with the same composition to form identical micelles without further purification of the polymers. Molecular-weights and molecular-weight distributions of block A is measured *via* GPC-MALS analysis of the first aliquot. The molecular-weight of the blockcopolymer is determined through the ratio of A/B and the molecular weight of the first block (A). Composition A/B [2VP/DAVP] is calculated *via* ¹H-NMR-spectroscopy of the dried blockcopolymer. For AB polymers the CH₂-signal of the phosphate-ester is compared with an aromatic proton of the P2VP-side chain (Fig. S7†). For ABB'

polymers the combined CH₃-signals of the phosphate-esters are used (Fig. 2). Blockcopolymers with a monomer feed of A/B 1 : 1 all show a similar ratio of A/B in the polymer regardless of whether AB or ABB' blockcopolymers are obtained (A/B = 1/0.7–1/0.8; Table 1, entry 1, 2, 5–7). In all blockcopolymers, roughly 80% of the respective dialkylvinylphosphonate is converted and incorporated in the polymer chain, independent from the used amount of monomer. For the composition of B/B' [DEVP/DPVP, DMVP] in case of PDMVP A(BB')² the proportion of PDEVP and PDMVP-signals in the ³¹P-NMR-spectrum can be used, as the calculation is consistent both for calculation *via* ¹H-NMR and *via* ³¹P-NMR-spectra. Due to overlapping of PDEVP and PDMVP-³¹P-signals, the composition in A(BB')¹ is calculated solely *via* ¹H-NMR-spectroscopy of the CH₃-signals (Fig. 2).¹⁵ Due to a perfect regulation of the polymer composition by the monomer feed, it is possible to incorporate only small amounts of DPVP/DMVP in the ABB' polymers. For A(BB')¹ 5% of block B consists of DPVP. Almost 10% of DMVP is contained in blockcopolymer A(BB')². The obtained amphiphilic polymers have a critical micelle concentration (CMC) above which they self-assemble to micelle structures. The CMC was determined by a dialysis method using Nile red, a water insoluble and fluorescent dye and was found to be at 0.13 mg mL⁻¹ (Fig. 3). In general, a lower CMC is observed for polymeric micelles in contrast to other surfactants (*ca.* 4–10 mg mL⁻¹) leading to a higher thermodynamic stability of the system.^{18,19} TEM measurements image the unimodal size distribution of these polymers (Fig. 3). Because the hydrophilic chain is longer or the same as the hydrophobic one, core-shell-type spherical micelles are observed, in which the hydrophobic core (P2VP) is shielded from the aqueous milieu by the hydrophilic segments (PDAVP). For the application of micelles in the human body a diameter of 10–100 nm is necessary, which is near to other natural vehicles, to avoid renal excretion and filtration and to ensure the cellular uptake without the recognition by the immune system.^{16,18–20}

Via REM-GTP it is possible to exactly tune the composition of the micelle structure through the monomer feed. Different feed

Table 1 AB and ABB'-block copolymers with different compositions produced with catalyst 1

Entry	Polymer	Feed ^a A _{eq} /B _{eq}	Composition A/B ^b [2VP/DEVP]	M _n (A) × 10 ^{4c} [g mol ⁻¹]	M(A _n) _{n,NMR} × 10 ^{4d} [g mol ⁻¹]	D ^e	LCST (H ₂ O) ^f [°C]	D _n ^g [nm]
1	AB ¹	2VP ₁₀₀ /DEVP ₁₀₀	1/0.8	2.5	5.6	1.06	43.5	46 ± 3
2	AB ²	2VP ₅₀ /DEVP ₅₀	1/0.8	1.3	2.9	1.04	—	—
3	AB ³	2VP ₅₀ /DEVP ₉₀	1/1.5	1.3	4.5	1.09	43.5	40 ± 5
4	AB ⁴	2VP ₅₀ /DEVP ₁₂₀	1/1.9	0.9	3.6	1.15	43.0	48 ± 4
5	AB ⁵	2VP ₂₀₀ /DEVP ₂₀₀	1/0.8	4.1	9.3	1.05	43.0	156 ± 16
Entry	Polymer	Feed ^a A _{eq} /B _{eq} /B' _{eq}	Composition A/BB' ^b [2VP/DAVP]	M _n (A) × 10 ^{4c} [g mol ⁻¹]	M(A _n) _{n,NMR} × 10 ^{4d} [g mol ⁻¹]	D ^e	LCST (H ₂ O) ^f [°C]	D _n ^g [nm]
6	A(BB') ¹	2VP ₁₀₀ /DEVP ₉₇ /DPVP ₃	1/0.8	2.4	4.8	1.07	38.5	62 ± 5
7	A(BB') ²	2VP ₁₀₀ /DEVP ₉₀ /DMVP ₁₀	1/0.7	2.0	3.7	1.05	48.5	48 ± 4

^a By weighing the monomer, [M]/[cat.] = eq., [cat.] = 41.7 μmol in 2.5 mL CH₂Cl₂. ^b Calculated from ¹H NMR spectroscopy. ^c Determined by GPC-MALS (M_w/M_n of the blockcopolymers). ^d Determined by ¹H NMR spectroscopy. ^e Polydispersity index. ^f Determined by temperature dependent UV/VIS measurements at transmittance decrease of 10%. ^g Measured by DLS. The micelle size is given as the average hydrodynamic diameter.



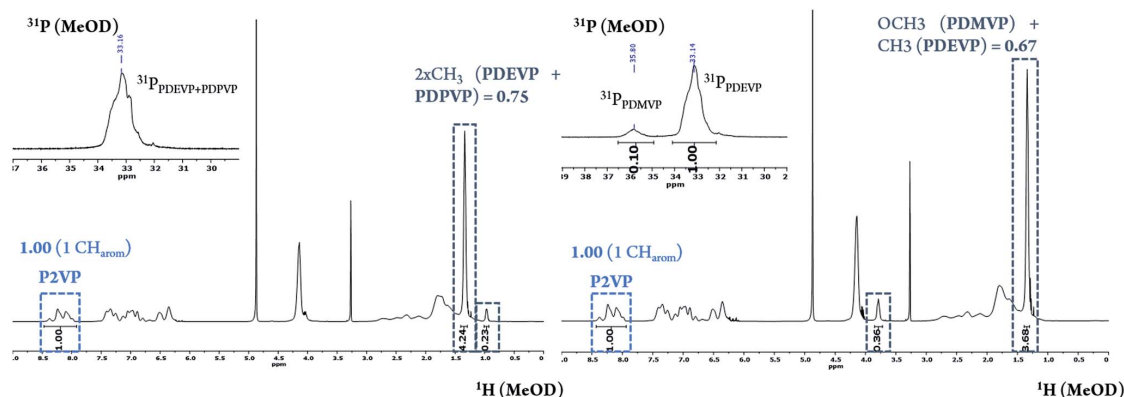


Fig. 2 ^1H - and ^{31}P -NMR spectrum of ABB^1 ($2\text{VP}_{100}/\text{DEVP}_{97}/\text{DPVP}_3$; Table 1, entry 6, left) and ABB^2 ($2\text{VP}_{100}/\text{DEVP}_{90}/\text{DMVP}_{10}$; Table 1, entry 7; right) in MeOD at 298 K. Assignment of the protons according to Rieger *et al.* overlapping of PDEVP and PDPVP- ^{31}P -signal.¹⁵

compositions were set to vary the chain length of the hydrophobic P2VP block and also the hydrophilic PDEVP block length was changed to analyze the differences in micelle formation (Table 1). The size of the micelles was determined by dynamic light scattering (DLS).

The measurements of all synthesized polymers (Table 1, entry 1–7) show that a minimum P2VP and PDEVP length is required to sustain the micelle formation in H_2O . At 2.5 wt%, fifty repeating units of 2VP and DEVP did not suffice for the formation of stable micelles in water (Table 1, entry 2). Upon increasing the chain length to 100/100 ratio between P2VP and PDEVP stable and perfectly sized (~ 50 nm) micelles can be observed (Table 1, entry 1).

The DLS-measurements underline the unimodal shape and the narrow size distribution of the AB-polymer (Fig. 3). Further increased chain length to 200/200 (P2VP/PDEVP, Table 1, entry 5) also resulted in stable micelles, but gave micelles with diameters of >100 nm and are therefore not suitable for targeting approaches. Whereas P2VP is insoluble in water under neutral conditions, a decrease of the pH-value to 5 in P2VP-PEO vehicles led to a protonation of the P2VP-block and in consequence to a dissociation of the membrane with subsequent

release of the encapsulated substance.²¹ These systems can be used for applications in drug delivery, because some cellular compartments (*e.g.* endosomal vesicles) show lower pH-values (5–6) than the one of normal blood (7.4). The pH-value is also effected by diseases as tumour cells are more acidic (pH \approx 6.5).^{18,20}

The pH-dependent solubility of our systems was investigated by titration with 0.1 M hydrochloric acid solution (Fig. S11†). The titration curve shows a high decrease to pH-value 4.5 after adding small amounts of HCl. In consequence, stable micelles are present at pH > 4.5 . This value of pH = 4.5 for dissolution of a P2VP-blockcopolymer is in agreement with other P2VP containing micelles where the dissolution occurs between pH = 4 and 5.^{17,21–23} To obtain multiresponsive micelles that are controllable not only *via* the pH-value, but also by temperature vinylphosphonates were introduced into the polymer. The suitability of phosphorous containing polymers for medical applications is well known, because of their high water solubility, thermal stability and non-toxicity.^{15,24} Therefore we performed temperature-dependent LCST-DLS measurements to show the reversible formation of micelles under hyperthermia. Below the LCST polymeric micelles are observed. When the

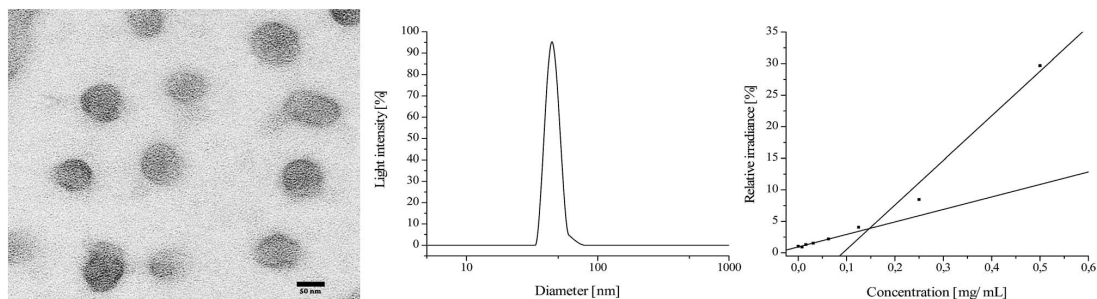


Fig. 3 Left: TEM-image of micelles from AB^1 (preparation see ESI†). Middle: dynamic light-scattering of micelles from AB^1 (2.5 mg mL^{-1}) in H_2O . Right: determination of critical micelle concentration (CMC) with Nile red. All figures for AB^1 ($2\text{VP}_{100}/\text{DEVP}_{100}$; Table 1, entry 1).



temperature is above the LCST a loaded drug can be released due to aggregation of the polymer. In the human body the drug would be released *e.g.* by a hyperthermic stimuli to the disease area.²⁰ The cloud points of PDEVVP homopolymers (230 kg mol⁻¹) was found to remain constant at low concentrations (0.1–2.5 wt%; 42 °C), but increases to 71 °C at high concentrations 67 wt%.^{15,25} The influence of P2VP on the LCST and the limits of adequate vinylphosphonate content within the polymer was tested in this study. These thermoresponsive measurements of the AB blockcopolymers (2.5 wt%) in H₂O show that the presence of P2VP and also the variation of chain length of PDEVVP (ratio: P2VP/PDEVVP 1/0.8–2.0; Table 1) have no measurable effect on the cloud points (43–43.5 °C) under the evaluated conditions. This is remarkable and can be used as an advantage over other thermoresponsive copolymers (poly-*N*-isopropylacrylamide (PNIPAm) or polyethyleneglycol (PEG)) as they show a significant influence of both, hydrophilic and hydrophobic, blocks on their LCST-behaviour.^{26,27} The independence of the LCST in P2VP-PDAVP polymers on the chain lengths and the P2VP-block in our study allows higher variation possibilities regarding the hydrophilic and hydrophobic chain segment as well as a better predictability and adjustability of the LCST. To test the influence of salts and buffer solutions on the LCST the cloud point of AB¹ was measured in PBS (phosphate buffered saline) (Fig. S13†). Due to a salting-out effect of the phosphate salt in PBS, which leads to a dehydration of the polymers, a decrease in the LCST of about 4 °C is observable. This decrease is lower than the ones of other stimuli responsive polymers *e.g.* PEG or PNIPAm resulting in a better applicability of our novel micelles in biomedical usage due to a lower impact of environmental conditions.^{15,28}

As a drawback, a release temperature of 44 °C which must be used for this micelles with an LCST at around 43 °C is not in the normal body temperature range which is between 36.2 and 37.5 °C.²⁹ Therefore our investigation was directed to the evaluation of ABB' blockcopolymers to proof the suitability of vinylphosphonates as substrates to tune the LCST in micellar

systems within a physiologically relevant temperature range for potential medical application. The introduction of small amounts of DMVP or DPVP (3–10 eq.) statistically incorporated into the DEVVP block has distinct influence and makes it possible to shift the cloud point of the copolymers (Fig. 4). The incorporation of at least 10 equivalents of hydrophobic DMVP suffice to increase the LCST up to 48.5 °C, while maintaining perfect control of the micellar architecture and without affecting the hysteresis upon cooling (Table 1, entry 7). Likewise, DPVP (even only 3 eq.) with its hydrophilic properties successfully decreases the LCST of ABB' block copolymers to 38.5 °C (Table 1, entry 6). For application in drug delivery a temperature of around 39 °C can be used which is near the normal body temperature range.

Conclusions

In summary, AB-blockcopolymers from 2VP and DAVP can be produced *via* REM-GTP with narrow molecular weight distribution and precise molecular-weight through variation of the monomer feed. These tailor-made blockcopolymers self-assemble into unimodal micelles at a low CMC, indicating a high thermodynamic stability. This stability in combination with the multiresponsive amphiphilic properties (pH-dependent solubility and LCST) of the micelles, which are investigated for the first time, making them adequate for targeting approaches. These micelles show several advantages over other micelle systems in matters of precise synthesis and exact control over the micelle structure. To use the lower critical solution temperature for release in the human body, the LCST has to be tuned to the physiologically relevant temperature range. In our study we showed, that only the vinylphosphonate block has influence on the thermoresponsive behaviour and can selectively be utilized to tune the LCST through the monomer feed. The observed a-P2VP-*b*-_{random}-(PDEVVP-*co*-PDMVP/PDPVP)-polymers in which small amounts of DMVP or DPVP are incorporated into the polymer chain shift the LCST of the micelles. Hydrophobic DMVP increases the LCST, whereas DPVP with its hydrophilic properties successfully decreases the LCST by maintaining perfect micelle structures. The possibility to tune the micelle structure *via* monomer feed, to generate desired properties, opens a new field for the application of amphiphilic micelles.

Acknowledgements

F. Adams thanks the Bavarian State Ministry of Environment and Consumer Protection for financial support within BayBio-tech research network. The authors thank Dr Marianne Hanzlik for the TEM measurements.

Notes and references

- 1 B. S. Soller, S. Salzinger and B. Rieger, *Chem. Rev.*, 2016, **116**, 1993–2022.
- 2 B. S. Soller, N. Zhang and B. Rieger, *Macromol. Chem. Phys.*, 2014, **215**, 1946–1962.

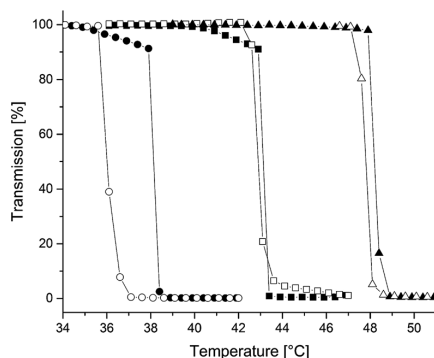


Fig. 4 Determination of the cloud points of AB (squares), A(BB')¹ (circles) and A(BB')² (triangles) block copolymers. The cloud point was determined at 10% decrease of transmittance for 2.5 wt% aqueous polymer solution.



- 3 E. Y. X. Chen, *Chem. Rev.*, 2009, **109**, 5157–5214.
- 4 H. Yasuda, M. Furo, H. Yamamoto, A. Nakamura, S. Miyake and N. Kibino, *Macromolecules*, 1992, **25**, 5115–5116.
- 5 E. Ihara, M. Morimoto and H. Yasuda, *Macromolecules*, 1995, **28**, 7886–7892.
- 6 B. S. Soller, Q. Sun, S. Salzinger, C. Jandl, A. Pöthig and B. Rieger, *Macromolecules*, 2016, **49**, 1582–1589.
- 7 B. S. Soller, S. Salzinger, C. Jandl, A. Pöthig and B. Rieger, *Organometallics*, 2015, **34**, 2703–2706.
- 8 S. Salzinger, B. S. Soller, A. Plikhta, U. B. Seemann, E. Herdtweck and B. Rieger, *J. Am. Chem. Soc.*, 2013, **135**, 13030–13040.
- 9 U. B. Seemann, J. E. Dengler and B. Rieger, *Angew. Chem., Int. Ed.*, 2010, **49**, 3489–3491.
- 10 P. T. Altenbuchner, F. Adams, A. Kronast, E. Herdtweck, A. Pöthig and B. Rieger, *Polym. Chem.*, 2015, **6**, 6796–6801.
- 11 J. F. Carpentier, *Organometallics*, 2015, **34**, 4175–4189.
- 12 P. T. Altenbuchner, B. S. Soller, S. Kissling, T. Bachmann, A. Kronast, S. I. Vagin and B. Rieger, *Macromolecules*, 2014, **47**, 7742–7749.
- 13 C.-X. Cai, L. Toupet, C. W. Lehmann and J.-F. Carpentier, *J. Organomet. Chem.*, 2003, **683**, 131–136.
- 14 N. Zhang, S. Salzinger, B. S. Soller and B. Rieger, *J. Am. Chem. Soc.*, 2013, **135**, 8810–8813.
- 15 N. Zhang, S. Salzinger and B. Rieger, *Macromolecules*, 2012, **45**, 9751–9758.
- 16 K. Kataoka, A. Harada and Y. Nagasaki, *Adv. Drug Delivery Rev.*, 2001, **47**, 113–131.
- 17 T. J. Martin, K. Procházka, P. Munk and S. E. Webber, *Macromolecules*, 1996, **29**, 6071–6073.
- 18 G. Gaucher, M.-H. Dufresne, V. P. Sant, N. Kang, D. Maysinger and J.-C. Leroux, *J. Controlled Release*, 2005, **109**, 169–188.
- 19 R. J. Stokes and D. F. Evans, *Fundamentals of Interfacial Engineering*, WILEY-VCH, 1997.
- 20 S. Ganta, H. Devalapally, A. Shahiwala and M. Amiji, *J. Controlled Release*, 2008, **126**, 187–204.
- 21 U. Borchert, U. Lipprandt, M. Bilanz, A. Kimpfler, A. Rank, R. Peschka-Süss, R. Schubert, P. Lindner and S. Förster, *Langmuir*, 2006, **22**, 5843–5847.
- 22 C. Tsitsilianis, D. Voulgaris, M. Štěpánek, K. Podhájecká, K. Procházka, Z. Tuzar and W. Brown, *Langmuir*, 2000, **16**, 6868–6876.
- 23 L. I. Atanase and G. Riess, *J. Colloid Interface Sci.*, 2013, **395**, 190–197.
- 24 G. David, C. Boyer, R. Tayou, S. Seabrook, B. Ameduri, B. Boutevin, G. Woodward and M. Destarac, *Macromol. Chem. Phys.*, 2008, **209**, 75–83.
- 25 S. Salzinger, U. B. Seemann, A. Plikhta and B. Rieger, *Macromolecules*, 2011, **44**, 5920–5927.
- 26 X. Zhao, W. Liu, D. Chen, X. Lin and W. W. Lu, *Macromol. Chem. Phys.*, 2007, **208**, 1773–1781.
- 27 Y. Yu, D. Hong, Z. Liu, F. Jia, Y. Zhou and C. Leng, *J. Polym. Res.*, 2013, **20**, 1–8.
- 28 J.-F. Lutz, Ö. Akdemir and A. Hoth, *J. Am. Chem. Soc.*, 2006, **128**, 13046–13047.
- 29 M. Sund-Levander, C. Forsberg and L. K. Wahren, *Scandinavian Journal of Caring Sciences*, 2002, **16**, 122–128.



5.5 Reprint permission of copyrighted content

Multiresponsive micellar block copolymers from 2-vinylpyridine and dialkylvinylphosphonates with a tunable lower critical solution temperature

F. Adams, P. T. Altenbuchner, P. D. L. Werz and B. Rieger, *RSC Adv.*, 2016, **6**, 78750

DOI: 10.1039/C6RA17160E

This article is licensed under a [Creative Commons Attribution-NonCommercial 3.0 Unported Licence](#). Material from this article can be used in other publications provided that the correct acknowledgement is given with the reproduced material and it is not used for commercial purposes.

Reproduced material should be attributed as follows:

- For reproduction of material from NJC:
[Original citation] - Published by The Royal Society of Chemistry (RSC) on behalf of the Centre National de la Recherche Scientifique (CNRS) and the RSC.
- For reproduction of material from PCCP:
[Original citation] - Published by the PCCP Owner Societies.
- For reproduction of material from PPS:
[Original citation] - Published by The Royal Society of Chemistry (RSC) on behalf of the European Society for Photobiology, the European Photochemistry Association, and RSC.
- For reproduction of material from all other RSC journals:
[Original citation] - Published by The Royal Society of Chemistry.

Information about reproducing material from RSC articles with different licences is available on our [Permission Requests page](#).

6 Yttrium-catalyzed synthesis of bipyridine-functionalized AB-block copolymers

6.1 Bibliographic data

Title: “Yttrium-Catalyzed Synthesis of Bipyridine-Functionalized AB-Block Copolymers: Micellar Support for Photocatalytic Active Rhenium-Complexes”

Status: Full paper, first published (Web): July 19, 2018

Journal: *ChemCatChem*, 2018, 10, 4309-4316.

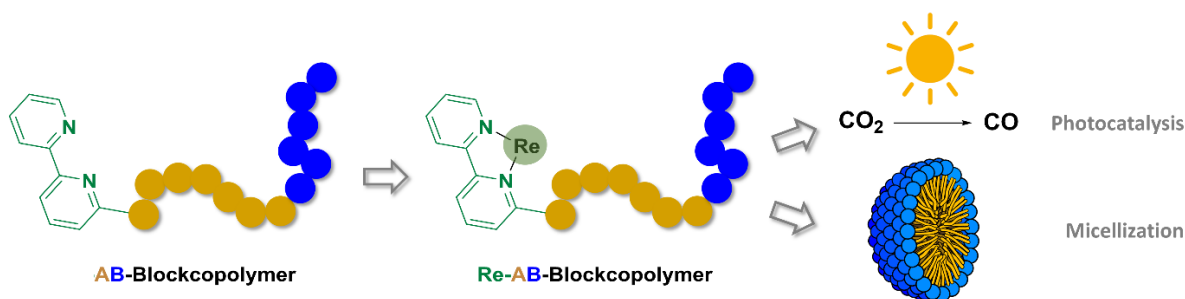
Publisher: WILEY-VCH Verlag GmbH & Co. KGaA

DOI: 10.1002/cctc.201801009

Authors: Friederike Adams^{*}, Markus Pschenitza^{*}, and Bernhard Rieger³

^{*}These authors contributed equally to this work

6.2 Abstract graphic (TOC)



³ F. Adams planned and executed all experiments and wrote the manuscript regarding the introduction, the synthesis of all yttrium species, the C-H-bond activation, the polymerizations und the polymer characterization. M. Pschenitza planned and executed all experiments and wrote the manuscript regarding the introduction, the synthesis of the rhenium complexes, DLS-measurements and photocatalysis. All work was supervised by B. Rieger.

6.3 Content

The high potential of rare-earth metal-mediated group-transfer polymerization (REM-GTP) is based on its ability to produce polymers with controllable molecular weights and narrow size distributions as well as the possibility to synthesize block copolymers effortlessly. Recently, our group used this polymerization method to synthesize block copolymers which form micelles in aqueous solutions. Based on these results, the synthesis of 2VP-DEVP-block copolymers *via* REM-GTP with bipyridine (bpy) as end-groups is described in this publication. To obtain these end-groups, C-H bond activations with α -methylated bipyridines were performed to obtain novel bpy-functionalized yttrium-catalysts (ONOO)^{tBu}Y(6-Me₂bpy) (6-Me₂bpy = 6,6'-dimethyl-2,2'-bipyridine) and (ONOO)^{tBu}Y(6-Mebpy). These catalysts were tested in the homopolymerization of 2VP, as well as for block copolymerization of 2VP with DEVP. The bpy end-groups in the block copolymers enable metal complexation shown by the reaction of bpy-2VP-DEVP-block copolymers with [Re(CO)₅Cl] providing a [Re(CO)₃(bpy)Cl] motif as the end-group. It is shown, that these Re-2VP-DEVP-block copolymers still form unimodal micelles in water. As the used block copolymers can enter cells and bipyridines are widely used ligands in metalorganic compounds, these bpy-block copolymers are a class of promising candidates as carriers for hydrophobic metal complexes. To proof that the polymer part of these systems does not influence the properties of the metalorganic complex and to open the door to a completely new field for REM-GTP block copolymers, we used the Re-2VP-DEVP-block copolymers in the photocatalytic reduction of CO₂ to CO. Comparing the catalytic performance of the rhenium functionalized block copolymers with its analogue polymer-free complex, the turnover numbers were not only retained with respect to the polymer-free system, but they even increased.

6.4 Manuscript



DOI: 10.1002/cctc.201801009

CHEMCATCHEM
Full Papers

Yttrium-Catalyzed Synthesis of Bipyridine-Functionalized AB-Block Copolymers: Micellar Support for Photocatalytic Active Rhenium-Complexes

F. Adams^{+, [a]}, M. Pschenitzka^{+, [a]} and B. Rieger^{*[a]}

Herein, *ortho*-methylated bipyridines are introduced as initiators in 2-aminoalkoxy-bis (phenolate) yttrium complexes. For this C–H bond activation (ONOO)^{tBu}Y(CH₂TMS)(thf) (1) (TMS = trimethylsilyl) is reacted with the respective bipyridine to obtain complexes (ONOO)^{tBu}Y(6-Me₂bpy) (2) and (ONOO)^{tBu}Y(6-Mebpy) (3). Both complexes were tested first in rare-earth metal-mediated group-transfer polymerization of 2-vinylpyridine (2VP). Complex 3 was further tested in block copolymerizations of 2VP and diethyl vinylphosphonate. The obtained initiator-P2VP-

PDEVP-block copolymers can selectively react with Re(CO)₂Cl at their bipyridine end-group. The obtained rhenium functionalized block copolymers are able to self-assemble to unimodal micelles in water, representing a possible carrier for hydrophobic metal containing complexes into cells. Furthermore, the Re-block copolymers sustain activity in the photocatalytic homogeneous CO₂ reduction and their performance exceed the catalytic activity of the analogue polymer-free system [Re(CO)₂(6-Mebpy)Cl] (4).

Introduction

Rare-earth metal-mediated group-transfer polymerization (REM-GTP) is an efficient method for the precise synthesis of polymers with controllable molecular weights and very narrow molar mass distributions.^[1] The living character of GTP and the high activity of rare-earth metals in this polymerization type allows the synthesis of block copolymers. By using various kinds of monomers, plenty of different block copolymers can be synthesized.^[2] The accessibility of phosphorus- and nitrogen-containing monomers in REM-GTP, especially, hydrophilic dialkyl vinylphosphonates (DAVP) with a lower critical solution temperature (LCST) and hydrophobic 2-vinylpyridine (2VP) with its pH-dependent solubility opens a new field of high performance polymers. In recent years, our group developed highly active 2-methoxyethylamino-bis (phenolate)-lanthanides with the general structure (ONOO)^{tBu}Y(CH₂TMS)(thf) (TMS = trimethylsilyl; ONOO)^{tBu} = 6,6'-(((2-methoxyethyl) azanediy)l)-bis (methylene)-bis (2,4-di-*tert*-butylphenolate)) in 2VP polymerization and reported on the application of these catalysts for copolymerization of 2VP among other polar vinyl monomers.^[3] Recently, we reported on the utilization of reversible multiresponsive AB, ABB' and BAB-block copolymers (A = poly (2-vinylpyridine) (P2VP), B = poly (diethyl vinylphosphonate) (PDEVP), B' = poly (di-*n*-propyl vinylphosphonate) (PDMVP) or poly (dimethyl vinyl-

phosphonate) (PDPVP)), which self-assemble to unimodal micelles over their critical micelle concentration (cmc). Rieger *et al.* investigated these polymers as potential nanocarrier in drug delivery systems, as these block copolymers are highly suitable systems for the transport of hydrophobic substances and controllable *via* pH-value and temperature.^[3c,4] As trivalent lanthanide-complexes are in addition able to perform σ -bond metathesis in a [2 σ + 2 σ]-cycloaddition, end-group functionalization is easily possible by using this form of C–H bond cleavage to introduce different types of initiators. These initiators serve then as end-groups in REM-GTP. C–H-bond activation of a variety of alkynes and heteroaromatic compounds such as 2,4,6-trimethylpyridine, 1-trimethylsilyl-1-propyne, or 2,3,5,6-trimethylpyrazine, was previously reported by the research groups of Rieger and Mashima. These C–H bond-activated molecules were introduced for improvements in initiator efficiency or to obtain bifunctional initiators.^[3b,5]

To further broaden the field of possible applications of AB-block copolymers synthesized by REM-GTP, *ortho*-methylated bipyridines (bpy) are employed as end-groups. In coordination chemistry of transition metals, these bipyridines are the most commonly used class of ligands.^[6] Differently substituted bipyridines or bipyridine frameworks are coordinated to a lot of transition metals which range from palladium and platinum^[7] to Mo,^[8] Fe,^[9] Co,^[10] Ni,^[11] Cu^[12] or Zn^[13]. In all these examples, a variety of applications are covered (e.g. epoxidation, enzymatic oxidation, interaction with DNA, electrocatalytic water oxidation, CO₂ capture *via* cycloaddition to epoxides etc.).^[8–10,12]

Another example for an application of bipyridines with transition metals is the homogeneous photocatalytic reduction of CO₂ using [Re(CO)₂(bpy)Cl] (5). Due to their ability to act as both photosensitizers and photocatalysts, and the high selectivity towards CO₂ reduction, these systems have been investigated for over 30 years. However, rhenium-based photocatalytic systems still lack sufficient stability for industrial

[a] F. Adams,^{*} M. Pschenitzka,^{*} Prof. Dr. B. Rieger
WACKER-Lehrstuhl für Makromolekulare Chemie
Catalysis Research Center
Department of Chemistry
Technische Universität München
Lichtenbergstr. 4
Garching bei München 85748 (Germany)
E-mail: rieger@tum.de

[†] These authors contributed equally to this work.

Supporting information for this article is available on the WWW under <https://doi.org/10.1002/cctc.201801009>

processes.^[14] In this context, **5** was tested in the electrocatalytic CO₂ reduction, dissolved in a brush polymer ion gel (PS–PEO–PS) or bound in a bipyridine macromolecular-structure.^[15] These approaches show the high potential of polymer/rhenium adducts for numerous applications. Polymeric Ru(bpy)₃²⁺ shows a preservation of luminescence properties of the metal after complexation to a bipyridine-polymer, which encouraged us to test rhenium complexes as end-groups in AB-block copolymers.^[16] So far, end-functionalized polymers have never been used for selective complexation of transition metals. In addition, photocatalytic CO₂ reduction has not been tested yet with polymer/metal adducts.

Providing such a versatile ligand as end-groups in P2VP-PDEV-Block copolymers offers the possibility to obtain a variety of bpy metal complexes in the core of a micelle. These micelles are known to penetrate cells and dissolve hydrophobic substances in aqueous solution. In addition, since the pH-dependent solubility of P2VP and the LCST of PDEV are preserved in block copolymers, the hydrophobic substance can be released *via* changes in temperature or pH and then used for its purpose at a place which hydrophobic substances would only hardly reach by themselves.^[3c,4]

Herein, bipyridine end-groups in P2VP-PDEV-Block copolymers are used to provide a [Re(CO)₃(bpy)Cl] motif for the synthesized polymers. The obtained Re-bpy-P2VP-PDEV-Block copolymers are a new class of photocatalytically active polymers which are investigated in homogeneous photocatalytic CO₂ reduction in this contribution.

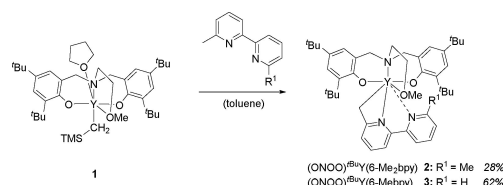
Results and Discussion

Synthesis of Yttrium bis (Phenolate) Complexes **2** and **3**

For the synthesis of (ONOO)^{tBu}Y(CH₂TMS)(thf) (**1**), one equivalent of the symmetric 2-methoxyethylamino-bis (phenolate) ligand was reacted with one equivalent of Y(CH₂TMS)₃(thf)₃, in a mixture of toluene/pentane at 0 °C and stirred overnight at room temperature.^[17] The symmetrically substituted ligand 2-methoxyethylamino-bis (phenolate) was synthesized *via* modified Mannich reaction of 2,3-di-*tert*-butylphenol with 2-methoxyethylamine in a formaldehyde solution.^[18]

Afterwards, we tested the reactivity of complex **1** towards 6,6'-dimethyl-2,2'-bipyridine (6-Me₂bpy) and 6-methyl-2,2'-bipyridine (6-Mebpy) to obtain bipyridine-functionalized yttrium bis (phenolate) complexes **2** and **3** (Scheme 1).

Time-resolved ¹H-NMR experiments of the reaction were performed at room temperature and 60 °C to investigate the tendency to activate these *ortho*-methylated bipyridines. These experiments revealed strongly varying ambitions for catalyst **1** to undergo C–H bond activation (SI, Figures S1 and S2). Very slow activation was observed at room temperature for 6-Me₂bpy. Increased temperatures (60 °C) led to changes in the reactivity and catalyst **1** was transformed to complex **2** in the presence of one equivalent of 6-Me₂bpy within 5 days (SI, Figure S1). A ratio of one regarding the ligand and the bipyridine in (ONOO)^{tBu}Y(6-Me₂bpy) was proven *via* ¹H-NMR



Scheme 1. C–H bond activation of **1** with 6-Me₂bpy and 6-Mebpy to obtain bipyridine-functionalized yttrium bis (phenolate) complexes **2** and **3**.

spectroscopy. Therefore, no dual C–H-bond activation took place and a monometallic structure is evident. Forcing a double C–H bond activation by increasing the amount of **1** was unsuccessful. In case of 6-Mebpy, full conversion was reached after 8 hours at room temperature and (ONOO)^{tBu}Y(6-Mebpy) (**3**) was obtained. For C–H bond activation with bis (phenolate) lanthanides this reaction time was until now the fastest, and the reaction proceeds in addition at room temperature which shows the high reactivity towards 6-Mebpy. For both C–H bond-activated compounds, centrifugation of a suspension in pentane afforded the desired complexes with the general structure (ONOO)^{tBu}Y(6-Me_nbpy)(thf) (n = 1 or 2) (Scheme 1). Both complexes were characterized *via* NMR-spectroscopy and elemental analysis. Complex **3** was isolated with a higher yield (62%) than **2** (28%) due to a better solubility of **2** in pentane. Remarkably, both complexes do not coordinate thf as observed so far for all investigated monometallic 2-aminoalkoxy-bis (phenolate) yttrium complexes with the general structure (ONOO)^{tBu}Y(initiator)(thf).^[19] In addition, **2** and **3** showed a purple to blue color, which is also found in complexes in which a substance is bound *via* a Y–N bond and an additional coordination of an intramolecular pyridine moiety is observed.^[20] All these findings suggest that the second nitrogen atom of the bipyridine moiety coordinates instead of a thf molecule.

Homopolymerization of 2-Vinylpyridine

The isolated catalysts **2** and **3** were employed in GTP of 2VP (first block in the block copolymers) to evaluate the general activities, initiator efficiencies, and microstructures of the isolated polymers. First, the initiation mechanisms of the C–H bond-activated complexes were elucidated *via* end-group analysis of oligomeric 2VP. ESI-MS was performed by reacting catalyst **3** with 30 equivalents of 2VP in toluene and immediate measurement in acetonitrile. Signals of the oligomers corresponding to initiator + n × M_{2VP} with either H⁺ or Na⁺ as charge carrier were observed (SI, Figure S3). The initiating groups were clearly visible in the ESI-MS; a nucleophilic transfer reaction of the initiator *via* monomer insertion into the Y–C bond is apparent, as also reported for other C–H bond-activated yttrium bis (phenolates).^[3b]

To determine conversions and kinetic parameters, aliquots were taken at regular time intervals during polymerization.

Conversion was then calculated gravimetrically. Absolute molecular masses and mass distributions were measured by gel-permeation chromatography (GPC) coupled with triple detection in dimethylformamide (dmf) as solvent (SI, Figure S9). The polymerization of 2VP with 2-methoxyethylamino-bis (phenolate)-catalysts **2** and **3** proceeds in a living fashion, as indicated by the narrow polydispersities ($1.05 \leq \bar{\xi} \leq 1.07$) and a linear relationship between molar masses and conversion (Figure 1, Table 1).

If the conversion is plotted against time, the polymerizations can be compared regarding the activity of the different catalysts. Complex **1**, known from the literature, has an initiator efficiency of 0.99 which means that 99% of the complex molecules are active in polymerization. As most of the complex molecules are active, the TOF (turnover frequency) and TOF* (normalized TOF) are nearly the same. Catalysts **2** and **3** both show a lower initiator efficiency and therefore a lower turnover frequency. By comparing only the two new catalysts, **3** shows a higher turnover frequency (TOF), because its initiator efficiency is higher. As expected, changing the initiator to a bipyridine did not impact the normalized turnover frequencies (TOF*) in comparison to catalyst **1** since the activity is determined in the propagation step and is solely influenced by the metal center and the ligand, which are identical in all complexes.^[3a,b] As the tacticity is also determined in the propagation step, catalyst **2**

and **3** produce atactic P2VP with the same tacticity as catalyst **1** (SI, Figure S5).^[17a]

Block Copolymerizations

The living nature of GTP allows the preparation of block copolymers of all *Michael*-type monomers among another. The first block must be the monomer with the lowest coordination strength to the metal center. Therefore, the synthesis of AB-block copolymers required the sequential addition of the monomers 2VP (A) and DEVP (B) (DEVP = diethyl vinylphosphonate) on the basis of their intrinsic coordination strength (DEVP > 2VP).^[2b,21] The block copolymerizations were carried out with catalyst **3**, as the activity and initiator efficiency was higher in 2VP polymerization than for **2**. In addition, catalyst **3** was isolated with a higher yield. After dissolving the calculated amount of **3** in dichloromethane, the respective equivalents of 2VP were added in one portion. The polymerization is quantitative after a short period of time (90 min) at room temperature as determined *via* activity measurements in homopolymerizations with 2VP (*vide supra*). Before adding monomer B, an aliquot sample was taken from the solution and quenched by the addition of CD₃OD. Conversion of 2VP was calculated *via* ¹H-NMR spectroscopy and GPC analysis was performed to determine the molar mass of the first block. Block

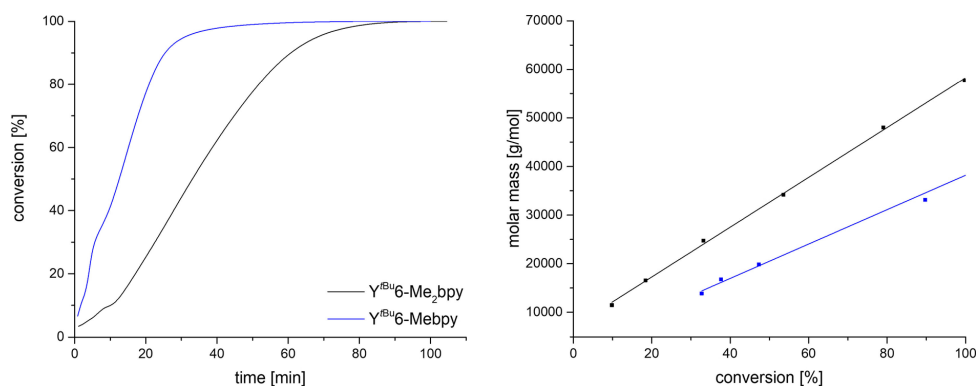


Figure 1. Left) Catalytic activity of catalysts **2** (black) and **3** (blue) ([cat.] = 135 μ mol, [2VP] = 27 mmol, toluene = 20 mL, T = 25 °C) measured by aliquot method. Right) Linear growth of the absolute molecular weight (M_n) (measured by GPC) as a function of monomer conversion (gravimetrically determined). Catalysts are abbreviated with Y^{8b}6-Me₂bpy and Y^{8b}6-Mebpy for clarity.

Entry	Catalyst	Time [min]	Conversion [%]	$M_{n,calc}$ [10^4 g/mol] ^[b]	$M_{n,GPC}$ [10^4 g/mol]	\bar{D} ^[c]	i ^[d]	I^* ^[e,f]	TOF ^[f] [h^{-1}]	TOF* ^[e] [h^{-1}]
1 ^[3a]	1	120	99	2.2	2.2	1.01	0.99	0.99	1100	1110
2	2	134	99	1.8	7.6	1.07	0.24	0.24	220	920
3	3	143	99	2.3	4.6	1.05	0.54	0.46	470	1000

[a] Reactions performed with [2VP] = 2.7 mmol, [2VP]/[Cat] = 200/1, at 25 °C in 2 mL solvent, conversions determined by ¹H-NMR-spectroscopy and $M_{n,GPC}$ determined as absolute molar masses by GPC coupled with triple detection in dmf; [b] $M_{n,calc}$ from $M_{n,calc} = M_{2VP} \times (([2VP]/[Cat]) \times \text{conversion})$; [c] Polydispersity calculated from $M_{w,GPC}/M_{n,GPC}$ determined by GPC; [d] $I = M_{n,calc}/M_{n,GPC}$ at the end of the reaction; [e] TOF* = TOF/ I^* ; normalized TOF for active metal centers; I^* = average I at the highest slope of the reaction; [f] Parameters calculated with reaction conditions stated in Figure 1.

Copolymers are achieved by the subsequent addition of DEVP to the reaction mixture which was then stirred overnight. The conversion of block B was determined via ^{31}P -NMR spectroscopy of an aliquot taken before quenching of the reaction. In all block copolymers, roughly 70 to 85% of DEVP were converted. The desired block copolymers were isolated and purified through quenching with methanol, precipitation from *n*-pentane and freeze-drying from benzene. All polymer samples showed monomodal distributions and very narrow molecular weight distributions ($\xi < 1.05$) (Table 2). No fractions of homopolymers were observed, which led to unimodal block copolymers in which all polymer chains had the same composition (SI, Figure S10, S11). Thus, GTP is a suitable method for generating tailor-made block copolymers effortlessly. The molecular weight of the block copolymer is determined through the ratio of A/B and the molecular weight of the first block (A). Composition A/B [2VP/DAVP] is calculated via ^1H -NMR spectroscopy of the freeze-dried block copolymer. The CH_2 -signal of the phosphate-ester (4 protons in total) was compared with an aromatic proton of the P2VP-side chain (SI, Figure S6, S7). It was possible to tune the composition of the copolymer through the monomer feed. Different feed compositions were set to vary the chain length of the P2VP and the PDEV block and the ratio of the two blocks to obtain different-sized block copolymers. Two block copolymers with higher molecular weights were synthesized which differed in their

composition (**AB**¹ and **AB**²; Table 2, Entry 1 and 2). **AB**¹ contains a larger P2VP block ($\text{P2VP}_{\text{eq.}}/\text{PDEV}_{\text{eq.}} = 300/235$), whereas **AB**² has a higher percentage of PDEV in its composition ($\text{P2VP}:\text{PDEV} = 1:1.24$). A second set of block copolymers was synthesized (**AB**³ and **AB**⁴) which shows lower molar masses (Table 2, Entry 3 and 4). Also in this case, the composition of the polymer was varied. To obtain micelles from **AB**¹–**AB**⁴, these block copolymers were dissolved in water (Table 2). Dynamic-light scattering (DLS) was used to determine the size of these micelles. The DLS-measurements underline the unimodal shape and the narrow size distribution of the AB-block copolymers (Figure 2, left, black graph). Core-shell-type spherical micelles are observed, in which the hydrophobic core (P2VP) is shielded from the aqueous milieu by the hydrophilic segments (PDEV).^[3c]

Micelles with a diameter of about 60–66 nm (**AB**¹ and **AB**²; Table 2, Entries 1 and 2) and those with a diameter of about 36–41 nm (**AB**³ and **AB**⁴; Table 2, entry 3 and 4) are obtained. The size of the micelles correlates exactly with the molar mass of the block copolymers. It seems, that only the length of the block copolymer has an influence on the size of the micelles. Different compositions do not affect the micellization. Larger micelles were not synthesized as the concentration of end-groups decreases drastically with increasing molecular weight of the block copolymer, hindering further end-group functionalization.

Entry	Block Copolymer	Feed ^[b] [A]/[B]	Conv. _A ^[c] [%]	$M_{n,\text{GPC,A}}$ ^[d] [10 ³ g/mol] ($M_{n,\text{calc,A}}$)	Conv. _B ^[e] [%]	$M_{n,\text{NMR,AB}}$ ^[f] [10 ³ g/mol]	\bar{D}_{AB} ^[g]	Composition ^[h] $A_{\text{eq.}}/B_{\text{eq.}}$	Ratio of A:B	$D_n^{[i]}$ [nm]	$D_{h,\text{Re}}^{[j]}$ [nm]	Cat. No. ^[i]
1	AB ¹	90/95	99	31.3 (9.6)	74	70.2	1.03	300/235	1 : 0.79	66 ± 3	62 ± 1	AB ¹ _{Re}
2	AB ²	60/110	99	23.5 (6.3)	70	68.3	1.05	220/275	1 : 1.24	60 ± 2	60 ± 1	AB ² _{Re}
3	AB ³	25/25	99	11.8 (2.1)	79	25.2	1.04	110/80	1 : 0.80	36 ± 2	33 ± 1	AB ³ _{Re}
4	AB ⁴	20/50	99	9.6 (2.1)	86	37.5	1.03	90/170	1 : 1.89	41 ± 1	38 ± 3	AB ⁴ _{Re}

[a] [Cat] = 42.8 μmol, 2.0 mL CH_2Cl_2 , r.t.; [b] [A] = [2VP]/[cat.]; [B] = [DEVP]/[cat.]; [c] Determined by ^1H -NMR spectroscopy; [d] $M_{n,\text{GPC,A}}$ = absolute molar mass of block A, determined by GPC with triple detection in dmf; $M_{n,\text{calc}} = M_{\text{VP}} \times (([2VP]/[\text{Cat}]) \times \text{conversion})$ in brackets; [e] Calculated from ^{31}P -NMR spectroscopy; [f] Determined by composition and $M_{n,\text{GPC,A}}$; [g] Determined by GPC (M_w/M_n of the block copolymers); [h] Calculated by ^1H -NMR spectroscopy; [i] Measured by DLS (with and without rhenium); the micelle size is given as the hydrodynamic diameter as the average number value of three independent runs with each 11 measurements; [j] Catalyst number for the respective rhenium-block copolymers

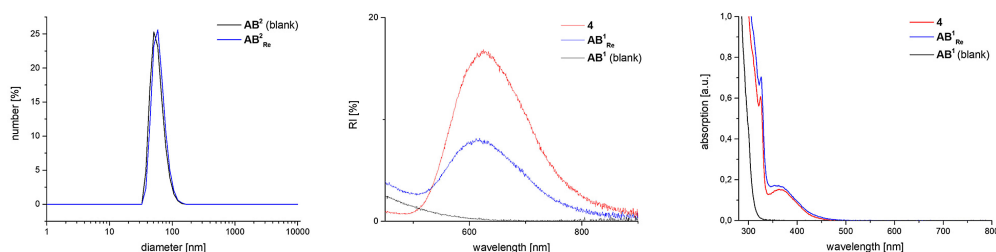


Figure 2. Left) DLS-spectra of micelles with 2.5 wt.% solutions in water from **AB**² (black) and **AB**²_{Re} (blue) (Table 2, Entry 2). Middle) PL-spectra of catalyst 4 (0.15 mM; red), **AB**¹ (3.20 mg in 2 mL dmf; black) and **AB**¹_{Re} (3.24 mg in 2 mL dmf; blue) Right) UV/Vis-spectra of catalyst 4 (red), **AB**¹ (black) and **AB**¹_{Re}. The same samples are used for PL and UV/Vis-measurements. All other block copolymers and rhenium-block copolymers show similar behavior and are not listed due to clarity reasons (SI, Figure S13, S14).

Synthesis and Properties of Rhenium-Block Copolymers

To test the ability of the bipyridine-functionalized block copolymers AB^1-AB^4 for metal complexation and subsequent micellization, $[Re(CO)_3Cl]$ was employed as possible example to get $[Re(CO)_3(6-Mebpy)Cl]$ moieties as end-groups in the polymers (Scheme 2). Due to the measurement of absolute molar masses of the first block *via* gel-permeation chromatography and a very narrow polydispersity of the block copolymers, the amount of end-groups are exactly definable. In addition, the Re-precursor $[Re(CO)_3Cl]$ does not show any absorption or photoluminescence and is photocatalytically inactive. Therefore, slight amounts of this precursor in the block copolymer as contamination does not interfere with further investigations on Re-block copolymers. After complexation, the resulting Re-block copolymers $AB^1_{Re}-AB^4_{Re}$ were compared to $[Re(CO)_3(4-Mebpy)Cl]$ (**4**) (Figure 2, middle and right), which is the analogue polymer-free complex. **4** is synthesized by reacting one equivalent of 6-methyl-2,2'-bipyridine with one equivalent of $[Re(CO)_3Cl]$ in toluene for 4 h at 100 °C.

AB^1_{Re} was tested in UV/VIS – and PL-spectroscopy in dmf and shows identical absorption and emission behavior as $[Re(CO)_3(6-Mebpy)Cl]$ (**4**). In PL-spectroscopy, both complexes show photoluminescence behavior exhibiting maxima at 620 nm. In the UV/VIS-measurements, **4** and AB^1_{Re} display similar absorption with maxima at 325 nm and 365 nm. Block copolymer AB^1 without rhenium does not show characteristic signals in PL- and UV/VIS-spectroscopy, indicating successful complexation of the rhenium at the bpy end-groups (Figure 2, middle and right). The block copolymers do not quench the optical characteristics of rhenium metals. The same results can be observed using AB^2-AB^4 in complexation reactions (SI, Figure S13, S14). Furthermore, complexation experiments with a 2VP-DEVP-block copolymer without bpy as end-group (SI, Table S1) do not lead to any maxima in PL- or UV/VIS-spectra after isolation of the polymer after the reaction, indicating that no complexation takes place without a bpy as end-group. DLS

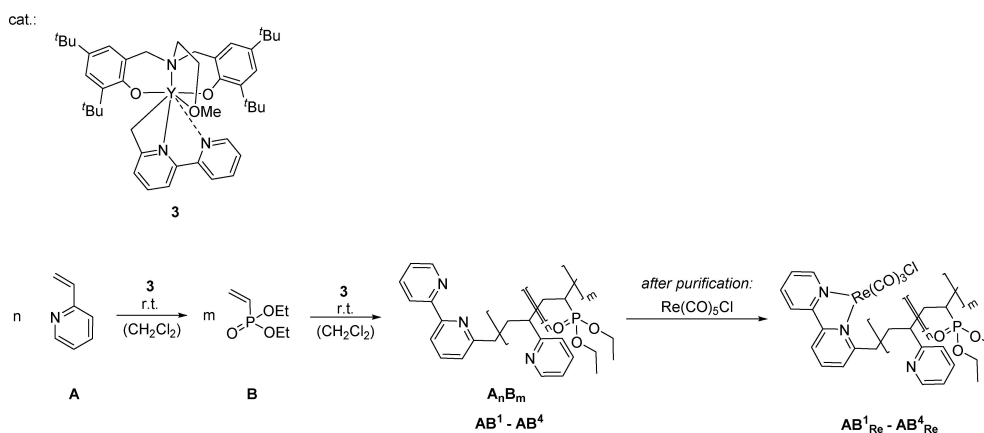
measurements of a 2.5 wt.% solution of $AB^1_{Re}-AB^4_{Re}$ in water prove that the Re-block copolymers successfully form micelles in water. The obtained diameters of the micelles do not differ from their unfunctionalized counterparts (Table 2, Figure 2 left).

UV/VIS spectra of a 0.8 wt.% solution of AB^2_{Re} in water shows identical absorption maxima as in dimethylformamide, but the intensity of the absorption seems to be lower than in dmf. In addition, micelles of AB^2 do not show any absorption (Figure S12). It seems, that rhenium-centers in the core of a micelle show similar absorption characteristics as in the flexible block copolymer in dimethylformamide. Water does not interfere with these rhenium-characteristics. These findings enable the use of rhenium in micelles.

In short, employing bipyridines as end-groups at 2VP-DEVP-block copolymers represent a new class of functional polymers, whose bpy motif can be used for metal complexation reactions. Both, the block copolymers with free bipyridines and those with metal-bpy-complexes show the same micellization and optical properties. As the micelles of 2VP-DEVP-block copolymers can enter cells, these systems could potentially be a shuttle for specific metal complexes.^[4]

Photocatalytic Reduction of CO₂

To ensure, that the connection of metal complexes to the block copolymer does not influence the properties of the complexes and to further broaden the field of potential applications for P2VP-PDEVP-block copolymers, the newly synthesized Re-block copolymers were, exemplary for possible reactions at metal centers, applied in photocatalytic reduction of CO₂, as the $[Re(CO)_3(bpy)Cl]$ motif is a well-known photocatalyst for the homogeneous photocatalytic reduction of CO₂. In the literature, a widely used system for homogeneous photocatalytic reduction of CO₂ is $[Re(CO)_3(bpy)Cl]$ (**5**) dissolved in dmf with triethanolamine (TEOA) as sacrificial electron donor. The bipyridines used for end-group functionalization are methy-



Scheme 2. Preparation of AB-block copolymers (A = P2VP; B = PDEVP) using catalyst **3**; complexation of a rhenium-precursor $[Re(CO)_3Cl]$.

lated in position 6, as this facilitates C–H-bond activation enabling synthesis of catalysts **2** and **3**. To evaluate how methyl groups in position 6 at the bpy influence the photocatalytic performance, $[\text{Re}(\text{CO})_3(6\text{-Me}_2\text{bpy})\text{Cl}]$ (**4**) and $[\text{Re}(\text{CO})_3(6\text{-Me}_2\text{bpy})\text{Cl}]$ (**6**) are synthesized and employed in the homogeneous photocatalytic reduction of CO_2 (Figure 3). The results are

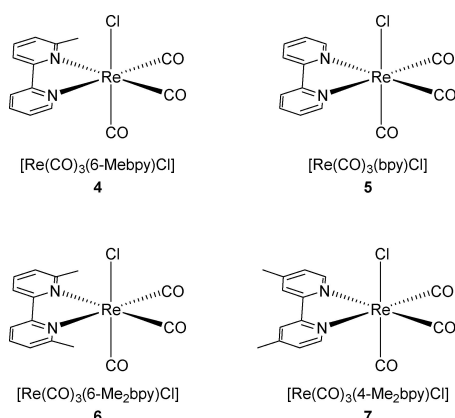


Figure 3. Structure of $[\text{Re}(\text{CO})_3(6\text{-Me}_2\text{bpy})\text{Cl}]$ (**4**), $[\text{Re}(\text{CO})_3(\text{bpy})\text{Cl}]$ (**5**), $[\text{Re}(\text{CO})_3(6\text{-Me}_2\text{bpy})\text{Cl}]$ (**6**) and $[\text{Re}(\text{CO})_3(4\text{-Me}_2\text{bpy})\text{Cl}]$ (**7**).

compared with two standard photocatalysts, $[\text{Re}(\text{CO})_3(\text{bpy})\text{Cl}]$ (**5**) and $[\text{Re}(\text{CO})_3(4\text{-Me}_2\text{bpy})\text{Cl}]$ (**7**) (Figure 3 and 5; SI, Table S2). The obtained results confirm the fact known in literature, that rhenium complexes containing a 4-Me₂bpy ligand (**7**) lead to lower TONs compared to rhenium complexes with a bpy ligand (**5**).^[22] Surprisingly, the synthesized catalysts **4** and **6** show the same catalytic stability as catalyst **5**, although they have one or two methyl groups at position 6 on the bipyridine. This proves that methyl groups in position 6 do not have the same negative influence on the electronic structure of the catalysts as methyl groups in position 4. The photocatalytic performance in homogeneous CO_2 reduction of the synthesized Re-block copolymers $\text{AB}^1_{\text{Re}}\text{--}\text{AB}^4_{\text{Re}}$ is shown in Figure 5 and compared with the analogue polymer-free complex **4**. According to DLS measurements, the block copolymers do not build micellar structures in dmf. The photocatalytic experiments using $\text{AB}^1_{\text{Re}}\text{--}\text{AB}^4_{\text{Re}}$ and **4** were performed under slightly different conditions (lower TEOA concentrations and smaller flasks, therefore different irradiation parameters) than the experiments in Figure 4, leading to lower TONs in this case. The results show a correlation between the length of the block copolymer and its catalytic activity, as block copolymers with longer chains (AB^1_{Re} and AB^2_{Re}) show higher TONs than block copolymers with shorter chains (AB^3_{Re} and AB^4_{Re}) (Figure 5, Table S3). Even more interestingly, employing the newly synthesized Re-block copolymers, higher TONs can be achieved compared to **4**. Potentially, the polymer chain arranges as a coil, protecting the active catalyst from negative effects like free radicals in the solution due to several types of functional groups on the polymer chain.

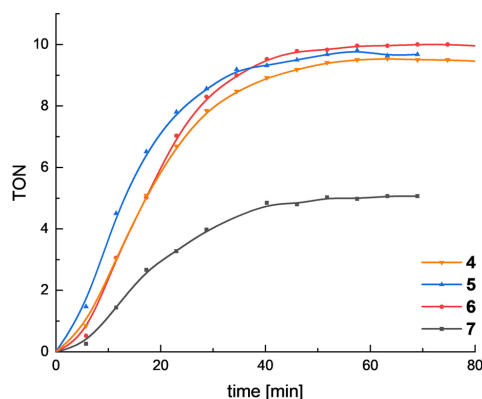


Figure 4. TON (CO) development during the photocatalytic reduction of CO_2 using catalyst **4–7**. Reaction conditions: Irradiation of CO_2 -saturated dmf/TEOA ([TEOA] = 1.7 M) solution containing 0.1 mM catalyst using an LED light source ($\lambda = 450$ nm).

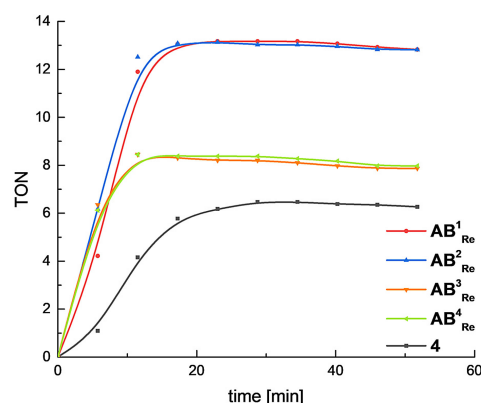


Figure 5. TON (CO) development during photocatalytic reduction of CO_2 using catalyst using $\text{AB}^1_{\text{Re}}\text{--}\text{AB}^4_{\text{Re}}$ and **4**. Reaction conditions: Irradiation of CO_2 -saturated dmf/TEOA ([TEOA] = 1.2 M) solution containing a 0.1 mM catalyst using an LED light source ($\lambda = 450$ nm).

In addition, deactivation processes might be prohibited. The longer the chain, the better is this shielding/prohibition effect. To elucidate the exact reasons, further investigations concerning the structure of the polymers in dmf and mechanistic studies have to be made. Applying equimolar amounts of **4** and an AB-block copolymer without bpy as end-group (SI, Table S1), no influence on the catalytic performance of **4** could be detected. These findings indicate that the rhenium core is protected from the block copolymer if its directly attached to the metal *via* the end-group. In all photocatalytic experiments carried out, CO was the only product detected by GC-analysis. ¹H-NMR spectroscopy of the reaction solution does not show any MeOH, formic acid or formaldehyde signals. In addition, no signals for ethanol or pyridine-species are visible,

therefore no decomposition of PDEVP or P2VP occurs during the reaction due to side reactions. Experiments either without catalyst, light, TEOA or CO₂ do not lead to any CO production.

In summary, attaching a photocatalytic active rhenium complex to a P2VP-PDEVP-block copolymer structure does not only retain the catalytic performance of the catalysts in CO₂ reduction with respect to the original system, but even increases it. This result broadens the possible applications of these block copolymers and proves that the performance of functional metal complexes does not suffer from the linkage to polymers.

A further idea is to use the micellization properties of the block copolymers to increase photocatalytic performance in CO₂ reduction in aqueous media. Changing the solvent of the photocatalytic experiments from dmf to water, no CO₂ conversion with catalyst **4** can be detected. Unfortunately, the micellization of the polymers does not help to circumvent this issue either, as **AB**¹_{Re} also shows no CO evolution at all. It seems, that processes related with the catalytic cycle of the reaction are suppressed or interfered even if the rhenium center is shielded from water. Applying different ratios of dmf to water, the block copolymer **AB**¹_{Re} always shows higher TONs than **4** (Table 3); using a ratio of 1:1 (dmf to water), the CO₂ conversion

Table 3. TON (CO) development during the photocatalytic reduction of CO₂ in different dmf/H₂O solvent mixtures using catalyst **4** and **AB**¹_{Re}.

dmf/H ₂ O	TON (CO) 4	TON (CO) AB ¹ _{Re}
0/1	0.0	0.0
1/1	0.6	2.1
0.75/0.25	6.2	12
1/0	6.5	13

[a] Reaction conditions: Irradiation of CO₂-saturated dmf/H₂O/TEOA solution ([TEOA] = 1.2 M) containing 0.1 mM catalyst using an LED light source (λ = 450 nm).

is nearly completely suppressed. At a ratio of 0.75 to 0.25, almost no difference to solutions with pure dmf can be observed. DLS measurements show that micelles are not built in water/dmf mixtures if the dmf ratio is high. Therefore, no difference is observed between the ratios 1:1 and 0.75 to 0.25 (dmf/water).

Conclusions

In summary, complexes **2** and **3** were synthesized via C–H bond activation of *ortho*-methylated bipyridines using a 2-aminoalkoxy-bis (phenolate) yttrium complex **1**. NMR-spectroscopy indicated coordination of the second pyridine moiety to the yttrium center via the nitrogen-atom instead coordination of a thf solvent-molecule. Complexes **2** and **3** were successfully tested in group-transfer polymerization of 2VP. Both catalysts showed a TOF* of about 1000 h⁻¹ and produced P2VP with narrow molecular mass distributions and controllable molecular weights. Tailor-made AB-block copolymers from 2VP and DEVP were synthesized via REM-GTP using 2-aminoalkoxy-bis (pheno-

late) yttrium bipyridine complex **3** with very narrow molecular weight distribution. Through variation of the monomer feed, block copolymers with different molecular weights and compositions are obtained. These block copolymers self-assemble to unimodal, perfectly-sized micelles, whose size can be exactly tuned via the polymer chain length. Complexation of [Re(CO)₅Cl] to the bpy end-groups of the block copolymers leads to a [Re(CO)₅(bpy)Cl] motif at the end of the polymers. These Re-block copolymer structures are still able to form micelles with the same size as the Re-free analogues, which demonstrates the possibility to use the bpy end-groups as ligand systems for metal complexation. In addition, a potential route to the application of the bpy-block copolymers as metal complex shuttles into cells is suggested within this contribution.

By testing the photocatalytic activity of the Re-block copolymers **AB**¹_{Re}–**AB**⁴_{Re} and comparing it to [Re(CO)₅(6-Mebpy)Cl] (**4**), it is shown that the attachment of a metal complex to the synthesized block copolymers does not negatively influence their catalytic properties. In fact, the Re-block copolymers even show higher TONs than the molecular catalyst **4**. Herein, 2VP-DEVP-block copolymers were used to enhance the catalytic activity in homogenous photocatalytic reduction of CO₂ for the first time.

Acknowledgements

F. Adams thanks the Bavarian State Ministry of Environment and Consumer Protection for its financial support within the BayBio-tech research network. M. Pschenitzka acknowledges the funding from DFG IRTG (2022). The authors declare no competing financial interests.

Conflict of Interest

The authors declare no conflict of interest.

Keywords: Block copolymers • Photocatalytic reduction of CO₂ • Rhenium-catalysts • Micellar systems • C–H bond activation

- [1] a) E. Y. Chen, *Chem. Rev.* **2009**, *109*, 5157–5214; b) B. S. Soller, S. Salzinger, B. Rieger, *Chem. Rev.* **2016**, *116*, 1993–2022.
- [2] a) B. S. Soller, N. Zhang, B. Rieger, *Macromol. Chem. Phys.* **2014**, *215*, 1946–1962; b) F. Adams, P. Pahl, B. Rieger, *Chem. Eur. J.* **2018**, *24*, 509–518.
- [3] a) P. T. Altenbuchner, B. S. Soller, S. Kissling, T. Bachmann, A. Kronast, S. I. Vagin, B. Rieger, *Macromolecules* **2014**, *47*, 7742–7749; b) F. Adams, M. R. Machat, P. T. Altenbuchner, J. Ehrmaier, A. Pothig, T. N. V. Karsili, B. Rieger, *Inorg. Chem.* **2017**, *56*, 9754–9764; c) F. Adams, P. T. Altenbuchner, P. D. L. Werz, B. Rieger, *RSC Adv.* **2016**, *6*, 78750–78754.
- [4] P. T. Altenbuchner, P. D. Werz, P. Schoppner, F. Adams, A. Kronast, C. Schwarzenbock, A. Pothig, C. Jandl, M. Haslbeck, B. Rieger, *Chem. Eur. J.* **2016**, *22*, 14576–14584.
- [5] a) B. S. Soller, S. Salzinger, C. Jandl, A. Pöthig, B. Rieger, *Organometallics* **2015**, *34*, 2703–2706; b) P. Pahl, C. Schwarzenbock, F. A. D. Herz, B. S. Soller, C. Jandl, B. Rieger, *Macromolecules* **2017**, *50*, 6569–6576; c) H. Kaneko, H. Nagae, H. Tsurugi, K. Mashima, *J. Am. Chem. Soc.* **2011**, *133*, 19626–19629.

- [6] C. Kaes, A. Katz, M. W. Hosseini, *Chem. Rev.* **2000**, *100*, 3553–3590.
- [7] A. J. Canty, B. W. Skelton, P. R. Traill, A. H. White, *Aust. J. Chem.* **1992**, *45*, 417.
- [8] F. E. Kühn, M. Groarke, É. Bencze, E. Herdtweck, A. Prazeres, A. M. Santos, M. J. Calhorda, C. C. Romão, I. S. Gonçalves, A. D. Lopes, M. Pillinger, *Chem. Eur. J.* **2002**, *8*, 2370.
- [9] J. Komoschinski, E. Steckhan, *Tetrahedron Lett.* **1988**, *29*, 3299–3300.
- [10] M. T. Carter, M. Rodriguez, A. J. Bard, *J. Am. Chem. Soc.* **1989**, *111*, 8901–8911.
- [11] S. Derien, E. Dunach, J. Perichon, *J. Am. Chem. Soc.* **1991**, *113*, 8447–8454.
- [12] a) S. M. Barnett, K. I. Goldberg, J. M. Mayer, *Nat. Chem.* **2012**, *4*, 498; b) Z. Dai, Q. Sun, X. Liu, L. Guo, J. Li, S. Pan, C. Bian, L. Wang, X. Hu, X. Meng, L. Zhao, F. Deng, F. S. Xiao, *ChemSusChem* **2017**, *10*, 1186–1192.
- [13] R. G. Inskeep, *J. Inorg. Nucl. Chem.* **1962**, *24*, 763–776.
- [14] a) A. J. Morris, G. J. Meyer, E. Fujita, *Acc. Chem. Res.* **2009**, *42*, 1983–1994; b) B. Kumar, M. Llorente, J. Froehlich, T. Dang, A. Sathrum, C. P. Kubiak, *Annu. Rev. Phys. Chem.* **2012**, *63*, 541–569; c) C. D. Windle, R. N. Perutz, *Coord. Chem. Rev.* **2012**, *256*, 2562–2570; d) H. Takeda, O. Ishitani, *Coord. Chem. Rev.* **2010**, *254*, 346–354; e) J. Hawecker, J.-M. Lehn, R. Ziessel, *Helv. Chim. Acta* **1986**, *69*, 1990–2012; f) J. Hawecker, J.-M. Lehn, R. Ziessel, *Chem. Commun.* **1983**, 536–538; g) R. Reithmeier, C. Bruckmeier, B. Rieger, *Catalysts* **2012**, *2*, 544–571; h) Y. Yamazaki, H. Takeda, O. Ishitani, *J. Photochem. Photobiol. C* **2015**, *25*, 106–137.
- [15] a) B. J. McNicholas, J. D. Blakemore, A. B. Chang, C. M. Bates, W. W. Kramer, R. H. Grubbs, H. B. Gray, *J. Am. Chem. Soc.* **2016**, *138*, 11160–11163; b) S. Sahu, P. L. Cheung, C. W. Machan, S. A. Chabolla, C. P. Kubiak, N. C. Gianneschi, *Chem. Eur. J.* **2017**, *23*, 8619–8622.
- [16] M. Furue, N. Kuroda, S.-i. Nozakura, *Chem. Lett.* **1986**, *15*, 1209–1212.
- [17] a) P. T. Altenbuchner, F. Adams, A. Kronast, E. Herdtweck, A. Pothig, B. Rieger, *Polym. Chem.* **2015**, *6*, 6796–6801; b) M. Bouyahyi, N. Ajellal, E. Kirillov, C. M. Thomas, J. F. Carpentier, *Chem. Eur. J.* **2011**, *17*, 1872–1883.
- [18] E. Y. Tshuva, S. Groysman, I. Goldberg, M. Kol, Z. Goldschmidt, *Organometallics* **2002**, *21*, 662–670.
- [19] J. F. Carpentier, *Organometallics* **2015**, *34*, 4175–4189.
- [20] a) C. T. Carver, P. L. Diaconescu, *J. Am. Chem. Soc.* **2008**, *130*, 7558–7559; b) G. Bombieri, F. Benetollo, W. T. Hawkins, A. Polo, L. M. Vallarino, *Polyhedron* **1989**, *8*, 1923–1931; c) R. Duchateau, E. A. C. Brussee, A. Meetsma, J. H. Teuben, *Organometallics* **1997**, *16*, 5506–5516.
- [21] N. Zhang, S. Salzinger, B. S. Soller, B. Rieger, *J. Am. Chem. Soc.* **2013**, *135*, 8810–8813.
- [22] M. Pschenitzka, S. Meister, A. von Weber, A. Kartouzian, U. Heiz, B. Rieger, *ChemCatChem* **2016**, *8*, 2688–2695.

Manuscript received: June 21, 2018
Accepted Article published: July 19, 2018
Version of record online: August 24, 2018

6.5 Reprint permission of copyrighted content

JOHN WILEY AND SONS LICENSE TERMS AND CONDITIONS

Nov 10, 2018

This Agreement between Friederike Adams ("You") and John Wiley and Sons ("John Wiley and Sons") consists of your license details and the terms and conditions provided by John Wiley and Sons and Copyright Clearance Center.

License Number	4465460095321
License date	Nov 10, 2018
Licensed Content Publisher	John Wiley and Sons
Licensed Content Publication	ChemCatChem
Licensed Content Title	Yttrium-Catalyzed Synthesis of Bipyridine-Functionalized AB-Block Copolymers: Micellar Support for Photocatalytic Active Rhenium-Complexes
Licensed Content Author	F. Adams, M. Pschenitza, B. Rieger
Licensed Content Date	Aug 24, 2018
Licensed Content Volume	10
Licensed Content Issue	19
Licensed Content Pages	8
Type of use	Dissertation/Thesis
Requestor type	Author of this Wiley article
Format	Print and electronic
Portion	Full article
Will you be translating?	No
Title of your thesis / dissertation	From Michael-type systems to biobased lactones: Designing novel polymer microstructures with modified bis(phenolate)lanthanides
Expected completion date	Nov 2018
Expected size (number of pages)	250
Requestor Location	Friederike Adams Zieblandstr. 47

7 Multiresponsive nanocarriers for drug delivery to cancer cells

7.1 Bibliographic data

Title: “Next Generation Multiresponsive Nanocarriers for Targeted Drug Delivery to Cancer Cells”

Status: Full paper, first published: August 19, 2016

Journal: *Chemistry – A European Journal*, 2016, 22, 14576-14584

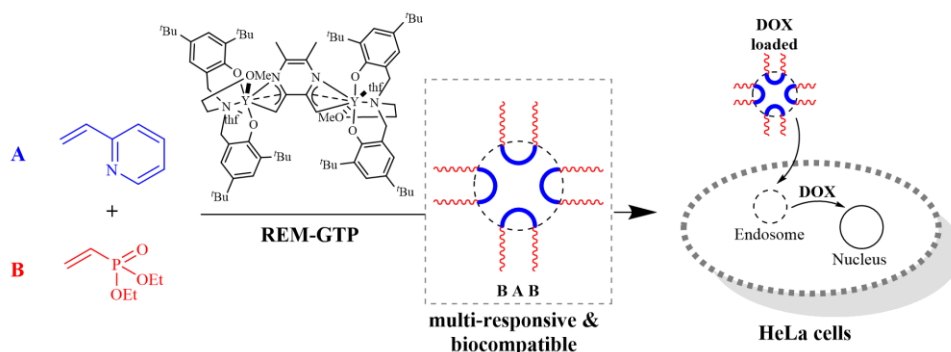
Publisher: WILEY-VCH Verlag GmbH & Co. KGaA

DOI: 10.1002/chem.201601822

Authors: Peter T. Altenbuchner*, Patrick D. L. Werz*, Patricia Schöppner*, Friederike Adams, Alexander Kronast, Christina Schwarzenböck, Alexander Pöthig, Christian Jandl, Martin Haslbeck, and Bernhard Rieger⁴

*These authors contributed equally to this work

7.2 Abstract graphic (TOC)



⁴ F. Adams executed all experiments regarding the yttrium-complex, the polymerization of 2-vinylpyridine and the activity measurements and helped with writing the manuscript. P. T. Altenbuchner planned all experiments, wrote the manuscript and performed block copolymerizations and polymer analytics. P. D. L. Werz helped with the polymer characterization, release studies and the preparation of the manuscript. P. Schöppner performed all *in vitro* and drug delivery studies and wrote this part of the manuscript. C. Jandl conducted the SC-XRD-measurement and processed the crystallographic data. C. Schwarzenböck, A. Kronast and M. Haslbeck helped with proofreading and discussions. All work was supervised by B. Rieger.

7.3 Content

Polymers with reversible and controllable thermoresponsive properties are in high demand. However, the intensely studied PNIPAAm or PEG systems all have significant disadvantages, e.g. long response time, lack of functionality, or loss of their functions in biological fluids. Thus, there is dire need for alternatives to broaden the choice of biocompatible, multi-stimuliresponsive polymers. The use of phosphorus-containing polymers in the past was mainly limited by the absence of efficient synthetic strategies. Advances in rare-earth metal-mediated group-transfer polymerization (REM-GTP) catalysis open up possibilities to combine the advantages of living ionic and coordinative polymerizations, making this method a versatile tool for the synthesis of tailor-made functional materials. Recently, our group and other researchers were able to extend REM-GTP from common (meth)acrylates and vinylphosphonates to several other monomer classes of interest, e.g. vinylpyridines. In this work, we report on multiresponsive, amphiphilic and biocompatible BAB block copolymers based on diethyl vinylphosphonate and 2-vinylpyridine for the application as drug delivery systems. The C-H bond activation of 2,3,5,6-tetramethylpyrazine with 2-methoxyethylamino-bis(phenolate)yttrium complexes enabled the synthesis of so far unattained well-defined b-PDEVp-a-P2VP-b-PDEVp (BAB) structures ($D \leq 1.20$). The polymerization follows the well-established rare-earth metal-mediated group-transfer polymerization mechanism. These BAB copolymers were employed as micellar, multiresponsive, nanocarriers with lower critical solution temperature and pH-dependent solubility. Their resilience to harsh biological conditions and drug loading and release capabilities of BAB block copolymers were tested. Drug delivery and release experiments with ovarian cancer cells (HeLa) demonstrated the biocompatibility of BAB micelles as well as their fast and efficient cellular uptake. *In vitro* studies demonstrated that doxorubicin (DOX) loaded BAB micelles can be successfully internalized into HeLa cells. The micelles are taken up *via* endocytosis, followed by the pH-driven release of the drug. Non-encapsulated DOX was used as control in comparison to the DOX-loaded micelles. Our investigations on cell viability revealed that BAB DOX-loaded micelles effectively induce cytotoxic effects on HeLa cells in a dose-dependent manner. In summary, we were able to introduce the next generation of multiresponsive, amphiphilic and biocompatible block copolymers for the application as versatile drug delivery system.

7.4 Manuscript



DOI: 10.1002/chem.201601822

CHEMISTRY
 A European Journal
 Full Paper

Polymers
Next Generation Multiresponsive Nanocarriers for Targeted Drug Delivery to Cancer Cells

 Peter T. Altenbuchner^{+,*^[a]}, Patrick D. L. Werz^{+,^[a]}, Patricia Schöppner^{+,^[b]}, Friederike Adams,^[a]
 Alexander Kronast,^[a] Christina Schwarzenböck,^[a] Alexander Pöthig,^[c] Christian Jandl,^[c]
 Martin Haslbeck,^[b] and Bernhard Rieger^{*^[a]}

Abstract: C–H bond activation of 2-methoxyethylamino-bis(phenolate)-yttrium catalysts allowed the synthesis of BAB block copolymers comprised of 2-vinylpyridine (2VP; monomer A) and diethylvinylphosphonate (DEVP; monomer B) as the A and B blocks, respectively, by rare-earth-metal-mediated group-transfer polymerization (REM-GTP). The inherent multi-stimuli-responsive character and drug-loading and -release capabilities were observed to be dependent on the chain length and monomer ratios. Cytotoxicity assays revealed the biocompatibility and nontoxic nature of the ob-

tained micelles toward ovarian cancer (HeLa) cells. The BAB block copolymers effectively encapsulated, transported, and released doxorubicin (DOX) within HeLa cells. REM-GTP enables access to previously unattainable vinylphosphonate copolymer structures, and thereby unlocks their full potential as nanocarriers for stimuli-responsive drug delivery in HeLa cells. The self-evident consequence is the application of these new micelles as potent drug-delivery vehicles with reduced side effects in future cancer therapies.

Introduction

Cancer remains a growing problem to society, although our understanding of its origin and development has vastly progressed in recent decades. The treatment of cancer is generally attempted by surgical removal of the affected tissue in combination with radiation and chemotherapy. Treatment with chemotherapeutic agents, in particular, is often accompanied by undesirable severe side effects, such as the development of drug resistance and severe cardiac toxicity, as observed for doxorubicin (DOX) based anticancer treatments.^[1] In general, these systemically administered therapeutic agents suffer from

numerous issues, for example, hydrophobicity, inefficient distribution, systemic toxicity, and low targeting capability. In turn, this decreases the efficiency of these treatments and puts extra strain on the patient by also affecting healthy tissue.^[2] Fundamental problems associated with drug administration, including poor selectivity between malignant and innocuous cells, difficulties in adjusting drug dosages, and various biological hurdles, can be addressed by nanomedicine. Thus, organic and inorganic nanoparticles with adjustable sizes have emerged as potent carrier systems for the cancer drugs.^[3] Polymeric nanocarriers, in particular, can be tailored with respect to size, chemical composition, shape, and surface properties. These carriers increase the solubility and protect the therapeutic agents against harsh biological conditions, and allow for controlled and targeted release of elevated dosages, which reduces off-target toxicity.^[3b] Furthermore, as drug carriers, polymeric micelles should be stable at low concentrations, which enables long in vivo circulation times and inhibits premature drug release.^[2]

The release mechanism of such polymer-based nanocarriers can be categorized into sustained and stimuli-responsive release, induced by changes in temperature or pH or by photochemical, enzymatic, or redox reactions, which leads to a sharp change in the properties of these carriers.^[3b,4] In particular, thermoresponsive and pH-sensitive triggers have received extensive attention. Exploiting pH changes within the various tissues and cellular compartments along the endocytic pathway and, in particular, in tumor cells has been a popular strategy for nanocarrier design.^[4a,5] Commonly used thermoresponsive polymers include poly(methylvinylether) (PMVE), poly(*N*-vinylcaprolactam) (PVCL), and poly(*N*-alkylacrylamide)s such as

[a] Dr. P. T. Altenbuchner,⁺ P. D. L. Werz,⁺ F. Adams, A. Kronast, C. Schwarzenböck, Prof. B. Rieger
 WACKER-Lehrstuhl für Makromolekulare Chemie
 Technische Universität München, Lichtenbergstraße 4
 85748 Garching bei München, (Germany)
 E-mail: rieger@tum.de
 pateraltenbuchner@gmail.com

[b] P. Schöppner,⁺ Dr. M. Haslbeck
 Center for Integrated Protein Science Munich (CIPSM) and
 Lehrstuhl für Biotechnologie
 Technische Universität München
 Lichtenbergstraße 4
 85748 Garching bei München (Germany)

[c] Dr. A. Pöthig, C. Jandl
 Department Chemie & Catalysis Research Center
 Technische Universität München
 Ernst-Otto-Fischer-Straße 1
 85748 Garching bei München (Germany)

[*] These authors contributed equally to this work.

Supporting information for this article is available on the WWW under <http://dx.doi.org/10.1002/chem.201601822>.

poly(*N*-isopropylacrylamide) (PNIPAM) and polyethylene glycol (PEG).^[6] Structurally versatile thermoresponsive materials based on ethylene oxide copolymers were prepared by Frey's group.^[7] Interesting phosphorous-containing macromolecules were generated by the group of Wurm by ring-opening polymerization (ROP), olefin metathesis, or ring-opening metathesis polymerization (ROMP) of cyclic phosphates and phosphonates.^[8] Biodegradable poly(phosphoester) (PPE) based polymeric micelles and shell cross-linked sphere-like nanoparticles have been prepared from amphiphilic block-graft terpolymers, and drug-release studies have demonstrated the applicability of PPE in nanotherapeutics.^[9]

However, suitable materials with thermoresponsive properties within the physiological range combined with hydrophilicity, biocompatibility, and resilience to harsh environmental conditions are scarce.^[10] Thus, a dire need exists to utilize alternative polymerization techniques and monomer feedstocks to obtain these useful materials while retaining biocompatibility and advantageous functionalities.

Currently, classic anionic atom-transfer radical polymerization (ATRP), radical addition-fragmentation chain transfer (RAFT), and ROP techniques are predominantly used to generate functional polymers for loading and release applications.^[11] REM-GTP of vinyl phosphonates and other heteroatom-containing monomers has received little attention in the field of drug delivery.^[12] However, REM-GTP offers access to strictly linear polymer growth and very narrow molecular-weight distributions ($D < 1.1$), and is applicable to a vast feedstock of monomers. In particular, dialkylvinyl phosphonates (DAVPs), which exhibit tunable thermoresponsive behavior, offer an alternative to the established polymers.^[13] Our group has made great progress in developing highly active catalysts for REM-GTP and elucidating their mechanism of action.^[14] The advent of 2-methoxyethylamino-bis(phenolate)-yttrium catalysts enabled the targeted synthesis of tactic, low molecular weight homo- and block-copolymers.^[15] Herein, we present the design and evaluation of amphiphilic block-copolymer structures and their application as next-generation multiresponsive nanodrug carriers for cancer treatment.

Results and Discussion

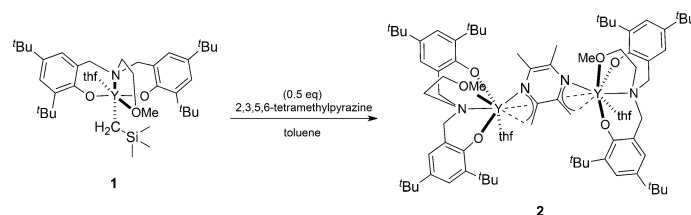
We previously reported the use of 2-methoxyethylamino-bis(phenolate)-yttrium catalysts for the polymerization of 2-vinylpyridine (2VP) and DAVPs.^[15] High initiator efficiencies allowed

the efficient synthesis of AB block copolymers with a broad feedstock of monomers. In particular, the combination of 2VP (monomer A) and diethylvinylphosphonate (DEVP; monomer B) resulted in a material with properties applicable for the generation of a new class of drug-delivery carriers. With a view toward the strict safety and functionality requirements in the field of drug delivery, we expected vinylphosphonate-based copolymers to exhibit properties compatible with biochemical environments. The block-copolymer architecture HLH (H = hydrophilic, L = lipophilic) has been demonstrated to increase the stability (lower critical micelle concentration (CMC)) of formed micelles relative to architecture LHL. This increased stability is attributed to the flower-like HLH polymer micelles being entropically disfavored compared to the loose-shell structure of LHL.^[16–17] Studies with polylactide (PLA) and PEG block copolymers (LHL and HLH architecture) have revealed that the HLH architecture brings additional size advantages because of its U-shaped self-assembly into micelles.^[18] Reports related to endgroup functionalization by C–H bond activation sparked our interest in evaluating our 2-methoxyethylamino-bis(phenolate)-yttrium alkyl complexes for their ability to activate the sigma bonds of heteroaromatic compounds, thereby introducing a bidirectional initiator and consequently accessing BAB-type copolymers.^[19] This intramolecular C–H bond activation of trivalent lanthanides and d^0 -transition metals is a common approach to C–H bond cleavage.

NMR spectroscopic experiments with complex **1** and 2,3,5,6-tetramethylpyrazine (TMpy) revealed an initial inability to activate the C–H bond at RT. However, at 60 °C selective and quantitative activation of TMpy was possible within 22 h (Scheme 1). ¹H NMR spectroscopic analysis indicated a successful double activation of TMpy (Figure 1), and attempts to crystallize compound **2** by slow diffusion of pentane into a saturated solution of **2** in THF at –30 °C gave crystals suitable for X-ray analysis (Figure 2).

Structure of the yttrium complex **2**

The bisphenolate ligand of complex **2** coordinates in a distorted octahedral fashion, which is similar to its coordination mode in the starting compound **1**. The most significant structural difference in **2** originates from the C–H-bond activation of TMpy and concomitant coordination to the metal center. The coordination mode of the initiator TMpy to the metal center is an unusual η^3 -(C,C,N)-aza-allylic coordination. The



Scheme 1. C–H activation of TMpy by alkyl yttrium complex **1** to form **2**.

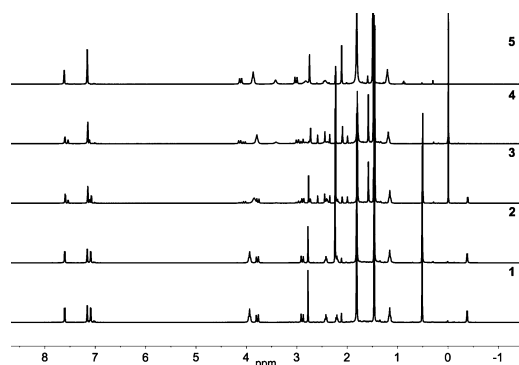


Figure 1. 1) The ^1H NMR spectrum of the isolated catalyst **2** in C_6D_6 . ^1H NMR spectra of the C–H bond activation of TMpy with catalyst **1** at 60°C in C_6D_6 at 2) 22 h, 3) 3 h, and 4) 0 h. 5) The ^1H NMR spectrum of the isolated catalyst **1** in C_6D_6 .

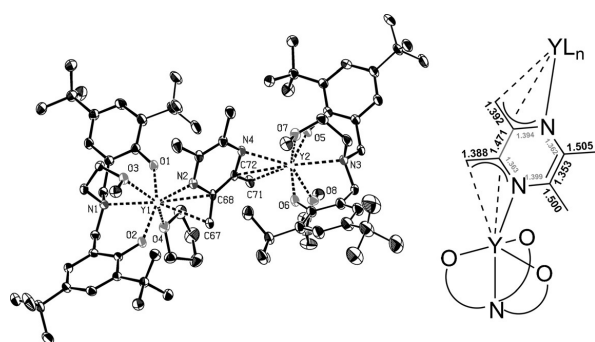


Figure 2. ORTEP representation and molecular structure of complex **2** with ellipsoids at the 50% probability level. Hydrogen atoms have been omitted for clarity. Selected bond lengths [Å] and angles [$^\circ$]: Y1–O1 2.129(2), Y1–O2 2.141(2), Y1–O3 2.446(2), Y1–O4 2.428(2), Y1–N1 2.605(2), Y1–N2 2.405(1), Y1–C67 2.637(2), Y1–C68 2.689(2), Y2–O5 2.148(2), Y2–O6 2.142(2), Y2–O7 2.461(2), Y2–O8 2.429(2), Y2–N3 2.596(2), Y2–N4 2.388(2), Y2–C71 2.628(2), Y2–C72 2.708(2), C67–C68 1.388(3), C68–C72 1.471(4), C68–N2 1.363(4), N2–C69 1.399(3), C69–C73 1.353(4), C71–C72 1.392(4), C67–C68–N2 118.4(2), C71–C72–N4 117.7(2).

Y–N bond in **2** (Y1–N2 = 2.405(1) Å, Y2–N4 = 2.388(2) Å) is shorter than the Y–C bonds (Y1–C68 = 2.689(2) Å, Y1–C67 = 2.637(2) Å, Y2–C71 = 2.628(2) Å, Y2–C72 = 2.708(2) Å), and therefore the initiator is mainly coordinated via the nitrogen atom. The C67–C68 and C71–C72 bond lengths (activated methyl groups of TMpy) are shorter than 1.4 Å, which lies between a carbon–carbon single- and double-bond length, which underlines the allylic character of the binding mode to Y.

The observed η^3 -(C,C,N)-aza-allylic coordination with **2** is intermediate between η^2 -allylic-amine and η^1 -amido-olefinic coordination, as described by Teuben's group.^[20] They reported that C–H bond activation with similar *ortho*-alkylpyridines resulted in longer C–C bond lengths (1.420–1.472 Å), which indi-

cates greater double-bond character in catalyst **2**.^[19b,21] Interestingly, adjacent rather than opposing methyl groups in TMpy were activated. The C–H bond activation has an additional effect on the aromaticity: loss of double-bond character is observed for the C68–C72 bond (1.471(4) Å) in favor of the η^3 -(C,C,N)-aza-allylic coordination to the yttrium center. Catalyst **2** enabled access to previously unattained vinylphosphonate-based block copolymers with the general BAB structure.

REM-GTP of Michael-type monomers

Polymer micelles can act as sophisticated vehicles for substance transport under harsh conditions. A direct correlation between polymer structure and subsequent micelle architecture has been reported, which profoundly influences drug-release and -loading characteristics.^[22] Prior to block-copolymerization experiments, catalyst **2** was used in the homopolymerization of DEVP and 2VP to evaluate its initiator efficiency and general activity. Concomitantly, the initiation mechanism was elucidated by endgroup analysis of oligomeric poly(2-vinylpyridine) (P2VP; see the Supporting Information). The initiating groups were clearly visible in the ESI mass spectra, therefore transfer of the coordinated ligand by insertion of a monomer into a Y–C bond during the initiation is evident. The excellent homopolymerization capabilities of catalyst **2** enabled us to investigate pathways to block-copolymer structures (Figure 3).

The desired block copolymers were isolated by precipitation from *n*-hexane after quantitative conversion of the monomers.

The exact length of the P2VP (monomer A) block was determined by gel-permeation chromatography with multi-angle light-scattering detection (GPC-MALS), and the chain length of poly(diethylvinylphosphonate) (PDEVP; monomer B) was calculated by correlation of the integrated area of the $-\text{OCH}_2$ peak of PDEVP to that of the $-\text{CH}_{\text{arom}}$ peak of P2VP in their respective ^1H NMR spectra (Figure 4, see also the Supporting Information). All synthesized homopolymers and copolymers were atactic and showed monomodal distributions with very narrow molecular-weight distributions ($\mathcal{D} \leq 1.20$) (Table 1, entries 1–

3). Amphiphilic polymers BAB₁–BAB₃ exhibit a CMC above which they self-assemble into micelle structures. The CMCs of our BAB polymers (0.1 and 0.2 mg mL^{−1}) were determined by using Nile red, a water-insoluble fluorescent dye (Figures 5 b). The TEM images highlight the unimodal size distribution (Figures 5 c). Light-scattering measurements of solutions of polymers BAB₁–BAB₃ in water (2.5 wt %) show hydrodynamic radii in the range 54–88 nm for the synthesized P2VP and PDEVP copolymers (Figures 5 d). This micelle size is ideal for the application of our polymers in drug delivery according to literature reports of high extravasation efficacy based on the enhanced permeability and retention (EPR) effect when micelles with sizes in the range 30–100 nm are employed.^[23] Hence, we investigated BAB₁–BAB₃ with different hydrophilic/hydrophobic

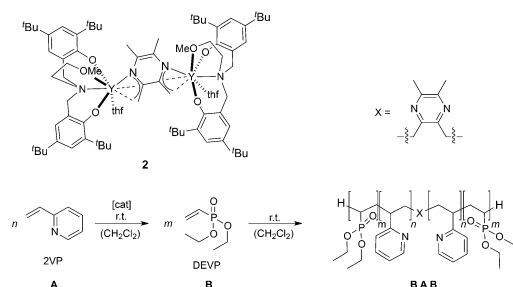


Figure 3. Sequential REM-GTP of 2VP and DEVP with catalyst **2** at RT (see Table 1).

block ratios in drug loading and release tests. We abstained from further increases in PDEVP block lengths because we did not want to impose size limits with regard to the ability of the

BAB micelles to penetrate cell membranes. Block copolymers tend to show prolonged or irreversible phase transitions.^[24] In our previous work, we showed that the lower critical solution temperatures (LCSTs) of polyvinylphosphonate homopolymers in aqueous media are relatively independent of concentration and that the polyvinylphosphonate homopolymers undergo a coil-globule phase transition similar to that of PNIPAM for example.^[13] Therefore, we performed temperature-dependent LCST dynamic light scattering (DLS) measurements, which nicely demonstrated the fast and reversible formation of micelles upon precipitation and re-dissolution cycles for BAB₁-BAB₃ (Table 1; see also the Supporting Information). Additional temperature-dependent UV/Vis measurements in deionized water, phosphate buffer solution (PBS), and Dulbecco's Modified Eagle's medium (DMEM) were performed to evaluate the influence of salts and other biologically relevant components on the LCST behavior. A typical salting-out effect due to partial dehydration of the macromolecules was observed; this effect

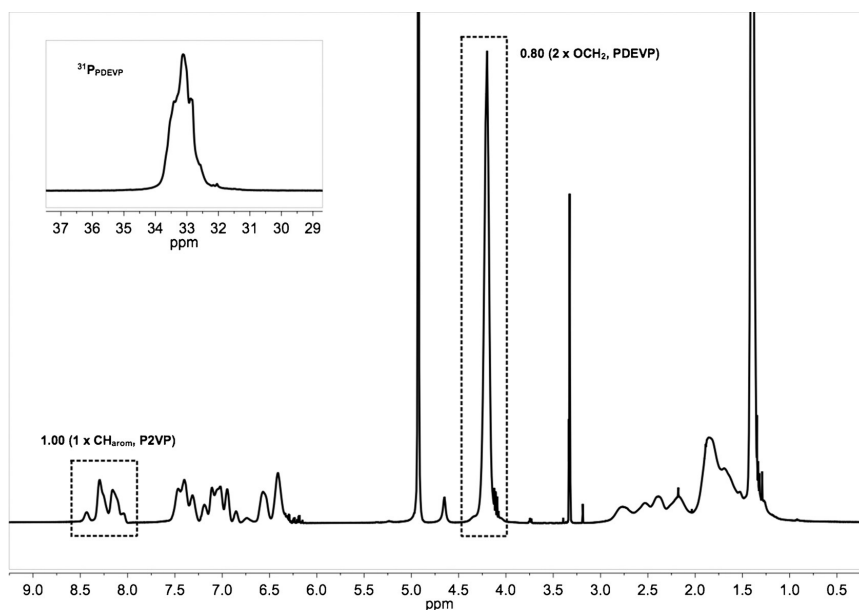
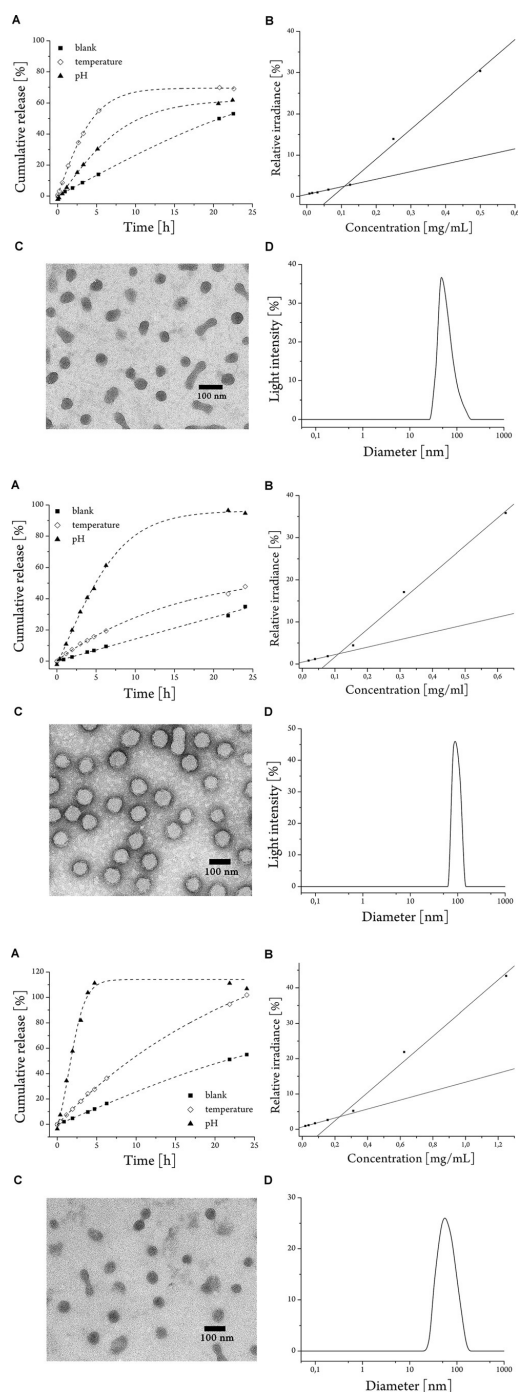


Figure 4. ¹H- and ³¹P NMR spectra of BAB₁ (Table 1, entry 1) in MeOD at 298 K.

Table 1. Block copolymers produced with catalyst 2 : BAB-type with different compositions.								
Entry	Polymer	Feed A _{eq} /B _{eq} ^[a]	Composition B/A [2VP/DEVP] ^[b]	M _n (A) [× 10 ⁴ g mol ⁻¹] ^[c]	M(BAB) _{n,NMR} [× 10 ⁴ g mol ⁻¹] ^[d]	Đ ^[c]	LCST (H ₂ O) [°C] ^[d]	D _h [nm] ^[e]
1	BAB ₁	2VP ₂₀₀ /DEVP ₂₀₀	1/0.8	4.1	8.9	1.12	43.5	72 ± 9
2	BAB ₂	2VP ₂₀₀ /DEVP ₂₅₀	1/1.1	5.0	12.8	1.11	43.0	54 ± 7
3	BAB ₃	2VP ₂₀₀ /DEVP ₄₀₀	1/2.1	4.4	18.1	1.20	43.5	88 ± 4

[a] By weighing the monomer, [M]/[cat] = equiv, [cat.] = 41.7 μmol in 2.5 mL CH₂Cl₂. [b] Calculated from the ¹H NMR spectrum. [c] Determined by GPC-MALS. [d] Determined by ¹H NMR spectroscopy. [e] Determined by temperature-dependent UV/Vis measurements at a 10% transmittance decrease. [f] The micelle size is an average hydrodynamic diameter.



reduced the LCST from 43 °C to 39 °C (cloud-point shift = 4 °C). More importantly, sharp phase transitions between the heating and cooling cycles in PBS or DMEM were observed for all three BAB copolymers with no increase in hysteresis compared to the measurements in water.

Fluorescein was used to assess the loading and release capabilities of copolymers BAB₁–BAB₃. The polymer and fluorescein were initially dissolved in DMSO then water was added dropwise. The resulting mixture was sonicated for 30 s to avoid agglomeration and subsequently dialyzed against water to obtain loaded micelles. Structurally the developed polymeric materials have bifunctional release properties, therefore we tested pH (pH 4.5) and temperature-triggered (44 °C) release separately. The release plots for BAB₁–BAB₃ highlight the differences in the release capabilities of the polymeric carriers (Figures 5 a). BAB₁ shows the lowest release efficiency of only 70% through temperature- and pH-triggered release. Loaded BAB₂ micelles gave quantitative cumulative release after 25 h at 44 °C. BAB₃ shows the best release properties with quantitative cumulative release triggered by temperature and pH.

The untriggered release is in accordance with the measured CMCs for BAB₁–BAB₃, and shows similar release properties for all three tested copolymers within 25 h (40–50%), which is an indicator of the micelle stability. The pH trigger for our BAB polymers can be used for a burst release, whereas the temperature trigger achieves a more-sustained release of the loaded substance for BAB₂ and BAB₃.

Given the similarity of vinylphosphonates to biologically relevant substances, we expected to achieve prolonged retention times because the vinylphosphonate corona should avoid recognition and sequestration by the reticuloendothelial system.

In general, macromolecules are taken up by the cell via receptor-mediated endocytosis, adsorptive endocytosis, or fluid-phase endocytosis.^[25] Because of the pH difference between the extracellular fluid region (pH 7.35–7.45) and the endosomes (pH 5.5–6.0), with further acidification in the lysosomal compartments (pH 4.5–5.0), pH-sensitive nanocarriers can release their cargo in response to decreasing pH following transport into the cell.^[26] However, bioactive molecules trapped in the endosome will be degraded by active enzymes in the lysosomal compartment.^[26a] Therefore, the bioactive drugs should have acid-resistant properties and the ability to penetrate endosomal membrane barriers to escape from the endosome.^[26a,27] These properties are not problematic for small chemotherapeutic drugs such as DOX.^[28] Additionally, the microenvironment of tumors is known to be slightly acidic (pH 5.7–6.8),^[29] which leads to a pH value in tumor tissues that is 0.5–1.0 units lower than in normal tissues.^[26b] Thus, acidification of the tumor microenvironment facilitates pH-sensitive nanocarriers to target cancer cells and release drugs in tumor tissues.^[26a]

Figure 5. A) Cumulative release of fluorescein from loaded BAB micelles: untriggered and pH- (pH 4.5 buffer solution) and temperature-triggered (44 °C). B) Determination of the CMC with Nile red. C) TEM images of the BAB micelles. D) Light-scattering measurement of micelles (2.5 mg mL⁻¹) in H₂O. BAB₁ (top), BAB₂ (middle), and BAB₃ (bottom).

Studies on the cellular uptake of loaded BAB₂ and BAB₃ micelles

In the next set of experiments, we evaluated whether loaded BAB₂ and BAB₃ micelles could be used as cellular drug-delivery systems. Thus, we investigated the cellular uptake of these micelles *in vitro* by fluorescence microscopy. As reported in the literature, Nile red fluoresces *in vitro* when it interacts with free lipids in the cytosol after being released from the carrier.^[30] BAB₂ and BAB₃ micelles loaded with Nile red were generated. After the treatment of ovarian cancer (HeLa) cells with the encapsulated Nile red micelles for 3 h at 37 °C in a humidified atmosphere of 5% CO₂, light microscopy images were collected. Nile red fluorescence was detected in the cytosol of HeLa cells treated with either BAB₂ (Figure 6a) or BAB₃ (Figure 6b) micelles loaded with Nile red. Additionally, no significant fluorescent intensity differences were observed, which demonstrates that both types of micelles could successfully enter the cells and that intracellular release of the drug from the micelles under acidic pH conditions was achieved.

We further analyzed whether the cell viability of the HeLa cells was affected by treatment with non-loaded BAB₂ or BAB₃ micelles. In the first step, HeLa cells were incubated for 3 h

under standard cell-culture conditions with increasing concentrations of the respective non-loaded micelles. Afterwards, the cell viability of each sample was determined by using alamarBlue to detect cell viability. No clear growth inhibition effects were identified for either of the non-loaded micelles (Figure 6c), even when the HeLa cells were incubated with 1 mg mL⁻¹ of non-loaded micelles. The nontoxic features of both micelle types *in vitro* suggest that these drug carrier systems are biocompatible and suitable for biomedical applications.

The release capabilities of BAB₃ micelles are superior to those of the BAB₂ micelles (Figure 6d), particularly for the temperature-triggered release. Therefore, BAB₃ micelles were identified as the carrier of choice for all subsequent *in vitro* studies. Hence, the following experiments were only performed with the BAB₃ block copolymer.

Intracellular DOX release and antitumor activity

As an effective strategy for clinical tumor treatment, chemotherapy plays an important role in tumor suppression and elimination.^[31] Thus, the development of suitable biodegradable drug-delivery systems for the controlled *in vitro* release of mainly insoluble anticancer drugs such as DOX has attracted increasing attention.^[32]

Consequently, we investigated whether DOX-loaded BAB₃ micelles could be efficiently internalized into HeLa cells. If DOX is released, the viability of the cancer cell will be decreased. To this end, we treated HeLa cells separately with 3 μg mL⁻¹ DOX-loaded BAB₃ micelles or non-encapsulated DOX under standard cell-culture conditions. After 3 and 6 h of incubation time the HeLa cells were observed by fluorescence microscopy. The nuclei of the cells were stained with Hoechst 33342, which resulted in visible blue fluorescence that was easily distinguished from the red autofluorescence of DOX. After treatment of the HeLa cells with DOX-loaded BAB₃ micelles for 3 h, free DOX was found in the cytosol, which was indicated by the corresponding red DOX fluorescence (Figure 7a). Additionally, some HeLa cells already show migration of DOX into the nucleus, indicated by the resulting purple fluorescence in the respective overlay image (Figure 7a). After a prolonged incubation time DOX fully co-localized with the nuclei of the HeLa cells (Figure 7b), which suggested successful internalization of the micelles and release of DOX within the cells. To exhibit anticancer activity, DOX must intercalate into DNA, and subsequently inhibit topoisomerase II to prevent replication within the tumor cells and induce cell death.^[2,32–33] Hence, the observed migration of DOX from the BAB₃ micelles into the nucleus is critical for its function as a therapeutic agent (Figure 7b). Similar results were obtained in our control experiments, in which HeLa cells were treated with non-encapsulated DOX (Figure 7c and d). The only difference is the faster internalization of free DOX than the DOX-loaded micelles into the nucleus. This difference appears to arise because of the diffusion-controlled release of non-encapsulated DOX^[33] within the HeLa cells. In the case of free DOX, co-localization of DOX and the nuclei was already visible after 3 h of incubation. (Figure 7c). By contrast, the

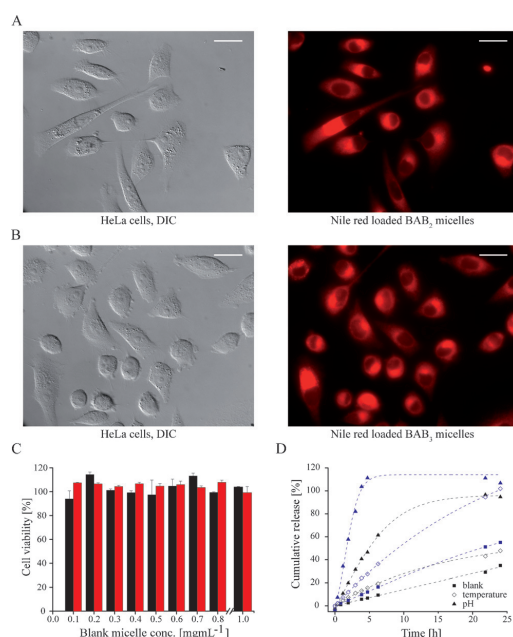


Figure 6. Studies on cellular uptake of BAB₂ and BAB₃ loaded micelles into HeLa cells. Light microscopy images of HeLa cells incubated with Nile red-loaded a) BAB₂ and b) BAB₃ micelles. Scale bar: 25 μm. Images were taken 3 h after treatment with Nile-red-loaded micelles. c) Analysis of the cell viability of HeLa cells as a function of increasing BAB₂ (red) and BAB₃ (black) micelle concentrations. All calculated cell viability values are the means of at least three independent measurements. The corresponding standard deviations are indicated. d) Release of fluorescein from BAB micelles at pH 4.5 and 42 °C; BAB₂ = blue, BAB₃ = black

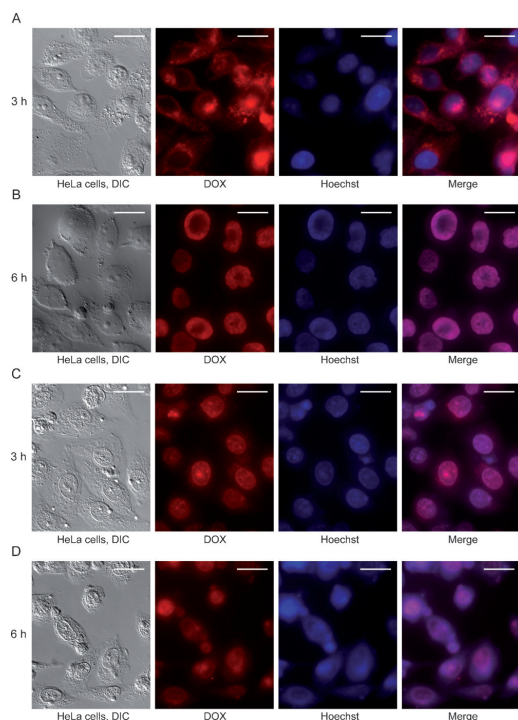


Figure 7. Localization studies of intracellular DOX release of DOX-loaded BAB₃ micelles and non-encapsulated DOX followed by fluorescence microscopy: Images of HeLa cells treated with a), b) DOX-loaded BAB₃ micelles or c), d) non-encapsulated DOX for a), c) 3 h or b), d) 6 h. For all experiments a concentration of 3 μg mL⁻¹ was used. Left to right: Images depict bright-field HeLa cells captured by differential interference contrast (DIC) microscopy, DOX fluorescence in cells (red), nuclei stained with Hoechst 33342 (blue), and overlays of the fluorescence images (scale bar: 25 μm).

DOX-loaded BAB₃ micelles first need to become protonated at lower pH values, leading to swelling and rapid disassembly in the acidic compartments (pH ≈ 5.0), which induced DOX release and distribution into the cytoplasm via BAB₃-micelle-facilitated endosomal escape.^[28,34]

From these results we concluded that, in contrast to non-encapsulated DOX, the DOX-loaded BAB₃ micelles mediate a more-sustained intracellular anticancer drug release. The observed delay was induced via the pH-controlled release mechanism. Further, we wanted to investigate the effect on cell viability of DOX-loaded BAB₃ micelles in HeLa cells. Therefore, the viability of cells treated with increasing concentrations of DOX-loaded BAB₃ micelles or free DOX was analyzed 3 h after incubation under standard cell-culture conditions by the addition of alamarBlue, and the results were compared. For the exact determination of the DOX-loading concentration, each loaded sample of DOX was separately measured by fluorescence spectroscopy (see Figure S24 in the Supporting Information). The fluorescence emission spectra clearly show that the DOX-

loaded BAB₃ micelles open under acidic conditions (purple in Figure S24), which is indicated by an increase in the fluorescence intensity relative to the corresponding spectra collected at pH 7.4 (red in Figure S24). Furthermore, comparison of the spectra of the DOX-loaded BAB₃ micelle at pH 2 (purple in Figure S24) and non-encapsulated DOX at pH 2 (blue in Figure S24) indicates explicit disruption of the micelles.

Figure 8 reveals that the cell viability of the HeLa cells treated with either DOX-loaded BAB₃ micelles or non-encapsulated DOX was significantly reduced. Given that non-loaded BAB₃ micelles were identified as nontoxic (Figure 6c), the reduced cell

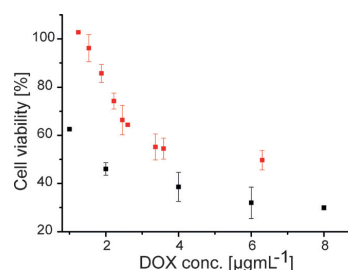


Figure 8. Analysis of the cell viability of DOX-loaded BAB₃ and non-encapsulated DOX treated HeLa cells: Studies of the cell viability of HeLa cells as a function of increasing DOX-loaded BAB₃ micelles (■) and non-encapsulated DOX (■) concentrations. All calculated cell viability values are means of at least three independent measurements. The corresponding standard deviations are indicated.

viability could only be explained by the high cytotoxicity of the released DOX. The IC₅₀ (half-maximal inhibitory concentration) values of the DOX-loaded BAB₃ micelles and non-encapsulated DOX in HeLa cells were determined to be 3.7 μg mL⁻¹^[32] and 1.9 μg mL⁻¹,^[1,5a] respectively, in good accordance with the literature data. Basically, the less-potent cytotoxicity of the DOX-loaded micelles relative to non-encapsulated DOX is due to prolonged release of DOX from the micelles.^[35] However, a comparison of the IC₅₀ value of the DOX-loaded BAB₃ micelles with other potential drug carrier systems, such as nanopolymerosomes, shows a four-fold higher cytotoxicity for DOX-loaded BAB₃ micelles combined with superior biocompatibility.^[1]

Hence, the DOX-loaded micelles show good apoptosis induction activity in HeLa cells. Consequently the designed BAB₃ micelles are potent candidates for a novel pH-controlled drug-delivery system with sustained release properties.

Conclusion

C–H bond activation with 2-methoxyethylamino-bis(phenolate)-yttrium catalysts enabled the synthesis of previously unattained PDEV-P2VP-PDEV (BAB) block copolymers. These micellar nanocarriers are based on 2VP and DEV and exhibit LCSTs within the physiological range and pH-dependent solubility. Under hydrophilic conditions and above their respective CMCs, these block copolymers are capable of spontaneously

self-assembling into micelles with unique properties. Studies of the stability and drug loading/release capabilities of the BAB block copolymers revealed different degrees of burst-release behavior in accordance with the vinylphosphonate block length. Drug-delivery and -release experiments with HeLa cells demonstrated the biocompatibility of the BAB micelles, as well as their fast and efficient cellular uptake. Additional studies on BAB block-copolymer micelles revealed excellent cellular uptake properties and concomitant in vitro biocompatibility of non-loaded BAB micelles. DOX-loaded BAB micelles were successfully internalized into HeLa cells, most likely because of the pH-triggered release of the drug under acidic conditions (pH 4.5) in the endosomal compartment. Observation of the migration process of the anticancer drug DOX into the nucleus of HeLa cells over time showed that co-localization of DOX with the nuclei of HeLa cells was more-rapidly achieved in cells treated with non-encapsulated DOX than in cells treated with DOX-loaded BAB₃ micelles. Hence, in contrast to the strictly diffusion-controlled delivery of non-encapsulated DOX, the drug-carrier system mediates the amount of intracellular anticancer drug available by delaying its release, apparently via a pH-controlled release and endosomal escape mechanism. Our investigations on cell viability revealed that DOX-loaded BAB₃ micelles effectively induced cytotoxic effects on HeLa cells in a dose-dependent manner. In addition, cytotoxicity was not observed in HeLa cells treated with non-loaded BAB₃ micelles. In summary, we have designed multiresponsive, amphiphilic, and biocompatible block copolymers for application in a versatile drug-delivery system. Our results underscore the great potential of polyvinylphosphonate- and polyvinylpyridine-based polymers as next-generation temperature- and pH-controlled drug-delivery systems.

Experimental Section

See the Supporting Information for experimental details.

Acknowledgements

The authors thank Dr. Marianne Hanzlik for the TEM measurements. The Deutsche Forschungsgemeinschaft (SFB 1035) and CIPSM are acknowledged for financial support.

Keywords: drug delivery · group-transfer polymerization · micelles · stimuli-responsive release · vinylphosphonates

- [1] M. Alibolandi, F. Sadeghi, K. Abnous, F. Atyabi, M. Ramezani, F. Hadizadeh, *Eur. J. Pharm. Biopharm.* **2015**, *94*, 521–531.
- [2] W. Chen, F. Meng, R. Cheng, C. Deng, J. Feijen, Z. Zhong, *J. Controlled Release* **2015**, *210*, 125–133.
- [3] a) R. Haag, F. Kratz, *Angew. Chem. Int. Ed.* **2006**, *45*, 1198–1215; b) T. Sun, Y. S. Zhang, B. Pang, D. C. Hyun, M. Yang, Y. Xia, *Angew. Chem. Int. Ed.* **2014**, *53*, 12320–12364.
- [4] a) Y. Sun, Y. Li, S. Nan, L. Zhang, H. Huang, J. Wang, *J. Colloid Interf. Sci.* **2015**, *458*, 119–129; b) S. Guragain, B. P. Bastakoti, V. Malgras, K. Nakashima, Y. Yamauchi, *Chem. Eur. J.* **2015**, *21*, 13164–13174.
- [5] a) L. Qiu, C. Y. Hong, C. Y. Pan, *Int. J. Nanomed.* **2015**, *10*, 3623–3640; b) A. E. Felber, M. H. Dufresne, J. C. Leroux, *Adv. Drug Deliv. Rev.* **2012**,

- 64*, 979–992; c) S. Binauld, M. H. Stenzel, *Chem. Commun.* **2013**, *49*, 2082–2102.
- [6] a) K. Knop, R. Hoogenboom, D. Fischer, U. S. Schubert, *Angew. Chem. Int. Ed.* **2010**, *49*, 6288–6308; *Angew. Chem.* **2010**, *122*, 6430–6452; b) C. d. I. H. Alarcon, S. Pennadam, C. Alexander, *Chem. Soc. Rev.* **2005**, *34*, 276–285; c) H. G. Schild, *Prog. Polym. Sci.* **1992**, *17*, 163–249.
- [7] a) B. Obermeier, F. Wurm, C. Mangold, H. Frey, *Angew. Chem. Int. Ed.* **2011**, *50*, 7988–7997; b) C. Mangold, F. Wurm, H. Frey, *Polymer Chem.* **2012**, *3*, 1714–1721.
- [8] a) T. Steinbach, S. Ritz, F. R. Wurm, *ACS Macro Lett.* **2014**, *3*, 244–248; b) F. Marsico, M. Wagner, K. Landfester, F. R. Wurm, *Macromolecules* **2012**, *45*, 8511–8518; c) T. Steinbach, E. M. Alexandrino, F. R. Wurm, *Polym. Chem.* **2013**, *4*, 3800–3806.
- [9] F. Zhang, S. Zhang, S. F. Pollack, R. Li, A. M. Gonzalez, J. Fan, J. Zou, S. E. Leininger, A. Pavia-Sanders, R. Johnson, L. D. Nelson, J. E. Raymond, M. Elsbahy, D. M. P. Hughes, M. W. Lenox, T. P. Gustafson, K. L. Wooley, *J. Am. Chem. Soc.* **2015**, *137*, 2056–2066.
- [10] J.-F. Lutz, Ö. Akdemir, A. Hoth, *J. Am. Chem. Soc.* **2006**, *128*, 13046–13047.
- [11] a) C. Boyer, V. Bulmus, T. P. Davis, V. Ladmiraal, J. Liu, S. Perrier, *Chem. Rev.* **2009**, *109*, 5402–5436; b) C. Boyer, N. A. Corrigan, K. Jung, D. Nguyen, T.-K. Nguyen, N. N. M. Adnan, S. Oliver, S. Shanmugam, J. Yeow, *Chem. Rev.* **2015**; c) J. K. Oh, *Soft Matter* **2011**, *7*, 5096–5108.
- [12] B. S. Soller, S. Salzinger, B. Rieger, *Chem. Rev.* **2016**, *116*, 1993–2022.
- [13] N. Zhang, S. Salzinger, B. Rieger, *Macromolecules* **2012**, *45*, 9751–9758.
- [14] a) U. B. Seemann, J. E. Dengler, B. Rieger, *Angew. Chem. Int. Ed.* **2010**, *49*, 3489–3491; *Angew. Chem.* **2010**, *122*, 3567–3569, 53489/3481-53489/3415; b) S. Salzinger, U. B. Seemann, A. Plikhta, B. Rieger, *Macromolecules* **2011**, *44*, 5920–5927; c) S. Salzinger, B. Rieger, *Macromol. Rapid Commun.* **2012**, *33*, 1327–1345; d) S. Salzinger, B. S. Soller, A. Plikhta, U. B. Seemann, E. Herdtweck, B. Rieger, *J. Am. Chem. Soc.* **2013**, *135*, 13030–13040.
- [15] a) P. T. Altenbuchner, B. S. Soller, S. Kissling, T. Bachmann, A. Kronast, S. I. Vagin, B. Rieger, *Macromolecules* **2014**, *47*, 7742–7749; b) P. T. Altenbuchner, F. Adams, A. Kronast, E. Herdtweck, A. Pöthig, B. Rieger, *Polym. Chem.* **2015**.
- [16] X. Zhao, W. Liu, D. Chen, X. Lin, W. W. Lu, *Macromol. Chem. Phys.* **2007**, *208*, 1773–1781.
- [17] a) Y. Yu, D. Hong, Z. Liu, F. Jia, Y. Zhou, C. Leng, *J. Polym. Res.* **2013**, *20*, 1–8; b) A. J. de Graaf, K. W. M. Boere, J. Kemmink, R. G. Fokink, C. F. van Nostrum, D. T. S. Rijkers, J. van der Gucht, H. Wienk, M. Baldus, E. Mastrobattista, T. Vermonden, W. E. Hennink, *Langmuir* **2011**, *27*, 9843–9848; c) S. H. Kim, W. H. Jo, *J. Chem. Phys.* **2002**, *117*, 8565–8572; d) N. P. Balsara, M. Tirrell, T. P. Lodge, *Macromolecules* **1991**, *24*, 1975–1986.
- [18] G. He, L. L. Ma, J. Pan, S. Venkatraman, *Int. J. Pharm.* **2007**, *334*, 48–55.
- [19] a) H. Kaneko, H. Nagae, H. Tsurugi, K. Mashima, *J. Am. Chem. Soc.* **2011**, *133*, 19626–19629; b) B. S. Soller, S. Salzinger, C. Jandl, A. Pöthig, B. Rieger, *Organometallics* **2015**.
- [20] R. Duchateau, E. A. C. Brussee, A. Meetsma, J. H. Teuben, *Organometallics* **1997**, *16*, 5506–5516.
- [21] B.-T. Guan, B. Wang, M. Nishiura, Z. Hou, *Angew. Chem. Int. Ed.* **2013**, *52*, 4418–4421; *Angew. Chem.* **2013**, *125*, 4514–4517.
- [22] A. O. Moughton, M. A. Hillmyer, T. P. Lodge, *Macromolecules* **2012**, *45*, 2–19.
- [23] J. Wang, W. Mao, L. L. Lock, J. Tang, M. Sui, W. Sun, H. Cui, D. Xu, Y. Shen, *ACS Nano* **2015**.
- [24] a) H. Ajiro, Y. Takahashi, M. Akashi, *Macromolecules* **2012**, *45*, 2668–2674; b) L. T. T. Trinh, H. M. L. Lambermont-Thijs, U. S. Schubert, R. Hoogenboom, A.-L. Kjoeniksen, *Macromolecules* **2012**, *45*, 4337–4345; c) S. Salzinger, S. Huber, S. Jaksch, P. Busch, R. Jordan, C. M. Papadakis, *Colloid Polym. Sci.* **2012**, *290*, 385–400.
- [25] S. Mukherjee, R. N. Ghosh, F. R. Maxfield, *Physiol. Rev.* **1997**, *77*, 759–803.
- [26] a) Z. Fang, L. Y. Wan, L. Y. Chu, Y. Q. Zhang, J. F. Wu, *Expert Opin. Drug Delivery* **2015**, 1–11; b) R. Haag, F. Kratz, *Angew. Chem. Int. Ed.* **2006**, *45*, 1198–1215; *Angew. Chem.* **2006**, *118*, 1218–1237.
- [27] S. Grijalvo, A. Avino, R. Eritja, *Expert Opin. Ther. Pat.* **2014**, *24*, 801–819.
- [28] a) L. Han, C. Tang, C. Yin, *Biomaterials* **2015**, *60*, 42–52; b) T. Liu, M. Wang, T. Wang, Y. Yao, N. Zhang, *Colloids Surf. B* **2015**, *126*, 531–540.
- [29] Y. Ping, J. Guo, H. Ejima, X. Chen, J. J. Richardson, H. Sun, F. Caruso, *Small* **2015**, *11*, 2032–2036.

- [30] P. Greenspan, E. P. Mayer, S. D. Fowler, *J. Cell. Biol.* **1985**, *100*, 965–973.
- [31] H. Cheng, J. Y. Zhu, X. D. Xu, W. X. Qiu, Q. Lei, K. Han, Y. J. Cheng, X. Z. Zhang, *ACS Appl. Mater. Interfaces* **2015**, *7*, 16061–16069.
- [32] Y. M. Li, T. Jiang, Y. Lv, Y. Wu, F. He, R. X. Zhuo, *Colloids Surf. B* **2015**, *132*, 54–61.
- [33] E. S. Kim, C. Durairaj, R. S. Kadam, S. J. Lee, Y. Mo, D. H. Geroski, U. B. Kompella, H. F. Edelhauser, *Pharm. Res.* **2009**, *26*, 1155–1161.
- [34] a) Y. Sun, Y. Li, S. Nan, L. Zhang, H. Huang, J. Wang, *J. Colloid Interface Sci.* **2015**, *458*, 119–129; b) R. Núñez-Lozano, M. Cano, B. Pimentel, G. de La Cueva-Mendez, *Curr. Opin. Biotechnol.* **2015**, *35*, 135–140.
- [35] W. Xun, H. Y. Wang, Z. Y. Li, S. X. Cheng, X. Z. Zhang, R. X. Zhuo, *Colloids Surf. B* **2011**, *85*, 86–91.

Received: April 18, 2016
Published online on August 19, 2016

Please note: Minor changes have been made to this manuscript since its publication in *Chemistry–A European Journal* Early View. The Editor.

7.5 Reprint permission of copyrighted content

JOHN WILEY AND SONS LICENSE TERMS AND CONDITIONS

Nov 10, 2018

This Agreement between Friederike Adams ("You") and John Wiley and Sons ("John Wiley and Sons") consists of your license details and the terms and conditions provided by John Wiley and Sons and Copyright Clearance Center.

License Number	4465460994521
License date	Nov 10, 2018
Licensed Content Publisher	John Wiley and Sons
Licensed Content Publication	Chemistry - A European Journal
Licensed Content Title	Next Generation Multiresponsive Nanocarriers for Targeted Drug Delivery to Cancer Cells
Licensed Content Author	Peter T. Altenbuchner, Patrick D. L. Werz, Patricia Schöppner, et al
Licensed Content Date	Aug 19, 2016
Licensed Content Volume	22
Licensed Content Issue	41
Licensed Content Pages	9
Type of use	Dissertation/Thesis
Requestor type	Author of this Wiley article
Format	Print and electronic
Portion	Full article
Will you be translating?	No
Title of your thesis / dissertation	From Michael-type systems to biobased lactones: Designing novel polymer microstructures with modified bis(phenolate)lanthanides
Expected completion date	Nov 2018
Expected size (number of pages)	250
Requestor Location	Friederike Adams Zieblandstr. 47

München, Bayern 80798

8 Group-transfer polymerization as a versatile tool for functional (co)polymers

8.1 Bibliographic data

Title: “Metal-Catalyzed Group-Transfer Polymerization: A Versatile Tool for Tailor-Made Functional (Co)Polymers”

Status: Concept Article, First published (Web): October 17, 2017

Journal: *Chemistry – A European Journal*, 2018, 24, 509-518

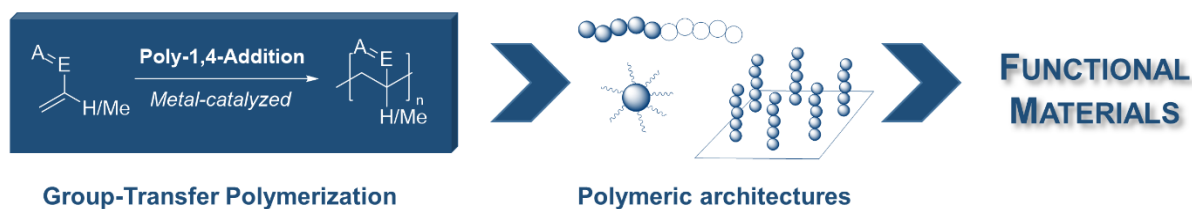
Publisher: WILEY-VCH Verlag GmbH & Co. KGaA

DOI: 10.1002/chem.201703965

Authors: Friederike Adams*, Philipp Pahl*, and Bernhard Rieger ⁵

*These authors contributed equally to this work

8.2 Abstract graphic (TOC)



⁵ F. Adams and P. Pahl wrote equal parts of this concept article. All work was supervised by B. Rieger.

8.3 Content

Polymers face challenging applications in health care, mobility, and the energy sector. To meet these demands precise synthesis of macromolecules is of special interest. In the last decades, various research groups reported on the homo- and copolymerizations of several types of polar vinyl monomers with metallocene and nonmetallocene catalysts bearing transition metals, rare-earth metals, and main group elements (e.g. aluminum) as active centers. This so-called metal-catalyzed group-transfer polymerization gives access to polymers with extraordinary narrow molecular weight distributions and the molecular weights are precisely controllable. The living fashion of this polymerization type allows the synthesis of block copolymers, which are tunable *via* the monomer feed. Besides the outstanding precision of GTP, the temperature-insensitivity and the extraordinary high polymerization rates can be emphasized regarding a broad range of monomers. Therefore, metal-catalyzed GTP provides a versatile method for the efficient, accurate and fast synthesis of a variety of functional polymers. However, unfortunately little attention is still being paid to GTP in comparison to other methods e.g. controlled radical techniques.

This concept article highlights the most important progress in the field of metal-catalyzed GTP with special emphasis on functional (co)polymers. A brief overview on different catalysts and their polymerization mechanisms is provided. The synthesis of homo-, block-, and star-shaped polymers is described in detail. Furthermore, recent advancements in applications, such as stimuli-responsive polymers, surface modifications, hybrid nanomaterials, and micellar structures as drug delivery system are presented.

8.4 Manuscript



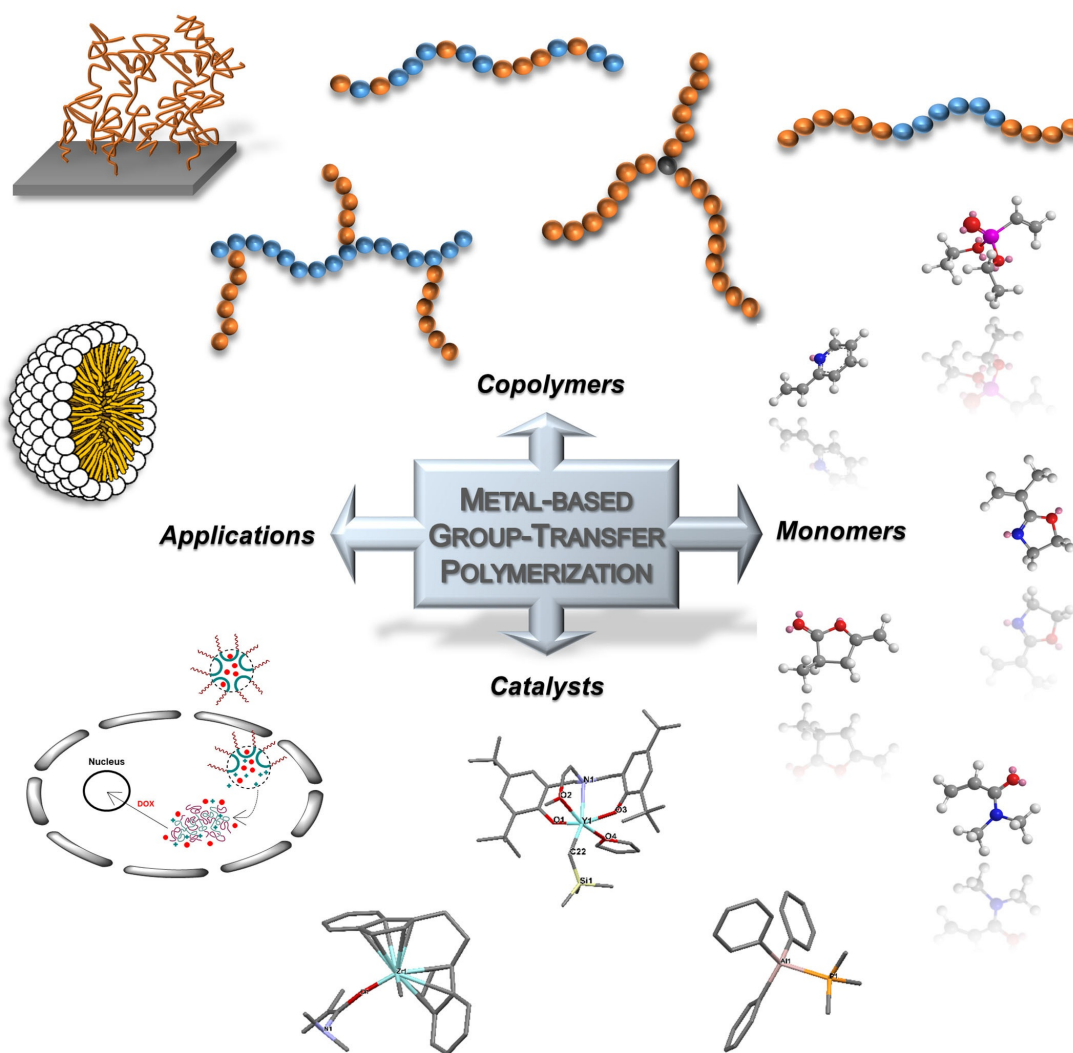
DOI: 10.1002/chem.201703965

CHEMISTRY
A European Journal
Concept

■ Copolymerization

Metal-Catalyzed Group-Transfer Polymerization: A Versatile Tool for Tailor-Made Functional (Co)Polymers

Friederike Adams[†], Philipp Pahl[†], and Bernhard Rieger^{*,[a]}



Abstract: Accommodating the increasing demand for tailor-made polymers is a major goal in polymer chemistry. Therefore, the investigation of polymerization techniques, which allow the precise synthesis of macromolecules is of exceptional interest. Ionic or controlled radical polymerization are capable living-type methods for the generation of uniform polymers. However, even these approaches reach their limits in certain issues. In the last decades, group-transfer polymerization (GTP) and especially metal-catalyzed GTP have proven to give access to a plethora of tailor-made homo- and copolymers based on α,β -unsaturated monomers. Thereby, GTP has established its potential in the development of functional and smart polymers. This concept article highlights the most significant progress in metal-catalyzed GTP with a focus on functional (co)polymers including different polymeric architectures and microstructures.

Introduction

The impressive diversity of plastics has put forth an application horizon, which exceeds far beyond ordinary consumer goods in the private sector. Based on the wide range of applications, the importance of plastics in industrial processing is steadily growing. Polymers, that bear specific chemical groups imparting new properties to materials for physical, chemical, biological, and pharmaceutical uses are called functional polymers. The conversion of light, phase separation, self-assembly, the transport of drugs, or the capture/transport of electric charge are only a few capabilities, illustrating the potential of these functional polymers for high-tech materials.^[1] Smart polymers, a special type of functional polymers, provide even more possibilities for advanced utilization, since their properties are reversibly switchable via various chemical or physical stimuli. The preparation of such customized polymers requires precise and targeted control of the mechanical and thermal properties through changes in composition, microstructure and molecular weight. Metal-catalyzed group-transfer polymerization (GTP) is an efficient method for the accurate and controllable polymerization of a variety of functionalized α,β -unsaturated monomers with narrow molecular weight distribution in a living fashion. Therefore, this polymerization type is predestinated for the synthesis of functional polymers including block, star- and graft-copolymers (Figure 1).^[2] In this concept article, we include the term “tacticity” as a characteristic of functional polymers,

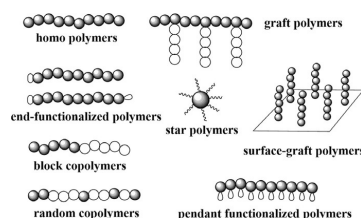


Figure 1. Different copolymers and polymeric materials. Adapted from reference^[12].

since the accurate control of stereoregularity enables the design of (co)polymers with tunable glass-transition/melting temperatures associated with designed stress-strain-properties. Stereo-regular polymers often exhibit physical and mechanical properties superior to their stereo-random analogues.^[3]


The original GTP dates back to 1983, when Webster et al.^[4] discovered the polymerization of Michael-type monomers using silyl ketene acetals (SKA) as initiators. The polymerization was supposed to proceed by repeated associative transfer of the organosilyl group to unreacted monomer. In fact, later studies revealed a dissociative mechanism, in which nucleophilic anions or metallic Lewis acids reversibly remove the silyl group at the SKA chain end, thereby forming the active enolate. Thus, the polymerization proceeds by the repeated attack of an enolate-species to a monomer in its 1,4-unsaturated form (poly-1,4-addition). Nevertheless, the deceptive term “group-transfer” has remained in literature.

Since the pioneering discovery of Webster et al., various modifications and different catalytically active systems were established. However, the scope of this article only covers, rare earth metal-mediated (REM-),^[5] transition-metal catalyzed,^[5a,6] and frustrated Lewis-pair catalyzed GTP,^[7] all being known to produce well controlled polymers. In brief, all methods have a similar propagation in common, proceeding through repeated 1,4-conjugate additions, in which the anionic enolate chain end is coordinated to a metal cation/atom.^[5a,7a,8] Consequently, GTP can be assigned as a special case of anionic polymerization.^[8,9] However, in anionic polymerizations, particularly the extent of reactions between initiators and ester groups, as well as backbiting, increases strongly with the temperature, making low temperatures ($-78\text{ }^{\circ}\text{C}$) prerequisite.^[9,10] In GTP, this major drawback is eliminated by the stabilization of the growing chain end.^[2] Therefore, GTP is less sensitive to temperature, allowing to perform polymerizations at up to $100\text{ }^{\circ}\text{C}$. This is advantageous from a practical as well as an economic perspective.^[10b]

An additional benefit of GTP lies in the broad scope of accessible monomers. Originally, GTP was restricted to α,β -unsaturated carbonyl compounds; however, extensive research has enlarged the variety of accessible monomers. By now, acrylates, acrylamides, vinylphosphonates, and vinylpyridines with a multitude of different functionalities (Figure 2) have been successfully homo- and copolymerized by various catalysts.^[7c,11]

[a] F. Adams,* P. Pahl,* Prof. Dr. B. Rieger
WACKER-Lehrstuhl für Makromolekulare Chemie
Catalysis Research Center, Department of Chemistry
Technische Universität München, Lichtenbergstr. 4, 85748 Garching bei
München (Germany)
E-mail: rieger@tum.de

[*] These authors contributed equally to this work.

 The ORCID identification number(s) for the author(s) of this article can be found under <https://doi.org/10.1002/chem.201703965>.

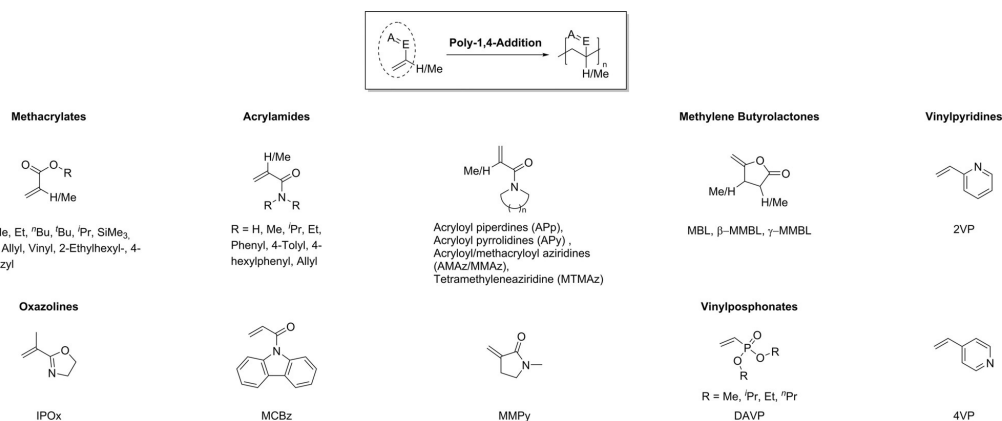
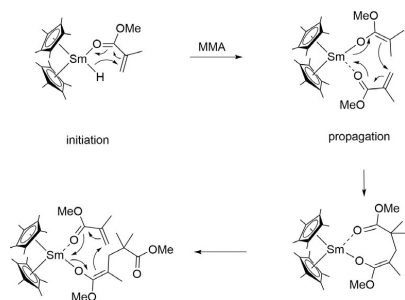


Figure 2. Scope of available monomers for metal-catalyzed GTP and general form of poly-1,4-addition with Michael-type vinyl monomers.^[7c,11]

Catalysts in Group-Transfer Polymerization

Metalloenes

Cyclopentadienyl ligands are ubiquitous in organometallic chemistry. Naturally, initial studies on metal-catalyzed GTP were conducted with metallocene complexes. In 1992, Yasuda et al. used a neutral samarocene $[(C_5Me_5)_2SmH]_2$ for the polymerization of methyl methacrylate (MMA). The catalyst was active over a broad temperature range between $-95^\circ C$ and $40^\circ C$. The produced poly(methyl methacrylate) (PMMA) showed low molecular weight distributions ($D < 1.05$) and high syndiotacticity of up to 95%. Yasuda et al. proposed a monometallic anionic coordination polymerization mechanism, in which the reaction is initiated by the attack of the hydride to the first MMA monomer. The subsequent propagation proceeds through the repeated 1,4-addition of the formed "SmO-C(OCH₃)-C(CH₃)(CH₂R)" to the next MMA molecule via an eight-membered cyclic intermediate (Scheme 1). The intramolecular repulsion of the two methyl groups of the involved MMA molecules in the cyclic intermediate was stated to be essential for the syndiospecific propagation.^[11g] Introduction of a



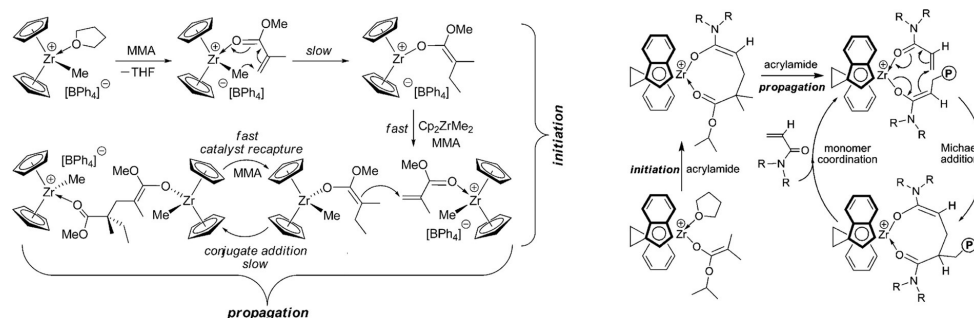
Scheme 1. Proposed Yasuda-type mechanism for syndiospecific MMA polymerization with $[(C_5Me_5)_2SmH]_2$.^[11g]

chiral neomenthyl moiety changed the stereospecificity of similar lanthanide-complexes (Y, La, Sm, Lu) from syndiotactic to isotactic with an increasing stereoregularity with decreasing temperatures. The resulting PMMA showed increasing polydispersities up to 7.9 at elevated temperatures.^[13]

Xu et al. described the synthesis of poly(allyl methacrylate) (PAMA) using $(C_5H_5)Y[Me_2SiCH_2C(N-2,6-iPr_2C_6H_3)_2](CH_2TMS)(THF)$ (in which TMS = trimethylsilyl).^[14] However, Rieger et al. mainly focused on the polymerization of phosphorous containing polymers through REM-GTP, since these polymers show high biocompatibility and water solubility, and are potential candidates for various applications.^[5b] In 2010, the polymerization of diethyl vinylphosphonate (DEVP) was introduced, which has been unapproachable by conventional techniques like radical or classical anionic polymerizations.^[5b] First investigations with Cp_2YbCl and Cp_2YbMe as catalysts revealed high activities and yielded high molecular weight polymers.^[15] In later studies the polymerization mechanism was elucidated (Yasuda-type) and further catalysts were introduced. In particular, simple Cp_3Ln ($Ln = Lu, Yb, Tm$) complexes produced well controlled polymers.^[16]

A special class of catalysts for GTP is zirconocene complexes. In 1992, parallel to the developments of Yasuda et al., Collins and Ward investigated the polymerization of MMA in the presence of a cationic and a neutral zirconocene as a two-component system $([Cp_2ZrMe(THF)][BPh_4])$ and Cp_2ZrMe_2 .^[6,17] The resultant syndiotactic PMMA was produced using chain-end control in a non-living fashion with low polydispersities ($D = 1.2-1.4$).^[6,18]

Related studies indicated, that the propagating step proceeds via a bimetallic intermediate in contrast to the monometallic Yasuda-type mechanism (Scheme 2, left). The synthesis of isotactic PMMA was enabled by introduction of a chiral initiator through an enantiomeric site-control mechanism.^[17] Further investigations on single component cationic zirconocene complexes uncovered that isotactic as well as syndiotactic PMMA are accessible depending on the symmetry of the



Scheme 2. Chain initiation and propagation steps in: Left: MMA polymerization by two-component system. (Reprinted with permission from ref. [5a]. Copyright 2009 American Chemical Society.) Right: DMAA polymerization with *ansa*-zirconocene cations. (Reprinted with permission from ref. [20b]. Copyright 2008 American Chemical Society.)

catalyst.^[3,19] Although MMA polymerization with $[\text{Me}_2\text{Cp}^*\text{IndZrMe}(\text{THF})][\text{BPh}_4]$ is highly isospecific at room temperature, symmetric $[\text{Me}_2\text{Cp}^*\text{ZrMe}(\text{THF})][\text{BPh}_4]$ leads to syndiotactic PMMA at low temperatures.^[3]

The scope of accessible monomers for zirconocene-mediated GTP was broadened in 2004 by Mariott and Chen. They introduced highly active chiral *ansa*-metallocenium enolate cations ($\text{rac}-(\text{C}_2\text{H}_4(\text{Ind})_2)\text{Zr}^+(\text{THF})[\text{OC}(\text{O}i\text{Pr})=\text{CMe}_2][\text{MeB}(\text{C}_6\text{F}_5)_3]^-$) for the isoselective polymerization of methacrylates (e.g., methyl- and *n*-butylmethacrylate) and various acrylamides. The polymerization proceeded in a living, monometallic and intramolecular coordinative-conjugate-addition mechanism via a cyclic ester enolate intermediate (Scheme 2, right).^[11d,e,20] As sustainability is an emerging topic in the field of macromolecular chemistry, Chen et al. investigated the polymerization catalysis of renewable methylene butyrolactones by GTP (Figure 1). The naturally occurring α -methylene- γ -butyrolactone (MBL) and the plant-biomass-derived γ -methyl- α -methylene- γ -butyrolactone (γ -MMBL) were polymerized by different lanthanocenes with high activities.^[21] Later, the same monomers and β -methyl- α -methylene- γ -butyrolactone (β -MMBL) were tested with the before mentioned *ansa*-zirconocenes resulting in low molecular weight distributions and highly isotactic P_i -MMBL. The obtained polymers show enhanced thermal properties reflected in high glass transition and decomposition temperatures (T_g up to 288 °C).^[20c,21a,22]

Non-metallocenes

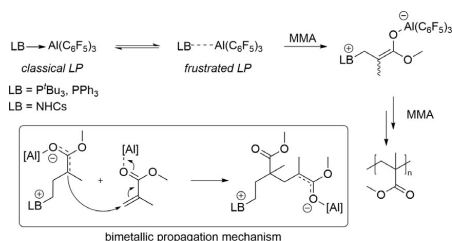
Investigations in organometallic chemistry, among other fields, aim at the development of new mono- and polydentate ligands in REM-GTP, which go beyond the previously described cyclopentadienyl systems.^[23] Since metallocene lanthanides were not yet considered for stereospecific polymerization beyond MMA and show an insufficient activity in polymerization of 2-vinylpyridine (2VP), 2-isopropenyl-2-oxazoline (IPOx) and *N,N'*-dimethylacrylamide (DMAA) also non-metallocene lanthanides were regarded.^[24] Carpentier et al. investigated the activity of bis(phenoxide)-yttrium complexes with two different initiators for the polymerization of MMA in 2003.^[25] Rieger

et al. utilized similar 2-aminoalkoxy-bis(phenolate)catalysts with the general form $(\text{ONOO})^R\text{Ln}(\text{CH}_2\text{TMS})(\text{THF})$ ($\text{Ln} = \text{Y}, \text{Lu}$) for the polymerization of 2VP, DMAA, DEVP and IPOx under mild conditions with moderate to exceptional activities.^[11b,26] In situ ATR-IR measurements assumed a monometallic Yasuda-type mechanism analogue to that of lanthanocenes. Rieger et al. attributed the different tendencies in activity for lanthanocenes and non-metallocene lanthanides to opposing trends in the impact of metal radius and monomer-type on the activation energy.^[11b]

In 2011, Mashima et al. showed that polymerization of 2VP is also possible with an en-diamido yttrium catalyst (in which en = ethylenediamine).^[27] Recently, two different approaches toward highly stereospecific 2VP-polymerization with non-metallocene lanthanides were established by the groups of Lu and Rieger.^[28] The group of Lu developed yttrium bis(phenolate)ether catalysts, in which the stereospecificity of the complex depended on the number of carbon atoms in the backbone of the ligand. P2VP with high isotacticity up to 97% was obtained.^[28c] The newly developed C_1 -symmetric $(\text{ONOO})^R\text{Y}(\text{CH}_2\text{TMS})(\text{THF})$ catalysts investigated by Rieger et al. revealed an impact of the steric bulk in the *ortho*-position of the phenolate rings on the isotacticity of the resulting P2VP. Isotacticities up to 92% were reached with a bis(phenolate) catalyst bearing a tris(3,5-dimethylphenyl)methyl-moiety.^[28a,b] With regard to the stereospecific polymerization of DMAA, the 2-aminoalkoxy-bis(phenolate)yttrium complexes and the before mentioned *ansa*-zirconocenium complexes are the only catalysts that produce highly isotactic PDMAA with isotacticities up to 99% in a living polymerization.^[11d,26]

Frustrated Lewis-pairs

In 2010, Chen et al. polymerized different methacrylates, acrylamides, methylene butyrolactones and DEVP via so called conjugate-addition polymerization with frustrated and classic Lewis pairs (Scheme 3). In particular, the polymerization with frustrated Lewis pairs (FLP), in which a Lewis acid and a Lewis base cannot form a Lewis adduct due to steric hindrance, possess great potential in GTP as the Lewis reactivity remains



Scheme 3. Classical and frustrated Lewis-pairs, the polymerization of MMA and the postulated bimetallic mechanism.^[7a]

unabated.^[7a,b,22] In 2016, Rieger et al. were able to broaden the scope of available monomers, including extended Michael systems such as 4-vinylpyridine, by using highly active combinations of phosphorus-containing Lewis bases and organoaluminum compounds. The group could influence the tacticity of poly(*t*BuMA) by the steric demand of the Lewis pairs. Sterically unhindered combinations afforded a facilitated initiation process, but a lower degree of tacticity ($rr = 61\%$).

Sterically more demanding pairs gave higher syndiotactic products ($rr = 78\%$); however, the molecular weight distribution was broadened.^[7c]

Utilization of C–H bond activation

Lanthanide complexes are able to perform σ -bond-metathesis in a $[2\sigma+2\sigma]$ -cycloaddition. This type of C–H bond activation of trivalent lanthanides and d^0 -transition metals is a common way for C–H-bond cleavage, as these metals do not possess any electrons for oxidative addition- and reductive elimination-reactions. C–H bond activation of a variety of alkynes and heteroaromatic compounds such as 2,4,6-trimethylpyridine (sym-collidine), 1-trimethylsilyl-1-propyne, or 2,3,5,6-trimethylpyrazine was previously reported by the groups of Rieger and Mashima (Figure 3).^[26,27,29]

As yttrium complexes with alkylinitiators, in general, show relatively low initiator efficiencies in the polymerization of

DEVP, heteroaromatic initiators can be introduced through σ -bond metathesis to improve the initiator efficiency. Inefficient initiation by deprotonation of the acidic α -CH is avoided and initiation by nucleophilic attack of the initiator to the first monomer takes place.^[16a, 30] Contrary to observations in DEVP and DMAA polymerization, 2-aminoalkoxy-bis(phenolate)yttrium complexes with heteroaromatic initiators showed a decreased efficiency in polymerization with electron-donating monomers (2VP and IPOx) as an overload of electron density is provoked at the yttrium center. Computational studies underlined that the coordination of nitrogen-donating monomers was hindered with these yttrium catalysts, if an electron-donating initiator was used.^[26]

In addition, the activation of 2,3,5,6-trimethylpyrazine with $(ONOO)^{tBu}Y(CH_2TMS)(THF)$ was of specific interest. The synthesis of B-A-X-A-B polymers (X = initiator, A = P2VP, B = PDEVP), which are suitable systems for drug delivery, was enabled with this system (vide infra).^[29c]

The latest research with $Cp_2YCH_2TMS(THF)$ as precursor complex gave a trinuclear catalyst by three-fold C–H bond activation of 1,3,5-tris(3,5-dimethyl-4-pyridinyl)benzene. This catalyst allowed the fast catalytic synthesis of star-shaped polymeric structures (vide infra).^[29d]

Yttrium ene-diamido complexes were also able to activate a plethora of different N-heteroaromatics and alkynes. These C–H-bond-activated molecules were introduced as end-capping functional groups in P2VP.^[27]

Functional (Co)polymers

Post-functionalizations

An efficient method for post-functionalized and cross-linked polymers is the chemoselective GTP of polar divinyl monomers (vinyl methacrylate, allyl methacrylate, etc.). Subsequent thio-ene-click chemistry of the pendant vinyl group leads to thio-ether bonds in the network.^[11c,14] A second approach for functional materials with these pendant groups is photocuring.

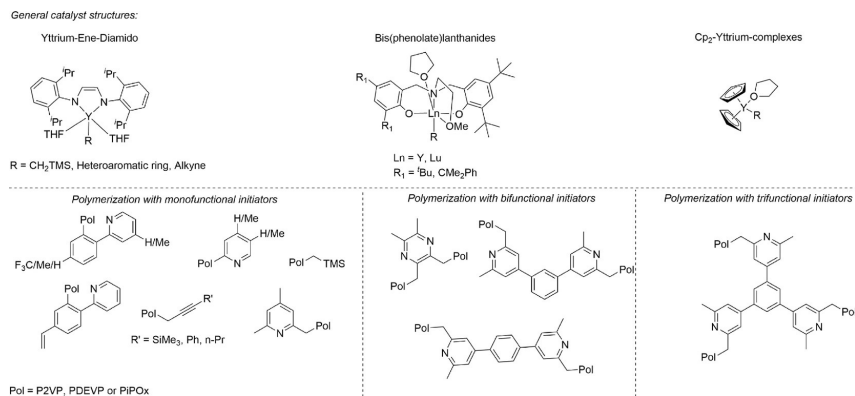


Figure 3. C–H bond activation of alkynes and heteroaromatics as a versatile tool for mono-, bi- and trifunctional initiators in REM-GTP.^[27,29c,30]

This approach produces a cross-linked, elastic, translucent, but colorless thin film.^[11c]

To address further topologies, the synthesis of bottle-brush polymers, also known as molecular polymer brushes, was accomplished by post-functionalization of PIPOx. A highly precise synthesis was achieved by the combination of REM-GTP of IPOx using Cp_2YbMe followed by living cationic ring-opening polymerization (LCROP) of 2-ethyl-2-oxazoline (EtOx). REM-GTP produced IPOx with remarkably narrow molecular weight distributions. By reaction with MeOTf, the polymer was converted into a macroinitiator. LCROP of EtOx yielded bottle-brush polymers with a high grafting density and uniform backbones and side chains. The defined nanoscaled structures were verified using AFM-analysis (Figure 4).^[31]

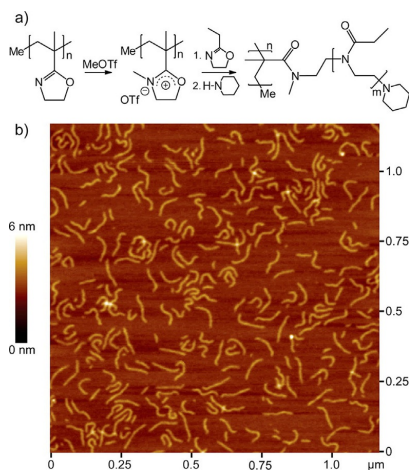


Figure 4. a) Preparation of the molecular brush P(IPOx-g-EtOx). b) AFM scan of P(IPOx-g-EtOx) on mica. (Reprinted from ref. [24]. Copyright 2013 American Chemical Society.)

Star-shaped polymers

Star-shaped polymers, based on the compact structure, exhibit exceptional physical properties distinctly different from their linear analogues. Thus, these polymers are ideal candidates for special applications, for example, in which low viscosities are needed.^[32] There are two conceptually different strategies for the synthesis; either living chain ends are reacted with a multifunctional core, the arm-first approach, or the structures are constructed by chain growth in several directions from a multi-

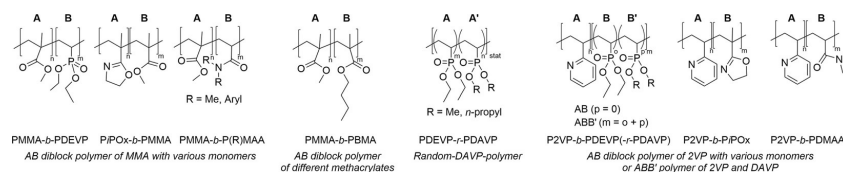


Figure 5. Examples of random- and block-copolymers synthesized using metal-catalyzed GTP.^[11a, b, 20a, b, d]

functional initiator, the core-first approach.^[33] In GTP, particularly the latter technique has proven to be conducive for the synthesis of defined polymers. Just recently, Rieger et al. synthesized star shaped PDEVP and PIPOx through REM-GTP. Therefore, a trinuclear complex was prepared by three fold C–H bond activation of 1,3,5-tris(3,5-dimethyl-4-pyridinyl)benzene with $Cp_2YCH_2TMS(THF)$ followed by polymerization in three directions (vide supra). As a result of incomplete initiation, short linear, long linear, and star shaped structures were observed. Visualization was achieved by transformation of PIPOx into P(IPOx-g-EtOx) and subsequent analysis with AFM. Based on the findings a detailed study on the initiator efficiency of multinuclear complexes was conducted.^[29d]

Block copolymers and micellar systems

The living nature of GTP allows the preparation of block copolymers of all Michael-type monomers among another. The first block has to be the monomer with lowest coordination strength to the metal center. In order to determine the relative coordination strength statistical copolymerizations were conducted revealing an order of $DAVP > (R)MAA > (R)MA > IPOX > 2VP$ (R = any substitution).^[20b, 24] Sequential addition of the monomer after the previous one is consumed entirely gives access to AB-, ABC-, and multiblock-copolymers (Figure 5). Rieger et al. studied the preparation of block copolymers of 2VP and IPOx with other monomers.^[11b, 24] 2VP and IPOx can only be polymerized as the first block because of the lowest coordination strength to the metal center. Block copolymers with all other Michael-monomers (DEVP, DMAA, IPOx, MMA) as the second block were realized.^[11b, 24] If monomers of the same class are used, block copolymers and random copolymers can be produced (Figure 5). Block copolymers are accessible by sequential addition, as described above.^[20d, 11g] Random copolymers are prepared by pre-addition mixing of monomers of the same kind (methacrylates, acrylates, DAVP, etc.) and subsequent addition to the catalyst.^[11a]

In 2006, Chen et al. utilized the diastereospecific ion-pairing polymerization (DIPP) of methacrylates in which both, the cation and the anion, can catalyze the polymerization, and in addition exhibit different stereospecificities. The isospecific polymerization by the cation, the syndiospecific polymerization of the anion, and the switching of the polymer chain led to an *iso*-block-*syndio* stereo-multi-block microstructure. A mixture of a Zr/B ion pair (isotactic block via zirconium ester enolate cation), a Zr/Al ion pair (syndiotactic block via enol aluminate anion) and a neutral zirconocene bis(ester)enolate (exchange of polymer chains) were efficient in DIPP of MMA.^[34] The

system was enhanced by using different combinations of neutral zirconocene bis(phenolate) esters and aluminum species and through the copolymerization of stereoblock-copolymers with different methacrylates (*n*Bu- or 2-ethylhexyl-MA).^[35]

Polymers with reversible and controllable stimuli-responsive properties are in high demand for medical applications. The accessibility of phosphorus- and nitrogen-containing monomers, especially hydrophilic DAVPs with a thermoresponsive behavior and hydrophobic ZVP with its pH-dependent solubility, enabled the synthesis of multiresponsive micelles via REM-GTP. Rieger et al. utilized 2-methoxyethylamino-bis(phenolate)-yttrium complexes as highly active catalysts for the generation of AB and ABB' block copolymers (Figure 5) and for the synthesis of B-A-X-A-B-systems (X = initiator, A = P2VP, B = PDEV, B' = PDMVP or PDPVP). For the synthesis of the latter system, a bifunctional tetramethylpyrazine initiator was introduced to the bis(phenolate) yttrium complexes (vide supra).^[29c,36] It was possible to exactly tune the composition of the copolymer through the monomer feed. Different feed compositions were set to vary the chain length of the P2VP and the PDEV block. DLS measurements showed that a minimum P2VP and PDEV length is required to sustain the micelle formation. The block copolymers possessing a ratio of at least P2VP/PDEV = 50:90 self-assemble to unimodal, perfectly-sized micelles above their critical micelle concentration (CMC; Figure 6 A and C). Moreover, the pH-dependent solubility of the P2VP fragment and the lower critical solution temperature (LCST) of PDEV were

preserved. Stable micelles were present at pH > 4.5. Remarkably, the presence of P2VP and also the variation of chain length of PDEV had no measurable effect on the cloud points which remained at 43.5 °C.^[36] These systems could therefore be used for applications in drug delivery and are controllable by temperature and pH-value. As a release temperature of 44 °C is not in the normal body temperature range, investigations were performed regarding the evaluation of ABB' block copolymers. Differently substituted DAVPs were incorporated to tune the LCST in micellar systems. Previous studies on DAVP-polymers showed that statistical copolymers exhibit a tunable LCST between 5 and 92 °C. The cloud points correlate linear with the content of hydrophilic/hydrophobic comonomer.^[11a] The same effect was shown in the block copolymers; the introduction of small amounts of dimethylvinylphosphonate (DMVP) or di-*iso*-propylvinylphosphonate (DPVP), statistically incorporated into the DEV block, shifted the cloud points. The incorporation of at least 10 equivalents of hydrophilic DMVP sufficed to increase the LCST up to 48.5 °C. Likewise, DPVP (3 equiv.), with its hydrophobic properties, successfully decreased the LCST to 38.5 °C (Figure 6 B).^[36] For the application of micelles in the human body a diameter of 10–100 nm is necessary, which is near to other natural vehicles. Therefore, only micelles with a diameter ≤ 100 nm were used. As the developed polymers have bifunctional release properties, pH (4.5) and temperature (44 °C) triggered release studies were conducted with fluorescein loaded B-A-X-A-B

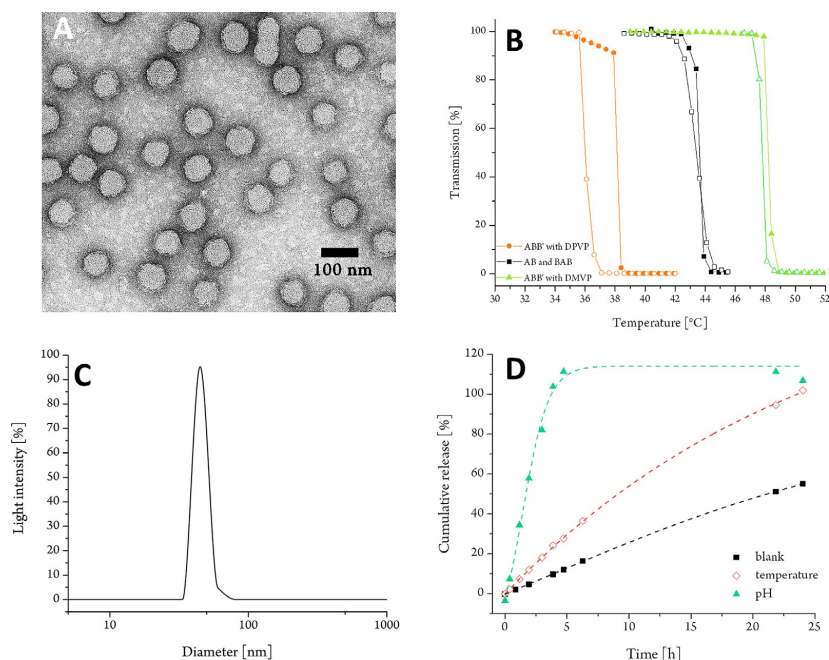


Figure 6. A) TEM image of a BAB micelle with $D_h = 54$ nm. B) Cloud points of AB and ABB' block copolymers. C) DLS of an AB micelle with $D_h = 46$ nm. D) Cumulative release of fluorescein from loaded BAB micelles ($D_h = 88$ nm; untriggered, pH (4.5)- and temperature (44 °C)-triggered). Adapted from ref. [36] (published by The Royal Society of Chemistry) and from ref. [29c].

(abbreviated: BAB)-micelles (Figure 6, D). The drug loading/release capabilities revealed different degrees of burst-release behavior in dependence of the vinylphosphonate block length. The BAB polymer with the shortest PDEVp chain length showed the lowest release efficiency. In all cases, it was shown that the pH-trigger can be used for a burst release, whereas temperature achieves a more sustained release of a loaded substance over a period of 25 hours. To test if these systems can act as cellular drug-delivery systems, cellular uptake of Nile-red colored micelles in ovarian cancer (HeLa) cells and pH-dependent release was investigated. A successful intracellular release was achieved, since Nile red fluoresces when it interacts with free lipids after being released from the carrier under acidic conditions (Figure 7, left). In addition, investigations in the *in vitro* release of the hydrophobic, insoluble anticancer drug doxorubicin (DOX) were performed. The release of DOX is associated with the decrease of the cancer cell viability. After verification that non-loaded BAB-micelles are non-toxic (Figure 7, middle), the observed reduced cell viability could be explained by the cytotoxicity of successfully released DOX (Figure 7, right).^[29c]

Polymers on surfaces

Surface-immobilized macromolecules have attracted great attention since the 1950s. The unique conformation, in which the polymer chains stretch along the direction normal to the grafting surface, offered a plethora of applications; for exam-

ple, prevention of flocculation of colloidal particles, adhesive materials, protein-resistant biosurfaces, chromatographic devices, lubricants, and chemical gates.^[37] In particular, smart polymers grafted onto surfaces show extraordinary properties. Most prominent is the use of polymers exhibiting a LCST. Taking advantage of the thermoresponsiveness, these polymers bound to surfaces reversibly and sharp changes their chemical and physical properties, such as hydrophilicity and layer thickness.

GTP, due to its living character, provides a strong method for the generation of uniform polymer brushes. Two decades after this initial finding,^[38] especially REM-GTP proved its worth for the synthesis of defined polymer brushes. Rieger et al. developed a strategy for the preparation of thermoresponsive and proton-conducting brush layers. Using photoactivated hydrosilylation, ethylene glycol dimethacrylate (EGDM) was grafted onto H-terminated silicon substrates; thereby constructing a PEGDM network covalently bound to silicon. Preserved methacrylate moieties were used to immobilize Cp_2YbMe . Starting from this catalyst loaded surface, DEVP, DMVP, DPVP and MMA were polymerized (Figure 8). AFM measurements confirmed a linear growth of layer thickness as a function of polymerization time (Figure 10, left). Investigation in the influence of the alkyl chain length of the PDAVP (DEVP, DMVP, DPVP) on the hydro/lipophilicity was performed by static water contact angle measurements (Figure 9a–c). In addition, a fully reversible change of the hydrophilicity was observed based on the LCST of PDEVp ($CA_{25^\circ C} = 46^\circ$; $CA_{50^\circ C} = 66^\circ$; Figure 9d and e).^[39,40]

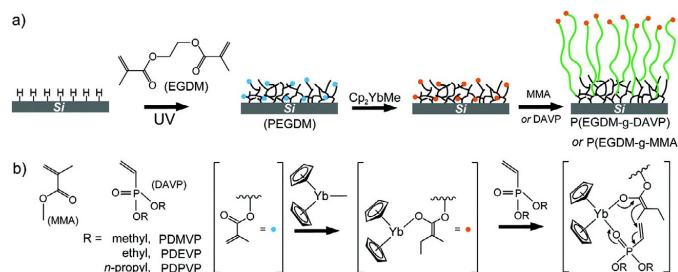


Figure 8. Preparation of the pre-coating PEGDM layer on a silicon substrate, catalyst immobilization, and subsequent SI-GTP of MMA or DAVP. (Reprinted from ref. [39]. Copyright 2012 American Chemical Society.)

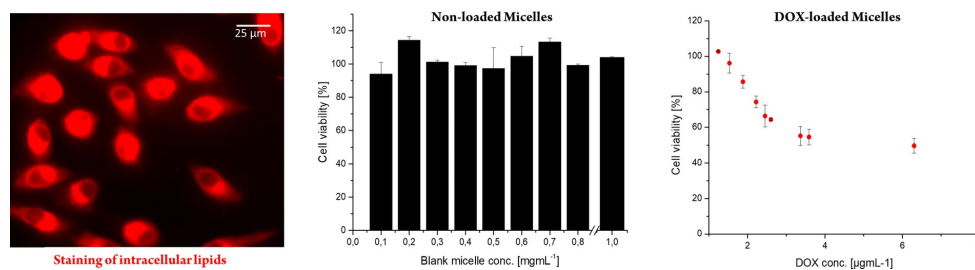


Figure 7. Left: Cellular uptake of Nile-red colored micelles and intracellular release. Middle: Analysis of the cell viability of increasing micelle concentration (BAB, $D_n = 88$ nm) using alamarBlue assay. Right: analysis of the cell viability of DOX-loaded BAB treated-HeLa cells as a function of increasing micelle concentration (BAB, $D_n = 88$ nm) using alamarBlue assay. Adapted from ref. [29c].

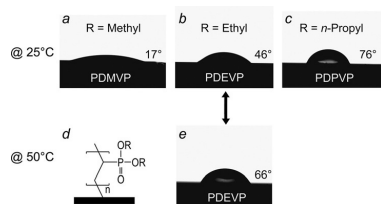


Figure 9. Molecular structure of PDAVP (d) and static water contact angle (CA) on different PDAVP coatings on silicon substrates at different temperatures. a–c) CA of PDMVP, PDEVP, and PDPVP brushes at 25 °C. e) CA of PDEVP brush at 50 °C. (Reprinted from ref. [39]. Copyright 2012 American Chemical Society.)

This concept was transferred to silicon nanocrystals (3 nm). With $\text{Cp}_2\text{YCH}_2\text{TMS}(\text{THF})$ as catalyst, thermoresponsive, red-light photoluminescent, and oxidation-stable hybrid silicon nanoparticles with a hydrodynamic radius of $441(\pm 96)$ nm ($T < \text{LCST}$) were yielded. Heating of the particles above 50 °C triggered collapsing of the polymer chains and thus a decrease in the hydrodynamic radius to 140 nm. Extended heating to 70 °C induced aggregate formation. These particles, under UV light, exhibited photoluminescence focused to a point.^[41]

Another class of well-investigated supports for grafting of polymer brushes are crosslinked polystyrene microspheres. These structures were reacted with EGDM yielding a covalently bound PEGDM network on the PS spheres. Again, the preserved methacrylate functionalities served as reactants for the REM-GTP catalyst (Cp_2YbMe). Subsequent addition of DEVP led to enolate-initiated polymerization on the surface. Analysis of the mass gain as a function of time in combination with monitoring the growth of the beads by SEM revealed a linear in-

crease for polymerization times up to 3 min (Figure 10, right, a–d). After this point, rupture of the particles occurred, which was attributed to accumulated repulsion between the grafted polymer chains and growth of chains inside the particles (Figure 10, right, e and f).^[42]

Conclusions

Metal-catalyzed GTP has made major contributions to the development of functional polymers. Considering catalyst design, a lot of effort was made to increase the performance in polymerization catalysis. The versatility and precision of this technique, as highlighted in this concept article, allow the polymerization of an enormous spectrum of monomers with remarkable control over the molecular weight and the stereoregularity. Moreover, different architectural structures (e.g. star-shaped polymers, polymers on surfaces), block copolymers, and post functionalizations were made accessible. The versatility of α,β -unsaturated monomers gives plenty of room for broadening the scope of application far beyond drug delivery systems and polymeric surfaces. Therefore, completely novel polymers are conceivable. In conclusion, metal-catalyzed GTP has clearly proven its worth in polymer chemistry; nevertheless, improvement in various directions is possible and necessary to expand the variety of functional polymers.

Acknowledgements

F.A. acknowledges support by the Bavarian State Ministry of the Environment and Consumer Protection via the project association "BayBiotech".

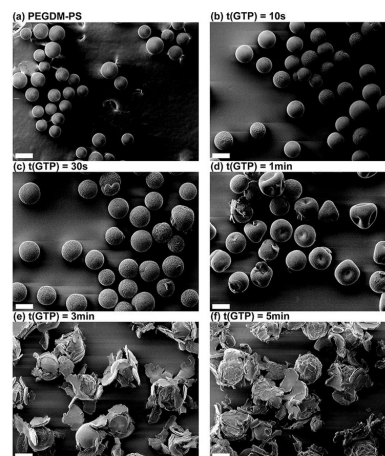
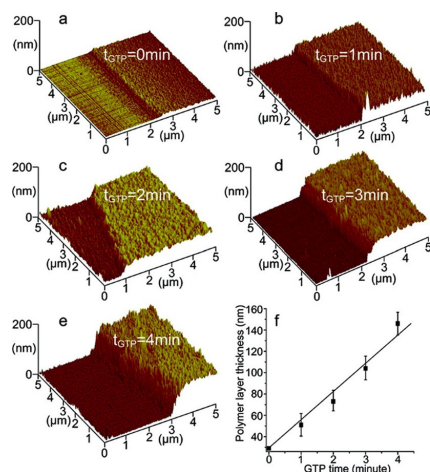


Figure 10. Left: Three-dimensional representation of AFM scans of a PEGDM film on silicon wafer and polymer brushes after SI-GTP of DEVP. a) SIPGP of EGDM for 30 min gives a PEGDM film with a thickness of $29(\pm 6)$ nm. b–e) SI-GTP of DEVP on the same substrate after 1, 2, 3, and 4 min results in $51(\pm 11)$, $73(\pm 9)$, $104(\pm 11)$, and $146(\pm 12)$ nm thick polymer brush layers, respectively. f) P(EGDM-g-DEVP) layer thickness as a function of SI-GTP time. (Reprinted from ref. [39]. Copyright 2012 American Chemical Society.) Right: SEM scans of PDEVP modified PS microspheres after SI-GTP for different reaction times: a) 0 s, b) 10 s, c) 30 s, d) 1 min, e) 3 min, and f) 5 min. Scale bar: 200 μm . (Reprinted with permission from ref. [42]. Copyright 2014 John Wiley and Sons.)

Conflict of interest

The authors declare no conflict of interest.

Keywords: copolymers · functional polymers · group-transfer polymerization · metal-catalyzed polymerization · Michael-type vinyl monomers

- [1] a) IUPAC, *Compendium of Chemical Terminology*, 2nd Ed. (the "Gold Book"), Blackwell Scientific Publications, Oxford, 1997; b) D. N. Schulz, A. O. Patil, in *Functional Polymers*, Vol. 704, ACS, 1998, pp. 1–14.
- [2] M. Rikkou-Kalourkoti, O. W. Webster, C. S. Patrickios, in *Encyclopedia of Polymer Science and Technology*, Wiley, 2002.
- [3] H. Frauenrath, H. Keul, H. Höcker, *Macromolecules* 2001, 34, 14–19.
- [4] a) O. W. Webster, W. R. Hertler, D. Y. Sogah, W. B. Farnham, T. V. RajanBabu, *J. Am. Chem. Soc.* 1983, 105, 5706–5708; b) D. Y. Sogah, W. R. Hertler, O. W. Webster, G. M. Cohen, *Macromolecules* 1987, 20, 1473–1488.
- [5] a) E. Y. X. Chen, *Chem. Rev.* 2009, 109, 5157–5214; b) B. S. Soller, S. Salzinger, B. Rieger, *Chem. Rev.* 2016, 116, 1993–2022.
- [6] S. Collins, D. G. Ward, *J. Am. Chem. Soc.* 1992, 114, 5460–5462.
- [7] a) Y. Zhang, G. M. Miyake, M. G. John, L. Falivene, L. Caporaso, L. Cavallo, E. Y. X. Chen, *Dalton Trans.* 2012, 41, 9119–9134; b) Y.-B. Jia, W.-M. Ren, S.-J. Liu, T. Xu, Y.-B. Wang, X.-B. Lu, *ACS Macro Lett.* 2014, 3, 896–899; c) M. G. M. Knaus, M. M. Giuman, A. Pöthig, B. Rieger, *J. Am. Chem. Soc.* 2016, 138, 7776–7781.
- [8] M. Rikkou-Kalourkoti, O. W. Webster, C. S. Patrickios, in *Encyclopedia of Polymer Science and Technology*, Wiley, 2014.
- [9] S. Bywater, *Makromolekulare Chemie Macromolecular Symposia* 1993, 67, 339–350.
- [10] a) O. Webster, *Adv. Polym. Sci.* 2004, 167, 1–34; b) O. W. Webster, *Makromolekulare Chemie Macromolecular Symposia* 1992, 60, 287–296.
- [11] a) N. Zhang, S. Salzinger, B. Rieger, *Macromolecules* 2012, 45, 9751–9758; b) P. T. Altenbuchner, B. S. Soller, S. Kissling, T. Bachmann, A. Kronast, S. I. Vagin, B. Rieger, *Macromolecules* 2014, 47, 7742–7749; c) F. Vidal, R. R. Gowda, E. Y. X. Chen, *J. Am. Chem. Soc.* 2015, 137, 9469–9480; d) W. R. Mariott, E. Y. X. Chen, *Macromolecules* 2004, 37, 4741–4743; e) G. Miyake, L. Caporaso, L. Cavallo, E. Y. X. Chen, *Macromolecules* 2009, 42, 1462–1471; f) H. Yasuda, H. Yamamoto, K. Yokota, S. Miyake, A. Nakamura, *J. Am. Chem. Soc.* 1992, 114, 4908–4910; g) H. Yasuda, *J. Organomet. Chem.* 2002, 647, 128–138.
- [12] B. S. Soller, N. Zhang, B. Rieger, *Macromol. Chem. Phys.* 2014, 215, 1946–1962.
- [13] M. A. Giardello, Y. Yamamoto, L. Brard, T. J. Marks, *J. Am. Chem. Soc.* 1995, 117, 3276–3277.
- [14] T. Xu, J. Liu, X.-B. Lu, *Macromolecules* 2015, 48, 7428–7434.
- [15] U. B. Seemann, J. E. Dengler, B. Rieger, *Angew. Chem. Int. Ed.* 2010, 49, 3489–3491; *Angew. Chem.* 2010, 122, 3567–3569.
- [16] a) S. Salzinger, B. S. Soller, A. Plikhta, U. B. Seemann, E. Herdtweck, B. Rieger, *J. Am. Chem. Soc.* 2013, 135, 13030–13040; b) S. Salzinger, U. B. Seemann, A. Plikhta, B. Rieger, *Macromolecules* 2011, 44, 5920–5927; c) B. S. Soller, Q. Sun, S. Salzinger, C. Jandl, A. Pöthig, B. Rieger, *Macromolecules* 2016, 49, 1582–1589.
- [17] S. Collins, D. G. Ward, K. H. Suddaby, *Macromolecules* 1994, 27, 7222–7224.
- [18] Y. Li, D. G. Ward, S. S. Reddy, S. Collins, *Macromolecules* 1997, 30, 1875–1883.
- [19] T. Stuhldreier, H. Keul, H. Höcker, *Macromol. Rapid Commun.* 2000, 21, 1093–1098.
- [20] a) W. R. Mariott, E. Y. X. Chen, *Macromolecules* 2005, 38, 6822–6832; b) G. M. Miyake, E. Y. X. Chen, *Macromolecules* 2008, 41, 3405–3416; c) X. Chen, L. Caporaso, L. Cavallo, E. Y. X. Chen, *J. Am. Chem. Soc.* 2012, 134, 7278–7281; d) A. Rodríguez-Delgado, E. Y.-X. Chen, *Macromolecules* 2005, 38, 2587–2594.
- [21] a) G. M. Miyake, S. E. Newton, W. R. Mariott, E. Y. X. Chen, *Dalton Trans.* 2010, 39, 6710–6718; b) Y. Hu, X. Xu, Y. Zhang, Y. Chen, E. Y. X. Chen, *Macromolecules* 2010, 43, 9328–9336.
- [22] Y. Zhang, G. M. Miyake, E. Y. X. Chen, *Angew. Chem. Int. Ed.* 2010, 49, 10158–10162; *Angew. Chem.* 2010, 122, 10356–10360.
- [23] Z. Hou, Y. Wakatsuki, *Coord. Chem. Rev.* 2002, 231, 1–22.
- [24] N. Zhang, S. Salzinger, B. S. Soller, B. Rieger, *J. Am. Chem. Soc.* 2013, 135, 8810–8813.
- [25] C.-X. Cai, L. Toupet, C. W. Lehmann, J.-F. Carpentier, *J. Organomet. Chem.* 2003, 683, 131–136.
- [26] F. Adams, M. R. Machat, P. T. Altenbuchner, J. Ehrmaier, A. Pothig, T. N. V. Karsili, B. Rieger, *Inorg. Chem.* 2017, 56, 9754–9764.
- [27] H. Kaneko, H. Nagae, H. Tsurugi, K. Mashima, *J. Am. Chem. Soc.* 2011, 133, 19626–19629.
- [28] a) P. T. Altenbuchner, F. Adams, A. Kronast, E. Herdtweck, A. Pöthig, B. Rieger, *Polym. Chem.* 2015, 6, 6796–6801; b) A. Kronast, D. Reiter, P. T. Altenbuchner, S. I. Vagin, B. Rieger, *Macromolecules* 2016, 49, 6260–6267; c) T.-Q. Xu, G.-W. Yang, X.-B. Lu, *ACS Catal.* 2016, 6, 4907–4913.
- [29] a) E. Ihara, K. Koyama, H. Yasuda, N. Kanehisa, Y. Kai, *J. Organomet. Chem.* 1999, 574, 40–49; b) B. S. Soller, S. Salzinger, C. Jandl, A. Pothig, B. Rieger, *Organometallics* 2015, 34, 2703–2706; c) P. T. Altenbuchner, P. D. Werz, P. Schöppner, F. Adams, A. Kronast, C. Schwarzenböck, A. Pöthig, C. Jandl, M. Haslbeck, B. Rieger, *Chem. Eur. J.* 2016, 22, 14576–14584; d) P. Pahl, C. Schwarzenböck, F. A. D. Herz, B. S. Soller, C. Jandl, B. Rieger, *Macromolecules* 2017, 50, 7458–7467.
- [30] B. S. Soller, S. Salzinger, C. Jandl, A. Pöthig, B. Rieger, *Organometallics* 2015, 34, 2703–2706.
- [31] N. Zhang, S. Salzinger, B. S. Soller, B. Rieger, *J. Am. Chem. Soc.* 2013, 135, 8810–8813.
- [32] a) M. Pitsikalis, S. Pispas, J. W. Mays, N. Hadjichristidis, *Adv. Polym. Sci.* 1998, 1–137; b) N. Hadjichristidis, M. Pitsikalis, H. Iatrou, P. Driva, G. Sakellariou, M. Chatzichristidi in *Polymer Science: A Comprehensive Reference Vol. 6* (Eds.: K. Matyjaszewski, M. Möller), Elsevier B. V., Amsterdam, 2012, Chapter 3, pp. 29–111.
- [33] M. K. Mishra, S. Kobayashi, *Star and Hyperbranched Polymers*, Marcel Dekker, New York, 1999.
- [34] E. Y. X. Chen, M. J. Cooney, *J. Am. Chem. Soc.* 2003, 125, 7150–7151.
- [35] Y. Ning, E. Y. X. Chen, *Macromolecules* 2006, 39, 7204–7215.
- [36] F. Adams, P. T. Altenbuchner, P. D. L. Werz, B. Rieger, *RSC Adv.* 2016, 6, 78750–78754.
- [37] B. Zhao, W. J. Brittain, *Prog. Polym. Sci.* 2000, 25, 677–710.
- [38] W. R. Hertler, D. Y. Sogah, F. P. Boettcher, *Macromolecules* 1990, 23, 1264–1268.
- [39] N. Zhang, S. Salzinger, F. Deubel, R. Jordan, B. Rieger, *J. Am. Chem. Soc.* 2012, 134, 7333–7336.
- [40] F. Deubel, B. Rieger, S. Salzinger, N. Zhang, *WO 2013072309 A1*, 2013, p. 44.
- [41] J. Kehrle, I. M. D. Höhle, Z. Yang, A.-R. Jochem, T. Helbich, T. Kraus, J. G. C. Veinot, B. Rieger, *Angew. Chem.* 2014, 126, 12702–12705.
- [42] J. Yang, Y. Liang, S. Salzinger, N. Zhang, D. Dong, B. Rieger, *J. Polym. Sci. Part A* 2014, 52, 2919–2925.

Manuscript received: August 23, 2017

Accepted manuscript online: October 17, 2017

Version of record online: November 23, 2017

8.5 Reprint permission of copyrighted content

JOHN WILEY AND SONS LICENSE TERMS AND CONDITIONS

Nov 10, 2018

This Agreement between Friederike Adams ("You") and John Wiley and Sons ("John Wiley and Sons") consists of your license details and the terms and conditions provided by John Wiley and Sons and Copyright Clearance Center.

License Number	4465470010915
License date	Nov 10, 2018
Licensed Content Publisher	John Wiley and Sons
Licensed Content Publication	Chemistry - A European Journal
Licensed Content Title	Metal-Catalyzed Group-Transfer Polymerization: A Versatile Tool for Tailor-Made Functional (Co)Polymers
Licensed Content Author	Friederike Adams, Philipp Pahl, Bernhard Rieger
Licensed Content Date	Nov 23, 2017
Licensed Content Volume	24
Licensed Content Issue	3
Licensed Content Pages	10
Type of use	Dissertation/Thesis
Requestor type	Author of this Wiley article
Format	Print and electronic
Portion	Full article
Will you be translating?	No
Title of your thesis / dissertation	From Michael-type systems to biobased lactones: Designing novel polymer microstructures with modified bis(phenolate)lanthanides
Expected completion date	Nov 2018
Expected size (number of pages)	250
Requestor Location	Friederike Adams Zieblandstr. 47

München, Bayern 80798

9 Tuning Material Properties of Poly(3-hydroxybutyrate): Isospecific Ring-Opening Polymerization of β -Butyrolactone

9.1 Bibliographic data

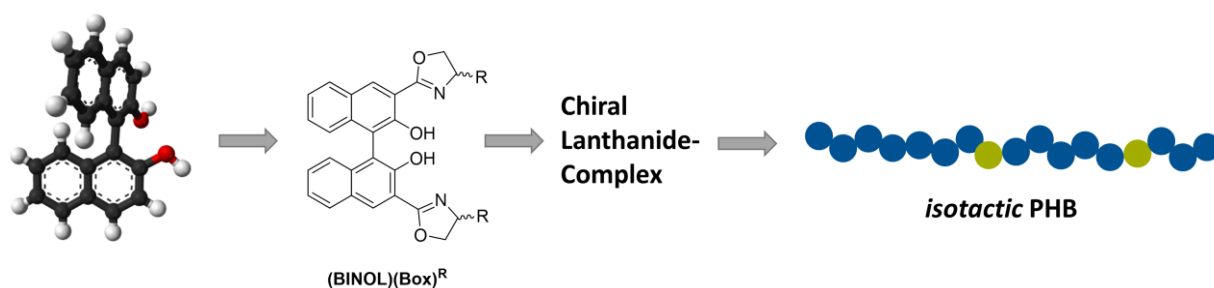
Title: “Process for polymerizing β -butyrolactone”

Status: Patent pending

Journal: Patent application

Authors: Friederike Adams, Bernhard Rieger (Technische Universität München)⁶

9.2 Abstract graphic (TOC)

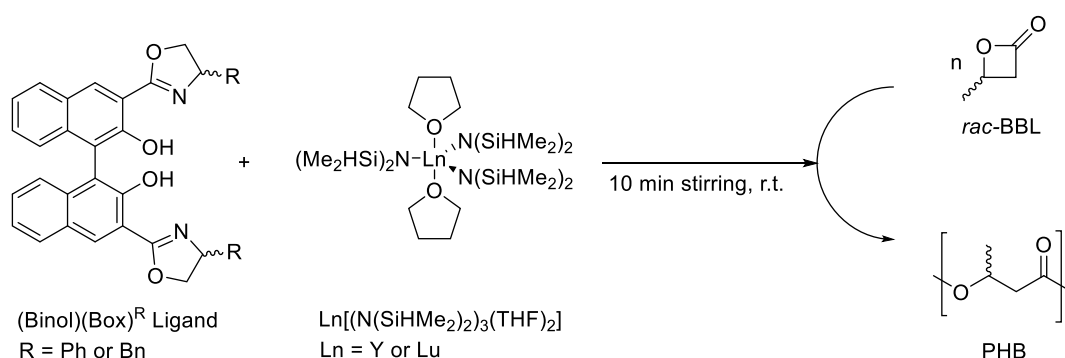


⁶ F. Adams planned and executed all experiments. All work was supervised by B. Rieger.

9.3 Content

With the advancement of technology, research on new materials such as novel polymers with optimized and designed properties is becoming more important. The use of thermoplastic polymers, such as poly(ethylene), poly(ethylene terephthalate) or poly(vinyl chloride), in households, the health sector or in industry is nowadays self-evident. However, as these polymers are not biodegradable, they become an ever-increasing problem for the environment. Since recycling is often not possible, too cumbersome or expensive, plastics are stored on landfills and are burned. Biological decomposition of plastics by microorganisms is therefore an alternative and efficient way to recycle polymers.^[153] Promising biodegradable materials are aliphatic polyesters such as poly(hydroxyalkanoates). A natural, biodegradable PHA is the strictly (*R*)-*isotactic* poly(3-hydroxybutyrate) (*nat*-PHB) produced by various microorganisms as energy and carbon storage.^[203] Due to its thermoplastic properties, which are very similar to the oil-based plastics, PHB is a conceivable alternative for petrochemical polymers. However, the application is limited because of its low thermostability and high crystallinity, which makes it brittle and hard to process.^[158] These drawback provoked an increasing research in transition and rare-earth catalysts to synthesis a less, but still (*R*)-*isotactic* form of PHB ($P_m = 0.60 - 0.80$) as this microstructure preserves its biodegradability and has, in addition, a lower melting-point and is less brittle.^[164-165, 204] Studies by various groups were concentrating on the ring-opening polymerization of *racemic* β -butyrolactone, a low cost feedstock derived from CO₂, for the synthesis of PHB. However, they were only able to produce *atactic* or *syndiotactic* PHB, which is not biodegradable.^[27, 70, 79] In search for more active and stereoselective catalysts for isoselective ring-opening polymerization of *racemic* BBL, our attention was directed to chiral rare-earth metal complexes. The introduction of a chiral ligand should be realized by using the versatile chiral agent 1,1'-binaphthol. The utilization of binaphthol in lanthanide complexes for asymmetric reactions was first published by *Shibasaki et al.* in 1992 for an enantioselective nitro-aldol reaction.^[200] Already there, it was apparent that the active structure was hard to isolate as a large radii of the lanthanide-ion suggest that the steric demand of one binaphthol is not sufficient for coordination. Just a few Binaphthol-derivatives were since then investigated in lanthanide chemistry, but in most of the cases the structures could not be synthesized, were complicated or could never been characterized crystallographically.^[201] The *in situ* generated lanthanide-catalyzed asymmetric 1,3-dipolar cycloaddition investigated by *Ohta et al.* in 2000 aroused our interest as a new efficient chiral 3,3'-bis(2-oxazolyl)-1,1'-bi-2-naphthol (BINOL-Box) ligand was developed. Nevertheless, also in this publication the catalyst structure was not isolated ^[202] In this contribution, we use this structure as a new building block in self-assembled yttrium complexes. To avoid the laborious and sometimes impossible isolation of defined active species, polymerizations are performed with an *in situ*

generated chiral catalyst from lanthanide precursors and a BINOL-Box ligand (Scheme 19).^[205] In this case, one equivalent of the respective ligand was stirred with one equivalent of the precursor for 10 minutes and then the respective amount of *rac*-BBL is added. After isolation of the polymers, they were characterized by nmr spectroscopy, DSC and GPC analysis. All precursor/ligand mixtures were active in the ring-opening polymerization of *rac*-BBL. Microstructural analysis by ¹³C nmr spectroscopy confirmed that *isotactically*-enriched to *isotactic* PHB was obtained with different tacticities. Some PHB samples had exactly the tacticity, as formulated in the goal of this project (Table 3- Table 5).



Scheme 19: *In situ* polymerizations of *rac*-BBL with different ligand/precursor combinations.

Table 3: ROP of *rac*-BBL with (BINOL)(Box)^R ligands [L] and Y[(N(SiHMe₂)₂)₃(thf)₂] [Y].^[a]

Entry	[L]	solvent	time [h]	conversion [%] ^[b]	$M_{n,\text{GPC}}$ [$\times 10^3$ g/mol] ^[c]	\bar{D} ^[d]	P_m ^[e]
1	(R)(R) ^{Ph}	DCM	18	7	70.1	1.62	0.70
2	(R)(R) ^{Ph}	Tol	18	17	51.1	1.49	0.66
3	(R)(R) ^{Ph}	thf	2	12	n.d.	n.d.	0.71
4	(S)(R) ^{Ph}	DCM	18	55	35.1	2.76	0.65
5	(S)(R) ^{Bn}	DCM	26	89	105.5	3.58	0.61
6	(S)(R) ^{Bn}	Tol	26	81	62.5	4.99	0.68
7 ^[e]	(S)(R) ^{Bn}	Tol	19	67	93.7	5.5	0.68

[a] All reactions were performed in 2mL of solvent with a ratio of [Y]/[L]/[BBL] = 1/1/200 and a concentration of [BBL] = 2.44 mol/L. DCM = dichloromethane, Tol = toluene, thf = tetrahydrofuran; n.d. = not determined [b] Conversion determined via ¹H nmr spectroscopy (integration of methyl group resonances of BBL and PHB) [c] M_n was calculated with GPC analysis in chloroform versus polystyrene standards. [d] $\bar{D} = M_w/M_n$ as determined *via* GPC [e] P_m is the probability of *racemic* linkages between monomer units and is determined by ¹³C nmr spectroscopy using the carbonyl region.

Tuning Material Properties of Poly(3-hydroxybutyrate): Isospecific Ring-Opening Polymerization of β -Butyrolactone

Table 4: ROP of *rac*-BBL with (BINOL)(Box)^R ligands [L] and Y[(N(SiHMe₂)₂)₃(thf)₂] [Y].^[a]

Entry	[L]	solvent	time [h]	conversion [%] ^[b]	M _n [× 10 ³ g/mol] ^[c]	Đ ^[d]	P _m ^[e]
1	(R)(R) ^{Ph}	Tol	17	10	112.5	6.54	0.73
2	(R)(R) ^{Ph}	DCM	17	5	146	2.65	0.74
2*	(R)(R) ^{Ph}	thf/DCM ^[f]	13	19	n.d.	n.d.	0.79
3	(R)(S) ^{Ph}	DCM	1.5	33	48.9	2.69	0.67
4	(R)(S) ^{Ph}	Tol	1.5	35	52.6	3.15	0.63
5 ^[g]	(R)(R) ^{Ph}	DCM	5	11	n.d.	n.d.	0.81

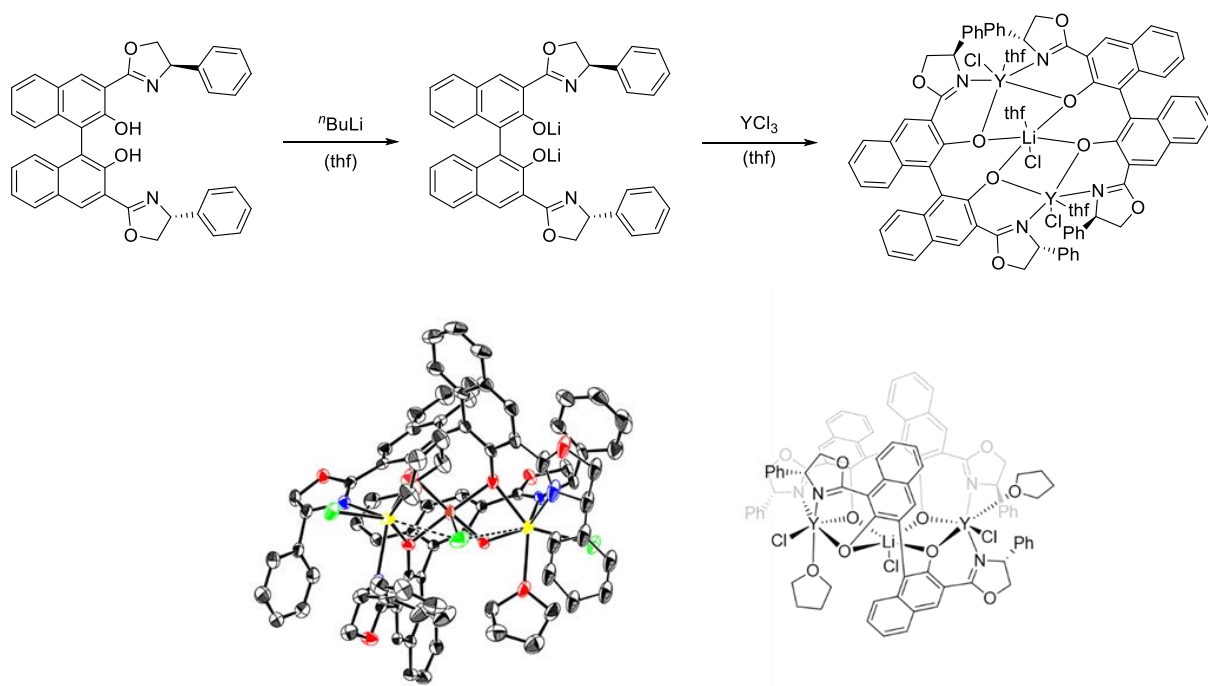
[a] All reactions were performed in 2mL of solvent with a ratio of [Y]/[L]/[BBL] = 1/1/400. DCM = dichloromethane, Tol = toluene, thf = tetrahydrofuran; n.d. = not determined [b] Conversion determined via ¹H nmr spectroscopy (integration of methyl group resonances of BBL and PHB) [c] M_n was calculated with GPC analysis in chloroform versus polystyrene standards. [d] Đ = M_w/M_n as determined *via* GPC [e] P_m is the probability of *racemic* linkages between monomer units and is determined by ¹³C nmr spectroscopy using the carbonyl region [f] Complexation in thf, reaction in DCM [g] 1000 eq. of *rac*-BBL.

Table 5: ROP of *rac*-BBL with (BINOL)(Box)^R ligands [L] and Lu[(N(SiHMe₂)₂)₃(thf)₂] [Lu].^[a]

Entry	Ligand	time [h]	conversion [%] ^[b]	M _n [× 10 ³ g/mol] ^[c]	Đ ^[d]	P _m ^[e]
1	(S)(R) ^{Ph}	19	58	23.4	2.14	0.52
2	(R)(R) ^{Ph}	19	26	1599.3	1.4	0.86
3	(S)(R) ^{Bn}	19	67	93.7	5.5	0.68
3	(R)(R) ^{Bn}	19	27	55.3	5.77	0.48

[a] All reactions were performed in 2mL of toluene with a ratio of [Lu]/[L]/[BBL] = 1/1/200 and a concentration of [BBL] = 2.44 mol/L. [b] Conversion determined via ¹H nmr spectroscopy (integration of methyl group resonances of BBL and PHB) [c] M_n was calculated with GPC analysis in chloroform versus polystyrene standards. [d] Đ = M_w/M_n as determined *via* GPC [e] P_m is the probability of *racemic* linkages between monomer units and is determined by ¹³C nmr spectroscopy using the carbonyl region.

In the further course of this work, a synthesis route *via* salt metathesis was developed in which formation of different undefined complexes is prevented by deprotonation of the binaphthol-OH groups (Scheme 20). During complexation with YCl_3 only one complex is formed indicated by 1H and DOSY nmr spectroscopy. The isolated complex was fully characterized *via* nmr spectroscopy and elemental analysis which prove a general complex structure of $[(BINOL)(Box)^{Ph}YCl(thf)]_2LiCl(thf)$. In addition, we were also able to grow crystals from a saturated tetrahydrofuran solution at room temperature with the structure $[(BINOL)(Box)^{Ph}YCl(thf)]_2LiCl$. A multimetallic structure in which two yttrium centers divide two binol-box ligands is present. All metal centers are located nearly in one plane and LiCl serves as a scaffold stabilizer as it is coordinating the four oxygen atoms of the two ligands in its favored planar fashion. In addition, each yttrium center is coordinated by a chloride and a thf-molecule. After activation with $K[N(SiMe_3)_2]$ or $Li[N(HSiMe_2)_2]$, the complex was also active ring-opening polymerization and produced PHB with an isotacticity of 76%.



Scheme 20: Synthesis and XRD-structure of $[(BINOL)(Box)^{Ph}YCl(thf)]_2LiCl$.

Tuning Material Properties of Poly(3-hydroxybutyrate): Isospecific Ring-Opening Polymerization of β -Butyrolactone

Table 6: ROP of *rac*-BBL with [(S)(R)(BINOL)(Box)^{Ph}YCl(thf)]₂LiCl(thf) and a co-catalyst. ^[a]

Entry	Co-catalyst [Co-Cat]	[M]/[Co- Cat]/[BBL]	time [h]	conversion [%] ^[b]	M _n [$\times 10^3$ g/mol] ^[c]	\bar{D} ^[d]	P _m ^[e]
1	K[N(SiMe ₃) ₂]	1/2/200	0.6	35	30.7	5.1	0.76
2	Li[N(HSiMe ₂) ₂]	1/2.2/200	25	12	4.8	1.40	0.76

[a] All reactions were performed in 2mL of toluene at room temperature. [b] Conversion determined via ¹H nmr spectroscopy (integration of methyl group resonances of BBL and PHB) [c] M_n was calculated with GPC analysis in chloroform versus polystyrene standards. [d] $\bar{D} = M_w/M_n$ as determined *via* GPC [e] P_m is the probability of *racemic* linkages between monomer units and is determined by ¹³C nmr spectroscopy using the carbonyl region.

9.4 Patent application



HOEFER & PARTNER

ETU171201PEP
22.12.2017

Applicant:
Technische Universität München
Arcisstraße 21
80333 München

Process for polymerizing β -butyrolactone

The present invention is concerned with a process for polymerizing racemic β -butyrolactone to obtain polymers with high isotacticity, and with a polymer obtained with this process.

5

Poly(3-hydroxybutyrate) (PHB) is a biopolymer that is produced by microorganisms. In its natural form it is a strictly isotactic polyester of the monomer 3-(R)-hydroxybutyric acid. This polymer is highly valuable as it is biodegradable, is a renewable resource, has barrier properties and has convenient thermoplastic properties similar to those of polypropylene.

10 Although natural PHB is a valuable resource, there are some properties which could be improved, in particular the thermoplastic properties. Moreover, it is desirable to provide a synthetic process for preparing these polymers.

15 It is known to produce PHB polymers by fermentation of glucose containing materials, i.e. food resources. From an ethical view it is not desirable to use food materials for the production of technical products. Moreover, using a fermentation process results in a polymer which is similar to the polymer produced by microorganisms, i.e. a highly isotactic (R)-polymer, and has the same disadvantages. Due to the high crystallinity of these polymers it is very brittle and has a melting temperature which is near the decomposition
20 temperature which makes its processability impossible.

β -butyrolactone as a monomer for PHB synthesis is obtainable by a synthesis method using propylene oxide and CO₂, i.e. readily available cheap products. However, this method yields racemic β -butyrolactone which consists of same amounts of (R)- and (S)- β -butyrolactone. It
25 is desirable to be able to use racemic β -butyrolactone for producing isotactic PHB.

Methods have been described for the synthesis of PHB polymers via a ring opening polymerization using different catalysts. Many catalysts have been developed in the past, but most of these catalysts produce only atactic or syndiotactic PHB polymers. These
30 syndiotactic or atactic PHB polymers have inferior properties than isotactic polymers. In particular they are not biodegradable and the thermoplastic properties are not optimal.

2

Thus, those PHB polymer products that are presently available are either not biodegradable or have less desirable mechanical properties.

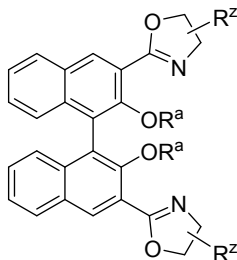
Although, it would be possible to prepare isotactic PHB polymers by using enantiomerically pure β -butyrolactone, i.e. either only the (R)-enantiomer or only the (S)-enantiomer, this option is not feasible as the separation of enantiomers is very time and cost consuming.

Thus, it is an object of the present invention to provide a process wherein racemic β -butyrolactone can be used and nevertheless an isotactic polymer can be obtained. Moreover, it was an object of the present invention to provide a process for preparing PHB polymers having improved mechanical properties but at the same time are biodegradable. Moreover, it was an object to provide a process for preparing a polymer with a predetermined percentage of isotacticity. It was another object of the present invention to provide a polymer that can be produced from monomers that are readily available and/or can be produced from cheap components. Furthermore, it was an object of the present invention to provide a polymer having barrier properties.

All these objects are obtained by using a process as defined in claim 1 and by polymers obtained by the processes described in this application.

20

A process for polymerizing β -butyrolactone with an isotacticity of at least 60% is provided which comprises contacting racemic β -butyrolactone or an enantiomer thereof with a catalyst/initiator system which comprises a rare earth metal, a chiral ligand, at least one nucleophilic ligand, at least one solvent ligand, and optionally an alkali based co-catalyst, wherein the chiral ligand is an enantiomer of a unit of formula I

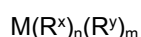


wherein each R^z independently is linear or branched, substituted or unsubstituted C₁-C₂₀ alkyl, substituted or unsubstituted C₆-C₂₀ aryl, substituted or unsubstituted C₅-C₂₀ heteroaryl, or halogen; wherein each R^a independently is H or an alkali metal.

30

The catalyst/initiator system that is used in the method of the present invention is based on a rare earth metal and comprises a chiral ligand as essential part of the system.

In one embodiment the catalyst/initiator system is obtained by contacting a chiral ligand of formula I with a compound of formula II:



and optionally an alkali based co-catalyst,
wherein M is a rare earth metal,
each R^x independently is a nucleophilic ligand,
10 each R^y independently is a solvent ligand,
n is an integer from 1-5, such as 1-3,
m is an integer from 0-5, such as 1-3 with the proviso that $n + m$ is an integer corresponding to the number of association/bonding sites of the rare earth metal, the upper limit of which is the number of available association/bonding sites on the rare earth metal, which is up to 9,
15 such as 5 or 6.

In another embodiment the catalyst/initiator system is obtained by contacting a chiral ligand of formula I with a rare earth metal compound of formula III $MX_3(R^y)_m$, wherein M is a rare earth metal, R^y and m are as defined above and each X independently is halogenide,
20 triflate, or C_1 - C_{20} alkoxide, and with a solvent, and optionally an alkali based co-catalyst, For activation the obtained complex is contacted with an alkali salt of a nucleophilic ligand (co-catalyst). When contacting these components a complex is obtained which comprises a rare earth metal atom bound/associated with the chiral ligand and with at least one nucleophilic ligand and/or solvent ligand. When this route is used, the complex can also include alkali
25 species, for example lithium or potassium halogenides.

The catalyst/initiator system can be obtained with or without a co-catalyst. Moreover, the catalyst/initiator system of the present invention can be obtained by first preparing a rare earth metal compound of formula II, wherein the rare earth metal atom carries already at
30 least one nucleophilic ligand and at least one solvent ligand. It is also possible to prepare the catalyst/initiator system in a one pot reaction, with or without a co-catalyst. Furthermore, after the reaction the complete catalyst/initiator system can be isolated or the reaction mixture can be used directly. In other words, the catalyst/initiator system can be either prepared in situ, i.e. the components of the system can be added to the monomer
35 composition and the system provides the catalytic activity directly. It is also possible to prepare the catalyst/initiator system separately, isolate it and to add it to the monomer composition.

Surprisingly it has been found that when using a catalyst/initiator system as defined in claim 1 it is possible to produce PHB polymers that have a predeterminable amount of isotacticity, a predeterminable amount of imperfections and combine mechanical strength with
5 biodegradability. Such biodegradable polymers can be used for many purposes, for example for packaging. Moreover, it has been found that these polymers still have highly desirable barrier properties, in particular have a high oxygen barrier. By introducing imperfections the mechanical properties are improved compared to natural occurring or microbial produced PHB polymers, i.e. the polymers produced with the process of the
10 present invention have a lower melting point, are less brittle and rigid and have a higher tensile strength.

These valuable properties are obtained by using the process of the present invention, in particular by using the catalyst/initiator system as defined in claim 1.

15

It has been found that a catalyst/initiator system comprising a rare earth metal based compound, a chiral ligand and optionally an alkali-based co-catalyst allows to polymerize racemic β -butyrolactone to obtain isotactic PHB with either a majority of (R)-enantiomers or a majority of (S)-enantiomers. Although a racemic mixture of monomers is used, the
20 polymer comprises only one type of enantiomers with some imperfections. These imperfections in the polymer introduced by the catalyst/initiator system of the present invention provide for the improved mechanical properties. The amount or percentage of imperfections can be controlled in the process of the present invention by parameters as disclosed below, and it should be low enough to maintain the biodegradability which is a
25 valuable property of the polymer.

The figures further explain the subject matter of the present invention.

Fig. 1 shows a conversion per time diagram for racemic β -butyrolactone using a catalyst/initiator system of the present invention.

30 Fig. 2 shows ^{13}C -NMR-spectrograms which are used to determine the microstructure of the polymer obtained with a process of the present invention. For analysis it is possible to either evaluate the carbonyl signal at 169 ppm (see Fig. 2a) or the methylene signal at 40 ppm (see Figs. 2b-d). The ratio between the isotactic part of the polymer (mm and rm) and the syndiotactic part (rr and mr) has been calculated for PHB examples in deuterated
35 chloroform with different isotacticity ratios from 0.70 to 0.88.

Fig. 3 shows the DSC diagram for a PHB example that has been obtained using the process of the present invention. It can be seen that the melting temperature T_m is 166°C and, thus, lower than the melting point of known polymers.

The following definitions are used in the present application.

The term "rare earth metal" refers to the group as defined by IUPAC, i.e. scandium, yttrium
5 and lanthanum and lanthanides. Specific examples of rare earth metals are yttrium and lutetium.

A "chiral ligand" refers to a unit that has an axial chirality and has at least one chiral center. Because of the axial chirality the unit can occur in at least two enantiomeric units, one of the
10 enantiomeric units ((R)- or (S)-compound) is used for the catalyst/initiator system of the present invention.

A "solvent ligand" is a ligand that is based on a solvent, such as tetrahydrofuran, and can associate with the rare earth metal.

15

A "nucleophilic ligand" is a ligand that can associate with the rare earth metal because of a nucleophilic site, such as nucleophilic nitrogen or nucleophilic carbon groups. Examples are substituted amido ligands, C_1 - C_{20} alkoxides and di- or trialkyl methyl-silyl groups. Otherwise the structure of the ligand is not critical as long as it does not interfere with
20 bonding/association of rare earth metal. Examples for a substituted amido ligand or carbon-ligand are $NR^bR^cR^d$, OR^b and CHR^bR^c , wherein each of R^b , R^c and R^d independently is H or a group selected from linear or branched, substituted or unsubstituted C_1 - C_{20} alkyl, substituted or unsubstituted C_6 - C_{20} aryl, substituted or unsubstituted C_5 - C_{20} heteroaryl, arylalkyl, silylalkyl, wherein the substitution can be as defined below.

25

The integer $n+m$ corresponds to the coordination number or number of association/bonding sites of the rare earth metal that is the core of the catalyst. The number of available sites for association or bonding with the rare earth metal is the number that is occupied by ligands. Rare earth metals normally have a coordination number of up to 9. Thus, the sum of n and
30 m can be an integer up to 9, such as 3, 4, or 6.

A linear or branched C_1 - C_{20} -alkyl is an alkyl group having 1 to 20 carbon atoms which can be in a line or can have branches, such as a C_1 - C_{10} alkyl group, particularly a C_1 - C_4 alkyl group. A substituted alkyl is an alkyl which is substituted with groups like OH, NH_2 , NHR,
35 NR_2 , OH, OR, SH, SR, halogen, wherein halogen comprises chlorine, iodine, fluorine, and bromine, wherein R is C_1 - C_4 -alkyl.

C_6 - C_{20} -aryl refers to an aromatic group, like benzyl, phenyl, naphthyl, biphenyl etc.

6

Arylalkyl refers to a C_6 - C_{20} -aryl group substituted with alkyl as defined above.

Silylalkyl refers to silyl units carrying one, two or three C_1 - C_4 -alkyl groups. such as $Si(alk)_3$,
5 $SiH(alk)_2$, $SiH_2(alk)$, wherein alk is C_1 - C_4 -alkyl.

Nucleophilic carbon groups are carbon comprising groups carrying 1-3 mono-, di- or trialkylsilyl units,

10 Alkoxide refers to an O-Alkyl group, wherein "alkyl" is a linear or branched C_1 - C_{20} -alkyl, as defined above, preferably an O- C_1 - C_{10} alkyl group.

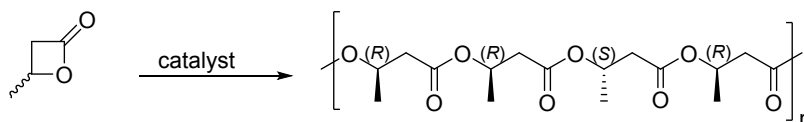
C_5 - C_{20} -heteroaryl refers to heteroaryl groups, i.e. aromatic groups comprising at least one heteroatom, wherein the heteroatom is selected from N, S, and O. Examples for heteroaryl
15 are furanyl, thienyl, pyrrolyl, pyridyl, isochinolyl, oxazolyl, isoxazolyl, thiazolyl, isothiazolyl etc.

The terms "halogen" or "halogenide" comprise chloro, fluoro, bromo, iodo, or chloride, fluoride, bromide, iodide, respectively.

20

A "monomer composition" is a composition comprising at least monomers to be polymerized, i.e. β -butyrolactone and can comprise additionally one or more solvents. If a copolymer shall be produced, the composition can comprise further monomers. As β -butyrolactone is fluid at room temperature, it can be used as it is. The monomer can also be
25 used in a solvent such as toluene.

For polymerizing β -butyrolactone having desirable properties a specific catalyst/initiator system is used. In general the polymerization can be summarized as follows:



(*rac*)-BBL

(*R*)-*isotactic* PHB with (*S*)-stereoerrors

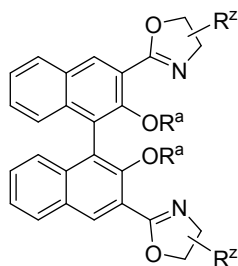
30

The catalyst/initiator system of the present invention comprises a rare earth metal based catalyst and a chiral ligand wherein the rare earth metal is in complex with the chiral ligand which occupies 4 association/bonding sites, at least some of the remaining

association/bonding sites of the rare earth metal are occupied by ligands, i.e. nucleophilic ligands and/or solvent ligands, and/or anions like halogenide, triflate, or C_1 - C_{20} alkoxide up to the coordination number.

- 5 The catalyst/initiator system of the present invention can be prepared by reacting a chiral ligand and a rare earth metal based compound. The chiral ligand is an important part of the system, as it provides for the incorporation of one type of enantiomer of β -butyrolactone in the polymer chain. The chiral ligand used according to the present invention is an enantiomer of a compound of formula I:

10



wherein R^a and R^z as defined above.

- 15 This compound is a substituted binaphthol, examples of which are well-known in the art under the name BINOL-box. Methods for producing these compounds are well-known to the skilled person and have been published in the literature, for example Kodama, H., Ito, J., Hori, K., Ohta, T., & Furukawa, I. (2000). Lanthanide-catalyzed asymmetric 1, 3-dipolar cycloaddition of nitrones to alkenes using 3, 3'-bis (2-oxazolyl)-1, 1'-bi-2-naphthol (BINOL-
20 Box) ligands. *Journal of Organometallic Chemistry*, 603(1), 6-12. The core of this compound is a binaphthyl group, i.e. two naphthyl groups connected by a 1-1 bond. Both carry a hydroxy group in position 2 and a heterocyclic group in position 3. This part of the core provides for the complex with the rare earth metal which is necessary for the catalytic activity. The two heterocyclic groups carry a group R^z at position 4 or 5, preferably at
25 position 4. R^z can be substituted or unsubstituted alkyl, substituted or unsubstituted aryl, heteroaryl, or halogen. This group is not critical as long as it does not interfere with or affect the bonding of the rare earth metal to the four specific association sites of this unit. R^z for example can be linear or branched alkyl, such as methyl, ethyl, n-propyl, n-butyl, isobutyl or isopropyl. The alkyl chain can be substituted by groups like hydroxy, amino, halogen. R^z
30 can also be an aryl group like phenyl or naphthyl or a heteroaryl group. R^z can be bound to the oxazolyl group in two configurations. For the chiral ligand of the present invention it is preferred that both groups R^z have the same configuration, i.e. are both (R) or both (S). Therefore, when it is referred to the chiral ligand the term "(R)(R)-BINOL box" means that

the two naphthyl rings are in (R) configuration and both R^z groups are in (R) configuration. An (S)(R)-BINOL box refers to a compound wherein the two naphthyl rings are in (S) configuration and both groups R^z are in (R) configuration etc.

5 The chiral ligand as defined above and in the claims is reacted/has been reacted with a rare earth metal based compound to obtain the system that provides activity as polymerization catalyst. In the catalyst/initiator complex in its active form the rare earth metal binds/coordinates with the chiral ligand via the two OR^a groups and via the nitrogen atoms of the heteroaryl rings.

10

Producing such complexes is known to the skilled person. There are different approaches to obtain such complexes. The active catalyst/initiator system, which activates a monomer for polymerization is a complex which is formed by contacting the chiral ligand with the rare earth metal based compound. This complex can be obtained either by separate reaction
15 and isolation of the complex or in situ.

In one approach the chiral ligand is contacted with a rare earth metal compound according to formula II. It has been found that a compound of formula II which comprises a nucleophilic ligand is active enough to combine with the OH groups of the chiral ligand
20 (amine elimination reaction), i.e. with R^a being H. In this approach no co-catalyst is necessary, although it can be used. Thus, in a variation of this method, an alkali compound like n-butyl lithium can be used to activate one or both OH groups of the chiral ligand for bonding. The alkali metal of the deprotonating agent in this approach can become part of the catalyst/initiator complex.

25

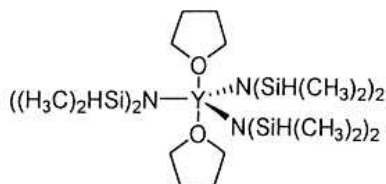
It is assumed without being bound by theory that some of the ligands of the rare earth metal compound of formula II are replaced by bonding/association with the chiral ligand but some remain. It is assumed that at least one nucleophilic ligand and at least one solvent ligand are necessary for the activity of the catalyst/initiator complex of the present invention. These
30 ligands can be provided by using a rare earth metal compound of formula II for preparing the complex. As outlined before, in the complex the rare earth metal in addition to the association with the chiral ligand associates with or carries further ligand(s), at least one nucleophilic ligand and/or at least one solvent ligand, to obtain a coordination number of 6, The solvent ligand can be provided by the rare earth metal compound of formula II or can
35 be attached from the reaction mixture, when said mixture comprises a solvent.

The solvent ligand is a solvent molecule, such as a molecule from the solvent used for dissolving the rare earth metal salt and/or the system or which is present in a compound of

formula II as R^y . A solvent ligand can be exchanged easily when contacted with a monomer. It can be any solvent that is used for this type of compounds and is able to coordinate to metal centers, such as tetrahydrofuran (THF), 1,4-dioxane or diethylether. Other solvents can also be used as long as they have no active proton, protic solvents like alcohols or acids are not suitable. Preferred are solvents that have oxygen but no active proton like dioxane, THF or ether.

The nucleophilic ligand can be a nitrogen and/or carbon and/or oxygen comprising group, for example a substituted amino or amido group, such as a dialkylamido, diarylamido or disilylalkylamido group carrying 1-3 trialkylsilyl units, such as $N(\text{SiH}(\text{alk})_2)_2$ or $N(\text{Si}(\text{alk})_3)_2$. Examples for carbon comprising nucleophilic groups are groups carrying 1-3 mono-, di- or trialkylsilyl units, such as $\text{CH}_2\text{Si}(\text{alk})_3$, $\text{CH}(\text{Si}(\text{alk})_3)_2$, $\text{CH}(\text{SiH}(\text{alk})_2)_2$, $\text{C}(\text{Si}(\text{alk})_3)_3$, wherein alk is C_1 - C_4 -alkyl.

Compounds that are well suited for this approach are yttrium compounds having 3 nucleophilic ligands and up to 3 solvent ligands. The number of ligands depends on the number of available association/binding sites of the metal. A useful rare earth compound is the following:

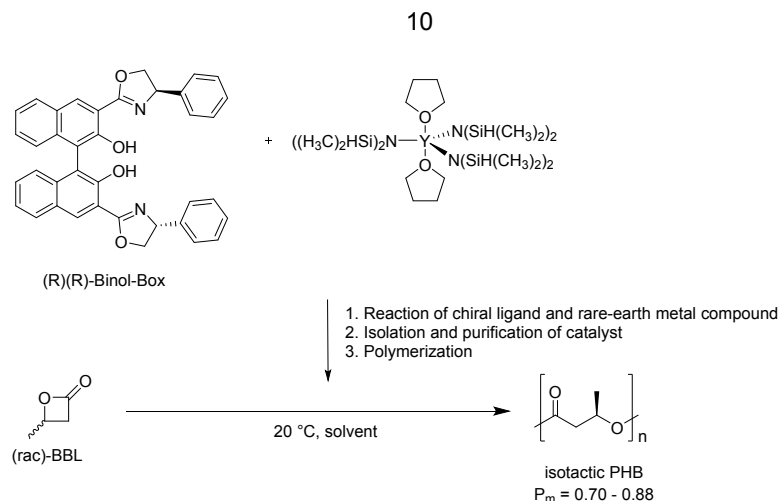


20

Without being bound by theory it is assumed that when contacting this type of rare earth metal compound with a chiral ligand some of the ligands are replaced by bonds to the chiral ligand, whereas some ligands remain which then provide for the catalytic activity for polymerization.

25

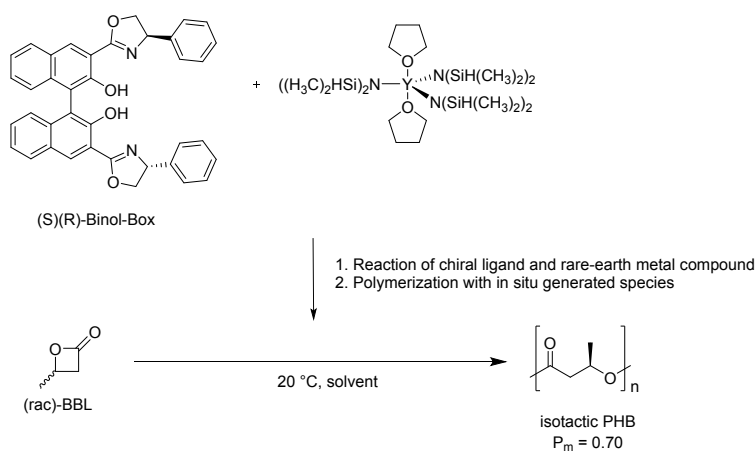
Tuning Material Properties of Poly(3-hydroxybutyrate): Isospecific Ring-Opening Polymerization of β -Butyrolactone



The catalyst/initiator complex obtained allows to polymerize β -butyrolactone at room temperature (about 20°C) and yields isotactic PHB with a P_m between about 0.6 and about 0.9, such as 0.7 to about 0.88, depending on the reaction conditions, the used solvents and the chirality of the chiral ligand with some imperfections.

It is assumed that when contacting the chiral ligand with a rare earth metal compound like the yttrium compound shown above, the core atom associates with the two hydroxy groups of the binaphthyl and with the two nitrogen atoms of the oxazole rings. This complex can be isolated by washing with an apolar solvent like pentane or diethylether. The catalyst/initiator system is very active and results in a high polymerization rate.

The catalyst/initiator complex can also be used without isolation as can be seen in scheme 2:

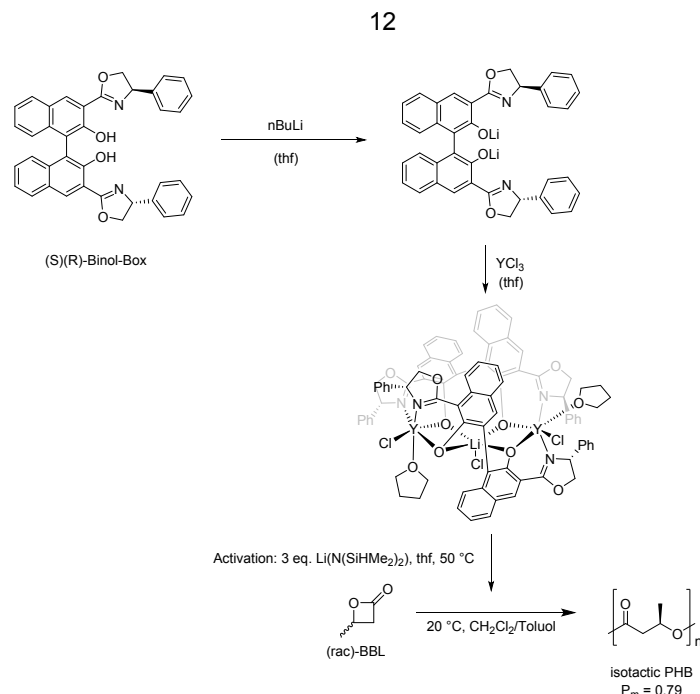


The reaction is carried out in a solvent like THF, 1,4-dioxane, diethylether or another solvent. The reactants are reacted at room temperature for some time, the reaction time is not critical, it can be a few minutes up to an hour, for example 10 to 40 minutes, but also longer, such as overnight. If an in situ catalyst/initiator system is used the reagents can be
5 reacted for some minutes up to a day or more, such as 0.5 to 24 hours or 1 to 12 hours, for example overnight.

As an example the active catalyst/initiator system is prepared in situ, the reaction mixture comprising the catalyst/initiator complex is used directly for polymerization of β -
10 butyrolactone. The polymerization can be carried out at room temperature (about 20°C). PHB is obtained with an isotacticity/ P_m of 0.70. Thus, when using an isolated catalyst/initiator complex the number of imperfections is lower than when using catalyst/initiator complex without isolation. This shows that one measure to control isotacticity of the polymer is to control the purity of the catalyst/initiator complex – the higher
15 the purity of the catalyst/initiator complex the lower the amount of imperfections and the higher the isotacticity.

In another embodiment the active catalyst/initiator system is prepared by deprotonating a chiral ligand of formula I and reacting it with a rare earth metal compound like yttrium
20 chloride as rare earth metal compound in the presence of an oxygen containing solvent which can serve as a solvent ligand R^y . Thereafter, the complex obtained is reacted with a co-catalyst and subsequently polymerization is performed as can be seen in Scheme 3

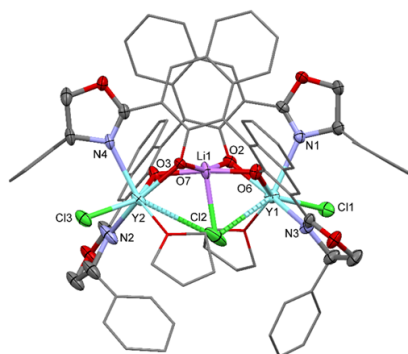
Tuning Material Properties of Poly(3-hydroxybutyrate): Isospecific Ring-Opening Polymerization of β -Butyrolactone



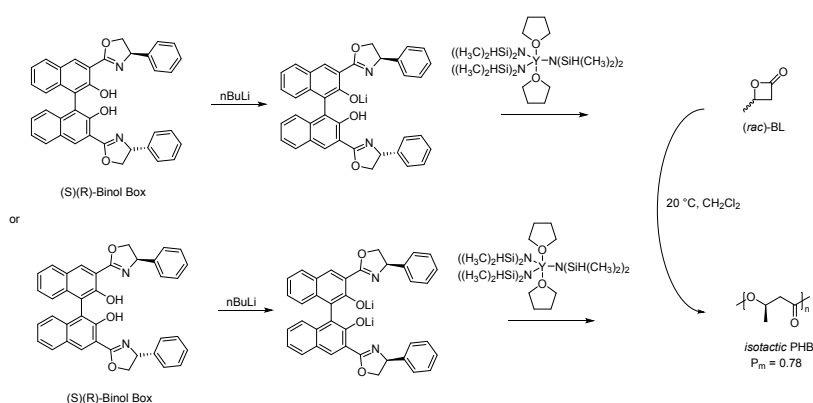
In this case the chiral ligand is activated by a deprotonating agent like $n\text{BuLi}$ and, thus, makes available the binding sites for the rare earth metal. Furthermore, the rare earth metal compound is added as rare earth metal salt, such as halogenide. After isolation the compound is activated with co-catalyst lithium bis(dimethyl)silyl amide (LIBDSA) to provide at least one nucleophilic ligand. The catalyst/initiator complex obtained is used for polymerization, it is active at room temperature and yields PHB with high isotacticity of 0.79. It has been found that the use of a co-catalyst reduces the number of imperfections and increases the degree of isotacticity. At the same time polymerization speed is reduced.

10

Without being bound by theory the structure of one embodiment of a catalyst/initiator complex of the present invention can be depicted as follows:



A further embodiment is shown in Scheme 4, where a deprotonating agent is used to deprotonate the OH groups of the chiral ligand and the activated chiral ligand then is reacted with a rare earth metal compound of formula II to form a catalyst/initiator complex of the present invention. This catalyst/initiator complex can be isolated by using a solvent like pentane. It is also possible to use the reaction mixture without isolation.



The catalyst/initiator system of the present invention that can be obtained as outlined above provides for stereospecific polymerization because of its structural composition. The catalyst/initiator system of the present invention comprises as essential part a chiral ligand, a 1,1'-binaphthol based ligand which is referred to as chiral ligand. As outlined before, this ligand has at least two chiral centers, the chirality of the binaphthol, and the position of the two substituents R^2 . Thus, the chiral ligand can be in (R)(R)-, (S)(R)-, (R)(S)- and (S)(S)- form. This form has an influence on the microstructure which is obtained for the polymer. It is easy to find out which monomer is preferred by a chosen catalyst/initiator complex by some routine tests.

For preparing the catalyst/initiator system of the present invention either the components can be reacted separately, isolated and then used in isolated form or the components can be mixed and the mixture can be used as it is without isolation.

It has been found that the purer the catalyst system is, the more selective it is, i.e. the higher the amount of isotacticity is. With the isolated catalyst/initiator system an isotacticity rate of up to about 0.9, such as 0.88 can be obtained. Thus, the degree of isotacticity can be controlled by using an isolated versus an in situ catalyst/initiator complex.

Critical for the catalyst/initiator system of the present invention is that it comprises a chiral ligand, a rare earth metal atom as core or catalytic atom, at least one nucleophilic ligand

and at least one solvent ligand which can be exchanged for a monomer for the polymerization reaction.

The catalyst/initiator system of the present invention selectively polymerizes one
5 enantiomer of β -butyrolactone, either (R)- β -butyrolactone or (S)- β -butyrolactone, with some imperfections, which is desirable.

The polymerization reaction takes place in solution. The β -butyrolactone can be used as solvent or a solvent that can dissolve the reactants can be used. Examples for useful
10 solvents are toluene, THF, 1,4-dioxane and diethylether. It is also possible to run the polymerization without a solvent because the monomer, i.e. β -butyrolactone, can serve as solvent itself. As, however, the system becomes more viscous when the polymer chains become longer, a solvent is advisable if high molecular weights are considered.

15 It was found that the slower the polymerization reaction is the more exact the monomers are added to the polymer chain so that the isotacticity becomes higher. On the other hand, when speed is increased, for example by increasing the temperature of the reaction the polymerization rate becomes faster and the number of imperfections increases. In this case isotacticity decreases.

20

Furthermore, it was found that the solvent ligand of the catalyst/initiator complex or, in case of an in situ catalyst/initiator complex, the solvent used, has an influence on isotacticity. Without being bound by theory it is assumed that this is due to the fact that the solvent ligand in the catalyst/initiator system has an influence on the type of monomers that is taken
25 up and added to the polymer chain. In this regard it was found that dichloromethane is a good solvent to obtain an isotacticity in the desired range, i.e. 60 to 80% isotacticity. Toluene is a solvent which increases the speed of polymerization. The solubility is not as high as with dichloromethane so that polymer chains precipitate when they become too long. Therefore, toluene can be used as solvent if polymers with a medium to low molecular
30 weight are desired. Furthermore, THF is a solvent that coordinates very well with the rare earth metal and can be added as ligand. Thereby, catalyst activity and polymerization speed can be decreased, which has an influence on isotacticity, it is lower.

Any factor, that has an influence on the the polymerization rate can also influence
35 isotacticity. Therefore, the ratio of monomer and catalyst can also influence isotacticity.

By controlling the isotacticity of the polymer built with the catalyst/initiator system of the present invention and by controlling the number of imperfections, it is possible to fine tune

the properties of the polymer that is obtained. Thereby the mechanical properties of the polymer can be optimized. By selecting the temperature, the solvent, the configuration of the chiral ligand and the ligands of the rare earth metal based catalyst it is possible to produce PHBs with different microstructures. This is particularly valuable.

5

Another aspect of the present invention are polymers that have been obtained with a method as described. These polymers are superior to known polymers as they have a high enough isotacticity to be biodegradable but have a controllable number of imperfections to allow for superior mechanical properties. A desirable range of isotacticity is 50 to 90%,
10 preferably 55 to 85 %, and in particular 60 to 80%.

The polymers obtained with the method of the present invention have been analyzed with methods as described in the following. To find the best suited catalyst/initiator system for a specific polymer experiments can be carried out as is explained in detail below.

15

NMR kinetic experiments can be carried out to determine catalyst activities as is known to the skilled person. For this purpose, conversions from NMR values are recorded in a conversion or turnover per time diagram. From the conversion rates it can be seen that either the S-monomer or the R-monomer is consumed as about 50% of the monomer is
20 consumed and about 50% of the monomer remain, this shows that only one of the enantiomers of the β -butyrolactone has been consumed, by analyzing which of both enantiomers remains in solution it can be analyzed which preference the system has. Fig. 1 shows a conversion per time diagram for racemic β -butyrolactone using a catalyst/initiator system as described in detail with reference to the schemes. From the curve it can be seen
25 that only one enantiomer was converted. To determine if a system is specific for R- or S-monomer, experiments with either R-monomer or S-monomer can be conducted.

Isotacticity is analyzed as is known in the art. ^{13}C -NMR-spectroscopy can be used to determine the microstructure of the polymer obtained with a process of the present
30 invention. For analysis it is possible to either evaluate the carbonyl signal at 169 ppm (see Fig. 2a) or the methylene signal at 40 ppm (see Figs. 2b-d). The ratio between the isotactic part of the polymer (mm and rm) and the syndiotactic part (rr and mr) has been evaluated.. Evaluated is the probability for meso-connections (P_m -value; meso = two adjacent centers having the same orientation). Fig. 2 shows some spectra of PHB examples in deuterated
35 chloroform with different isotacticity ratios from 0.70 to 0.88.

The thermal properties of the polymer can be evaluated by DSC determination. It is the object of the present invention to provide polymers having a lower melt temperature than

the isotactic PHBs known in the art. Fig. 3 shows the DSC diagram for a PHB example that has been obtained using the process of the present invention. It can be seen that the melting temperature T_m is 166°C and, thus, lower than the melting point of known polymers.

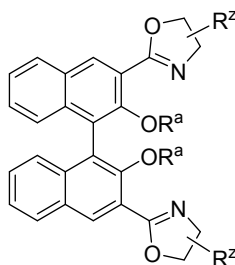
- 5 For molecular weight determinations, GPC analysis can be used as is known in the art, For polymers produced with the catalyst/initiator system of the present invention GPC analysis was carried out on a Polymer Laboratories GPC50 Plus chromatograph. As eluent, chloroform was used. Polystyrene standards were used for calibration.

- 10 It was found that the polymers obtained with a process of the present invention have very valuable properties. The mechanical properties are similar to those of petroleum based polymers like isotactic polypropylene and, therefore, can be used for similar applications, such as packaging. PHB polymers of the state of the art have a melting point which is close to the decomposition point, processability of these polymers is restricted. In contrast thereto
15 the polymers obtained with the process of the present invention have a much better processability because their melting point is lower. Furthermore it has been found that when using the process of the present invention polymers are obtained which have a higher tensile strength than those isotactic PHBs known from the prior art. Thus, with the process of the present invention it is possible to improve the mechanical properties of PHB
20 polymers. As those polymers have only some imperfections but otherwise are highly isotactic, they have a high biodegradability and can be used as biodegradable polymers. Furthermore, it has been found that other useful properties like barrier properties are maintained with the polymers of the present invention.

- 25 In summary the present invention provides a process for obtaining very valuable polymers with predeterminable parameters.

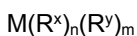
Claims

1. A process for polymerizing β -butyrolactone comprising contacting racemic β -butyrolactone or an enantiomer thereof with a catalyst/initiator system which comprises a rare earth metal, a chiral ligand, at least one nucleophilic ligand, at least one solvent ligand, and optionally an alkali based co-catalyst, wherein the chiral ligand is an enantiomer of a unit of formula I



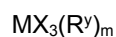
- 10 wherein each R^z independently is linear or branched, substituted or unsubstituted C_1 - C_{20} alkyl, substituted or unsubstituted C_6 - C_{20} aryl, substituted or unsubstituted C_5 - C_{20} heteroaryl, or halogen;
wherein each R^a independently is H or an alkali metal.

- 15 2. The process of claim 1 wherein the catalyst/initiator system is a rare earth metal based complex which has been obtained by contacting a chiral ligand of formula I with a compound of formula II:



- 20 and optionally an alkali based co-catalyst,
wherein M is a rare earth metal,
each R^x independently is a nucleophilic ligand,
each R^y independently is a solvent ligand,
n is an integer from 1-5,
m is an integer from 0-5 with the proviso that $n + m$ is an integer corresponding to the
25 number of available association/bonding sites of the rare earth metal.

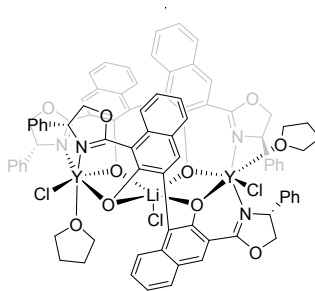
3. The process of claim 1, wherein the catalyst/initiator system is a rare earth metal based complex which has been obtained by contacting a chiral ligand of formula I with a rare earth metal compound of formula III, a solvent, and optionally an alkali based
30 co-catalyst,
wherein the earth metal based compound is a compound of formula III



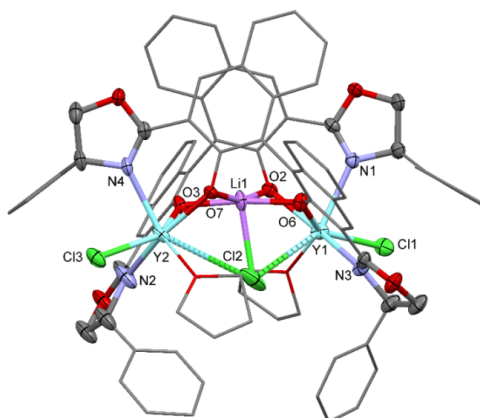
- wherein M is a rare earth metal,
each X independently is halogenide, triflate, or C₁-C₂₀ alkoxide;
each R^y independently is a solvent ligand,
m is an integer from 0-5 and
- 5 contacting the complex obtained with an alkali salt of a nucleophilic ligand.
4. The process of one of the preceding claims wherein the catalyst/initiator system is prepared in situ.
- 10 5. The process of one of claims 1-3 wherein the catalyst/initiator system is isolated from the reaction mixture and added to a monomer composition comprising β -butyrolactone.
6. The process of one of the preceding claims wherein the rare earth metal is yttrium,
15 lutetium, scandium, ytterbium, terbium, samarium, lanthanum or a lanthanide, wherein optionally the rare earth metal is yttrium.
7. The process of one of the preceding claims wherein n is 1-3 and m is 1-3.
- 20 8. The process of one of the preceding claims wherein the monomer is racemic β -butyrolactone.
9. The process of one of the preceding claims wherein the nucleophilic ligand is an amido group, an alkoxide or a di- or trialkyl methyl-silyl group, preferably a group
25 selected from NR^bR^cR^d, OR^b and CHR^bR^c, wherein each of R^b, R^c, and R^d independently is H or a group selected from linear or branched, substituted or unsubstituted C₁-C₂₀ alkyl, C₆-C₂₀ aryl, arylalkyl, silylalkyl.
10. The process of one of the preceding claims wherein at least one nucleophilic ligand is
30 n N(SiHMe₂)₂ group.
11. The process of one of the preceding claims wherein at least one solvent ligand is tetrahydrofuran.
- 35 12. The process of one of the preceding claims wherein the co-catalyst is a lithium salt (LiN(SiHMe₂)₂) or wherein the co-catalyst is a potassium salt (K(N(SiMe₃)₂).

19

13. The process of one of the preceding claims wherein the catalyst has one of the following formulae:



5



14. Polyhydroxybutyrate polymer obtained with a process of one of claims 1-13.
- 10 15. Polyhydroxybutyrate polymer of claim 14 having a P_m between 0.6 and 0.9.

9.5 Designation of inventor

Form 1002 - 1: Public inventor(s)

Designation of inventor

User reference: ETU171201PEP
Application No:

Public

Inventor	Name: ADAMS Friederike Address: [REDACTED] Germany The applicant has acquired the right to the European patent: Under agreement:
Inventor	Name: RIEGER Bernhard Address: [REDACTED] Germany The applicant has acquired the right to the European patent: Under agreement:

Signature(s)

Place:
Date: **23 December 2017**
Signed by: **Gabriele Leissler-Gerstl 13242**
Representative name: **Gabriele Leißler-Gerstl**
Capacity: **(Representative)**

10 Tuning Material Properties of Poly(3-hydroxybutyrate): Copolymerization with sustainable lactones

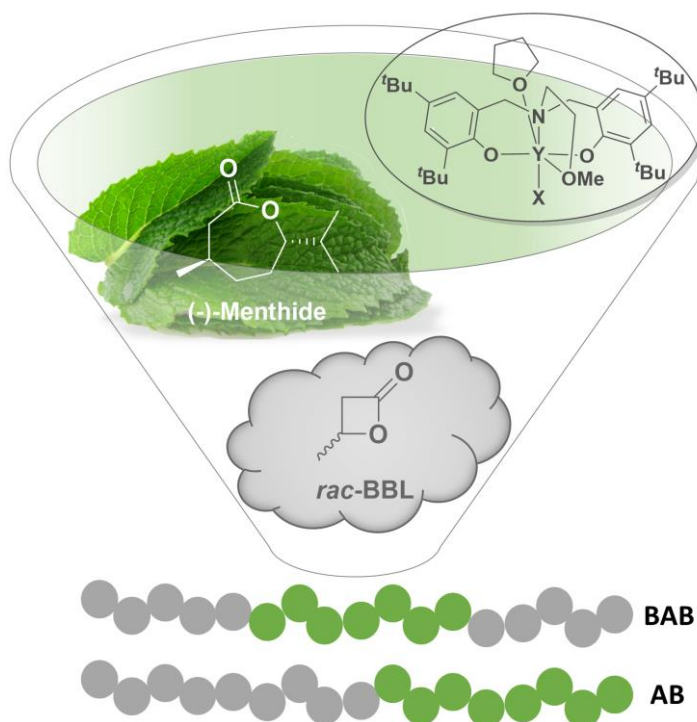
10.1 Bibliographic data

Title: “(Co)polymerization of (-)-Menthide and β -Butyrolactone catalyzed by Heteroaromatic Yttrium-bis(phenolates): Tuning Material Properties of Sustainable Polyesters”

Status: Full paper, In preparation

Authors: Friederike Adams, Thomas M. Pehl, Moritz Kränzlein, Sebastian A. Kernbichl, and Bernhard Rieger⁷

10.2 Abstract graphic (TOC)



⁷ F. Adams planned and executed all experiments and wrote the manuscript. T. M. Pehl, S. A. Kernbichl and M. Kränzlein helped with measurements and proofreading of the manuscript. All work was supervised by B. Rieger.

10.3 Content

The demand and production of plastics which derive from petrol-based chemicals is still increasing drastically. Therefore, the substitution of petrochemical-based plastics with polymers that are based on renewable resources is imperative. Poly(hydroxyalkanoates) are a promising class of biocompatible polymers, while poly(3-hydroxybutyrate) represents one of the most commonly used PHA. Besides naturally occurring *isotactic* PHB, a well-known synthesis route is the ring-opening polymerization of *racemic* β -butyrolactone. As *rac*-BBL is synthetically available from carbon dioxide, it is a promising monomer for PHB production. However, despite the high internal strain of the four-membered ring, BBL is instead a reluctant monomer, as it is less reactive than lactide or ϵ -caprolactone. According to studies of *Carpentier et al.*, stereoselective bis(phenolate)yttrium catalysts are a class of complexes that perform fast ROP of BBL to obtain semicrystalline *syndiotactic* PHB. In this manuscript, heteroaromatic pyridine-based initiators attached to bis(phenolate)yttrium complexes are proven as efficient catalysts for syndiospecific BBL polymerization. Especially, a bimetallic aminoalkoxy-bis(phenolate)yttrium complex with a bifunctional tetramethylpyrazine initiator showed his high potential in ROP which opened the pathway to BAB polymers *via* chain-growth in two directions. These BAB block copolymers were used to modulate the stress-strain properties of PHB, which is often brittle and hard to process, by combining it with a soft amorphous polyester. (-)-menthone, which derives from the plant mint, can be converted to the corresponding lactone (-)-menthide. Herein, the first lanthanide-based catalysts are reported that can polymerize (-)-menthide to amorphous poly((-)-menthide) under mild conditions with very low molar mass distributions. On basis of these two polyesters, we produced AB and BAB block copolymers using poly((-)-menthide) as the first block (A) and *syndiotactic* PHB as the second one *via* simple sequential addition in a one-pot reaction. For the AB-polymers a bis(phenolate) complex with a bis(dimethylsilyl)amide initiator was used. Block copolymer formation was verified by GPC- and ^1H nmr analysis and *via* DOSY nmr spectroscopy by comparison the block copolymers to a blend from PHB and PM. DSC, TGA, XRD and stress-strain measurements were used to study the influence of different composition and molar masses on the mechanical and thermal properties of the block copolymers. Two glass transition temperatures, obtained using DSC analysis, strongly indicate a microphase separation of PHB and PM on molecular scale, which was further supported by XRD measurements. In scope of application of these sustainable polyesters, hot-molding was performed, which offers an advantage compared to *isotactic* PHB from natural sources. The specimens were analyzed in stress-strain measurements. The *syndiotactic* PHB is less brittle than *isotactic* PHB resulting in a lower *Young's*-modulus. Incorporating PM in the structure, the elastic modulus is further lowered with increasing the elongation at break.

10.4 Manuscript Draft

(Co)polymerization of (-)-Menthide and β -Butyrolactone catalyzed by Heteroaromatic Yttrium-bis(phenolates): Tuning Material Properties of Sustainable Polyesters

Friederike Adams,^[a] Thomas M. Pehl,^[a] Moritz Kränzlein,^[a] Sebastian A. Kernbichl,^[a] and Bernhard Rieger*^[a]

[a] F. Adams, T. M. Pehl, M. Kränzlein, S. A. Kernbichl, Prof. Dr. Dr. h.c. B. Rieger

WACKER-Chair of Macromolecular Chemistry

Catalysis Research Center

Department of Chemistry

Technical University Munich

Lichtenbergstr. 4, 85748 Garching bei München (Germany)

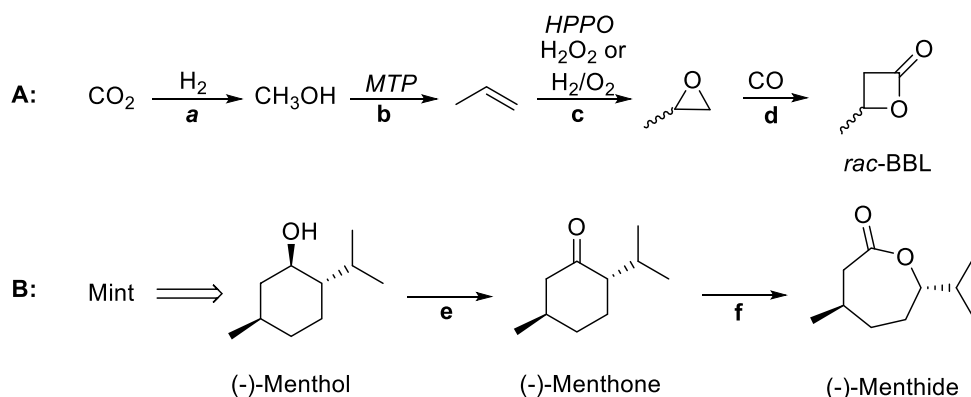
E-mail: rieger@tum.de

Abstract

By introducing three new pyridine-based heteroaromatic initiators to yttrium-bis(phenolate) complexes, efficient catalysts for ring-opening polymerization of *rac*-BBL and (-)-menthide were obtained. These catalysts produce poly(3-hydroxybutyrate) (PHB) and poly((-)-menthide) (PM) even at room temperature. For BBL, *syndiotactic* PHB is obtained which shows narrower molar mass distributions than PHB produced with similar nitrogen-containing initiators. (-)-Menthide can be polymerized with very narrow PDI under mild conditions. In addition, AB- and BAB-copolymers from PM (A) and PHB (B) were synthesized. Special interest is laid on the BAB-copolymer, which is accessible through introduction of a bifunctional pyrazine initiator to the yttrium-complexes, enabling chain growth in two directions. Block copolymers are analyzed using DSC, TGA, XRD, nmr and stress-strain measurements. These measurements confirmed a microphase separation within the semicrystalline BAB-materials. Regarding the mechanical behavior, two hot-moldable PHB-based polymers – a homopolymer and a BAB-copolymer- with tunable elastic modulus were obtained.

Introduction

Nowadays, the growing limitation of raw materials rises to the challenge of having an economical handling of fossil resources. In addition, the demand and production of plastics which derive from petrol-based chemicals is still increasing drastically. Therefore, the substitution of petrochemical-based plastics with polymers that are based on renewable resources is imperative. Polyesters built up the fourth largest group of natural biomacromolecules, following the three major groups nucleic acids, proteins and polysaccharides.^[1] This class provides us with important polymers such as poly(ethylene terephthalate).^[1] In addition, poly(hydroxyalkanoate)s (PHA) are a well-known class of polyesters, in which poly(3-hydroxybutyrate) (PHB) is one of the most commonly used PHA. When it is synthesized naturally *via* microorganisms, it serves as an intracellular carbon and energy storage compound in the cell cytoplasm and is biodegradable.^[2-4] Therefore, PHB is a conceivable alternative for petrochemical polymers. However, the application is limited because of its low thermostability and high crystallinity which makes it brittle and hard to process.^[5] This drawback provoked an increasing research to produce PHB with various microstructures from small molecules. A potential chemical synthesis route is thereby the ring-opening polymerization (ROP) of *racemic* β -butyrolactone (BBL). As BBL can be produced from carbon dioxide *via* industrial relevant reactions, it is an interesting monomer for sustainable PHB production (Scheme 1A).^[6-12]



Scheme 1: A. Synthesis of *rac*-BBL: a) Catalytic Hydrogenative Conversion of Carbon Dioxide to Methanol^[6]; b) Methanol-to-Propylene(MTP)-Process^[27]; c) Epoxidation of propylene (e.g. HPPO-process)^[7-10]; d) Ring expansion of propylene oxide^[11-12]. B. Synthesis of (-)-Menthide: e) Oxidation of (-)-Menthol^[28]; f) Baeyer-Villiger-Oxidation^[29-30]

Despite the high internal strain of the four-membered ring, BBL is instead a reluctant monomer, as it is less reactive than lactide or ϵ -caprolactone.^[13-14] Therefore, it is hard to polymerize and only a small class of main-group,^[15-16] transition (e.g. zinc)^[17-19] and rare-earth complexes are able to perform these

reactions. Special emphasize was given to the rare-earth metal (REM) catalyzed ROP as these REM-complexes are a promising class of catalysts in matters of activity and stereospecificity.^[20-21] Compared to other catalyst systems, in particular yttrium complexes supported by single-site dianionic aminoalkoxy-bis(phenolate) ligands provide the opportunity of a rapid and controlled ROP resulting in high-molecular-weight PHB under mild conditions.^[20-26] According to studies of *Carpentier et al.*, stereoselective aminoalkoxy-bis(phenolate)yttrium amido catalysts **1** ((ONOO)^{tBu}Y(N(SiHMe₂)₂)(thf)) in which ONOO^{tBu} = 6,6'-(((2-methoxyethyl)azane-diyl)-bis(methylene))-bis(2,4-di-*tert*-butylphenolate)) can be used for syndiospecific ROP of *rac*-BBL.^[22] To our knowledge, besides often used bis(di- or trimethylsilyl)amide (bdsa, btsa), trimethylsilyl and *iso*-propanol initiators,^[22-24, 31-36] further efficient initiators were not investigated in REM-mediated ROP of *rac*-BBL.

Besides ring-opening polymerization, *Rieger et al.* established isostructural bis(phenolate) complexes **2-4** with heteroaromatic initiators as multifunctional catalysts in REM-mediated group-transfer polymerization (GTP) of different *Michael*-type vinyl monomers.^[37-39] As heteroaromatic initiators, that coordinate to the yttrium center *via* η^3 -(C,C,N)-*aza*-allylic binding, are not yet known for initiating ring-opening polymerization, herein, these complexes are established as efficient initiators for syndiospecific BBL-polymerization (Scheme 2). Under tension, highly *isotactic* and *syndiotactic* PHB has a high *Young's* modulus and fractures at very low strains, and is therefore unsuitable for use in numerous applications where elasticity is necessary.^[5] Modulation of the stress-strain properties can be reached by incorporation of PHB into block copolymers, which still remain rare in literature. They are restricted to oligomeric forms or commercially available natural PHB as macroinitiators for different polymerization-types (e.g. radical or thermal) in which modifications prior to polymerization are necessary. In addition, hot molding is not possible, because the melting point is near the dissociation temperature. Furthermore, amorphous PHB was used in combination with lactide, β -malolactone, or epoxides and carbon dioxide.^[40-48] Block copolymers with semicrystalline, *syndiotactic* PHB are not yet accessible or published.

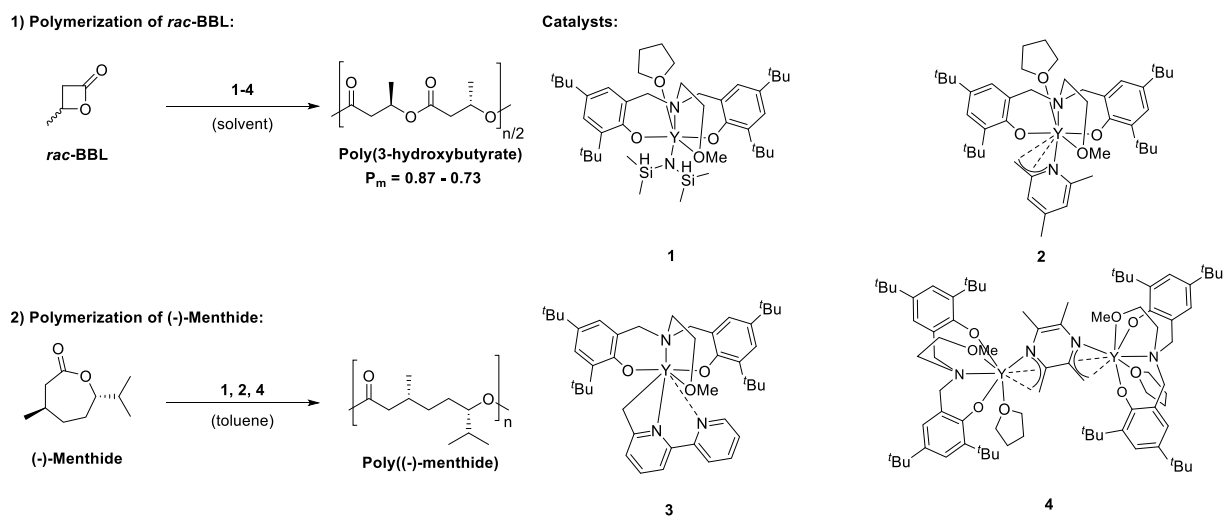
Beyond carbon dioxide, various natural products can be used for the preparation of biobased polymers. An important class among these are terpenes. The naturally occurring, cyclic representatives such as (-)-menthone can be converted to the corresponding lactones, which can be used as monomers for ring-opening polymerization (Scheme 1B). As a result, cyclic terpenes offer the possibility to produce polymers from renewable raw materials.^[29, 49-51] (-)-Menthide derives from the monoterpeneic alcohol (-)-menthol, which is extracted from plants of the genus *Mentha* (mint).^[52] In 1958, *Hall* and *Schneider* first performed polymerization of (-)-menthide with sodium as catalyst. Since then, only very little research was performed on (-)-menthide.^[53] Only since 2005, the groups of *Tolman* and *Hillmyer* used

zinc- and tin-species for menthane-polymerization.^[29-30, 54] Since then, poly((-)-menthane) (PM) has been the subject for the production of thermoplastic elastomers in combination with lactide, γ -methyl- α -methylene- γ -butyrolactone or Tulipalin A (α -methylene- γ -butyrolactone).^[30, 54-57] To obtain thermoplastic elastomers BAB block copolymers are necessary in which a “hard” *semi* crystalline B-segment (high T_g) is combined with a “soft” amorphous A-segment (low T_g). As both segments are immiscible, microphase separation occurs providing the desired combination of elastic and thermoplastic properties. Herein, the first lanthanide-based catalysts **1**, **2** and **4** are reported that are able to polymerize (-)-menthane to poly((-)-menthane) under mild conditions with low molar mass distributions (Scheme 2). To modulate the stress-strain properties of PHB, AB- and BAB-block copolymers, are developed in a one-pot reaction with the respective catalysts, (-)-menthane (block A) and *rac*-BBL (block B). As the BAB blockcopolymer are in detail B-A-X-A-B-systems (X = initiator, A = PM, B = PHB), the bifunctional tetramethylpyrazine initiator of catalyst **4** was used to obtain chain-growth in two directions. For the AB-polymers catalyst **1** was used. Block copolymer formation was verified by GPC-, ¹H nmr-analysis and via DOSY nmr-spectroscopy by comparison to a blend from PHB and PM. DSC, TGA, SAXS, powder-XRD and stress-strain measurements were used to study the mechanical and thermal properties of the block copolymers.

Results and Discussion

Polymerization of *rac*-BBL

Catalysts **2-4** were employed in ROP of *rac*-BBL to evaluate the general activities and initiator efficiencies of the catalysts, and the microstructures of the isolated PHB. These were then compared to the ones of complex **1**, which is known from literature, and also bears a nitrogen-atom in its initiator. It is therefore the complex with the highest similarity to **2-4**. $[(\text{ONOO})^{\text{tBu}}\text{Y}(\text{bdsa})(\text{thf})]$ (**1**) is accessible in good yield through a procedure from literature by reacting an yttrium-bdsa-precursor $[\text{Y}(\text{N}(\text{SiHMe}_2)_2)_3(\text{thf})_2]$ with one equivalent of the ligand $\text{H}_2(\text{ONOO})^{\text{tBu}}$ at room temperature.^[58-59] Catalysts **2-4** were synthesized *via* C-H-bond activation of the respective heteroaromatics (**2** = 2,4,6-trimethylpyridine (*sym*-collidine); **3** = 6-methyl-2,2'-bipyridine (6-Mebpy), **4** = 2,3,5,6-tetramethylpyrazine (TMPy)) with $[(\text{ONOO})^{\text{tBu}}\text{Y}(\text{CH}_2\text{TMS})(\text{thf})]$ (TMS = trimethylsilyl) in moderate to good yields.^[37-39] In case of complex **4**, a bimetallic complex is obtained in which the activated tetramethylpyrazine serves as a bifunctional initiator. All other complexes exist as monometallic ones with the general structures $[(\text{ONOO})^{\text{tBu}}\text{Y}(\text{sym-collidine})(\text{thf})]$ (**2**) and $[(\text{ONOO})^{\text{tBu}}\text{Y}(6\text{-Mebpy})]$ (**3**) (Scheme 2).



Scheme 2: Left) 1) Polymerization of *rac*-BBL to poly(3-hydroxybutyrate) with catalysts 1-4. 2) Polymerization of (-)-menthido to poly((-)-menthido) with catalysts 1, 2, and 4. Right) Catalysts 1-4 that are used in ROP of *rac*-BBL and menthido and that differ in their nucleophilic initiator.

First, the initiation mechanisms of the C-H bond-activated complexes was elucidated *via* end-group analysis of oligomeric BBL. ESI-MS analysis was performed by reacting catalyst 4 with 13 equivalents of *rac*-BBL in toluene and immediate measurement in acetonitrile. Complex 4 was chosen as the attachment of the bifunctional tetramethylpyrazine initiator to the polymer chain is mandatory for chain-growth in two directions, enabling BAB-blockcopolymers. In addition, previous ESI-MS studies with catalyst 1 showed the absence of bis(dimethylsilyl)amine-end-groups at the polymer chains, probably due to ESI-MS fragmentation reactions.^[26] By using catalyst 4, elimination of the initiator is not possible, as it is embedded in the middle of the polymer chain. Signals of the oligomers corresponding to $M_{\text{initiator}} + n \times M_{\text{BBL}} + \text{Na}^+$ as charge carrier or with an olefinic end-group (crotonate) due to ESI-MS fragmentation (*McLafferty* rearrangement^[60]) were observed (Figure 1, left). The initiating groups were clearly visible in the ESI-MS; a nucleophilic transfer reaction of the initiator *via* monomer insertion into the Y-C bond (attack of the nucleophilic initiator to the carbonyl of the lactone) is apparent.

To investigate the relative activities of the catalysts among each other, the polymerization of BBL was conducted in an autoclave with *in situ* IR monitoring. A concentration of $[\text{BBL}] = 2.49 \text{ mmol/mL}$ and a ratio of $[\text{BBL}]/[\text{cat}] = 600$ in 6 mL of dichloromethane were chosen as parameters to prevent precipitation of the polymer. Conversions were then calculated *via* ^1H nmr spectroscopy before quenching the reaction with dichloromethane and precipitation of the polymer from methanol.

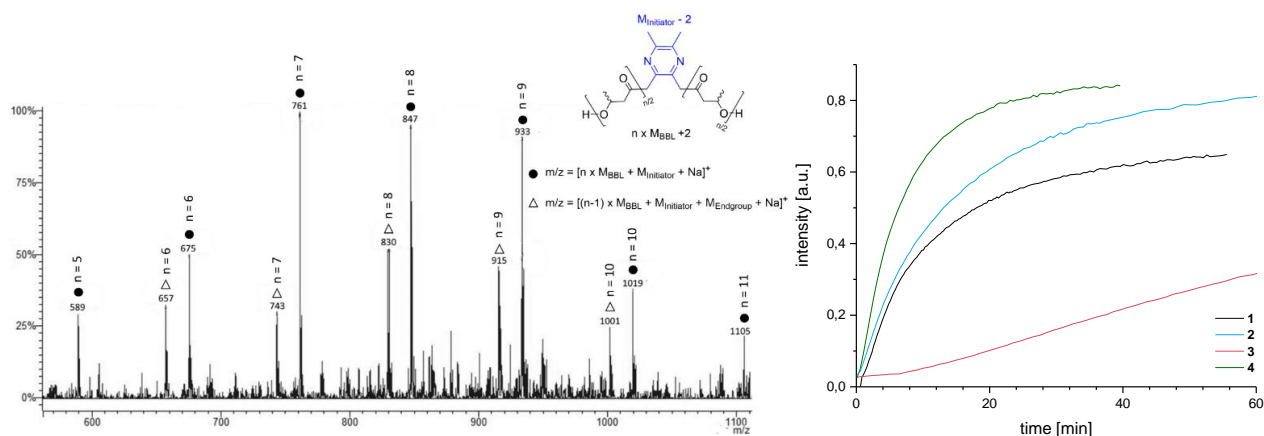


Figure 1: Left) End-group analysis via ESI-MS measured in acetonitrile with catalyst **4** and *rac*-BBL (7 μmol of catalyst, 93 μmol *rac*-BBL, 0.5 ml toluene, 20 $^{\circ}\text{C}$). Right) Polymerization of BBL with catalysts **1-4** (conditions: see Table 1) monitored by *in situ* IR spectroscopy ($\nu_{\text{C}=\text{O}}$, PHB = 1750 cm^{-1}).

Molecular weights and weight distributions were measured by gel-permeation chromatography (GPC) in chloroform relative to polystyrene standards. Catalysts **1** is already known from literature to polymerize BBL, but was also tested in BBL-polymerization for comparison reasons. All catalysts were active in ROP of *rac*-BBL, however *in situ* IR measurements reveal a higher activity of catalysts **2** and **4** in comparison to complex **1**, due to a higher increase of the carbonyl-stretching bond of the built PHB ($\nu_{\text{C}=\text{O}} = 1750 \text{ cm}^{-1}$) with time (Figure 1, right). Since the activity is determined in the propagation step and is solely influenced by the metal center and the ligand, which are identical in all complexes, the higher “activity” in these measurements correlates with a higher initiator efficiency of the complexes. In case of catalyst **4**, a higher activity is expected as chain growth in two directions with two catalytic centers is possible. The molar masses of PHB produced with catalyst **1** are in accordance with polymerization results from literature under similar conditions (toluene instead of dichloromethane), but in no event we could reach full conversion (Table 1, Entry 1).^[23] These findings, in addition with a broader molar mass distribution, were also observed in previous studies with complex **1** during polymerizations of *rac*-BBL.^[26] All other heteroaromatic complexes, even the bimetallic one, produced PHB with lower polydispersities (Table 1, Entries 2-4). But by comparison of the three novel complexes for ROP, bimetallic **4** showed the highest \bar{D} due to chain growth in two directions. Nevertheless, it was the only catalyst which could reach nearly full conversion. As the initiator efficiency of this complex was the highest, it produced PHB with the lowest molar mass due to a higher accordance between calculated and observed molar mass. As the activity/initiator efficiency of complex **3** was drastically lower than the ones of all other complexes, it was not further investigated in this contribution. The absence of thf as coordinating solvent in **3** might be decisive for the low initiator efficiency, as the thf molecule exchanges with the first BBL-molecules in the initial step of the initiation process. The

tacticity of the investigated PHBs is determined with help of the carbonyl carbon signal in the ^{13}C nmr spectrum of the polymers. In all cases, *syndiotactic* PHB with tacticities between 84 – 87% is obtained when performing polymerizations with catalysts **1-4** in dichloromethane at room temperature.

Table 1: Results of BBL-polymerization performed with catalysts **1-4** in an autoclave with *in situ* IR monitoring.^a

Entry	Catalyst	Time [min]	Conversion [%] ^b	$M_{n,\text{GPC}}$ [$\times 10^3$ g/mol] ^c	Đ^d	P_r^e
1	1	56	72	66.1	1.86	0.84
2	2	73	84	91.9	1.64	0.84
3	3	305	66	68.9	1.42	0.87
4	4	39	98	52.8	1.75	0.85

^a Reactions performed with $[\text{BBL}] = 14.9$ mmol; $[\text{Cat}]/[\text{BBL}] = 1/600$, at 25 °C in 6 mL dichloromethane. ^b Conversion determined *via* ^1H nmr spectroscopy (integration of methyl group resonance of BBL and PHB) ^c $M_{n,\text{GPC}}$ measured *via* GPC in chloroform as eluent at room temperature relative to polystyrene standards. ^d Polydispersity calculated from $M_{w,\text{GPC}}/M_{n,\text{GPC}}$ as determined by GPC ^e P_r is the probability of *racemic*-linkages between monomer units and was determined by ^{13}C nmr spectroscopy from the carbonyl region.

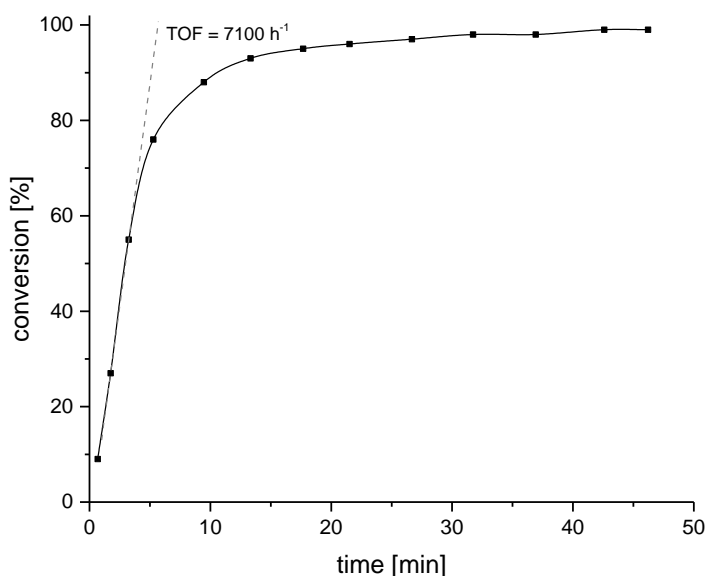


Figure 2: Catalytic activity of catalyst **4** ($[\text{BBL}] = 14.9$ mmol; $[\text{Cat}]/[\text{BBL}] = 1/600$, at 25 °C in 6 mL dichloromethane) measured *via* aliquot method.

To numeralize the relative activities measured by *in situ* IR spectroscopy, aliquots of the polymerization with the fastest catalyst **4** were taken at regular time intervals and quenched by addition to CDCl₃ (same conditions as stated in Table 1). Conversions were measured *via* ¹H nmr spectroscopy and plotted against time, to determine the activity (Figure 2). Due to the high initiator efficiency, a turn-over frequency (TOF) of 7100 h⁻¹ was calculated, which is higher in comparison to TOFs determined for previous investigated lanthanide bis(phenolate)amide complexes.^[26]

As known from the literature, the solvent can have a major effect on the activity and stereospecificity of the catalysts, therefore, polymerizations were also conducted in toluene (Table 2). A concentration of BBL with [BBL] = 2.49 mmol/mL and a ratio of [BBL]/[Y] = 200 were chosen as parameters as these were shown to be the best ones in literature.^[22] Comparing the catalysts **1**, **2** and **4** with respect to their influence on the polymerization, same trends as for polymerization in dichloromethane are observable. Full conversion is only reached with catalyst **4** after a short period of time (Table 2, Entry 7). After the same time interval catalyst **2** only shows 75% conversion (Table 2, Entry 4). Almost complete reaction is achieved after a reaction time of about 10 minutes. Comparing the molecular weights of the synthesized polymers, much smaller molar masses are obtained when using catalyst **4** than using catalyst **1** or **2**, even though higher molar masses were calculated for catalyst **4** due to a higher conversion of *rac*-BBL. Thus, catalyst **4** has a much higher initiator efficiency among the observed catalysts with respect to the polymerization of *rac*-BBL. Comparing these results to Entries 6 and 8 with significantly longer reaction times, the average molecular weights decrease, whereas the polydispersities of the polymers increase. Side reactions, termination reactions and transesterifications might be the reason, which occur more frequently when high conversions are reached. This was also proven by plotting the molar masses versus conversions of the aliquots taken for the activity measurement. Polydispersities increased drastically with higher conversions (SI, Figure S36). Therefore, it was attempted to terminate the polymerizations quickly after reaching high conversions, to obtain polymers with high molecular weights and low molar mass distributions. Polymerizations of catalyst **1** and **4** were also conducted at elevated temperatures of 60 °C and 100 °C to examine the influence of temperature on the activity and the microstructure of the polymers. Catalyst **1** is still active at 100 °C (Table 2, Entry 2) and also catalyst **4** shows a high activity at 60 °C (Table 2, Entry 9). In case of catalyst **1**, elevated temperature polymerizations afforded polymers with lower average molecular weights and higher polydispersities compared to polymerizations at room-temperature. Also, in case of catalyst **4** the molar mass distribution is broader. In both cases, *syndiotactic* PHB with P_r = 0.73 is obtained which is slightly less *syndiotactic* than PHB prepared in toluene at room temperature (P_r up to 0.78). As both catalysts still show a high activity and sustain the semicrystallinity of the obtained PHB (Figure 4), elevated temperatures can be used for copolymerizations.

Table 2: Results of BBL polymerization performed with catalysts **1**, **2** and **4** in toluene.^a

Entry	Catalyst	Time [min]	Conversion [%] ^b	M _{n,calc} g/mol] ^c	[x10 ³ M _{n,GPC} g/mol] ^d	[x10 ³ Đ ^e	P _r ^f
1	1	21	81	13.7	24.2	1.98	0.77
2 ^g	1	8	68	12.1	16.9	2.51	0.73
3 ^{g,h}	1	15.75	59	20.3	31.7	1.85	0.74
4	2	6.5	75	12.0	28.3	1.36	0.77
5	2	9	91	14.7	31.5	1.76	n.d.
6	2	47	>99	16.3	23.2	1.91	n.d.
7	4	6.5	>99	15.1	15.0	1.56	0.78
8	4	101	>99	17.3	14.2	2.07	n.d.
9 ⁱ	4	6.5	98	16.8	15.1	1.72	0.73

^a Reactions performed with [BBL] = 4.98 mmol; [Cat]/[BBL] = 1/200, at 25 °C in 2 mL toluene except from entry 2,3 and 9. ^b Conversion determined *via* ¹H nmr spectroscopy (integration of methyl group resonance of BBL and PHB). ^c M_{n,calc} calculated from M_{n,calc} = M × (([M]/[Cat]) × conversion) ^d M_{n,GPC} measured *via* GPC in chloroform as eluent at room temperature relative to polystyrene standards. ^e Polydispersity calculated from M_{w,GPC}/M_{n,GPC} as determined by GPC ^f P_r is the probability of *racemic*-linkages between monomer units and was determined by ¹³C nmr spectroscopy from the carbonyl region ^g performed at 100°C ^h performed with 400 eq. of BBL in 4 mL toluene in double scale ⁱ performed at 60 °C.

Polymerization of (-)-menthide

In addition to the polymerization of *rac*-BBL, polymerizations of (-)-menthide were also performed with catalysts **1,2** and **4**. (-)-Menthide was synthesized in a *Baeyer-Villiger* oxidation from (-)-menthone according to literature with *meta*-chloroperbenzoic acid or Oxone®.^[30, 54] After twofold sublimation, the purity of the monomer was verified *via* nmr spectroscopy, elemental and GC-MS analysis (SI, Figure S2 and S3).

First, the initiation mechanism of the complexes was elucidated with catalyst **1** and **4** by end-group ESI-MS analysis of oligomeric (-)-menthide. 5 (cat. **1**) and 17 (cat. **4**) equivalents of menthide are reacted with the respective catalyst in toluene followed by immediate ESI-MS measurement in acetonitrile. Oligomers prepared with catalyst **4** show signals corresponding to $M_{\text{initiator}} + n \times M_{(-)\text{-menthide}}$ with either Na^+ or K^+ as charge carrier (SI, Figure S21). As the initiating groups are clearly visible in the ESI-MS; attack of the nucleophilic initiator to the carbonyl of the lactone is apparent, generating poly((-)-menthide) with the desired structure. In case of catalyst **1**, as expected, an absence of the bdsa-group at the oligomers is observed indicating that in the ESI-MS an olefinic end-group or a cyclic oligomer with either Na^+ or K^+ as charge carrier is formed due to elimination of the bdsa-group (SI, Figure S22).

Afterwards, catalysts **1** and **2** were tested in polymerizations of (-)-menthide with different monomer-to-catalyst ratios and different temperatures (Table 3, Entries 1-5). All polymerizations were conducted in toluene. Polymerizations in chloroform or dichloromethane showed insufficient activity of the catalysts. Absolute molecular weights and weight distributions were measured by gel-permeation chromatography (GPC) coupled with triple detection in tetrahydrofuran (thf) as solvent. The dn/dc was determined *via* GPC measurement of three samples with different concentrations of polymers with various molar masses. It was determined as 0.067 mL/g. Conversions were determined by ^1H nmr spectroscopy in CDCl_3 . The polymers were obtained by precipitation from methanol. ^1H nmr and ^{13}C nmr spectroscopy underlined the successful polymerization as all signals of the PM repeating units agree with those of PM reported in literature (SI, Figure S9 and S10).^[29] Compared to the polymerization of *rac*-BBL very long reaction times are necessary, however only low yields of 50 – 82 % are obtained. Especially, an increase in the monomer-to-catalyst ratio from 100 to 200 led to a drastic decrease in conversion even when higher temperatures (100 °C) are used. Even, a further increase in reaction time did not led to an increase in conversion (Table 3, Entry 3 and 4). To investigate, if full conversion is possible when using catalyst **1**, the kinetics of the polymerization of menthide were investigated by taking aliquots. The polymerization is carried out using 74.7 μmol of catalyst **1** and 100 or 200 eq. of (-)-menthide in toluene. At regular intervals samples were taken to calculate the conversion via ^1H nmr spectroscopy and molar masses by GPC measurements in chloroform. Plotting the conversion against time, a maximum conversion of 80% in case of using 100 eq. and 45% in case of using 200 eq. (-)-menthide is reached (SI, S37). The polymerization of (-)-menthide proceeds in a living fashion, as indicated by very narrow polydispersities ($1.01 \leq \text{Đ} \leq 1.12$) of all polymer samples when using catalysts **1** and **2** even after long reaction times and a linear relationship when plotting molar masses versus conversion (SI, Figure S38).

Table 3: Results of (-) menthilde polymerization performed with catalysts **1**, **2** and **4**.^a

Entry	Catalyst	[Cat]/[M]	Temp. [°C]	Time [h]	Conversion [%] ^b	M _{n,calc} [x10 ³ g/mol] ^c	M _{n,GPC} [x10 ³ g/mol] ^d	I ^e	Đ ^f
1	1	100	r.t.	18	63	10.7	33.4	0.32	1.07
2	1	100	100	1.5	82	12.5	19.0	0.66	1.06
3	1	200	100	21	50	17.0	28.8	0.60	1.08
4	1	200	100	91	50	17.1	29.9	0.57	1.12
5	2	100	r.t.	19	52	8.9	16.6	0.54	1.00
6	4	100	r.t.	18.5	89	15.2	23.7	0.65	1.16 ^g
7	4	100	60	19	96	16.4	21.4	0.77	1.12 ^g

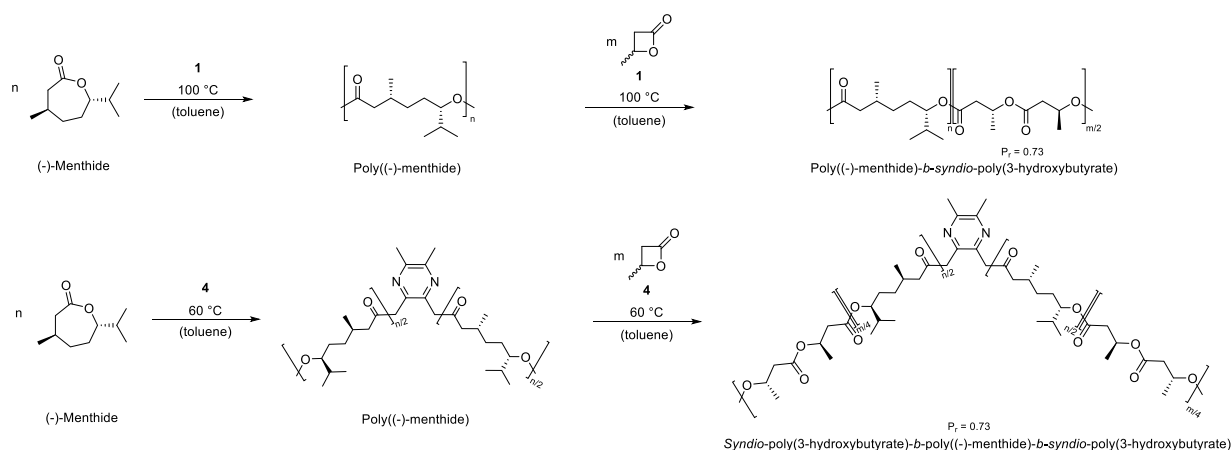
^a Reactions performed with [Cat] = 24.9 μmol in 0.5 mL toluene; [M] = menthilde; r.t. = room temperature; ^b Conversion determined *via* ¹H nmr spectroscopy (integration of methine group resonance of the iso-propyl group of menthilde and PM) ^c M_{n,calc} calculated from M_{n,calc} = M × (([M]/[Cat]) × conversion) ^d M_{n,GPC} measured *via* GPC in thf as eluent at room temperature with triple detection as absolute molar masses. ^e Initiator efficiency; I = M_{n,calc}/M_{n,GPC} at the end of the reaction ^f Polydispersity calculated from M_{w,GPC}/M_{n,GPC} determined by GPC. ^g slightly bimodal distribution.

Remarkably, and in contrast to BBL-polymerization, a longer reaction-time had no effect on the molecular weights or the molar mass distributions, which confirms the living-type of the reaction and the absence of side and termination reactions (Table 3, Entry 3 vs. Entry 4). To overcome the limited conversions, complex **4** was introduced as catalyst (Table 3, Entries 6 + 7). This complex was able to polymerize menthilde with nearly full conversion while maintaining good control over the molar masses. Due to chain growth in two directions, the polydispersities of the obtained PM showed bimodal distributions and therefore broader polydispersities than polymers produced with catalyst **1** and **2**. As absolute molecular weights are obtained, the polymerizations can be analyzed regarding the initiator efficiencies of the catalysts. Complex **1** has an initiator efficiency of 0.33 when using 100 eq. of menthilde which means that 33% of the complex molecules are active in polymerization. By increasing the temperature an increase in initiator efficiency up to 0.66 can be reached, observable by a higher accordance between calculated and obtained molar masses. The two C-H bond activated complexes **2** and **4** show increased initiator efficiency in comparison to **1** of up to 65% already observed in polymerizations performed at room temperature. Increasing the temperature to 60 °C led to an increase

of initiator efficiency to 77% when using complex **4**. By comparing these two catalysts among each other, complex **4** shows only a slightly higher efficiency than complex **2**.

Block copolymers from PM and PHB

The living nature of ROP of (-)-menthide allows the preparation of block copolymers with PHB. The first block must be (-)-menthide, statistical copolymerizations or polymerizations with BBL as first block led only to PHB-homopolymer. A higher coordination strength of BBL to the yttrium-center is assumed. Therefore, the synthesis of AB- and BAB-polymers required the sequential addition of first (-)-menthide and then BBL in a one pot reaction. Block copolymerizations were carried out with catalyst **1** to obtain AB-block copolymers and with catalyst **4** to enable BAB-polymers which are in detail B-A-X-A-B-polymers (X = tetramethylpyrazine initiator, A = PM, B = PHB) (Scheme 3). Temperatures of 100 °C (catalyst **1**) and 60 °C (catalyst **4**) were used to increase the initiator efficiency and activity of the complexes and to lower the melting temperature of the PHB-block enabling polymer processing via hot molding. Higher temperatures were not used to sustain the semicrystallinity of PHB. After weighing the calculated amount of (-)-menthide in a screw cap vial and heating to the respective temperature in a copper-bath in the glovebox, the calculated amount of catalyst **1** or **4** is dissolved in a minimum of toluene (0.5 mL) and added to the molten (-)-menthide. Then, the polymerization is stirred for 2 to 6.5 hours. Before adding *rac*-BBL, an aliquot sample was taken from the solution and quenched by the addition of CDCl₃.



Scheme 3: Polymerization procedure for block copolymerizations with (-)-menthide and *rac*-BBL using catalysts **1** and **4**.

Conversion of (-)-menthide was calculated *via* ¹H nmr spectroscopy and GPC analysis in thf was performed to determine the absolute molar mass of the first block. Block copolymers are achieved by the subsequent addition of *rac*-BBL to the reaction mixture which was then stirred overnight at the

respective temperature. The conversion of block B was determined *via* ^1H nmr spectroscopy of an aliquot taken before quenching of the reaction with methanol. The desired block copolymers were isolated and purified through washing with methanol and drying of the polymer overnight in a vacuum oven at 60 °C. The molecular weight of the block copolymer is determined through the ratio of PM/PHB (A/B) and the molecular weight of the first block (A). Composition A/B is calculated *via* ^1H nmr spectroscopy of the dried polymer. The methine signal of PHB was compared with the methine-proton of the *iso*-propyl group of PM (Figure 3, right and SI, S11 and S13). It was possible to tune the composition of the copolymer through the monomer feed. Different feed compositions were set to vary the chain length of the PM and the PHB block and the ratio of the two blocks to obtain different-sized block copolymers (Table 4). It was found that the conversion of (-)-menthicide is increased in this block copolymerizations, because the monomer-to-catalyst ratio was decreased.

Table 4: Results of block copolymerizations with (-)-menthicide and *rac*-BBL performed with catalysts 1 and 4.^a

Entry	Cat.	[Cat]/[M]/ [BBL]	Time _A [h]	Conv. _A ^b [%]	M _{nA,GPC} [x10 ³ g/mol] ^c	D _A ^d	Time _B [h]	Conv. _B ^b [%]	M _{nAB,nmr} [x10 ³ g/mol] ^e	D _{AB} ^f	P _r ^g	PM/ PHB ^h	T _g [°C] ⁱ	T _m [°C] ⁱ
1	AB ¹	1	1/50/200	2	89	16.2	1.04	10.5	47	32.2	1.53	0.73	33/67 -21 (PM) 5 (PHB)	-
2	AB ²	1	1/75/150	6.5	92	28.9	1.01	3	51	41.4	1.38	n.d.	54/46 -22 (PM) 4 (PHB)	-
3	BAB ¹	4	1/50/200	2	73	10.8	1.21 ^j	16	95	44.3	1.79	0.73	14/86 -20 (PM) 3 (PHB)	108 (PHB)
4	BAB ²	4	1/75/150	2.5	77	19.0	1.06 ^j	15	97	42.0	1.69	n.d.	30/70 -20 (PM) 4 (PHB)	116 (PHB)
5 ^k	BAB ³	4	1/100/100	2.5	74	22.3	1.26 ^j	15.5	>99	36.7	1.64	0.73	44/56 -21 (PM) 1 (PHB)	110 (PHB)
6	BAB ⁴	4	1/75/50	4	86	19.0	1.04 ^j	17	>99	24.4	1.40	n.d.	77/23 -22 (PM)	-

^a Reactions performed with [Cat] = 24.9 μmol in 0.5 mL toluene; [M] = menthicide; ^b Conversion determined *via* ^1H nmr spectroscopy ^c M_{n,GPC} measured *via* GPC in thf as eluent at room temperature with triple detection as absolute molar masses.

^d Polydispersity calculated from M_{w,GPC}/M_{n,GPC} determined by GPC in thf. ^e Determined *via* composition and M_{nA,GPC} ^f Polydispersity calculated from M_{w,GPC}/M_{n,GPC} determined by GPC in chloroform ^g P_r is the probability of *racemic*-linkages between monomer units and was determined by ^{13}C nmr spectroscopy from the carbonyl region ^h Calculated *via* ^1H nmr spectroscopy (a(PM)/b(PHB)) as depicted in Figure 3, right) ⁱ Determined *via* DSC-analysis ^j slightly bimodal distribution. ^k performed in double scale.

Using catalyst **1** and 50 to 75 eq. of (-)-menthicide nearly full conversion is reached in up to 7 hours. The conversion of *rac*-BBL was not quantitative when using catalyst **1** and reached only about 50%. By using

catalyst **4**, full conversion of *rac*-BBL was obtained. The successful synthesis of the copolymer is confirmed by the monomodal molecular weight distributions in the GPC. In addition, a shift of the GPC-signal from Block A to the AB and BAB block copolymers is observed when measuring both samples on a chloroform-GPC (Figure 3, middle and SI, S28). No fractions of homopolymers, but a broadening in polydispersity (up to 1.79) was detected as also observed during BBL-homopolymerization.

DOSY nmr studies were used to further confirm the successful linkage between the PM- and the PHB-block. DOSY nmr spectra of all blockcopolymers (AB¹, AB² and BAB¹ – BAB⁵) were measured under the same conditions (SI, S15 – S18). In all cases, independent from the composition or the molecular weights of the respective PM or PHB blocks, solely one set of signals corresponding to only one diffusion coefficient was observable in these spectra. Therefore, a linkage of the two blocks is expected in all polymers. To further evaluate these findings a blend of PHB and PM analogue to the composition of AB¹ is prepared and also analyzed *via* DOSY nmr spectroscopy (SI, S19). In this spectrum, two sets of signals are visible each for the PHB and the PM diffusion coefficient.

Transesterification would be significant if additional PM carbonyl peaks are observed in the ¹³C nmr spectra (Figure 3, left and SI, S12 and S14). Only minimal transesterification reactions are observed for PM-PHB block copolymers as only two distinct carbonyl signals, associated with the carbonyl groups of PM and PHB, are visible and the carbonyl signal of PM shows only very little additional peaks.

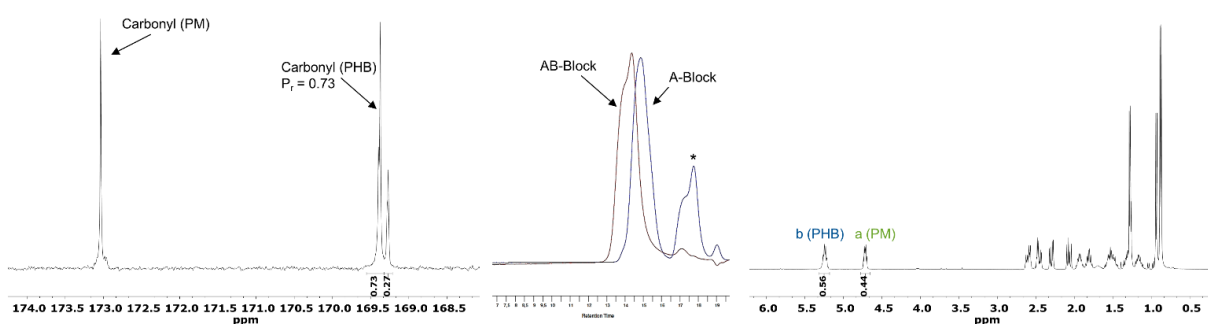


Figure 3: Left) Carbonyl signals of ¹³C nmr spectrum of AB¹ (full spectrum see SI, S12) measured in CDCl₃. Middle) Shift of signal in GPC from block A (blue) to AB¹ (red). Both samples are measured on a GPC in chloroform (* = residual menthene in aliquot sample). Right) ¹H nmr spectrum of BAB³ measured in CDCl₃. Calculation of PHB/PM via comparison of the methine-signals a and b (full spectrum see SI, S13).

Thermal and mechanical properties of block copolymers

DSC analysis was used to determine the immiscibility and morphology of the polymers. Thermal analysis of a PM-PHB blend by DSC revealed two glass transition temperature to those of the PHB and

PM segments indicating the immiscibility and phase separation within the material (SI, S47). Microphase separation of PHB-b-PM-b-PHB is necessary to obtain the mechanical properties analog to thermoplastic elastomers. Afterwards all AB and BAB copolymers were analyzed via DSC analysis. In comparison to the blend, the AB polymers indeed showed a separation of the glass transition temperatures indicating an immiscibility, but in addition an absence of the melting point of PHB was observed, leading to an amorphous material (Figure 4). In contrast, the BAB polymers showed different signals in the DSC subject to their composition. All triblock polymers showed a glass transition temperature which belongs to the PM-block. This T_g was not affected by the composition or the molar mass and remained at -20 to -22 °C in all samples. BAB⁵, with the lowest content of PHB, shows solely a T_g corresponding to PM. The T_m of PHB is only slightly visible, the T_g of PHB is not apparent. Since the peak of the melting temperature of PHB in BAB⁵ is extremely low, it can be assumed that there are nearly no crystalline domains in the copolymer. With a higher PHB content, all BAB polymers show two glass transition temperatures, for PM and PHB each, and a melting point corresponding to PHB, which suggests the phase separation of the polymers within the material and the existence of a semicrystalline polymer. The melting point of PHB in these block copolymers is between 108 and 116 °C (Table 4) which is slightly lower than the T_m of PHB with the same syndiotacticity of 73% and a similar molar mass of the PHB block (Table 2, Entry 9, T_m = 122 °C, SI, S43). The same effect is slightly visible by looking at the glass transition temperatures. The amorphous PM seems to lower the T_m and T_g in the block copolymers and therefore the crystallinity of the PHB domains.

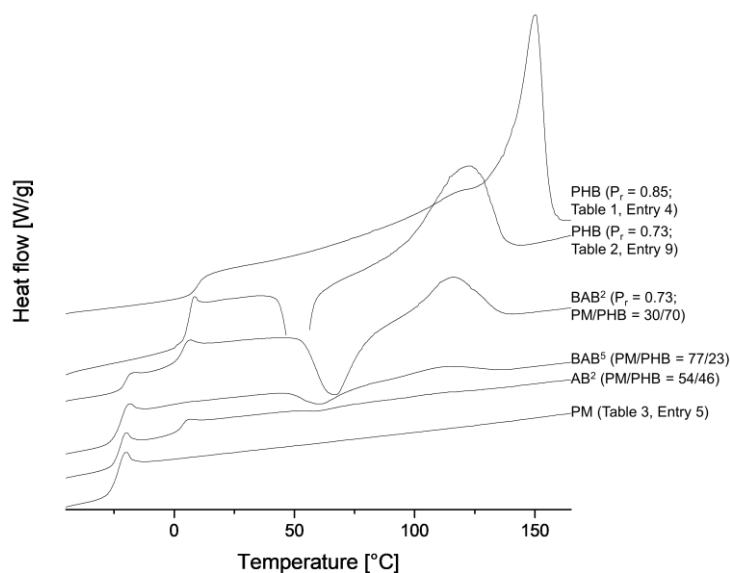


Figure 4: DSC curves of different PHB, PM, AB and BAB polymers. Section from the third cycle (-50 to 160 °C) measured with exo down mode. Peak of pre-crystallization temperature of PHB (P_r = 0.73) is omitted for clarity. For full spectra see SI.

To additionally determine the effect of the amorphous PM on the crystallinity of PHB, power-XRD measurements were performed with different crystalline PHB ($P_r = 0.85$ and 0.73), BAB¹ and BAB³ samples (SI, S48). After background correction of the diffractograms, the crystalline part of PHB is assigned to the reflexes at 10.7° , 15.4° , 19.0° , 22.3° , 24.9° and 28.0° based on the diffraction of the PHB sample with the highest crystallinity ($P_r = 0.85$) (Figure 5; orange diffractogram). Compared to the PHB sample with lower syndiotacticity (green diffractogram), the amount of crystallinity in the polymer decreases as especially the reflex at 15.4° starts to broaden and therefore it seems as if the reflexes 10.7° and 15.4° even slightly increase in their intensity. Therefore, amorphous regions of PHB seem to mainly increase between 10 and 20° , the reflex at 22.3° is only decreasing in its intensity but is not broadened showing that in this region only crystalline parts are visible. The broadening occurs as with less stereoregularity the polymer chains tend to rather form amorphous sections instead of crystalline parts. As pure PM and the AB polymers occur solely in an amorphous state, X-Ray diffraction of these samples cannot provide useful information. However, when examining PHB-PM-PHB triblock copolymers, the behavior of the crystalline parts of PHB in presence of amorphous PM can be observed using XRD. Regarding the amorphous parts of the polymers, the area between 10.7° to 19.0° and the reflex at 22.3° seem to be of interest. Comparing the PHB sample with $P_r = 0.73$ with BAB¹ (blue diffractogram) which has the same P_r and only a low amount of PM, solely an increase in amorphous background between 15° and 19° is observed resulting in an increase of the reflex 15.4° . Reflexes 22.3° , 24.9° and the amorphous region between 10.7 and 15.4° are unaffected.

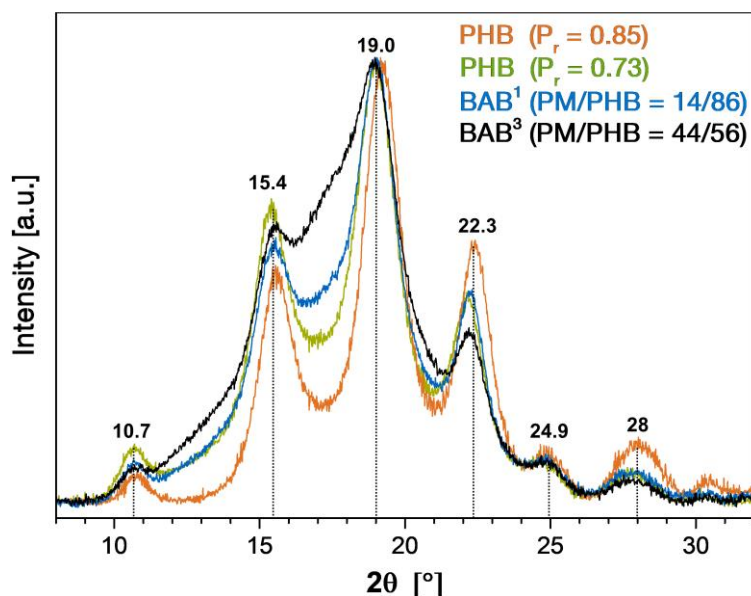


Figure 5: Powder XRD measurements with background correction of PHB (orange, $P_r = 0.85$; Table 1, Entry 4), PHB (green, $P_r = 0.73$; Table 2, Entry 9), BAB¹ (blue, $P_r = 0.73$, PM/PHB = 14/86, Table 4, Entry 3) and BAB³ (black, $P_r = 0.73$, PM/PHB = 44/56, Table 4, Entry 5).

With increasing PM-to-PHB ratio (BAB³; black diffractogram), all reflexes in the area between 10° and 22° seem to strongly broaden and a high increase in amorphous background signal can be seen. Further, the intensity of the reflex at 22.3° is decreasing, similar to the observations between the two PHB samples. In conclusion, the crystallinity of the PHB section in the BAB block copolymers decreases with higher (-)-menthide content (decrease of reflex at 22.3°) as well as more amorphous background diffraction can be observed due to a higher amount of amorphous poly(menthide) between 10° and 20°.

To investigate the influence of tacticity/crystallinity of syndiotactic PHB and PM on the stress strain-properties of PHB (co)polymers, PHB ($P_r = 0.74$, $T_m = 117$ °C; Table 2, Entry 3) and BAB³ ($P_r = 0.73$, $T_m = 110$ °C, PM/PHB = 44/56, Table 4, Entry 5) were measured on a *Zwick-Roell* machine. These two samples were produced in double scale to isolate enough sample material. Afterwards they were processed *via* hot molding under vacuum at 117 °C into dog-bone shaped specimens. To perform this polymer processing technique, polymerizations were conducted at higher temperatures to lower the melting temperature of PHB (*vide supra*). Hot molding with natural and highly crystalline PHB is only hardly possible due to dissociation processes. A specimen that consist of PHB with a syndiotacticity of 74% (Table 2. Entry 3) shows a high *Young's* modulus of ca. 195 MPa which is about 20-times lower in comparison to highly tactic PHB and is therefore less brittle and more easy to process.^[5]

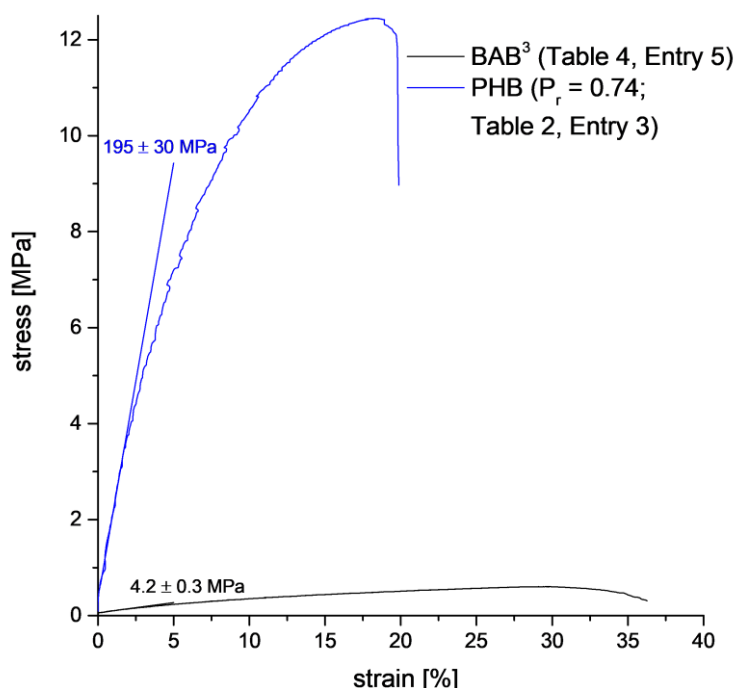


Figure 6: Stress-Strain curve of PHB ($P_r = 0.74$; Table 2, Entry 3) and BAB³ ($P_r = 0.73$, PM/PHB = 44/56, Table 4, Entry 5).

In addition, it shows an improved elongation at break of 18%. Incorporation of PM into BAB blockcopolymers had a drastic effect on the stiffness of the material. BAB³ with a PM/PHB ratio of 44/56 shows an about 50-times reduced *Young's* modulus (4.2 MPa) while increasing the elongation at a break by two times (ca. 35%). However, this elongation is still amendable.

Further investigations on the influence of the PM/PHB ratio on the *Young's* modulus and elastic properties (cyclic stress-strain measurements) are ongoing work and exceed the scope of this contribution.

Conclusion

Three heteroaromatic pyridine-based bis(phenolate)yttrium complexes were successfully tested in the ring-opening polymerization of *rac*-BBL and (-)-menthide for the synthesis of sustainable polyesters. The activities of these catalysts in ROP of *rac*-BBL were analyzed *via in situ* IR-monitoring. Although all four described catalysts 1-4 were able to polymerize *rac*-BBL, the 6-Mebpy based catalyst 3 has not been investigated further due to its deficient performance during ROP. The *sym*-collidine catalyst 2 and tetramethylpyrazine-based 4 (TOF = 7100 h⁻¹) however showed high activity and allow polymerization of BBL with increased conversions and narrower molar mass distributions even at room temperature in comparison to catalyst 1 bearing a bis(dimethylsilyl)amide initiator. The obtained PHB samples further showed a semicrystallinity resulting from a *syndiotactic* microstructure. The yttrium complexes also showed activity in ROP of (-)-menthide. Amorphous poly((-)-menthide) was obtained using mild conditions with very low polydispersities. Apart from the homopolymerization, the catalysts gave access to AB and BAB block copolymers. The bimetallic catalyst system 4 was used to obtain BAB-blockcopolymers from PM (block A) and PHB (block B). The BAB-system was expected to show microphase separation as semicrystalline PHB segments are enclosed in an amorphous PM matrix. Block copolymer formation was verified by GPC-, 1D and 2D nmr analysis *via* comparison to a blend from PHB and PM. DSC, TGA, XRD and stress-strain measurements were used to study the mechanical and thermal properties of the block copolymers. Two glass transition temperatures obtained using DSC analysis strongly indicate an immiscibility of PHB and PM on molecular scale. To support this thesis, XRD measurements are applied, further confirming a microphase separation. In scope of application of these sustainable polyesters, mechanical properties of a *syndiotactic* PHB and a BAB-blockcopolymer were measured. Both polymers could be processed by hot-molding, which offers an advantage compared to *isotactic* PHB from natural sources. The *syndiotactic* PHB is less brittle than *isotactic* PHB resulting in a lower *Young's*-modulus. Incorporating PM in the structure, the elastic modulus is further lowered with increasing the elongation at break.

Experimental Section

Homopolymerization Procedure for *rac*-BBL

24.9 μmol (1.0 eq.) of the respective catalyst are dissolved in 2 ml of toluene in a screw cap vials in the glove box and 4.98 mmol (200 eq.) *racemic* β -butyrolactone are added in one portion. After stirring for the stated time at the respective temperature, the reaction is quenched by addition of 1.5 mL deuterated chloroform. To determine the conversion an aliquot (0.4 mL) is taken from this solution and measured by ^1H nmr spectroscopy. The polymers are precipitated by addition of the reaction mixtures to methanol (100 ml) and the solution is decanted off. Relative molecular weights and molar mass distributions are measured *via* GPC in chloroform.

Homopolymerization Procedure for *rac*-BBL with *in situ* Monitoring

All Polymerizations with *in situ* monitoring are performed using a React-IR/MultiMax four-autoclave system (Mettler-Toledo). The 50 mL steel autoclaves are equipped with a diamond window, a mechanic stirring and a heating device. The autoclaves were heated to 130 $^{\circ}\text{C}$ under vacuum prior to polymerization.

For these polymerizations 24.9 μmol of the respective complex are dissolved in 6.0 mL dichloromethane and taken to a syringe. 14.9 mmol BBL (600 eq.) are stored in a second syringe. The two syringes were rapidly transported to the reactor using a vial equipped with an injection septum. The autoclave was stored under argon atmosphere at room temperature and the two syringes were transferred into the reactor. An IR-spectrum is then taken every 30 seconds. After the given time an aliquot was taken to determine the conversion via ^1H nmr spectroscopy in CDCl_3 . Chloroform was added to the reaction mixture to stop the polymerization and the polymer was precipitated by addition of the reaction solution to methanol (100 ml). The solution was decanted off. Relative molecular weights and molar mass distribution are measured *via* GPC in chloroform.

Kinetic Measurements of *rac*-BBL by Aliquot Method

To a solution of 24.9 μmol of catalyst **4** in 6.0 mL dichloromethane at room temperature, 14.9 mmol BBL (600 eq.) were added in one portion. Aliquots were taken from the reaction solution at regular time intervals and quenched by addition of CDCl_3 . For each aliquot, the conversion is determined *via* ^1H nmr spectroscopy and the molecular weight and polydispersity of the polymer sample is determined by GPC analysis in chloroform.

Homopolymerization Procedure for (-)-menthide

After dissolving the calculated amount of catalyst (24.9 μmol) in toluene (0.5 ml), this solution is added to the respective equivalents of (-)-menthide which is pre-heated to the respective temperature in a copper-bath in the glove box. The reaction mixture is stirred for the given time, then an aliquot was taken and quenched by the addition of CDCl_3 (calculation of conversion *via* ^1H nmr spectroscopy). The reaction is quenched by addition of methanol. The polymer is precipitated in methanol, the solvent is decanted off or the polymer is isolated *via* centrifugation and the polymer is dried under vacuum at 60 $^\circ\text{C}$ overnight. Absolute molecular weights and molar mass distributions were measured *via* GPC in tetrahydrofuran.

Kinetic Measurements of (-)-Menthide by Aliquot Method

After dissolving 74.7 μmol (1.0 eq.) of catalyst **1** in 1.5 mL of toluene, this solution is added to the respective equivalents of (-)-menthide. At regular intervals, aliquots are taken from the reaction solution which are quenched by addition of CDCl_3 . For each aliquot, the conversion is determined *via* ^1H nmr spectroscopy and molecular weight and polydispersity of the polymer sample is determined by GPC analysis in chloroform.

Copolymerization Procedure

After dissolving the calculated amount of catalyst **1** or **4** (24.9 μmol) in toluene (0.5 ml) at room temperature, this solution is added to the respective equivalents of (-)-menthide pre-heated to 60 $^\circ\text{C}$ or 100 $^\circ\text{C}$ in a copper-bath in the glove box. The reaction mixture was stirred for a given time-interval. One aliquot (0.1 ml) was taken and quenched by the addition of 0.4 ml CDCl_3 (calculation of conversion of (-)-menthide *via* ^1H nmr spectroscopy) while the calculated amount of *rac*-BBL was added to the reaction solution and stirred overnight at the respective temperature. Before quenching a second aliquot is taken and quenched with 0.5 ml CDCl_3 to calculate the conversion of BBL *via* ^1H nmr spectroscopy. The polymers were precipitated and quenched by addition of methanol. The polymer sample of the first aliquot (block A) is dried overnight, the absolute molecular weight and polydispersity of the polymer is determined by GPC analysis in tetrahydrofuran. The polydispersity of the block copolymer is determined by GPC analysis in chloroform. A ^1H nmr spectrum of the block copolymer is in CDCl_3 taken to determine the ratio of PHB/PM.

Acknowledgements

The manuscript was written through contribution of all authors. Friederike Adams thanks the Bavarian State Ministry of Environment and Consumer Protection for financial support within BayBiotech research network. The authors thank Daniel Melzer for help with XRD measurements.

There are no conflicts of interest to declare.

Keywords: Ring-opening Polymerization • Block Copolymers • Yttrium Bis(phenolate) Catalyst • Material Properties • Sustainable Lactones

References

- [1] S. Kobayashi, *Proc. Japan Acad.* **2010**, *86*, 338-365.
- [2] F. P. Delafield, M. Doudoroff, N. J. Palleroni, C. J. Lusty, R. Contopoulos, *J. Bacteriol.* **1965**, *90*, 1455-1466.
- [3] J. M. Merrick, M. Doudoroff, *J. Bacteriol.* **1964**, *88*, 60-71.
- [4] P. A. Holmes, *Phys. Technol.* **1985**, *16*, 32-36.
- [5] R. Reichardt, B. Rieger, *Adv. Polym. Sci.* **2012**, *245*, 49-90.
- [6] G. A. Olah, A. Goepfert, G. K. Prakash, *J. Org. Chem.* **2009**, *74*, 487-498.
- [7] X. Zuwei, Z. Ning, S. Yu, L. Kunlan, *Science* **2001**, *292*, 1139-1141.
- [8] E. E. Stangland, K. B. Stavens, R. P. Andres, W. N. Delgass, *J. Catal.* **2000**, *191*, 332-347.
- [9] T. Hayashi, K. Tanaka, M. Haruta, *J. Catal.* **1998**, *178*, 566-575.
- [10] V. Russo, R. Tesser, E. Santacesaria, M. Di Serio, *Ind. Eng. Chem. Res.* **2013**, *52*, 1168-1178.
- [11] V. Mahadevan, Y. D. Y. L. Getzler, G. W. Coates, *Angew. Chem. Int. Ed.* **2002**, *114*, 2905-2908.
- [12] J. T. Lee, P. J. Thomas, H. Alper, *J. Org. Chem.* **2001**, *66*, 5424-5426.
- [13] P. Dubois, O. Coulembier, J.-M. Raquez, *Handbook of ring-opening polymerization*, John Wiley & Sons, **2009**.
- [14] J. F. Carpentier, *Macromol. Rapid Commun.* **2010**, *31*, 1696-1705.

- [15] E. D. Cross, L. E. N. Allan, A. Decken, M. P. Shaver, *J. Polym. Sci., A: Polym. Chem.* **2013**, *51*, 1137-1146.
- [16] J. S. Klitzke, T. Roisnel, E. Kirillov, O. d. L. Casagrande, J.-F. Carpentier, *Organometallics* **2014**, *33*, 309-321.
- [17] L. R. Rieth, D. R. Moore, E. B. Lobkovsky, G. W. Coates, *J. Am. Chem. Soc.* **2002**, *124*, 15239-15248.
- [18] C. Guillaume, J.-F. Carpentier, S. M. Guillaume, *Polymer* **2009**, *50*, 5909-5917.
- [19] B. M. Chamberlain, M. Cheng, D. R. Moore, T. M. Ovitt, E. B. Lobkovsky, G. W. Coates, *J. Am. Chem. Soc.* **2001**, *123*, 3229-3238.
- [20] C. M. Thomas, *Chem. Soc. Rev.* **2010**, *39*, 165-173.
- [21] J.-F. Carpentier, *Organometallics* **2015**, *34*, 4175-4189.
- [22] A. Amgoune, C. M. Thomas, S. Ilinca, T. Roisnel, J.-F. Carpentier, *Angew. Chem. Int. Ed.* **2006**, *45*, 2782-2784.
- [23] N. Ajellal, M. Bouyahyi, A. Amgoune, C. M. Thomas, A. Bondon, I. Pillin, Y. Grohens, J.-F. Carpentier, *Macromolecules* **2009**, *42*, 987-993.
- [24] N. Ajellal, J. F. Carpentier, C. Guillaume, S. M. Guillaume, M. Helou, V. Poirier, Y. Sarazin, A. Trifonov, *Dalton Trans.* **2010**, *39*, 8363-8376.
- [25] M. Bouyahyi, N. Ajellal, E. Kirillov, C. M. Thomas, J.-F. Carpentier, *Chem. Eur. J.* **2011**, *17*, 1872-1883.
- [26] P. T. Altenbuchner, A. Kronast, S. Kissling, S. I. Vagin, E. Herdtweck, A. Pöthig, P. Deglmann, R. Loos, B. Rieger, *Chem. Eur. J.* **2015**, *21*, 13609-13617.
- [27] H. Koempel, W. Liebner, in *Studies in Surface Science and Catalysis, Vol. 167*, Elsevier, **2007**, pp. 261-267.
- [28] S. O. Nwaukwa, P. M. Keehn, *Tetrahedron Lett.* **1982**, *23*, 35-38.
- [29] D. Zhang, M. A. Hillmyer, W. B. Tolman, *Biomacromolecules* **2005**, *6*, 2091-2095.

- [30] J. Shin, M. T. Martello, M. Shrestha, J. E. Wissinger, W. B. Tolman, M. A. Hillmyer, *Macromolecules* **2011**, *44*, 87-94.
- [31] N. Ajellal, D. M. Lyubov, M. A. Sinenkov, G. K. Fukin, A. V. Cherkasov, C. M. Thomas, J.-F. Carpentier, A. A. Trifonov, *Chem. Eur. J.* **2008**, *14*, 5440-5448.
- [32] J. Fang, M. J. L. Tschan, T. Roisnel, X. Trivelli, R. M. Gauvin, C. M. Thomas, L. Maron, *Polym. Chem.* **2013**, *4*, 360-367.
- [33] E. Grunova, E. Kirillov, T. Roisnel, J.-F. Carpentier, *Organometallics* **2008**, *27*, 5691-5698.
- [34] A. Amgoune, C. M. Thomas, J.-F. Carpentier, *Macromol. Rapid Commun.* **2007**, *28*, 693-697.
- [35] E. Grunova, E. Kirillov, T. Roisnel, J.-F. Carpentier, *Dalton Trans.* **2010**, *39*, 6739-6752.
- [36] Y. J. Luo, W. Y. Li, D. Lin, Y. M. Yao, Y. Zhang, Q. Shen, *Organometallics* **2010**, *29*, 3507-3514.
- [37] F. Adams, M. R. Machat, P. T. Altenbuchner, J. Ehrmaier, A. Pothig, T. N. V. Karsili, B. Rieger, *Inorg. Chem.* **2017**, *56*, 9754-9764.
- [38] P. T. Altenbuchner, P. D. Werz, P. Schöppner, F. Adams, A. Kronast, C. Schwarzenböck, A. Pöthig, C. Jandl, M. Haslbeck, B. Rieger, *Chem. Eur. J.* **2016**, *22*, 14576-14584.
- [39] F. Adams, M. Pschenitzka, B. Rieger, *ChemCatChem* **2018**, *10*, 4309-4316.
- [40] D. C. Aluthge, C. Xu, N. Othman, N. Noroozi, S. G. Hatzikiriakos, P. Mehrkhodavandi, *Macromolecules* **2013**, *46*, 3965-3974.
- [41] S. Kernbichl, M. Reiter, F. Adams, S. Vagin, B. Rieger, *J. Am. Chem. Soc.* **2017**, *139*, 6787-6790.
- [42] H. Arslan, A. Menteş, B. Hazer, *J. Appl. Polym. Sci.* **2004**, *94*, 1789-1796.
- [43] H. Arslan, B. Hazer, M. Kowalczyk, *J. Appl. Polym. Sci.* **2002**, *85*, 965-973.
- [44] H. Arslan, N. Yeşilyurt, B. Hazer, *J. Appl. Polym. Sci.* **2007**, *106*, 1742-1750.
- [45] S. Nguyen, R. H. Marchessault, *Macromol. Biosci.* **2004**, *4*, 262-268.
- [46] X. Zhang, H. Yang, Q. Liu, Y. Zheng, H. Xie, Z. Wang, R. Cheng, *J. Polym. Sci., A: Polym. Chem.* **2005**, *43*, 4857-4869.
- [47] I. Yu, T. Ebrahimi, S. G. Hatzikiriakos, P. Mehrkhodavandi, *Dalton Trans.* **2015**, *44*, 14248-14254.

- [48] C. G. Jaffredo, J.-F. Carpentier, S. M. Guillaume, *Macromolecules* **2013**, *46*, 6765-6776.
- [49] J. R. Lowe, W. B. Tolman, M. A. Hillmyer, *Biomacromolecules* **2009**, *10*, 2003-2008.
- [50] J. R. Lowe, M. T. Martello, W. B. Tolman, M. A. Hillmyer, *Polym. Chem.* **2011**, *2*, 702-708.
- [51] S. A. Gurusamy-Thangavelu, S. J. Emond, A. Kulshrestha, M. A. Hillmyer, C. W. Macosko, W. B. Tolman, T. R. Hoye, *Polym. Chem.* **2012**, *3*, 2941-2948.
- [52] M. L. Gupta, A. Prasad, M. Ram, S. Kumar, *Biores. Technol.* **2002**, *81*, 77-79.
- [53] H. Hall Jr, A. Schneider, *J. Am. Chem. Soc.* **1958**, *80*, 6409-6412.
- [54] C. L. Wanamaker, L. E. O'Leary, N. A. Lynd, M. A. Hillmyer, W. B. Tolman, *Biomacromolecules* **2007**, *8*, 3634-3640.
- [55] K. Ding, A. John, J. Shin, Y. Lee, T. Quinn, W. B. Tolman, M. A. Hillmyer, *Biomacromolecules* **2015**, *16*, 2537-2539.
- [56] J. Shin, Y. Lee, W. B. Tolman, M. A. Hillmyer, *Biomacromolecules* **2012**, *13*, 3833-3840.
- [57] C. L. Wanamaker, M. J. Bluemle, L. M. Pitet, L. E. O'Leary, W. B. Tolman, M. A. Hillmyer, *Biomacromolecules* **2009**, *10*, 2904-2911.
- [58] E. Y. Tshuva, S. Groysman, I. Goldberg, M. Kol, Z. Goldschmidt, *Organometallics* **2002**, *21*, 662-670.
- [59] C.-X. Cai, L. Toupet, C. W. Lehmann, J.-F. Carpentier, *J. Organomet. Chem.* **2003**, *683*, 131-136.
- [60] Z. Jedliński, G. Adamus, M. Kowalczyk, R. Schubert, Z. Szewczuk, P. Stefanowicz, *Rapid. Commun. Mass Spectrom.* **1998**, *12*, 357-360

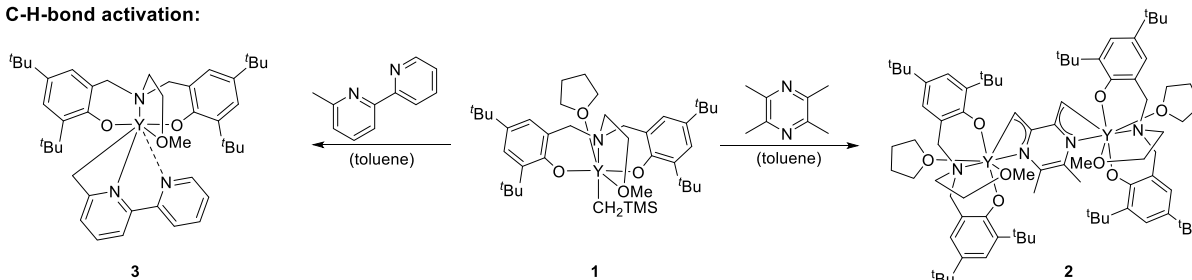
11 Summary and outlook

11.1 Group-transfer polymerization

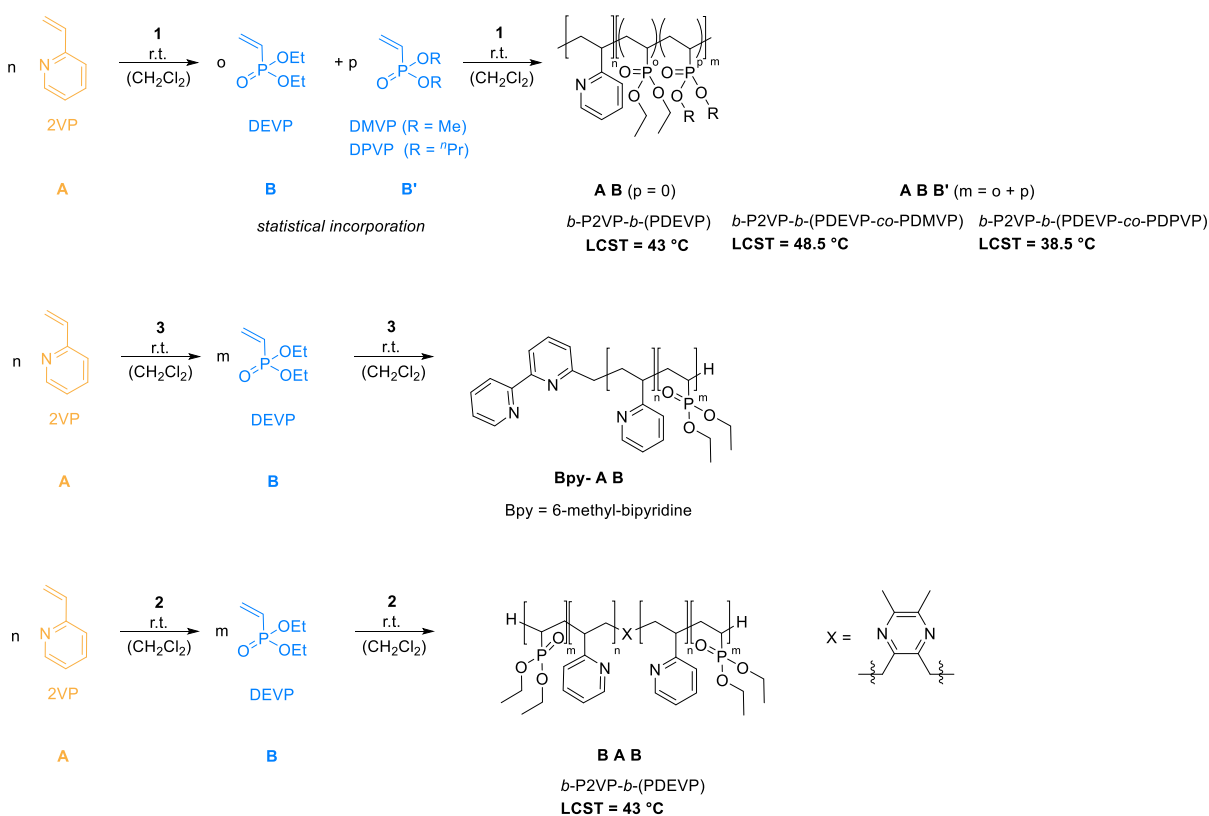
In this thesis, we establish REM-GTP with nonmetallocene bis(phenolate)lanthanides as a multifunctional method for the efficient synthesis of new, high performance and high precision polymers with variable tacticity, controllable molecular weights and narrow molar mass distributions. The present fundamental study of isostructural 2-methoxyethylamino-bis(phenolate)lanthanide complexes combines the experimental findings of REM-GTP with in-depth quantum chemical calculations on the initiation process of this polymerization offering deeper insight into the ongoing initiation and reaction mechanism and the electronic properties of the catalysts. This analysis included the differentiation of electron-donating and non-donating vinyl monomers, the impact of the ionic radius of the metal centers (yttrium and lutetium) and the comparison of two initiators (highly nucleophilic alkylinitiators vs. electron-donating heteroaromatics). The investigation examines the effect of these parameters on the activity, initiator efficiency and tacticity of the obtained polymers and enables the possibility to generate a toolbox of different catalysts, in which each individual one is favored for a monomer or stereoselectivity. A higher acidity of lutetium leads to an improved activity in 2-vinylpyridine polymerization (highest declared normalized turn over frequency by the time). The strongly basic, alkylinitiators are inefficient and slow at initiating the polymerization of DEVP as deprotonation of the acidic α -CH occurs and no initiation *via* nucleophilic attack of the strongly basic initiator to the first monomer takes place. To avoid side reactions and to improve the initiator efficiency, heteroaromatic initiators can be introduced *via* σ -bond metathesis. Contrary to observations in DEVP and DMAA polymerization (non-donating monomers), 2-aminoalkoxy-bis(phenolate)yttrium complexes with heteroaromatic initiators show a decreased efficiency in polymerization with electron-donating monomers (2VP and IPOx) as an overload of electron density is provoked at the yttrium center. Computational studies underline that a coordination of nitrogen-donating monomers (containing a free electron pair) is hindered with yttrium catalysts when also an electron-donating initiator is used. For polymerization of DMAA and DEVP, C-H bond activation of a pyridine-based substrate is shown to be a versatile tool towards efficient initiators. These boosted initiator efficiencies enable a highly isoselective polymerization of DMAA, because low-temperature polymerizations are possible. Nonmetallocene complexes with heteroaromatic initiators were not only synthesized for the improvement of DEVP and DMAA polymerization, but also for end-group functionalization of 2VP polymerization and copolymerizations of 2VP with DEVP. The use of hydrophilic dialkyl vinylphosphonates with a thermoresponsive behavior and hydrophobic 2-vinylpyridine with its pH-dependent solubility enable the synthesis of novel multiresponsive micelles. We utilize

2-methoxyethylamino-bis(phenolate)yttrium catalysts with a CH₂TMS (**1**) or tetramethylpyrazine (**2**) initiator as highly active catalysts for the generation of AB and ABB' block copolymers and for the synthesis of B-A-X-A-B systems (X = tetramethylpyrazine initiator, A = P2VP, B = PDEVp, B' = PDMVP or PDPVP) (PDPVP = poly(di-*n*-propyl vinylphosphonate) (Scheme 21). It is possible to exactly tune the composition of the copolymer through the monomer feed. Different feed compositions are set to vary the chain length of the P2VP and the PDEVp block.

C-H-bond activation:

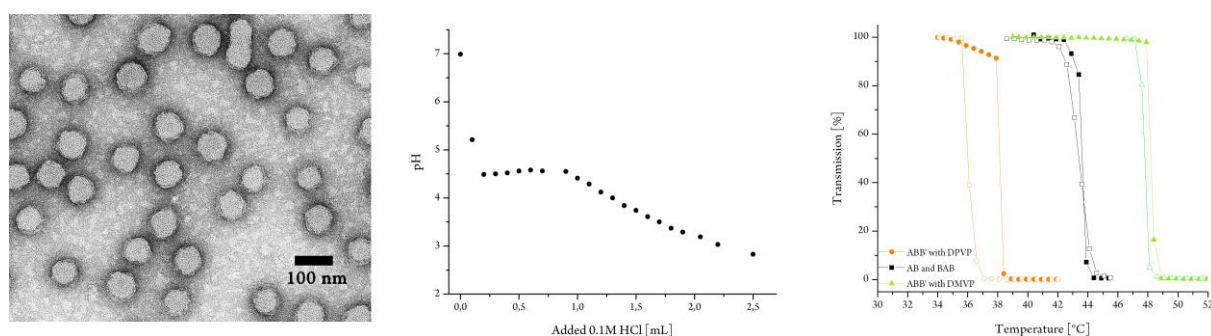


Polymer synthesis:



Scheme 21: Synthesis of multiresponsive AB, ABB' and BAB copolymers with versatile 2-methoxyethylamino-bis(phenolate)yttrium catalysts **1-3**.

DLS-measurements show that a minimum P2VP and PDEVP length is required in AB-polymers to sustain the micelle formation. The block copolymers which have a ratio of at least 50/90 self-assemble to unimodal, perfectly-sized micelles above their critical micelle concentration (CMC) and exhibit pH-dependent solubility and a lower critical solution temperature (Scheme 22). The pH-dependent solubility was investigated by titration with hydrogenchloride-solution. Stable micelles are present at $\text{pH} > 4.5$. Remarkably, the presence of P2VP and the variation of the chain length of PDEVP have no measurable effect on the cloud points which are always at 43-43.5 °C. As a release temperature of 44 °C is not in the normal body temperature range, investigations were performed regarding the evaluation of ABB' block copolymers. Differently substituted dialkyl vinylphosphonates were incorporated into the DEVP-block to tune the LCST in micellar P2VP-PDEVP-systems. The incorporation of at least 10 equivalents of hydrophilic dimethyl vinylphosphonate suffice to increase the LCST up to 48.5 °C. Likewise, more hydrophobic di-*n*-propyl vinylphosphonate (3 eq.) successfully decreases the LCST of ABB' block copolymers to 38.5 °C.



Scheme 22: Left) TEM image of a BAB micelle with $D_h = 54$ nm. Middle) Titration curve of an AB-polymer with 0.1 M hydrogen chloride solution. Right) Cloud points of AB, BAB and ABB' block copolymers.

To assess the loading and release capabilities of the BAB polymers fluorescein was used and pH (4.5) and temperature (44 °C) triggered release studies were conducted as the polymers have bifunctional properties. The drug loading/release capabilities reveal different degrees of burst-release behavior in dependence with the vinylphosphonate block length. The BAB polymer with the shortest PDEVP chain length shows the lowest release efficiency. The pH-trigger can be used for a burst release while temperature achieves a more sustained release of the loaded substance over a period of 25 hours. To test if these systems can act as cellular drug-delivery systems, cellular uptake of Nile-red colored micelles to ovarian cancer cells (HeLa-cells) and pH-dependent release was tested. Intracellular release can be achieved under acidic conditions, as Nile-red fluoresces when it interacts with free lipids after being released from the carrier. Investigations on an *in vitro* release of the insoluble anti-cancer drug doxorubicin were also performed. The release of DOX is associated with the decrease of the cancer cell

viability. Given that non-loaded BAB-micelles were identified as non-toxic, the observed reduced cell viability could be explained by the cytotoxicity of successfully released DOX.

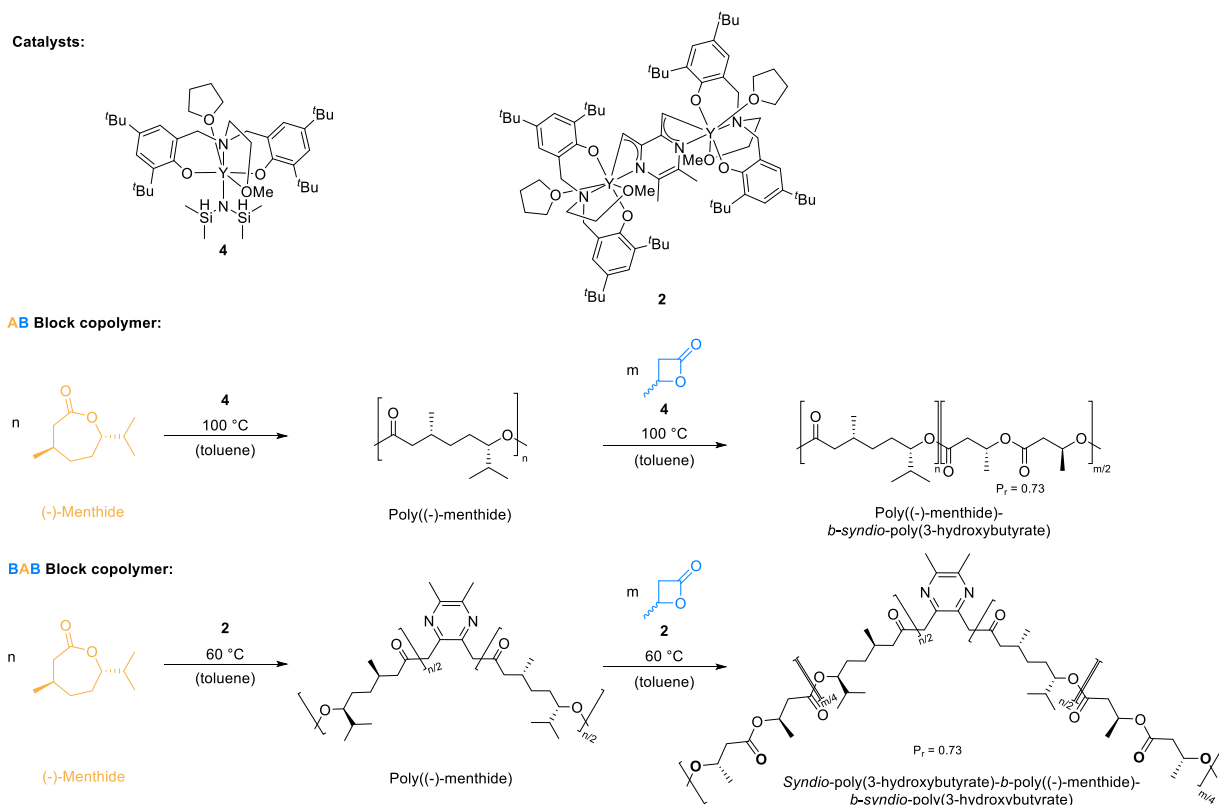
To address a completely new field for 2VP-DEVP block copolymers, *ortho*-methylated bipyridines are introduced as initiators in 2-aminoalkoxy-bis(phenolate)yttrium complexes (**2**) that serve than as end-groups in GTP (Scheme 21). The bpy end-groups enable metal complexation shown by the reaction of bpy-2VP-DEVP block copolymers with $[\text{Re}(\text{CO})_5\text{Cl}]$ generating a $[\text{Re}(\text{CO})_3(\text{bpy})\text{Cl}]$ motif at the end of each polymer chain. It is shown, that these Re-2VP-DEVP block copolymers still form unimodal micelles in water. The hydrophobic core (P2VP) containing the hydrophobic rhenium complex is shielded from the aqueous milieu by the hydrophilic segments (PDEVP), representing a possible carrier for hydrophobic metal-containing complexes into cells. To proof that the polymer part of these systems does not influence the properties of the metalorganic complex, we used the Re-2VP-DEVP-block copolymers in photocatalytic reduction of CO_2 to CO. Remarkably, the catalytic performance (turnover number) of the rhenium-functionalized block copolymers were increased in comparison to its analogue polymer-free complex.

11.2 Ring-opening polymerization

Poly(hydroxyalkanoates) are a promising class of biodegradable and biocompatible polymers, whereas poly(3-hydroxybutyrate) represents one of the most common PHA. Besides naturally occurring PHB, a promising synthesis route is the ROP of *racemic* β -butyrolactone. As *rac*-BBL is synthetically available from carbon dioxide, it is an interesting monomer for PHB production. According to studies of *Carpentier* and *Rieger et al.*, stereoselective aminoalkoxy-bis(phenolate)yttrium-amido catalysts can be used for syndiospecific ROP of *rac*-BBL. To our knowledge, besides often used bis(di- or trimethylsilyl)amide, CH_2TMS and *iso*-propanol, further efficient initiators were not investigated in REM-mediated ROP of BBL. In this thesis, heteroaromatic initiators, which coordinate to the yttrium center *via* η^3 -(C,C,N)-*aza*-allylic binding, which were not yet known for initiating ROP of BBL, were proven as efficient catalysts for syndiospecific BBL polymerization. Besides carbon dioxide as a carbon source, various natural products can be used for the preparation of biobased polymers. An important class among these are terpenes. These naturally occurring, cyclic representatives such as (-)-menthone and (-)-carvone can be converted to the corresponding lactones. Herein, the first lanthanide-based catalysts are reported that can polymerize (-)-menthide to poly((-)-menthide) under mild conditions with very low molecular weight distributions.

Under tension, highly stereoregular PHB, which is obtained with these yttrium-catalysts, fractures at very low strains and is therefore unsuitable for applications where elasticity is necessary. Improvement

of the stress-strain properties is reached by incorporation of *syndiotactic* PHB into block copolymers for the first time *via* simple sequential addition of the respective monomers to the reaction mixture in a one-pot reaction. We produced AB block copolymers using poly((-)-menthite) as the first block (A) and *syndiotactic* PHB as the second one (B) with a bis(phenolate)yttrium-bdsa complex (**4**). DOSY nmr studies, GPC- and DSC-measurements reveal the linkage between the two blocks by comparison with a blend from PM and PHB. A separation of the glass transition temperatures is observed in the DSC-curve of the polymer blend and the AB-polymers, which suggests the phase separation of the polymers within the materials. However, a lack of the melting temperature of the AB-polymers is observed, leading to an amorphous material. To obtain thermoplastic elastomers, we also developed ABA block copolymers, by using the bifunctional tetramethylpyrazine bis(phenolate) catalyst (**2**) (Scheme 23).

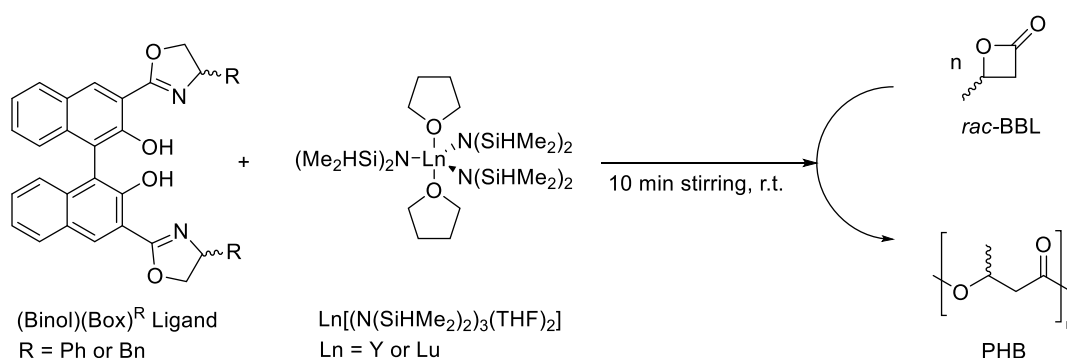


Scheme 23: Polymerization procedure for block copolymerizations with (-)-menthite and *rac*-BBL using a bds- (**4**) and a tetramethylpyrazine-(**2**) bis(phenolate) catalyst.

Mechanical and thermal properties were analyzed by DSC-, TGA-, XRD- and stress-strain-measurements. In scope of application of these sustainable polyesters, stress-strain curves of a *syndiotactic* PHB and a BAB-block copolymer were measured. Both polymers could be processed by hot-molding, which offers an advantage compared to *isotactic* PHB from natural sources. The *syndiotactic* PHB is less brittle than *isotactic* PHB resulting in a lower *Young's*-modulus. Incorporating

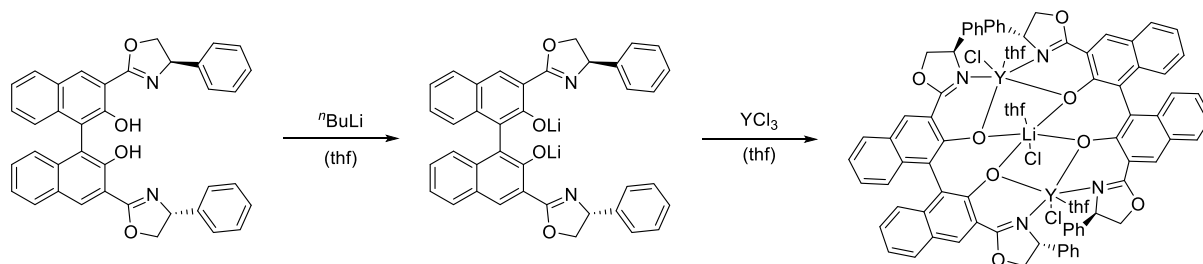
PM in the structure, the elastic modulus is further lowered with increasing the elongation at break. Further studies on the correlation of the block length of each monomer with the mechanical and thermal properties of BAB-polymers are an ongoing work that is not reported in this thesis. In addition, DMA-measurements could be performed.

In the last part of the thesis, the stereoselective ring-opening polymerization of *racemic* BBL to (*R*)-*isotactic*-enriched to *isotactic* PHB was realized by introduction of a new ligand to yttrium complexes. It was possible to synthesize a (*R*)(*R*)-, (*S*)(*S*)-, (*R*)(*S*)- and (*S*)(*R*)- (BINOL)(Box)^{phenyl} ligand, as well as the (*R*)(*R*)- and (*S*)(*R*)- (BINOL)(Box)^{benzyl} ligands. All ligands were used for an *in situ* polymerization with a Ln(bdsa)₃(thf)₂ (Ln = Y or Lu) precursor (Scheme 24).



Scheme 24: *In situ* polymerizations of *rac*-BBL with different ligand/precursor combinations.

All precursor/ligand mixtures are active in the ring-opening polymerization of *rac*-BBL. Microstructural analysis by ¹³C nmr spectroscopy confirmed that *isotactic*-enriched to *isotactic* PHB with different tacticities was obtained. In the next step, we tested the complexation reaction *via* amine elimination with Y(bdsa)₃(thf)₂ which is the commonly used route to nonmetallocene yttrium-complexes. However, this reaction leads to different species that are detectable *via* ¹H nmr spectroscopy. In the further course of this work, a synthesis route *via* salt metathesis was developed in which formation of several species is prevented by deprotonation of the binaphthol-OH groups. In the first step a deprotonation with *n*-butyllithium generates the lithiated ligand detectable *via* shift of the oxazoline protons in the ¹H nmr spectrum. During complexation with YCl₃ only one complex is formed indicated by ¹H and DOSY nmr spectroscopy (Scheme 25). A splitting of the oxazoline-protons shows a highly chiral surrounding in the catalyst structure. A complex structure of [(BINOL)(Box)^{Ph}YCl(thf)]₂LiCl(thf) was proven *via* several analytic methods including crystallographic analysis.



Scheme 25: Synthesis of $[(\text{BINOL})(\text{Box})^{\text{Ph}}\text{YCl}(\text{thf})]_2\text{LiCl}(\text{thf})$ via salt metathesis reaction of YCl_3 with $\text{Li}_2(\text{BINOL})(\text{Box})^{\text{Ph}}$.

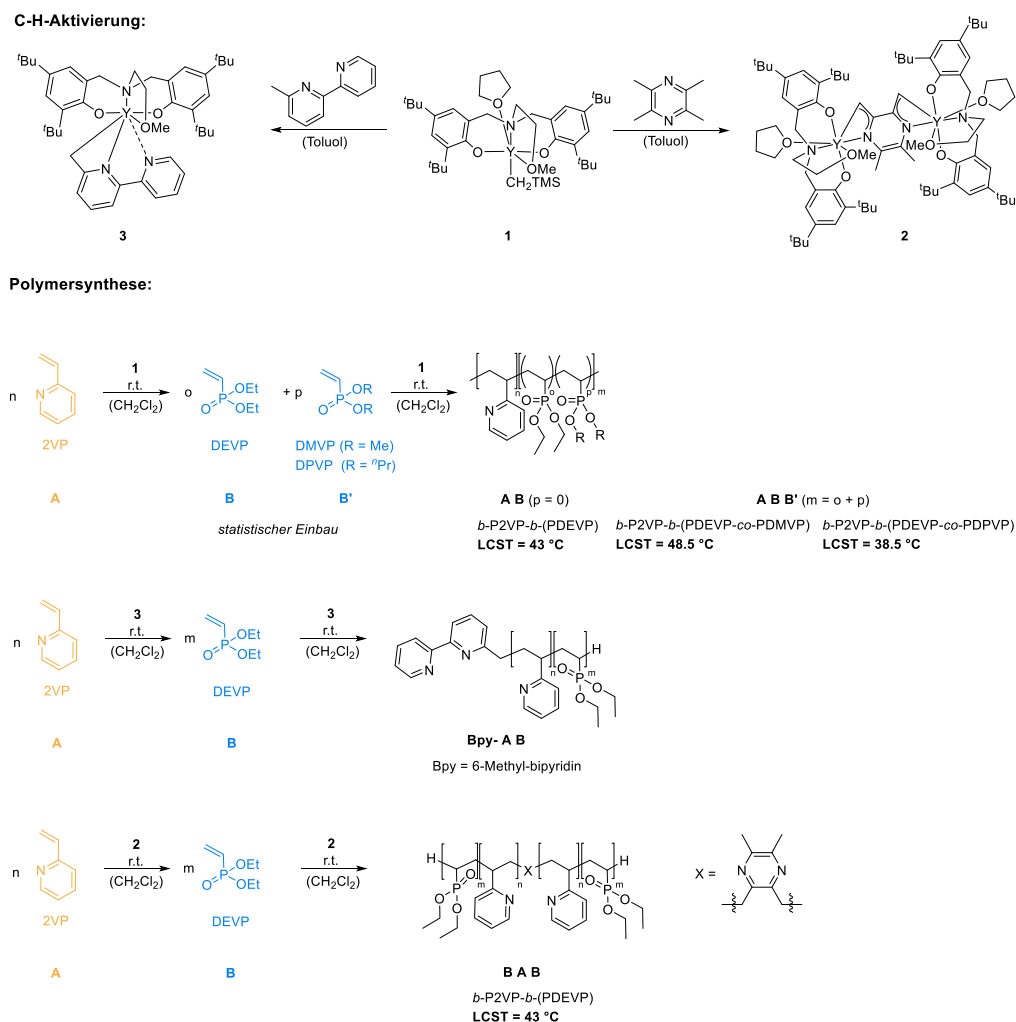
This complex is also active in ring-opening polymerization after activation with alkali-metal nucleophiles (Li-bdsa, K-btsa) and produces PHB with an isotacticity of 78%. Further activity studies and investigations in the microstructure were carried out in the further course of the project, but were only partially successful and must be continued.

12 Zusammenfassung und Ausblick

12.1 Gruppentransferpolymerisation

In dieser Arbeit wurde die Seltenerdmetall-katalysierte Gruppentransferpolymerisation (REM-GTP) mit Bis(phenolat)-Lanthanoiden als Methode zur effizienten Synthese von neuen, hochleistungsfähigen und maßgeschneiderten Polymeren mit variabler Taktizität, kontrollierbaren Molekulargewichten und engen Molmassenverteilungen untersucht. Die durchgeführte Studie über isostrukturelle 2-Methoxyethylamino-bis(phenolat)-Lanthanoid-Komplexen kombiniert die experimentellen Ergebnisse der REM-GTP mit detaillierten quantenchemischen Rechnungen über den Initiierungsprozess dieser Polymerisationsart. Diese Rechnungen geben einen genauen Einblick in den Initiations- und Reaktionsmechanismus und in die elektronischen Eigenschaften der Katalysatoren. Diese Analyse umfasst die Differenzierung von elektronen-donierenden und nicht-donierenden *Michael*-Monomeren, den Einfluss des Ionenradius der Metallzentren im Komplex (Yttrium und Lutetium) und den Unterschied zweier Initiatoren (stark nukleophile Alkylinitiatoren gegenüber elektronen-donierenden Heteroaromaten). Die Untersuchung beinhaltet den Einfluss dieser Parameter auf die Aktivität, Initiatoreffektivität und Taktizität der erhaltenen Polymere und ermöglicht, einen „Baukasten“ verschiedener Katalysatoren zu erzeugen, in dem jeder Einzelne für ein bestimmtes Monomer oder eine bestimmte Stereoselektivität bevorzugt ist. Die höhere Azidität von Lutetium führt zu einer verbesserten Aktivität bei der 2VP-Polymerisation (höchste deklarierte normalisierte Umkehrfrequenz zu diesem Zeitpunkt). Die stark basischen Alkylinitiatoren sind jedoch ineffizient und langsam bei der Initiierung der Polymerisation von DEVP, da eine Deprotonierung des aziden α -CH-Atoms stattfindet und daher keine Initiierung über einen nukleophilen Angriff des stark basischen Initiators auf das erste Monomer erfolgen kann. Um Nebenreaktionen zu vermeiden und die Initiatoreffektivität zu verbessern wurden heteroaromatische Initiatoren über eine σ -Bindungsmetathese eingeführt. Jedoch zeigen die untersuchten Komplexe mit diesen Initiatoren eine verminderte Effizienz bei der Polymerisation mit elektronenschiebenden Monomeren (2VP und IPOx), da eine Überladung an Elektronendichte am Yttriumzentrum erzeugt wird. DFT-Studien stützen die These, dass eine Koordination von Stickstoff-donierenden Monomeren (die ein freies Elektronenpaar besitzen) mit Yttriumkatalysatoren gehindert ist, wenn auch ein Heteroaromat (ebenfalls N-donierend) als Initiator verwendet wird. Im Gegensatz dazu wurde für die Polymerisationen von DMAA und DEVP gezeigt, dass die CH-Aktivierung eines Substrats auf Pyridinbasis eine vielseitige Methode für effiziente Initiatoren ist. Diese gesteigerten Initiatoreffektivitäten ermöglichen zusätzlich eine hoch isoselektive Polymerisation von DMAA, da Polymerisationen bei niedrigen Temperaturen (-78 °C) möglich sind. Die untersuchten Komplexe wurden zusätzlich zur Endgruppenfunktionalisierung von P2VP und für

Copolymerisationen von 2VP mit DEVP angewendet. Die Kombination von hydrophilem Polydialkylvinylphosphonaten, mit einem thermoresponsiven Verhalten, und hydrophobem Poly-2-vinylpyridin, mit seiner pH-abhängigen Löslichkeit, ermöglicht die Synthese neuer multiresponsiver Mizellen. 2-Methoxyethylamino-bis(phenolat)-Yttrium-Komplexe mit einem CH₂TMS- (1) oder Tetramethylpyrazin-Initiator (2) wurden als Katalysatoren zur Herstellung von AB- und ABB'-Blockcopolymeren und zur Synthese von BAXAB-Systemen (X = Tetramethylpyrazin-Initiator, A = P2VP, B = PDEVP, B' = PDMVP oder PDPVP) verwendet (Schema 1). Es ist möglich, die Zusammensetzung des Copolymers präzise durch die Verhältnisse der Monomere zueinander zu bestimmen. Verschiedene Monomer-Zusammensetzungen können verwendet werden, um die Kettenlänge des P2VP- und des PDEVP-Blocks zu variieren und Copolymere mit verschiedenen molaren Massen zu erhalten.



Schema 1: Synthese multiresponsiver AB, ABB' und BAB Copolymere mit verschiedenen Bis(phenolat)-Katalysatoren 1-3.

DLS-Messungen der AB-Polymere zeigen, dass eine Mindestlänge der P2VP- und PDEV-Blöcke erforderlich ist, um die Mizellenbildung zu gewährleisten. Die Blockcopolymere, die ein Verhältnis von mindestens 50/90 besitzen, bilden unimodale, perfekt geformte Micellen oberhalb ihrer kritischen Mizellenbildungskonzentration (Abbildung 1). Außerdem zeigen die Polymere eine pH-abhängige Löslichkeit und eine untere kritische Lösungstemperatur (LCST). Die pH-abhängige Löslichkeit wurde durch Titration mit Salzsäure-Lösung untersucht. Stabile Micellen sind bei $\text{pH} > 4,5$ vorhanden. Bemerkenswerterweise hat das Vorhandensein von P2VP und auch die Variation der Kettenlänge von PDEV keinen messbaren Effekt auf die kritische Lösungstemperatur der Copolymere, welche immer zwischen 43 und $43,5$ °C liegt. Da eine Temperatur von etwa 44 °C nicht im Körpertemperaturbereich liegt, wurden Untersuchungen zur Synthese von ABB'-Blockcopolymeren durchgeführt. Verschiedene substituierte Dialkylvinylphosphonate wurden statistisch in den PDEV-Block eingebaut, um die temperaturabhängige Löslichkeit dieser mizellaren Systeme zu verändern. Der Einbau von zehn Äquivalenten hydrophilem Dimethylvinylphosphonat reicht aus, um die kritische Lösungstemperatur auf $48,5$ °C zu erhöhen. In ähnlicher Weise verringert hydrophobes Di-*n*-propylvinylphosphonat (3 Äq.) erfolgreich diesen Wert auf $38,5$ °C.

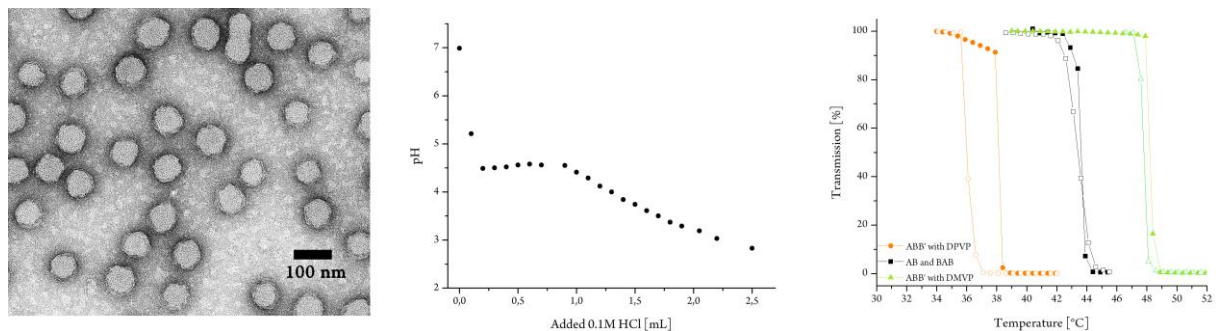


Abbildung 1: Links) TEM-Bild einer BAB-Micelle mit $D_h = 54$ nm. Mitte) Titrationskurve eines AB-Polymers mit $0,1$ M Salzsäure. Rechts) LCST-Messungen von AB, BAB und ABB' Blockcopolymeren.

Zur Untersuchung der Beladungs- und Freisetzungsfähigkeiten der BAB-Polymere wurde Fluorescein verwendet. Es wurden pH- ($4,5$) und temperatur- (44 °C) abhängige Messungen durchgeführt, da die Polymere bifunktionelle Eigenschaften aufweisen. Diese Messungen zeigen unterschiedliches Freisetzungsverhalten von Fluorescein in Abhängigkeit der Vinylphosphonatblocklänge des Polymers. Das BAB-Polymer mit der kürzesten PDEV-Kettenlänge zeigt dabei die niedrigste Freisetzungseffizienz. Außerdem kann die pH-Abhängigkeit für eine sehr schnelle Freisetzung verwendet werden, während die temperatur-gesteuerte Freisetzung der geladenen Substanz über einen Zeitraum von 25 Stunden nur verzögert erreicht wird. Um zu testen, ob diese Systeme als zelluläre Wirkstoffabgabesysteme wirken können, wurde die zelluläre Aufnahme von Nilrot gefärbten Micellen

in Eierstockkrebs-Zellen und anschließende pH-abhängige Freisetzung getestet. Die intrazelluläre Freisetzung wird unter sauren Bedingungen erreicht, da Nilrot fluoresziert, wenn es mit freien Lipiden interagiert, nachdem es vom Träger freigesetzt wurde. Untersuchungen zu einer *in-vitro* Freisetzung des unlöslichen Krebsmedikaments Doxorubicin wurden ebenfalls durchgeführt. Die Freisetzung von DOX geht mit der Abnahme der Lebensfähigkeit von Krebszellen einher. Nach Verifikation, dass nicht-beladene BAB-Micellen nicht toxisch sind, konnte die beobachtete verringerte Zellebensfähigkeit durch die Zytotoxizität von erfolgreich freigesetztem DOX aus den Mizellen erklärt werden.

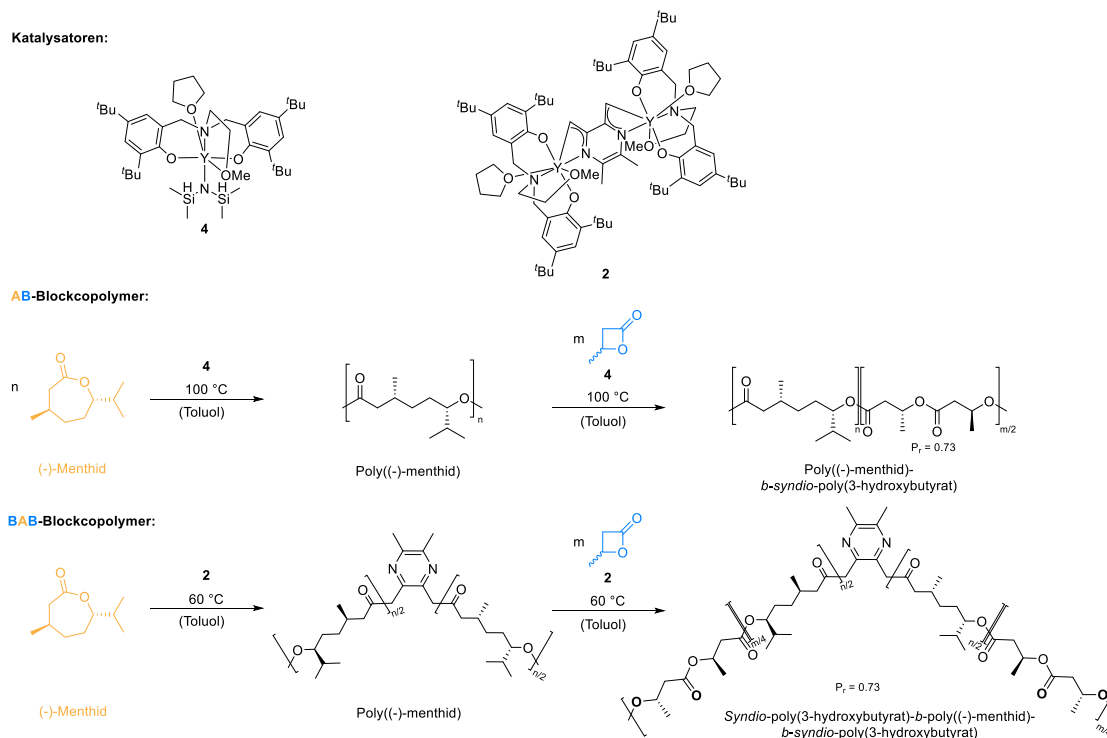
Um ein neues Anwendungsgebiet für 2VP-DEVP-Blockcopolymerer zu adressieren, wurden *ortho*-methylierte Bipyridine als Initiatoren in 2-Aminoalkoxy-bis(phenolat)-Yttrium-Komplexe eingeführt, die dann als Endgruppen in der GTP dienen. Die bpy-Endgruppen ermöglichen eine Metallkomplexierung, die durch die Reaktion von bpy-2VP-DEVP-Blockcopolymeren mit $[\text{Re}(\text{CO})_5\text{Cl}]$ nachgewiesen wurde und ein $[\text{Re}(\text{CO})_3(\text{bpy})\text{Cl}]$ -Motiv am Ende jeder Polymerkette erzeugt. Es konnte außerdem gezeigt werden, dass diese Re-2VP-DEVP-Blockcopolymerer in Wasser weiterhin Mizellen bilden. Der hydrophobe Kern (P2VP), der den ebenfalls hydrophoben Rheniumkomplex enthält, wird durch die hydrophilen Segmente (PDEVP) vom wässrigen Milieu abgeschirmt. Dadurch wird ein möglicher Träger für hydrophobe metallhaltige Komplexe in Zellen erhalten. Um nachzuweisen, dass der Polymeranteil dieser Systeme die Eigenschaften des metallorganischen Komplexes nicht beeinflusst, verwendeten wir die Re-2VP-DEVP-Blockcopolymerer zur photokatalytischen Reduktion von CO_2 zu CO. Bemerkenswert ist dabei, dass die katalytische Leistung (Umsatzzahl) des Rhenium-Zentrums in den funktionalisierten Blockcopolymeren im Vergleich zu dem analogen Polymer-freien Komplex höher ist.

12.2 Ringöffnungspolymerisation

Poly(hydroxyalkanoate) sind eine vielseitige Klasse von biologisch abbaubaren und biokompatiblen Polymeren, in der Poly(3-hydroxybutyrat) eines der häufigsten PHAs darstellt. Ein vielversprechender Syntheseweg ist, neben natürlich vorkommendem (R)-PHB, die Ringöffnungspolymerisation von *racemischem* β -Butyrolacton. Da *rac*-BBL synthetisch aus Kohlenstoffdioxid zugänglich ist, ist es ein interessantes Monomer für die nachhaltige PHB-Produktion. Nach Untersuchungen von *Carpentier* und *Rieger et al.* können stereoselektive Aminoalkoxy-bis(phenolat) Yttrium-amido-Katalysatoren für die *syndio*-spezifische ROP von *rac*-BBL verwendet werden. Neben häufig verwendeten Bis(di- oder trimethylsilyl)amid-, CH_2TMS - und *iso*-Propanol-Initiatoren wurden keine weitere effiziente Initiatoren in der REM-vermittelten ROP von BBL untersucht. In dieser Arbeit stellten sich heteroaromatische Initiatoren, die über eine η^3 -(C,C,N)-Aza-Allylische-Bindung an das Yttriumzentrum koordinieren und

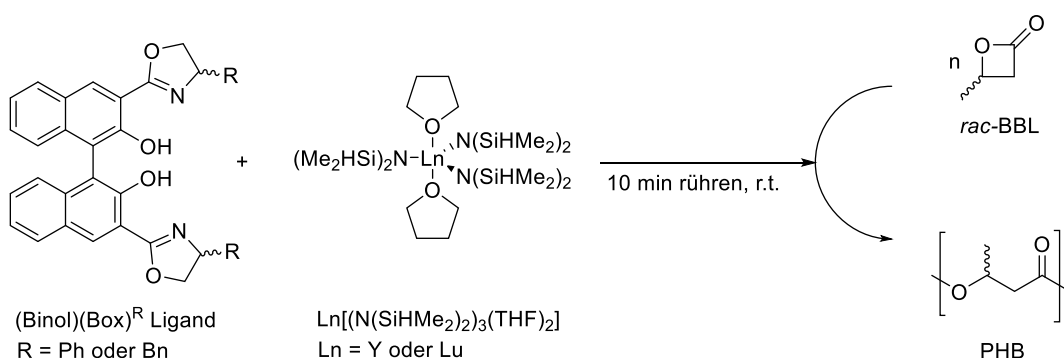
bisher nicht als Initiatoren in der ROP getestet wurden, als effiziente Katalysatoren für die *syndio*-spezifische BBL-Polymerisation heraus. Neben Kohlendioxid als Kohlenstoffquelle können verschiedene weitere natürliche Produkte für die Herstellung von biobasierten Polymeren verwendet werden. Eine wichtige Klasse unter diesen sind die Terpene. Die natürlich vorkommenden cyclischen Vertreter wie (-)-Menthon können in die entsprechenden Lactone umgewandelt werden. In dieser Arbeit wurden die ersten Katalysatoren auf Lanthanoidbasis beschrieben, die in der Lage sind, (-)-Menthide zu Poly((-)-menthid) unter milden Bedingungen mit sehr niedrigen Molekulargewichtsverteilungen zu polymerisieren.

Unter Zug-Belastung bricht taktisches PHB, welches mit diesen Yttrium-Katalysatoren erhalten wird, bei sehr geringen Dehnungen und ist daher für Anwendungen, bei denen Elastizität notwendig ist, ungeeignet. Die Verbesserung der Zug-Dehnungs-Eigenschaften wurde durch erstmalige Einarbeitung von *syndiotaktischem* PHB in Blockcopolymeren durch einfache sequentielle Zugabe der jeweiligen Monomere zum Reaktionsgemisch erreicht. AB-Blockcopolymeren mit Poly((-)-menthid) als ersten Block (A) und *syndiotaktischem* PHB als zweitem Block (B) wurde über Verwendung des Bis(phenolat)-Yttrium-bdsa-Komplex (4) erhalten. DOSY-NMR-Untersuchungen, GPC- und DSC-Messungen zeigen die Verknüpfung zwischen den beiden Blöcken im Vergleich zu einer Mischung aus PM- und PHB-Homopolymeren. Eine Trennung der Glasübergangstemperaturen in der DSC-Kurve wird sowohl für das Polymerblend als auch für die AB-Polymeren beobachtet, was auf die Phasentrennung der Polymeren innerhalb der Materialien hindeutet. Jedoch zeigt sich für die AB-Polymeren eine Abwesenheit des Schmelzpunktes, wodurch ein amorphes Material erhalten wird. Um thermoplastische Elastomere zu erhalten, wurden daher ABA-Blockcopolymeren unter Verwendung des bifunktionellen Tetramethylpyrazin-Bis(phenolat)-Katalysators (2) hergestellt (Schema 2). Mechanische und thermische Eigenschaften wurden mittels DSC-, TGA-, XRD- und Zug-Dehnungs-Messungen analysiert. Um die Anwendbarkeit der Polyester zu testen, wurden die mechanischen Eigenschaften eines *syndiotaktischen* PHBs und eines BAB-Blockcopolymeren gemessen. Beide Proben können über Heißpressen hergestellt werden, was ein Vorteil gegenüber natürlichem PHB darstellt. Zug-Dehnungs-Messungen zeigen, dass das *syndiotaktische* PHB weniger brüchig ist als *isotaktisches* PHB, nachgewiesen durch ein niedrigeres Elastizitätsmodul. Wenn Polymenthid in die Struktur eingebaut wird, wird das Elastizitätsmodul weiter verringert und die Dehnbarkeit steigt. Weitere Studien zur Korrelation der Blocklänge jedes Monomers mit den mechanischen und thermischen Eigenschaften von BAB-Polymeren sind noch nicht vollständig untersucht worden. Zusätzlich könnten DMA-Messungen durchgeführt werden.



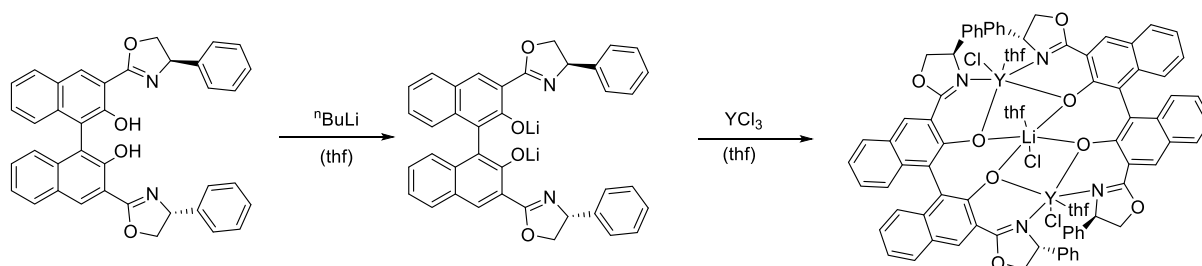
Schema 2: Synthese von Blockcopolymeren mit (-)-Menthid und *rac*-BBL hergestellt mit *bsda*-(4) und tetramethylpyrazin-(2) bis(phenolat)yttrium-Katalysatoren.

Im letzten Teil dieser Arbeit wurde die stereoselektive ROP von *racemischem* BBL zu (R) -*isotaktisch*-angereichertem zu *isotaktischem* PHB durch Einführung eines neuen Liganden in Yttriumkomplexe realisiert. Es war möglich, einen (*rac*)(R)-, (R)(R)-, (S)(S)-, (R)(S)- und (S)(R)-(BINOL)(Box)^{Phenyl}-Liganden zu synthetisieren, sowie die (R)(R)- und (S)(R)-(BINOL)(Box)^{Benzyl}-Liganden. Alle Liganden wurden für eine *in-situ* Polymerisation von BBL mit einem Ln(*bsda*)₃(thf)₂-Vorläuferkomplex (Ln = Y oder Lu) verwendet (Schema 3).



Schema 3: *In-situ* Polymerisation von *rac*-BBL mit verschiedenen Ligand/Vorläuferkomplex Kombinationen.

Alle Vorläufer/Ligand-Mischungen sind aktiv in der ROP von *rac*-BBL. Die Mikrostruktur des Polymers kann durch ^{13}C -NMR-Spektroskopie analysiert werden und diese Messungen bestätigten, dass *isotaktisch*-angereichertes bis *isotaktisches* PHB mit unterschiedlichen Taktizitäten erhalten wurde. Im nächsten Schritt wurde die Komplexierungsreaktion über die Amin-Eliminierungs-Reaktion mit $\text{Y}(\text{bdsa})_3(\text{thf})_2$ nach dem üblicherweise verwendeten Weg für Bis(phenolat)-Yttrium-Komplexe getestet. Diese Reaktion führt jedoch zu verschiedenen Spezies, wie ^1H -NMR-Spektroskopie zeigt. Im weiteren Verlauf dieser Arbeit wurde ein Syntheseweg über Salzmetathese entwickelt, bei dem die Bildung mehrerer Spezies durch Deprotonierung der Binaphthol-OH-Gruppen verhindert wird. Im ersten Schritt erzeugt eine Deprotonierung mit *n*-Butyllithium den lithiierten Liganden, der über die Verschiebung der Oxazolinprotonen im ^1H -NMR-Spektrum nachweisbar ist. Während der Komplexierung mit YCl_3 wird nur ein Komplex gebildet, wie ^1H - und DOSY-NMR-Spektroskopie bestätigt. Eine Aufspaltung der Oxazolin-Protonen zeigt eine stark chirale Umgebung in der Katalysatorstruktur. Eine Struktur der Form $[(\text{BINOL})(\text{Box})^{\text{Ph}}\text{YCl}(\text{thf})]_2\text{LiCl}(\text{thf})$ wurde über mehrere analytische Methoden einschließlich kristallographischer Analyse nachgewiesen (Schema 4).



Schema 4: Synthese von $[(\text{BINOL})(\text{Box})^{\text{Ph}}\text{YCl}(\text{thf})]_2\text{LiCl}(\text{thf})$ über Salzmetathese mit YCl_3 und $\text{Li}_2(\text{BINOL})(\text{Box})^{\text{Ph}}$.

Dieser Komplex ist ebenfalls aktiv in der Ringöffnungspolymerisation und nach der Aktivierung (mit K-btsa, Li-bdsa) erzeugt dieser PHB mit einer Isotaktizität von 76%. Weitere Aktivitätsstudien und Untersuchungen der Mikrostruktur wurden im weiteren Verlauf dieser Arbeit durchgeführt, waren jedoch nur teilweise erfolgreich und müssen fortgesetzt werden.

13 References

- [1] K. Horie, *Macromol. Chem. Phys.* **2003**, *204*, 1134-1136.
- [2] P. M. Hergenrother, *High Perform. Polym.* **2003**, *15*, 3-45.
- [3] https://www.plasticseurope.org/application/files/2815/1689/9283/2006compelling_fact_PubJan2008.pdf, Status: July 2018.
- [4] <https://committee.iso.org/files/live/sites/tc61/files/The%20Plastic%20Industry%20Berlin%20Aug%202016%20-%20Copy.pdf>. Status: July 2018.
- [5] https://www.plasticseurope.org/application/files/5715/1717/4180/Plastics_the_facts_2017_FINAL_for_website_one_page.pdf, Status: July 2018.
- [6] A. H. Tullo, *Chemical & Engineering News* **2016**, *94*, 23-24.
- [7] E. R. Larson, *Thermoplastic Material Selection: A Practical Guide*, Elsevier Science, **2015**.
- [8] M. M. S. Koltzenburg, O. Nuyken, *Polymere: Synthese, Eigenschaften und Anwendungen*, Springer Spektrum, Berlin, Heidelberg, **2004**.
- [9] H. G. Elias, *Macromolecules: Volume 4: Applications of Polymers*, Wiley, **2009**.
- [10] R. B. Seymour, G. B. Kauffman, *J. Chem. Educ.* **1992**, *69*, 311.
- [11] V. Arrighi, J.M.G Cowie, *Polymers: Chemistry and Physics of Modern Materials, Third Edition*, CRC Press, New York, **2008**.
- [12] R. Benhamou, *Technology and Culture* **2001**, *42*, 571-573.
- [13] A. Shenoy, *Thermoplastic Melt Rheology and Processing*, CRC Press, **1996**.
- [14] *Selecting Thermoplastics for Engineering Applications, Second Edition*, Taylor & Francis, **1997**.
- [15] R. D. Maier, M. Schiller, *Handbuch Kunststoff Additive*, Carl Hanser Verlag GmbH & Company KG, **2016**.
- [16] C. A. Heaton, *The Chemical Industry*, Springer Netherlands, **2012**.
- [17] F. Adams, P. Pahl, B. Rieger, *Chem. Eur. J.* **2018**, *24*, 509-518.
- [18] D. N. Schulz, O. P. Abhimanyu, in *Functional Polymers, Vol. 704*, American Chemical Society, **1998**, pp. 1-14.
- [19] B. S. Soller, N. Zhang, B. Rieger, *Macromol. Chem. Phys.* **2014**, *215*, 1946-1962.
- [20] D. K. Dimov, T. E. Hogen-Esch, *Macromolecules* **1995**, *28*, 7394-7400.
- [21] Y. E. Shapiro, *Bulletin of Magnetic Resonance* **1985**, *7*, 27-58.
- [22] D. Steinborn, *Grundlagen der metallorganischen Komplexkatalyse, Vol. 2*, Vieweg + Teubner, Wiesbaden, **2010**.
- [23] W. Kaminsky, *Polyolefins: 50 Years After Ziegler and Natta II: Polyolefins by Metallocenes and Other Single-Site Catalysts, Vol. 258*, Springer, **2013**.
- [24] W.-F. Su, in *Principles of Polymer Design and Synthesis*, Springer Berlin Heidelberg, Berlin, Heidelberg, **2013**, pp. 219-232.

- [25] B. Rieger, A. Künkel, G. W. Coates, R. Reichardt, E. Dinjus, T. A. Zevaco, *Synthetic Biodegradable Polymers, Vol. 245*, Springer Science & Business Media, **2012**.
- [26] P. Dubois, O. Coulembier, J.-M. Raquez, *Handbook of ring-opening polymerization*, John Wiley & Sons, **2009**.
- [27] J.-F. Carpentier, *Macromol. Rapid Commun.* **2010**, *31*, 1696-1705.
- [28] Z. Grobelny, A. Stolarzewicz, B. Morejko, W. Pisarski, A. Maercker, A. Skibiński, S. Krompiec, J. Rzepa, *Macromolecules* **2006**, *39*, 6832-6837.
- [29] Z. Jedliński, M. Kowalczyk, P. Kurcok, G. Adamus, A. Matuszowicz, W. Sikorska, R. A. Gross, J. Xu, R. W. Lenz, *Macromolecules* **1996**, *29*, 3773-3777.
- [30] L. R. Rieth, D. R. Moore, E. B. Lobkovsky, G. W. Coates, *J. Am. Chem. Soc.* **2002**, *124*, 15239-15248.
- [31] S. Penczek, M. Cypryk, A. Duda, P. Kubisa, S. Słomkowski, *Prog. Polym. Sci.* **2007**, *32*, 247-282.
- [32] N. C. Billingham, M. G. Proctor, J. D. Smith, *J. Organomet. Chem.* **1988**, *341*, 83-93.
- [33] A. Hamitou, T. Ouhadi, R. Jerome, P. Teyssié, *J. Polym. Sci. Pol. Chem.* **1977**, *15*, 865-873.
- [34] T. Ouhadi, A. Hamitou, R. Jérôme, P. Teyssié, *Macromolecules* **1976**, *9*, 927-931.
- [35] W. J. Evans, H. Katsumata, *Macromolecules* **1994**, *27*, 2330-2332.
- [36] M. Yamashita, Y. Takemoto, E. Ihara, H. Yasuda, *Macromolecules* **1996**, *29*, 1798-1806.
- [37] E. Martin, P. Dubois, R. Jérôme, *Macromolecules* **2003**, *36*, 5934-5941.
- [38] W. M. Stevels, M. J. K. Ankoné, P. J. Dijkstra, J. Feijen, *Macromolecules* **1996**, *29*, 8296-8303.
- [39] W. M. Stevels, M. J. K. Ankoné, P. J. Dijkstra, J. Feijen, *Macromolecules* **1996**, *29*, 3332-3333.
- [40] E. Martin, P. Dubois, R. Jérôme, *Macromolecules* **2000**, *33*, 1530-1535.
- [41] K. Tortosa, T. Hamaide, C. Boisson, R. Spitz, *Macromol. Chem. Phys.* **2001**, *202*, 1156-1160.
- [42] M. Save, M. Schappacher, A. Soum, *Macromol. Chem. Phys.* **2002**, *203*, 889-899.
- [43] A. L. Borgne, C. Pluta, N. Spassky, *Macromol. Rapid Commun.* **1994**, *15*, 955-960.
- [44] A. Le Borgne, N. Spassky, *Polymer* **1989**, *30*, 2312-2319.
- [45] B. Wu, R. W. Lenz, *Macromolecules* **1998**, *31*, 3473-3477.
- [46] S. Bloembergen, D. A. Holden, T. L. Bluhm, G. K. Hamer, R. H. Marchessault, *Macromolecules* **1989**, *22*, 1656-1663.
- [47] R. W. Lenz, J. Yang, B. Wu, C. J. Harlan, A. R. Barron, *Can. J. Microbiol.* **1995**, *41*, 274-281.
- [48] C. K. Williams, N. R. Brooks, M. A. Hillmyer, W. B. Tolman, *Chem. Commun.* **2002**, 2132-2133.
- [49] C. K. Williams, L. E. Breyfogle, S. K. Choi, W. Nam, V. G. Young, M. A. Hillmyer, W. B. Tolman, *J. Am. Chem. Soc.* **2003**, *125*, 11350-11359.
- [50] C. M. Silvernail, L. J. Yao, L. M. R. Hill, M. A. Hillmyer, W. B. Tolman, *Inorg. Chem.* **2007**, *46*, 6565-6574.
- [51] D. Zhang, M. A. Hillmyer, W. B. Tolman, *Biomacromolecules* **2005**, *6*, 2091-2095.

- [52] B. M. Chamberlain, M. Cheng, D. R. Moore, T. M. Ovitt, E. B. Lobkovsky, G. W. Coates, *J. Am. Chem. Soc.* **2001**, *123*, 3229-3238.
- [53] C. Guillaume, J.-F. Carpentier, S. M. Guillaume, *Polymer* **2009**, *50*, 5909-5917.
- [54] S. Inoue, S. Jacob, M. Jiang, J. P. Kennedy, M. Li, H. Sugimoto, M. Xiang, H. Zhou, *Polymer Synthesis Polymer-Polymer Complexation*, Springer Berlin Heidelberg, **2003**.
- [55] S. Inoue, *J. Polym. Sci. Pol. Chem.* **2000**, *38*, 2861-2871.
- [56] N. Ajellal, J. F. Carpentier, C. Guillaume, S. M. Guillaume, M. Helou, V. Poirier, Y. Sarazin, A. Trifonov, *Dalton Trans.* **2010**, *39*, 8363-8376.
- [57] A. Kronast, M. Reiter, P. T. Altenbuchner, C. Jandl, A. Pöthig, B. Rieger, *Organometallics* **2016**, *35*, 681-685.
- [58] S. Vagin, M. Winnacker, A. Kronast, P. T. Altenbuchner, P. Deglmann, C. Sinkel, R. Loos, B. Rieger, *ChemCatChem* **2015**, *7*, 3963-3971.
- [59] R. Reichardt, S. Vagin, R. Reithmeier, A. K. Ott, B. Rieger, *Macromolecules* **2010**, *43*, 9311-9317.
- [60] M. Zintl, F. Molnar, T. Urban, V. Bernhart, P. Preishuber-Pflügl, B. Rieger, *Angew. Chem. Int. Ed.* **2008**, *47*, 3458-3460.
- [61] Y. Hori, T. Hagiwara, *Int. J. Biol. Macromol.* **1999**, *25*, 237-245.
- [62] J. E. Kemnitzer, S. P. McCarthy, R. A. Gross, *Macromolecules* **1993**, *26*, 1221-1229.
- [63] J. E. Kemnitzer, S. P. McCarthy, R. A. Gross, *Macromolecules* **1993**, *26*, 6143-6150.
- [64] H. R. Kricheldorf, S.-R. Lee, N. Scharnagl, *Macromolecules* **1994**, *27*, 3139-3146.
- [65] C.-X. Cai, L. Toupet, C. W. Lehmann, J.-F. Carpentier, *J. Organomet. Chem.* **2003**, *683*, 131-136.
- [66] C.-X. Cai, A. Amgoune, C. W. Lehmann, J.-F. Carpentier, *Chem. Commun.* **2004**, 330-331.
- [67] A. Amgoune, C. M. Thomas, T. Roisnel, J.-F. Carpentier, *Chem. Eur. J.* **2005**, *12*, 169-179.
- [68] A. Amgoune, C. M. Thomas, J. F. Carpentier, *Macromol. Rapid Commun.* **2007**, *28*, 693-697.
- [69] E. Y. Tshuva, S. Groysman, I. Goldberg, M. Kol, Z. Goldschmidt, *Organometallics* **2002**, *21*, 662-670.
- [70] A. Amgoune, C. M. Thomas, S. Ilinca, T. Roisnel, J.-F. Carpentier, *Angew. Chem. Int. Ed.* **2006**, *45*, 2782-2784.
- [71] N. Ajellal, M. Bouyahyi, A. Amgoune, C. M. Thomas, A. Bondon, I. Pillin, Y. Grohens, J.-F. Carpentier, *Macromolecules* **2009**, *42*, 987-993.
- [72] L. Clark, M. G. Cushion, H. E. Dyer, A. D. Schwarz, R. Duchateau, P. Mountford, *Chem. Commun.* **2010**, *46*, 273-275.
- [73] H. E. Dyer, S. Huijser, N. Susperregui, F. Bonnet, A. D. Schwarz, R. Duchateau, L. Maron, P. Mountford, *Organometallics* **2010**, *29*, 3602-3621.
- [74] K. Nie, L. Fang, Y. Yao, Y. Zhang, Q. Shen, Y. Wang, *Inorg. Chem.* **2012**, *51*, 11133-11143.
- [75] T. Zeng, Q. Qian, B. Zhao, D. Yuan, Y. Yao, Q. Shen, *RSC Adv.* **2015**, *5*, 53161-53171.
- [76] M. Bouyahyi, N. Ajellal, E. Kirillov, C. M. Thomas, J.-F. Carpentier, *Chem. Eur. J.* **2011**, *17*, 1872-1883.

- [77] Y. Chapurina, J. Klitzke, O. d. L. Casagrande Jr, M. Awada, V. Dorcet, E. Kirillov, J.-F. Carpentier, *Dalton Trans.* **2014**, *43*, 14322-14333.
- [78] E. Grunova, E. Kirillov, T. Roisnel, J.-F. Carpentier, *Dalton Trans.* **2010**, *39*, 6739-6752.
- [79] P. T. Altenbuchner, A. Kronast, S. Kissling, S. I. Vagin, E. Herdtweck, A. Pöthig, P. Deglmann, R. Loos, B. Rieger, *Chem. Eur. J.* **2015**, *21*, 13609-13617.
- [80] Z. Zhang, X. Xu, W. Li, Y. Yao, Y. Zhang, Q. Shen, Y. Luo, *Inorg. Chem.* **2009**, *48*, 5715-5724.
- [81] Y. J. Luo, W. Y. Li, D. Lin, Y. M. Yao, Y. Zhang, Q. Shen, *Organometallics* **2010**, *29*, 3507-3514.
- [82] X. Liu, X. Shang, T. Tang, N. Hu, F. Pei, D. Cui, X. Chen, X. Jing, *Organometallics* **2007**, *26*, 2747-2757.
- [83] J. S. Klitzke, T. Roisnel, E. Kirillov, O. d. L. Casagrande, J.-F. Carpentier, *Organometallics* **2014**, *33*, 309-321.
- [84] M. Sinenkov, E. Kirillov, T. Roisnel, G. Fukin, A. Trifonov, J.-F. Carpentier, *Organometallics* **2011**, *30*, 5509-5523.
- [85] Y. Yao, Z. Zhuo, c. zhang, Y. Luo, Y. Wang, D. Yuan, D. Cui, *Chem. Commun.* **2018**.
- [86] K. Nie, W. Gu, Y. Yao, Y. Zhang, Q. Shen, *Organometallics* **2013**, *32*, 2608-2617.
- [87] M. Mazzeo, R. Tramontano, M. Lamberti, A. Pilone, S. Milione, C. Pellicchia, *Dalton Trans.* **2013**, *42*, 9338-9351.
- [88] E. Grunova, E. Kirillov, T. Roisnel, J.-F. Carpentier, *Organometallics* **2008**, *27*, 5691-5698.
- [89] A. Alaaeddine, C. M. Thomas, T. Roisnel, J.-F. Carpentier, *Organometallics* **2009**, *28*, 1469-1475.
- [90] T. V. Mahrova, G. K. Fukin, A. V. Cherkasov, A. A. Trifonov, N. Ajellal, J.-F. Carpentier, *Inorg. Chem.* **2009**, *48*, 4258-4266.
- [91] N. Ajellal, D. M. Lyubov, M. A. Sinenkov, G. K. Fukin, A. V. Cherkasov, C. M. Thomas, J.-F. Carpentier, A. A. Trifonov, *Chem. Eur. J.* **2008**, *14*, 5440-5448.
- [92] T. V. Mahrova, G. K. Fukin, A. V. Cherkasov, A. A. Trifonov, N. Ajellal, J.-F. Carpentier, *Inorg. Chem.* **2009**, *48*, 4258-4266.
- [93] R. Ligny, M. M. Hänninen, S. M. Guillaume, J. F. Carpentier, *Angew. Chem. Int. Ed.* **2017**, *56*, 10388-10393.
- [94] R. Ligny, M. M. Hänninen, S. M. Guillaume, J.-F. Carpentier, *Chem. Commun.* **2018**, *54*, 8024-8031.
- [95] C. G. Jaffredo, Y. Chapurina, E. Kirillov, J.-F. Carpentier, S. M. Guillaume, *Chem. Eur. J.* **2016**, *22*, 7629-7641.
- [96] O. W. Webster, W. R. Hertler, D. Y. Sogah, W. B. Farnham, T. V. RajanBabu, *J. Am. Chem. Soc.* **1983**, *105*, 5706-5708.
- [97] D. Y. Sogah, W. R. Hertler, O. W. Webster, G. M. Cohen, *Macromolecules* **1987**, *20*, 1473-1488.
- [98] R. P. Quirk, J. Ren, *Macromolecules* **1992**, *25*, 6612-6620.
- [99] A. H. E. Mueller, *Macromolecules* **1994**, *27*, 1685-1690.
- [100] O. W. Webster, *Adv. Polym. Sci.* **2004**, *167*, 1-34.

- [101] M. Rikkou-Kalourkoti, O. W. Webster, C. S. Patrickios, in *Encyclopedia of Polymer Science and Technology*, John Wiley & Sons, Inc., **2002**.
- [102] S. Bywater, *Macromol. Symp.* **1993**, *67*, 339-350.
- [103] E. Y. X. Chen, *Chem. Rev.* **2009**, *109*, 5157-5214.
- [104] Y. Zhang, G. M. Miyake, M. G. John, L. Falivene, L. Caporaso, L. Cavallo, E. Y. X. Chen, *Dalton Trans.* **2012**, *41*, 9119-9134.
- [105] H. Yasuda, *J. Organomet. Chem.* **2002**, *647*, 128-138.
- [106] W. J. Evans, L. A. Hughes, D. K. Drummond, H. Zhang, J. L. Atwood, *J. Am. Chem. Soc.* **1986**, *108*, 1722-1723.
- [107] Y. Hajime, I. Eiji, N. Yuu, K. Takamaro, M. Masakazu, N. Mitsufumi, in *Functional Polymers, Vol. 704*, American Chemical Society, **1998**, pp. 149-162.
- [108] M. A. Giardello, Y. Yamamoto, L. Brard, T. J. Marks, *J. Am. Chem. Soc.* **1995**, *117*, 3276-3277.
- [109] S. Collins, D. G. Ward, *J. Am. Chem. Soc.* **1992**, *114*, 5460-5462.
- [110] S. Collins, D. G. Ward, K. H. Suddaby, *Macromolecules* **1994**, *27*, 7222-7224.
- [111] H. Frauenrath, H. Keul, H. Höcker, *Macromolecules* **2001**, *34*, 14-19.
- [112] T. Stuhldreier, H. Keul, H. Höcker, *Macromol. Rapid Commun.* **2000**, *21*, 1093-1098.
- [113] W. R. Mariott, E. Y. X. Chen, *Macromolecules* **2005**, *38*, 6822-6832.
- [114] W. R. Mariott, E. Y. X. Chen, *Macromolecules* **2004**, *37*, 4741-4743.
- [115] G. M. Miyake, E. Y. X. Chen, *Macromolecules* **2008**, *41*, 3405-3416.
- [116] G. Miyake, L. Caporaso, L. Cavallo, E. Y. X. Chen, *Macromolecules* **2009**, *42*, 1462-1471.
- [117] X. Chen, L. Caporaso, L. Cavallo, E. Y. X. Chen, *J. Am. Chem. Soc.* **2012**, *134*, 7278-7281.
- [118] A. Rodriguez-Delgado, E. Y.-X. Chen, *Macromolecules* **2005**, *38*, 2587-2594.
- [119] G. M. Miyake, S. E. Newton, W. R. Mariott, E. Y. X. Chen, *Dalton Trans.* **2010**, *39*, 6710-6718.
- [120] Y. Zhang, G. M. Miyake, E. Y. X. Chen, *Angew. Chem. Int. Ed.* **2010**, *122*, 10356-10360.
- [121] S. Salzinger, B. Rieger, *Macromol. Rapid Commun.* **2012**, *33*, 1327-1345.
- [122] U. B. Seemann, J. E. Dengler, B. Rieger, *Angew. Chem. Int. Ed.* **2010**, *49*, 3489-3491.
- [123] S. Salzinger, U. B. Seemann, A. Plikhta, B. Rieger, *Macromolecules* **2011**, *44*, 5920-5927.
- [124] J. Parvole, P. Jannasch, *Macromolecules* **2008**, *41*, 3893-3903.
- [125] S. Salzinger, B. S. Soller, A. Plikhta, U. B. Seemann, E. Herdtweck, B. Rieger, *J. Am. Chem. Soc.* **2013**, *135*, 13030-13040.
- [126] N. Zhang, S. Salzinger, B. S. Soller, B. Rieger, *J. Am. Chem. Soc.* **2013**, *135*, 8810-8813.
- [127] Z. Hou, Y. Wakatsuki, *Coord. Chem. Rev.* **2002**, *231*, 1-22.
- [128] P. T. Altenbuchner, B. S. Soller, S. Kissling, T. Bachmann, A. Kronast, S. I. Vagin, B. Rieger, *Macromolecules* **2014**, *47*, 7742-7749.
- [129] H. Kaneko, H. Nagae, H. Tsurugi, K. Mashima, *J. Am. Chem. Soc.* **2011**, *133*, 19626-19629.

- [130] P. T. Altenbuchner, F. Adams, A. Kronast, E. Herdtweck, A. Pöthig, B. Rieger, *Polym. Chem.* **2015**, *6*, 6796-6801.
- [131] T.-Q. Xu, G.-W. Yang, X.-B. Lu, *ACS Catal.* **2016**, *6*, 4907-4913.
- [132] G. Natta, G. Mazzanti, P. Longi, G. Dall'Asta, F. Bernardini, *J. Polym. Sci.* **1961**, *51*, 487-504.
- [133] K. Matsuzaki, T. Kanai, T. Matsubara, S. Matsumoto, *J. Polym. Sci. Pol. Chem.* **1976**, *14*, 1475-1484.
- [134] T. E. Hogen-Esch, C. F. Tien, *J. Polym. Sci. Polym. Lett.* **1979**, *17*, 431-436.
- [135] A. Soum, M. Fontanille, *Die Makromolekulare Chemie* **1980**, *181*, 799-808.
- [136] A. Soum, M. Fontanille, *Die Makromolekulare Chemie* **1982**, *183*, 1145-1159.
- [137] A. Kronast, D. Reiter, P. T. Altenbuchner, S. I. Vagin, B. Rieger, *Macromolecules* **2016**, *49*, 6260-6267.
- [138] C. Yan, T.-Q. Xu, X.-B. Lu, *Macromolecules* **2018**.
- [139] S. G. Alan, I. G. Karen, in *Activation and Functionalization of C-H Bonds*, Vol. 885, American Chemical Society, **2004**, pp. 1-43.
- [140] S. C. Pan, *J. Org. Chem.* **2012**, *8*, 1374-1384, No. 1159.
- [141] B. A. Arndtsen, R. G. Bergman, T. A. Mobley, T. H. Peterson, *Acc. Chem. Res.* **1995**, *28*, 154-162.
- [142] J. A. Labinger, J. E. Bercaw, *Nature* **2002**, *417*, 507-514.
- [143] P. L. Watson, *J. Am. Chem. Soc.* **1983**, *105*, 6491-6493.
- [144] P. L. Watson, *Chem. Commun.* **1983**, 276-277.
- [145] J. E. Huheey, E. A. Keiter, R. L. Keiter, *Anorganische Chemie - Prinzipien von Struktur und Reaktivität*, Vol. 4, De Gruyter, Berlin, **2012**.
- [146] R. Duchateau, C. T. van Wee, A. Meetsma, J. H. Teuben, *J. Am. Chem. Soc.* **1993**, *115*, 4931-4932.
- [147] R. Duchateau, E. A. C. Brussee, A. Meetsma, J. H. Teuben, *Organometallics* **1997**, *16*, 5506-5516.
- [148] R. Duchateau, C. T. van Wee, J. H. Teuben, *Organometallics* **1996**, *15*, 2291-2302.
- [149] H. Nagae, A. Kundu, H. Tsurugi, K. Mashima, *Organometallics* **2017**, *36*, 3061-3067.
- [150] Y. Shibata, H. Nagae, S. Sumiya, R. Rochat, H. Tsurugi, K. Mashima, *Chem. Sci.* **2015**, *6*, 5394-5399.
- [151] B. S. Soller, S. Salzinger, C. Jandl, A. Pöthig, B. Rieger, *Organometallics* **2015**, *34*, 2703-2706.
- [152] P. Pahl, C. Schwarzenböck, F. A. D. Herz, B. S. Soller, C. Jandl, B. Rieger, *Macromolecules* **2017**, *50*, 6569-6576.
- [153] Y. Tokiwa, B. P. Calabia, C. U. Ugwu, S. Aiba, *Int. J. Mol. Sci.* **2009**, *10*, 3722-3742.
- [154] C. R. Y. Zhu, C. K. Williams, *Nature* **2016**, *540*, 354-362.
- [155] H. F. J. Rass-Hansen, B. Jorgensen, C. H. Christensen, *J. Chem. Technol. Biotechnol.* **2007**, *82*, 329-333.
- [156] M. A. H. B. J. O'Keefe, W. B. Tolman, *J. Chem. Soc.* **2001**, 2215-2224.

- [157] S. Kobayashi, *Proc. Japan Acad.* **2010**, *86*, 338-365.
- [158] R. Reichardt, B. Rieger, *Adv. Polym. Sci.* **2012**, *245*, 49-90.
- [159] T. Tanio, T. Fukui, Y. Shirakura, T. Saito, K. Tomita, T. Kaiho, S. Masamune, *Eur. J. Biochem.* **1982**, *124*, 71-77.
- [160] F. P. Delafield, M. Doudoroff, N. J. Palleroni, C. J. Lusty, R. Contopoulos, *J. Bacteriol.* **1965**, *90*, 1455-1466.
- [161] J. M. Merrick, M. Doudoroff, *J. Bacteriol.* **1964**, *88*, 60-71.
- [162] P. A. Holmes, *Phys. Technol.* **1985**, *16*, 32-36.
- [163] C. J. Lusty, M. Doudoroff, *Proc. Natl. Acad. Sci. USA.* **1966**, *56*, 960-965.
- [164] H. Abe, I. Matsubara, Y. Doi, Y. Hori, A. Yamaguchi, *Macromolecules* **1994**, *27*, 6018-6025.
- [165] N. Tanahashi, Y. Doi, *Macromolecules* **1991**, *24*, 5732-5733.
- [166] G. A. Olah, A. Goepfert, G. K. Prakash, *J. Org. Chem.* **2009**, *74*, 487-498.
- [167] X. Zuwei, Z. Ning, S. Yu, L. Kunlan, *Science* **2001**, *292*, 1139-1141.
- [168] E. E. Stangland, K. B. Stavens, R. P. Andres, W. N. Delgass, *J. Catal.* **2000**, *191*, 332-347.
- [169] T. Hayashi, K. Tanaka, M. Haruta, *J. Catal.* **1998**, *178*, 566-575.
- [170] V. Russo, R. Tesser, E. Santacesaria, M. Di Serio, *Ind. Eng. Chem. Res.* **2013**, *52*, 1168-1178.
- [171] V. Mahadevan, Y. D. Y. L. Getzler, G. W. Coates, *Angew. Chem. Int. Ed.* **2002**, *114*, 2905-2908.
- [172] J. T. Lee, P. J. Thomas, H. Alper, *J. Org. Chem.* **2001**, *66*, 5424-5426.
- [173] J. F. Carpentier, *Organometallics* **2015**, *34*, 4175-4189.
- [174] M. Zintl, F. Molnar, T. Urban, V. Bernhart, P. Preishuber-Pflügl, B. Rieger, *Angew. Chem. Int. Ed.* **2008**, *120*, 3508-3510.
- [175] S. I. Vagin, R. Reichardt, S. Klaus, B. Rieger, *J. Am. Chem. Soc.* **2010**, *132*, 14367-14369.
- [176] C. M. Thomas, *Chem. Soc. Rev.* **2010**, *39*, 165-173.
- [177] H. Koempel, W. Liebner, in *Studies in Surface Science and Catalysis, Vol. 167*, Elsevier, **2007**, pp. 261-267.
- [178] E. Breitmaier, in *Terpene: Aromen, Düfte, Pharmaka, Pheromone*, Vieweg+Teubner Verlag, Wiesbaden, **1999**, pp. 123-126.
- [179] J. R. Lowe, W. B. Tolman, M. A. Hillmyer, *Biomacromolecules* **2009**, *10*, 2003-2008.
- [180] J. R. Lowe, M. T. Martello, W. B. Tolman, M. A. Hillmyer, *Polym. Chem.* **2011**, *2*, 702-708.
- [181] S. C. Knight, C. P. Schaller, W. B. Tolman, M. A. Hillmyer, *RSC Adv.* **2013**, *3*, 20399-20404.
- [182] R. Hopp, *Adv. Tobacco Science* **1993**, *19*, 3.
- [183] S. O. Nwaukwa, P. M. Keehn, *Tetrahedron Lett.* **1982**, *23*, 35-38.
- [184] J. Shin, M. T. Martello, M. Shrestha, J. E. Wissinger, W. B. Tolman, M. A. Hillmyer, *Macromolecules* **2011**, *44*, 87-94.
- [185] M. A. H. D. Zhang, W. B. Tolman, *Biomacromolecules* **2005**, *6*, 2091-2095.

-
- [186] A. K. S. H. K. Jr. Hall, *J. Am. Chem. Soc.* **1958**, *80*, 6409-6412.
- [187] M. T. M. J. Shin, M. Shrestha, J. E. Wissinger, W. B. Tolman, M. A. Hillmyer, *Macromolecules* **2011**, *22*, 87-94.
- [188] Y. L. J. Shin, W. B. Tolman, M. A. Hillmyer, *Biomacromolecules* **2012**, *13*, 3833-3840.
- [189] S. Koltzenburg, M. Maskos, O. Nuyken, *Polymere- Synthese, Eigenschaften und Anwendungen*, Springer Spektrum, Heidelberg, **2014**.
- [190] <https://commons.wikimedia.org/wiki/File:CrystTPE.svg>. Status: August 2018.
- [191] C. L. Wanamaker, L. E. O'Leary, N. A. Lynd, M. A. Hillmyer, W. B. Tolman, *Biomacromolecules* **2007**, *8*, 3634-3640.
- [192] C. L. Wanamaker, M. J. Bluemle, L. M. Pitet, L. E. O'Leary, W. B. Tolman, M. A. Hillmyer, *Biomacromolecules* **2009**, *10*, 2904-2911.
- [193] M. A. Hillmyer, W. B. Tolman, *Acc. Chem. Res.* **2014**, *47*, 2390-2396.
- [194] J. Shin, Y. Lee, W. B. Tolman, M. A. Hillmyer, *Biomacromolecules* **2012**, *13*, 3833-3840.
- [195] S. A. Gurusamy-Thangavelu, S. J. Emond, A. Kulshrestha, M. A. Hillmyer, C. W. Macosko, W. B. Tolman, T. R. Hoye, *Polym. Chem.* **2012**, *3*, 2941-2948.
- [196] P. T. Altenbuchner, B. S. Soller, S. Kissling, T. Bachmann, A. Kronast, S. I. Vagin, B. Rieger, *Macromolecules* **2014**, *47*, 7742-7749.
- [197] H. Yasuda, *J. Organomet. Chem.* **2002**, *647*, 128-138.
- [198] N. Zhang, S. Salzinger, B. Rieger, *Macromolecules* **2012**, *45*, 9751-9758.
- [199] S. S. Pennadam, K. Firman, C. Alexander, D. C. Górecki, *J. of Nanobiotechnol.* **2004**, *2*, 8.
- [200] H. Sasai, T. Suzuki, S. Arai, T. Arai, M. Shibasaki, *J. Am. Chem. Soc.* **1992**, *114*, 4418-4420.
- [201] H. C. Aspinall, *Chem. Rev.* **2002**, *102*, 1807-1850.
- [202] H. Kodama, J. Ito, K. Hori, T. Ohta, I. Furukawa, *J. Organomet. Chem.* **2000**, *603*, 6-12.
- [203] A. A. Chowdhury, *Arch. Microbiol.* **1963**, *47*, 167-200.
- [204] B. M. Bachmann, D. Seebach, *Macromolecules* **1999**, *32*, 1777-1784.
- [205] J. M. Brunel, *Chem. Rev.* **2005**, *105*, 857-898.

14 Appendix

14.1 Supporting Information: “Toolbox of Nonmetallocene Lanthanides: Multifunctional Catalysts in Group-Transfer Polymerization”

Supporting Information for the Manuscript Entitled

Toolbox of Non-Metallocene-Lanthanides: Multifunctional Catalysts in Group-Transfer Polymerization

Friederike Adams^{††}, Martin R. Machat^{††}, Peter T. Altenbuchner^{††}, Johannes Ehrmaier[§], Alexander Pöthig[‡], Tolga N. V. Karsili[§], and Bernhard Rieger^{††*}

^{††}WACKER-Lehrstuhl für Makromolekulare Chemie, Technische Universität München, Lichtenbergstraße 4, 85748 Garching bei München, Germany

[§] Chair of Theoretical Chemistry, Technische Universität München, Lichtenbergstraße 4, 85748 Garching bei München, Germany

[‡]Department Chemie & Catalysis Research Center, Technische Universität München, Ernst-Otto-Fischer-Straße 1, 85748 Garching bei München, Germany.

Table of Contents

1. Experimental procedure.....	2
2. NMR Kinetics of C-H-bond activation	11
3. X-ray diffraction analysis of complex 1b (CCDC 1547971).....	13
4. Polymerization results of DEVP and IPOx polymerization.....	17
5. Polymer Analytics.....	18
2VP Polymerization.....	18
DEVP Polymerization	26
DMAA Polymerization	32
6. Computational methods	41
7. Literature.....	62

1. Experimental procedure

Materials and Methods.

All reactions were carried out under argon atmosphere using standard Schlenk or glovebox techniques. All glassware was heat dried under vacuum prior to use. Unless otherwise stated, all chemicals were purchased from Sigma-Aldrich, Acros Organics, or ABCR and used as received. Toluene, thf, diethylether, dichloromethane and pentane were dried using a MBraun SPS-800 solvent purification system. Hexane was dried over 3 Å molecular sieves. The monomers 2-vinylpyridine, diethyl vinylphosphonate, and N,N-dimethylacrylamide were dried over calcium hydride and distilled prior to use.

The precursor complexes $\text{Ln}(\text{CH}_2\text{TMS})_3(\text{thf})_2$, Ligands L1 and L2, as well as complex 1a and 3a are prepared according to literature procedure.¹⁻²

NMR spectra were recorded on a Bruker AVIII-300 and AVIII-500 Cryo spectrometer. Unless otherwise stated, ¹H- and ¹³C-NMR spectroscopic chemical shifts δ are reported in ppm. δ (1H) is calibrated to the residual proton signal, δ (13C) to the carbon signal of the solvent. Unless otherwise stated, coupling constants J are averaged values and refer to couplings between two protons. Deuterated solvents were obtained from Sigma-Aldrich and dried over 3 Å molecular sieves.

Elemental analyses were measured at the Laboratory for Microanalysis at the Institute of Inorganic Chemistry at the Technische Universität München.

Single Crystal X-ray Crystallography was performed in the SCXRD laboratory of the Catalysis Research Center at Technische Universität München.

Homopolymerization Procedures.

For 2VP and DEVP: To a solution of 13.5 μmol catalyst (1.0 eq.) in 2 mL toluene at room temperature, 2.7 mmol monomer (200 eq.; 27 mmol [M]/ 20 mL toluene) was added in one portion. The polymerization is quenched by addition of methanol. Conversion is determined by ¹H-NMR-spectroscopy of an aliquot taken before quenching of the reaction. The polymers were precipitated by addition of the reaction mixtures to pentane (100 mL) and the solution was decanted off. Residual solvent was removed by freeze-drying from benzene (P2VP) or water (PDEVP) (100 mL) over night. Molecular weights and polydispersities are measured via GPC.

For DMAA: To a solution of 21.4 μmol catalyst (1.0 eq.) in 3.49 g dichloromethane at a certain temperature in a heat-dried pressure schlenk-flask, 4.3 mmol monomer in 1.00 g dichloromethane (200 eq.) was added in

one portion. If no polymerization takes place, the mixture is warmed-up and the temperature is noted were the polymerization starts. Polymerizations at 0 °C and -20 °C were performed analogous in a glovebox and are thermostatted with a cryo-cooled vessel. The polymerization is quenched by addition of methanol. Conversion is determined by ¹H-NMR-spectroscopy of an aliquot taken before quenching of the reaction. The polymers were precipitated by addition of the reaction mixtures to pentane (100 mL) and the solution was decanted off. Residual solvent was removed by freeze-drying from water (100 mL) over night. Molecular weights and polydispersities are measured *via* GPC.

Kinetic measurements of 2-vinylpyridine by aliquots method.

To a solution of 135 μmol catalyst in 20 mL toluene at room temperature, the corresponding amount of monomer (27 mmol, 200 eq.) was added in one portion. Aliquots were taken from the reaction solution at regular time intervals and quenched by addition of MeOH. Solvent and not polymerized monomer were removed by drying the polymers under vacuum at 60 °C overnight. For each aliquot, the conversion is determined gravimetrically and the molecular weight of the polymer is determined by GPC-MALS analysis.

Characterization of Polymer-Samples.

The tacticity determination of P2VP was performed by ¹³C-NMR-spectroscopy at room temperature. Spectra for the analysis of P2VP quaternsry carbon atom mm, mr/rm and rr triads were recorded with a sample concentration of 15% (w/w; 75 mg/0.6 mL CD₃OD) on a AVIII 500 Cryo spectrometer and analyzed according to literature.³⁻⁴

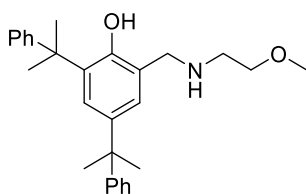
The tacticity determination of PDMAA was performed by ¹H-NMR-spectroscopy of the main-chain methylene-proton signal of PDMAA. Spectra for the analysis of m and r-dyads were recorded analogous to *Kakuchi et al.* with a sample concentration of 4% (w/w; 25 mg/0.6 mL DMSO-d₆) at 140 °C.⁵

Gel permeation chromatography (GPC) was carried out with samples of 5 mg/mL concentration on a Varian LC-920 equipped with two PL Polargel columns. As eluent a mixture of THF/water (1:1; v:v), 9 g/L tetrabutylammonium bromide (TBAB) and 680 mg/L_{THF} 3,5-di-tert-butyl-4-hydroxytoluene (BHT) was used. Absolute molecular weights have been determined online by multiangle light scattering (MALS) analysis using a Wyatt Dawn Heleos II in combination with a Wyatt Optilab rEX as concentration source.

Proligand Synthesis^{4,6}

2-(((2-Methoxyethyl)amino)methyl)-4,6-bis(2-phenylpropan-2-yl)phenol: 2-methoxyethylenamine (1.0 eq.) is added to a solution of the respective 2-hydroxybenzaldehyde (1.0 eq.) in methanol/chloroform (1:1, v:v). The reaction mixture is heated to reflux for 24 hours. The reaction mixture is then cooled to 0 °C

and NaBH₄ (2.1 eq.) is added in small portions. The reaction is kept at 50 °C for 48 h. After cooling to room temperature, the solution is acidified by adding concentrated HCl. All volatiles are removed under vacuum and the residue is dissolved in saturated aqueous Na₂CO₃. The aqueous layer is extracted with chloroform and the combined organic layers are dried over anhydrous MgSO₄, filtrated and concentrated *in vacuo*. Recrystallization from ethanol leads to the desired product (yield: 74%) as a yellow powder.



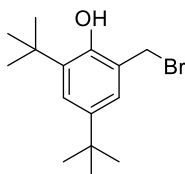
¹H-NMR (300 MHz, CDCl₃, 298 K): δ (ppm) = 7.37 – 7.12 (m, 11H, H_{arom}), 6.81 (d, ⁴J = 2.2 Hz, 1H, H_{arom}), 3.87 (s, 2H), 3.43 (t, ³J = 5.0 Hz, 2H), 3.26 (s, 3H), 2.74 (t, ³J = 5.0 Hz, 2H), 1.69 (s, 6H, CMe₂Ph), 1.64 (s, 6H, CMe₂Ph).

¹³C-NMR (75 MHz, CDCl₃, 298 K): δ (ppm) = 154.2, 151.5, 151.4, 139.9, 135.2, 128.0, 127.8, 126.9, 125.6, 125.5, 125.0, 124.9, 122.2, 70.9, 58.9, 52.8, 47.8, 42.5, 42.2, 31.2, 29.7.

ESI-MS (EtOAc): 418.3 [M]⁺

2-(Bromomethyl)-4,6-di-tert-butylphenol:^{7,9} NaBH₄ (2.0 eq.) is slowly added to a stirred solution of the respective 2-hydroxybenzaldehyde (1.0 eq.) in methanol. The solution is stirred at room temperature for 1 h. All volatiles are removed in vacuum and the resulting residue is dissolved in water. The resulting aqueous mixture is neutralized with glacial acetic acid and extracted with CH₂Cl₂. The combined organic layers are dried with anhydrous MgSO₄ and concentrated to give a white solid which is immediately converted in the next step.

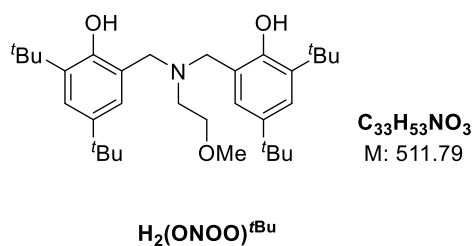
PBr₃ (0.5 eq.) is added to a stirred solution of 2-hydroxybenzyl alcohol (1.0 eq.) in chloroform. The mixture is stirred for 1 h at room temperature. Within 5 minutes cold water is added with vigorous stirring. The organic layer is separated and the aqueous residue is extracted with chloroform. The combined organic layers are dried with anhydrous MgSO₄ and concentrated *in vacuo* to yield the desired product (yield: 95%) as a brown oil.



$^1\text{H-NMR}$ (300 MHz, CDCl_3 , 298 K): δ (ppm) = 7.34 (d, $^4J = 2.5$ Hz, 1H, H_{arom}), 7.11 (d, $^4J = 2.5$ Hz, 1H, H_{arom}), 4.59 (s, 2H, CH_2), 1.44 (s, 9H, ^tBu), 1.30 (s, 9H, ^tBu).

$^{13}\text{C-NMR}$ (75 MHz, CDCl_3 , 298 K): δ (ppm) = 151.7, 143.0, 137.2, 125.8, 124.8, 123.3, 35.0, 34.4, 32.8, 31.6, 30.0.

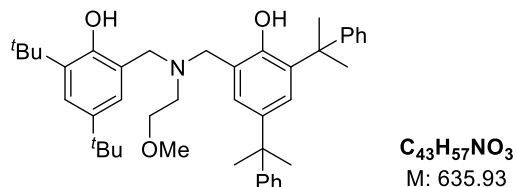
$\text{H}_2(\text{ONOO})^{\text{tBu}}$ (L1): A solution of 2.0 equivalents of 2,4-di-*tert*-butylphenol, 1.0 equivalents 2-methoxyethylamine and aqueous formaldehyde-solution (36% in water; 3.0 eq.) in methanol is refluxed for 10 days. The mixture was cooled and the colorless solid was separated *via* filtration. After double recrystallization from ethanol the product is yielded (yield: 45%) as colorless crystals.



$^1\text{H-NMR}$ (300 MHz, CDCl_3 , 300 K): δ (ppm) = 8.52 (s, 2H, OH), 7.21 (d, $^4J = 2.5$ Hz, 2H, H_{arom}), 6.88 (d, $^4J = 2.5$ Hz, 2H, H_{arom}), 3.74 (s, 4H, ArCH_2), 3.56 (t, $^3J = 5.1$ Hz, 2H, $\text{H}_{\text{sidearm}}$), 3.47 (s, 3H, OMe), 2.75 (t, $^3J = 5.1$ Hz, 2H, $\text{H}_{\text{sidearm}}$), 1.41 (s, 18H, ^tBu), 1.27 (s, 18H, ^tBu).

$^{13}\text{C-NMR}$ (75 MHz, CDCl_3 , 300 K): δ (ppm) = 153.0, 140.8, 136.1, 125.0, 123.5, 121.7, 71.5, 58.9, 58.2, 51.5, 35.1, 34.2, 31.8, 29.7.

$\text{H}_2(\text{ONOO})^{\text{tBu,CM}_2\text{Ph}}$ (L2): One equivalent of the methylbromide is dissolved in tetrahydrofuran and added dropwise to a solution of one equivalent of the respective secondary amine in tetrahydrofuran. The solution is stirred for 30 minutes at room temperature before 1.5 equivalents of triethylamine are added slowly. The solution is heated up to 75 °C for 14 hours. The solid is filtered off and the solvent is removed *in vacuo*. A column chromatographic purification (SiO_2 , hexane / EtOAc = 12: 1) yields the desired product (yield: 49%) as a white powder.



H₂(ONO)tBuMe₂Ph

DC: $R_f = 0.46$ (hexane/EtOAc = 12:1) [UV]

¹H-NMR (300 MHz, CDCl₃, 300 K): δ (ppm) = 7.37 – 7.11 (m, 12H, H_{arom}), 6.91 (d, ⁴J = 2.4 Hz, 1H, H_{arom}), 6.83 (d, ⁴J = 2.4 Hz, 1H, H_{arom}), 3.68 (s, 2H), 3.61 (s, 2H), 3.27 (t, ³J = 5.4 Hz, 2H, H_{sidearm}), 3.17 (s, 3H, OMe), 2.59 (t, ³J = 5.4 Hz, 2H, H_{sidearm}), 1.71 (s, 6H, CMe₂Ph), 1.64 (s, 6H, CMe₂Ph), 1.42 (s, 9H, tBu), 1.29 (s, 9H, tBu).

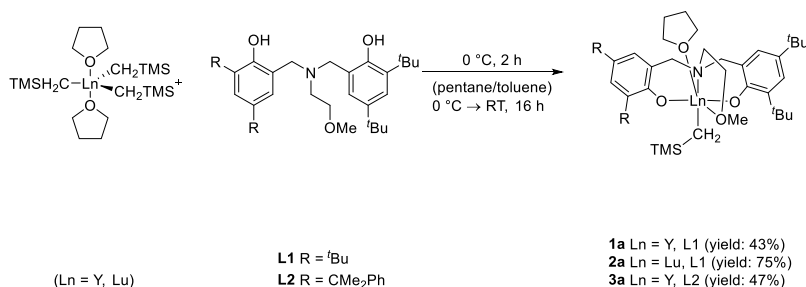
¹³C-NMR (75 MHz, CDCl₃, 300 K): δ (ppm) = 153.3, 151.7, 151.2, 150.2, 140.7, 140.4, 135.7, 135.4, 128.0, 127.8, 127.4, 126.7, 125.9, 125.4, 125.4, 124.8, 124.4, 123.1, 122.8, 121.6, 71.0, 58.5, 58.3, 56.0, 51.4, 42.5, 41.9, 34.9, 34.0, 31.7, 31.0, 29.6, 29.3.

EA: calculated: C 81.22 H 9.03 N 2.20

found: C 81.39 H 9.24 N 2.01

ESI-MS (iso-propanol): 636.6 [M]⁺

Complex synthesis.

General procedure for the synthesis of $(\text{ONOO})^{\text{R}}\text{Ln}(\text{CH}_2\text{TMS})(\text{thf})$ **1a-3a**:

One equivalent of proligand $\text{H}_2(\text{ONOO})^{\text{R}}$ (L1 or L2) in toluene is added to a stirred solution of one equivalent of $\text{Ln}(\text{CH}_2\text{TMS})_3(\text{thf})_2$ in pentane at 0°C . The resulting solution is stirred overnight at room temperature. The solvent is removed in vacuo and the resulting solid is washed with pentane.

 $(\text{ONOO})^{\text{tBu}}\text{Y}(\text{CH}_2\text{TMS})(\text{thf})$ (**1a**)¹⁰

Yield: 43% (colorless powder)

¹H-NMR (300 MHz, C₆D₆, 300 K): δ (ppm) = 7.61 (d, ⁴J = 2.6 Hz, 2H, H_{arom}), 7.09 (d, ⁴J = 2.6 Hz, 2H, H_{arom}), 4.00 – 3.89 (m, 4H, H_{thf}), 3.78 (d, ²J = 12.4 Hz, 2H, ArCH₂), 2.89 (d, ²J = 12.4 Hz, 2H, ArCH₂), 2.78 (s, 3H, OMe), 2.42 (t, ³J = 5.4 Hz, 2H, H_{sidearm}), 2.20 (t, ³J = 5.4 Hz, 2H, H_{sidearm}), 1.81 (s, 18H, ^tBu), 1.46 (s, 18H, ^tBu), 1.19 – 1.11 (m, 4H, H_{thf}), 0.52 (s, 9H, H_{TMS}), -0.38 (d, ²J_{V,H} = 3.3 Hz, 2H, CH₂TMS).

¹³C-NMR (126 MHz, C₆D₆, 300 K): δ (ppm) = 161.6 (d, ²J_{C,Y} = 1.8 Hz), 136.8, 136.6, 125.6, 124.4, 124.1, 74.0, 71.7, 64.9, 61.3, 49.3, 35.6, 34.3, 32.3, 30.3, 25.4, 25.1, 4.9.

 $(\text{ONOO})^{\text{tBu}}\text{Lu}(\text{CH}_2\text{TMS})(\text{THF})$ (**2a**):

Yield: 75% (colorless powder)

¹H-NMR (300 MHz, C₆D₆, 300 K): δ (ppm) = 7.63 (d, ⁴J = 2.6 Hz, 2H, H_{arom}), 7.08 (d, ⁴J = 2.6 Hz, 2H, H_{arom}), 3.97 (s, 4H, H_{thf}), 3.81 (d, ²J = 12.4 Hz, 2H, ArCH₂), 2.87 (d, ²J = 12.4 Hz, 2H, ArCH₂), 2.78 (s, 3H, OMe), 2.43 (t, ³J = 5.5 Hz, 2H, H_{sidearm}), 2.17 (t, ³J = 5.5 Hz, 2H, H_{sidearm}), 1.81 (s, 18H, ^tBu), 1.47 (s, 18H, ^tBu), 1.23 – 1.09 (m, 4H, H_{thf}), 0.51 (s, 9H, H_{TMS}), -0.50 (s, 2H, CH₂TMS).

$^{13}\text{C-NMR}$ (126 MHz, C_6D_6 , 300 K): δ (ppm) = 162.1, 137.1, 136.6, 125.5, 124.5, 123.9, 74.4, 72.3, 64.9, 61.7, 49.4, 35.6, 34.2, 32.3, 30.3, 29.6, 25.0, 5.0.

EA	calculated:	C 58.34	H 8.36	N 1.66
	found:	C 58.73	H 8.57	N 1.73

(ONOO)^tBu,CMe₂PhY(CH₂TMS)(thf)(3a):⁴

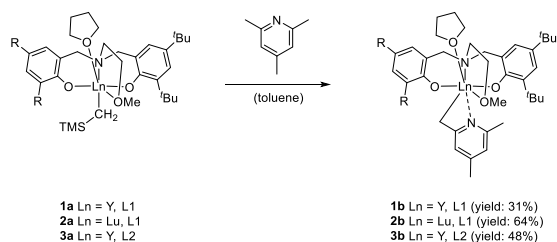
Yield: 47% (white powder)

$^1\text{H-NMR}$ (300 MHz, C_6D_6 , 300 K): δ (ppm) = 7.68 (d, $^4J = 2.6$ Hz, 1H, H_{arom}), 7.58 (d, $^2J = 2.6$ Hz, 1H, H_{arom}), 7.50 (d, $^3J = 7.5$ Hz, 2H, H_{arom}), 7.46 – 7.40 (m, 2H, H_{arom}), 7.25 – 7.18 (m, 4H, H_{arom}), 7.11 (t, $^3J = 7.5$ Hz, 1H, H_{arom}), 7.00 (d, $^4J = 2.6$ Hz, 1H, H_{arom}), 6.97 (t, $^3J = 7.5$ Hz, 1H, H_{arom}), 6.88 (d, $^4J = 2.6$ Hz, 1H, H_{arom}), 3.63 – 3.28 (m, 6H, $\text{ArCH}_2 + \text{H}_{\text{thf}}$), 2.72 (s, 3H), 2.64 (m, 2H, ArCH_2), 2.49 – 2.37 (m, 2H), 2.16 – 2.10 (m, 1H), 2.07 (s, 3H), 2.02 (m, 1H), 1.80 (m, 18H), 1.45 (s, 9H), 1.14 – 1.05 (m, 4H, H_{thf}), 0.49 (s, 9H, H_{TMS}), -0.55 – -0.65 (m, 2H, CH_2TMS).

$^{13}\text{C-NMR}$ (126 MHz, C_6D_6 , 300 K): δ (ppm) = 161.6 (d, $^2J_{\text{C,Y}} = 2.4$ Hz), 161.2 (d, $^2J_{\text{C,Y}} = 2.4$ Hz), 136.7, 136.5, 136.2, 136.1, 128.5, 128.4, 128.3, 128.1, 127.9, 127.3, 126.4, 125.9, 125.8, 125.6, 124.5, 124.4, 124.3, 124.0, 73.9, 71.3, 64.6, 64.2, 61.2, 49.0, 42.7, 42.6, 35.6, 34.4, 34.2, 32.4, 32.3, 31.7 (d, $^1J_{\text{C,Y}} = 14.9$ Hz), 30.4, 28.2, 25.2, 25.0, 24.9, 22.7.

EA:	calculated:	C 69.44	H 8.46	N 1.59
	found:	C 68.99	H 8.48	N 1.61

General procedure for the synthesis of C-H-bond activated complexes (1b-3b):



One equivalent of the respective CH₂TMS-complex (**1a-3a**) and one equivalent of 2,4,6-collidine are dissolved in toluene and stirred over a specified period of time at a certain temperature. The solvent is removed in vacuo and the raw product is recrystallized from pentane.

(ONOO)^{tBu}Y((4,6-dimethylpyridin-2-yl)methyl)(THF) (1b):

The yellow reaction mixture is stirred overnight at 60 °C.

Yield: 31% (yellow powder)

¹H-NMR (300 MHz, C₆D₆, 300 K): δ (ppm) = 7.58 (d, ⁴J = 2.6 Hz, 2H, H_{arom}), 7.14 (d, ⁴J = 2.6 Hz, 2H, H_{arom}), 6.57 (s, 1H, H_{arom,pyr}), 5.76 – 5.68 (s, 1H, H_{arom,pyr}), 4.08 (d, ²J = 12.6 Hz, 2H, ArCH₂), 3.77 – 3.64 (br, 4H, H_{thf}), 2.98 (d, ²J = 12.6 Hz, 2H, ArCH₂), 2.80 (d, ²J_{H,Y} = 2.9 Hz, 2H, Ar_{pyr}CH₂), 2.76 (t, ³J = 5.4 Hz, 2H, H_{sidearm}), 2.58 (s, 3H, CH₃), 2.40 (t, ³J = 5.4 Hz, 2H, H_{sidearm}), 2.14 (s, 3H, CH₃), 2.01 (s, 3H, CH₃), 1.65 (s, 18H, tBu), 1.48 (s, 18H, tBu), 1.18 – 1.09 (br m, 4H, H_{thf}).

¹³C-NMR (75 MHz, C₆D₆, 300 K): δ (ppm) = 167.4 (d, ²J_{C,Y} = 1.0 Hz), 161.7 (d, ²J_{C,Y} = 2.6 Hz), 155.8, 145.4, 136.6, 136.4, 125.8, 124.5, 124.1, 116.0, 109.0, 72.8, 70.8, 65.2, 59.5, 52.8 (d, ¹J_{C,Y} = 6.8 Hz), 49.5, 35.4, 34.3, 32.3, 30.3, 25.1, 23.5, 21.3.

EA:	calculated:	C 68.33	H 8.79	N 3.54
	found:	C 68.60	H 9.05	N 3.67

(ONOO)^{tBu}Lu((4,6-dimethylpyridin-2-yl)methyl)(THF) (2b):

The yellow reaction mixture is stirred for nine days at 80 °C.

Yield: 64% (yellow powder)

¹H-NMR (500 MHz, C₆D₆, 300 K): δ (ppm) = 7.59 (d, ⁴J = 2.6 Hz, 2H, H_{arom}), 7.05 (d, ⁴J = 2.6 Hz, 2H, H_{arom}), 6.67 (s, 1H, H_{arom,pyr}), 5.91 (s, 1H, H_{arom,pyr}), 3.81 (d, ²J = 12.7 Hz, 2H, ArCH₂), 3.74 (t, J = 6.4 Hz, 2H), 3.12 (d, ²J = 12.7 Hz, 2H, ArCH₂), 2.81 (s, 3H, CH₃), 2.69 (t, ³J = 5.4 Hz, 2H, H_{sidearm}), 2.60 (s, 2H, Ar_{pyr}CH₂), 2.22 (s, 5H, CH₃ + CH₂), 2.00 (s, 3H, CH₃), 1.62 (s, 18H, tBu), 1.46 (s, 18H, tBu), 1.17 – 1.11 (m, 2H).

^{13}C -NMR (126 MHz, C_6D_6 , 300 K): δ (ppm) = 167.4 (d, $^2J_{\text{C,Y}} = 1.0$ Hz), 161.7 (d, $^2J_{\text{C,Y}} = 2.6$ Hz), 155.8, 145.4, 136.6, 136.4, 125.8, 124.5, 124.1, 116.0, 109.0, 72.8, 70.8, 65.2, 59.5, 52.8 (d, $^1J_{\text{C,Y}} = 6.8$ Hz), 49.5, 35.4, 34.3, 32.3, 30.3, 25.1, 23.5, 21.3.

EA:	calculated:	C 61.63	H 7.93	N 3.19
	found:	C 61.65	H 8.05	N 3.08

(ONOO)^tBu,CM₂Ph₂Y((4,6-dimethylpyridin-2-yl)methyl)(THF)(3b):

The yellow reaction mixture is stirred for six days at room temperature.

Yield: 48% (yellow powder)

^1H -NMR (500 MHz, C_6D_6 , 300 K): δ (ppm) = 7.64 (d, $^4J = 2.6$ Hz, 1H, H_{arom}), 7.54 (d, $^4J = 2.6$ Hz, 1H, H_{arom}), 7.45 (d, $^3J = 7.6$ Hz, 2H, H_{arom}), 7.37 (d, $^3J = 7.6$ Hz, 2H, H_{arom}), 7.26 – 7.22 (m, 3H, H_{arom}), 7.13 – 7.09 (m, 3H, H_{arom}), 7.05 (d, $^4J = 2.6$ Hz, 1H, H_{arom}), 6.92 (d, $^4J = 2.6$ Hz, 1H, H_{arom}), 6.60 (s, 1H, $\text{H}_{\text{arom,pyr}}$), 5.77 (s, 1H, $\text{H}_{\text{arom,pyr}}$), 3.87 – 3.66 (m, 2H, ArCH_2), 3.30 (br s, 4H, H_{thf}), 2.94 – 2.80 (m, 2H), 2.74 – 2.59 (m, 2H), 2.55 (s, 2H), 2.53 (s, 3H), 2.31 – 2.08 (m, 5H), 2.03 (s, 3H), 1.92 (s, 3H), 1.83 (s, 3H), 1.81 (s, 3H), 1.69 (s, 3H), 1.57 (s, 9H, *t*Bu), 1.46 (s, 9H, *t*Bu), 1.16 (t, $^3J = 6.3$ Hz, 4H, H_{thf}).

^{13}C -NMR (75 MHz, C_6D_6 , 300 K): δ (ppm) = 167.5, 161.6, 161.1, 155.8, 153.2, 152.5, 145.5, 136.7, 136.5, 136.4, 135.8, 127.5, 127.3, 126.6, 125.8, 125.7, 125.19, 124.7, 124.3, 124.2, 124.0, 116.4, 109.2, 72.5, 70.1, 64.1, 59.6, 52.5, 49.2, 42.7, 42.2, 35.4, 34.28, 32.3, 31.8, 31.7, 30.3, 30.2, 27.9, 25.2, 24.4, 23.6, 22.7, 21.2, 20.5, 14.3.

EA:	calculated:	C 72.19	H 8.04	N 3.06
	found:	C 71.85	H 8.08	N 3.08

2. NMR Kinetics of C-H-bond activation

Complex 1a to 1b:

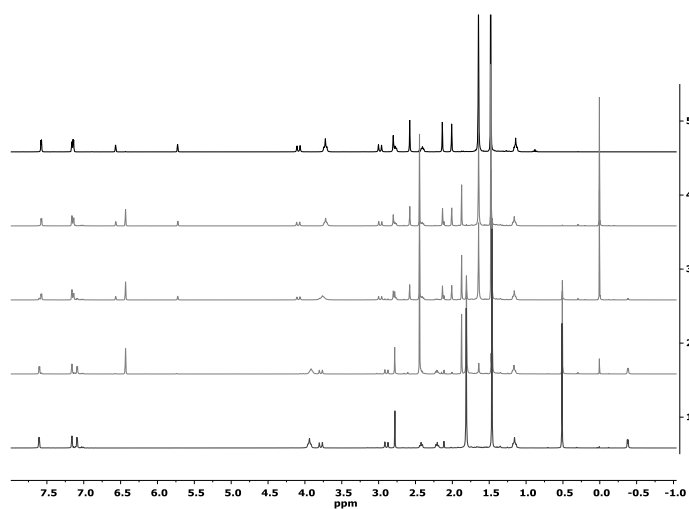


Figure S1: $^1\text{H-NMR}$ -kinetic for the C-H-bond activation of *sym*-collidine with complex **1a** in C_6D_6 . **1.** Complex **1a**. **2.** Immediate after addition of *sym*-collidine. **3.** 40 Min; 60 °C. **4.** 4 hours; 60 °C. **5.** Complex **1b**.

Complex 2a to 2b:

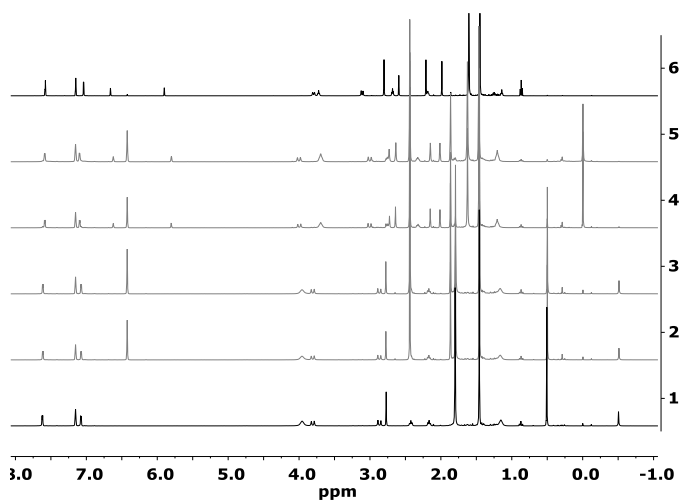


Figure S2: $^1\text{H-NMR}$ -kinetic for the C-H-bond activation of *sym*-collidine with complex **2a** in C_6D_6 . **1.** Complex **2a**. **2.** Immediate after addition of *sym*-collidine. **3.** 90 Min; 25 °C. **4.** 4 days; 70 °C. **5.** 9 days; 80 °C. **6.** Complex **2b**.

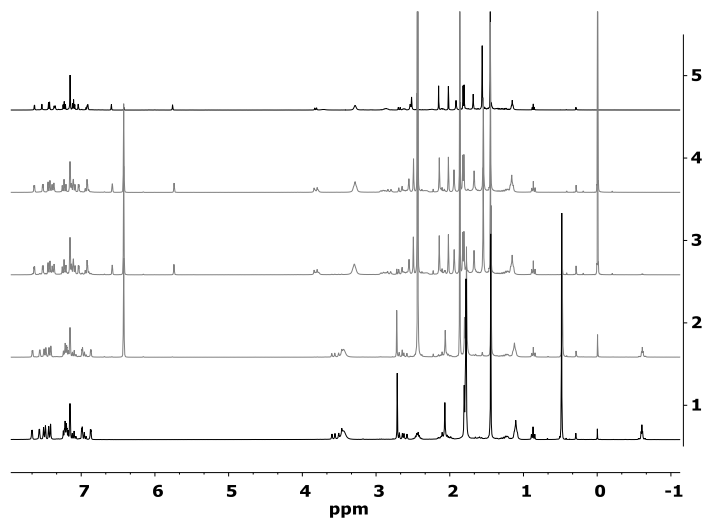
Complex 3a to 3b:

Figure S 3: ^1H -NMR-kinetic for the C-H-bond activation of *sym*-collidine with complex **3a** in C_6D_6 . **1.** Complex **3a**. **2.** Immediate after addition of *sym*-collidine. **3.** 24 hours; 25 °C. **4.** 6 days; 25 °C. **5.** Complex **3b**.

3. X-ray diffraction analysis of complex 1b (CCDC 1547971)

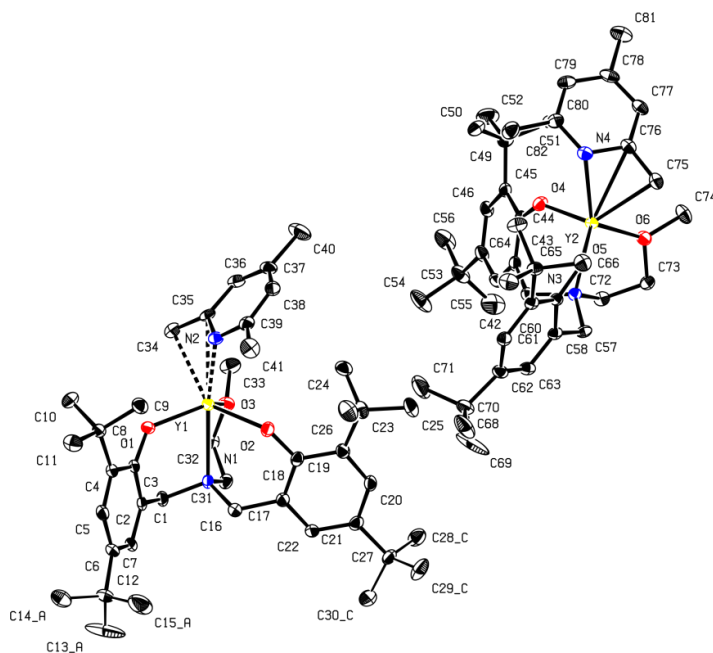


Figure S 4: Molecular structure of complex 1b (two independent molecules). Ellipsoids are shown at the 50% probability level. Hydrogen atoms are omitted for clarity.

A clear pale yellow fragment-like specimen of $C_{82}H_{122}N_4O_6Y_2$, approximate dimensions 0.231 mm x 0.232 mm x 0.246 mm, was used for the X-ray crystallographic analysis. The X-ray intensity data were measured on a Bruker Kappa APEX II CCD system equipped with a MONTEL mirror monochromator and a Mo FR591 rotating anode ($\lambda = 0.71073 \text{ \AA}$).

A total of 2585 frames were collected. The total exposure time was 14.36 hours. The frames were integrated with the Bruker SAINT software package using a narrow-frame algorithm. The integration of the data using a monoclinic unit cell yielded a total of 101335 reflections to a maximum θ angle of 25.39° (0.83 \AA resolution), of which 14469 were independent (average redundancy 7.004, completeness = 99.7%, $R_{\text{int}} = 4.57\%$) and 12448 (86.03%) were greater than $2\sigma(F^2)$. The final cell constants of $a = 30.729(3) \text{ \AA}$, $b = 17.3329(14) \text{ \AA}$, $c = 14.8368(12) \text{ \AA}$, $\beta = 91.915(4)^\circ$, volume = $7898.0(11) \text{ \AA}^3$, are based upon the refinement of the XYZ-centroids of 9998 reflections above $20 \sigma(I)$ with $4.537^\circ < 2\theta < 50.47^\circ$. Data were corrected for absorption effects using the multi-scan method (SADABS). The ratio of minimum to maximum apparent transmission was 0.901. The calculated minimum and maximum transmission coefficients (based on crystal size) are 0.7070 and 0.7210.

The final anisotropic full-matrix least-squares refinement on F^2 with 951 variables converged at $R1 = 3.44\%$, for the observed data and $wR2 = 7.86\%$ for all data. The goodness-of-fit was 1.113. The largest peak in the final

difference electron density synthesis was $0.367 \text{ e}^-/\text{\AA}^3$ and the largest hole was $-0.377 \text{ e}^-/\text{\AA}^3$ with an RMS deviation of $0.052 \text{ e}^-/\text{\AA}^3$. On the basis of the final model, the calculated density was 1.209 g/cm^3 and $F(000)$, 3072 e^- .

Table S 1 Sample and crystal data for complex 1b.

Identification code	AltPe4 AP6270-123	
Chemical formula	$\text{C}_{82}\text{H}_{122}\text{N}_4\text{O}_6\text{Y}_2$	
Formula weight	1437.65	
Temperature	123(2) K	
Wavelength	0.71073 \AA	
Crystal size	0.231 x 0.232 x 0.246 mm	
Crystal habit	clear pale yellow fragment	
Crystal system	monoclinic	
Space group	$P 2_1/c$	
Unit cell dimensions	$a = 30.729(3) \text{\AA}$	$\alpha = 90^\circ$
	$b = 17.3329(14) \text{\AA}$	$\beta = 91.915(4)^\circ$
	$c = 14.8368(12) \text{\AA}$	$\gamma = 90^\circ$
Volume	7898.0(11) \AA^3	
Z	4	
Density (calculated)	1.209 g/cm^3	
Absorption coefficient	1.514 mm^{-1}	
F(000)	3072	

Table S 2 Data collection and structure refinement for complex 1b.

Diffractometer	Bruker Kappa APEX II CCD
Radiation source	FR591 rotating anode, Mo
Theta range for data collection	1.35 to 25.39°
Index ranges	$-36 \leq h \leq 34$, $-20 \leq k \leq 20$, $-17 \leq l \leq 17$
Reflections collected	101335
Independent reflections	14469 [R(int) = 0.0457]

Coverage of independent reflections	99.7%
Absorption correction	multi-scan
Max. and min. transmission	0.7210 and 0.7070
Refinement method	Full-matrix least-squares on F ²
Refinement program	SHELXL-2014 (Sheldrick, 2014)
Function minimized	$\Sigma w(F_o^2 - F_c^2)^2$
Data / restraints / parameters	14469 / 60 / 951
Goodness-of-fit on F ²	1.113
Δ/σ_{\max}	0.002
Final R indices	12448 data; I>2 σ (I) R1 = 0.0344, wR2 = 0.0756 all data R1 = 0.0442, wR2 = 0.0786
Weighting scheme	$w=1/[\sigma^2(F_o^2)+(0.0196P)^2+9.1903P]$ where $P=(F_o^2+2F_c^2)/3$
Largest diff. peak and hole	0.367 and -0.377 e \AA^{-3}
R.M.S. deviation from mean	0.052 e \AA^{-3}

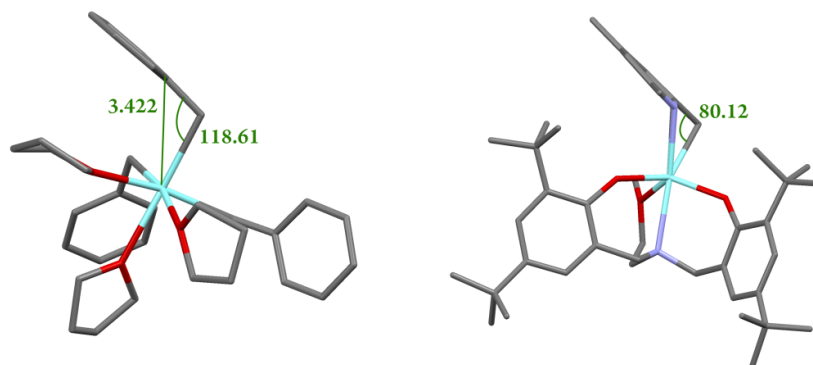


Figure S 5: Ellipsoid-style representation of $[\text{Y}(\text{CH}_2\text{Ph})_3(\text{thf})_3]^{11}$ (left) and $[(\text{ONOO})^{\text{tBu}}\text{Y}(\text{coll})]$ (**1b**) (right). The $\text{C}_a\text{-Y-C}_{\text{ipso}}$ angle is marked. For $[\text{Y}(\text{CH}_2\text{Ph})_3(\text{thf})_3]$, the Y-C_{ipso} bond is labeled in green.

Table S 3 Selected bond lengths (Å) and angles (°) for $[\text{Y}(\text{CH}_2\text{Ph})_3(\text{thf})_3]^{11}$ and **1b**.

	$[\text{Y}(\text{CH}_2\text{Ph})_3(\text{thf})_3]$ [a] ¹¹	$[(\text{ONOO})^{\text{tBu}}\text{Y}(\text{coll})]$	$[(\text{ONOO})^{\text{tBu}}\text{Y}(\text{coll})]$ (DFT)	$[(\text{ONOO})^{\text{tBu}}\text{Lu}(\text{coll})]$ (DFT)
Ln-C_α	2.460(2)	2.608(2)	2.548	2.511
Ln-C_{ipso}	3.387(3)	2.740(2)	2.868	2.870
Ln-C_{ortho/N}	4.160 ^[b]	2.3950(19)	2.426	2.403
C_α-C_{ipso}	1.466(2)	1.400(4)	1.455	1.482
C_α-Ln-C_{ipso}	117.17 ^[d]	80.12(14)	87.03	87.96

[a] Average values [b] No accuracy given in CCDC data

4. Polymerization results of DEVP and IPOx polymerization

Table S 4 REM-GTP polymerization results of catalyst 1-3 of DEVP.^[a]

Entry	[Cat]	Time [min]	Conversion [%]	$M_{n,calc}$ ($\times 10^4$) [g/mol] ^[b]	$M_{n,exp}$ ($\times 10^4$) [g/mol]	\bar{D} ^[c]	I ^[d]
1 ²	1a	198	99	3.3	9.0	1.10	0.36
2	2a	70	55	1.7	7.9	1.50	0.23
3	2a	1260	99	2.7	8.8	1.48	0.31
4	3a	202	99	3.2	6.9	1.14	0.46
5	1b	225	99	3.3	4.5	1.03	0.73
6	2b	240	99	3.2	4.6	1.14	0.68
7	3b	150	99	3.4	4.2	1.04	0.80

[a] reactions performed with [DEVP] = 27 mmol, [DEVP]/[Cat] = 200/1, at 25 °C in 20 mL solvent, conversions determined by ³¹P-NMR spectroscopy and $M_{n,exp}$ determined by GPC-MALS. [b] $M_{n,calc}$ from $M_{n,calc} = M \times (([M]/[Cat]) \times \text{conversion})$. [c] Polydispersity calculated from $M_{w,exp}/M_{n,exp}$ determined by GPC-MALS [d] $I = M_{n,calc}/M_{exp}$

Table S 5 REM-GTP polymerization results of catalyst 1a-1b of IPOx.^[a]

Entry	[Cat]	Time [min]	Conversion [%]	$M_{n,calc}$ ($\times 10^4$) [g/mol] ^[b]	$M_{n,exp}$ ($\times 10^4$) [g/mol]	\bar{D}	I ^[c]
1 ²	1a	10	99	2.2	2.4	1.01	0.93
2	1b	90	99	2.2	4.6	1.05	0.48

[a] reactions performed with [IPOx] = 27 mmol, [IPOx]/[Cat] = 200/1, at 25 °C in 20 mL solvent, conversions determined by ¹H-NMR spectroscopy and $M_{n,exp}$ determined by GPC-MALS. [b] $M_{n,calc}$ from $M_{n,calc} = M \times (([M]/[Cat]) \times \text{conversion})$. [c] Polydispersity calculated from $M_{w,exp}/M_{n,exp}$ determined by GPC-MALS [d] $I = M_{n,calc}/M_{exp}$

5. Polymer Analytics

2VP Polymerization

ESI-MS of Oligomeric 2VP:

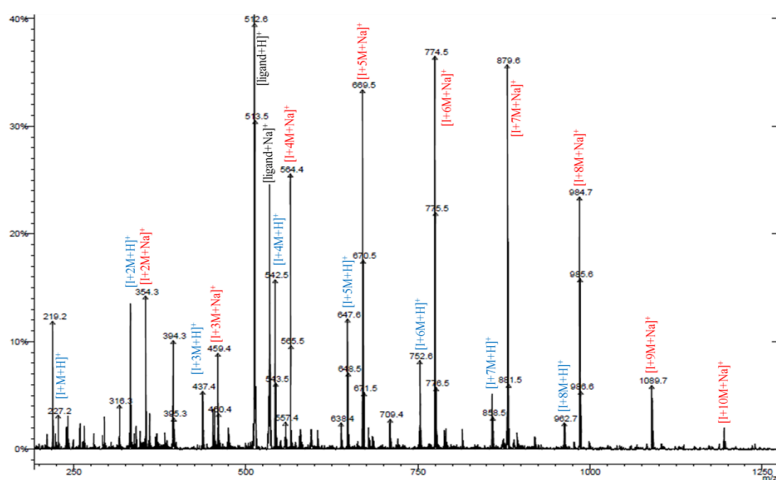


Figure S6: Endgroup analysis ESI-MS measured in *i*PrOH; Catalyst **1b** (40 μ mol of catalyst, 0.4 mmol 2VP, 0.5 mL C_6D_6 , 20 $^\circ C$).

NMR-spectra:

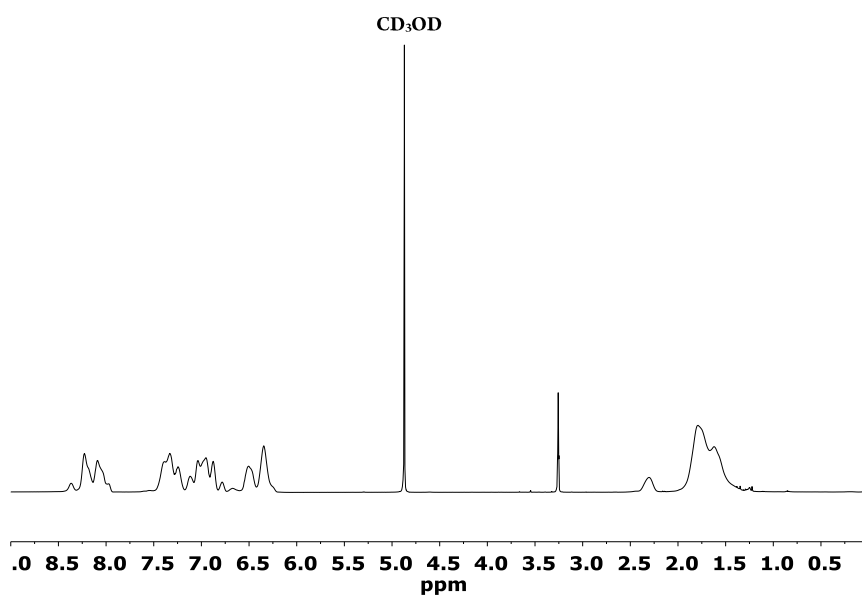


Figure S7: 1H -NMR-spectra of atactic P2VP produced by catalyst **1a** (500 MHz, Cryo, CD_3OD).

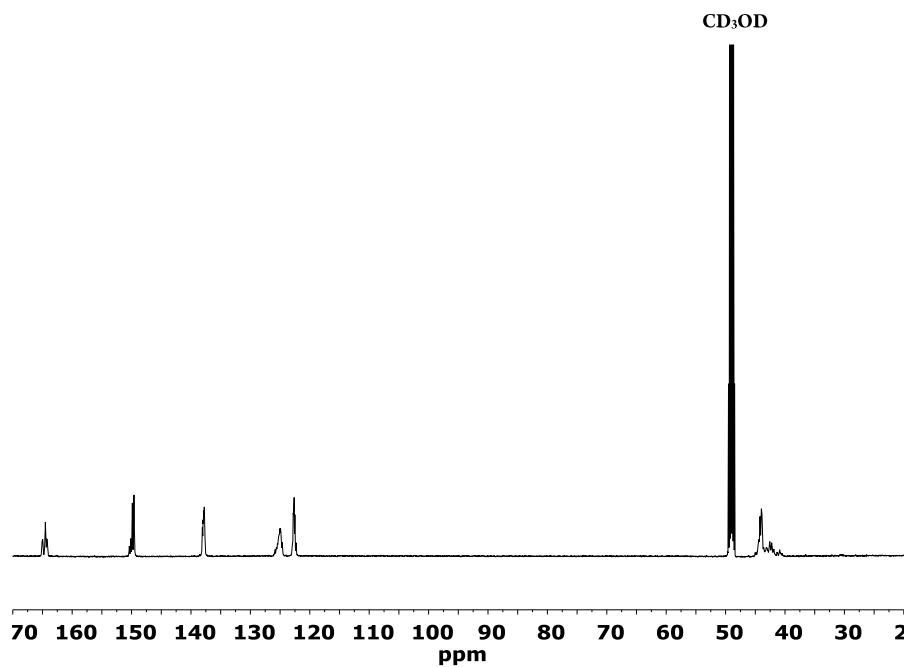


Figure S8: ^{13}C -NMR-spectrum of atactic P2VP produced by catalyst 1a (500 MHz, Cryo, CD_3OD).

Kinetic measurements:

Complex 1a:²

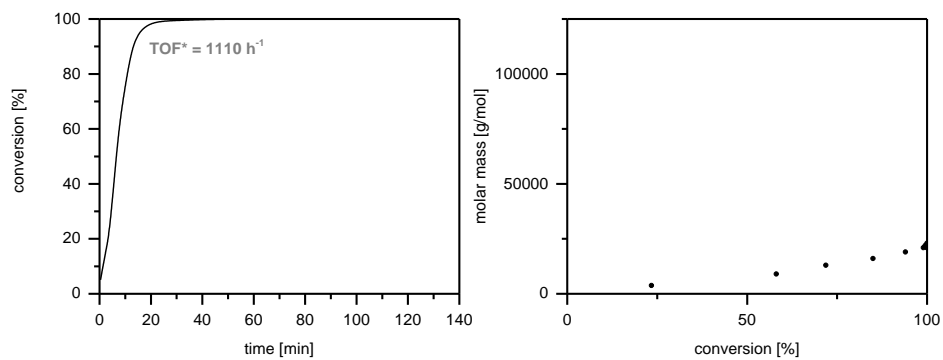


Figure S9: **Left:** Determination of catalytic activity of complex 1a. **Right:** Growth of the absolute molecular weight (M_n) determined by GPC-MALS as a function of monomer conversion. Catalyst: 1.43 μmol ; 2VP: 27.0 mmol; Toluene: 20 mL; 25 °C.

Complex 2a:

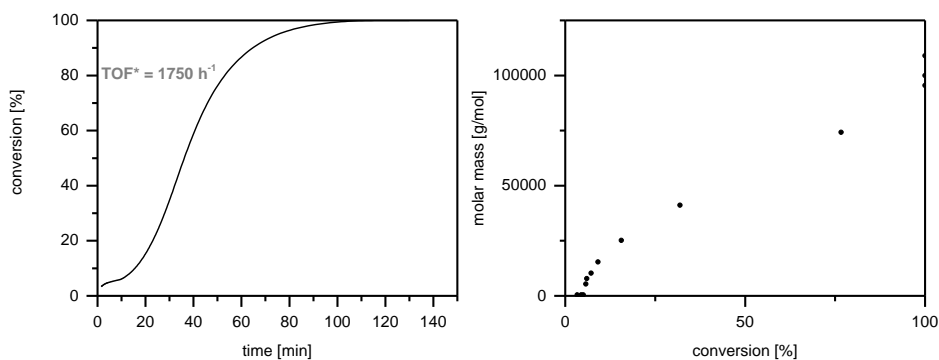


Figure S 10: Left: Determination of catalytic activity of complex **2a**. Right: Growth of the absolute molecular weight (M_n) determined by GPC-MALS as a function of monomer conversion. Catalyst: 1.43 μmol ; 2VP: 27.0 mmol; Toluene: 20 mL; 25 °C. Non-linear relationship in the area of small molecular masses due to a higher divergence of the gravimetric method with small masses and a short induction phase at the beginning of the polymerization.

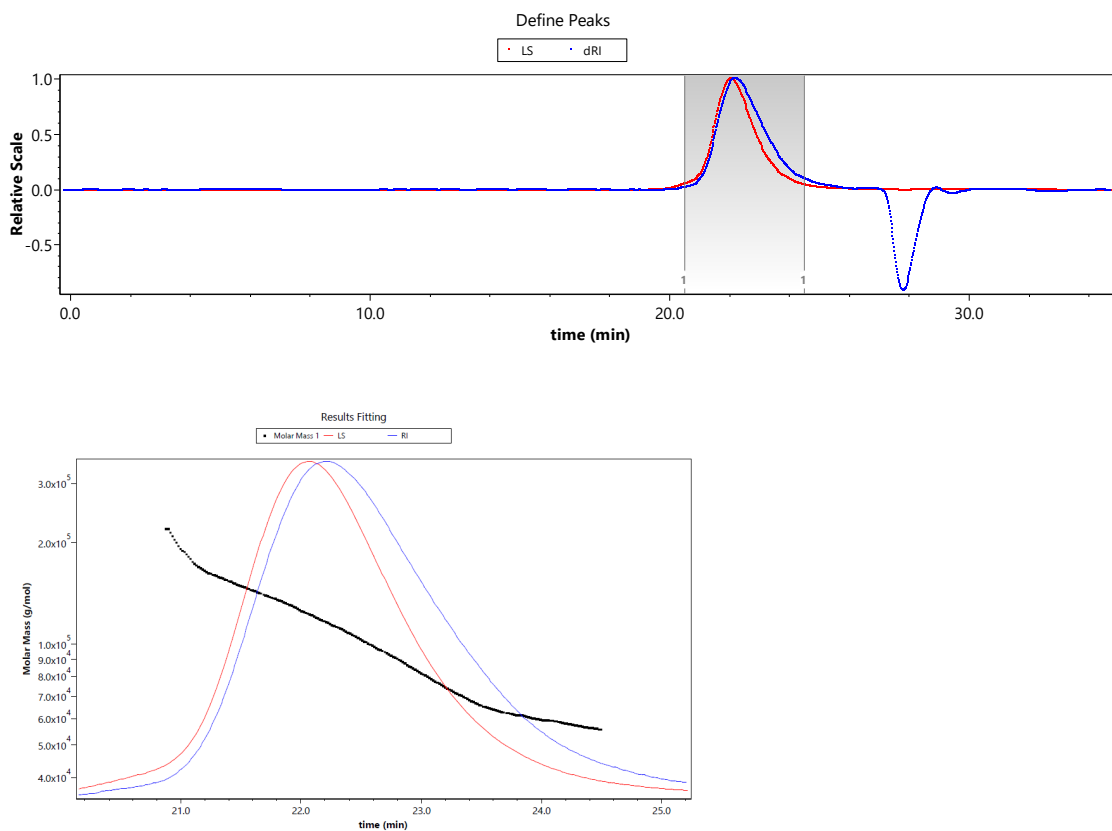


Figure S 11: GPC trace of P2VP produced with catalyst **2a** at the end of the reaction.

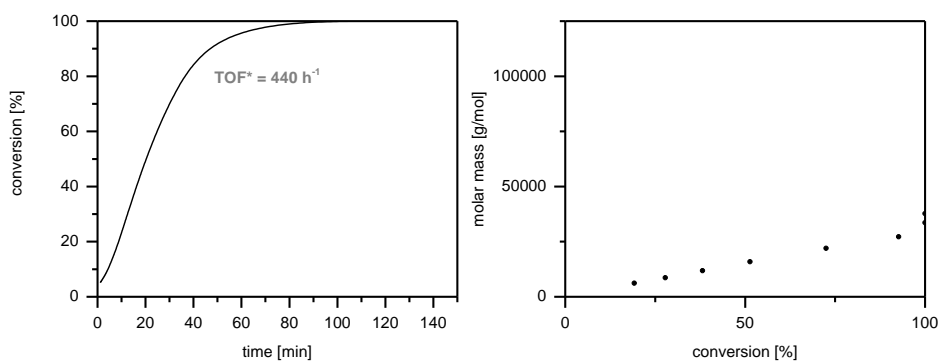
Complex 3a:

Figure S 12: Left: Determination of catalytic activity of complex **3a**. Right: Growth of the absolute molecular weight (M_n) determined by GPC-MALS as a function of monomer conversion. Catalyst: 1.43 μmol ; 2VP: 27.0 mmol; Toluene: 20 mL; 25 °C.

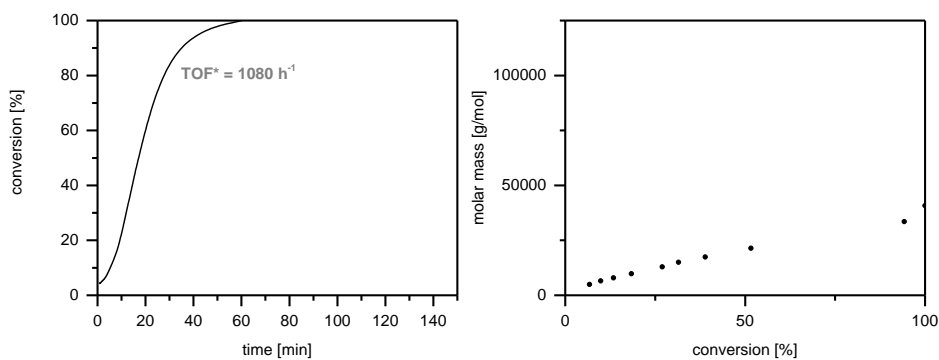
Complex 1b:

Figure S 13: Left: Determination of catalytic activity of complex **1b**. Right: Growth of the absolute molecular weight (M_n) determined by GPC-MALS as a function of monomer conversion. Catalyst: 1.43 μmol ; 2VP: 27.0 mmol; Toluene: 20 mL; 25 °C.

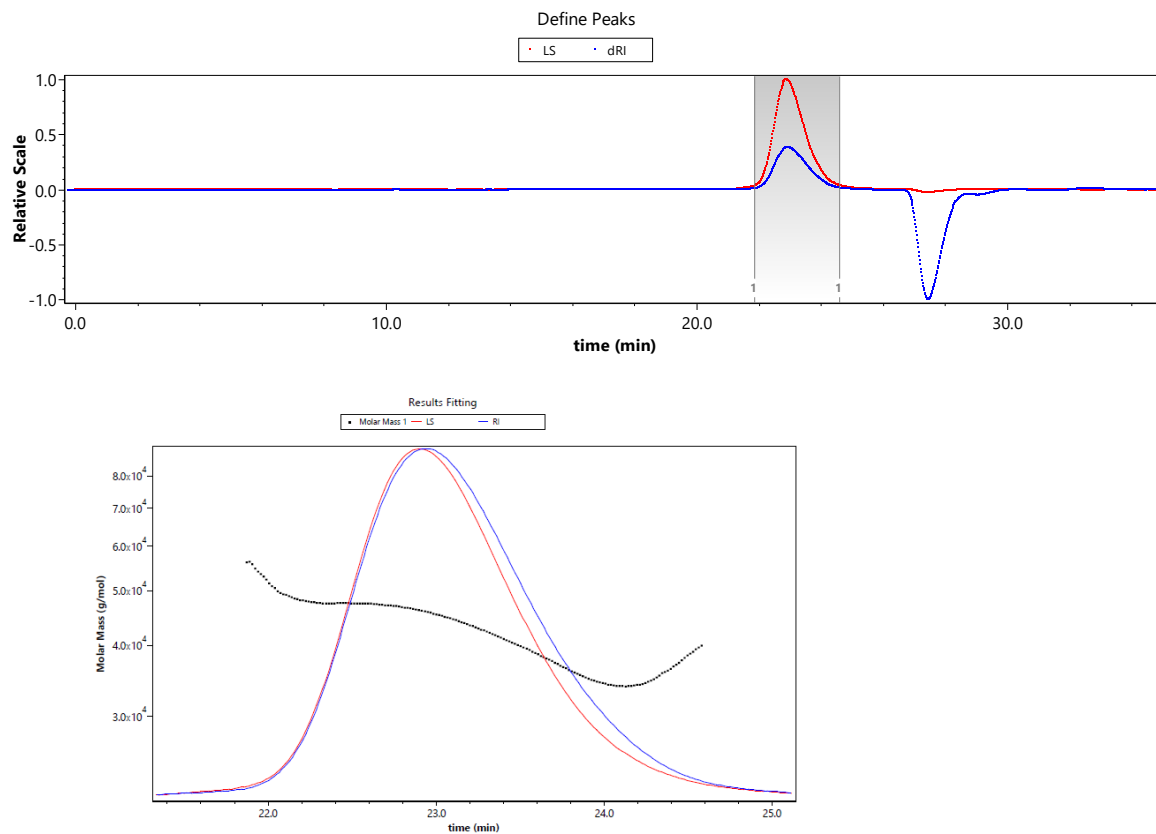


Figure S 14: GPC trace of P2VP produced with catalyst **1b** at the end of the reaction.

Complex 2b:

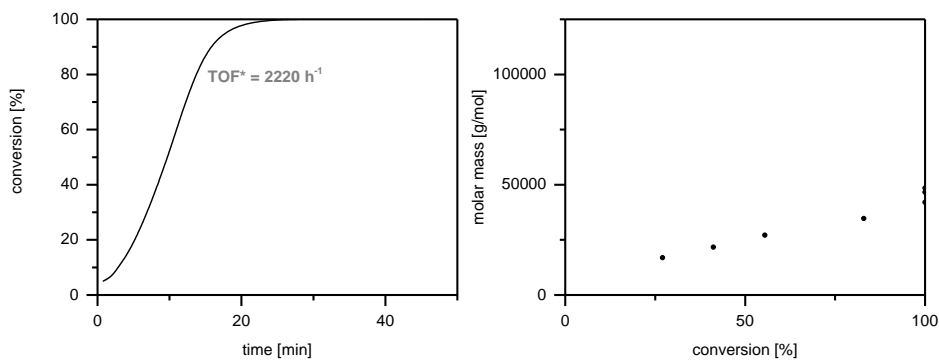


Figure S 15: **Left:** Determination of catalytic activity of complex **2b**. **Right:** Growth of the absolute molecular weight (M_n) determined by GPC-MALS as a function of monomer conversion. Catalyst: $1.43 \mu\text{mol}$; 2VP: 27.0 mmol ; Toluene: 20 mL ; 25°C .

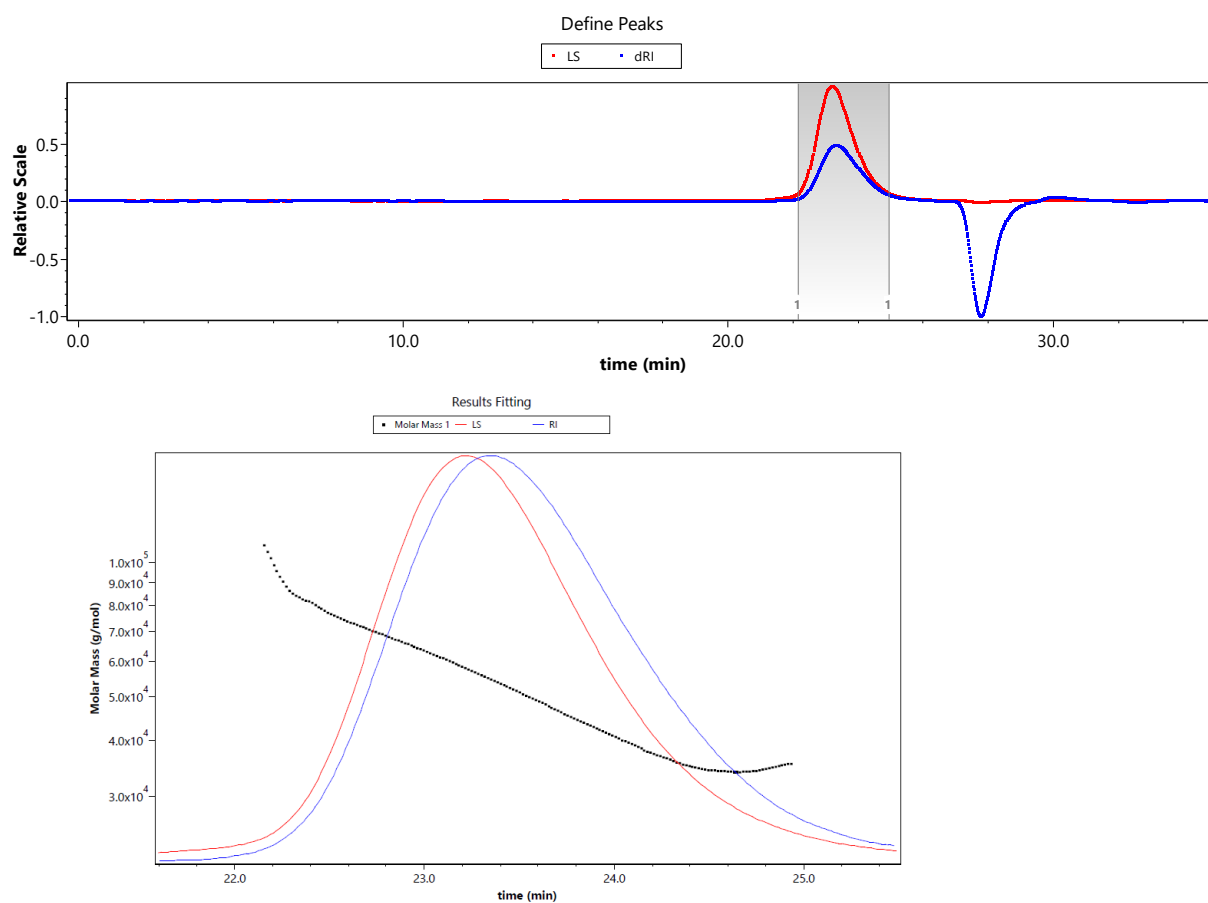


Figure S 16: GPC trace of P2VP produced with catalyst **2b** at the end of the reaction.

Complex 3b:

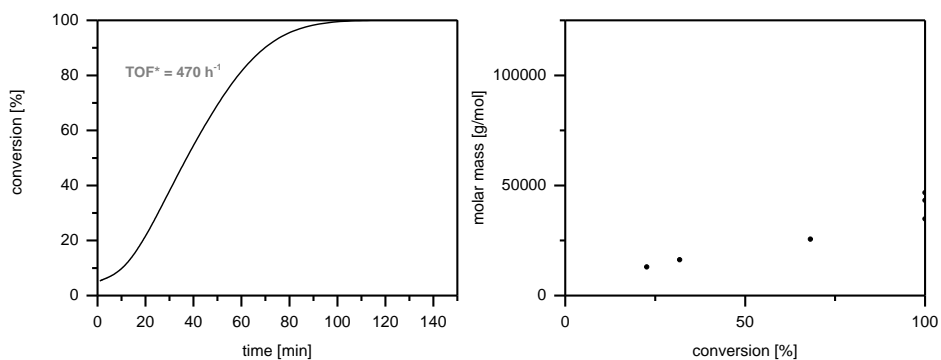


Figure S 17: Left: Determination of catalytic activity of complex **3b**. Right: Growth of the absolute molecular weight (M_n) determined by GPC-MALS as a function of monomer conversion. Catalyst: $1.43 \mu\text{mol}$; 2VP: 27.0 mmol; Toluene: 20 mL; 25°C .

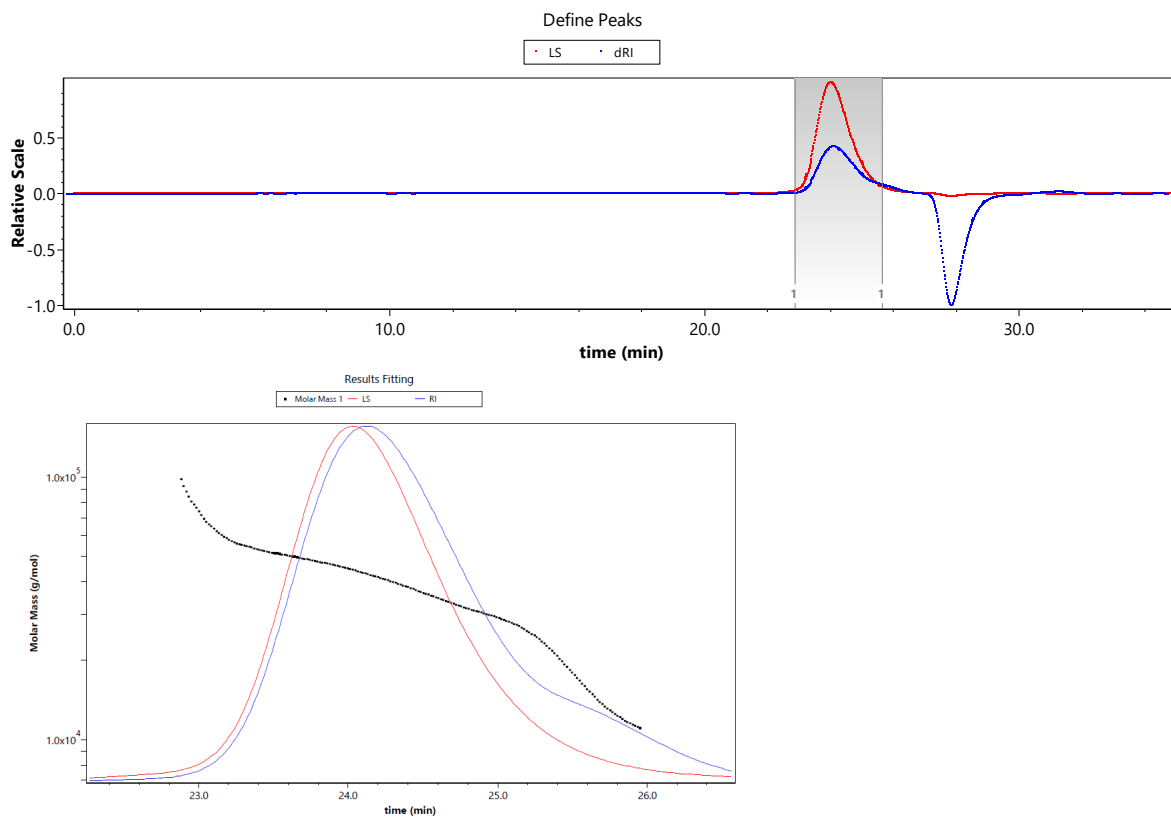


Figure S 18: GPC trace of P2VP produced with catalyst **3b** at the end of the reaction.

TGA:

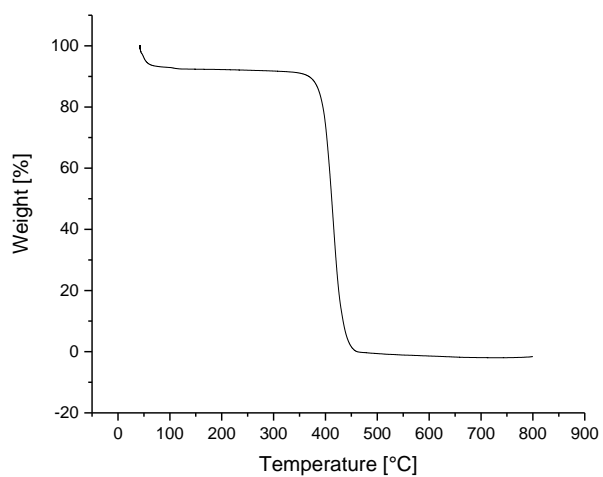


Figure S19: TGA thermogram für atactic P2VP produced with catalyst **1b**. $T_{\text{onset}} = 395$ °C.

DSC:

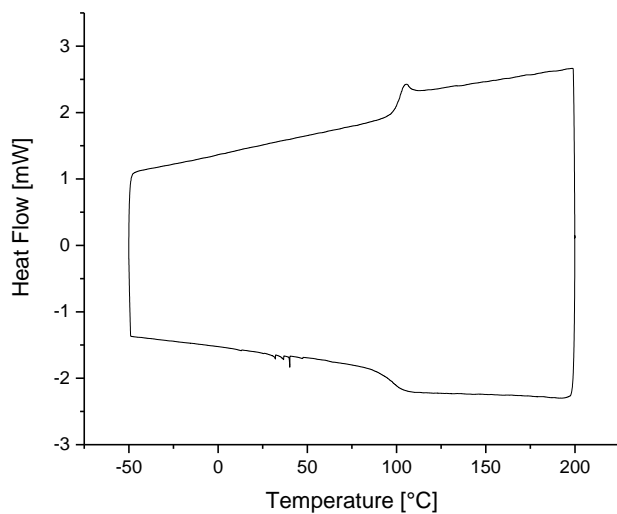
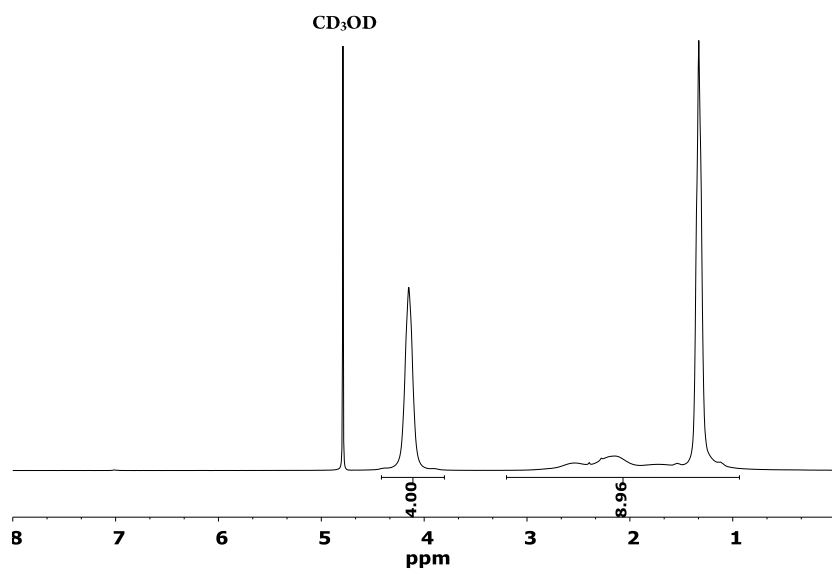
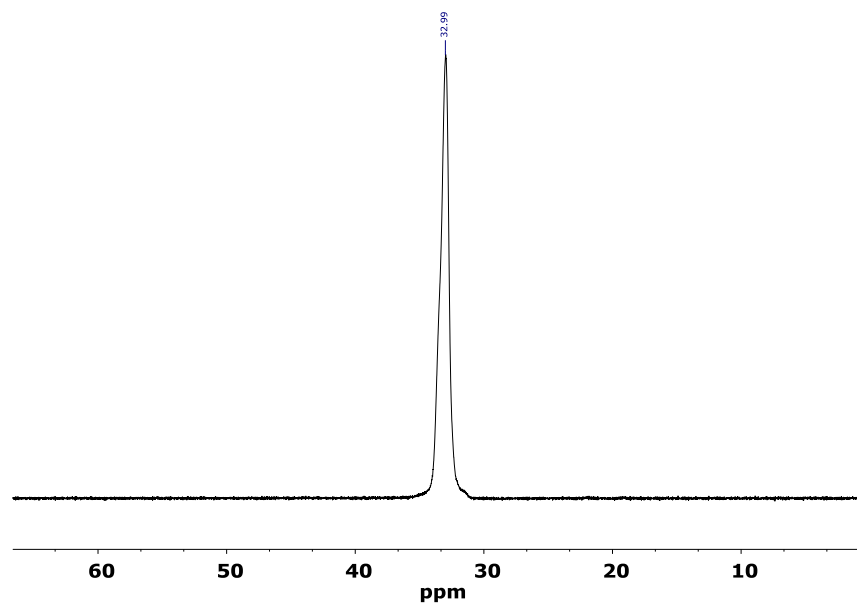


Figure S20: DSC thermogramm für P2VP produced with catalyst **1b**. $T_g = 102$ °C. Exo down.

DEVP Polymerization

NMR spectra:

**Figure S21:** ^1H -NMR-spectra of PDEVp produced by catalyst **1b** (300 MHz, CD_3OD).**Figure S22:** ^{31}P -NMR-spectra of PDEVp produced by catalyst **1b** (203 MHz, CD_3OD).

GPC traces:

Catalyst 1a:

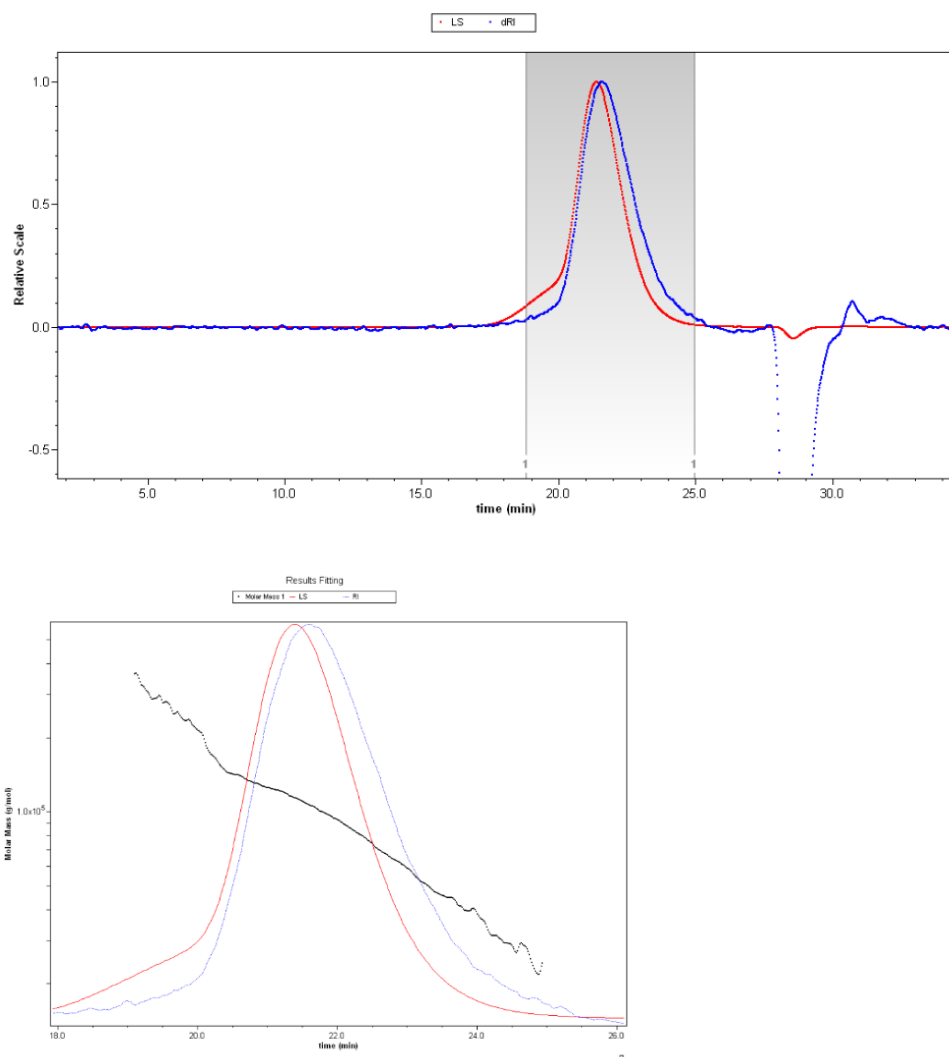


Figure S23: GPC trace of PDEVP produced with catalyst **1a** at the end of the reaction.²

Catalyst 2a:

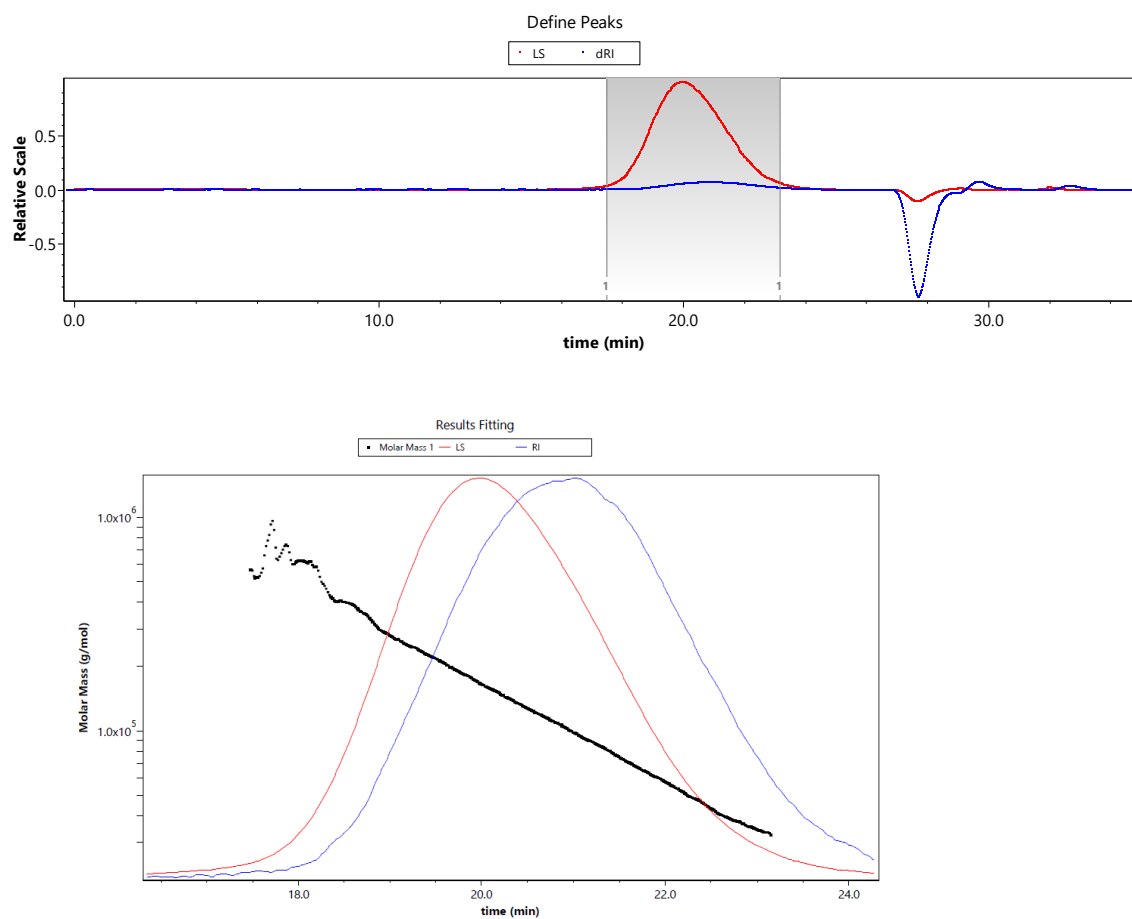


Figure S24: GPC trace of PDEVP produced with catalyst 2a at the end of the reaction (Entry 3, Table S3).

Catalyst 1b:

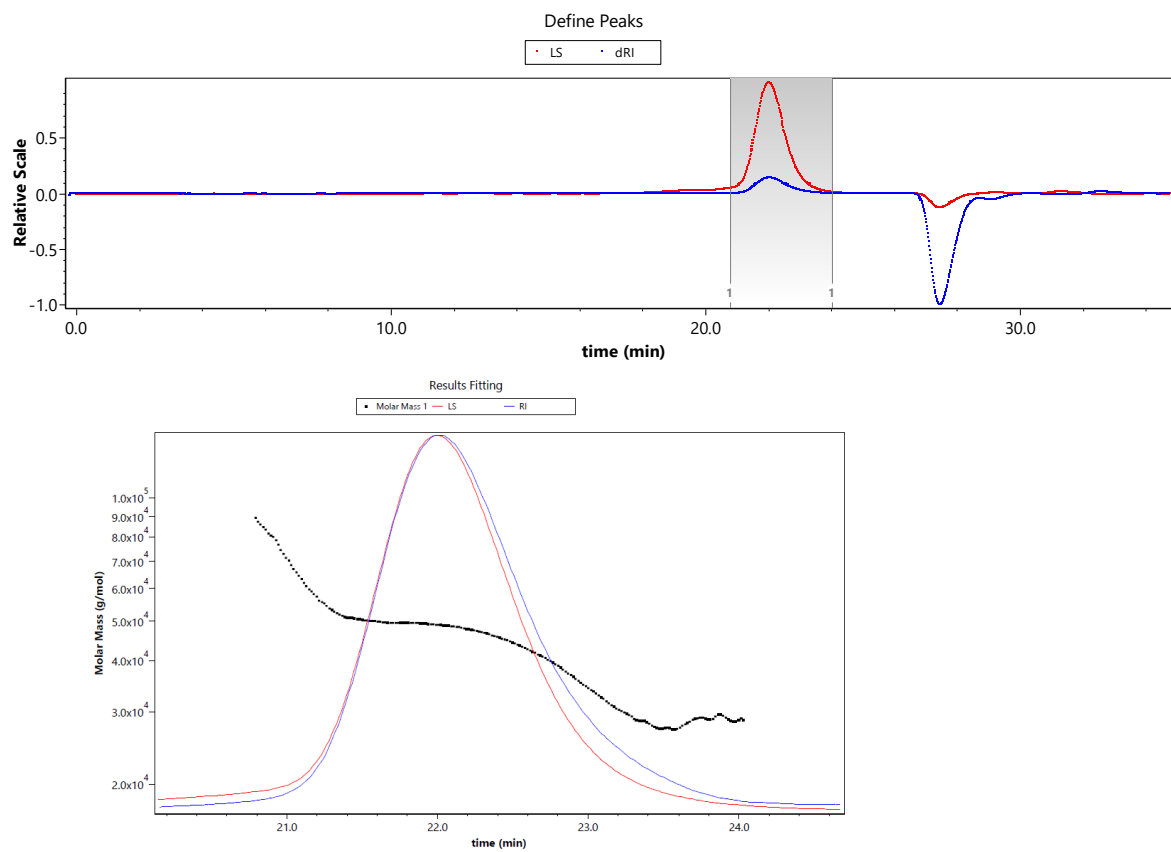


Figure S25: GPC trace of PDEVP produced with catalyst **1b** at the end of the reaction.

Catalyst 2b:

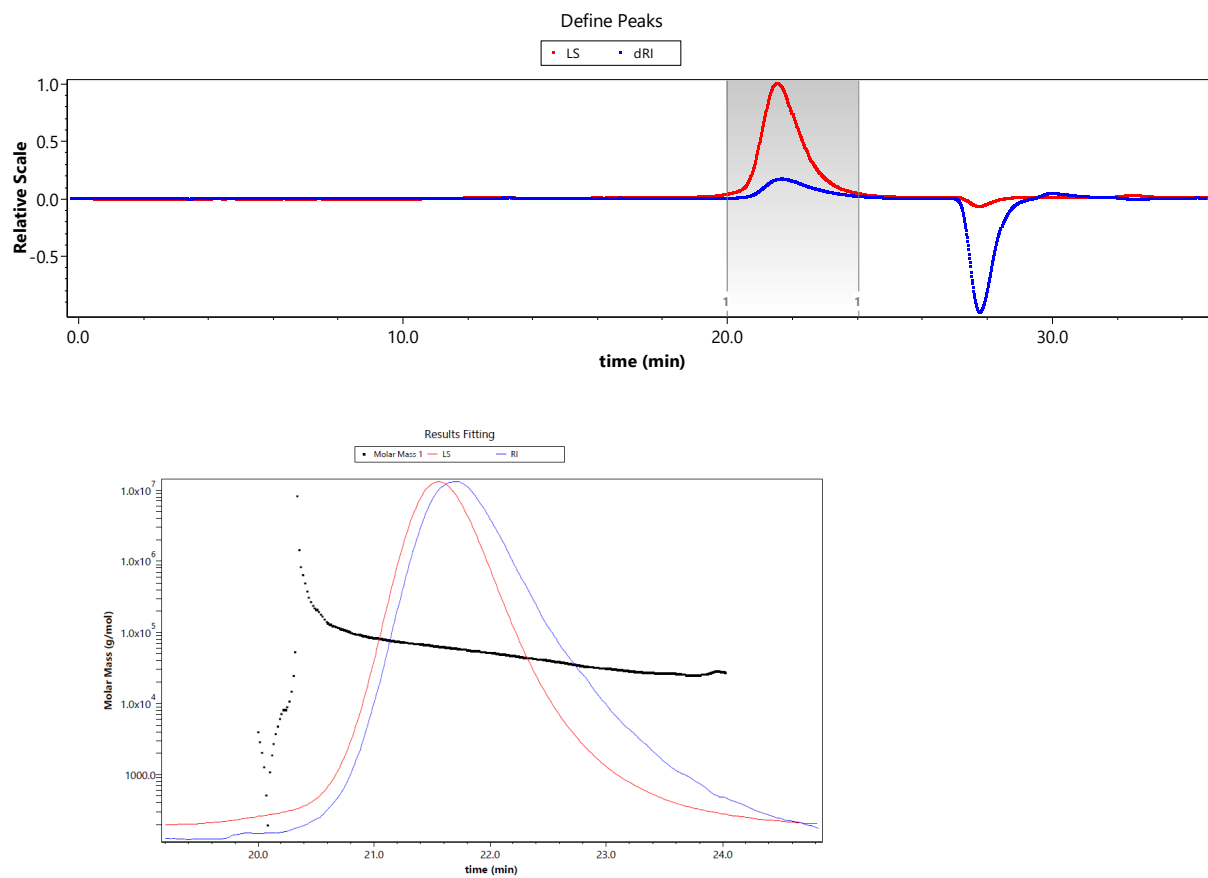


Figure S26: GPC trace of PDEVp produced with catalyst **2b** at the end of the reaction.

Catalyst 3b:

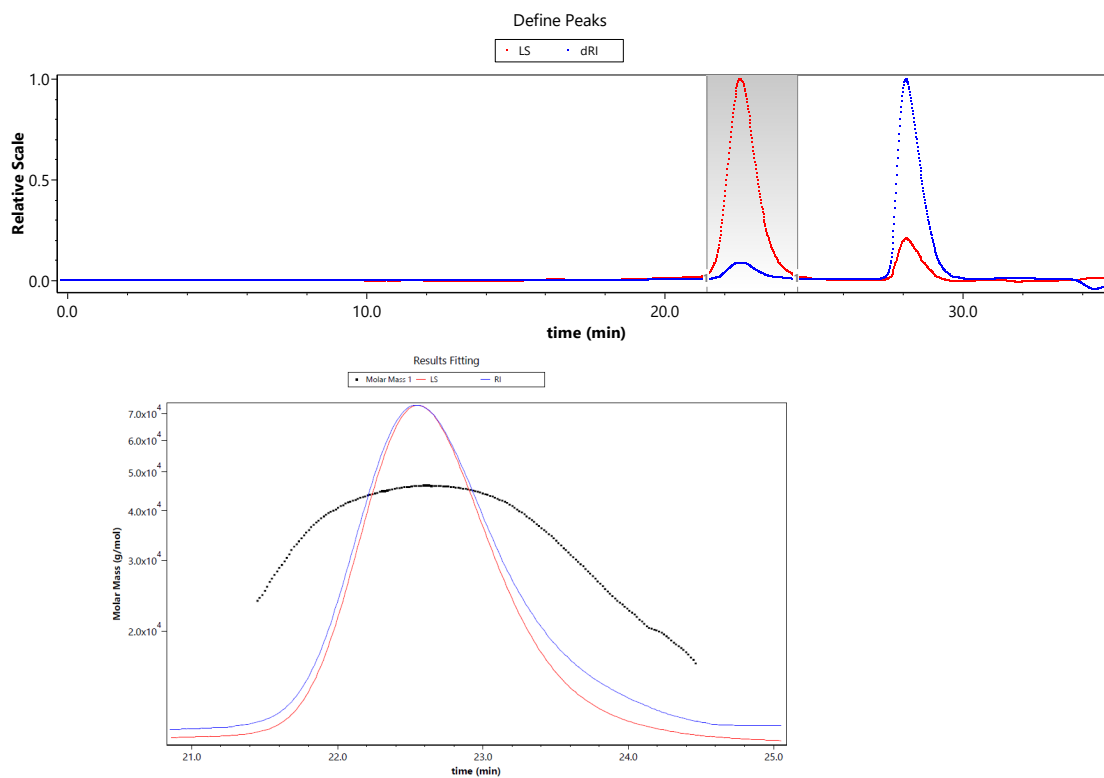


Figure S27: GPC trace of PDEVP produced with catalyst 3b at the end of the reaction.

TGA:

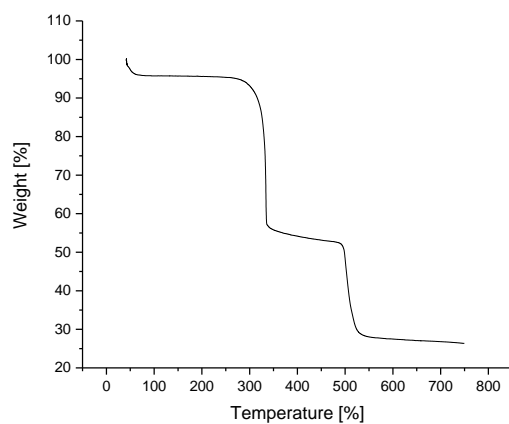


Figure S28: TGA thermogram for PDEVP produced with catalyst 1b.

DMAA Polymerization

PDMAA produced with catalyst **1a** at -50°C :

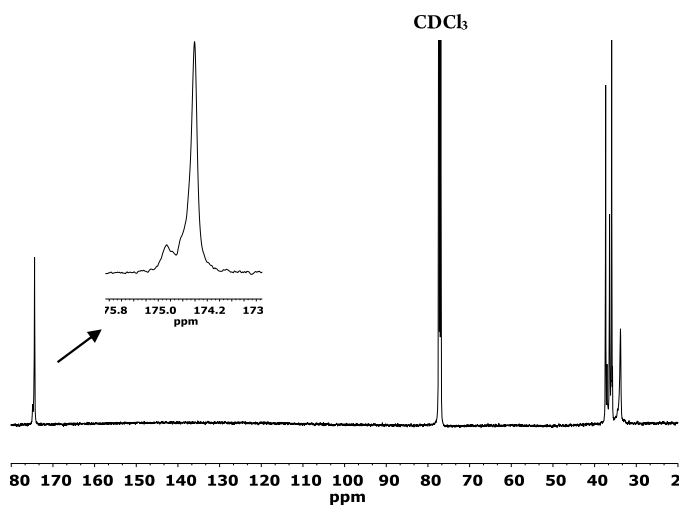


Figure S 29: ^{13}C -NMR spectra and ^{13}C -carbonyl region of PDMAA produced with catalyst **1a** at -50°C (126 MHz, CDCl_3 , 25°C).

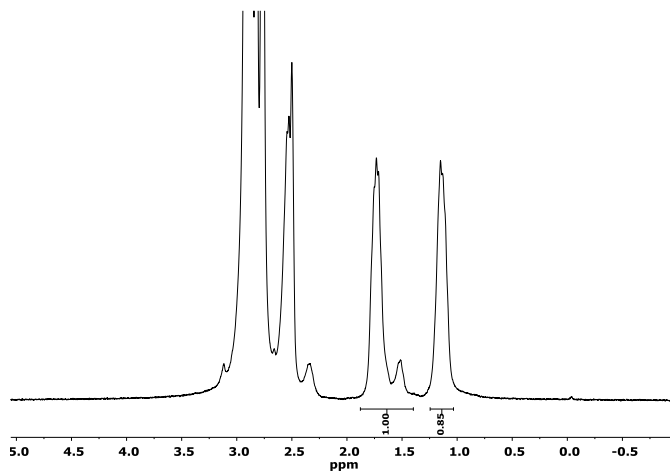


Figure S 30: ^1H -NMR spectra of PDMAA prepared by catalyst **1a** at -50°C (300 MHz, $\text{DMSO}-d_6$, 140°C). Main-chain methylene-proton signal is used for the determination of tacticity according to *Kakuchi et al.*⁵

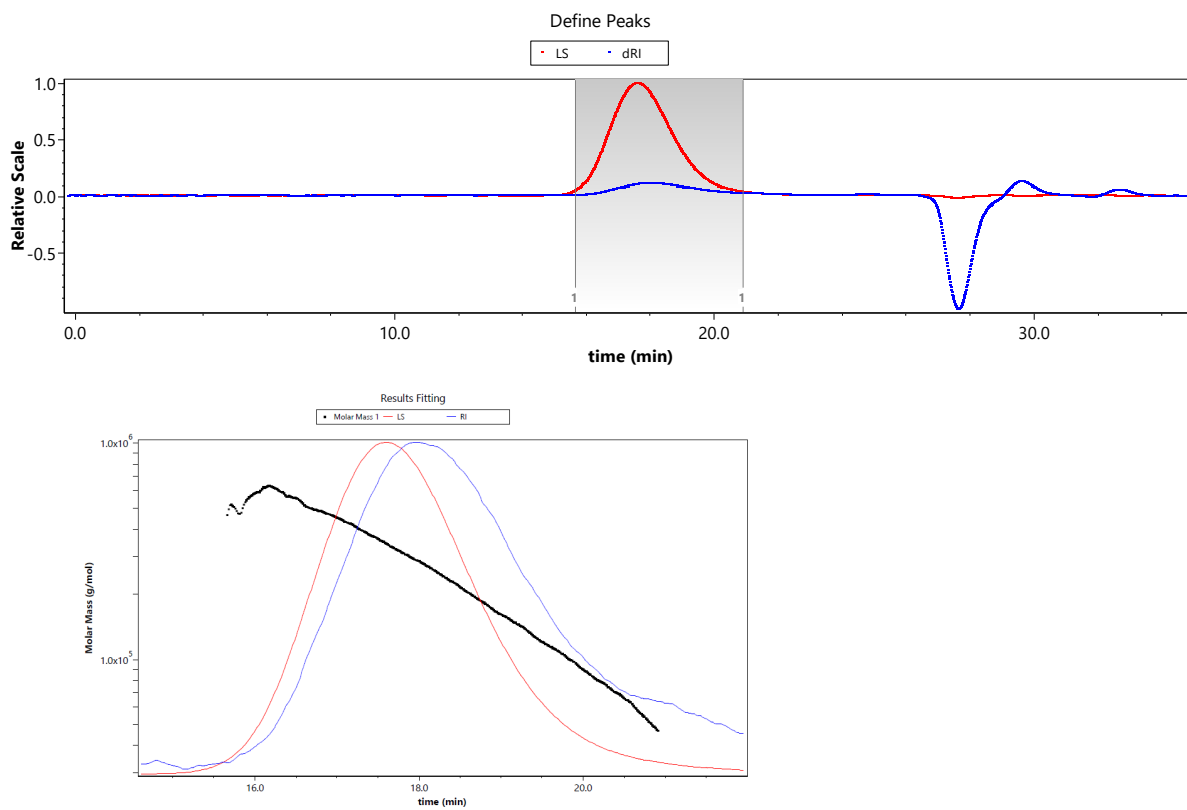


Figure S31: GPC trace of PDMAA produced with catalyst **1a** at $-50\text{ }^\circ\text{C}$ at the end of the reaction.

PDMAA produced with catalyst **1a** at $0\text{ }^\circ\text{C}$:

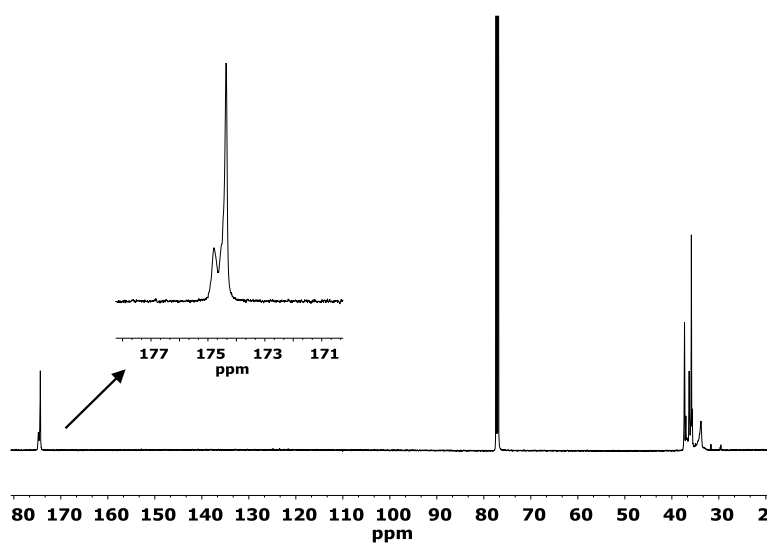


Figure S32: ^{13}C -NMR spectra and ^{13}C -carbonyl region of PDMAA produced with catalyst **1a** at $0\text{ }^\circ\text{C}$ (126 MHz, CDCl_3 , $25\text{ }^\circ\text{C}$).

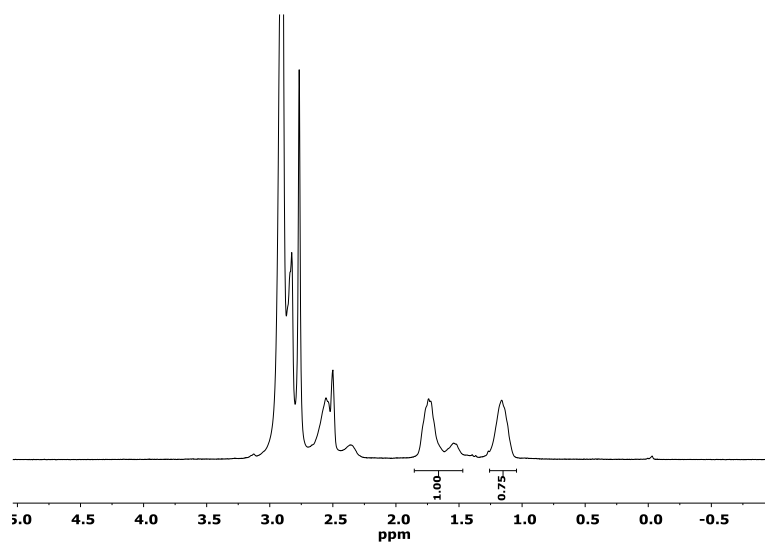


Figure S 33: ^1H -NMR spectra of PDMAA prepared by catalyst **1a** at $0\text{ }^\circ\text{C}$ (300 MHz, DMSO-d_6 , $140\text{ }^\circ\text{C}$). Main-chain methylene-proton signal is used for the determination of tacticity according to *Kakuchi et al.*⁵

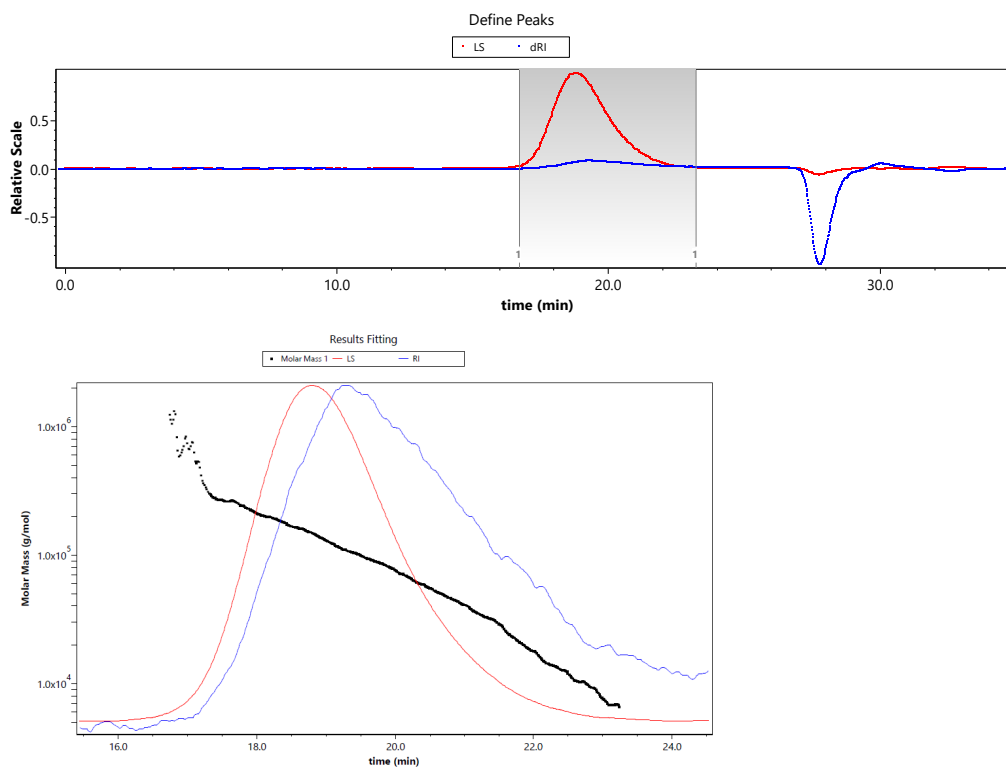


Figure S 34: GPC trace of PDMAA produced with catalyst **1a** at $0\text{ }^\circ\text{C}$ at the end of the reaction.

PDMAA produced with catalyst **2a** at -20°C:

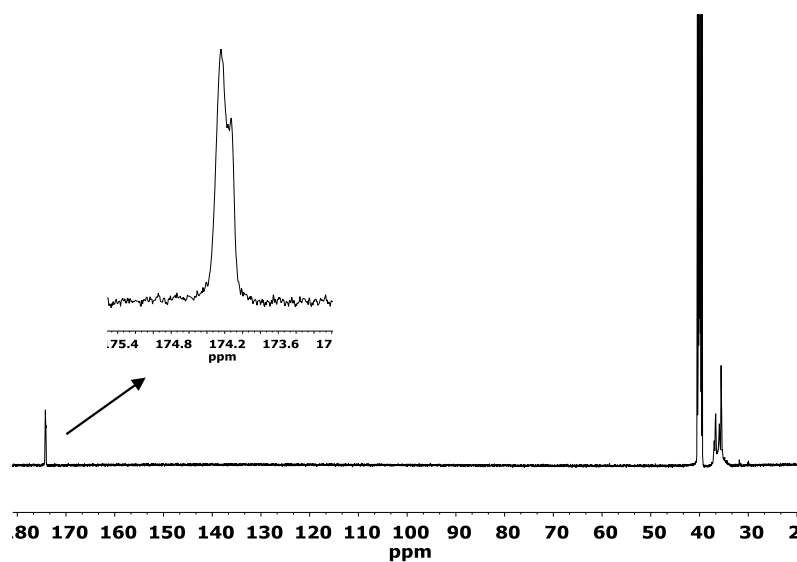


Figure S 35: ^{13}C -NMR spectra and ^{13}C -carbonyl region of PDMAA produced with catalyst **2a** at -20 °C (126 MHz, CDCl_3 , 25 °C).

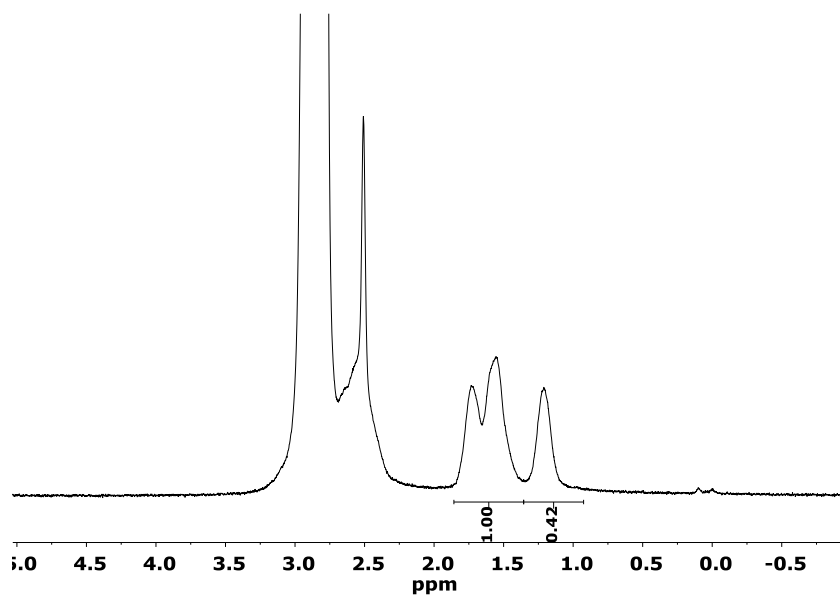


Figure S 36: ^1H -NMR spectra of PDMAA prepared by catalyst **2a** at -20 °C (300 MHz, DMSO-d_6 , 140 °C). Main-chain methylene-proton signal is used for the determination of tacticity according to *Kakuchi et al.*⁵

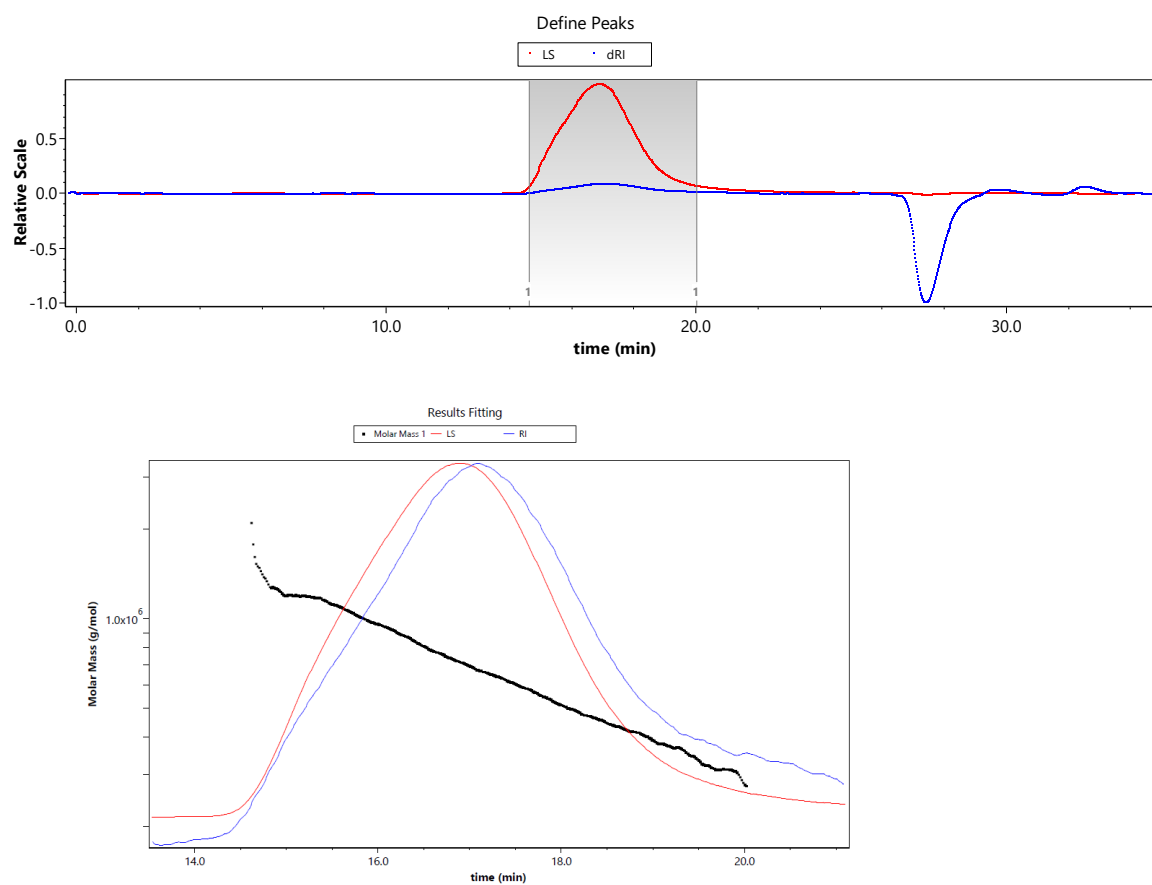


Figure S37: GPC trace of PDMAA produced with catalyst **2a** at -20°C at the end of the reaction.

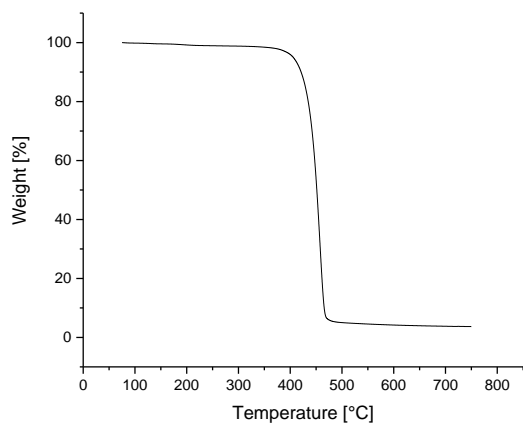


Figure S38: TGA thermogram for PDMAA produced with catalyst **2a** at -20 °C. $T_{\text{onset}} = 436$ °C.

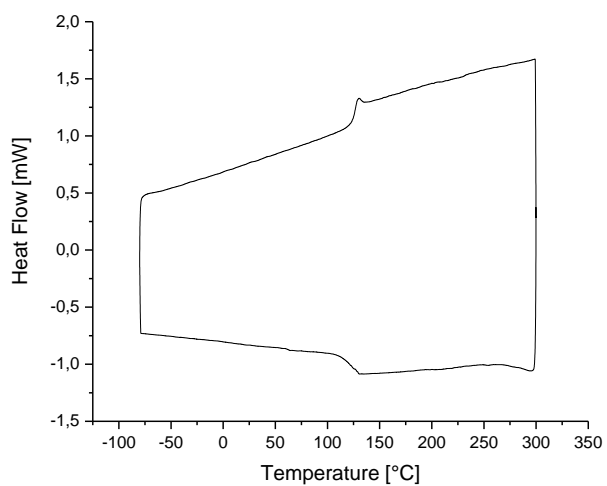


Figure S39: DSC thermogramm für PDMAA produced with catalyst **2a** at -20 °C. $T_g = 127$ °C. Exo down.

PDMAA produced with catalyst **1b** at -78 °C

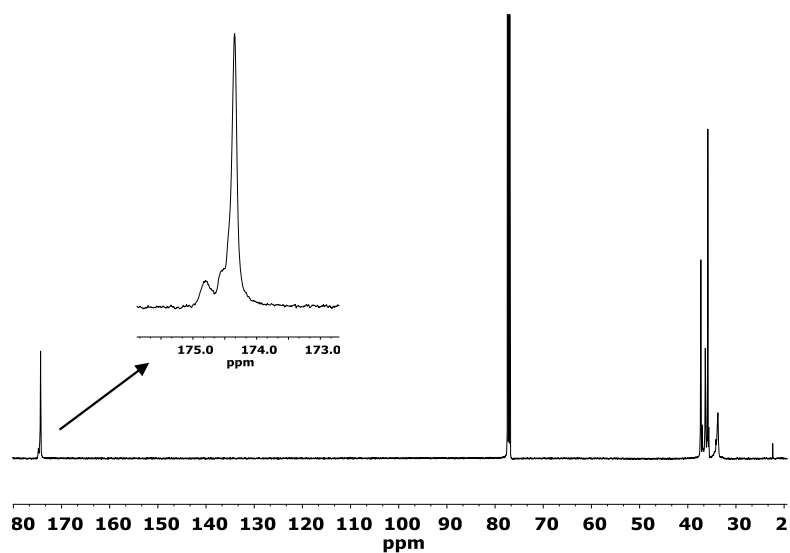


Figure S 40: ¹³C-NMR spectra and ¹³C-carbonyl region of PDMAA produced with catalyst **1b** at -78 °C (126 MHz, CDCl₃, 25 °C).

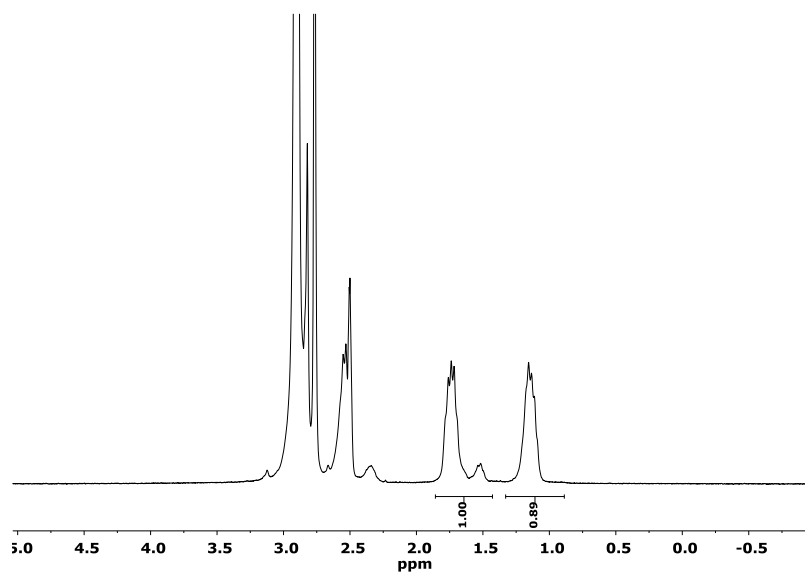


Figure S 41: ¹H-NMR spectra of PDMAA prepared by catalyst **1b** at -78 °C (300 MHz, DMSO-d₆, 140 °C). Main-chain methylene-proton signal is used for the determination of tacticity according to *Kakuchi et al.*⁵

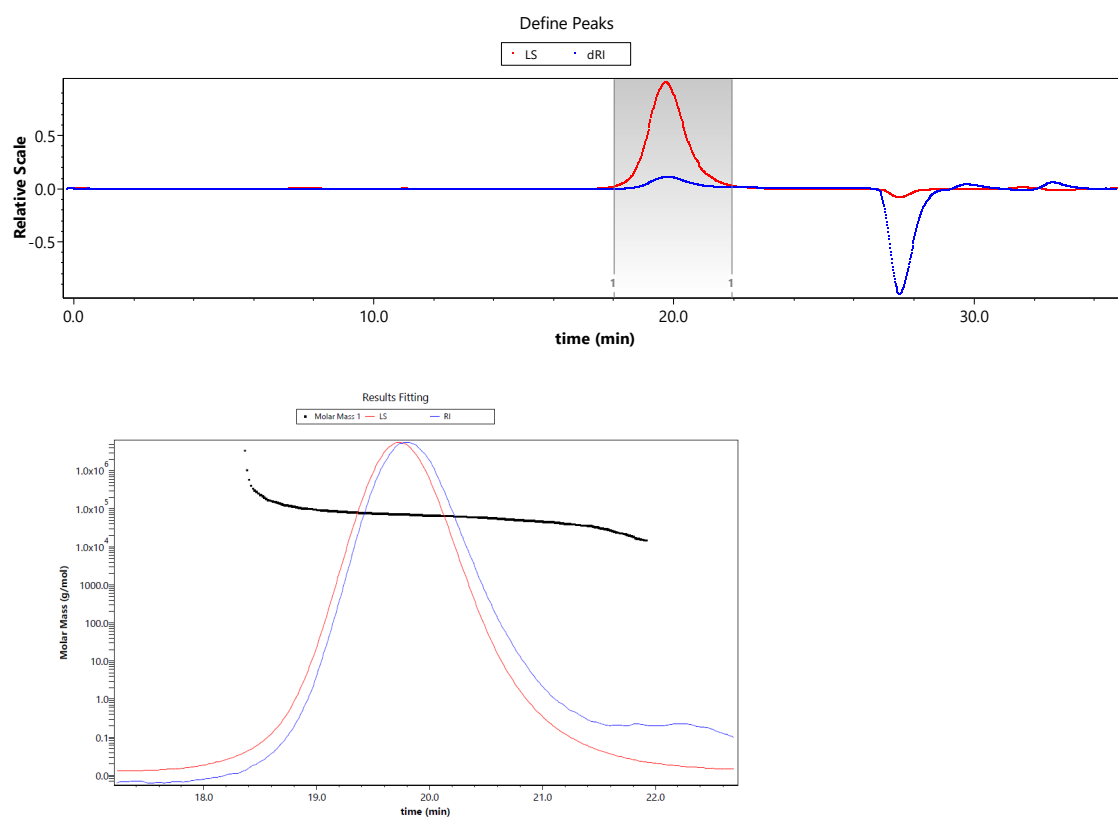


Figure S42: GPC trace of PDMAA produced with catalyst **1b** at -78 °C at the end of the reaction.

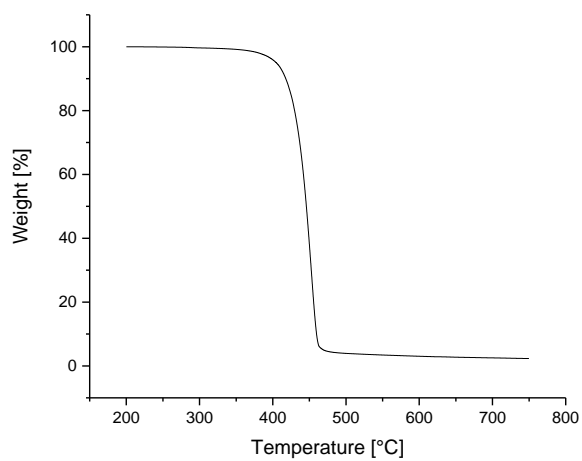


Figure S43: TGA thermogram for PDMAA produced with catalyst **1b** at $-78\text{ }^{\circ}\text{C}$. $T_{\text{onset}} = 431\text{ }^{\circ}\text{C}$.

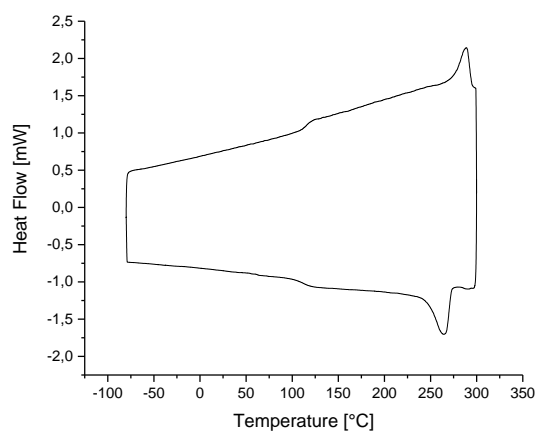


Figure S44: DSC thermogram für PDMAA produced with catalyst **1b** at $-78\text{ }^{\circ}\text{C}$. $T_g = 115\text{ }^{\circ}\text{C}$. $T_{\text{cryst}} = 265\text{ }^{\circ}\text{C}$. $T_m = 289\text{ }^{\circ}\text{C}$. Exo down.

6. Computational methods

Complete List of authors of Gaussian 09:

Gaussian 09, Revision B.01; M. J. Frisch, G. W. Trucks, H. B. Schlegel, G. E. Scuseria, M. A. Robb, J. R. Cheeseman, G. Scalmani, V. Barone, G. A. Petersson, H. Nakatsuji, X. Li, M. Caricato, A. Marenich, J. Bloino, B. G. Janesko, R. Gomperts, B. Mennucci, H. P. Hratchian, J. V. Ortiz, A. F. Izmaylov, J. L. Sonnenberg, D. Williams-Young, F. Ding, F. Lipparini, F. Egidi, J. Goings, B. Peng, A. Petrone, T. Henderson, D. Ranasinghe, V. G. Zakrzewski, J. Gao, N. Rega, G. Zheng, W. Liang, M. Hada, M. Ehara, K. Toyota, R. Fukuda, J. Hasegawa, M. Ishida, T. Nakajima, Y. Honda, O. Kitao, H. Nakai, T. Vreven, K. Throssell, J. A. Montgomery, Jr., J. E. Peralta, F. Ogliaro, M. Bearpark, J. J. Heyd, E. Brothers, K. N. Kudin, V. N. Staroverov, T. Keith, R. Kobayashi, J. Normand, K. Raghavachari, A. Rendell, J. C. Burant, S. S. Iyengar, J. Tomasi, M. Cossi, J. M. Millam, M. Klene, C. Adamo, R. Cammi, J. W. Ochterski, R. L. Martin, K. Morokuma, O. Farkas, J. B. Foresman, and D. J. Fox, Gaussian, Inc., Wallingford CT, 2010.

Geometries for the Lutetium complex were optimized with the same method as for the yttrium complexes, but the Stevens/Basch/Krauss ECP split valence basis set (CEP-31G) was used instead of LanL2DZ

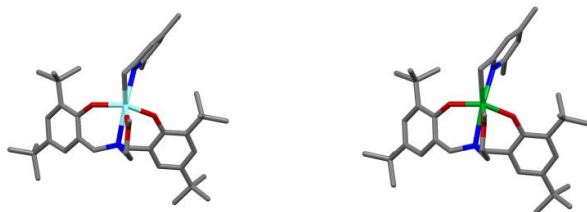


Figure S45: Calculated isolated structures of 1b' (left) and 2b' (right) (1b and 2b, but without attached THF molecule; light blue = yttrium; green = lutetium; red = oxygen; blue = nitrogen; gray = carbon).

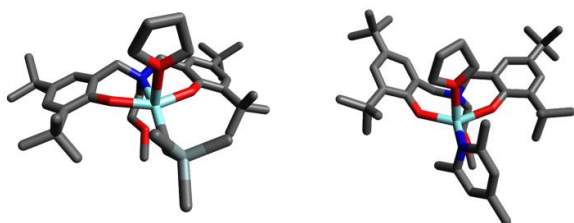


Figure S46: Calculated isolated structures of 1a (left) and 1b (right) (with attached THF molecule; light blue = yttrium; red = oxygen; blue = nitrogen; light gray = silicon; gray = carbon).

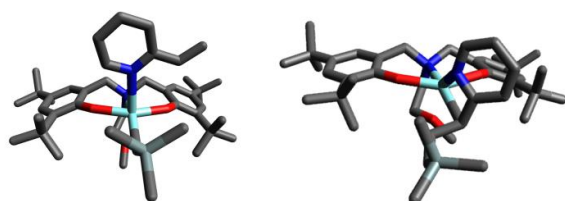


Figure S47: Calculated isolated structures of Ia (left) and IIa (right) (light blue = yttrium; red = oxygen; blue = nitrogen; light gray = silicon; gray = carbon).

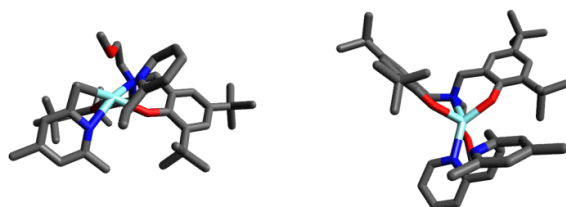


Figure S48: Calculated isolated structures of Ib (left) and IIb (right) (light blue = yttrium; red = oxygen; blue = nitrogen; gray = carbon).

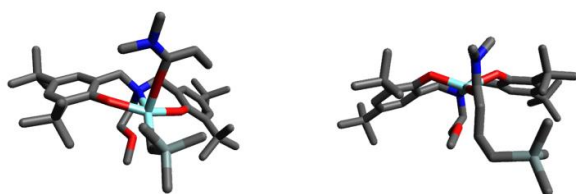


Figure S49: Calculated isolated structures of I_c (left) and II_c (right) (light blue = yttrium; red = oxygen; blue = nitrogen; light gray = silicon; gray = carbon).

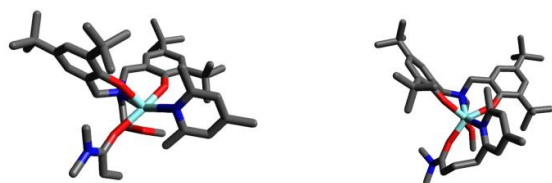


Figure S50: Calculated isolated structures of I_d (left) and II_d (right) (light blue = yttrium; red = oxygen; blue = nitrogen; gray = carbon).

XYZ coordinates of optimized geometries (in Å):

<u>1a:</u>							
Y	-0.007202	1.022089	-0.078102	C	1.124747	1.953329	3.079532
Si	-0.123501	4.783659	-0.769244	H	1.511941	0.946013	3.262150
O	-2.109396	0.578901	0.154704	H	1.879359	2.539048	2.551891
O	0.220126	-0.277474	-2.154361	C	0.576933	2.621769	4.352204
O	2.092530	0.611529	0.280787	H	0.652425	3.713306	4.278476
O	-0.059712	1.814179	2.170761	H	1.124201	2.301275	5.244667
N	-0.005230	-1.573017	0.395637	C	-0.910954	2.186896	4.377462
C	-3.002478	-0.451696	0.132369	H	-1.010508	1.168195	4.772338
C	-4.333702	-0.313787	-0.385794	H	-1.533160	2.853198	4.983784
C	-5.156520	-1.455660	-0.375775	C	-1.300873	2.233938	2.894531
H	-6.163579	-1.360374	-0.766918	H	-1.550551	3.250120	2.568589
C	-4.754073	-2.723143	0.112072	H	-2.089237	1.543817	2.589795
C	-3.449079	-2.821255	0.621560	C	0.004456	3.035847	-1.453087
H	-3.084853	-3.764111	1.021214	H	0.948359	2.960884	-2.030475
C	-2.580187	-1.711085	0.640664	H	-0.826186	2.894014	-2.174804
C	-1.215764	-1.843965	1.282308	C	0.247247	6.137743	-2.070689
H	-1.123456	-1.135826	2.118656	H	0.148299	7.148695	-1.647596
H	-1.119845	-2.859995	1.704505	H	-0.443330	6.058295	-2.922312
C	-0.069332	-2.344469	-0.879381	H	1.269772	6.034998	-2.461845
H	0.327613	-3.367968	-0.754082	C	1.113525	5.067393	0.662246
H	-1.123268	-2.426147	-1.161087	H	1.119766	6.120498	0.977820
C	0.685262	-1.674964	-2.028928	H	2.135764	4.801484	0.357690
H	0.453725	-2.203902	-2.965014	H	0.852741	4.453867	1.535324
H	1.768803	-1.666211	-1.875436	C	-1.881452	5.125252	-0.105072
C	0.478937	0.285767	-3.487012	H	-1.946412	6.121951	0.354768
H	0.115843	1.312322	-3.472802	H	-2.185753	4.382569	0.645015
H	-0.062362	-0.300585	-4.241005	H	-2.619074	5.083516	-0.918760
H	1.556384	0.273381	-3.697954	C	-4.844805	1.039139	-0.938250
C	1.215392	-1.895730	1.235027	C	-3.980524	1.465639	-2.161174
H	1.128778	-1.254794	2.124961	H	-4.329867	2.431403	-2.553495
H	1.130363	-2.941965	1.580267	H	-4.058533	0.721396	-2.966228
C	2.585360	-1.702486	0.616594	H	-2.930828	1.566008	-1.877142
C	3.466046	-2.793042	0.530448	C	-4.757422	2.127159	0.172151
H	3.107829	-3.771757	0.847256	H	-5.089931	3.098125	-0.220875
C	4.788513	-2.642945	0.064319	H	-3.729200	2.229618	0.526478
C	5.191596	-1.339539	-0.296043	H	-5.402259	1.862820	1.022061
H	6.205971	-1.197106	-0.643804	C	-6.321466	0.972645	-1.409640
C	4.351988	-0.204999	-0.229688	H	-6.624477	1.962315	-1.775780
C	3.007995	-0.397415	0.222468	H	-7.002629	0.698868	-0.592783
				H	-6.460924	0.259536	-2.233209

C -5.742520 -3.912254 0.075727
C -7.003047 -3.572167 0.925053
H -6.727912 -3.388827 1.971910
H -7.721435 -4.403596 0.897378
H -7.511122 -2.675394 0.550750
C -6.178489 -4.189471 -1.393661
H -5.311970 -4.457256 -2.012563
H -6.653900 -3.311207 -1.846533
H -6.898536 -5.019003 -1.431093
C -5.119718 -5.213159 0.642361
H -4.236061 -5.522979 0.068666
H -5.853530 -6.028190 0.589981
H -4.825161 -5.097558 1.693745
C 5.725401 -3.871129 -0.021161
C 5.106994 -4.935918 -0.975279
H 4.118182 -5.262475 -0.629948
H 5.753138 -5.823125 -1.032273
H 4.992203 -4.529053 -1.988679
C 7.132862 -3.508960 -0.558183
H 7.643207 -2.787434 0.092961
H 7.085747 -3.085405 -1.569994
H 7.754503 -4.412882 -0.604347
C 5.897939 -4.497865 1.394573
H 6.348742 -3.774643 2.086517
H 6.548843 -5.382162 1.347506
H 4.935544 -4.810880 1.817961
C 4.870122 1.196136 -0.637770
C 4.065200 1.716316 -1.864872
H 4.418994 2.715518 -2.156299
H 3.001029 1.782474 -1.627777
H 4.198799 1.044735 -2.725306
C 6.370991 1.188919 -1.031275
H 6.677871 2.211180 -1.288602
H 6.566755 0.555661 -1.906916
H 7.010840 0.848035 -0.206515
C 4.703716 2.186657 0.552119
H 5.048037 3.189386 0.261371
H 5.299913 1.857157 1.414373
H 3.654792 2.247836 0.851885

1b:

Y 0.039228 -1.258066 -0.526132
O 1.877569 -0.208966 -0.047319
O -2.119958 -1.071820 -0.809613
O 0.963080 -1.192717 -2.831384
N -0.193386 1.128930 -1.609622
N 0.571088 -3.370606 0.698859
C 0.225124 2.112777 -0.537157
H -0.360843 1.839332 0.347749
H -0.107320 3.122360 -0.835979
C 1.718841 2.180042 -0.246024
C 2.493262 1.002666 -0.017865
C 3.906667 1.135526 0.216546
C 4.448199 2.433101 0.260348
H 5.511563 2.535457 0.447359
C 3.693824 3.615347 0.065399
C 2.325313 3.453142 -0.202661
H 1.698461 4.321764 -0.386928
C 4.807861 -0.111404 0.394243
C 4.332188 -0.941969 1.620392
H 4.956147 -1.839401 1.736584
H 3.295392 -1.253866 1.485081
H 4.411110 -0.347969 2.542063
C 4.735556 -0.989111 -0.891260
H 5.334768 -1.901450 -0.760316
H 5.134394 -0.438498 -1.755160
H 3.702257 -1.275563 -1.102012
C 6.297349 0.254239 0.626718
H 6.879457 -0.669942 0.738592
H 6.437910 0.845985 1.541179
H 6.722419 0.813241 -0.217573
C 4.386113 4.996062 0.139934
C 4.999282 5.196965 1.557634
H 5.512942 6.166666 1.621377
H 5.728454 4.413226 1.796135
H 4.216100 5.170942 2.326636
C 3.402564 6.163409 -0.126183
H 3.937785 7.119909 -0.062568
H 2.590374 6.186514 0.612244
H 2.956212 6.097298 -1.127299
C 5.522984 5.076154 -0.921669
H 6.030532 6.049589 -0.868075
H 5.117761 4.954425 -1.934843

H	6.277906	4.295741	-0.767348	H	1.367306	0.042433	-4.486826
C	-1.608907	1.428038	-2.047442	C	1.590525	-2.299294	-3.558879
H	-1.800088	0.778988	-2.911517	H	2.493002	-1.932867	-4.066915
H	-1.640540	2.472666	-2.407936	H	0.886817	-2.724875	-4.285905
C	-2.752503	1.217637	-1.072311	H	1.856993	-3.056296	-2.822569
C	-3.070269	-0.107106	-0.658883	C	-0.460906	-3.693592	-1.433994
C	-4.381423	-0.379929	-0.140604	H	-1.438096	-3.386531	-1.065034
C	-5.205062	0.728899	0.143151	H	-0.476447	-4.157096	-2.417426
H	-6.185061	0.539202	0.567323	C	0.525347	-4.101050	-0.504854
C	-4.844876	2.073787	-0.115692	C	1.521070	-5.115272	-0.751417
C	-3.621239	2.285212	-0.776904	H	1.509780	-5.630030	-1.709386
H	-3.334469	3.284291	-1.094969	C	2.402028	-5.497630	0.251292
C	-4.922700	-1.831360	-0.028751	C	2.309529	-4.847392	1.522288
C	-4.121827	-2.692554	0.987484	H	2.949296	-5.156568	2.343672
H	-4.520318	-3.716769	1.000266	C	1.411278	-3.793013	1.700235
H	-4.211230	-2.285143	2.004106	C	3.418619	-6.601665	0.041608
H	-3.066445	-2.738282	0.712710	H	3.265852	-7.417495	0.761822
C	-4.824336	-2.493272	-1.437380	H	4.440684	-6.226459	0.191515
H	-5.185986	-3.530415	-1.395446	H	3.355073	-7.023313	-0.967766
H	-3.788485	-2.499627	-1.789210	C	1.340926	-3.062254	3.022103
H	-5.438156	-1.945021	-2.164986	H	1.917045	-3.589240	3.790006
C	-6.412117	-1.872170	0.405924	H	0.301708	-2.973090	3.360461
H	-6.749464	-2.916645	0.428853	H	1.751485	-2.051257	2.925921
H	-7.059969	-1.329227	-0.294377	O	-0.480958	-0.341933	1.726858
H	-6.561318	-1.455610	1.411566	C	-1.690646	-0.797316	2.481744
C	-5.809680	3.220305	0.267464	C	-1.542281	-0.226015	3.904555
C	-5.233822	4.615522	-0.084065	C	-0.612876	0.996244	3.703517
H	-5.937445	5.397028	0.231797	C	0.359344	0.500016	2.626162
H	-5.075851	4.729547	-1.164641	H	-2.561203	-0.399510	1.956901
H	-4.278106	4.799827	0.424440	H	-2.512056	0.047945	4.332540
C	-7.160293	3.053403	-0.490283	H	-0.092128	1.287689	4.622033
H	-7.856352	3.859740	-0.218914	H	0.815323	1.284434	2.025639
H	-7.642692	2.098137	-0.250338	H	-1.184145	1.859250	3.339665
H	-7.002228	3.085246	-1.576113	H	1.150273	-0.126836	3.051050
C	-6.080289	3.185209	1.800756	H	-1.067808	-0.955088	4.573115
H	-6.778667	3.984260	2.086997	H	-1.705816	-1.888910	2.447431
H	-5.147665	3.325175	2.363372				
H	-6.518263	2.228639	2.110791				
C	0.698633	1.213435	-2.809422	<u>1b'</u>			
H	1.727468	1.334193	-2.466791	Y	-0.111869	-1.371889	0.976543
H	0.445610	2.094212	-3.429027	O	-1.782669	-0.293648	0.169315
C	0.628447	-0.039772	-3.677016	O	1.981025	-1.173607	0.619183
H	-0.361608	-0.210643	-4.121326	O	-0.550695	-0.905767	3.336327
				N	0.354085	1.088837	1.561553

N	-0.534986	-3.099217	-0.673471	C	4.076219	-0.569056	-0.515941
C	0.045134	1.883062	0.303980	C	4.983148	0.473630	-0.789010
H	0.562707	1.361041	-0.512610	H	5.825198	0.258438	-1.437947
H	0.513560	2.877445	0.387081	C	4.867835	1.784898	-0.267425
C	-1.428768	2.066485	-0.013453	C	3.789213	2.032619	0.598695
C	-2.301193	0.944982	-0.084941	H	3.664989	3.010108	1.056896
C	-3.687822	1.149854	-0.389780	C	4.289921	-1.992351	-1.086103
C	-4.109286	2.468928	-0.644824	C	3.102082	-2.381292	-2.012597
H	-5.154145	2.632192	-0.884006	H	3.265402	-3.383642	-2.434090
C	-3.255355	3.597177	-0.607669	H	3.015024	-1.670538	-2.846898
C	-1.910674	3.364708	-0.274416	H	2.163159	-2.391978	-1.455429
H	-1.209498	4.192805	-0.216284	C	4.390333	-3.011506	0.087868
C	-4.689234	-0.030915	-0.427753	H	4.504224	-4.031376	-0.306280
C	-4.248543	-1.066265	-1.501805	H	3.491925	-2.975585	0.709567
H	-4.948140	-1.914326	-1.520170	H	5.262300	-2.789120	0.718403
H	-3.249078	-1.446634	-1.285741	C	5.593501	-2.108540	-1.919012
H	-4.242098	-0.607363	-2.500346	H	5.700241	-3.142056	-2.273336
C	-4.742333	-0.716711	0.970263	H	6.484723	-1.868193	-1.324074
H	-5.441255	-1.564950	0.948974	H	5.578930	-1.456331	-2.802703
H	-5.089379	-0.007965	1.735515	C	5.912035	2.860981	-0.646652
H	-3.754783	-1.087419	1.256762	C	5.614620	4.229262	0.017262
C	-6.131285	0.422174	-0.778316	H	6.375636	4.960550	-0.285269
H	-6.788838	-0.456909	-0.792625	H	5.635189	4.161954	1.113104
H	-6.184637	0.890305	-1.770196	H	4.635374	4.622686	-0.286192
H	-6.535637	1.126438	-0.038868	C	7.329764	2.403524	-0.192112
C	-3.820249	5.002890	-0.918562	H	8.082283	3.155961	-0.467119
C	-4.421821	5.019212	-2.355208	H	7.616717	1.454300	-0.660178
H	-4.833375	6.011465	-2.587851	H	7.362861	2.264069	0.896333
H	-5.230388	4.286307	-2.463726	C	5.913870	3.066798	-2.190526
H	-3.652536	4.781557	-3.101344	H	6.660650	3.820777	-2.476839
C	-2.733067	6.104616	-0.844642	H	4.929700	3.406706	-2.538597
H	-3.179110	7.080247	-1.078392	H	6.153473	2.137494	-2.721053
H	-1.925124	5.926186	-1.566328	C	-0.544439	1.451426	2.696634
H	-2.290372	6.173714	0.158008	H	-1.571981	1.456232	2.328511
C	-4.938061	5.359599	0.105575	H	-0.325130	2.465810	3.080188
H	-5.359417	6.350463	-0.114975	C	-0.434873	0.466936	3.861528
H	-4.537855	5.375686	1.127926	H	0.516936	0.546365	4.404195
H	-5.758056	4.631753	0.078249	H	-1.257894	0.645612	4.567972
C	1.799441	1.283805	1.967218	C	-0.761381	-1.907849	4.392258
H	1.982469	0.596649	2.804151	H	-1.700794	-1.693532	4.918587
H	1.918343	2.314611	2.347048	H	0.081620	-1.890142	5.096154
C	2.851874	1.028425	0.906518	H	-0.813474	-2.868879	3.882340
C	2.961527	-0.263967	0.329488	C	-0.186029	-3.846674	1.576340

H	0.912166	-3.802167	1.528262	H	-5.114279	0.009325	1.708082
H	-0.515044	-4.518816	2.371075	H	-3.758303	-1.060190	1.229240
C	-0.825935	-4.062363	0.287108	C	-6.177338	0.417146	-0.817815
C	-1.768780	-5.090418	-0.017465	H	-6.826384	-0.476119	-0.825199
H	-2.016341	-5.817334	0.751367	H	-6.240661	0.882908	-1.816777
C	-2.315346	-5.190492	-1.299407	H	-6.589507	1.122718	-0.075170
C	-1.929194	-4.231602	-2.278723	C	-3.921734	5.067666	-0.971761
H	-2.328077	-4.286959	-3.287534	C	-4.535168	5.077983	-2.414136
C	-1.060961	-3.190363	-1.933260	H	-4.967022	6.070098	-2.642092
C	-3.282671	-6.298890	-1.663580	H	-5.335656	4.326808	-2.520148
H	-2.871602	-6.931564	-2.462308	H	-3.761420	4.853734	-3.169207
H	-4.230599	-5.885558	-2.034165	C	-2.842512	6.192480	-0.900023
H	-3.503763	-6.940015	-0.803298	H	-3.306566	7.167682	-1.130002
C	-0.688771	-2.098064	-2.909533	H	-2.032121	6.025541	-1.630517
H	-1.194913	-2.236449	-3.870308	H	-2.393800	6.264388	0.106177
H	0.393978	-2.083244	-3.082156	C	-5.046732	5.407669	0.065111
H	-0.975225	-1.118421	-2.505892	H	-5.487167	6.397859	-0.154381
2b':				H	-4.639007	5.429377	1.091392
Lu	-0.096198	-1.266377	0.924150	H	-5.858907	4.661885	0.041148
O	-1.778761	-0.238537	0.112317	C	1.773462	1.402663	1.934751
O	1.969843	-1.045453	0.533600	H	1.959092	0.713665	2.776881
O	-0.549149	-0.839925	3.250566	H	1.869417	2.439929	2.318104
N	0.329471	1.180429	1.506758	C	2.841568	1.169398	0.872072
N	-0.488015	-2.921380	-0.773307	C	2.953276	-0.124371	0.263371
C	0.027087	1.975489	0.236082	C	4.080434	-0.408658	-0.597343
H	0.559930	1.452436	-0.576484	C	4.994394	0.654437	-0.852626
H	0.486459	2.979190	0.322277	H	5.840763	0.455779	-1.508408
C	-1.457603	2.142720	-0.086251	C	4.871114	1.967296	-0.299762
C	-2.320301	0.995465	-0.148219	C	3.779770	2.197954	0.581140
C	-3.726271	1.182498	-0.442771	H	3.648183	3.168791	1.061466
C	-4.176065	2.509844	-0.697846	C	4.302594	-1.827266	-1.200286
H	-5.229429	2.658346	-0.928599	C	3.108771	-2.206434	-2.139349
C	-3.330040	3.661555	-0.665535	H	3.273320	-3.210621	-2.573070
C	-1.963078	3.449310	-0.341388	H	3.024858	-1.482517	-2.971102
H	-1.268928	4.289328	-0.287627	H	2.163712	-2.220203	-1.580832
C	-4.718010	-0.018945	-0.469473	C	4.410916	-2.877069	-0.040830
C	-4.268795	-1.063231	-1.545708	H	4.538178	-3.892317	-0.460609
H	-4.971563	-1.917329	-1.560631	H	3.506223	-2.864628	0.582981
H	-3.262941	-1.441432	-1.325763	H	5.284056	-2.657045	0.600088
H	-4.262615	-0.604928	-2.551543	C	5.614516	-1.919465	-2.042705
C	-4.757031	-0.702578	0.941188	H	5.723499	-2.949931	-2.423838
H	-5.448403	-1.565592	0.925153	H	6.510010	-1.689571	-1.439147
				H	5.595919	-1.242182	-2.914632

C	5.915459	3.062931	-0.660792	Ia:		
C	5.612331	4.422886	0.041944	Y	0.016111	0.962963 -0.240434
H	6.373591	5.168589	-0.247365	Si	-0.059372	4.677191 -1.145737
H	5.637277	4.327634	1.141486	O	-2.082645	0.480626 -0.122567
H	4.624992	4.820347	-0.250952	O	0.198610	-0.509487 -2.198571
C	7.346536	2.599010	-0.221318	O	2.138277	0.555837 0.015607
H	8.098126	3.365476	-0.486714	N	0.035023	-1.576482 0.444228
H	7.635680	1.655439	-0.713298	C	-2.951974	-0.569781 -0.059948
H	7.386489	2.435824	0.870135	C	-4.249612	-0.538623 -0.670773
C	5.908995	3.306762	-2.209003	C	-5.058006	-1.683137 -0.533421
H	6.656890	4.074275	-2.481850	H	-6.041863	-1.669100 -0.988697
H	4.916124	3.653688	-2.545654	C	-4.668633	-2.854653 0.160355
H	6.149293	2.385288	-2.765051	C	-3.388636	-2.853952 0.738758
C	-0.591977	1.538632	2.636099	H	-3.032893	-3.723238 1.285422
H	-1.619820	1.537644	2.253810	C	-2.535782	-1.736221 0.638741
H	-0.379615	2.556446	3.028357	C	-1.189522	-1.761989 1.333100
C	-0.482979	0.536465	3.801927	H	-1.132608	-0.958909 2.082002
H	0.458363	0.630439	4.370717	H	-1.089619	-2.717599 1.877196
H	-1.331324	0.679289	4.495036	C	0.002390	-2.470467 -0.750563
C	-0.768188	-1.861118	4.298355	H	0.455723	-3.453333 -0.532507
H	-1.733414	-1.667745	4.797787	H	-1.046718	-2.635853 -1.010598
H	0.057214	-1.821250	5.030819	C	0.709700	-1.876064 -1.971326
H	-0.780612	-2.823807	3.777945	H	0.473215	-2.487993 -2.854278
C	-0.114661	-3.716263	1.474649	H	1.795470	-1.823261 -1.847920
H	0.994285	-3.692096	1.434703	C	0.389528	-0.048428 -3.580071
H	-0.435508	-4.441343	2.235119	H	-0.001960	0.966976 -3.630696
C	-0.709645	-3.957857	0.138672	H	-0.164633	-0.704687 -4.263783
C	-1.539945	-5.070482	-0.238258	H	1.457501	-0.048916 -3.833917
H	-1.730313	-5.859692	0.490837	C	1.251755	-1.788902 1.322884
C	-2.064597	-5.155149	-1.550323	H	1.173494	-1.035132 2.119827
C	-1.757187	-4.102783	-2.477755	H	1.163547	-2.779119 1.804670
H	-2.136562	-4.136812	-3.499933	C	2.616058	-1.693896 0.667230
C	-0.981040	-2.996231	-2.054621	C	3.485026	-2.795374 0.721818
C	-2.927627	-6.340959	-1.987942	H	3.126161	-3.712248 1.187502
H	-2.479471	-6.856351	-2.856375	C	4.795836	-2.733089 0.205123
H	-3.934372	-6.002205	-2.292811	C	5.196552	-1.507503 -0.366798
H	-3.043515	-7.074523	-1.174235	H	6.200576	-1.434775 -0.762813
C	-0.690011	-1.818328	-2.979364	C	4.366957	-0.366218 -0.454164
H	-1.187753	-1.949952	-3.952436	C	3.040301	-0.468015 0.072113
H	0.394801	-1.713680	-3.149166	C	0.019553	2.885402 -1.721153
H	-1.051472	-0.881795	-2.521719	H	0.932026	2.771020 -2.341134
				H	-0.847753	2.708236 -2.390847
				C	-0.105601	5.927082 -2.595449

H	-0.157794	6.965519	-2.235268	H	7.648721	-2.900829	0.191957
H	-0.979694	5.748386	-3.237974	H	7.053794	-3.452881	-1.391287
H	0.792730	5.831389	-3.222068	H	7.732832	-4.617345	-0.240676
C	1.471621	5.127260	-0.093862	C	5.921336	-4.371294	1.781868
H	1.477716	6.198960	0.151797	H	6.389749	-3.553462	2.344666
H	2.400190	4.903100	-0.638122	H	6.567652	-5.256940	1.858109
H	1.496561	4.567766	0.851049	H	4.967345	-4.608777	2.268436
C	-1.625388	4.998831	-0.100891	C	4.880064	0.940677	-1.110302
H	-1.696999	6.057835	0.186367	C	4.019263	1.272952	-2.364623
H	-1.634008	4.401190	0.820602	H	4.367942	2.207391	-2.826492
H	-2.532566	4.744127	-0.667086	H	2.969179	1.394833	-2.090105
C	-4.741796	0.699087	-1.461474	H	4.103619	0.471843	-3.113206
C	-3.797100	0.952968	-2.673142	C	6.357781	0.836891	-1.571861
H	-4.132704	1.835229	-3.236821	H	6.659815	1.792350	-2.020154
H	-3.801850	0.089791	-3.353580	H	6.501150	0.056581	-2.330993
H	-2.773696	1.126633	-2.333959	H	7.037150	0.634551	-0.733186
C	-4.755328	1.953650	-0.540097	C	4.792660	2.119470	-0.097142
H	-5.116088	2.828465	-1.099357	H	5.174856	3.042054	-0.556509
H	-3.752950	2.172039	-0.166592	H	5.396566	1.907897	0.796173
H	-5.428172	1.797204	0.314996	H	3.757318	2.289718	0.205730
C	-6.178282	0.516966	-2.018986	N	0.155110	1.948769	2.167141
H	-6.467354	1.424200	-2.565339	C	1.461381	2.162954	2.512299
H	-6.914459	0.364229	-1.218374	C	1.844999	2.776778	3.710469
H	-6.246244	-0.325970	-2.719521	H	2.194432	1.814806	1.792463
C	-5.640281	-4.054175	0.253963	C	0.839451	3.191928	4.604148
C	-6.949118	-3.613420	0.974334	H	2.897778	2.924050	3.926895
H	-6.733639	-3.268580	1.994033	C	-0.500255	2.970313	4.266315
H	-7.655158	-4.453561	1.035700	H	1.096632	3.676567	5.542321
H	-7.447135	-2.793878	0.442306	C	-0.835635	2.342874	3.041143
C	-5.993016	-4.560308	-1.176219	H	-1.290306	3.281164	4.940663
H	-5.091085	-4.899856	-1.702288	C	-2.232161	2.075406	2.643013
H	-6.456611	-3.772147	-1.781676	C	-3.332653	2.364762	3.374138
H	-6.698188	-5.401606	-1.122302	H	-2.355173	1.593333	1.675514
C	-5.036705	-5.241712	1.045576	H	-3.302622	2.840679	4.352307
H	-4.121761	-5.622477	0.572494	H	-4.319785	2.125431	2.989383
H	-5.760203	-6.066669	1.082633				
H	-4.798757	-4.961604	2.080223				
C	5.721085	-3.969630	0.290379	II:			
C	5.073091	-5.162199	-0.474087	Y	-0.010265	0.517953	0.318756
H	4.089965	-5.419798	-0.061092	Si	2.564428	5.508800	-0.978544
H	5.710486	-6.054917	-0.406328	O	-2.124609	0.404453	0.689204
H	4.938407	-4.915937	-1.535622	O	-0.221186	-0.336964	-1.904817
C	7.119222	-3.710904	-0.326139	O	1.944458	-0.385080	0.463060
				N	-0.493320	-2.083631	0.391761

C	-3.214630	-0.378252	0.432961	H	3.523220	6.657793	-3.009024
C	-4.491400	0.156430	0.054452	H	4.795145	5.797794	-2.119970
C	-5.513796	-0.763245	-0.250540	C	-4.752738	1.681941	0.021698
H	-6.478784	-0.368694	-0.548498	C	-3.830509	2.365926	-1.028499
C	-5.368364	-2.170335	-0.182226	H	-4.029487	3.446977	-1.056729
C	-4.121699	-2.657517	0.243543	H	-4.023360	1.961018	-2.032679
H	-3.957463	-3.725922	0.355924	H	-2.778403	2.214480	-0.779039
C	-3.060245	-1.784977	0.556251	C	-4.471940	2.276522	1.433554
C	-1.787360	-2.335672	1.153038	H	-4.621740	3.365638	1.422413
H	-1.630108	-1.888626	2.145434	H	-3.445763	2.070609	1.746576
H	-1.900450	-3.424206	1.300297	H	-5.158398	1.844942	2.174970
C	-0.566223	-2.613539	-1.007096	C	-6.218738	2.027877	-0.350236
H	-0.191440	-3.649186	-1.064475	H	-6.342663	3.118528	-0.333777
H	-1.619261	-2.621190	-1.308827	H	-6.935512	1.602814	0.364542
C	0.231002	-1.747368	-1.992539	H	-6.483856	1.679875	-1.357867
H	0.094290	-2.100585	-3.022986	C	-6.558425	-3.089516	-0.542795
H	1.294907	-1.732854	-1.754548	C	-7.763422	-2.784548	0.395892
C	-1.191961	0.092668	-2.919759	H	-7.494676	-2.963999	1.444946
H	-1.395997	1.144909	-2.716964	H	-8.618482	-3.427391	0.143831
H	-2.118832	-0.487790	-2.836769	H	-8.090797	-1.741490	0.308498
H	-0.751549	-0.022063	-3.917838	C	-6.987705	-2.837872	-2.018755
C	0.597897	-2.733892	1.224316	H	-6.164374	-3.068289	-2.707936
H	0.590625	-2.191980	2.183207	H	-7.279235	-1.793283	-2.182315
H	0.290492	-3.772124	1.440761	H	-7.845434	-3.472142	-2.283057
C	2.012205	-2.757169	0.688733	C	-6.206574	-4.591532	-0.395973
C	2.691309	-3.983119	0.597658	H	-5.378207	-4.881470	-1.056193
H	2.138482	-4.897134	0.810482	H	-7.076946	-5.203762	-0.665739
C	4.060343	-4.046461	0.267970	H	-5.929579	-4.844215	0.635949
C	4.719252	-2.817669	0.054388	C	4.772957	-5.416147	0.174078
H	5.775316	-2.838259	-0.178536	C	4.081524	-6.290860	-0.913551
C	4.087236	-1.555716	0.126621	H	3.019336	-6.449319	-0.689297
C	2.688417	-1.530668	0.425542	H	4.562642	-7.276905	-0.976846
C	2.081869	3.927835	-1.949976	H	4.149461	-5.811229	-1.898907
C	3.295487	5.050386	0.714775	C	6.270549	-5.283917	-0.200748
H	3.613817	5.950563	1.258894	H	6.829000	-4.709354	0.549601
H	4.173769	4.398602	0.606748	H	6.404500	-4.797804	-1.175937
H	2.565564	4.521257	1.340451	H	6.724367	-6.281979	-0.260085
C	1.092744	6.692564	-0.753931	C	4.684217	-6.147641	1.546497
H	1.419042	7.630227	-0.282122	H	5.171968	-5.557436	2.333063
H	0.315065	6.251489	-0.120172	H	5.179783	-7.127272	1.492926
H	0.639837	6.948098	-1.722283	H	3.643252	-6.314190	1.849808
C	3.892788	6.414128	-2.002819	C	4.885357	-0.254340	-0.128764
H	4.192427	7.355945	-1.522204	C	4.375193	0.395870	-1.447468

H	4.882072	1.355251	-1.625530	H	-5.954049	1.974753	-0.387785
H	3.300366	0.577367	-1.396287	C	-4.282488	3.283226	-0.076105
H	4.579879	-0.261891	-2.303857	C	-2.888309	3.302755	0.131281
C	6.408662	-0.504808	-0.288309	H	-2.369039	4.251306	0.261022
H	6.915339	0.458949	-0.429240	C	-4.905622	-0.554628	-0.380661
H	6.639452	-1.127753	-1.162719	C	-4.347336	-1.271153	-1.643570
H	6.840974	-0.981072	0.601661	H	-4.824078	-2.253899	-1.765663
C	4.700519	0.730941	1.062481	H	-3.269304	-1.419895	-1.561587
H	5.239771	1.668106	0.863134	H	-4.552680	-0.674652	-2.543537
H	5.107557	0.296011	1.985885	C	-4.691032	-1.446658	0.877818
H	3.644833	0.958820	1.224829	H	-5.192464	-2.415652	0.742576
N	0.359848	2.431761	1.696310	H	-5.117667	-0.962595	1.768446
C	0.201455	2.704370	3.025915	H	-3.628247	-1.629351	1.050711
C	-0.589258	3.751671	3.492531	C	-6.436246	-0.387615	-0.575100
H	0.716715	2.037668	3.714538	H	-6.889250	-1.380160	-0.699752
C	-1.297775	4.530449	2.530511	H	-6.676883	0.200290	-1.470877
H	-0.682232	3.942321	4.556435	H	-6.914222	0.088503	0.291814
C	-1.132800	4.286416	1.173337	C	-5.078283	4.609156	-0.120747
H	-1.958735	5.328338	2.862124	C	-4.538588	5.503852	-1.275950
C	-0.220543	3.268212	0.728038	H	-5.088884	6.454614	-1.315925
H	-1.654456	4.880675	0.428348	H	-4.652412	4.998392	-2.243653
C	0.054318	2.928983	-0.640563	H	-3.474615	5.735808	-1.144134
C	1.495557	2.719395	-1.152607	C	-4.910253	5.366963	1.229707
H	-0.581238	3.446443	-1.363094	H	-5.454870	6.321562	1.206333
H	2.162618	2.487737	-0.309999	H	-3.856248	5.586361	1.440289
H	2.995050	3.584211	-2.466780	H	-5.302011	4.767465	2.062140
H	1.374027	4.204396	-2.748988	C	-6.593406	4.385792	-0.356356
H	1.547327	1.850641	-1.831870	H	-7.109861	5.354669	-0.377140
<u>I_h</u>				H	-7.044618	3.784695	0.443859
Y	-0.120193	-1.129867	0.652430	H	-6.785936	3.884097	-1.313486
O	-1.974819	-0.263182	0.067180	C	1.370382	1.737704	1.745005
O	1.529703	-0.166018	-0.395008	H	1.776237	0.966272	2.412352
O	-0.151593	-0.825782	3.158967	H	1.373108	2.686199	2.313157
N	-0.058069	1.351729	1.457331	C	2.293240	1.901192	0.551451
N	-0.647278	-3.048933	-0.857300	C	2.371316	0.906938	-0.465563
C	-0.627171	2.208356	0.343879	C	3.323543	1.091684	-1.529093
H	-0.113965	1.891207	-0.569623	C	4.145404	2.233069	-1.490408
H	-0.350741	3.260311	0.526762	H	4.865672	2.366126	-2.290078
C	-2.130804	2.121245	0.169882	C	4.083751	3.226261	-0.485335
C	-2.760026	0.854018	0.002386	C	3.130697	3.034412	0.526112
C	-4.174764	0.796381	-0.198169	H	3.022890	3.766751	1.322304
C	-4.884457	2.017193	-0.232225	C	3.408232	0.108939	-2.720420
				C	2.068196	0.199526	-3.507443

H	2.044064	-0.539230	-4.321132	C	-0.958911	-3.266319	-2.177410
H	1.953807	1.199281	-3.948019	C	-4.015463	-5.563368	-1.968353
H	1.221333	0.015427	-2.843079	H	-3.701669	-6.373660	-2.640596
C	3.650617	-1.342293	-2.218916	H	-4.760054	-4.963589	-2.510898
H	3.671059	-2.039345	-3.069273	H	-4.510012	-6.012339	-1.099877
H	2.866674	-1.648603	-1.525373	C	-0.139761	-2.530043	-3.209068
H	4.617498	-1.411386	-1.700399	H	-0.291724	-2.954582	-4.207377
C	4.554898	0.449155	-3.709313	H	0.926520	-2.562178	-2.964570
H	4.562199	-0.296608	-4.515349	H	-0.431399	-1.472628	-3.244861
H	5.538997	0.422059	-3.222145	N	2.402198	-2.408061	1.564296
H	4.423644	1.434245	-4.175793	C	3.020620	-1.670785	2.524160
C	5.021848	4.453321	-0.551782	C	4.347399	-1.869858	2.928747
C	4.815187	5.418550	0.642798	H	2.420955	-0.892208	2.982739
H	5.505526	6.267916	0.555695	C	5.086308	-2.892387	2.302397
H	5.013589	4.923615	1.602821	H	4.785902	-1.238325	3.694888
H	3.793917	5.821191	0.666929	C	4.463195	-3.667221	1.317785
C	6.506562	3.983326	-0.538703	H	6.123423	-3.073113	2.572432
H	7.183794	4.846226	-0.609764	C	3.112544	-3.418714	0.963545
H	6.725405	3.314422	-1.379654	H	5.014103	-4.450634	0.808675
H	6.734800	3.440930	0.388276	C	2.404976	-4.217749	-0.057458
C	4.751972	5.247825	-1.864093	C	2.836306	-5.385699	-0.584694
H	5.420875	6.117449	-1.933150	H	1.451120	-3.811383	-0.385789
H	3.714967	5.606852	-1.894117	H	3.766820	-5.869100	-0.292955
H	4.915449	4.625659	-2.752190	H	2.240510	-5.904078	-1.330816
C	-0.877277	1.455335	2.696528				
H	-1.912738	1.228934	2.435549	II:			
H	-0.856983	2.480392	3.114521	Y	-0.392869	-0.029772	1.144243
C	-0.403416	0.487554	3.777642	O	0.138874	1.752794	0.105666
H	0.521339	0.819506	4.270971	O	0.214478	-1.806228	0.207855
H	-1.186332	0.378977	4.541362	O	0.164023	0.700453	3.368350
C	-0.069607	-1.895921	4.162775	N	2.100987	-0.025693	1.462646
H	-1.062223	-2.070727	4.595461	N	-5.129670	-0.913671	-1.400031
H	0.643304	-1.610967	4.949532	C	2.697719	0.480543	0.154747
H	0.272376	-2.790208	3.649427	H	2.236742	-0.122371	-0.634898
C	-0.906374	-3.480734	1.477035	H	3.774199	0.247220	0.149924
H	0.159832	-3.665476	1.639825	C	2.517269	1.959595	-0.135243
H	-1.534735	-3.861549	2.282211	C	1.217580	2.543886	-0.201792
C	-1.368174	-3.715043	0.138511	C	1.083815	3.920454	-0.563150
C	-2.516288	-4.492809	-0.220112	C	2.263987	4.643956	-0.843317
H	-3.095093	-4.956963	0.573821	H	2.164616	5.684509	-1.121193
C	-2.835390	-4.706867	-1.557574	C	3.559986	4.091487	-0.783401
C	-2.011438	-4.103739	-2.553613	C	3.655499	2.733895	-0.418843
H	-2.221287	-4.260611	-3.607936	H	4.630864	2.252933	-0.361561

C	-0.302697	4.605694	-0.637771	H	-2.219279	-4.330113	-1.528330
C	-1.202964	3.860194	-1.665578	H	-1.433878	-3.426936	-0.218213
H	-2.210947	4.299871	-1.675430	H	-1.044706	-5.144030	-0.468237
H	-1.281104	2.800582	-1.415716	C	-0.012180	-4.943544	-3.007440
H	-0.783132	3.947199	-2.676882	H	-0.974729	-5.059907	-3.521636
C	-0.964718	4.590119	0.771908	H	0.232768	-5.907349	-2.541393
H	-1.968214	5.036671	0.727065	H	0.746164	-4.721946	-3.770485
H	-0.363692	5.173362	1.483453	C	4.784874	-5.052782	-1.146051
H	-1.056634	3.569593	1.150521	C	6.040151	-4.726373	-0.297826
C	-0.217780	6.087772	-1.089663	H	6.872236	-5.372392	-0.606632
H	-1.232424	6.504881	-1.134747	H	5.864200	-4.899862	0.772117
H	0.226326	6.187959	-2.088687	H	6.361171	-3.684665	-0.431137
H	0.360699	6.703292	-0.387988	C	4.430418	-6.553060	-0.922810
C	4.839448	4.901034	-1.101114	H	5.279696	-7.193227	-1.199563
C	5.589398	4.241321	-2.296214	H	3.568032	-6.858939	-1.527033
H	6.510981	4.794786	-2.524713	H	4.184822	-6.742755	0.130257
H	4.959244	4.236147	-3.194964	C	5.146096	-4.831560	-2.644839
H	5.866335	3.202919	-2.076785	H	5.993403	-5.469287	-2.933110
C	5.774705	4.911410	0.144411	H	5.424144	-3.785473	-2.828630
H	6.697546	5.467041	-0.072614	H	4.303887	-5.073616	-3.304075
H	6.057867	3.895181	0.445492	C	2.457716	0.863660	2.610917
H	5.278354	5.389978	0.998960	H	2.333586	1.898359	2.281377
C	4.532982	6.371436	-1.481345	H	3.512742	0.730760	2.910740
H	5.470981	6.899130	-1.698210	C	1.561997	0.625727	3.826340
H	4.030613	6.907244	-0.665296	H	1.720725	-0.351719	4.301953
H	3.900995	6.436303	-2.376506	H	1.735968	1.413437	4.571764
C	2.559011	-1.451680	1.734057	C	-0.820742	0.921738	4.447320
H	1.939270	-1.828482	2.561714	H	-0.527078	1.811407	5.018094
H	3.600208	-1.417139	2.097248	H	-0.868530	0.036759	5.092160
C	2.487525	-2.421311	0.566173	H	-1.787640	1.075660	3.968650
C	1.270957	-2.604332	-0.139421	C	-3.248280	0.465064	-0.630491
C	1.181566	-3.585458	-1.175060	C	-4.569121	0.320499	-1.362631
C	2.341195	-4.336011	-1.448145	C	-5.183806	1.436056	-1.979671
H	2.289443	-5.086577	-2.229214	H	-4.696202	2.407410	-1.941781
C	3.571765	-4.171869	-0.766346	C	-6.411681	1.283438	-2.646836
C	3.618682	-3.196682	0.244125	C	-6.984686	-0.009520	-2.667717
H	4.535698	-3.029880	0.802285	H	-7.932652	-0.181097	-3.171808
C	-0.134719	-3.807308	-1.958661	C	-6.322705	-1.081576	-2.040545
C	-0.515095	-2.504461	-2.723000	C	-7.105637	2.453678	-3.316101
H	-1.461409	-2.646686	-3.262485	H	-8.044403	2.700326	-2.800887
H	0.261883	-2.242893	-3.454708	H	-7.359116	2.221589	-4.358900
H	-0.638325	-1.665966	-2.033117	H	-6.475244	3.349880	-3.311538
C	-1.278833	-4.198010	-0.976010	C	-6.887308	-2.485039	-2.038108

H -7.851259 -2.536122 -2.556691
H -7.019071 -2.836440 -1.007395
H -6.187481 -3.176770 -2.523685
N -2.249896 -0.903470 2.264993
C -1.851377 -2.050490 2.936364
C -2.586594 -2.698618 3.906833
H -0.883332 -2.457961 2.635887
C -3.886335 -2.153682 4.233980
H -2.213272 -3.602976 4.375272
C -4.349790 -1.049677 3.564810
H -4.497950 -2.632494 4.996224
C -3.560179 -0.387791 2.521094
H -5.334301 -0.639069 3.777726
C -4.057790 0.695554 1.826297
C -3.354510 1.351553 0.664743
H -5.063750 1.030109 2.064555
H -3.865740 2.286434 0.400739
H -2.510498 0.915893 -1.312859
H -2.921736 -0.550148 -0.370123
H -2.334638 1.691696 0.938075

I_g

Y 8.3268209 3.0787644 21.9811471
Si 7.8902389 6.5173208 20.4581732
O 9.9490564 3.4372072 23.3850856
O 6.7913340 2.6998251 23.9268988
O 6.9391651 1.8197352 20.8545688
N 8.6572516 0.7198892 23.1075352
C 10.5581502 2.8990488 24.4390052
C 11.1220791 3.6918504 25.5007109
C 11.7440105 3.0136322 26.5645588
H 12.1747450 3.6170514 27.3753980
C 11.8512356 1.6068079 26.6661901
C 11.2894307 0.8583039 25.6199838
H 11.3373968 -0.2413124 25.6316231
C 10.6567122 1.4760909 24.5229719
C 10.1291604 0.6265337 23.3933105
H 10.6365354 0.8956584 22.4385918
H 10.3923852 -0.4403728 23.5965951
C 7.8462093 0.5633507 24.3310320
H 7.6262412 -0.5095694 24.5500231
H 8.4495001 0.9559759 25.1741530

C 6.5289529 1.3297596 24.2892365
H 6.0729163 1.3048838 25.3051360
H 5.8025469 0.8912370 23.5721820
C 5.7280199 3.5813759 24.3021794
H 6.0100967 4.5968441 23.9749806
H 5.5896150 3.5648603 25.4057304
H 4.7754348 3.2892077 23.8080624
C 8.3486980 -0.2973271 22.0569313
H 8.9885249 -0.0302085 21.1848535
H 8.7041312 -1.2958186 22.4133015
C 6.9141490 -0.4336273 21.6063870
C 6.2459252 -1.6573945 21.7687363
H 6.7817432 -2.4750742 22.2800603
C 4.9370890 -1.8616426 21.2902817
C 4.3331118 -0.7724415 20.6285098
H 3.3172235 -0.9052202 20.2390479
C 4.9493358 0.4825931 20.4331170
C 6.2776287 0.6683489 20.9479179
C 7.3512369 5.2926342 21.7671723
H 6.2480292 5.1594328 21.6431216
H 7.4939924 5.8021890 22.7530216
C 6.9250124 8.1691304 20.5132780
H 7.2637710 8.8778054 19.7269233
H 7.0517300 8.6708565 21.4960880
H 5.8368463 7.9999544 20.3680781
C 7.6364536 5.7998529 18.7034186
H 7.9058909 6.5370143 17.9175691
H 6.5786295 5.5045908 18.5398655
H 8.2606770 4.8951622 18.5480061
C 9.7399996 6.9567868 20.6421763
H 10.0602767 7.6997244 19.8811768
H 10.3881586 6.0617412 20.5332725
H 9.9479098 7.3918978 21.6422785
C 11.0432480 5.2366424 25.4789301
C 9.5591639 5.6843372 25.4826696
H 9.4886991 6.7925210 25.4576745
H 9.0451694 5.3317059 26.4009232
H 9.0214959 5.2841447 24.6033396
C 11.7522259 5.7842002 24.2143209
H 11.7038161 6.8935356 24.1931210
H 11.2734472 5.4012582 23.2946759
H 12.8229276 5.4915692 24.2063076
C 11.7260860 5.8769052 26.7069332

H 11.6428013 6.9811166 26.6396710
H 12.8061486 5.6296956 26.7630921
H 11.2514224 5.5681931 27.6608910
C 12.5595373 0.9689724 27.8810866
C 14.0319759 1.4502477 27.9349037
H 14.5798428 1.1537887 27.0169471
H 14.5594409 1.0099722 28.8078631
H 14.1007395 2.5531193 28.0236352
C 11.8370829 1.3897072 29.1861137
H 10.7812160 1.0492943 29.1825773
H 11.8329041 2.4903597 29.3179747
H 12.3377035 0.9479276 30.0738954
C 12.5601678 -0.5718888 27.8080564
H 11.5310030 -0.9855914 27.7933736
H 13.0750476 -0.9938660 28.6956728
H 13.0917867 -0.9432944 26.9081536
C 4.2390043 -3.2258258 21.4850461
C 4.1503222 -3.5542069 22.9971898
H 5.1528487 -3.5975200 23.4688114
H 3.6620382 -4.5387216 23.1591511
H 3.5585712 -2.7858283 23.5359846
C 2.8087021 -3.2376143 20.9075383
H 2.8010716 -3.0448469 19.8154567
H 2.1598858 -2.4804718 21.3932000
H 2.3421723 -4.2306559 21.0724089
C 5.0572071 -4.3318141 20.7707166
H 5.1300089 -4.1300128 19.6823344
H 4.5792450 -5.3255853 20.9048561
H 6.0900953 -4.4006002 21.1680287
C 4.2082242 1.6203937 19.6913732
C 3.9971372 2.8207703 20.6487835
H 3.4757717 3.6499771 20.1252221
H 4.9641769 3.2047561 21.0235499
H 3.3710954 2.5233684 21.5161324
C 2.8191854 1.1827855 19.1782425
H 2.3398068 2.0302984 18.6464854
H 2.1393324 0.8856009 20.0028513
H 2.8839235 0.3368313 18.4635120
C 5.0365245 2.0744059 18.4626773
H 4.5145562 2.8943767 17.9252543
H 5.1740942 1.2343984 17.7500490
H 6.0314057 2.4407900 18.7753534
N 10.3621254 2.4012292 18.1053326

C 11.2782546 2.3551497 16.9688279
C 8.9952238 1.9569228 17.8243607
C 10.6993848 2.7979703 19.3631253
O 9.8126329 2.8813983 20.2568179
C 12.1173299 3.0994881 19.6911775
C 12.4655224 3.4735607 20.9407134
H 12.8881328 2.9843879 18.9165996
H 11.7093638 3.5762808 21.7388973
H 13.5173581 3.6768297 21.1921438
H 9.0254768 0.9644586 17.3288929
H 8.4874148 2.6735889 17.1456811
H 8.4195425 1.8836534 18.7641223
H 10.7347639 2.6856233 16.0614733
H 11.6542463 1.3246292 16.7880158
H 12.1358723 3.0342552 17.1065979

II:

Y 0.215325 -0.083945 -0.687616
Si -3.729771 -5.054538 2.152736
O -1.443726 1.083328 -1.344135
O 0.768610 0.042464 1.604670
O 2.219851 -0.137081 -1.439135
N 1.020114 2.312206 -0.096093
C -2.111935 2.195797 -0.900892
C -3.538621 2.246110 -0.795091
C -4.103281 3.424600 -0.270328
H -5.182548 3.472885 -0.178101
C -3.352678 4.553066 0.141152
C -1.957790 4.479647 -0.009752
H -1.330494 5.325892 0.257607
C -1.336129 3.325784 -0.528470
C 0.147265 3.333671 -0.824803
H 0.298489 3.127180 -1.892284
H 0.552025 4.340023 -0.620292
C 0.896951 2.474063 1.383376
H 1.446987 3.364765 1.739499
H -0.163839 2.630417 1.607996
C 1.402074 1.259176 2.163347
H 1.105546 1.344718 3.217860
H 2.487650 1.135586 2.091855
C 1.018686 -1.168702 2.410715
H 0.562485 -1.999769 1.874838
H 0.554005 -1.048648 3.396609

H	2.099830	-1.323783	2.508926	C	-4.912806	5.400749	1.956045
C	2.434838	2.539632	-0.610457	H	-4.262606	5.003703	2.746768
H	2.330703	2.584116	-1.702236	H	-5.658523	4.632395	1.719348
H	2.767173	3.535317	-0.267549	H	-5.445782	6.275196	2.354623
C	3.509541	1.519360	-0.290941	C	-3.093624	6.918888	1.116654
C	4.669233	1.909680	0.399336	H	-2.401361	6.582062	1.899971
H	4.726567	2.928723	0.780012	H	-3.654466	7.775154	1.513608
C	5.753811	1.026285	0.579570	H	-2.501973	7.276569	0.263722
C	5.632555	-0.259191	0.008580	C	7.013694	1.494406	1.346507
H	6.462036	-0.945279	0.114852	C	6.619342	1.927974	2.789723
C	4.495652	-0.704916	-0.703436	H	5.881360	2.739869	2.780718
C	3.400046	0.203163	-0.826850	H	7.502396	2.283620	3.338528
C	-1.821423	-5.211815	2.181554	H	6.187709	1.084565	3.345082
C	-4.228696	-3.247157	2.477176	C	8.088521	0.383914	1.459501
H	-5.321282	-3.147251	2.539968	H	8.446415	0.061512	0.473400
H	-3.879669	-2.587464	1.672213	H	7.708781	-0.497398	1.992878
H	-3.806469	-2.880148	3.423531	H	8.953543	0.764705	2.018188
C	-4.420303	-6.148580	3.552285	C	7.651990	2.709035	0.608729
H	-5.518245	-6.110406	3.581754	H	7.952993	2.430367	-0.409254
H	-4.049370	-5.823210	4.534424	H	8.542646	3.060571	1.147945
H	-4.128286	-7.199642	3.417617	H	6.951498	3.549687	0.531727
C	-4.483288	-5.634909	0.506084	C	4.443901	-2.118618	-1.333980
H	-5.581040	-5.588294	0.540770	C	3.319368	-2.964049	-0.665975
H	-4.200812	-6.673146	0.282170	H	3.318669	-3.982253	-1.078896
H	-4.139295	-5.005247	-0.323061	H	2.332702	-2.532129	-0.847561
C	-4.422520	1.059579	-1.250267	H	3.483516	-3.040479	0.418963
C	-4.108319	-0.203166	-0.394380	C	5.776735	-2.893339	-1.157943
H	-4.765531	-1.032077	-0.692919	H	5.691306	-3.868525	-1.654614
H	-4.282014	-0.001421	0.671960	H	6.012407	-3.081550	-0.101582
H	-3.073899	-0.528515	-0.526319	H	6.623279	-2.362740	-1.613476
C	-4.151804	0.758868	-2.754351	C	4.167961	-1.999830	-2.862393
H	-4.734609	-0.116209	-3.075249	H	4.087428	-3.001250	-3.308216
H	-3.091404	0.556544	-2.924804	H	4.988829	-1.467952	-3.362882
H	-4.447606	1.613452	-3.378209	H	3.236994	-1.458530	-3.047460
C	-5.937686	1.357776	-1.098418	N	-0.903791	-3.521532	-2.444616
H	-6.509598	0.495181	-1.464028	C	-0.990131	-4.893337	-2.948330
H	-6.246346	2.232489	-1.686179	C	-1.581186	-2.528865	-3.295167
H	-6.223841	1.523166	-0.050983	C	-0.894478	-3.315396	-1.034933
C	-4.079749	5.797824	0.701495	O	-0.531483	-2.046049	-0.668100
C	-5.036641	6.376071	-0.382967	C	-1.170466	-4.300411	-0.127791
H	-4.474319	6.678537	-1.275887	C	-1.017147	-4.154268	1.372969
H	-5.568801	7.256213	0.004227	H	-1.486203	-5.273264	-0.492846
H	-5.786440	5.638592	-0.693295	H	-2.652915	-2.766257	-3.437688

H	-1.104099	-2.489312	-4.283314	H	3.957134	7.142248	0.272548
H	-1.525595	-1.537733	-2.840975	H	3.685114	5.847979	1.465587
H	-0.759802	-4.894519	-4.021139	H	2.464152	6.182607	0.225681
H	-1.992564	-5.346660	-2.816386	C	4.028901	5.564362	-2.007699
H	-0.257917	-5.526846	-2.436688	H	4.435719	6.572938	-2.168467
H	0.048725	-4.245979	1.659245	H	2.963800	5.585879	-2.269438
H	-1.330845	-3.144849	1.681092	H	4.531754	4.876174	-2.700122
H	-1.540660	-6.220542	1.835964	C	5.767254	5.162278	-0.238568
H	-1.513561	-5.164543	3.239924	H	6.144836	6.179007	-0.410644
				H	6.328304	4.482212	-0.892924
				H	5.988314	4.896418	0.803238
I₄:				C	-1.776405	1.111317	-1.748999
Y	0.169612	-1.304514	-0.436284	H	-2.057153	0.186101	-2.266882
O	1.872154	-0.116388	0.126508	H	-1.982955	1.950514	-2.437169
O	-1.518983	-0.453656	0.673889	C	-2.654940	1.297040	-0.521923
O	1.077566	-1.172747	-2.797115	C	-2.508281	0.487652	0.642063
N	-0.280257	1.039026	-1.523513	C	-3.403300	0.710674	1.749101
N	0.883292	-2.960639	1.290662	C	-4.414424	1.678322	1.599205
C	0.177104	2.087647	-0.530247	H	-5.093944	1.834940	2.429347
H	-0.275051	1.815549	0.427771	C	-4.588794	2.473026	0.442803
H	-0.240114	3.066218	-0.822981	C	-3.673902	2.268432	-0.601284
C	1.681034	2.222790	-0.374364	H	-3.738637	2.865163	-1.507435
C	2.475435	1.103899	0.024330	C	-3.218422	-0.017660	3.103458
C	3.866954	1.304941	0.304742	C	-1.862218	0.451349	3.707649
C	4.400064	2.598943	0.109499	H	-1.644106	-0.085856	4.641736
H	5.452052	2.747774	0.312204	H	-1.898472	1.526192	3.931141
C	3.642753	3.707548	-0.321779	H	-1.047143	0.271275	3.003559
C	2.269211	3.486842	-0.546077	C	-3.224136	-1.561954	2.920482
H	1.627702	4.312254	-0.852041	H	-3.070930	-2.056807	3.890379
C	4.754479	0.165167	0.866145	H	-2.435400	-1.874064	2.233898
C	4.165794	-0.299997	2.229933	H	-4.194335	-1.895236	2.523996
H	4.754099	-1.135243	2.635395	C	-4.331982	0.322311	4.130326
H	3.134063	-0.634956	2.108025	H	-4.142533	-0.233856	5.058017
H	4.187096	0.522668	2.958002	H	-5.328389	0.034747	3.767495
C	4.800332	-1.040351	-0.115510	H	-4.349625	1.389536	4.386437
H	5.446434	-1.831225	0.291014	C	-5.725779	3.519496	0.385655
H	5.209559	-0.734098	-1.089559	C	-5.745753	4.295094	-0.955497
H	3.801249	-1.454166	-0.260185	H	-6.569193	5.021480	-0.950944
C	6.219584	0.613071	1.115128	H	-5.897920	3.623096	-1.810558
H	6.786307	-0.235011	1.521822	H	-4.812306	4.850544	-1.115800
H	6.283086	1.432042	1.843508	C	-7.102092	2.809150	0.550517
H	6.718293	0.931984	0.189540	H	-7.919058	3.544634	0.536423
C	4.246229	5.116199	-0.531677	H	-7.160592	2.259099	1.497505
C	3.543395	6.133801	0.415331				

H -7.269616 2.092455 -0.264457
 C -5.547656 4.554159 1.536139
 H -6.353106 5.301720 1.509443
 H -4.587290 5.077437 1.441859
 H -5.569473 4.071130 2.520395
 C 0.427515 1.189510 -2.830466
 H 1.458462 1.493105 -2.627891
 H -0.035118 1.982152 -3.448580
 C 0.433853 -0.125979 -3.607468
 H -0.576160 -0.495236 -3.804945
 H 0.967758 -0.017501 -4.562029
 C 2.523539 -1.321382 -3.003612
 H 3.062118 -0.429911 -2.663766
 H 2.724082 -1.513091 -4.066785
 H 2.819675 -2.181948 -2.402770
 C 0.853107 -3.827256 -0.928988
 H -0.230657 -3.955238 -0.925569
 H 1.349414 -4.366448 -1.734911
 C 1.490191 -3.797864 0.348681
 C 2.709805 -4.477334 0.683642
 H 3.195939 -5.079347 -0.080019
 C 3.209447 -4.429000 1.981053
 C 2.496135 -3.665416 2.952364
 H 2.845764 -3.620187 3.979812
 C 1.369470 -2.929834 2.573204
 C 4.464609 -5.178922 2.380217
 H 4.257258 -5.889971 3.191966
 H 5.233863 -4.485298 2.747824
 H 4.886173 -5.737987 1.537261
 C 0.661255 -2.033133 3.558369
 H 1.041567 -2.187972 4.573851
 H -0.417408 -2.216520 3.548377
 H 0.813329 -0.979483 3.293849
 N -3.623778 -3.266603 -1.774034
 C -4.597170 -4.217543 -2.351347
 C -3.957824 -2.697516 -0.450060
 C -2.453291 -2.931313 -2.390131
 O -1.618672 -2.129733 -1.839994
 C -2.159804 -3.523509 -3.726694
 C -0.920687 -3.447175 -4.260031
 H -2.958553 -4.029830 -4.259860
 H -0.113347 -2.958127 -3.718805
 H -0.703233 -3.889364 -5.230091

H -4.035528 -3.501204 0.293038
 H -4.915740 -2.165195 -0.503313
 H -3.179665 -2.002491 -0.139135
 H -5.361231 -4.423917 -1.598108
 H -4.122901 -5.168054 -2.618679
 H -5.097315 -3.801997 -3.235826

II:

Y 0.100346 -1.045441 0.549534
 O -1.873001 -0.380185 -0.071751
 O 1.789922 -0.058954 -0.308493
 O -0.994083 -1.031396 2.805454
 N -0.080097 1.343946 1.461929
 N -0.292210 -2.602605 -1.510809
 C -0.709047 2.177047 0.353480
 H -0.153712 1.926239 -0.557643
 H -0.517788 3.242583 0.560361
 C -2.202102 1.977278 0.162231
 C -2.736688 0.669391 -0.048497
 C -4.151534 0.513363 -0.211580
 C -4.950450 1.677738 -0.199025
 H -6.018198 1.561135 -0.330059
 C -4.440413 2.981300 -0.020229
 C -3.048700 3.098098 0.171837
 H -2.601731 4.078473 0.332853
 C -4.788344 -0.889803 -0.368918
 C -4.204472 -1.610289 -1.618577
 H -4.657270 -2.606693 -1.727178
 H -3.123518 -1.724504 -1.522023
 H -4.419769 -1.036994 -2.531176
 C -4.489214 -1.735063 0.905635
 H -4.881591 -2.755635 0.786501
 H -4.967473 -1.285343 1.786955
 H -3.412293 -1.787998 1.085391
 C -6.328961 -0.833330 -0.541928
 H -6.715894 -1.855886 -0.644848
 H -6.620656 -0.276651 -1.442574
 H -6.826541 -0.376957 0.324083
 C -5.330406 4.246318 -0.017057
 C -4.877184 5.205637 -1.157507
 H -5.491172 6.117436 -1.161520
 H -4.976823 4.718414 -2.136199
 H -3.828818 5.505797 -1.039529

C	-5.193747	4.981254	1.349567	H	3.530285	5.676738	-2.127406
H	-5.806826	5.893550	1.360193	H	4.964984	4.787784	-2.668325
H	-4.155194	5.272718	1.549034	C	-0.905837	1.371340	2.712009
H	-5.525066	4.334115	2.172467	H	-1.958761	1.374060	2.423852
C	-6.829804	3.920844	-0.234710	H	-0.712828	2.290512	3.294169
H	-7.413325	4.851028	-0.226920	C	-0.666271	0.154483	3.602379
H	-7.225085	3.272969	0.558682	H	0.369863	0.073347	3.962801
H	-7.002322	3.427047	-1.199851	H	-1.337155	0.202124	4.472840
C	1.314934	1.848566	1.770340	C	-1.141642	-2.261948	3.595464
H	1.770266	1.107762	2.445110	H	-1.879738	-2.093498	4.391573
H	1.221924	2.789297	2.341131	H	-0.172290	-2.575421	4.000047
C	2.262825	2.096502	0.607927	H	-1.514634	-3.026845	2.910478
C	2.566459	1.063094	-0.320344	C	-0.022429	-4.576341	-0.044251
C	3.677647	1.224514	-1.212859	C	-0.363743	-3.969081	-1.384139
C	4.329330	2.473134	-1.215606	C	-0.675156	-4.795694	-2.479011
H	5.157406	2.614014	-1.901090	H	-0.725420	-5.870227	-2.326409
C	3.982340	3.552674	-0.368921	C	-0.911518	-4.242715	-3.750774
C	2.953669	3.323483	0.559881	C	-0.834774	-2.841454	-3.860881
H	2.680116	4.094672	1.274984	H	-1.017292	-2.356111	-4.815429
C	4.203955	0.048914	-2.075138	C	-0.536592	-2.042119	-2.741318
C	3.123784	-0.447249	-3.076291	C	-1.214689	-5.112349	-4.952325
H	3.543685	-1.232696	-3.721107	H	-0.299598	-5.302123	-5.531188
H	2.775752	0.373360	-3.719010	H	-1.932434	-4.628707	-5.625310
H	2.270570	-0.860152	-2.538209	H	-1.623357	-6.083797	-4.652550
C	4.603041	-1.124884	-1.129906	C	-0.523314	-0.538065	-2.882961
H	4.948003	-1.985928	-1.720661	H	-0.399800	-0.253454	-3.933091
H	3.753379	-1.440091	-0.517598	H	-1.465735	-0.120518	-2.512285
H	5.420092	-0.821442	-0.460935	H	0.287636	-0.084146	-2.307288
C	5.458726	0.436459	-2.902015	N	2.187020	-3.345823	3.677160
H	5.801192	-0.442661	-3.463374	C	2.682172	-4.527624	4.390544
H	6.289388	0.765246	-2.264109	C	2.886294	-2.096033	4.031067
H	5.242217	1.230773	-3.629299	C	1.827157	-3.505983	2.302375
C	4.748354	4.892210	-0.471109	O	1.276500	-2.407864	1.730671
C	4.227869	5.947220	0.537824	C	1.970033	-4.674371	1.597013
H	4.789587	6.882842	0.416817	C	1.532383	-4.718286	0.150422
H	4.356335	5.614422	1.576350	H	2.442453	-5.544905	2.036060
H	3.165362	6.172324	0.376413	H	3.973899	-2.159238	3.839196
C	6.261560	4.659298	-0.184518	H	2.737581	-1.869027	5.095330
H	6.817861	5.603527	-0.269261	H	2.485173	-1.280979	3.425850
H	6.701680	3.945365	-0.891108	H	2.773215	-4.290544	5.457715
H	6.408889	4.261825	0.828210	H	3.671302	-4.867968	4.028790
C	4.587013	5.478682	-1.905088	H	1.974665	-5.356617	4.279925
H	5.142687	6.422385	-1.999031	H	1.863671	-5.651900	-0.323957

H -0.496915 -5.559902 0.055892
H -0.410863 -3.949627 0.765331

H 2.010480 -3.894885 -0.401743

7. Literature

1. Hultzs, K. C.; Voth, P.; Beckerle, K.; Spaniol, T. P.; Okuda, J., Single-Component Polymerization Catalysts for Ethylene and Styrene: Synthesis, Characterization, and Reactivity of Alkyl and Hydrido Yttrium Complexes Containing a Linked Amido-Cyclopentadienyl Ligand. *Organometallics* **2000**, *19* (3), 228-243.
2. Altenbuchner, P. T.; Soller, B. S.; Kissling, S.; Bachmann, T.; Kronast, A.; Vagin, S. I.; Rieger, B., Versatile 2-Methoxyethylaminobis(Phenolate)Yttrium Catalysts: Catalytic Precision Polymerization of Polar Monomers Via Rare Earth Metal-Mediated Group Transfer Polymerization. *Macromolecules* **2014**, *47* (22), 7742-7749.
3. Brigodiot, M.; Cheradame, H.; Fontanille, M.; Vairon, J. P., Microstructure of Poly(2-Vinylpyridine): Correlation between ¹³C and ¹H NMR Determinations. *Polymer* **1976**, *17* (3), 254-256.
4. Altenbuchner, P. T.; Adams, F.; Kronast, A.; Herdtweck, E.; Pöthig, A.; Rieger, B., Stereospecific Catalytic Precision Polymerization of 2-Vinylpyridine Via Rare Earth Metal-Mediated Group Transfer Polymerization with 2-Methoxyethylamino-Bis(Phenolate)-Yttrium Complexes. *Polym. Chem.* **2015**, *6* (38), 6796-6801.
5. Fuchise, K.; Sakai, R.; Satoh, T.; Sato, S.-i.; Narumi, A.; Kawaguchi, S.; Kakuchi, T., Group Transfer Polymerization Of n,N-Dimethylacrylamide Using Nobel Efficient System Consisting of Dialkylamino Silyl Enol Ether as an Initiator and Strong Brønsted Acid as an Organocatalyst. *Macromolecules* **2010**, *43* (13), 5589-5594.
6. Tshuva, E. Y.; Groysman, S.; Goldberg, I.; Kol, M.; Goldschmidt, Z., [Onxo]-Type Amine Bis(Phenolate) Zirconium and Hafnium Complexes as Extremely Active 1-Hexene Polymerization Catalysts. *Organometallics* **2002**, *21* (4), 662-670.
7. Wong, Y.-L.; Tong, L. H.; Dilworth, J. R.; Ng, D. K. P.; Lee, H. K., New Dioxo-Molybdenum(VI) and -Tungsten(VI) Complexes with N-Capped Tripodal N₂O₂ Tetradentate Ligands: Synthesis, Structures and Catalytic Activities Towards Olefin Epoxidation. *Dalton Transactions* **2010**, *39* (19), 4602-4611.
8. Barroso, S.; de Aguiar, S. R. M. M.; Munhá, R. F.; Martins, A. M., New Zirconium Complexes Supported by N-Heterocyclic Carbene (Nhc) Ligands: Synthesis and Assessment of Hydroamination Catalytic Properties. *Journal of Organometallic Chemistry* **2014**, *760* (0), 60-66.
9. Konkol, M.; Nabika, M.; Kohno, T.; Hino, T.; Miyatake, T., Synthesis, Structure and A-Olefin Polymerization Activity of Group 4 Metal Complexes with [Osso]-Type Bis(Phenolate) Ligands. *J. Organomet. Chem.* **2011**, *696* (9), 1792-1802.
10. Amgoune, A.; Thomas, C. M.; Roisnel, T.; Carpentier, J.-F., Ring-Opening Polymerization of Lactide with Group 3 Metal Complexes Supported by Dianionic Alkoxy-Amino-Bisphenolate Ligands: Combining High Activity, Productivity, and Selectivity. *Chem. Eur. J.* **2005**, *12* (1), 169-79.
11. Harder, S.; Ruspic, C.; Bhriain, N. N.; Berkermann, F.; Schürmann, M., Benzyl Complexes of Lanthanide (II) and Lanthanide (III) Metals: Trends and Comparisons. *Zeitschrift für Naturforschung B* **2008**, *63* (3), 267-274.

14.2 Supporting Information: “Multiresponsive micellar block copolymers from 2-vinylpyridine and dialkylvinylphosphonates with a tunable lower critical solution temperature”

Supporting Information for the Manuscript Entitled

Multiresponsive Micellar Block Copolymers from 2-Vinylpyridine and Dialkylvinylphosphonates with a Tunable Lower Critical Solution Temperature

Friederike Adams, Peter T. Altenbuchner*, Patrick D. L. Werz, and Bernhard Rieger*

WACKER-Lehrstuhl für Makromolekulare Chemie, Technische Universität München, Lichtenbergstraße 4, 85747 Garching b. München, Germany.

Table of Contents

1. Experimental procedure.....	2
2. Polymerization results.....	5
3. Characterization of micelles.....	11

Experimental procedure

Materials and Methods.

All reactions were carried out under argon atmosphere using standard Schlenk or glovebox techniques. All glassware was heat dried under vacuum prior to use. Unless otherwise stated, all chemicals were purchased from Sigma-Aldrich, Acros Organics, or ABCR and used as received. Toluene, thf, diethylether dichloromethane and pentane were dried using a MBraun SPS-800 solvent purification system. Hexane was dried over 3 Å molecular sieves. Compound $Y(CH_2Si(CH_3)_3(thf)_2)$, $LiCH_2TMS$ and catalyst 1 are prepared according to literature procedures.¹⁻⁴ Monomers 2-vinylpyridine (2VP) and the dialkyl vinyl phosphonates (DAVP) were dried over calcium hydride and distilled prior to use.

NMR spectra were recorded on a Bruker AVIII-300 and AVIII-500 Cryo spectrometer. Unless otherwise stated, 1H - and ^{13}C -NMR spectroscopic chemical shifts δ are reported in ppm relative to the residual proton signal of the solvent. δ (1H) is calibrated to the residual proton signal, δ (^{13}C) to the carbon signal of the solvent. Unless otherwise stated, coupling constants J are averaged values and refer to couplings between two protons. Deuterated solvents were obtained from Sigma-Aldrich and dried over 3 Å molecular sieves.

Copolymerization Procedures.

After dissolving the calculated amount of catalyst in dichloromethane at room temperature, the respective equivalents of 2-vinylpyridine were added in one portion. The reaction mixture was stirred for 90 minutes. One aliquot (0.1 mL) was taken and quenched by the addition of 0.4 mL CD_3OD (calculation of conversion of 2-vinylpyridine via 1H -NMR) while the calculated amount of a second monomer (or mixture of two dialkyl vinyl phosphonates) was added to the reaction solution, stirred over night and quenched by addition of 0.5 mL methanol. Before quenching an aliquot (0.1 mL) is, once again, taken and quenched with 0.5 mL CD_3OD to calculate the conversion of vinylphosphonates via ^{31}P -NMR-spectroscopy. The polymers were precipitated by addition of the reaction mixtures to pentane (150 mL) and decanted from solution. Residual solvent was removed by freeze-drying from benzene or water (100 mL) over night. The polymer of the aliquot of the first polymerization-sequence is dried under vacuum at 60 °C overnight.

Characterization of Polymer Samples.

Molecular-weights and molecular-weight-distributions of the first polymerization sequence are measured via GPC-MALS analysis of the first aliquot. Ratio of A/B [2VP/DAVP] is calculated via 1H -NMR-spectroscopy of the dried blockcopolymer. The molecular-weight of the blockcopolymer is determined through the ratio of A/B and the molecular weight of the first block (A). Molecular-weight-distributions are measured via GPC-MALS analysis.

Gel permeation chromatography (GPC) was carried out with samples of 5 mg/mL concentration on a Varian LC-920 equipped with two PL Polargel columns. As eluent a mixture of THF/water (1:1; v:v), 9 g/L tetrabutylammonium bromide (TBAB) and 680 mg/L_{THF} 3,5-di-tert-butyl-4-hydroxytoluene (BHT) was used. Absolute molecular weights have been determined online by multiangle light scattering (MALS) analysis using a Wyatt Dawn Heleos II in combination with a Wyatt Optilab rEX as concentration source.

Lower critical solution temperature (LCST)-measurements were carried out on a Cary 50 UV-Vis spectrophotometer from Varian. The LCST was determined by spectrophotometric detection of the changes in transmittance at $\lambda = 500$ nm of the aqueous polymer solutions. The heating/cooling rate was 1.0 K/min in steps of 1 K followed by a 5 min period of constant temperature to ensure equilibration. For determination of the transition hysteresis, equilibration periods of 3, 1.5, 0.75, 0.5, and 0.25 min or no equilibration period was used. The cloud point was defined as the temperature corresponding to a 10% decrease in optical transmittance.

Preparation of Micelles

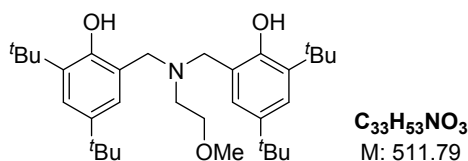
To obtain Nile red-loaded micelles, firstly Nile red was dissolved in DMSO ($c = 0.3$ mg/mL). Under continuous stirring the Nile red solution was added dropwise to the freshly prepared blank-micelle solution (Micelle/Nile-Red = 1/10). The mixture was then stirred for 1 hour followed by overnight dialysis against water (MWCO: 6000 – 8000). Afterwards non-encapsulated Nile red was removed by an additional centrifugation step at 4000 rpm for 10 min at room temperature. The supernatant was transferred into a new reaction tube.

TEM images

High-resolution transmission electron microscopy (TEM) was performed on a JEOL JEM100CX using an accelerating voltage of 100 kV. Samples were prepared from a dilute aqueous solution using a 2% uranyl acetate solution as the negative stain. TEM images were prepared from aqueous solution of the micelles on a copper tape and dried until the water disappeared and measured immediately.

Ligand synthesis.**H₂(ONOO)^{tBu} 5**

A solution of 2.0 equivalents of 2,4-di-tert-butylphenol, 1.0 equivalents 2-methoxyethylamine and aqueous formaldehyde-solution (36% in water; 3.0 eq.) in methanol were refluxed for 10 days. The mixture was cooled and the colorless solid was separated via filtration. After double recrystallization from ethanol the product is yielded as colorless crystals.

**H₂(ONOO)^{tBu}**

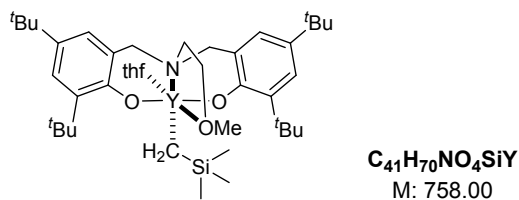
Yield: 45% (colorless crystals)

¹H-NMR (300 MHz, CDCl₃, 300 K): δ (ppm) = 8.52 (s, 2H, OH), 7.21 (d, ⁴J = 2.5 Hz, 2H, H_{arom}), 6.88 (d, ⁴J = 2.5 Hz, 2H, H_{arom}), 3.74 (s, 4H, ArCH₂), 3.56 (t, ³J = 5.1 Hz, 2H, H_{sidearm}), 3.47 (s, 3H, OMe), 2.75 (t, ³J = 5.1 Hz, 2H, H_{sidearm}), 1.41 (s, 18H, ^tBu), 1.27 (s, 18H, ^tBu).

¹³C-NMR (75 MHz, CDCl₃, 300 K): δ (ppm) = 153.0, 140.8, 136.1, 125.0, 123.5, 121.7, 71.5, 58.9, 58.2, 51.5, 35.1, 34.2, 31.8, 29.7.

Complex synthesis.**(ONOO)^{tBu}Y(CH₂TMS)(thf)(1)⁶**

One equivalent of proligand H₂(ONOO)^{tBu} in toluene is added to a stirred solution of Y(CH₂Si(CH₃)₃)₃(thf)₂ in pentane at 0 °C. The resulting solution is stirred overnight at room temperature. The solvent is removed *in vacuo* and the resulting solid is washed and recrystallized from pentane.



Yield: 43% (colorless powder)

¹H-NMR (300 MHz, C₆D₆, 300 K): δ (ppm) = 7.61 (d, ⁴J = 2.6 Hz, 2H, H_{arom}), 7.09 (d, ⁴J = 2.6 Hz, 2H, H_{arom}), 4.00 – 3.89 (m, 4H, H_{THF}), 3.78 (d, ²J = 12.4 Hz, 2H, ArCH₂), 2.89 (d, ²J = 12.4 Hz, 2H, ArCH₂), 2.78 (s, 3H, OMe), 2.42 (t, ³J = 5.4 Hz, 2H, H_{sidearm}), 2.20 (t, ³J = 5.4 Hz, 2H, H_{sidearm}), 1.81 (s, 18H, ^tBu), 1.46 (s, 18H, ^tBu), 1.19 – 1.11 (m, 4H, H_{THF}), 0.52 (s, 9H, H_{TMS}), -0.38 (d, ²J_{V,H} = 3.3 Hz, 2H, CH₂TMS).

$^{13}\text{C-NMR}$ (126 MHz, C_6D_6 , 300 K): δ (ppm) = 161.6 (d, $^2J_{\text{C,Y}} = 1.8$ Hz), 136.8, 136.6, 125.6, 124.4, 124.1, 74.0, 71.7, 64.9, 61.3, 49.3, 35.6, 34.3, 32.3, 30.3, 25.4, 25.1, 4.9.

1. Polymerization results

GPC traces.

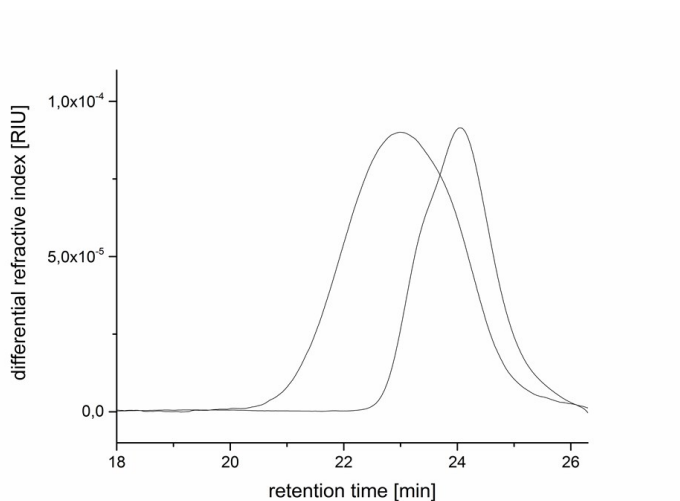


Figure S 1: GPC-traces of blockcopolymer AB (2VP₁₀₀/DEVP₁₀₀; entry 1, table 1). Right: P2VP Homopolymer before addition of Block B. Left: Blockcopolymer.

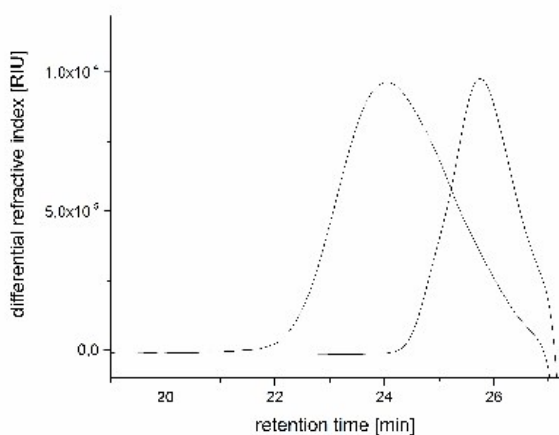


Figure S 2: GPC-traces of Blockcopolymer AB (2VP₅₀/DEVP₅₀; entry 2, table 1). Right: P2VP Homopolymer before addition of Block B. Left: Blockcopolymer.

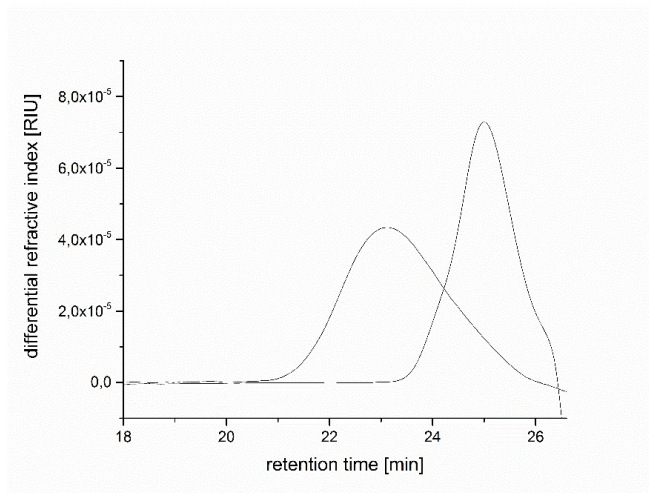


Figure S 3: GPC-traces of blockcopolymer AB (2VP₅₀/DEVP₉₀; entry 3, table 1). Right: P2VP Homopolymer before addition of Block B. Left: Blockcopolymer.

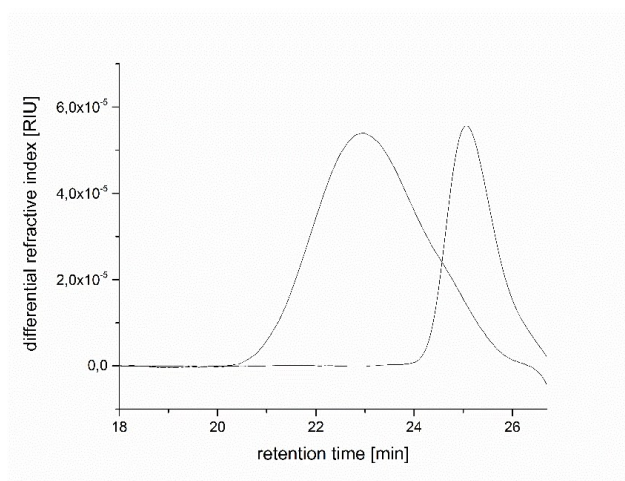


Figure S 4: GPC-traces of blockcopolymer AB (2VP₅₀/DEVP₁₂₀; entry 4, table 1). Right: P2VP Homopolymer before addition of Block B. Left: Blockcopolymer.

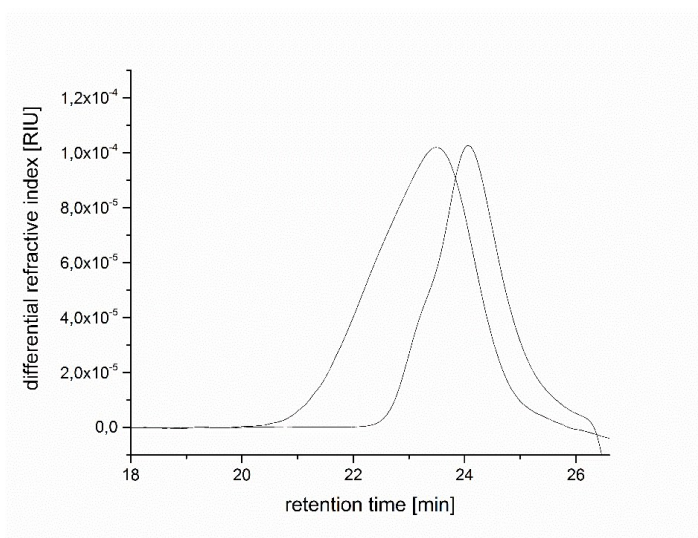


Figure S 5: GPC-traces of blockcopolymer ABB' ($2VP_{100}/DEVP_{97}/DPVP_3$; entry 6, table 1). Right: P2VP Homopolymer before addition of Block B. Left: Blockcopolymer.

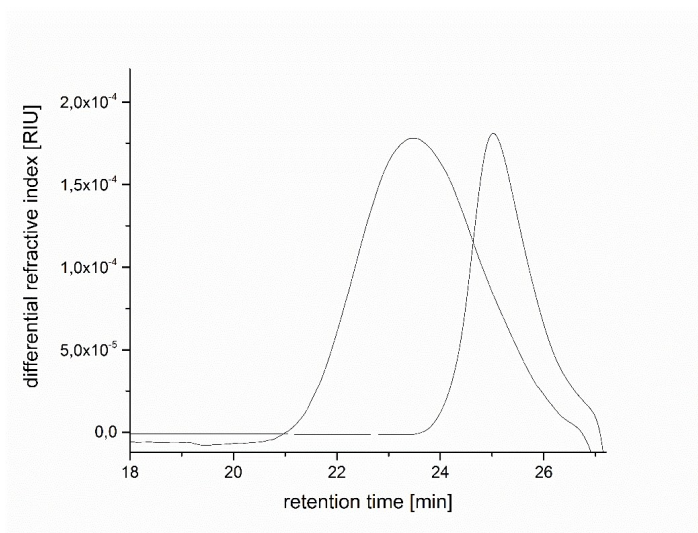
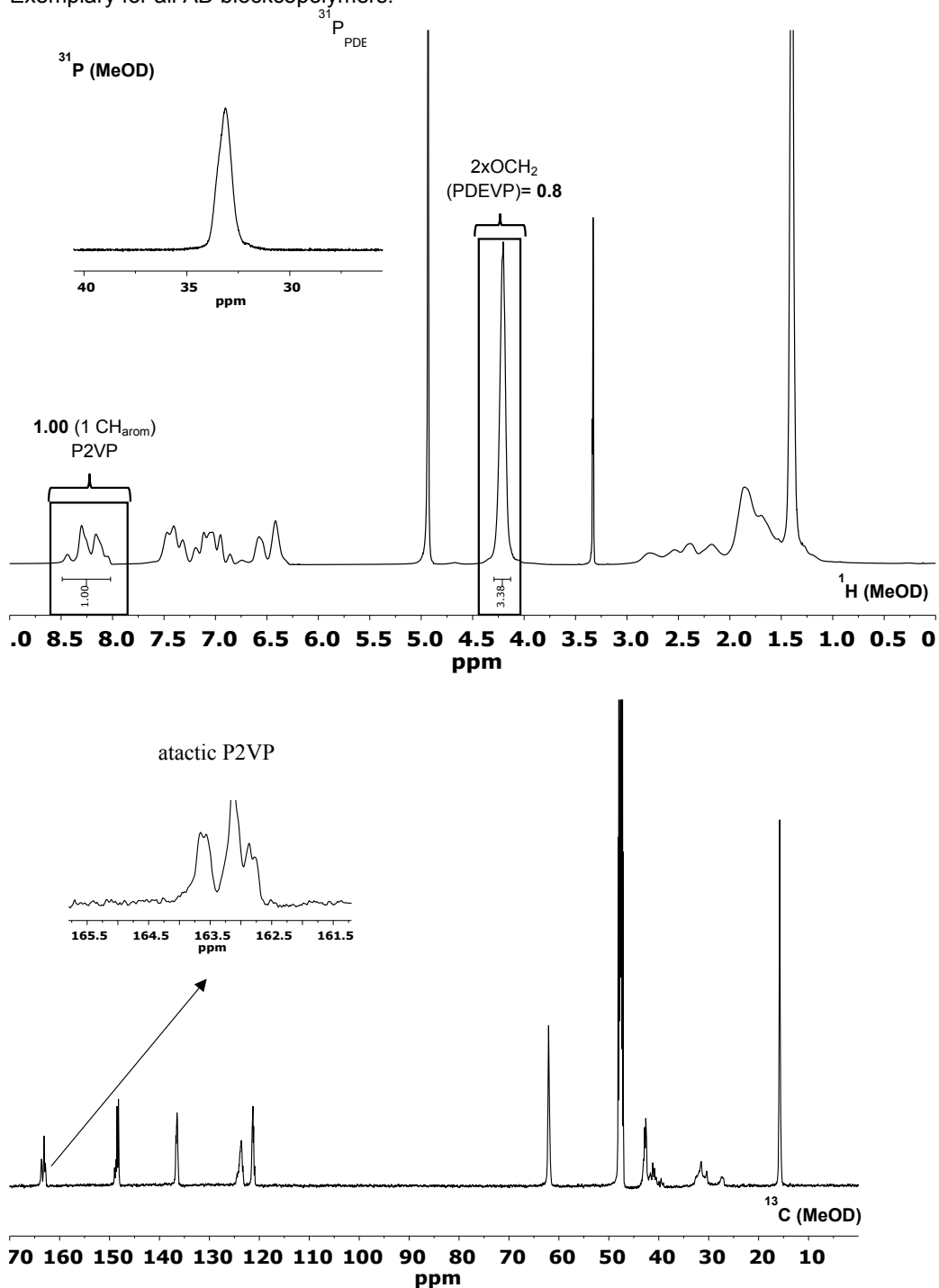


Figure S 6: GPC-traces of blockcopolymer ABB' ($2VP_{100}/DEVP_{90}/DMVP_{10}$; entry 7, table 1). Right: P2VP Homopolymer before addition of Block B. Left: Blockcopolymer.

Blockcopolymers.

Exemplary for all AB-blockcopolymers:

**Figure S 7:** ^1H -, ^{31}P - and ^{13}C -NMR spectrum of AB (2VP₁₀₀/DEV_P₁₀₀; entry 1, table 1) in MeOD at 298 K.

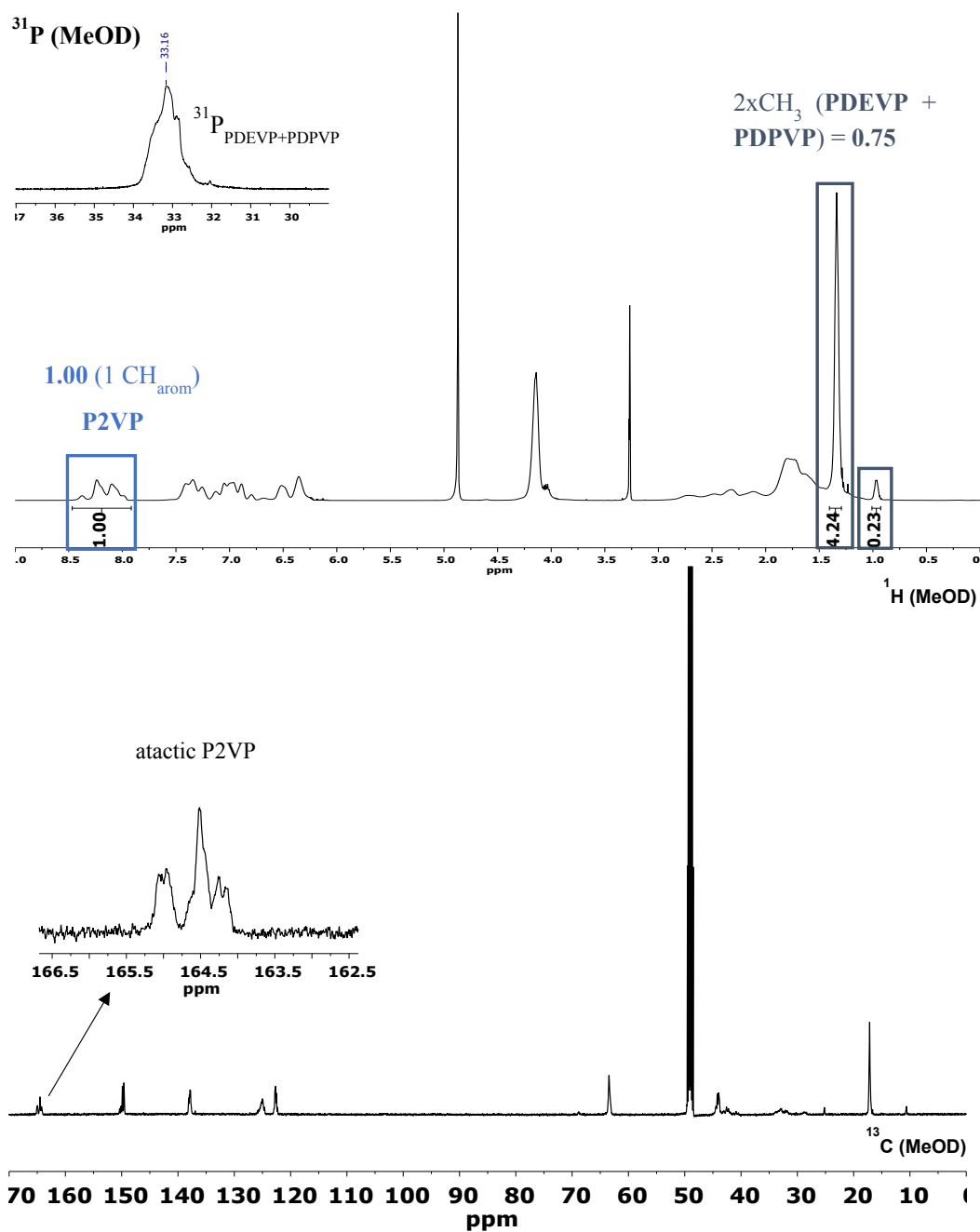


Figure S 8: ^1H -, ^{31}P - and ^{13}C -NMR spectrum of ABB' (2VP₁₀₀/DEVP₉₀/DPVP₁₀; entry 6, table 1) in MeOD at 298 K. Assignment of the Protons according to *Rieger et al.* Overlapping of PDEVP and PDPVP- ^{31}P -signal. ⁷

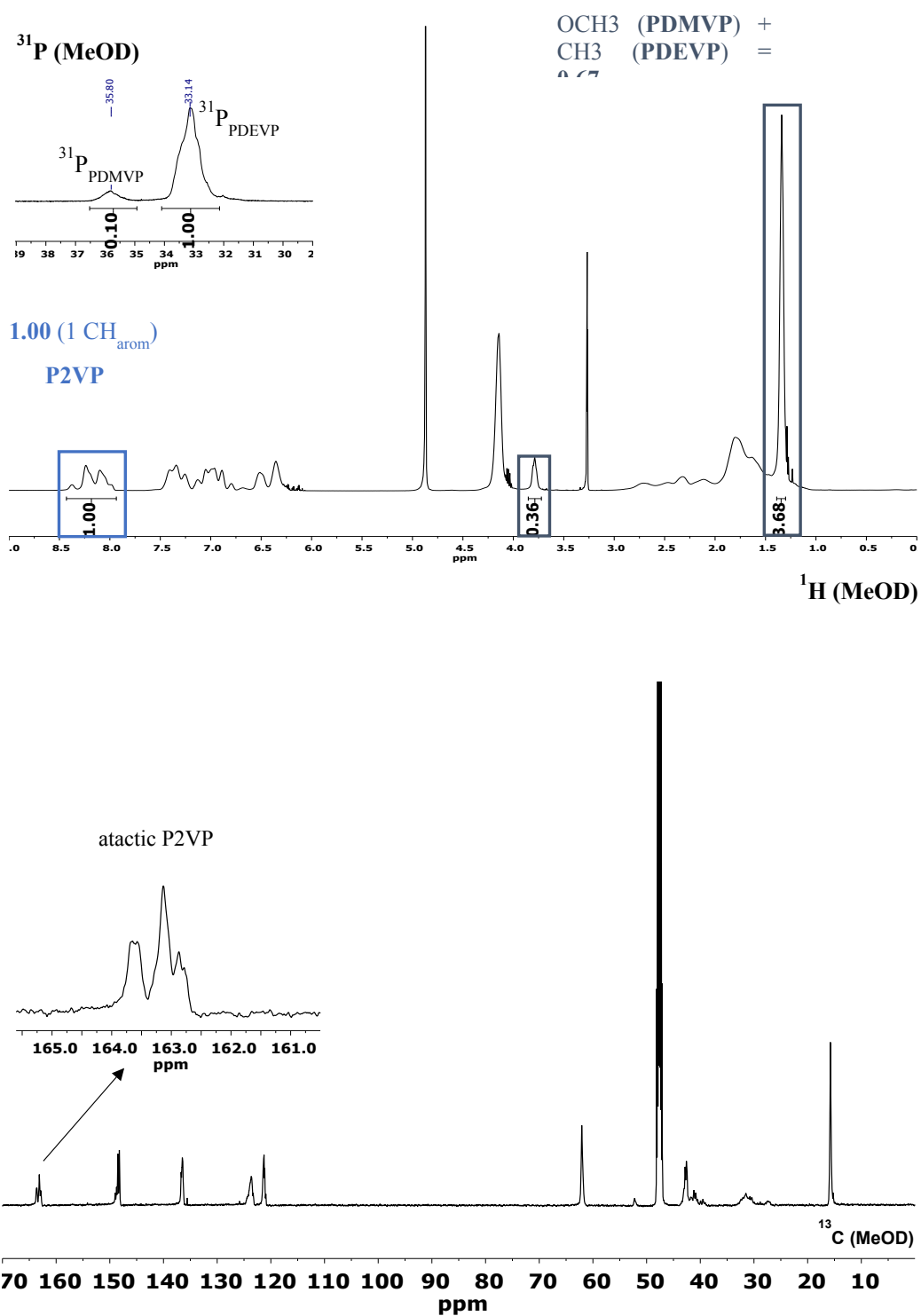


Figure S 9: ^1H -, ^{31}P - and ^{13}C -NMR spectrum of ABB' (2VP₁₀₀/DEV₉₀/DMVP₁₀; entry 8 table 1) in MeOD at 298 K. Assignment of the Protons according to Rieger et al.⁷

2. Characterization of micelles

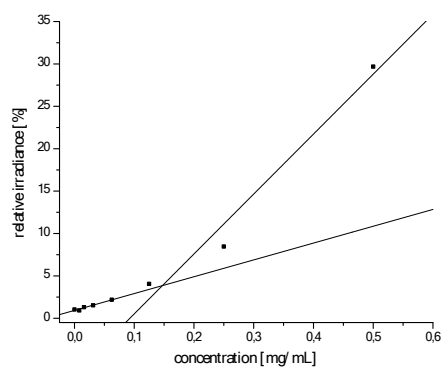


Figure S 10: Determination of critical micelle concentration (CMC) with Nile red for AB (2VP₁₀₀/DEVP₁₀₀; entry 1 table 1).

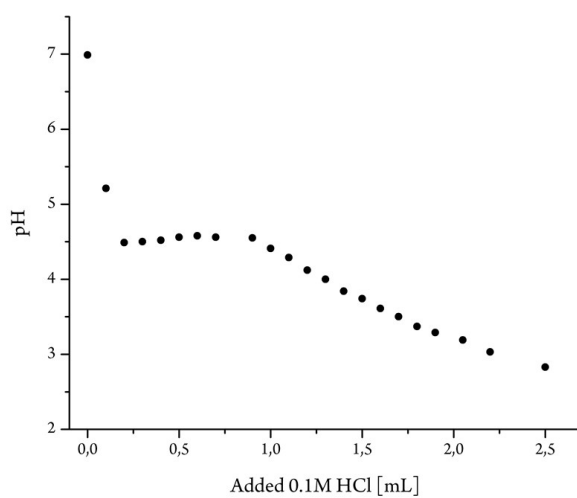


Figure S 11: Titrationcurve of AB₁ (2VP₁₀₀/DEVP₁₀₀; entry 1 table 1) with 0.1 M hydrogenchloride-solution.

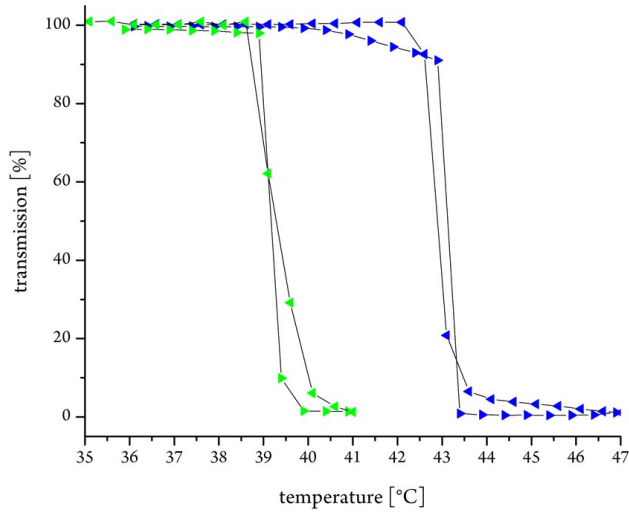


Figure S 12: LCST-UV/VIS-measurement of blockcopolymer AB¹ (2VP₁₀₀/DEVP₁₀₀; entry 1 table 1). The cloud point was determined at 10% decrease of transmittance for 2.5 wt % aqueous polymer solution (blue: deionized, green: PBS puffer).

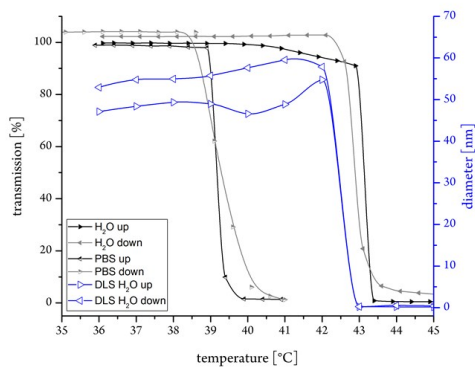


Figure S 13: LCST-UV/VIS-measurement and DLS-measurement of blockcopolymer AB¹ (2VP₁₀₀/DEVP₁₀₀; entry 1 table 1) in H₂O and PBS buffer solution.

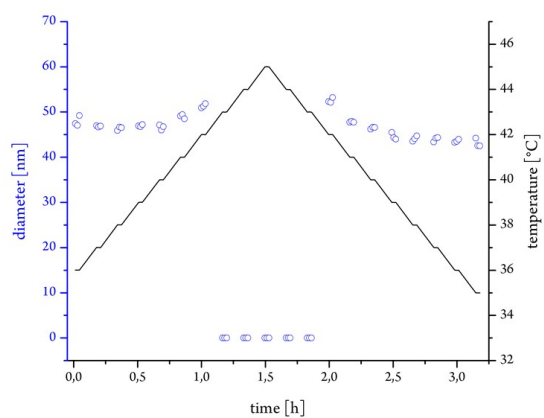


Figure S 14: LCST-DLS-measurement of blockcopolymer AB¹ (2VP₁₀₀/DEVP₁₀₀; entry 1 table 1).

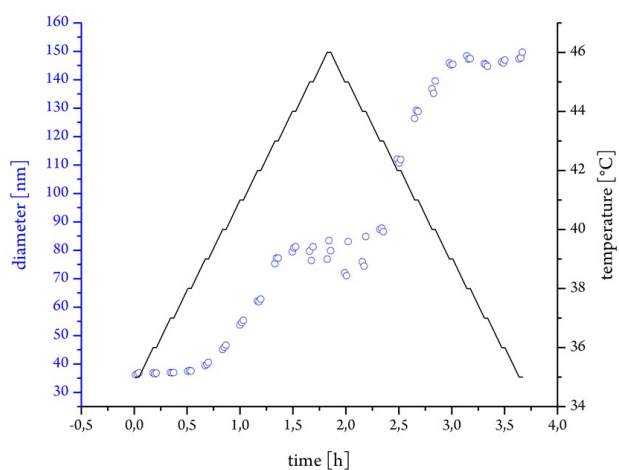


Figure S 15: LCST-DLS-measurement of blockcopolymer AB² (2VP₅₀/DEVP₅₀; entry 2 table 1).

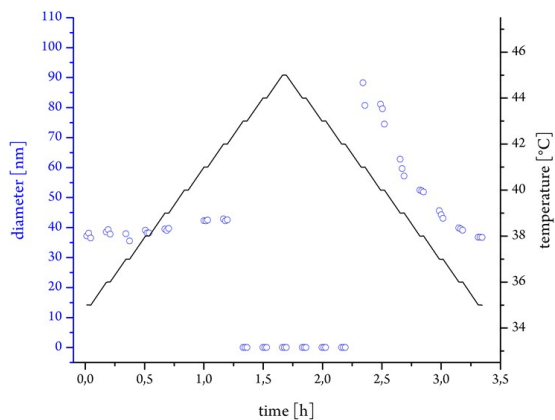


Figure S 16: LCST-DLS-measurement of blockcopolymer AB³ (2VP₅₀/DEVP₉₀; entry 3 table 1).

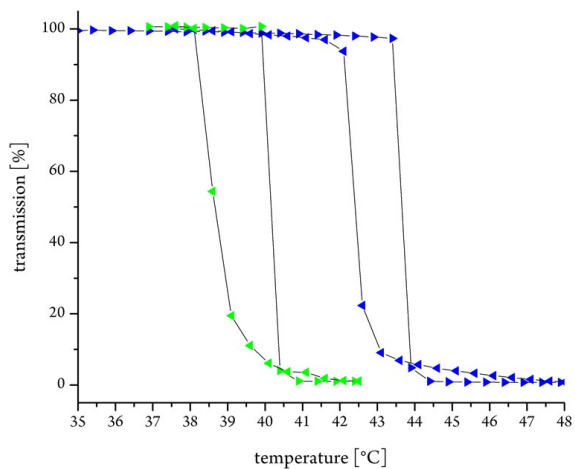


Figure S 17: LCST-UV/VIS-measurement of blockcopolymer AB³ (2VP₅₀/DEVP₉₀; entry 3 table 1). The cloud point was determined at 10% decrease of transmittance for 2.5 wt % aqueous polymer solution (blue: deionized, green: PBS puffer).

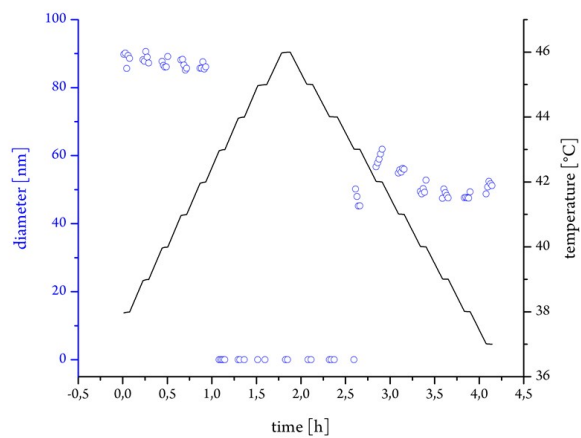


Figure S 18: LCST-DLS-measurement of blockcopolymer AB⁴ (2VP₅₀/DEVP₁₂₀; entry 4 table 1).

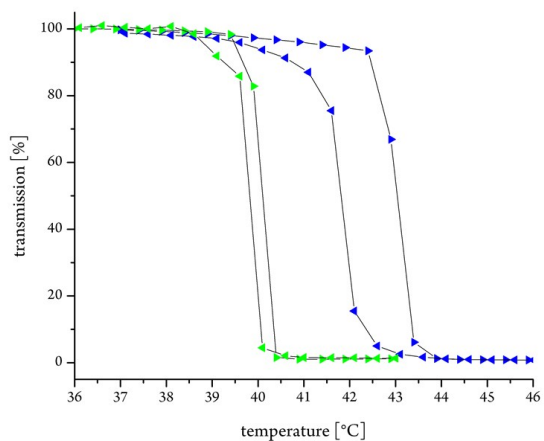


Figure S 19: LCST-UV/VIS-measurement of blockcopolymer AB⁴ (2VP₅₀/DEVP₁₂₀; entry 4 table 1). The cloud point was determined at 10% decrease of transmittance for 2.5 wt % aqueous polymer solution (blue: deionized, green: PBS puffer).

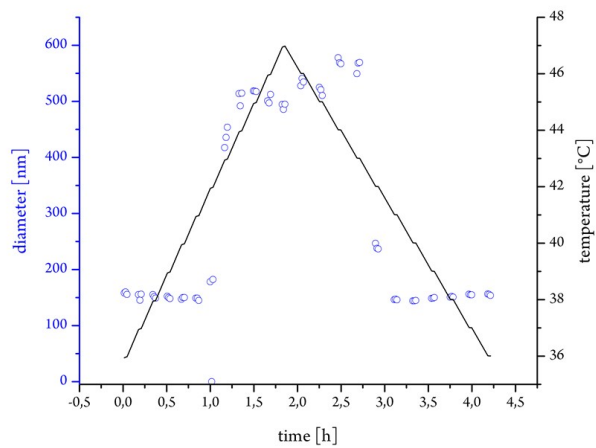


Figure S 20: LCST-DLS-measurement of blockcopolymer AB⁵ (2VP₂₀₀/DEVP₂₀₀; entry 5 table 1).

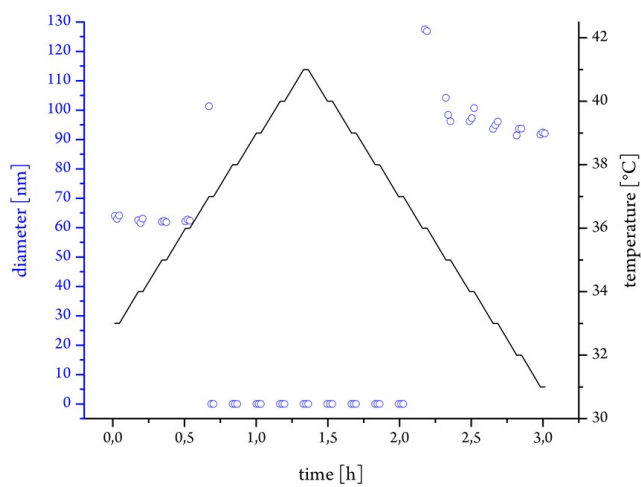


Figure S 21: LCST-DLS-measurement of blockcopolymer ABB'¹ (2VP₁₀₀/DEVP₉₀/DPVP₁₀; entry 6, table 1).

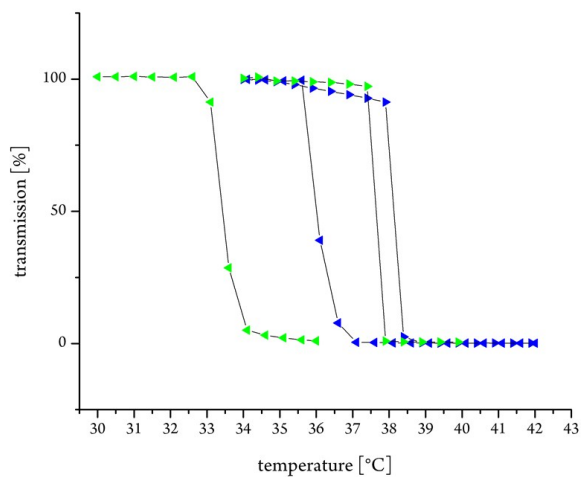


Figure S 22: LCST-UV/VIS-measurement of blockcopolymer ABB^{'1} (2VP₁₀₀/DEVP₉₀/DPVP₁₀; entry 6, table 1). The cloud point was determined at 10% decrease of transmittance for 2.5 wt % aqueous polymer solution (blue: deionized, green: PBS puffer).

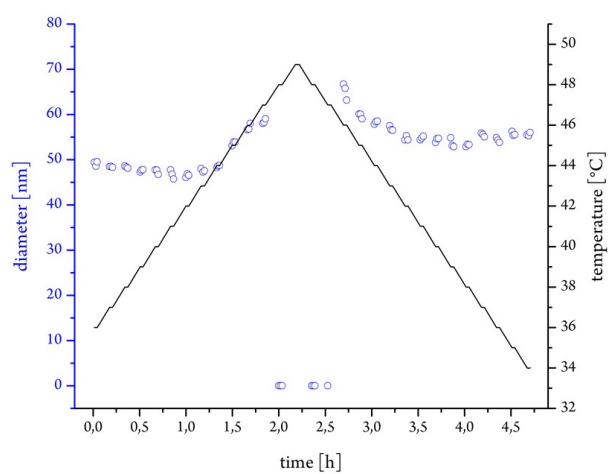


Figure S 23: LCST-DLS-measurement of blockcopolymer ABB^{'2} (2VP₁₀₀/DEVP₉₀/DMVP₁₀; entry 7, table 1).

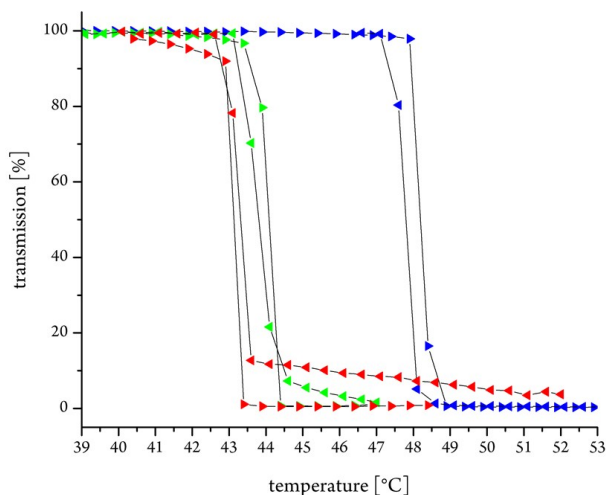


Figure S 24: LCST-UV/VIS-measurement of blockcopolymer ABB'² (2VP₁₀₀/DEVP₉₀/DMVP₈; entry 7, table 1). The cloud point was determined at 10% decrease of transmittance for 2.5 wt % aqueous polymer solution (blue: deionized, green: PBS puffer, red: DMEM puffer).

1. Altenbuchner, P. T.; Soller, B. S.; Kissling, S.; Bachmann, T.; Kronast, A.; Vagin, S. I.; Rieger, B., *Macromolecules* **2014**, *47* (22), 7742-7749.
2. Hultsch, K. C.; Voth, P.; Beckerle, K.; Spaniol, T. P.; Okuda, J., *Organometallics* **2000**, *19* (3), 228-243.
3. Vaughn, G. D.; Krein, K. A.; Gladysz, J. A., *Organometallics* **1986**, *5* (5), 936-42.
4. Cai, C.-X.; Toupet, L.; Lehmann, C. W.; Carpentier, J.-F., *J. Organomet. Chem.* **2003**, *683* (1), 131-136.
5. Tshuva, E. Y.; Groyzman, S.; Goldberg, I.; Kol, M.; Goldschmidt, Z., *Organometallics* **2002**, *21* (4), 662-670.
6. Amgoune, A.; Thomas, C. M.; Roisnel, T.; Carpentier, J.-F., *Chem. Eur. J.* **2005**, *12* (1), 169-79.
7. Zhang, N.; Salzinger, S.; Rieger, B., *Macromolecules* **2012**, *45* (24), 9751-9758.

14.3 Supporting Information: “Yttrium-Catalyzed Synthesis of Bipyridine-Functionalized AB-Block Copolymers: Micellar Support for Photocatalytic Active Rhenium-Complexes”

Supporting Information

© Copyright Wiley-VCH Verlag GmbH & Co. KGaA, 69451 Weinheim, 2018

Yttrium-Catalyzed Synthesis of Bipyridine-Functionalized AB-Block Copolymers: Micellar Support for Photocatalytic Active Rhenium-Complexes

F. Adams⁺, M. Pschenitza⁺, and B. Rieger^{*}

Supporting Information for the Manuscript Entitled

Yttrium-catalyzed Synthesis of Bipyridine-functionalized AB-Block Copolymers: Micellar Support for Photocatalytic active Rhenium-Complexes

F. Adams, † M. Pschenitza, † and B. Rieger*

WACKER-Lehrstuhl für Makromolekulare Chemie,
Catalysis Research Center
Department of Chemistry
Technische Universität München

Table of Contents

1. Experimental procedure.....	2
2. NMR Kinetics of C-H bond activation.....	12
3. ESI-MS of Oligomeric 2VP	14
4. NMR-spectra of P2VP.....	15
5. NMR-spectra of P2VP-PDEV block copolymers.....	17
6. GPC traces of polymers.....	20
7. Supplementary UV/VIS and PL Spectra	23
8. AB-Block copolymer produced with catalyst 1.....	25
9. Photocatalytic Reduction of CO ₂	25
10. Literature.....	26

1. Experimental procedure

Materials and Methods.

All reactions were carried out under argon atmosphere using standard Schlenk or glovebox techniques. All glassware was heat dried under vacuum prior to use. Unless otherwise stated, all chemicals were purchased from Sigma-Aldrich, Acros Organics, or ABCR and used as received. Toluene, thf, diethylether, dichloromethane and pentane were dried using a MBraun SPS-800 solvent purification system. Hexane was dried over 3 Å molecular sieves. The monomers 2-vinylpyridine and diethyl vinylphosphonate were dried over calcium hydride and distilled prior to use.

The precursor complex $Y(CH_2TMS)_3(thf)_2$, the 2-methoxyethylamino-bis(phenolate) ligand as well as complex **1** are prepared according to literature procedure.^{1, 2} 6-Methyl-2,2'-bipyridine is prepared according to literature procedure and stored over 3 Å molecular sieves.³

NMR spectra were recorded on a Bruker AVIII-300, AVIII-500 and AVIII-500 Cryo spectrometer. Unless otherwise stated, ¹H-, ³¹P and ¹³C-NMR spectroscopic chemical shifts δ are reported in ppm. δ (¹H) is calibrated to the residual proton signal, δ (¹³C) to the carbon signal of the solvent. Unless otherwise stated, coupling constants *J* are averaged values and refer to couplings between two protons. Deuterated solvents were obtained from Sigma-Aldrich and dried over 3 Å molecular sieves.

Elemental analysis was measured at the Laboratory for Microanalysis at the Institute of Inorganic Chemistry at the Technical University of Munich.

UV/VIS spectra were obtained using a Varian Cary 50 spectrophotometer in a UV quartz cuvette (10 mm).

GC analysis was performed using a Varian 490 gas chromatographer equipped with a 1 m COX column and a GC thermal conductivity detector. He (5.0) was used as the carrier gas.

Photoluminescence spectra were recorded on a AVA-Spec 2048 spectrometer (AVANTES) with a current Controller as 365nm light source (Prizmatix). A 90° cuvette holder and a 40 mm × 10 mm × 2 mm quartz glass cuvette were used for the measurements.

DLS measurements were performed at a Zetasizer Nano ZS (Malvern). The diameter was averaged over three independent values consisting each of 10 measurements. The standard deviation was determined based on these three data points.

Homopolymerization Procedures.

To a solution of 13.5 μmol catalyst (1.0 eq.) in 2 ml toluene at room temperature, 2.7 mmol 2-vinylpyridine (200 eq.) were added in one portion. The polymerization is quenched by addition of methanol after the respective polymerization time. Conversion is determined by ^1H NMR spectroscopy of an aliquot taken before quenching of the reaction. The polymers were precipitated by addition of the reaction mixtures to pentane (100 ml) and the solution was decanted off. Residual solvent was removed by freeze-drying from benzene (100 ml) over night. Molecular weights and polydispersities are measured *via* GPC.

Kinetic Measurements of 2-vinylpyridine by Aliquots Method.

To a solution of 135 μmol catalyst in 20 ml toluene at room temperature, the corresponding amount of monomer (27 mmol, 200 eq.) was added in one portion. Aliquots were taken from the reaction solution at regular time intervals and quenched by addition of MeOH. Solvent and not polymerized monomer were removed by drying the polymers under vacuum at 60 °C overnight. For each aliquot, the conversion is determined gravimetrically and the molecular weight of the polymer is determined by GPC analysis.

Copolymerization Procedures.

After dissolving the calculated amount of catalyst (0.0428 mmol) in dichloromethane (2 ml) at room temperature, the respective equivalents of 2-vinylpyridine were added in one portion. The reaction mixture was stirred for 90 minutes. One aliquot (0.1 ml) was taken and quenched by the addition of 0.4 ml CD_3OD (calculation of conversion *via* ^1H NMR spectroscopy) while the calculated amount of DEVP was added to the reaction solution, stirred overnight and quenched by addition of 0.5 ml MeOH. Before quenching an aliquot (0.1 ml) is, once again, taken and quenched with 0.5 ml CD_3OD to calculate the conversion of DEVP *via* ^{31}P NMR spectroscopy. The polymers were precipitated by addition of the reaction mixtures to pentane (150 ml) and decanted from solution. Residual solvent was removed by freeze-drying from benzene (100 ml) overnight. The polymer of the aliquot of the first polymerization-sequence is dried under vacuum at 60 °C overnight.

Characterization of Polymer-Samples.

Absolute molecular weights and polydispersities were measured *via* gel permeation chromatography (GPC) with samples of 2-3 mg/ml concentration on an *Agilent* PL-50 equipped with two PL Polargel-M columns at 30 °C. As eluent a mixture of DMF and 0.025 mol/l lithium bromide was used. Absolute molecular weights have been determined online by triple analysis using two angle light scattering, a refractometer and viscometer.

The dn/dc was determined via measurement of three different concentrations of an analytical standard P2VP sample bought from Sigma-Aldrich ($M_n = 35\,000$ g/mol; $M_w = 37\,000$ g/mol). It was determined as 0.149.

The tacticity determination of P2VP was performed by ^{13}C -NMR-spectroscopy at room temperature. Spectra for the analysis of P2VP mm, mr/rm and rr triads were recorded with a sample concentration of 15% (w/w; 75 mg/0.6 mL CD_3OD) on a AVIII 500 Cryo spectrometer and analyzed according to literature.^{4,5}

Photocatalytic Experiments.

Irradiation experiments were performed either in a 160 ml Schlenk tube (for catalysts **4-7**) or in a 15 ml Schlenk tube (for catalysts $\text{AB}^1_{\text{re}} - \text{AB}^4_{\text{re}}$ and **4**) using LEDs ($\lambda=450$ nm, $4.14 \cdot 10^{-6}$ Einstein/s). Reaction vessels were wrapped in an aluminum foil prior to sample preparation and unwrapped just before irradiation experiments. DMF/TEOA solutions containing the required rhenium catalyst in the desired concentration were saturated with CO_2 by bubbling for at least 15 min and sealed with a septum. The pressure was adjusted to 140 kPa. Irradiation experiments were performed in a dark room. For GC analysis 100 μl samples from the headspace above the solution were injected directly into the micro gas chromatograph. TONs were determined from the point at which catalyst activity fully ceased or from the point measured last and were defined as $\text{TON} = n(\text{CO})/n(\text{cat.})$, in which cat. represents the investigated catalytic system or mixture.

Irradiation sources

TUM LED control unit:

$I = \text{constant}$

→ Constant photon flux

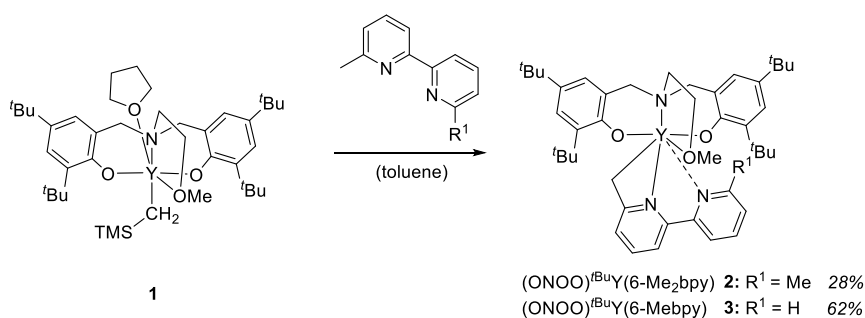
- Power supply 220–240 V//50 Hz
- Eight LEDs ($\lambda = 450$ nm) independently switchable and tuneable
- Air cooling system
- Irradiation power tuneable via current



Left: TUM LED Control Unit. Right: Irradiation of catalytic mixture with 450 nm LEDs.

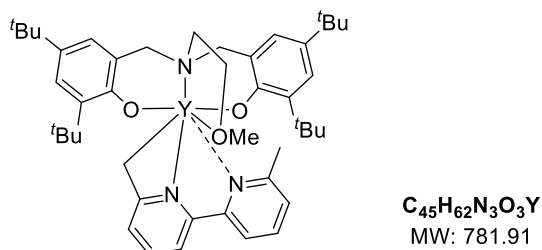
Complex Synthesis.

General procedure for the synthesis of C-H bond activated complexes:



One equivalent of **1** and one equivalent of the respective bipyridine-derivative are dissolved in toluene and stirred over a specified period of time at a certain temperature. The solvent is removed *in vacuo* and the raw product is washed with pentane and isolated *via* centrifugation.

(ONOO)^{tBu}Y((6'-methyl-[2,2'-bipyridin]-6-yl)methyl) (**2**):



The yellow to greenish reaction mixture is stirred for 5 days at 60 °C.

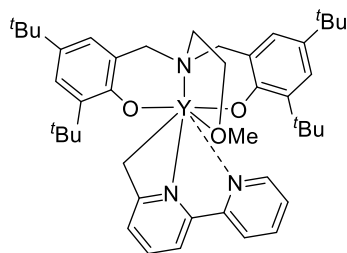
Yield: 28% (blue powder)

¹H NMR (300 MHz, C₆D₆, 300 K): δ (ppm) = 7.55 (d, ⁴J = 2.5 Hz, 2H, H_{phenolate}), 7.10 (d, J = 8.1 Hz, 1H), 7.04 (d, ⁴J = 2.5 Hz, 2H, H_{phenolate}), 6.88 (t, J = 7.8 Hz, 1H), 6.44 (d, J = 7.5 Hz, 1H), 6.21 (d, J = 5.0 Hz, 2H), 5.69 (d, J = 4.7 Hz, 1H), 3.66 (s, 6H), 3.13 (s, 3H), 2.88 (t, ³J = 5.2 Hz, 2H, CH_{2,sidearm}), 2.72 (s, 3H), 2.26 (t, ³J = 5.2 Hz, 2H, CH_{2,sidearm}), 1.45 (d, J = 3.5 Hz, 36H, ^tBu).

$^{13}\text{C NMR}$ (126 MHz, C_6D_6 , 300 K): δ (ppm) = 161.1, 158.6, 157.8, 156.3, 150.1, 138.0, 137.2, 136.3, 130.4, 125.7, 124.2, 124.1, 123.4, 122.0, 117.4, 98.0, 72.7, 67.5, 62.4, 60.7, 54.1, 35.2, 34.3, 32.2, 30.4, 25.0.

EA:	calculated:	C 69.12	H 7.99	N 5.37
	found:	C 68.97	H 8.10	N 5.25

(ONOO) $^{\text{tBu}}\text{Y}([2,2'\text{-bipyridin}]\text{-6-yl-methyl})$ (**3**):



$\text{C}_{44}\text{H}_{60}\text{N}_3\text{O}_3\text{Y}$
MW: 767.89

The purple reaction mixture is stirred for 12 hours at room temperature.

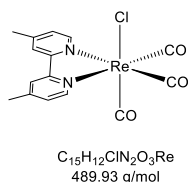
Yield: 62% (purple powder)

$^1\text{H NMR}$ (500 MHz, C_6D_6 , 300 K): δ (ppm) = 8.82 (s, 1H), 7.55 (d, $^4J = 2.6$ Hz, 2H, $H_{\text{phenolate}}$), 7.12 (s, 1H), 7.03 ($^4J = 2.6$ Hz, 2H, $H_{\text{phenolate}}$), 6.91 (td, $J = 7.8, 1.6$ Hz, 1H), 6.58 (t, $J = 6.4$ Hz, 1H), 6.42 (d, $J = 4.5$ Hz, 2H), 3.91 (s, 1H), 3.60 (s, 2H), 3.39 (s, 2H), 2.91 – 2.70 (m, 5H), 2.54 – 2.41 (m, 2H), 1.51 (s, 18H, 'Bu), 1.46 (s, 18H, 'Bu).

$^{13}\text{C NMR}$ (126 MHz, C_6D_6 , 300 K): δ (ppm) = 161.6, 150.8, 149.3, 138.4, 137.0, 136.1, 125.8, 124.7, 124.0, 23.5, 123.2, 122.2, 120.9, 120.2, 118.3, 110.2, 99.6, 73.6, 63.9, 60.3, 35.3, 32.3, 30.1, 24.6.

EA:	calculated:	C 68.82	H 7.88	N 5.47
	found:	C 68.03	H 7.66	N 5.48

[Re(CO)₃(4-Me₂bpy)Cl] (**7**):



4,4'-Dimethyl-2,2'-bipyridine (76.40 mg, 415 μmol, 1.0 eq.) and [Re(CO)₅Cl] (150.0 mg, 415 μmol, 1.0 eq.) were refluxed for 3 h in dry toluene (10 ml) under argon. After cooling to room temperature, the yellow precipitate was filtered off, washed with toluene (10 ml) and diethyl ether (2 × 10 ml) and dried under vacuum.

Yield: 193.0 mg (394 μmol, 95%).

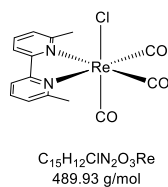
¹H NMR (300 MHz, CDCl₃, 298 K): δ (ppm) = 8.81 (d, *J* = 5.6 Hz, 2H), 7.91 (s, 2H), 7.26 (d, *J* = 5.6 Hz, 2H), 2.50 (s, 6H)

¹³C NMR (75 MHz, CDCl₃, 298 K): δ (ppm) = 155.53, 152.73, 151.34, 128.04, 123.88, 21.83

UV/VIS (DMF): λ_{max} = 363 nm

EA:	calculated:	C 36.77	H 2.47	N 5.72
	found:	C 37.54	H 2.45	N 5.79

[Re(CO)₃(6-Me₂bpy)Cl] (**6**):



6,6'-Dimethyl-2,2'-bipyridine (76.40 mg, 415 μmol, 1.0 eq.) and [Re(CO)₅Cl] (150.0 mg, 415 μmol, 1.0 eq.) were refluxed for 4 h in dry toluene (7 ml) under argon. After cooling to room temperature, the yellow precipitate was filtered off, washed with toluene (10 ml) and diethyl ether (2 × 10 ml) and dried under vacuum.

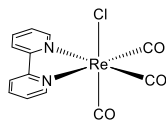
Yield: 172.0 mg (351 μmol, 85%).

$^1\text{H NMR}$ (300 MHz, Acetone- d_6 , 298 K): δ (ppm) = 8.44 (d, J = 8.1 Hz, 2H), 8.15 (t, J = 7.9 Hz, 2H), 7.72 (d, J = 7.6 Hz, 2H), 3.11 (s, 6H)

UV/VIS (DMF): λ_{max} = 365 nm

EA:	calculated:	C 36.77	H 2.47	N 5.72
	found:	C 36.85	H 2.46	N 5.72

$[\text{Re}(\text{CO})_3(\text{bpy})\text{Cl}]$ (**5**):



$\text{C}_{13}\text{H}_{18}\text{ClN}_2\text{O}_3\text{Re}$
461.88 g/mol

2,2'-Bipyridine (64.48 mg, 419 μmol , 1.0 eq.) and $[\text{Re}(\text{CO})_5\text{Cl}]$ (150.5 mg, 416 μmol , 1.0 eq.) were refluxed for 3 h in dry toluene (10 ml) under argon. After cooling to room temperature, the yellow precipitate was filtered off, washed with toluene (10 ml) and diethyl ether (2×10 ml) and dried under vacuum.

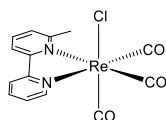
Yield: 164.4 mg (365 μmol , 86%).

$^1\text{H NMR}$ (300 MHz, CDCl_3 , 298 K): δ (ppm) = 8.18-8.11 (m, 2H), 8.02 (td, J = 7.9, 1.6 Hz, 2H), 7.49 (ddd, J = 7.3, 5.5, 1.3 Hz, 2H)

UV/VIS (DMF): λ_{max} = 369 nm

EA:	calculated:	C 33.81	H 1.75	N 6.07
	found:	C 33.88	H 1.67	N 6.03

$[\text{Re}(\text{CO})_3(6\text{-Mebpy})\text{Cl}]$ (**4**):



$\text{C}_{14}\text{H}_{10}\text{ClN}_2\text{O}_3\text{Re}$
475.90 g/mol

6-Methyl-2,2'-bipyridine (70.60 mg, 415 μmol , 1.0 eq.) and $[\text{Re}(\text{CO})_5\text{Cl}]$ (150.0 mg, 415 μmol , 1.0 eq.) were refluxed for 4 h in dry toluene (7 ml) under argon. After cooling to room temperature, the yellow precipitate was filtered off, washed with toluene (10 ml) and diethyl ether (2×10 ml) and dried under vacuum.

Yield: 175.0 mg (368 μmol , 89%).

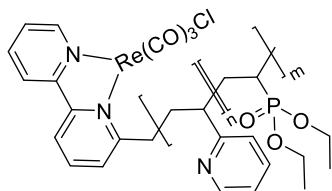
$^1\text{H NMR}$ (300 MHz, Acetone- d_6 , 298 K): δ (ppm) = 9.17 (ddd, $J = 5.5, 1.6, 0.8$ Hz, 1H), 8.48 (dt, $J = 8.3, 1.1$ Hz, 1H), 8.42 – 8.34 (m, 1H), 8.28 (ddd, $J = 8.3, 7.6, 1.6$ Hz, 1H), 8.15 (t, $J = 7.9$ Hz, 1H), 7.78 – 7.74 (m, 1H), 7.72 (ddd, $J = 7.6, 5.5, 1.3$ Hz, 1H), 3.12 (s, 3H)

UV/VIS (DMF): $\lambda_{\text{max}} = 365$ nm

PL (DMF): $\lambda_{\text{max}} = 620$ nm

EA:	calculated:	C 35.33	H 2.12	N 5.89
	found:	C 35.18	H 2.01	N 5.85

Re-2VP-DEVP-block copolymers ($\mathbf{AB}^1_{\text{Re}} - \mathbf{AB}^4_{\text{Re}}$):



Equimolar amounts of the respective block copolymer $\mathbf{AB}^1 - \mathbf{AB}^4$ and $[\text{Re}(\text{CO})_5\text{Cl}]$ were refluxed overnight in dry toluene (10 ml) under argon. After cooling to room temperature, the solvent was removed and the yellow product was dried under vacuum.

UV/VIS (DMF): $\lambda_{\text{max}} = 365 \text{ nm}$

PL (DMF): $\lambda_{\text{max}} = 620 \text{ nm}$.

2. NMR Kinetics of C-H bond activation

Conversion of Complex 1 to 2:

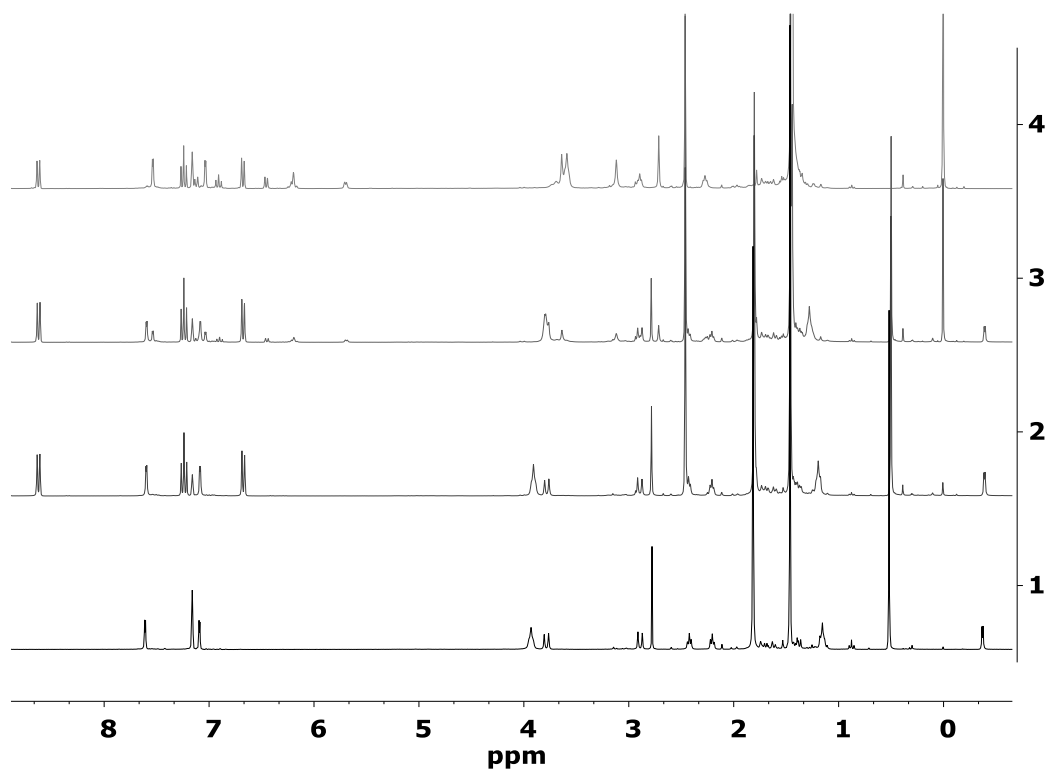


Figure S1: ¹H NMR kinetic for the C-H bond activation of 6,6'-dimethyl-2,2'-bipyridine with complex **1** in C₆D₆. **1)** Complex **1**. **2)** Immediate after addition of 6,6'-dimethyl-2,2'-bipyridine. **3)** 120 Min; 60 °C. **4)** 4 days; 60 °C.

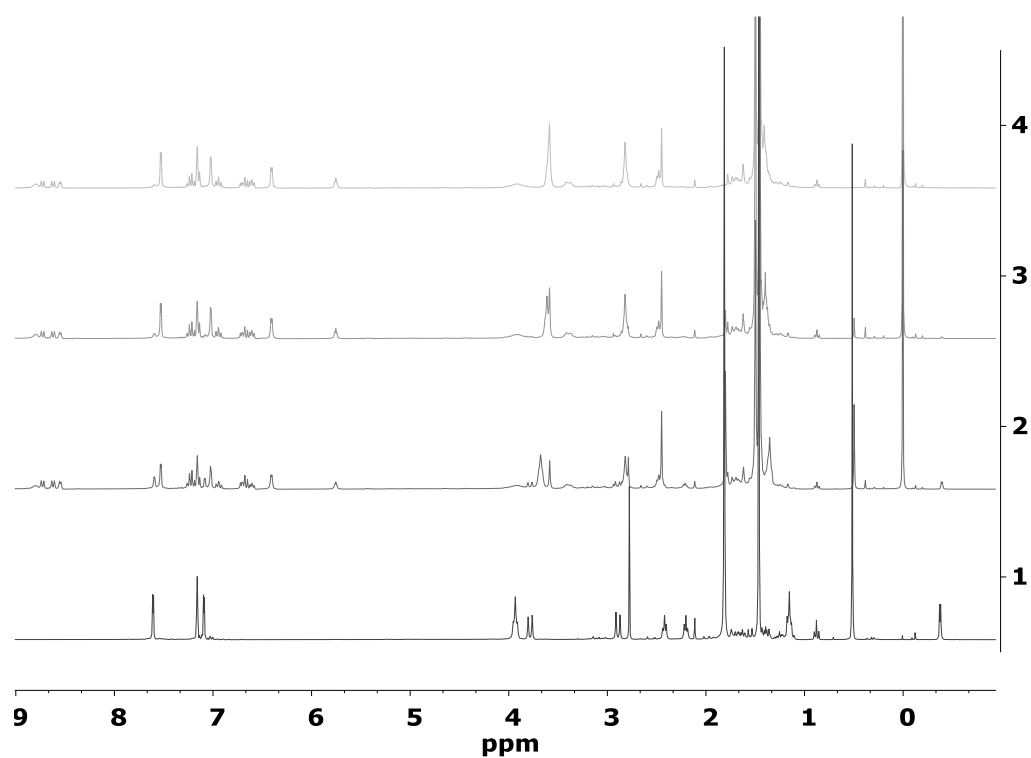
Conversion of Complex 1 to 3:

Figure S2: ¹H NMR kinetic for the C-H bond activation of 6-methyl-2,2'-bipyridine with complex 1 in C₆D₆. 1.) Complex 1. 2) Immediate after addition of 6-methyl-2,2'-bipyridine. 3) 2 h; 25 °C. 4) 8 h; 25 °C.

3. ESI-MS of Oligomeric 2VP

Oligomer produced with catalyst 3

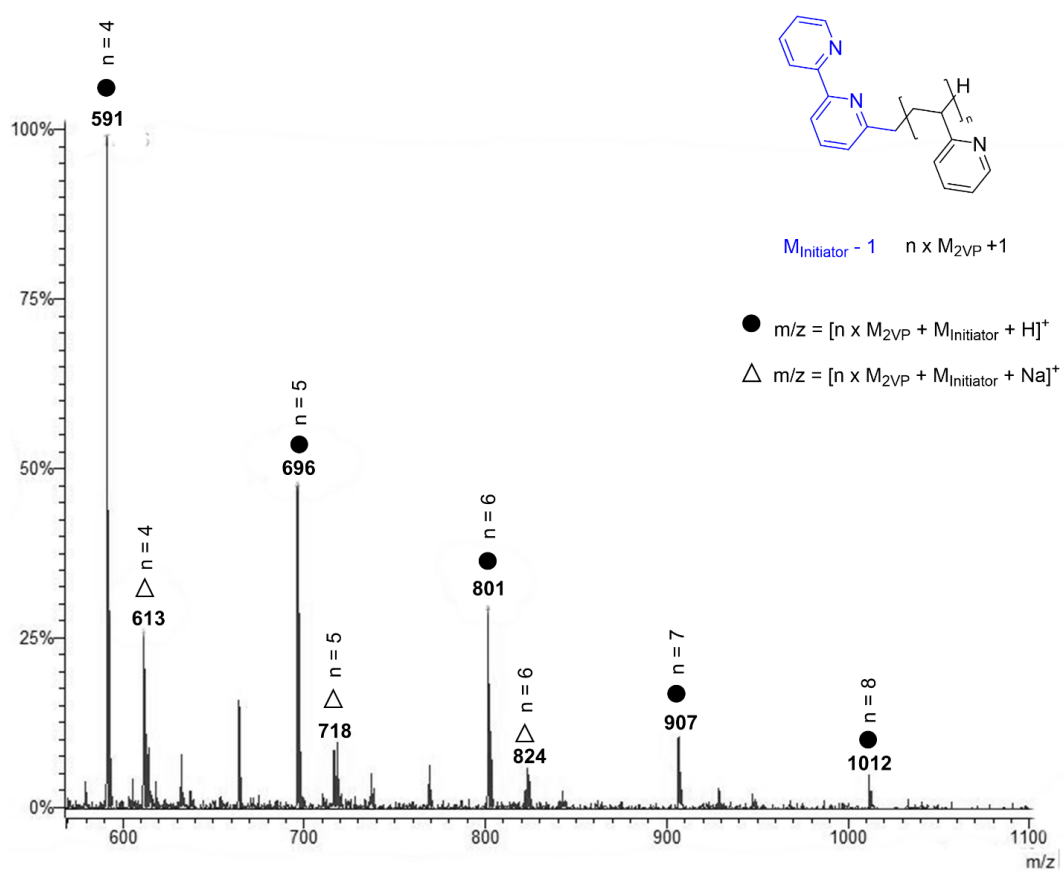


Figure S3: End-group analysis ESI-MS measured in acetonitrile with catalyst 3 and 2-vinylpyridine (11 μmol of catalyst, 0.38 mmol 2VP, 2 ml toluene, 20 $^{\circ}\text{C}$).

4. NMR-spectra of P2VP

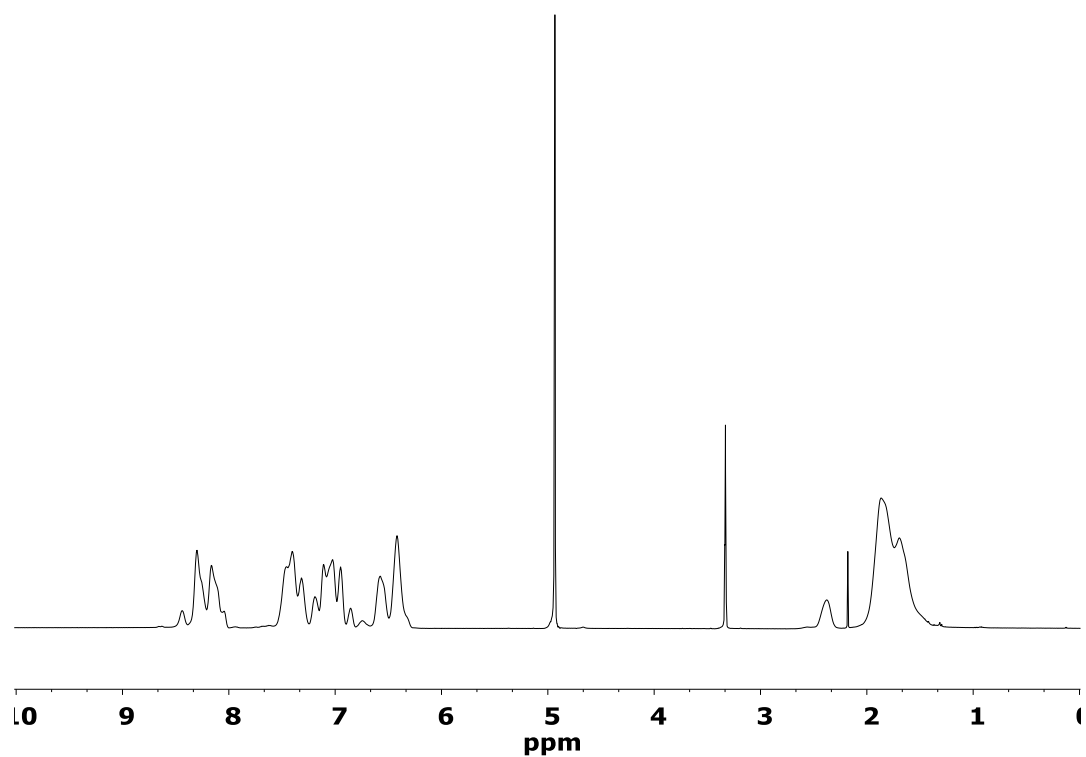


Figure S4: ¹H-NMR spectrum of P2VP produced with catalyst **3** (Table 1, Entry 3, CD₃OD, 500 MHz)

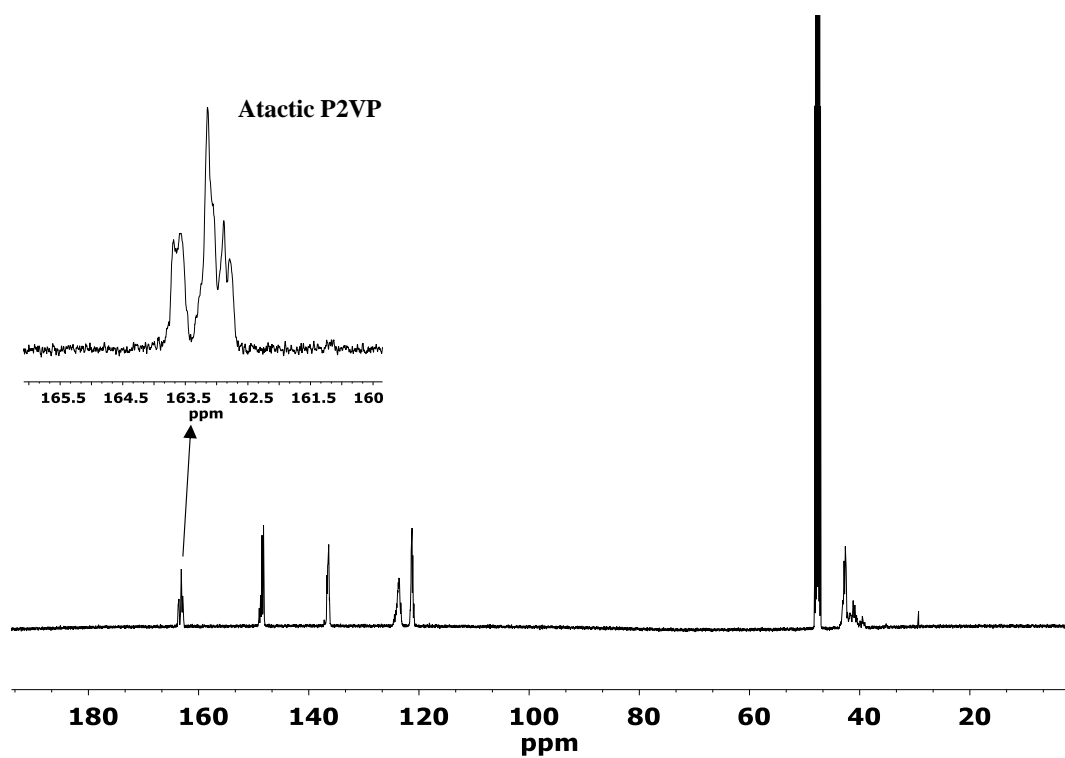


Figure S5: ^{13}C -NMR spectrum of P2VP produced with catalyst 3 (Table 1, Entry 3, CD_3OD , 126 MHz)

5. NMR-spectra of P2VP-PDEVp block copolymers

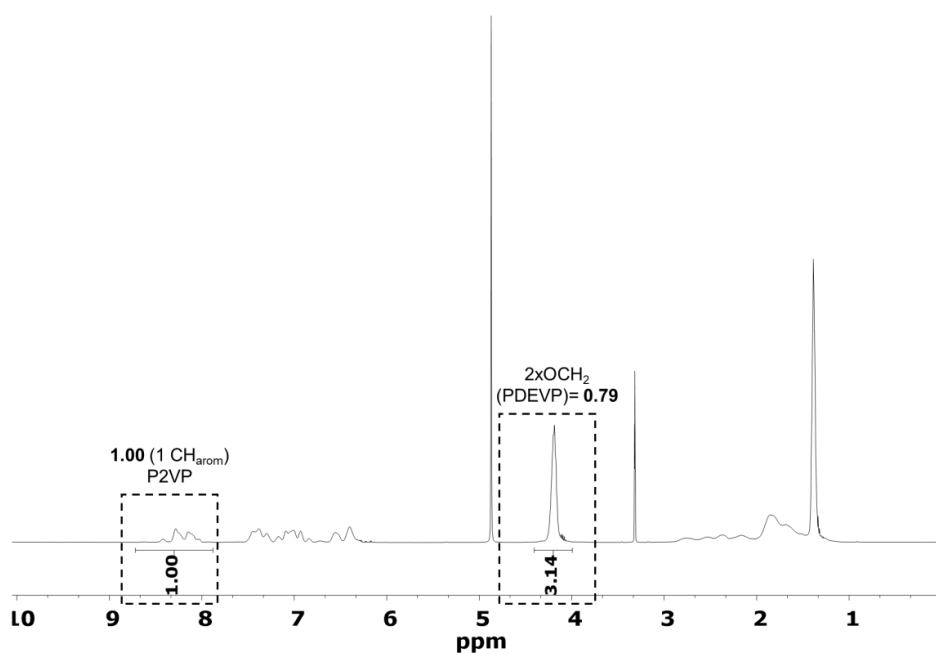


Figure S6: $^1\text{H-NMR}$ spectrum of a P2VP-PDEVp block copolymer produced with catalyst **3** (Table 2, Entry 1, CD_3OD , 500 MHz)

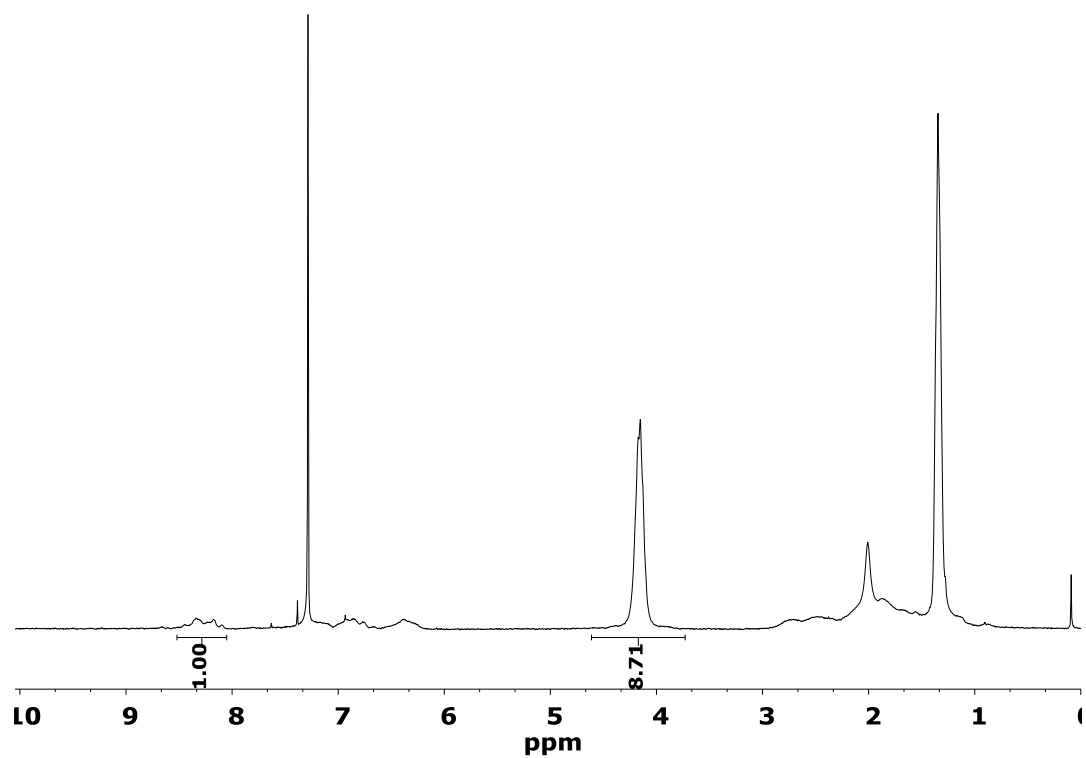


Figure S7: ¹H-NMR spectrum of a P2VP-PDEV block copolymer produced with catalyst **3** (Table 2, Entry 4, CDCl₃, 500 MHz)

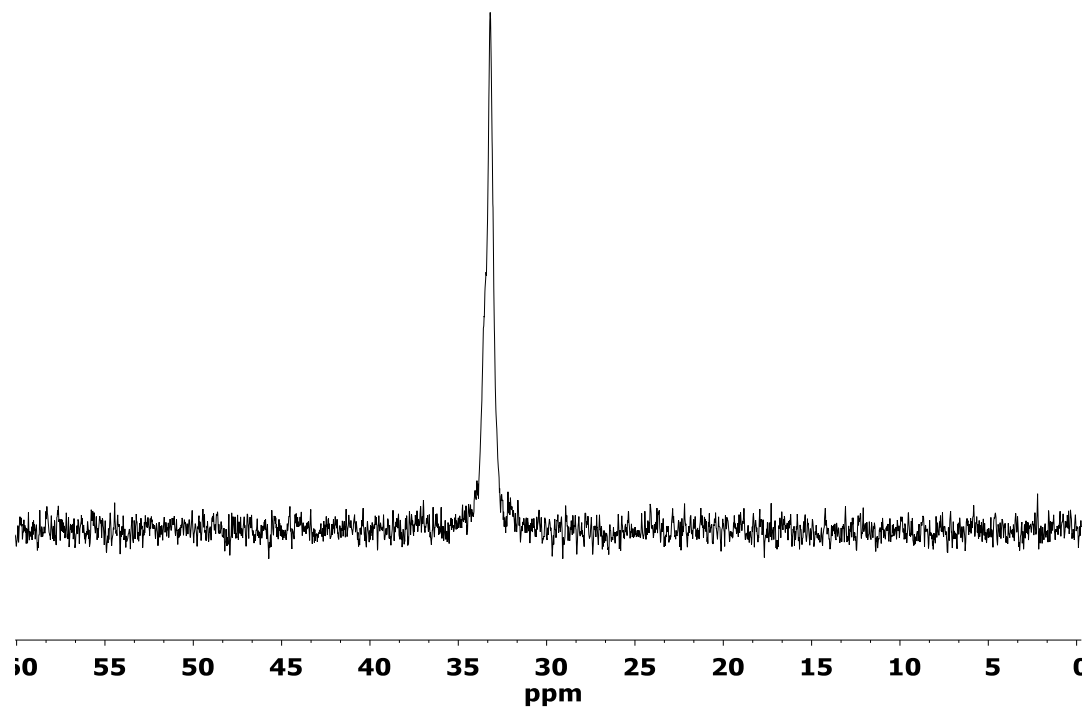
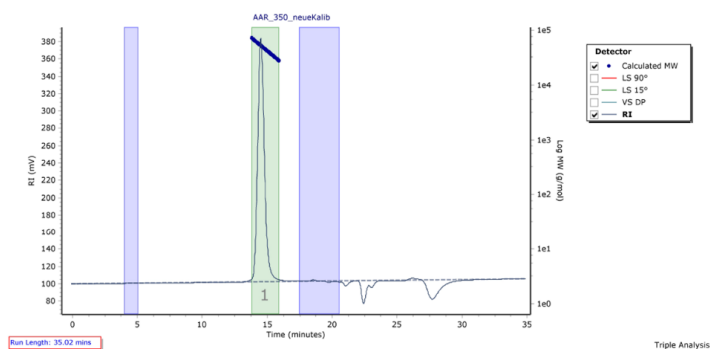


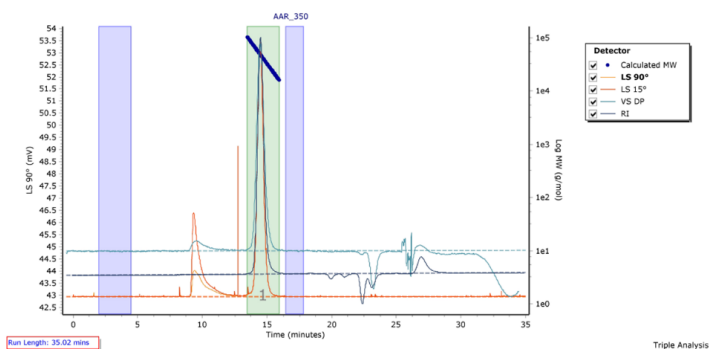
Figure S8: ^{31}P -NMR spectrum of a P2VP-PDEVp block copolymer produced with catalyst **3** (Table 2, Entry 4, CDCl_3 , 122 MHz)

6. GPC traces of polymers

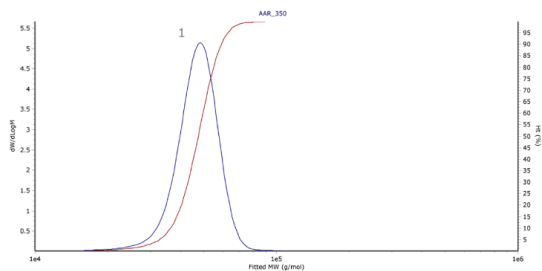
Chromatogram Plot



Chromatogram Plot



Distribution Plot

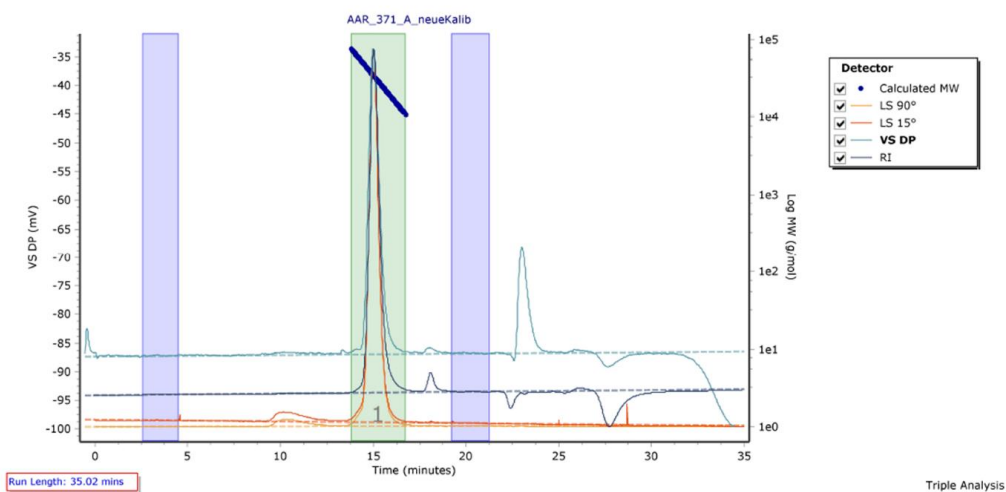


Molecular Weight Averages

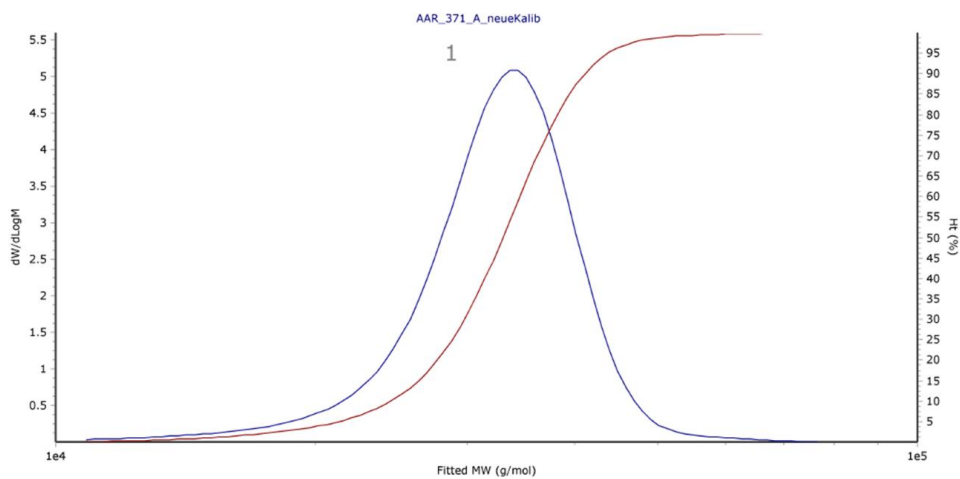
Peak	Mp (g/mol)	Mn (g/mol)	Mw (g/mol)	Mz (g/mol)	Mz+1 (g/mol)	Mv (g/mol)	PD
Peak 1	48475	45583	47612	49461	51253	49040	1.045

Figure S9: GPC trace of P2VP produced with catalyst **3** (Table 1, Entry 3). GPC-trace of the light-scattering detectors show signals at 10 min, which are not detectable *via* RI (first chromatogram); therefore these signals do not belong to polymeric material.

Chromatogram Plot



Distribution Plot

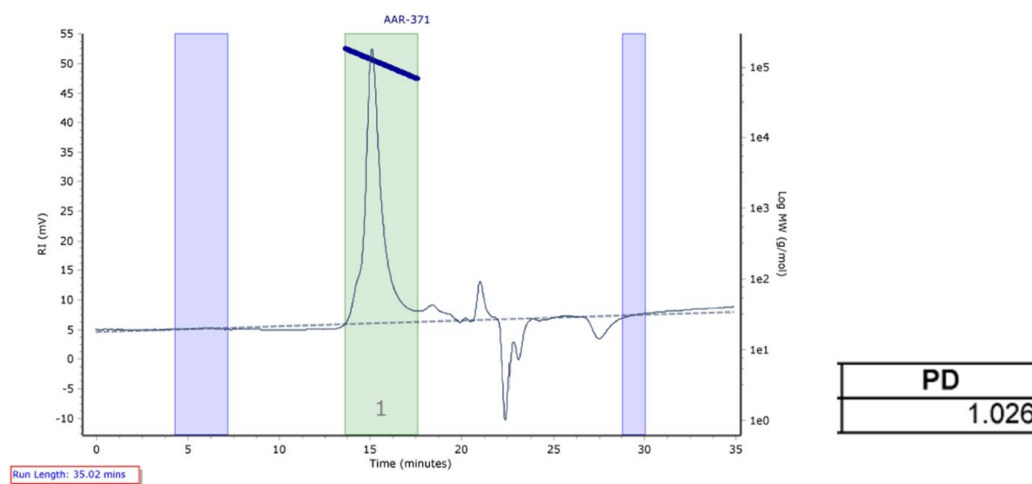


Molecular Weight Averages

Peak	Mp (g/mol)	Mn (g/mol)	Mw (g/mol)	Mz (g/mol)	Mz+1 (g/mol)	Mv (g/mol)	PD
Peak 1	34022	31282	32975	34470	35903	33933	1.054

Figure S10: GPC trace of P2VP block A of a AB^1 produced with catalyst 3 (Table 2, Entry 1). GPC-trace of the light-scattering detectors show signals at 10 min, which are not detectable *via* RI; therefore these signals do not belong to polymeric material.

Chromatogram Plot



Distribution Plot

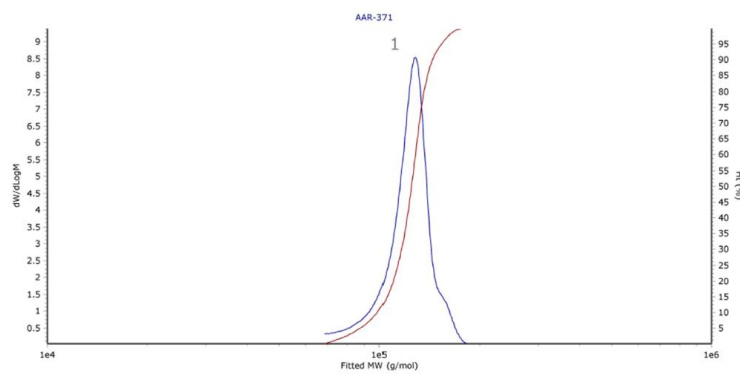


Figure S11: Polydispersity determination with the RI detector of the GPC of AB¹ produced with catalyst 3 (Table 2, Entry 1).

7. Supplementary UV/VIS and PL Spectra

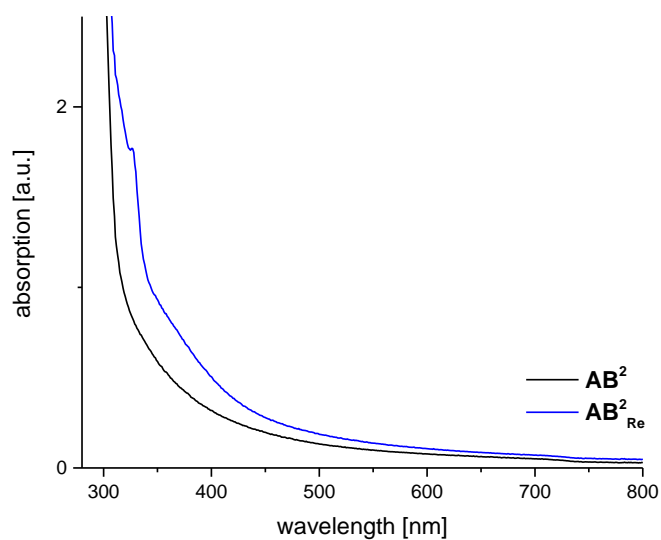


Figure S12: UV/VIS spectra of 0.8 wt.% solutions in water of AB^2 (black) and AB^2_{Re} (blue) in water.

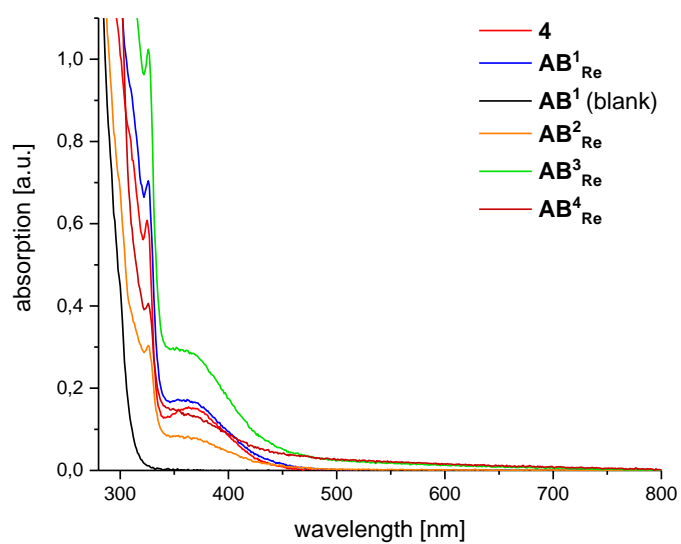


Figure S13: UV/VIS spectra of catalyst 4, AB^1 , AB^1_{Re} , AB^2_{Re} , AB^3_{Re} , and AB^4_{Re} .

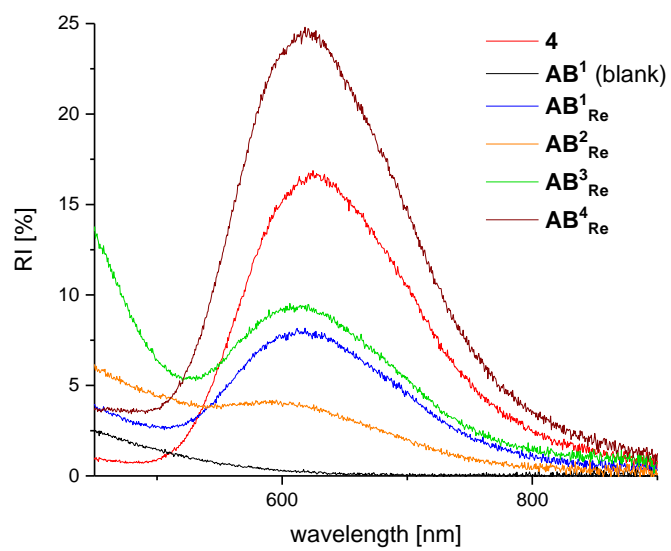


Figure S14: PL spectra of catalyst **4**, **AB¹**, **AB¹_{Re}**, **AB²_{Re}**, **AB³_{Re}**, and **AB⁴_{Re}**.

8. AB-Block copolymer produced with catalyst 1

Table S1: Synthesis of unfunctionalized P2VP-DEVP block copolymer produced with catalyst 1. ^[a]

Feed ^[b] [A]/[B]	Conversion _A ^[c] [%]	M _{n, GPC, A} ^[d] [10 ³ g/mol]	Conversion _B ^[e] [%]	M _{n, NMR, AB} ^[f] [10 ³ g/mol]	D _{AB} ^[g]	Composition ^[h] A _{eq} /B _{eq.} (ratio A:B)
50/90	99	13.2	83	44.7	1.09	125/190 (1:1.53)

[a] [Cat] = 21.4 μmol, 2.5 mL CH₂Cl₂, r.t. [b] [A] = [2VP]/[cat.]; [B] = [DEVP]/[cat.] [c] Determined via ¹H-NMR spectroscopy [d] M_{n, GPC, A} = absolute molar mass of block A, determined by GPC with multi angle light scattering in thf/water (1:1; v:v), 9 g/L tetrabutylammonium bromide (TBAB) and 680 mg/L THF 3,5-di-tert-butyl-4-hydroxytoluene (BHT) [e] Calculated from ³¹P-NMR spectroscopy [f] Determined via composition and M_{n, GPC, A} [g] Determined by GPC (M_w/M_n of the block copolymers) [h] Calculated via ¹H-NMR spectroscopy .

9. Photocatalytic Reduction of CO₂

In all photocatalytic experiments carried out, CO was the only product detected by GC-analysis. ¹H-NMR spectroscopy of the reaction solution does not show any MeOH, formic acid or formaldehyde signals. In addition, no signals for ethanol or pyridine-species are visible, therefore no decomposition of PDEVP or P2VP occurs during the reaction due to side reactions. Experiments either without catalyst, light, TEOA or CO₂ do not lead to any CO production.

Table S2: TONs (CO) during photocatalytic reduction of CO₂ using catalyst 4-7. Reaction conditions: Irradiation of CO₂-saturated DMF/TEOA ([TEOA]=1.7 M) solution containing 0.1 mM catalyst using LED light source (λ = 450 nm).

Catalyst	TON
7	5.1
6	10
5	9.7
4	9.5

Table S3: TONs (CO) during photocatalytic reduction of CO₂ using AB¹_{Re} – AB⁴_{Re} and **4**. Reaction conditions: Irradiation of CO₂-saturated DMF/TEOA ([TEOA]=1.2 M) solution containing 0.1 mM catalyst using LED light source (λ = 450 nm).

Catalyst	TON
4	6.5
AB¹_{Re}	13
AB²_{Re}	13
AB³_{Re}	8.5
AB⁴_{Re}	8.5

10.Literature

1. K. C. Hultsch, P. Voth, K. Beckerle, T. P. Spaniol and J. Okuda, *Organometallics*, 2000, **19**, 228-243.
2. P. T. Altenbuchner, B. S. Soller, S. Kissling, T. Bachmann, A. Kronast, S. I. Vagin and B. Rieger, *Macromolecules* 2014, **47**, 7742-7749.
3. S. A. Savage, A. P. Smith and C. L. Fraser, *J. Org. Chem.*, 1998, **63**, 10048-10051.
4. M. Brigodiot, H. Cheradame, M. Fontanille and J. P. Vairon, *Polymer*, 1976, **17**, 254-256.
5. P. T. Altenbuchner, F. Adams, A. Kronast, E. Herdtweck, A. Pöthig and B. Rieger, *Polym. Chem.*, 2015, **6**, 6796-6801.

14.4 Supporting Information: “Next Generation Multiresponsive Nanocarriers for Targeted Drug Delivery to Cancer Cells”

CHEMISTRY

A European Journal

Supporting Information

Next Generation Multiresponsive Nanocarriers for Targeted Drug Delivery to Cancer Cells

Peter T. Altenbuchner^{+, *^[a]} Patrick D. L. Werz^{+, ^[a]} Patricia Schöppner^{+, ^[b]} Friederike Adams,^[a]
Alexander Kronast,^[a] Christina Schwarzenböck,^[a] Alexander Pöthig,^[c] Christian Jandl,^[c]
Martin Haslbeck,^[b] and Bernhard Rieger^{*,^[a]}

chem_201601822_sm_miscellaneous_information.pdf

Supporting Information for the Manuscript Entitled Next Generation of Multi-Responsive Nanocarriers for the Targeted Drug Delivery to Cancer Cells

Peter T. Altenbuchner*,^{¶[a]} Patrick D. L. Werz,^{¶[a]} Patricia Schöppner,^{¶[b]} Friederike Adams,^[a]
Alexander Kronast,^[a] Christina Schwarzenböck,^[a] Alexander Pöthig,^[c] Christian Jandl,^[c] Martin
Haslbeck,^[b] and Bernhard Rieger*^[a]

[a] Dr. P.T. Altenbuchner, P.D.L. Werz, F. Adams, A. Kronast, C. Schwarzenböck, Prof. Rieger
WACKER-Lehrstuhl für Makromolekulare Chemie,
Technische Universität München, Lichtenbergstraße 4, 85748 Garching bei München, Germany

[b] P. Schöppner, Dr. M. Haslbeck
Center for Integrated Protein Science Munich (CIPSM) and Lehrstuhl für Biotechnologie, Technische Universität München, Lichtenbergstraße 4, 85748
Garching bei München, Germany

[c] Dr. A. Pöthig, C. Jandl
Department Chemie & Catalysis Research Center, Technische Universität München, Ernst-Otto-Fischer-Straße 1, 85748 Garching bei München,
Germany

Table of Contents

1. Experimental procedure	2
2. NMR-kinetic-investigations	9
3. Crystallographic Details	11
4. Polymerization investigations	16
5. NMR-Analysis of Polymers	21
6. Characterization of micelles	29

1. Experimental procedure

Materials and Methods.

All reactions were carried out under argon atmosphere using standard Schlenk or glovebox techniques. All glassware was heat dried under vacuum prior to use. Unless otherwise stated, all chemicals were purchased from Sigma-Aldrich, Acros Organics, or ABCR and used as received. Toluene, thf, diethylether dichloromethane and pentane were dried using a MBraun SPS-800 solvent purification system. Hexane was dried over 3 Å molecular sieves. The precursor complexes $Y(CH_2Si(CH_3)_3)_3(thf)_2$ and $LiCH_2TMS$ and catalysts **1** are prepared according to literature procedures.¹ 2-vinylpyridine (2VP) and the diethyl vinyl phosphonate (DEVP) was dried over calcium hydride and distilled prior to use. NMR spectra were recorded on a Bruker AVIII-300 and AVIII-500 Cryo spectrometer. Unless otherwise stated, ¹H- and ¹³C-NMR spectroscopic chemical shifts δ are reported in ppm relative to the residual proton signal of the solvent. δ (¹H) is calibrated to the residual proton signal, δ (¹³C) to the carbon signal of the solvent. Unless otherwise stated, coupling constants J are averaged values and refer to couplings between two protons. Deuterated solvents were obtained from Sigma-Aldrich and dried over 3 Å molecular sieves.

Elemental analyses were measured at the Laboratory for Microanalysis at the Institute of Inorganic Chemistry at the Technische Universität München.

Single Crystal X-ray Crystallography was performed in the SCXRD laboratory of the Catalysis Research Center at Technische Universität München. Additional crystallographic information is given below.

Homopolymerization Procedures.

To a solution of 13.5 μ mol catalyst (1.0 eq.) in 2 mL toluene at room temperature, 2.7 mmol monomer (200 eq.; 27 mmol [2VP]/ 20 mL toluene) was added in one portion. The polymerization is quenched by addition of methanol. Conversion is determined by ¹H-NMR-spectroscopy of an aliquot taken before quenching of the reaction. The polymers were precipitated by addition of the reaction mixtures to pentane (100 mL) and the solution was decanted of. Residual solvent was removed by freeze-drying from benzene (100 mL) over night. Molecular weights and polydispersities are measured via GPC.

Copolymerization Procedures.

After dissolving the calculated amount of catalyst in dichloromethane at room temperature, the respective equivalents of 2-vinylpyridine were added in one portion. The reaction mixture was stirred for 90 minutes. One aliquot (0.1 mL) was taken and quenched by the addition of 0.4 mL CD₃OD (calculation of conversion of 2-vinylpyridine via ¹H-NMR) in an NMR-tube while the calculated amount of a second monomer (or mixture of two dialkyl vinyl phosphonates) was added to the

reaction solution, stirred overnight and quenched by addition of 0.5 mL MeOH. Before quenching an aliquot is taken and quenched with 0.5 mL CD₃OD in an NMR tube to calculate the conversion of vinylphosphonates via ³¹P-NMR-spectroscopy. The polymers were precipitated by addition of the reaction mixtures to pentane (150 mL) and decanted from solution. Residual solvent was removed by freeze-drying from benzene or water (100 mL) over night. The polymer of the aliquot of the first polymerization-sequence is dried under vacuum at 60 °C overnight.

Molecular-weights and molecular-weight-distributions of the first polymerization sequence are measured via GPC-MALS analysis of the first aliquot. Composition A/B [2VP/DEVP] is determined via ¹H-NMR-spectroscopy of the dried block copolymer. The molecular-weight of the block copolymer is determined with the help of the composition A/B and the molecular weight of the first block. Molecular-weight-distributions are determined via GPC-MALS analysis.

Kinetic measurements of 2-vinylpyridine by aliquots method.

To a solution of 135 μmol catalyst in 20 mL toluene at room temperature, the corresponding amount of monomer (27 mmol, 200 eq.) was added in one portion. Aliquots were taken from the reaction solution at regular time intervals and quenched by addition of MeOH. Solvent and not polymerized monomer were removed by drying the polymers under vacuum at 60 °C overnight. For each aliquot, the conversion is determined gravimetrically and the molecular weight of the polymer is determined by GPC-MALS analysis.

Characterization of Polymer-Samples.

The tacticity determination of P2VP was performed by ¹³C-NMR-spectroscopy at room temperature. Spectra for the analysis of P2VP *mm*, *mr/rm* and *rr* triads were recorded with a sample concentration of 15% (w/w; 75 mg/0.6 mL CD₃OD) on a AVIII 500 Cryo spectrometer and analyzed according to literature.²

Gel permeation chromatography (GPC) was carried out with samples of 5 mg/mL concentration on a Varian LC-920 equipped with two PL Polargel columns. As eluent a mixture of THF/water (1:1; v:v), 9 g/L tetrabutylammonium bromide (TBAB) and 680 mg/L_{THF} 3,5-di-tert-butyl-4-hydroxytoluene (BHT) was used. Absolute molecular weights have been determined online by multiangle light scattering (MALS) analysis using a Wyatt Dawn Heleos II in combination with a Wyatt Optilab rEX as concentration source.

Lower critical solution temperature (LCST)-measurements were carried out on a Cary 50 UV-Vis spectrophotometer from Varian. The LCST was determined by spectrophotometric detection of the changes in transmittance at $\lambda = 500$ nm of the aqueous polymer solutions (2.5mg/mL). The heating/cooling rate was 1.0 K/min in steps of 1 K followed by a 5 min period of constant temperature to ensure equilibration. For determination of the transition hysteresis, equilibration periods of 3, 1.5, 0.75, 0.5, and 0.25 min or no equilibration period was used. The cloud point was defined as the temperature corresponding to a 10% decrease in optical transmittance.

Preparation of micelles.

To obtain Nile red-loaded micelles, firstly Nile red was dissolved in DMSO ($c = 0.3 \text{ mg/mL}$). Under continuous stirring the Nile red solution was added dropwise to the freshly prepared blank-micelle solution (Micelle/Nile-Red = 1/10). The mixture was then stirred for 1 hour followed by overnight dialysis against water (MWCO: 6000 – 8000). Afterwards non-encapsulated Nile red was removed by an additional centrifugation step at 4000 rpm for 10 min at room temperature. The supernatant was transferred into a new reaction tube.

The preparation of fluorescein-loaded micelles were performed in the same way.

For the preparation of DOX-loaded micelles 1.5 equivalents of triethylamine were added dropwise to a DOX-HCl DMSO solution and stirred for 1 hour in a cold water bath. Afterwards the DOX DMSO solution was added slowly to the freshly prepared blank-micelle solution under continuous stirring. The mixture was then stirred for 1 hour followed by overnight dialysis against water (MWCO: 6000 – 8000). Free Doxorubicine aggregates were separated from the DOX-loaded micelles by centrifugation of the dialyzed solution at 4.000 rpm for 10 min and transfer of the supernatant DOX-loaded micelle solution to a fresh Eppendorf tube.

For the calculation of the exact DOX concentration in the DOX-loaded micelles a standard curve of DOX fluorescence intensity against DOX concentration ranging from $0.05 \mu\text{g mL}^{-1}$ to $2.00 \mu\text{g mL}^{-1}$ was determined. Here for the DOX fluorescence was measured on a spectrofluorometer FP-8500 (excitation wavelength: 505 nm, emission wavelength: 556 nm, slit width: 5nm, Jasco, Großumstadt, Germany) at room temperature. Prior the fluorescence measurements of the DOX-loaded micelles, the encapsulated DOX was extracted by an acidic pH shift to pH 2, leading to the disruption of the micelles. Before the addition of HCl to the aqueous solution 10-fold dilutions of the DOX-loaded micelles were prepared for extraction.

Fluorescence spectroscopy measurements.

To study the drug release of DOX-loaded BAB₃ micelles at acidic pH conditions *in vitro*, emission fluorescence spectra of BAB₃ micelles, DOX-loaded micelles and non-encapsulated DOX were recorded by direct excitation of DOX at 505 nm (slit width: 5nm). The measurements were carried out on a spectrofluorometer FP-8500 (Jasco, Großumstadt, Germany) at room temperature. Spectra were measured at pH = 7.4 and pH = 2.0 and compared to the respective non-encapsulated DOX emission spectra. To achieve the full disruption of the BAB₃ micelles or the DOX-loaded BAB₃ micelles, the pH was shifted from pH 7.4 to pH 2 and the samples were incubated for additional 3 h at room temperature prior the measurements. A concentration of $1 \mu\text{g mL}^{-1}$ of DOX-loaded micelles was used.

Cumulative release

Fluorescein-loaded micelles were prepared as mentioned above. One batch of freshly prepared micelles was splitted into three equal parts of 15 mL each and filled into dialysis tubes (MWCO: 6.000 – 8.000). The first sample (reference) was put into 500 mL deionized water, the second sample into

4

500 mL deionized water and put into a preheated water bath (44 °C) (temperature release), and the third sample was put into 100 mL Britton-Robinson buffer (pH = 4.5) (pH release). Samples of 1 mL were drawn regularly for 24 h and the beaker refilled with the appropriate amount of fresh water/buffer. The samples were then measured via fluorescence spectrometer and quantitatively analyzed against a freshly prepared calibration curve consisting of 10 known concentrations.

Cell culture.

In vitro studies on non-loaded micelles, Nile red-loaded micelles, and DOX-loaded micelles were performed in HeLa cells. Cells were cultured in Dulbecco's Modified Eagle Medium (Invitrogen molecular probes, Darmstadt, Germany) equipped with 10 % (v/v) Fetal Calf Serum (BioConcept, Allschwil, Switzerland) at 37 °C in a humidified atmosphere containing 5 % CO₂. For splitting and sub-culturing of cells Trypsin-EDTA 0.5 % (Invitrogen molecular probes, Darmstadt, Germany) was used.

Cellular uptake of loaded micelles.

To analyze the cellular uptake of the different micelles (BAB₂, BAB₃), HeLa cells were grown overnight on CC2-coated 2-well glass slides (Nalgen Nunc International, Roskilde, Denmark, 3 x 10⁴ cells/well). HeLa cells were then treated with Nile red-loaded micelles and incubated for additional 3 hours at 37 °C in a humidified atmosphere containing 5 % CO₂.

The intracellular drug release was studied with DOX-loaded micelles or non-encapsulated DOX at a final concentration of 3 µg mL⁻¹, by treatment of HeLa cells, for 3 h or 6 h at 37 °C in a humidified atmosphere containing 5 % CO₂. The nuclei were stained with Hoechst 33342 (Sigma-Aldrich, St. Louis, USA) for 5 min at room temperature. After washing the cells three times with DPBS (Invitrogen molecular probes, Darmstadt, Germany) the cells were further analyzed by fluorescence light microscopy using a Zeiss Axiovert 200 microscope (Zeiss, Jena, Germany), equipped with a Hamamatsu C4742-95 camera (Hamamatsu, Herrsching, Germany). Pictures were taken with a 63 x oil lenses. Images were processed with ImageJ.

Cell viability studies.

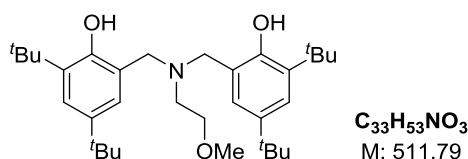
The growth inhibition of DOX on HeLa cells, was determined by analyzing the cell viability of HeLa cells in presence of increasing concentrations of non-encapsulated DOX (1 µg mL⁻¹ to 8 µg mL⁻¹) and DOX-loaded micelles (1.2 µg mL⁻¹ to 6.3 µg mL⁻¹). Prior to the addition of non-encapsulated DOX or DOX-loaded micelles to the HeLa cells, cells were grown overnight in Sigma[®] Cell Culture 24-well plates (Sigma-Aldrich, St. Louis, USA, 1 x 10⁴ cells/well). After 3 hours of incubation at 37 °C in a humidified atmosphere with 5% CO₂, the cell viability of the treated cells was determined using the AlamarBlue[®] Cell Viability Reagent (Invitrogen molecular probes, Darmstadt, Germany) according to the manufacturer's instruction. Untreated HeLa cells were used as a positive control. For determination of the exact loaded DOX concentration additional fluorescence spectroscopy measurements (Ex.: 505 nm) were performed with every loaded sample of DOX. Prior to the

fluorescence emission measurements of the respective DOX-loaded micelles, aqueous 10-fold dilutions were prepared and the encapsulated DOX was then extracted by an acidic pH shift to pH 2, leading to the disruption of the micelles. For the calculation of the respective DOX-loaded concentrations the linear fit equation $y = 424.65x + 31.233$ was used. The standard curve was achieved by measuring fluorescent emission spectra of non-encapsulated DOX at 505 nm excitation, with increasing concentrations of DOX ($0.05 \mu\text{g mL}^{-1}$ to $2.00 \mu\text{g mL}^{-1}$) at acidic pH conditions (pH = 2). Plotted are the DOX concentrations against the corresponding fluorescence intensities at 556 nm of each DOX concentration measured.

To exclude a negative influence of the non-loaded micelles on the cell viability, additional cell viability measurements were performed with increasing concentrations of non-loaded micelles ($100 \mu\text{g mL}^{-1}$ to $1000 \mu\text{g mL}^{-1}$). Shown are mean values of at least three independent biological replicates and the respective standard deviations are indicated.

Ligand synthesis: **$\text{H}_2(\text{ONOO})^{\text{tBu}}$**

A solution of 2.0 equivalents of 2,4-di-tert-butylphenol, 1.0 equivalents 2-methoxyethylamine and aqueous formaldehyde-solution (36% in water; 3.0 eq.) in methanol were refluxed for 10 days. The mixture was cooled and the colorless solid was separated via filtration. After double recrystallization from ethanol the product is yielded as colorless crystals.

 **$\text{H}_2(\text{ONOO})^{\text{tBu}}$**

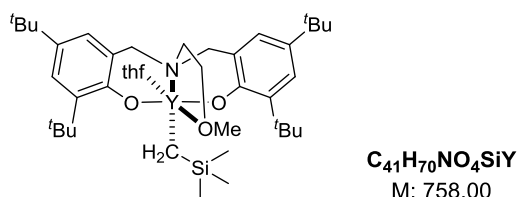
Yield: 45% (colorless crystals)

$^1\text{H-NMR}$ (300 MHz, CDCl_3 , 300 K): δ (ppm) = 8.52 (s, 2H, OH), 7.21 (d, $^4J = 2.5$ Hz, 2H, H_{arom}), 6.88 (d, $^4J = 2.5$ Hz, 2H, H_{arom}), 3.74 (s, 4H, ArCH_2), 3.56 (t, $^3J = 5.1$ Hz, 2H, $\text{H}_{\text{sidearm}}$), 3.47 (s, 3H, OMe), 2.75 (t, $^3J = 5.1$ Hz, 2H, $\text{H}_{\text{sidearm}}$), 1.41 (s, 18H, tBu), 1.27 (s, 18H, tBu).

$^{13}\text{C-NMR}$ (75 MHz, CDCl_3 , 300 K): δ (ppm) = 153.0, 140.8, 136.1, 125.0, 123.5, 121.7, 71.5, 58.9, 58.2, 51.5, 35.1, 34.2, 31.8, 29.7.

Complex synthesis: **$(\text{ONOO})^{\text{tBu}}\text{Y}(\text{CH}_2\text{TMS})(\text{thf})$ (**1**)⁴**

One equivalent of proligand $\text{H}_2(\text{ONOO})^{\text{tBu}}$ in toluene is added to a stirred solution of $\text{Y}(\text{CH}_2\text{Si}(\text{CH}_3)_3)(\text{thf})_2$ in pentane at 0 °C. The resulting solution is stirred overnight at room temperature. The solvent is removed *in vacuo* and the resulting solid is washed and recrystallized from pentane.



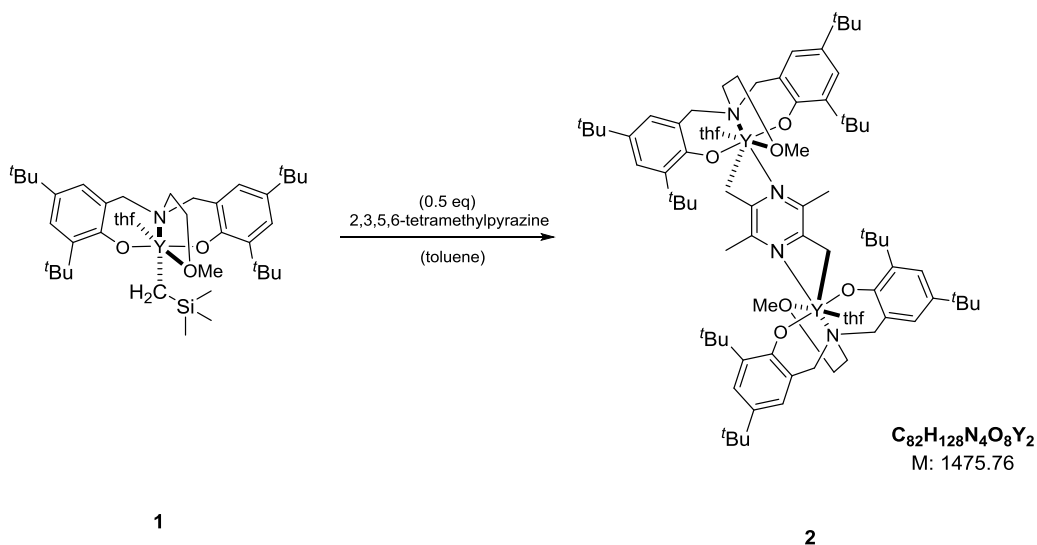
Yield: 43% (colorless solid)

$^1\text{H-NMR}$ (300 MHz, C_6D_6 , 300 K): δ (ppm) = 7.61 (d, $^4J = 2.6$ Hz, 2H, H_{arom}), 7.09 (d, $^4J = 2.6$ Hz, 2H, H_{arom}), 4.00 – 3.89 (m, 4H, H_{THF}), 3.78 (d, $^2J = 12.4$ Hz, 2H, ArCH_2), 2.89 (d, $^2J = 12.4$ Hz, 2H, ArCH_2), 2.78 (s, 3H, OMe), 2.42 (t, $^3J = 5.4$ Hz, 2H, $\text{H}_{\text{sidearm}}$), 2.20 (t, $^3J = 5.4$ Hz, 2H, $\text{H}_{\text{sidearm}}$), 1.81 (s, 18H, tBu), 1.46 (s, 18H, tBu), 1.19 – 1.11 (m, 4H, H_{THF}), 0.52 (s, 9H, H_{TMS}), -0.38 (d, $^2J_{\text{Y,H}} = 3.3$ Hz, 2H, CH_2TMS).

^{13}C -NMR (126 MHz, C_6D_6 , 300 K): δ (ppm) = 161.6 (d, $^2J_{\text{C,Y}} = 1.8$ Hz), 136.8, 136.6, 125.6, 124.4, 124.1, 74.0, 71.7, 64.9, 61.3, 49.3, 35.6, 34.3, 32.3, 30.3, 25.4, 25.1, 4.9.

$(\text{ONOO})^{\text{Bu}}\text{Y}(\text{THF})_2((\text{dimethylpyrazine-diy})\text{dimethyl})$ (2)

Compound 1 (1.0 eq) is dissolved in toluene and 0.5 equivalents of 2,3,5,6-tetramethylpyrazine is added. The solution is stirred over night at 60 °C. The solvent is removed and residue is washed with pentane. The compound is recrystallized from a saturated pentane/thf (5/1) solution at -30 °C.



Yield: 65% (orange solid)

^1H -NMR (300 MHz, C_6D_6 , 300 K): δ (ppm) = 7.61 (d, $^4J = 2.5$ Hz, 4H, H_{arom}), 7.16 (d, $^4J = 2.5$ Hz, 4H, H_{arom}), 4.13 (d, $^3J = 12.5$ Hz, 4H), 3.85 (br s, 8H, H_{THF}), 3.42 (br s, 4H), 3.00 (d, $^2J = 12.5$ Hz, 4H), 2.82 (s, 4H), 2.74 (s, 6H, *OMe*), 2.44 (s, 4H), 2.10 (s, 6H, *Me*_{TPPy}), 1.80 (s, 36H, *t*Bu), 1.48 (s, 36H, *t*Bu), 1.20 (br s, 8H, H_{THF}).

^{13}C -NMR (126 MHz, C_6D_6 , 300 K): δ (ppm) = 162.0 (d, $^2J_{\text{C,Y}} = 2.4$ Hz), 152.4, 136.9, 136.3, 125.8, 124.5, 124.2, 123.1, 72.7, 70.8, 65.3, 59.6, 55.8, 49.3, 35.8, 34.3, 32.3, 30.7, 25.2, 18.9.

EA: calculated: C 66.74 H 8.74 N 3.80

found: C 66.38 H 8.82 N 3.90

2. NMR-kinetic-investigations

CH-bond activation of 2,3,5,6-tetramethylpyrazine with complex 1

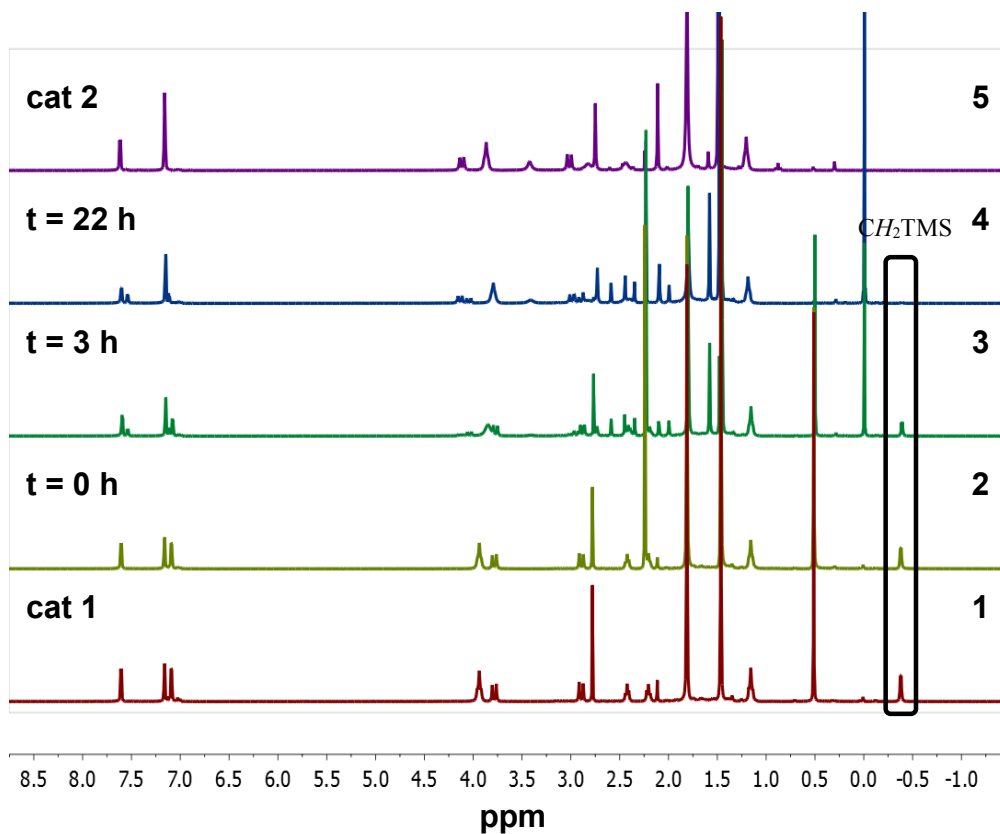
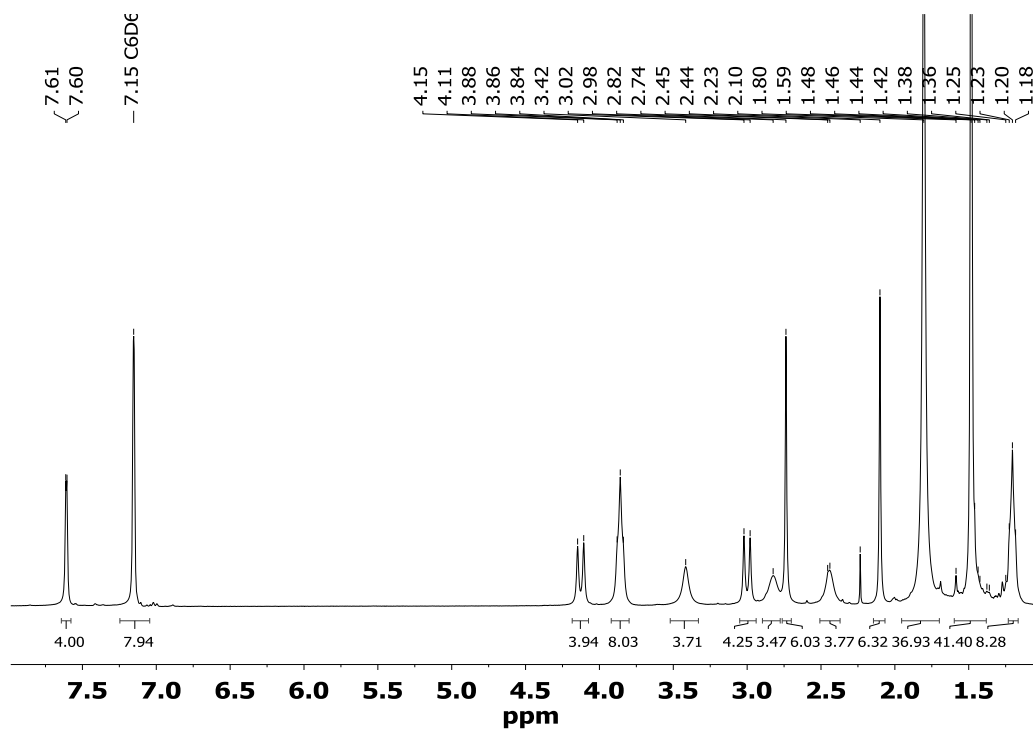


Figure S 1: Time resolved ¹H-NMR-spectra of the C-H-bond activation of 2,3,5,6-tetramethylpyrazine with catalyst 1 and ¹H NMR spectrum of the isolated catalyst 2 in C₆D₆.

¹H-NMR-spectrum of catalyst 2 after recrystallization**Figure S 2:** ¹H-NMR-spectrum of catalyst 2 in C₆D₆.

3. Crystallographic Details

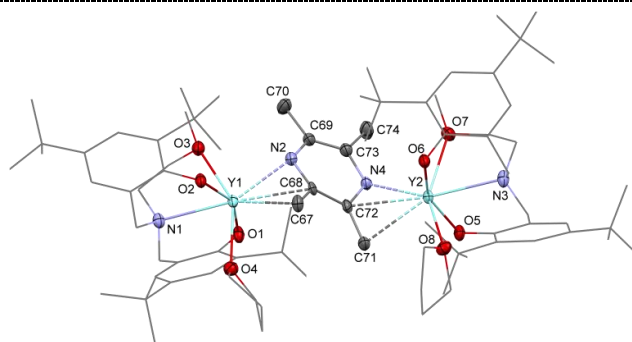
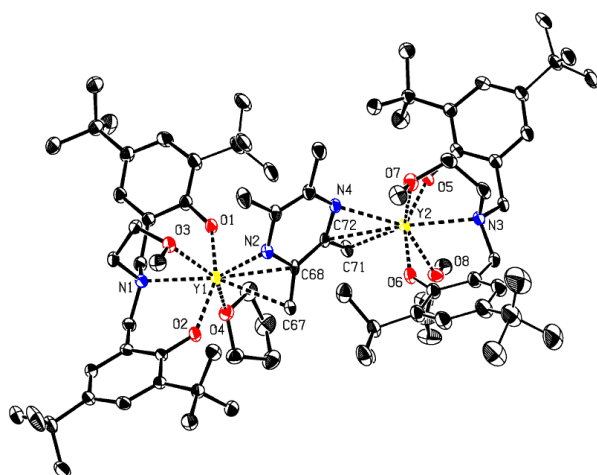
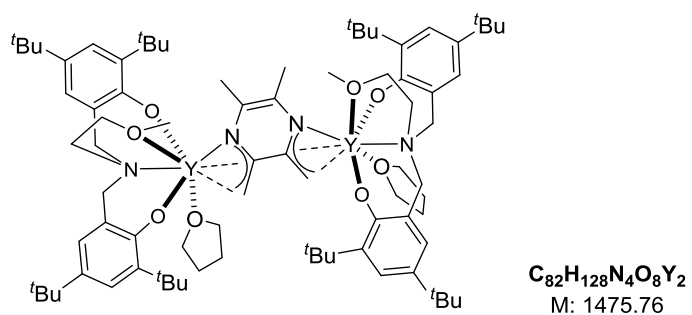
General.

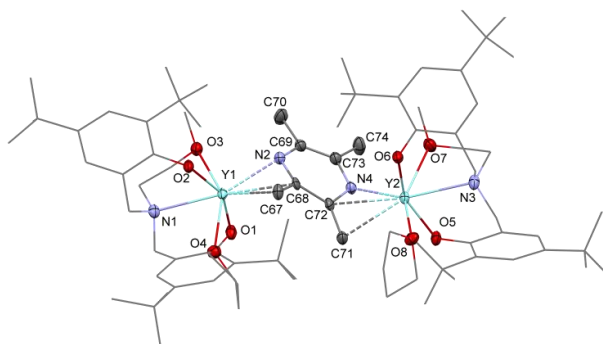
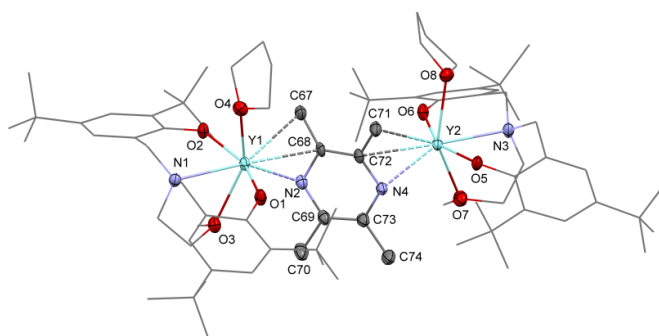
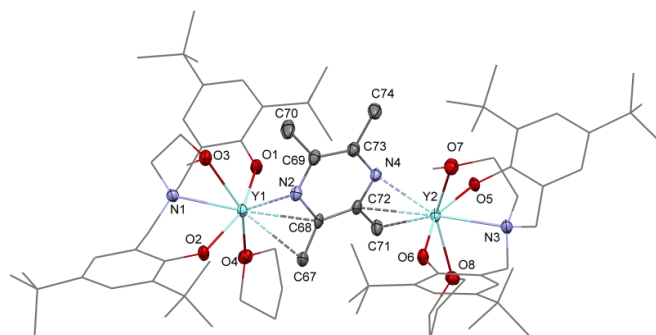
Data were collected on an X-ray single crystal diffractometer equipped with a CCD detector (APEX II, κ -CCD), a rotating anode FR591 and a Montel mirror optic using the SMART software package.⁽ⁱ⁾ The measurements were performed on single crystals coated with perfluorinated ether. The crystals were fixed on the top of a glass fiber and transferred to the diffractometer. Crystals were cooled under a stream of cold nitrogen. A matrix scan was used to determine the initial lattice parameters. Reflections were merged and corrected for Lorentz and polarization effects, scan speed, and background using SAINT.⁽ⁱⁱ⁾ Absorption corrections, including odd and even ordered spherical harmonics were performed using SADABS.⁽ⁱⁱⁱ⁾ Space group assignments were based upon systematic absences, *E* statistics, and successful refinement of the structures. Structures were solved by direct methods with the aid of successive difference Fourier maps,⁽ⁱⁱⁱ⁾ and were refined against all data using the APEX 2 software⁽ⁱ⁾ in conjunction with SHELXL-97 or SHELXL-2014^(iv) and SHELXLE^(v). Methyl hydrogen atoms were refined as part of rigid rotating groups, with a C–H distance of 0.98 Å and $U_{\text{iso(H)}} = 1.5 \cdot U_{\text{eq(C)}}$. Other H atoms were placed in calculated positions and refined using a riding model, with methylene and aromatic C–H distances of 0.99 and 0.95 Å, respectively, and $U_{\text{iso(H)}} = 1.2 \cdot U_{\text{eq(C)}}$. Non-hydrogen atoms were refined with anisotropic displacement parameters. Full-matrix least-squares refinements were carried out by minimizing $\sum w(F_o^2 - F_c^2)^2$ with SHELXL-97^(iv) weighting scheme. Neutral atom scattering factors for all atoms and anomalous dispersion corrections for the non-hydrogen atoms were taken from *International Tables for Crystallography*.^(vi) Disordered groups were treated with a split layer refinement and appropriate constraints were applied to stabilize the refinement. The unit cell of compound 2 contains four disordered molecules of pentane with partial occupancy which were treated as a diffuse contribution to the overall scattering without specific atom positions by SQUEEZE/PLATON.^(vii) Images of the molecular structure in the single crystal were generated with Mercury (Version 3.5.1).^(viii)

References:

- (i) APEX suite of crystallographic software. APEX 2 Version 2013.4. Bruker AXS Inc., Madison, Wisconsin, USA (2013).
- (ii) SAINT, Version 8.27b and SADABS Version 2012/1. Bruker AXS Inc., Madison, Wisconsin, USA (2012).
- (iii) Sheldrick, G. M. "SHELXS-97", Program for Crystal Structure Solution. Göttingen, (1997).
- (iv) Sheldrick, G. M. "SHELXL-97", University of Göttingen, Göttingen, Germany, (1998). *or* Sheldrick, G. M. "SHELXL-2014", University of Göttingen, Göttingen, Germany, (2014).
- (v) Hueschle, C. B., Sheldrick, G. M. & Dittrich, B. "SHELXLE", *J. Appl. Cryst.* **2011**, *44*, 1281- 1284.
- (vi) International Tables for Crystallography, Vol. C, Tables 6.1.1.4 (pp. 500-502), 4.2.6.8 (pp. 219-222), and 4.2.4.2 (pp. 193-199), Wilson, A. J. C., Ed., Kluwer Academic Publishers, Dordrecht, The Netherlands, 1992.
- (vii) Spek, A. L. "PLATON", A Multipurpose Crystallographic Tool, Utrecht University, Utrecht, The Netherlands, (2011).
- (viii) Macrae, C. F.; Bruno, I. J.; Chisholm, J. A.; Edgington, P. R.; McCabe, P.; Pidcock, E.; Rodriguez-Monge, L.; Taylor, R.; van de Streek, J.; Wood, P. A. *J. Appl. Cryst.* **2008**, *41*, 466-470.

Compound 2





Diffractometer operator C. Jandl
 scanspeed 10 s per frame
 dx 45 mm
 3234 frames measured in 9 data sets
 phi-scans with delta_phi = 0.5
 omega-scans with delta_omega = 0.5

Crystal data

$C_{82}H_{128}N_4O_8Y_2$	$F(000) = 1580$
$M_r = 1475.71$	

Triclinic, <i>P</i>	$D_x = 1.065 \text{ Mg m}^{-3}$
Hall symbol: <u>-P 1</u>	Melting point: ? K
$a = 15.1659 (4) \text{ \AA}$	Mo $K\alpha$ radiation, $\lambda = 0.71073 \text{ \AA}$
$b = 16.9562 (5) \text{ \AA}$	Cell parameters from <u>9760</u> reflections
$c = 21.1958 (6) \text{ \AA}$	$\theta = 2.5\text{--}26.4^\circ$
$\alpha = 92.612 (1)^\circ$	$\mu = 1.30 \text{ mm}^{-1}$
$\beta = 110.767 (2)^\circ$	$T = 123 \text{ K}$
$\gamma = 112.591 (1)^\circ$	Block, yellow
$V = 4600.0 (2) \text{ \AA}^3$	$0.59 \times 0.34 \times 0.25 \text{ mm}$
$Z = 2$	

Data collection

<u>Bruker APEX-II CCD diffractometer</u>	<u>16865</u> independent reflections
Radiation source: <u>rotating anode FR591</u>	<u>13736</u> reflections with $i > 2\sigma(i)$
<u>MONTEL optic monochromator</u>	$R_{\text{int}} = 0.053$
Detector resolution: <u>16 pixels mm⁻¹</u>	$\theta_{\text{max}} = 25.4^\circ$, $\theta_{\text{min}} = 1.5^\circ$
<u>phi- and ω-rotation scans</u>	$h = -18 \text{ } 18$
Absorption correction: <u>multi-scan SADABS, Bruker, 2008b</u>	$k = -20 \text{ } 20$
$T_{\text{min}} = 0.527$, $T_{\text{max}} = 0.745$	$l = -25 \text{ } 25$
<u>94197</u> measured reflections	

Refinement

Refinement on F^2	Secondary atom site location: <u>difference Fourier map</u>
Least-squares matrix: <u>full</u>	Hydrogen site location: <u>mixed</u>
$R[F^2 > 2\sigma(F^2)] = 0.037$	<u>H-atom parameters constrained</u>
$wR(F^2) = 0.102$	$W = 1/[\Sigma^2(FO^2) + (0.0524P)^2 + 2.7062P]$ <u>WHERE $P = (FO^2 + 2FC^2)/3$</u>
$S = 1.04$	$(\Delta/\sigma)_{\text{max}} = 0.003$
<u>16865</u> reflections	$\Delta\rho_{\text{max}} = 0.76 \text{ e \AA}^{-3}$
<u>1067</u> parameters	$\Delta\rho_{\text{min}} = -0.95 \text{ e \AA}^{-3}$

<u>612</u> restraints	Extinction correction: <u>none</u>
- constraints	Extinction coefficient: -
Primary atom site location: <u>structure-invariant</u> <u>direct methods</u>	

4. Polymerization investigations

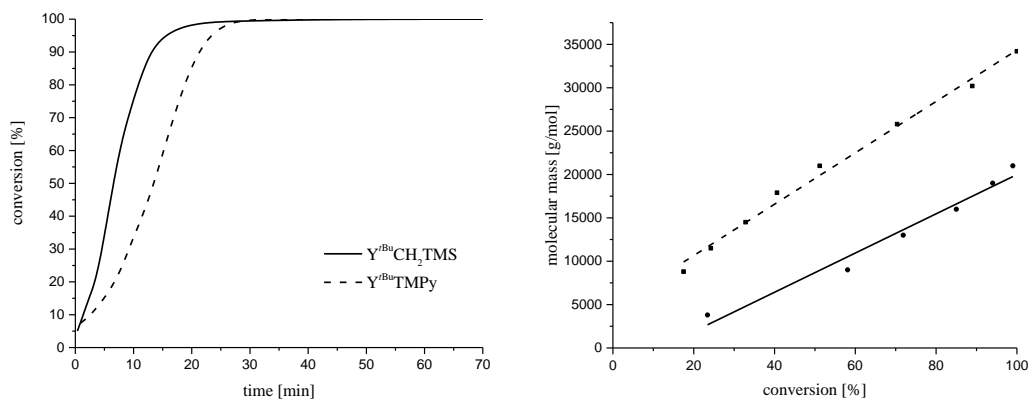


Figure S 3: Polymerization of 2VP with catalysts 1 and 2 (catalyst 135 μ mol, 2VP 27 mmol, toluene 20 mL, T = 25 $^{\circ}$ C) (Left) Conversion against time for catalysts 1 (black) and 2 (dashed). (Right) Linear growth of the absolute molecular weight (M_n) for catalyst 1 (black) and 2 (dashed) determined by GPC-MALS as a function of monomer conversion (determined gravimetrically).

Table S 1: Homopolymerization of 2VP with catalyst 1 and 2.^[a]

[Cat]	Time [min]	Conversion [%]	$M_{n,calc}$ ($\times 10^4$) [g/mol] ^[b]	$M_{n,exp}$ ($\times 10^4$) [g/mol]	M_w/M_n	I^* [c]	TOF ^[d] [h ⁻¹]
1	90	99	2.1	2.3	1.01	0.99	1100
2	165	99	2.0	3.8	1.06	0.53	600

[a] reactions performed with [2VP] = 27 mmol, [2VP]/[Cat] = 200/1, at 25 °C in 20 mL toluene, conversions determined by ¹H-NMR and $M_{n,exp,d}$ determined by GPC-MALS, [b] $M_{n,calc} = M \times (([M]/[Cat]) \times \text{conversion})$ [c] $I^* = M_{n,calc}/M_{n,exp}$; I^* at the end of the reaction [d] $\text{TOF}^* = \text{TOF}/I^*$.

Table S 2: Homopolymerization of DEVP with catalyst 1^{1a} and 2.^[a]

[Cat]	Time [min]	Conversion [%]	$M_{n,calc}$ ($\times 10^4$) [g/mol] ^[b]	$M_{n,exp}$ ($\times 10^4$) [g/mol]	\bar{D}	I^* [c]
1	198	99	3.3	9.0	1.10	0.36
2	60	99	3.4	3.5	1.07	0.97

[a] reactions performed with [DEVP] = 27 mmol, [DEVP]/[Cat] = 200/1, at 25 °C in 20 mL toluene, conversions determined by ³¹P-NMR and $M_{n,exp,d}$ determined by GPC-MALS. [b] $M_{n,calc}$ from $M_{n,calc} = M \times (([M]/[Cat]) \times \text{conversion})$. [c] $I^* = M_{n,calc}/M_{n,exp}$; I^* at the end of the reaction.

The homopolymerizations of 2VP and DEVP with catalyst 1 proceeds in a living fashion, as discernable by the narrow polydispersity and the good match between experimentally determined and the theoretically expected M_n values. To further examine the character of the polymerization, aliquots were taken at regular time intervals during the polymerization of 2VP and analyzed by gel permeation chromatography multi angle light scattering (GPC-MALS) to obtain the absolute molecular mass (M_n). The molecular mass was plotted against the monomer conversion as can be seen Figure S 3. The plots reveal a linear relationship between M_n and conversion while retaining a very narrow \bar{D} throughout the polymerization ($\bar{D} < 1.11$). A general improvement of the initiation for DEVP is observed for catalyst 2 compared to the CH₂TMS initiator of complex 1. Strongly basic CH₂TMS initiator leads to an initiation via deprotonation of the acidic α -CH while Tmpy can emulate the active propagating species. This indicates that, Tmpy can initiate via an eight-electron process and not via a six-electron initiation step. In our polymerization experiments, we found very high initiator efficiencies of up to 97% for DEVP with catalyst 2 while retaining perfect control over polydispersities (< 1.07).

Initiation:

First, the initiation mechanism was elucidated by end-group analysis of oligomeric P2VP generated by reacting catalyst 2 with 10 equivalents of 2VP and monitoring the reaction *via* NMR. The subsequent ESI-MS analysis found signals corresponding to $n \times M_{\text{Mon}} + M_{\text{I}}$ with either H^+ or Na^+ as charge carrier ($M_{\text{I}} = \text{TMPy}$) (Figure S 4). The initiating groups were clearly visible in the ESI-MS, therefore a transfer of the coordinated ligand via a monomer insertion into an yttrium-carbon-bond during the initiation is evident.

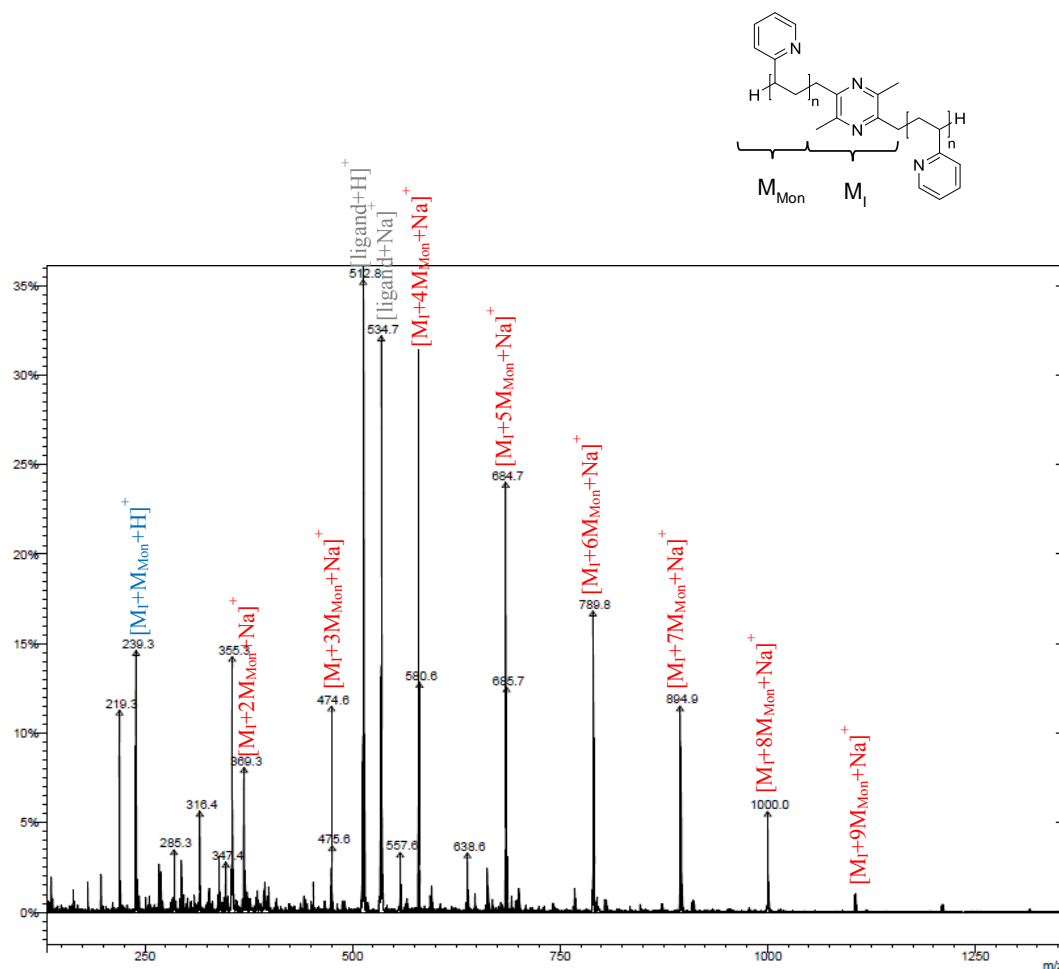
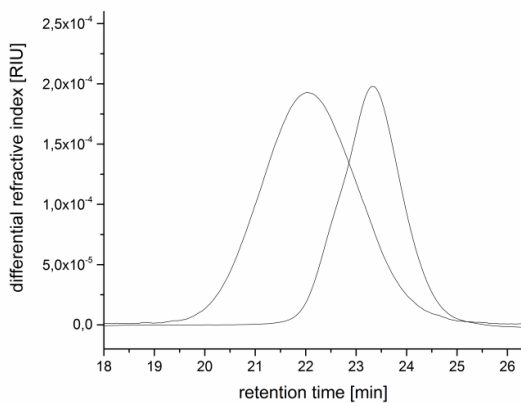
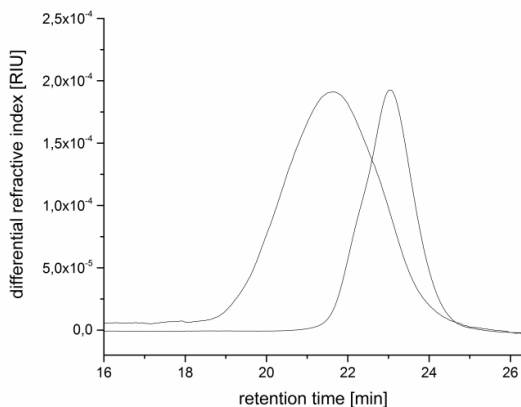


Figure S 4: Endgroup analysis ESI-MS measured in *i*PrOH; Catalyst 2 (40 μmol of catalyst, 0.4 mmol 2VP, 0.5 mL C_6D_6 , 20 $^\circ\text{C}$).

Table S 3: Block copolymers produced with catalyst 2: Type BAB with different compositions.

Entry	Polymer	Feed ^[a] A _{eq} /B _{eq}	Composition B/A/B ^[b] [2VP / DEVP]	M _n (A) * 10 ⁴ ^[c] [g/mol]	M(AB) _{n,NMR} * 10 ⁴ ^[d] [g/mol]	Đ ^[e]	LCST (H ₂ O) ^[d] [°C]	D _h ^[f] [nm]
1	BAB ₁	2VP ₂₀₀ /DEVP ₂₀₀	1 / 0.8	4.1	8.9	1.12	43.5	72 ± 9
2	BAB ₂	2VP ₂₀₀ /DEVP ₂₅₀	1 / 1.1	5.0	12.8	1.11	43.0	54 ± 7
3	BAB ₃	2VP ₂₀₀ /DEVP ₄₀₀	1 / 2.1	4.4	18.1	1.20	43.5	88 ± 4

[a] By weighing the monomer, [M]/[cat] = eq., [cat] = 41.7 μmol in 2.5 mL CH₂Cl₂. [b] Calculated from ¹H NMR spectroscopy. [c] Determined by GPC-MALS. [d] Determined by ¹H NMR spectroscopy. [e] Determined by temperature dependent UV/VIS measurements at a 10% transmittance decrease. [f] The micelle size is an average hydrodynamic diameter.

GPC traces:**Figure S 5:** GPC-traces of blockcopolymer BAB₁ (2VP₂₀₀/DEVP₂₀₀; entry 9, table S 3).**Figure S 6:** GPC-traces of blockcopolymer BAB₂ (2VP₂₀₀/DEVP₂₅₀; entry 10, table S 3).

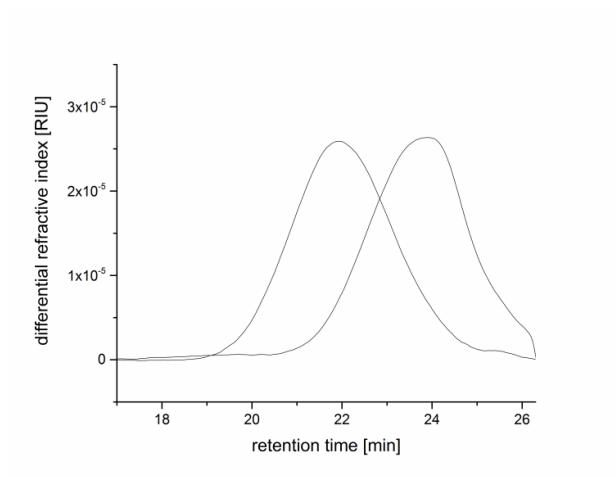


Figure S 7: GPC-traces of blockcopolymer BAB₃ (2VP₂₀₀/DEVP₄₀₀; entry 11, table S 3).

5. NMR-Analysis of Polymers

P2VP:

Produced with Catalyst 1

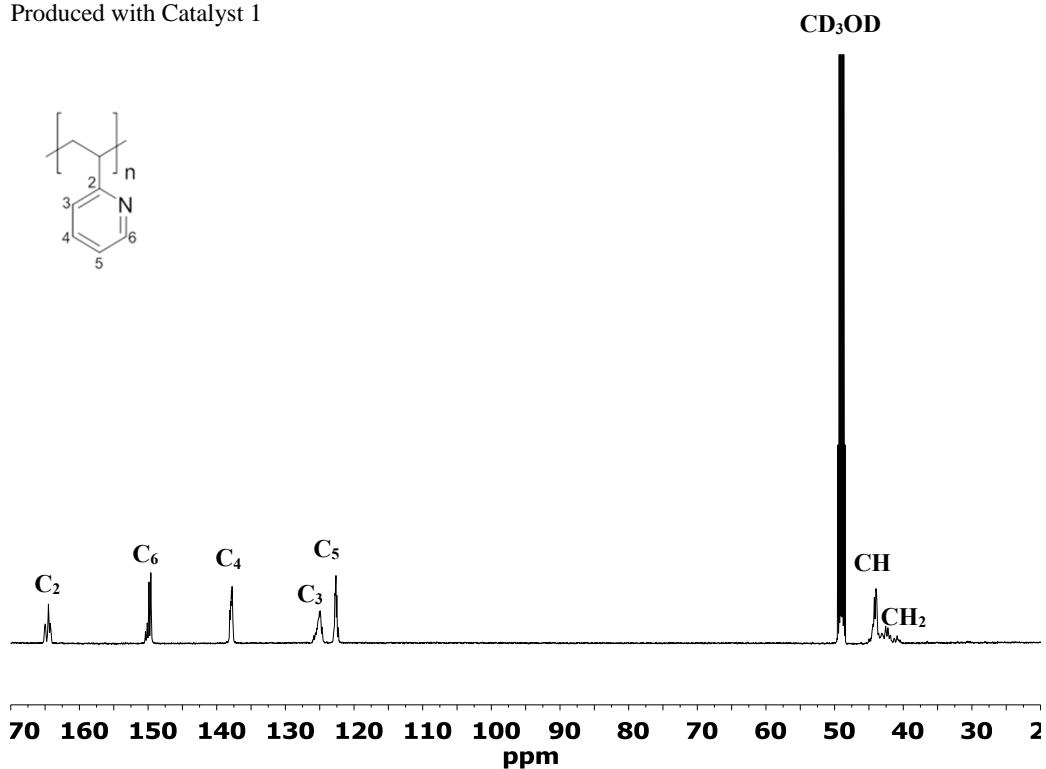


Figure S 8: ^{13}C -NMR-spectrum of atactic P2VP produced by catalyst 1 (500 MHz, Cryo, CD_3OD). Assignment according to Matsumoto and coworkers ⁵

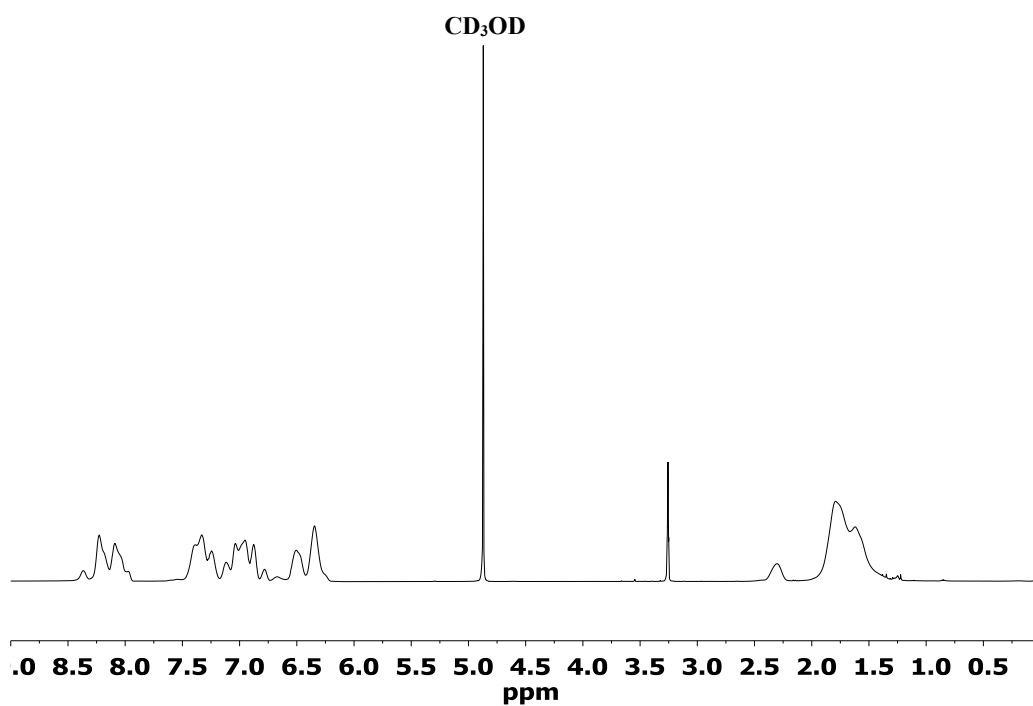


Figure S 9: ¹H-NMR-spectra of atactic P2VP produced by catalyst 1 (500 MHz, Cryo, CD₃OD).

Produced with catalyst 2

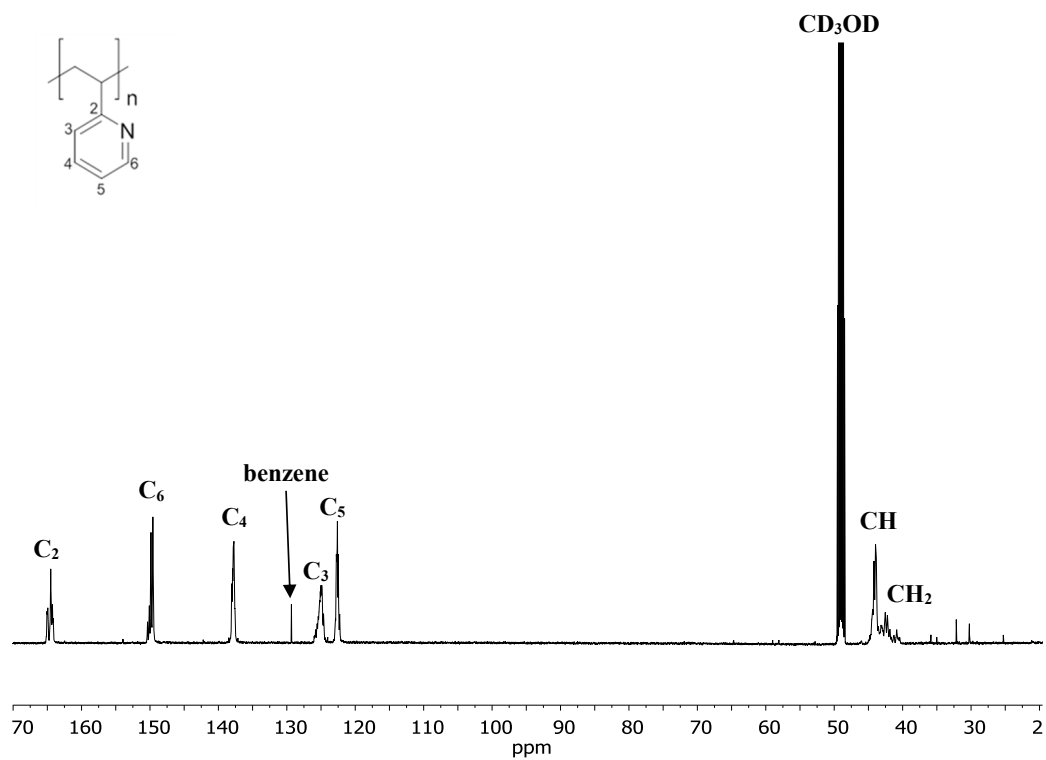


Figure S 10: ^{13}C -NMR-spectrum of atactic P2VP produced by catalyst 2 (500 MHz, Cryo, CD_3OD). Assignment according to Matsumoto and coworkers ⁵

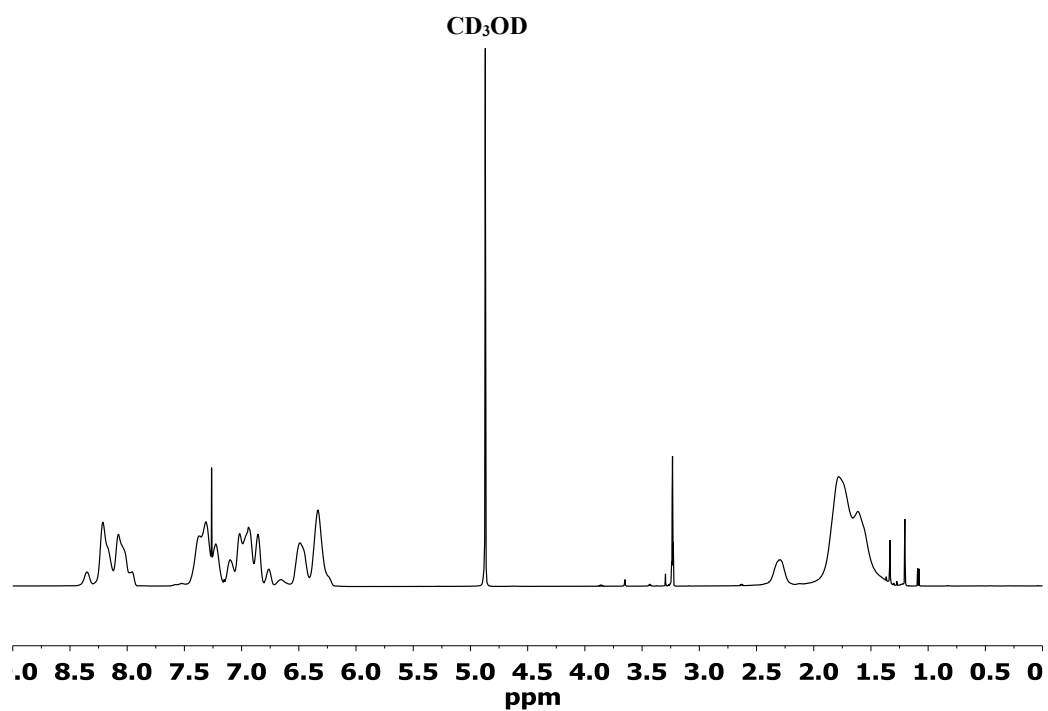


Figure S 11: ^1H -NMR-spectrum of atactic P2VP produced by catalyst 2 (500 MHz, Cryo, CD_3OD).

PDEVF:

Produced with catalyst 2

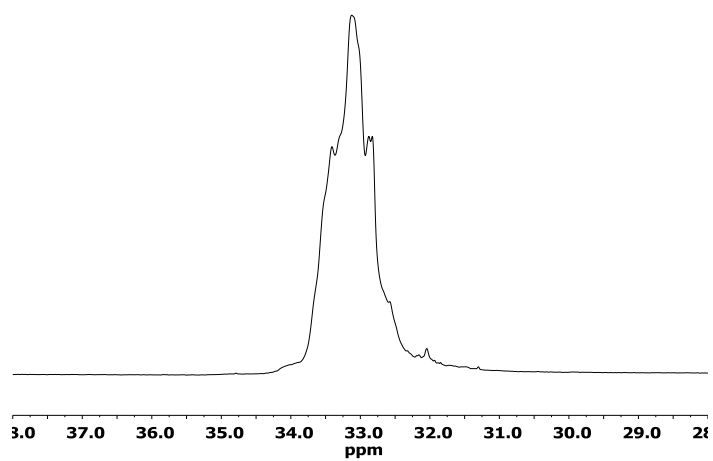


Figure S 12: ^{31}P -NMR-Spectrum of PDEVF produced with catalyst 2 (measured in CD_3OD).

Tacticity of P2VP:

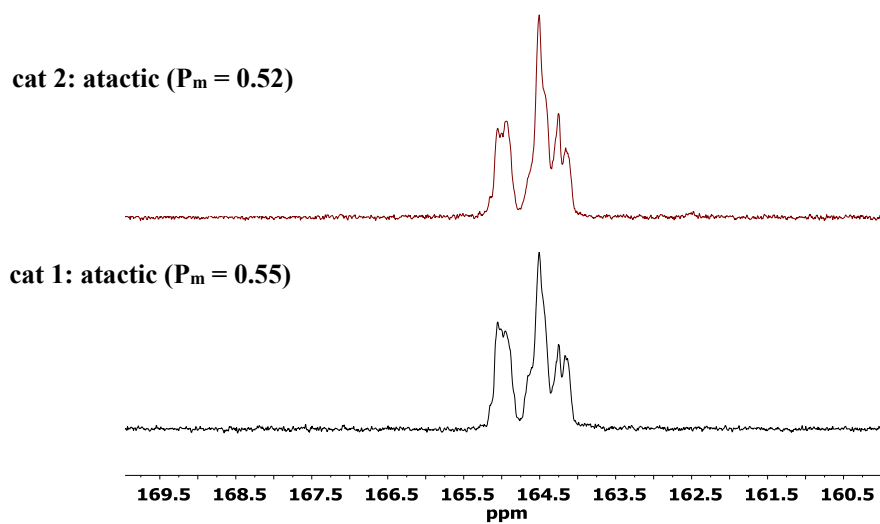


Figure S 13: Comparison of ^{13}C -NMR-spectra of the quaternary carbon atom produced by catalyst 1 (black) and catalyst 2 (red).

Blockcopolymers:

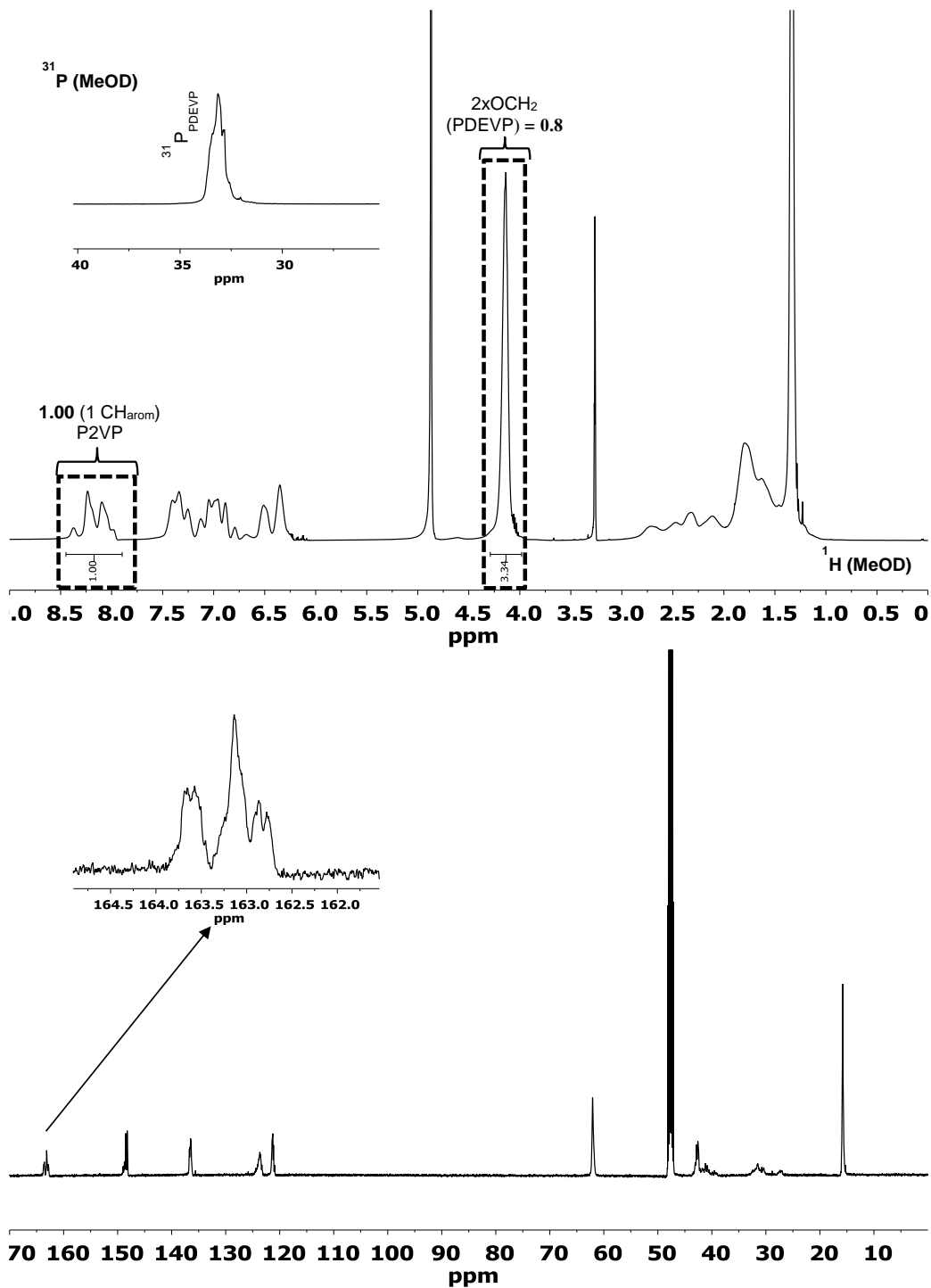


Figure S 14: ¹H-, ³¹P- and ¹³C-NMR spectrum of BAB₁ (2VP₂₀₀/DEVP₂₀₀; entry 1, table S 3) in MeOD at 298 K.

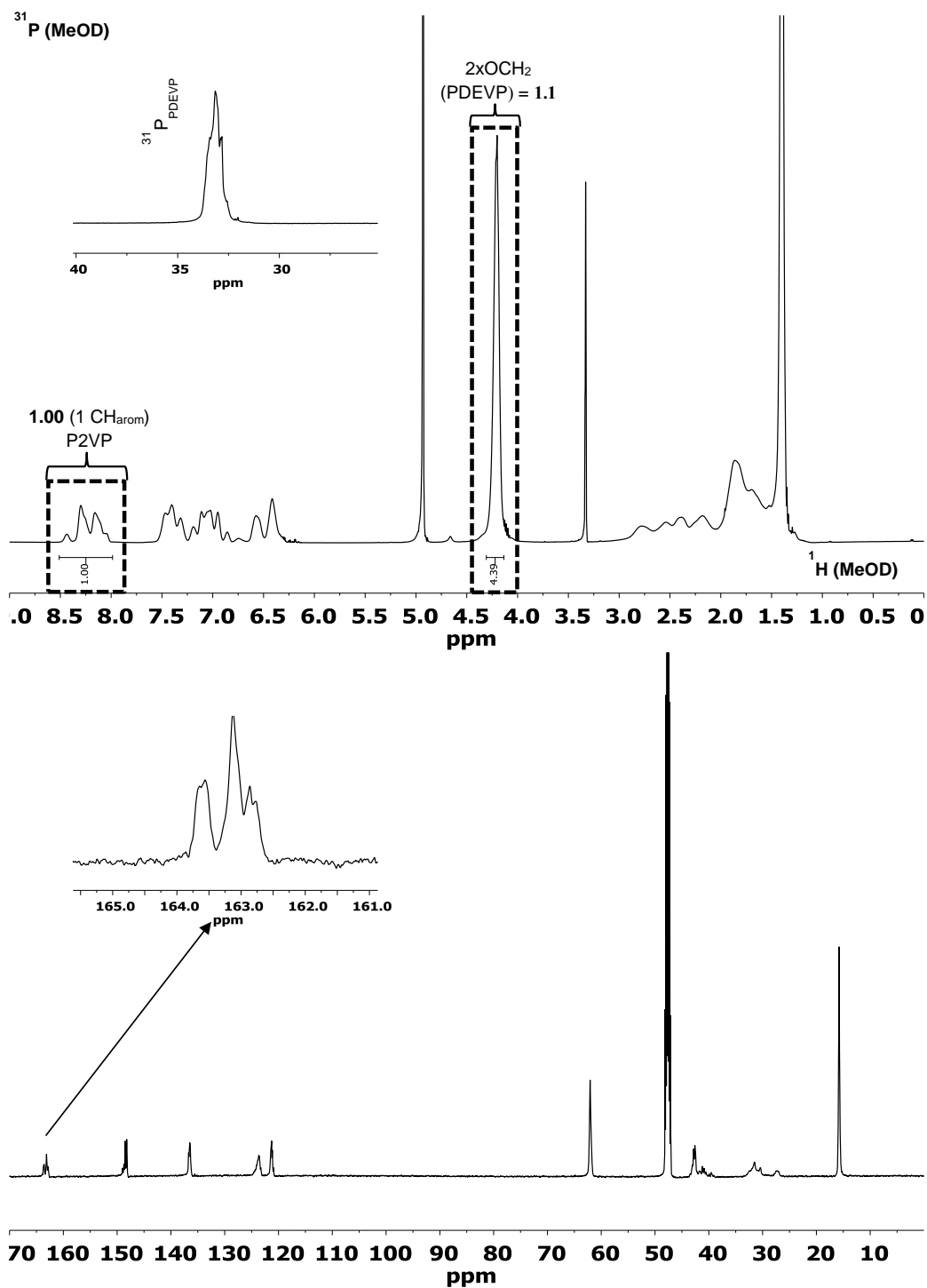


Figure S 15: ¹H-, ³¹P- and ¹³C-NMR spectrum of BAB₂ (2VP₂₀₀/DEVP₂₅₀; entry 2, table S 3) in MeOD at 298 K.

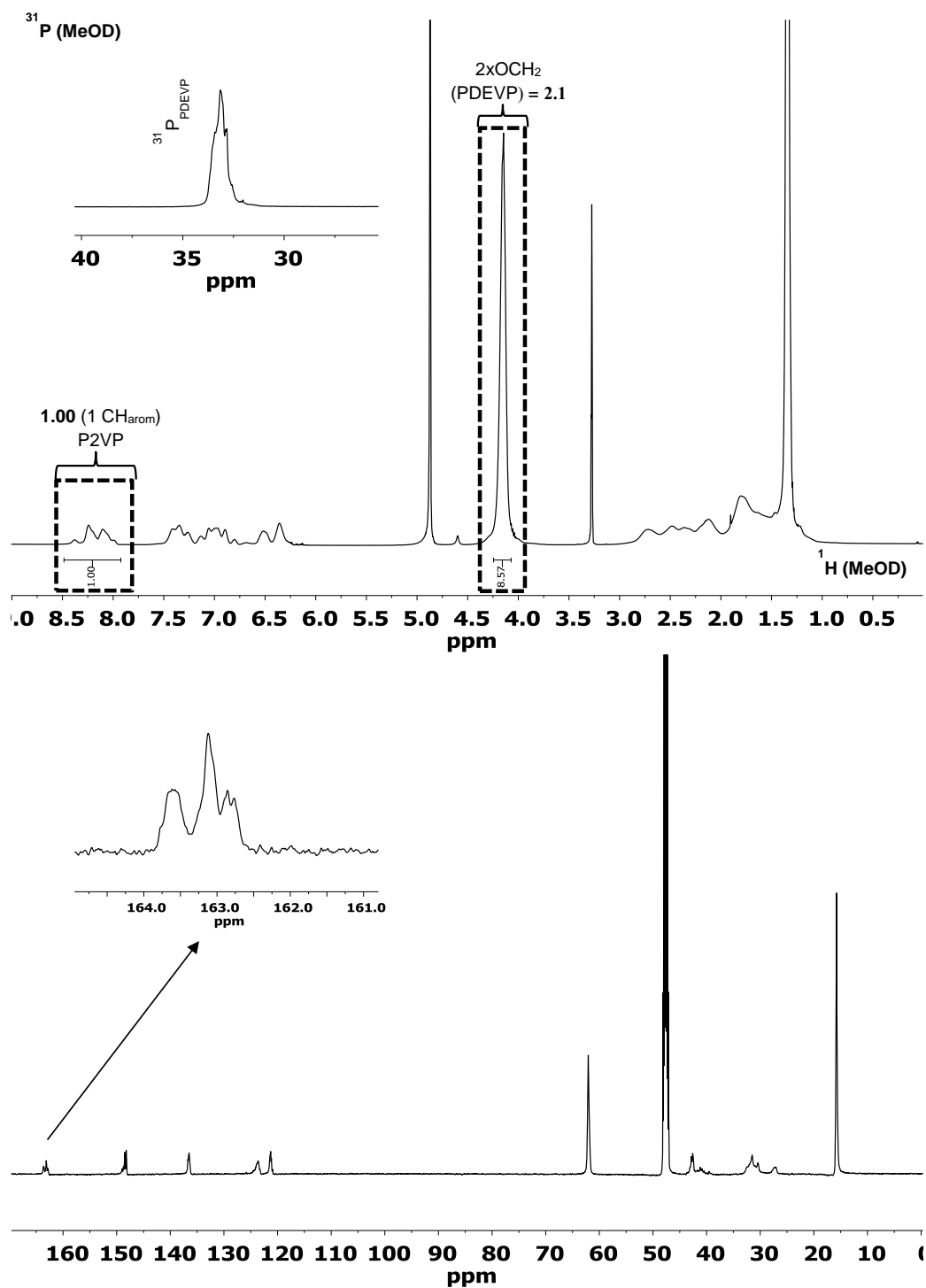


Figure S 16: ¹H-, ³¹P- and ¹³C-NMR spectrum of BAB₃ (2VP₂₀₀/DEVP₄₀₀; entry 3 table S 3) in MeOD at 298 K.

6. Characterization of micelles

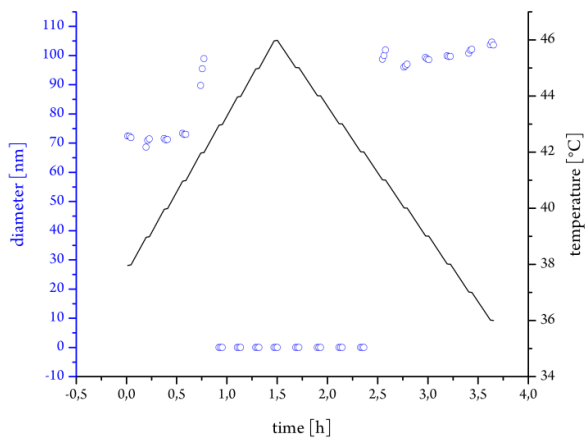


Figure S 17: LCST-DLS-measurement of blockcopolymer BAB₁ (2VP₂₀₀/DEVP₂₀₀; entry 1 table S 3).

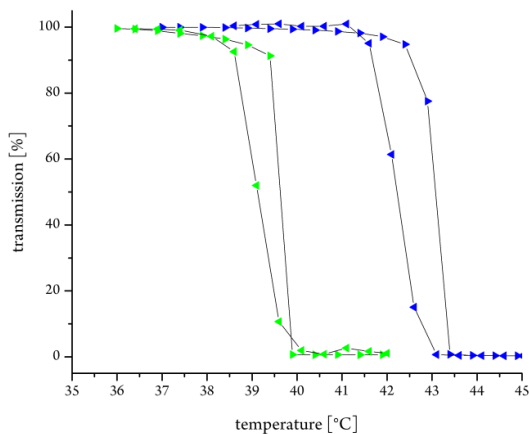


Figure S 18: LCST-UV/VIS-measurement of blockcopolymer BAB₁ (2VP₂₀₀/DEVP₂₀₀; entry 1, table S 3). The cloud point was determined at 10% decrease of transmittance for 2.5 wt % aqueous polymer solution (blue: deionized, green: PBS buffer).

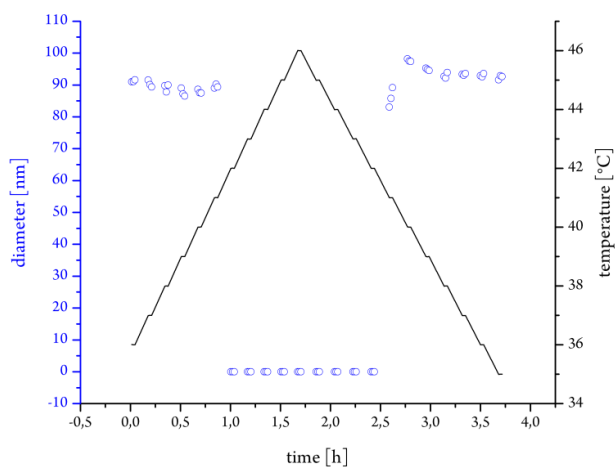


Figure S 19: LCST-DLS-measurement of blockcopolymer BAB₂ (2VP₂₀₀/DEVP₂₅₀; entry 2, table S 3).

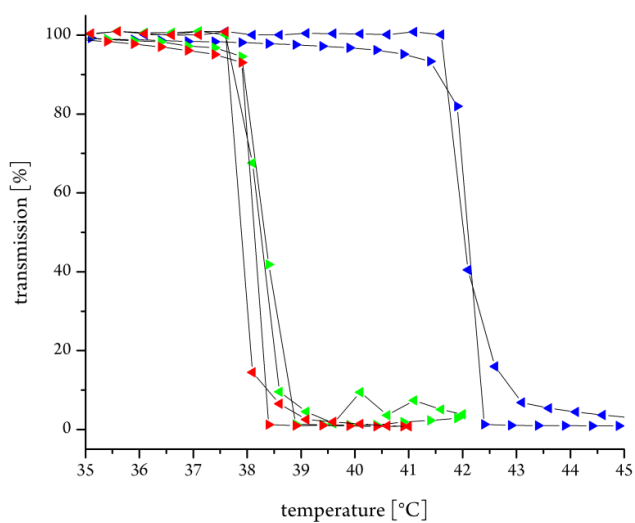


Figure S 20: LCST-UV/VIS-measurement of blockcopolymer BAB₂ (2VP₂₀₀/DEVP₂₅₀; entry 2, table S 3). The cloud point was determined at 10% decrease of transmittance for 2.5 wt % aqueous polymer solution (blue: deionized, green: PBS buffer, red: DMEM buffer).

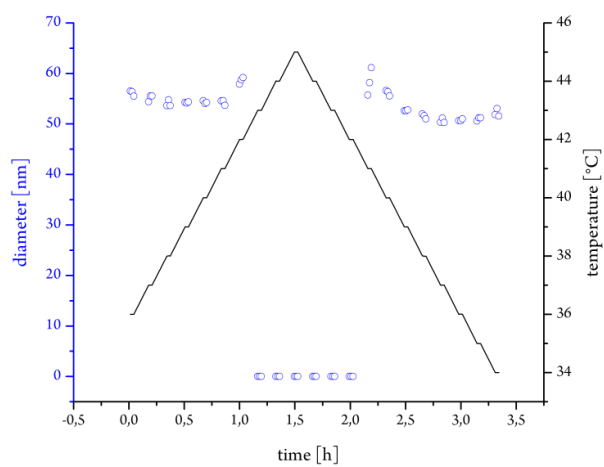


Figure S 21: LCST-DLS-measurement of blockcopolymer BAB₃ (2VP₂₀₀/DEVP₄₀₀; entry 3, table S 3).

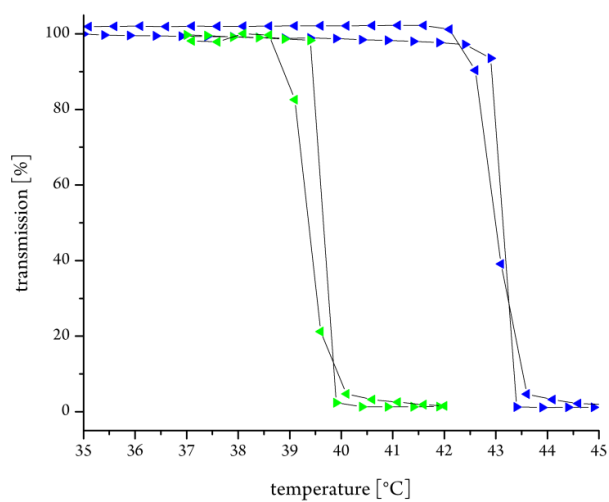


Figure S 22: LCST-UV/VIS-measurement of blockcopolymer BAB₃ (2VP₂₀₀/DEVP₄₀₀; entry 3, table S 3). The cloud point was determined at 10% decrease of transmittance for 2.5 wt % aqueous polymer solution (blue: deionized, green: PBS buffer).

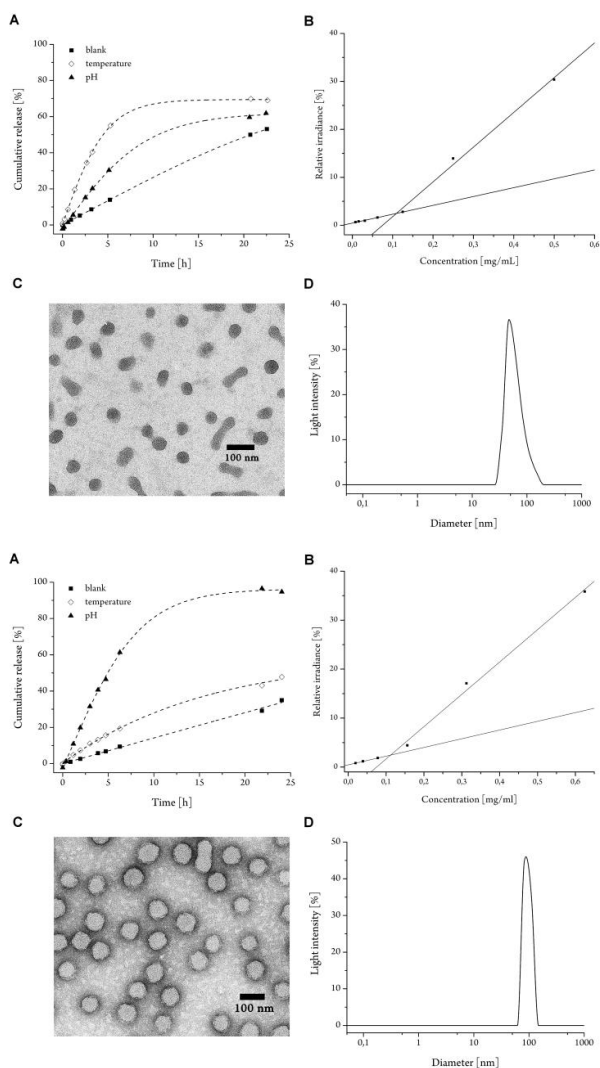


Figure S 23 (top) A: Cumulative release of fluorescein from loaded micelles (BAB₁, entry 1): untriggered and triggered with pH (4.5 buffer solution) and temperature (44 °C); B: Determination of critical micelle concentration (CMC) with Nile red; C: TEM-picture image of AB micelles; D: Light scattering measurement of BAB micelles (2.5 mg/mL) in H₂O. (bottom) A: Cumulative release of fluorescein from loaded micelles (BAB₂, entry 2): untriggered and triggered with pH (4.5 buffer solution) and temperature (44 °C); B: Determination of critical micelle concentration (CMC) with Nile red; C: TEM-picture image of AB micelles; D: Light scattering measurement of BAB micelles (2.5 mg/mL) in H₂O.

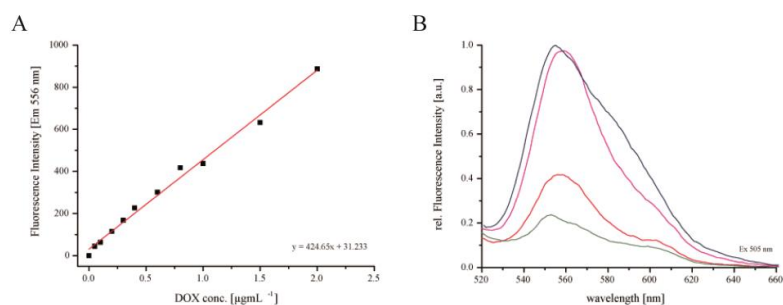


Figure S 24 A: Standard curve of DOX fluorescence intensity against DOX concentration ranging from $0.05 \mu\text{g mL}^{-1}$ to $2.00 \mu\text{g mL}^{-1}$ at acidic pH conditions ($\text{pH} = 2$). The respective fluorescence intensities were measured on a spectrofluorometer FP-8500 at room temperature (excitation wavelength: 505 nm, emission wavelength: 556 nm, slit width: 5nm). The exact DOX-loaded micelle concentrations were determined by the use of the linear fit equation $y=424.65x + 31.233$. B: Fluorescence emission spectra of Blank BAB_3 micelles, DOX-loaded BAB_3 micelles and non-encapsulated DOX, measured at $\text{pH} 7.4$ and $\text{pH} 2.0$, respectively (FP-8500 spectrofluorometer, excitation wavelength: 505 nm, slit width: 5nm). Blank BAB_3 micelles: green ($\text{pH} = 7.4$ and $\text{pH} = 2.0$), DOX-loaded BAB_3 micelles: red ($\text{pH} = 7.4$), purple ($\text{pH} = 2.0$), non-encapsulated DOX: blue ($\text{pH} = 7.4$ and $\text{pH} = 2.0$).

1. (a) Altenbuchner, P. T.; Soller, B. S.; Kissling, S.; Bachmann, T.; Kronast, A.; Vagin, S. I.; Rieger, B., Versatile 2-Methoxyethylaminobis(phenolate)yttrium Catalysts: Catalytic Precision Polymerization of Polar Monomers via Rare Earth Metal-Mediated Group Transfer Polymerization. *Macromolecules* **2014**, *47* (22), 7742-7749; (b) Hultsch, K. C.; Voth, P.; Beckerle, K.; Spaniol, T. P.; Okuda, J., Single-Component Polymerization Catalysts for Ethylene and Styrene: Synthesis, Characterization, and Reactivity of Alkyl and Hydrido Yttrium Complexes Containing a Linked Amido-Cyclopentadienyl Ligand. *Organometallics* **2000**, *19* (3), 228-243; (c) Vaughn, G. D.; Krein, K. A.; Gladysz, J. A., Synthesis and reactivity of metallacyclic manganese α -(silyloxy)alkyl complexes [cyclic] (CO)₄MnC(R)(OSi(CH₃)₃)P(C₆H₅)₂. A new thermodynamic driving force for carbonyl insertion. *Organometallics* **1986**, *5* (5), 936-42; (d) Cai, C.-X.; Toupet, L.; Lehmann, C. W.; Carpentier, J.-F., Synthesis, structure and reactivity of new yttrium bis(dimethylsilyl)amido and bis(trimethylsilyl)methyl complexes of a tetradentate bis(phenoxide) ligand. *J. Organomet. Chem.* **2003**, *683* (1), 131-136.
2. (a) Brigodiot, M.; Cheradame, H.; Fontanille, M.; Vairon, J. P., Microstructure of poly(2-vinylpyridine): correlation between ¹³C and ¹n.m.r. determinations. *Polymer* **1976**, *17* (3), 254-256; (b) Altenbuchner, P. T.; Adams, F.; Kronast, A.; Herdtweck, E.; Pöthig, A.; Rieger, B., Stereospecific catalytic precision polymerization of 2-vinylpyridine via rare earth metal-mediated group transfer polymerization with 2-methoxyethylamino-bis(phenolate)-yttrium complexes. *Polym. Chem.* **2015**, *6* (38), 6796-6801.
3. Tshuva, E. Y.; Groysman, S.; Goldberg, I.; Kol, M.; Goldschmidt, Z., [ONXO]-Type Amine Bis(phenolate) Zirconium and Hafnium Complexes as Extremely Active 1-Hexene Polymerization Catalysts. *Organometallics* **2002**, *21* (4), 662-670.
4. Amgoune, A.; Thomas, C. M.; Roisnel, T.; Carpentier, J.-F., Ring-opening polymerization of lactide with group 3 metal complexes supported by dianionic alkoxy-amino-bisphenolate ligands: combining high activity, productivity, and selectivity. *Chemistry* **2005**, *12* (1), 169-79.
5. Matsuzaki, K.; Kanai, T.; Matsubara, T.; Matsumoto, S., Stereoregularity of poly(2-vinylpyridine) determined by ¹H-NMR and ¹³C-NMR spectroscopy. *Journal of Polymer Science: Polymer Chemistry Edition* **1976**, *14* (6), 1475-1484.

14.5 Supporting Information: “Process for polymerizing β -butyrolactone”

Supporting Information for the Patent Application Entitled

“Process for polymerizing β -butyrolactone”

Materials and Methods.

All reactions were carried out under argon atmosphere using standard Schlenk or glovebox techniques. All glassware was heat dried under vacuum prior to use. Unless otherwise stated, all chemicals were purchased from Sigma-Aldrich, Acros Organics, or ABCR and used as received. Toluene, thf, diethylether, dichloromethane and pentane were dried using a MBraun SPS-800 solvent purification system. Hexane was dried over 3 Å molecular sieves. The monomer, β -butyrolactone, was dried over calcium hydride and distilled prior to use.

NMR spectra were recorded on a Bruker AVIII-300, AVIII-400, AVIII-500 and AVIII-500 Cryo spectrometer. Unless otherwise stated, ^1H - and ^{13}C -NMR spectroscopic chemical shifts δ are reported in ppm. δ (1H) is calibrated to the residual proton signal, δ (13C) to the carbon signal of the solvent. Unless otherwise stated, coupling constants J are averaged values and refer to couplings between two protons. Deuterated solvents were obtained from Sigma-Aldrich and dried over 3 Å molecular sieves.

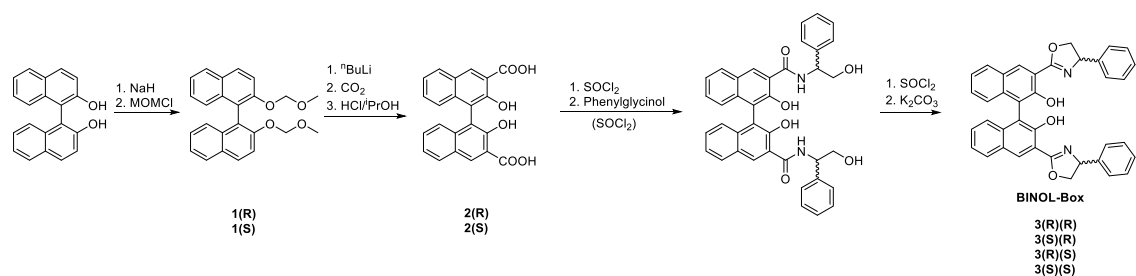
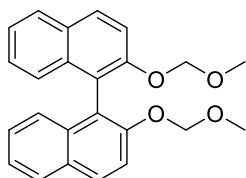
Elemental analyses were measured at the Laboratory for Microanalysis at the Institute of Inorganic Chemistry at the Technische Universität München.

Single Crystal X-ray Crystallography was performed in the SCXRD laboratory of the Catalysis Research Center at Technische Universität München.

The tacticity determination of PHB was performed by ^{13}C -NMR-spectroscopy at room temperature. Spectra for the analysis of PHB mm, mr/rm and rr triads were recorded with a sample concentration of 15 mg/0.6 mL CDCl_3 on a AVIII 500 Cryo spectrometer and analyzed according to literature.

DSC measurements are carried out on a TA Instruments DSC-Q2000 with heating rates of 10 K/min.

Synthesis route

Synthesis of 2,2'-bis(methoxymethoxy)-1,1'-binaphthalene (**1**)

C₂₄H₂₂O₄
MW: 374,44

1

9.76 g Binaphthol (34.0 mmol, 1.0 eq.) in DMF (100 ml) are slowly added to a stirred suspension of 5.76 g NaH (60% dispersion in mineral oil, 144 mmol, 4.3 eq.) in 100 ml DMF at 0 °C under argon atmosphere. The reaction mixture is stirred at 0 °C for 30 minutes, then 10.4 mL chloromethyl methyl ether (132 mmol, 4.0 eq.) are added in one portion. The ice bath is removed after 5 minutes and again 1.6 ml MOMCl (26.3 mmol, 0.6 eq.) are added. The mixture is stirred at room temperature for 3 hours, then the reaction solution is poured into 300 ml of water. The aqueous phase is extracted with diethylether (2 × 400 mL) and the organic phase is washed with water (4 × 200 mL) and NaCO_{3,aq.} (300 mL), dried over MgSO₄ and filtered. The solvent is removed in vacuo and the product is obtained as a colorless solid. The product is recrystallized from methanol to obtain colorless crystals.

1(R): yield: 92% (31.3 mmol, 11.7 g)

¹H NMR (300 MHz, CDCl₃, 298 K): δ (ppm) = 7.98 (d, ³J = 9.0 Hz, 2H), 7.90 (d, ³J = 8.1 Hz, 2H), 7.61 (d, ³J = 9.0 Hz, 2H), 7.37 (ddd, J = 8.1, 6.5, 1.5 Hz, 2H), 7.29 – 7.16 (m, 4H, overlapping with residual proton signal of CDCl₃), 5.11 (d, ²J = 6.8 Hz, 2H, CH'H''), 5.01 (d, ²J = 6.8 Hz, 2H, CH'H''), 3.17 (s, 6H, CH₃).

¹³C NMR (75 MHz, CDCl₃, 298 K): δ (ppm) = 152.7, 134.1, 130.0, 129.5, 127.9, 126.4, 125.6, 124.1, 121.4, 117.4, 95.3, 55.9.

EA: calculated: C 76.99 H 5.92

found: C 76.80 H 5.99

1(S): yield: 89% (30.3 mmol, 11.3 g)

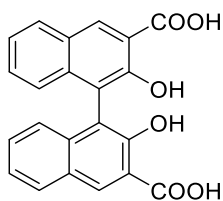
¹H NMR (300 MHz, CDCl₃, 298 K): δ (ppm) = 7.97 (d, ³J = 9.0 Hz, 2H), 7.89 (d, ³J = 8.1 Hz, 2H), 7.60 (d, ³J = 9.0 Hz, 2H), 7.36 (ddd, J = 8.1, 6.5, 1.5 Hz, 2H), 7.29 – 7.15 (m, 4H, overlapping with residual proton signal of CDCl₃), 5.10 (d, ²J = 6.8 Hz, 2H, CH'H''), 5.00 (d, ²J = 6.8 Hz, 2H, CH'H''), 3.17 (s, 6H, CH₃).

¹³C NMR (75 MHz, CDCl₃, 298 K): δ (ppm) = 152.7, 134.1, 130.0, 129.5, 128.0, 126.4, 125.6, 124.1, 121.4, 117.4, 95.3, 55.9.

EA: calculated: C 76.99 H 5.92

found: C 76.69 H 5.91

Synthesis of 2,2'-dihydroxy-[1,1'-binaphthalene]-3,3'-dicarboxylic acid (**2**)



C₂₂H₁₄O₆
MW: 374,35

2

25.0 mL ⁿButyllithium solution (2.5 M in hexane, 62.5 mmol, 2.6 eq.) are slowly added to a stirred solution of 9.00 g 2,2'-bis (methoxymethoxy) -1,1'-binaphthyl **1** (24.0 mmol, 1.0 eq.) in 100 mL THF at 0 °C. After stirring for 2 hours at 0 °C., carbon dioxide is passed into the solution with a syringe *via* a separate flask filled with dry ice. The reaction is quenched by addition of 100 mL water after 4 hours. The aqueous phase is washed with diethyl ether (2 × 50 mL) and then acidified to pH = 2 with an aqueous 5% hydrogen chloride solution. The aqueous phase is then extracted with ethyl acetate (3 × 100 mL). The combined ethyl acetate phases are extracted with brine, dried over MgSO₄, filtered and the solvent is removed under vacuum.

The protection group is removed by dissolving the product in THF and cooling to 0 °C. 80 mL of a 5-6 N hydrogen chloride solution in *iso*-propanol is added and stirred for 2 hours at room temperature. The solvent is removed under vacuum, the residue is dissolved in ethyl acetate and then washed with water (2 × 100 mL), dried over MgSO₄, filtered and the solvent is removed under vacuum. The product is washed with cold chloroform and is isolated as a yellow powder.

2(R): yield: 35 % (8.49 mmol, 3.19 g)

¹H NMR (300 MHz, DMSO-d₆, 298 K): δ (ppm) = 11.23 (br s, 2H), 8.75 (s, 2H), 8.10 (dd, ³J = 6.3, 3.0 Hz, 2H), 7.37 (dd, ³J = 6.3, 3.0 Hz, 4H), 7.11 – 6.81 (m, 2H).

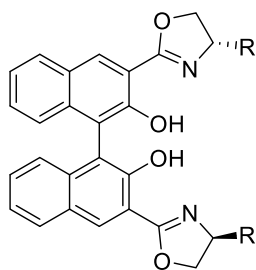
^{13}C NMR (75 MHz, DMSO- d_6 , 298 K): δ (ppm) = 172.1, 154.1, 136.5, 132.6, 129.8, 129.3, 126.7, 124.0, 123.7, 116.3, 114.6.

2(S): yield: 46 % (11.1 mmol, 4.17 g)

^1H NMR (300 MHz, DMSO- d_6 , 298 K): δ (ppm) = 11.25 (br s, 2H), 8.74 (s, 2H), 8.16 – 8.04 (m, 2H), 7.47 – 7.26 (m, 4H), 7.07 – 6.88 (m, 2H).

^{13}C NMR (75 MHz, DMSO- d_6 , 298 K): δ (ppm) = 172.1, 154.1, 136.5, 132.6, 129.9, 129.3, 126.7, 124.0, 123.7, 116.3, 114.7.

Synthesis of 3,3-bis(4-phenyl-4,5-dihydrooxazol-2-yl)-[1,1'-binaphthalene]-2,2'-diol ($\text{H}_2[(\text{Binol-Box})^{\text{Ph}}]$) (**3**):



3

A solution of 7.00 g **2** (1.0 eq.) in 60 ml of thionyl chloride is refluxed for 5 h at 80 °C. Afterwards, thionyl chloride is removed in vacuo and the residue is dissolved in 100 mL dichloromethane. A solution of (R)-phenylglycinol/(S)-phenylglycinol,(R)-phenylalaninol, etc. (2.2 eq.) and triethylamine (1.6 eq) in 60 ml of dichloromethane are added at 0 °C and the solution is stirred at room temperature overnight. A solution of thionyl chloride (5 eq.) in 50 ml of dichloromethane is added dropwise and stirred overnight at room temperature. The reaction is terminated by the addition of water (150 mL). The aqueous and organic phases are separated and the aqueous one is extracted with dichloromethane (3 x 150 mL). The organic phases are then combined, dried over magnesium sulfate, filtrated and the solvent is removed under reduced pressure. A solution of potassium carbonate (5.5 eq) in 50 ml of water is added to the residue dissolved in 50 ml of acetonitrile and refluxed overnight at 100 °C. The solvent is removed and the residue is dissolved in dichloromethane (200 mL) and water (170 mL), then the organic phase is extracted with a 1.0 M hydrochloric acid solution (100 mL) and the aqueous phase with dichloromethane (100 mL). After combining the organic phases and drying over magnesium sulfate, the solvent is removed under reduced pressure. For purification, the crude product is purified via column chromatography (hexane: EtOAc = 5:1, SiO_2) and recrystallized from ethylacetate to give a colorless to pale yellow solid.

3(S)(R)^{Ph}:

Yield: 31%

DC: $R_f = 0.45$ (ⁿhexan:EtOAc = 5:1) [UV]

¹H-NMR (330 MHz, CDCl₃, 300 K): δ (ppm) = 12.17 (s, 2H, OH), 8.51 (s, 2H), 7.94-7.89 (m, 2H, CH_{arom}), 7.36-7.24 (m, 16H, CH_{arom}), 5.52 (t, ³J = 9.2, 2H), 4.91 (t, ³J = 9.2, 2H), 4.35 (t, ³J = 9.2, 2H, CH₂).

¹³C-NMR (500 MHz, CDCl₃, 300 K): δ (ppm) = 165.99, 153.00, 140.91, 136.06, 130.14, 129.14, 128.65, 128.44, 127.68, 127.13, 126.41, 124.74, 123.44, 116.60, 112.58, 73.84, 68.98.

EA: Calculated: C 79.15 H 4.89 N 4.86

Measured: C 78.96 H 4.91 N 4.87

3(S)(R)^{Bn}:

DC: $R_f = 0.47$ (ⁿhexan:EtOAc = 5:1) [UV]

¹H-NMR (330 MHz, CDCl₃, 300 K): δ (ppm) = 12.12 (s, 2H, OH), 8.42 (s, 2H), 7.90-7.87 (m, 2H, CH_{arom}), 7.31-7.19 (m, 16H, CH_{arom}), 4.68 (p, ³J = 7.7 Hz, 2H, CH), 4.51 (t, ³J = 8.9 Hz, 2H, OCH₂), 4.21 (t, ³J = 8.1 Hz, 2H, OCH₂), 3.13 (dd, ²J = 6.3 Hz, ³J = 13.9 Hz, 2H, ArCH₂), 2.81 (dd, ²J = 6.3 Hz, ³J = 13.9 Hz, 2H, ArCH₂).

¹³C-NMR (500 MHz, CDCl₃, 300 K): δ (ppm) = 165.26, 152.99, 137.38, 135.93, 129.90, 129.08, 128.95, 128.51, 128.32, 127.07, 126.50, 124.62, 123.35, 116.52, 112.70, 71.25, 66.98, 41.59.

EA: Calculated: C 79.45 H 5.33 N 4.63

Measured: C 79.49 H 5.53 N 4.50

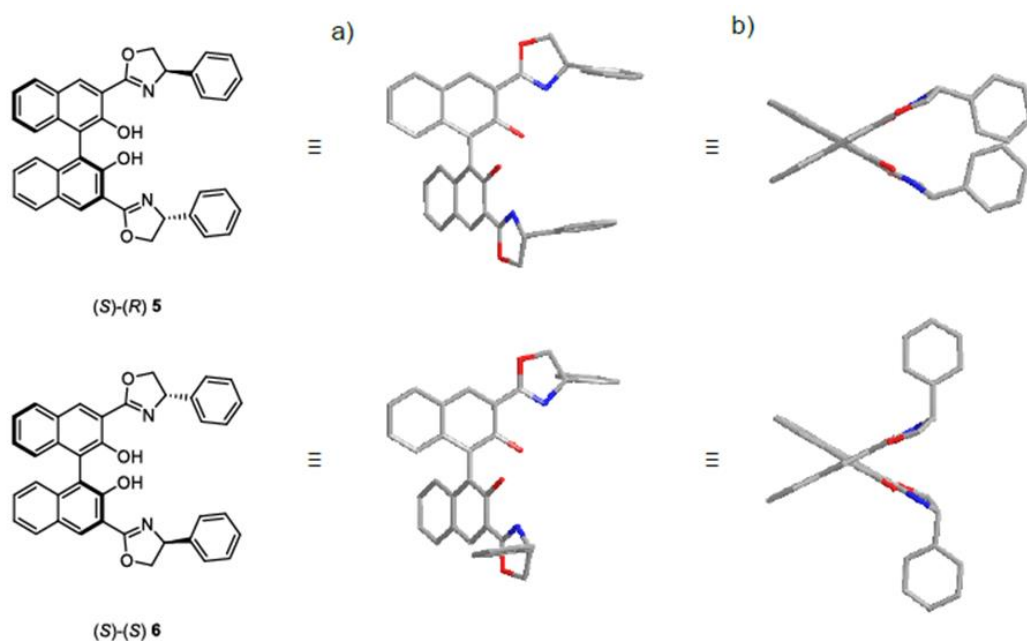
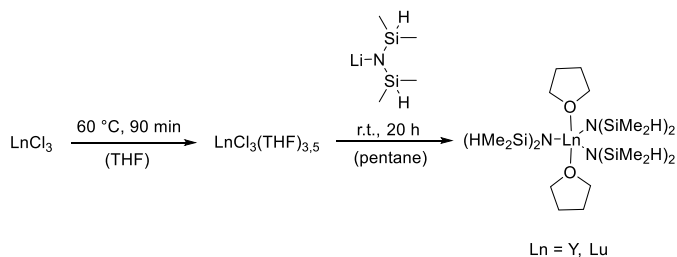


Figure S 1: Computational prediction of the geometry of the (S)(R)- and (S)(S)-(Binol)(Box)^{Ph} ligands.

Synthesis of $\text{Ln}(\text{N}(\text{SiMe}_2\text{H})_2)_3(\text{THF})_2$:



In a heated round bottom Schlenk flask a suspension of 2.20 g YCl_3 (11.20 mmol, 1.00 eq.) in tetrahydrofuran (120 ml) is stirred for 90 min at 70 °C. After solvent evaporation under vacuum the received colorless solid is suspended in pentane (100 ml) and 4.31 g lithium-bis(dimethylsilyl)amide (31.20 mmol, 2.75 eq.) are added carefully. The suspension is stirred at room temperature for 22 h. The residue is washed two times with pentane (25 ml) and is subsequently recrystallized from pentane. After solvent removal and drying, 4.30 g of precursor $\text{Y}(\text{N}(\text{SiMe}_2\text{H})_2)_3(\text{THF})$ (6.82 mmol, 61%) is obtained as colorless solid.

$\text{Y}(\text{N}(\text{SiMe}_2\text{H})_2)_3(\text{THF})_2$:

$^1\text{H NMR}$ (500 MHz, $\text{THF-}d_8$, 298 K): δ (ppm) = 4.78 (hept, $^3J = 3.0$ Hz, 3H, SiH), 0.10 (d, $^3J = 3.0$ Hz, 18H, CH_3).

$^{29}\text{Si NMR}$ (99 MHz, $\text{THF-}d_8$, 298 K): δ (ppm) = -23.96.

$^{13}\text{C NMR}$ (126 MHz, $\text{THF-}d_8$, 298 K): δ (ppm) = 45.9.

$^1\text{H-NMR}$ (330 MHz, C_6D_6 , 300 K): δ (ppm) = 4.99 (p, $^4J = 3.0$ Hz, 6H, SiH), 3.78 (s, 8H, H_{thf}), 1.35-1.30 (m, 8H, H_{thf}), 0.39 (d, $^3J = 3.0$ Hz, 36H, SiMe).

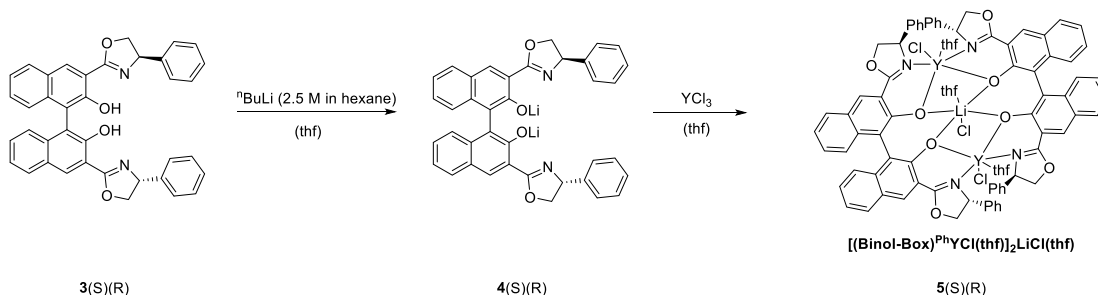
$^{13}\text{C-NMR}$ (500 MHz, C_6D_6 , 300 K): δ (ppm) = 71.0, 25.2, 3.3.

$^{29}\text{Si-INEPT-NMR}$ (500 MHz, C_6D_6 , 300 K): δ (ppm) = 22.91.

General *in situ* polymerization procedure:

Polymerization of rac-BBL was carried out in a glovebox for the stated periods. The polymerization was performed using a ratio of lanthanide to ligand to monomer ratio of 1:1:200 or 1:1:400. Therefore, one equivalent of [M] and one equivalent of the ligand is dissolved in 1 mL of the respective solvent each. Subsequently, the two solutions are combined and stirred for 10 minutes. The polymerization was initiated by addition of the respective amount of the monomer in one portion. After the stated time, the polymerization is quenched by addition of deuterated chloroform. An aliquot sample is taken to determine the conversion via ^1H nmr-spectroscopy. The polymer is precipitated in methanol and dried overnight.

Salt metathesis:



Synthesis of $\text{Li}_2[(\text{Binol-Box})^{\text{Ph}}]$ (**4**):

1.30 g of **3** (2.25 mmol, 1.0 eq.) were dissolved in 25 ml thf under argon atmosphere and were cooled to 0 °C. 3.05 mL n-Butyllithium (2.5 M in hexane, 2.2 eq.) were slowly added and the reaction mixture was stirred at room temperature for 2 hours. The lithiated ligand $\text{Li}_2[(\text{Binol-Box})^{\text{Ph}}]$ **4** was used for the next step without isolation and further purification.

¹H NMR (300 MHz, THF-*d*₆, 298 K): δ(ppm) = 8.27 (s, 2H), 7.58 – 6.78 (m, 8H), 5.29 (t, *J* = 9.6 Hz, 2H), 4.39 (dd, *J* = 9.6, 8.1 Hz, 2H), 3.77 (dd, *J* = 9.6, 8.1 Hz, 2H).

Synthesis of [(Binol-Box)^{Ph}YCl(thf)]₂LiCl(thf) (5**):**

One equivalent of anhydrous YCl₃ (440 mg, 2.25 mmol) was suspended in 30 mL thf and heated for 90 minutes at 60 °C. The solution of **4** in thf is added dropwise at room temperature and the reaction mixture is stirred over night. The solvent is removed in vacuo and the residue is washed five times with 40 mL toluene *via* whatman filtration. The solvent is removed under reduced pressure. Precipitation from thf/pentane at 0 °C led to a yellow solid. Recrystallization from thf at -20 °C led to crystals suitable for X-ray analysis.

5(S)(R)^{Ph}:

Yield: 1.28 g (1.66 mmol, 73%)

¹H NMR (500 MHz, CDCl₃, 298 K): δ (ppm) = 8.44 (s, 1H), 7.79 (d, *J* = 8.2 Hz, 1H), 7.70 (d, *J* = 8.2 Hz, 1H), 7.46 (s, 1H), 7.35– 7.13 (m, 9H, overlapping with residual proton signal of solvent), 7.05 (t, *J* = 7.6 Hz, 2H), 6.98 (t, *J* = 7.6 Hz, 2H), 6.92 (t, *J* = 7.6 Hz, 2H), 6.39 (d, *J* = 8.7 Hz, 1H), 5.74 (t, *J* = 9.5 Hz, 1H), 5.54 (dd, *J* = 9.2, 5.1 Hz, 1H), 4.54 (t, *J* = 9.5 Hz, 1H), 4.24 (t, *J* = 9.2 Hz, 1H), 4.07 (dd, *J* = 9.2, 5.1 Hz, 1H), 3.88 (t, *J* = 9.5 Hz, 1H), 3.49 (s, 6H), 3.34 (s, 6H), 1.70 – 1.42 (m, 12H).

¹³C NMR (126 MHz, CDCl₃, 298 K): δ (ppm) = 168.8, 167.3, 160.3, 157.12, 141.3, 141.0, 137.9, 137.50, 132.5, 132.4, 130.2, 129.0, 128.8, 128.7, 128.3, 128.0 (d, *J*_{Y,C} = 6.8 Hz), 127.7, 127.5 (d, *J*_{Y,C} = 6.0 Hz), 126.3, 125.0, 124.7, 120.7, 119.5, 116.9, 116.3, 74.4, 73.9, 70.8, 69.6, 68.62, 25.3.

EA: calculated: C 63.80 H 4.62 N 3.38

found: C 63.44 H 4.71 N 3.43

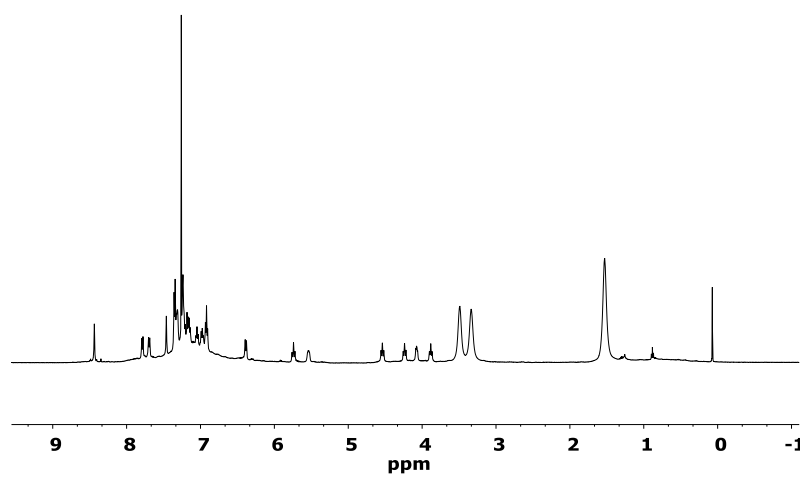


Figure S 2: $^1\text{H-NMR}$ spectrum of $5(\text{S})(\text{R})^{\text{Ph}}$ in CD_2Cl_2 .

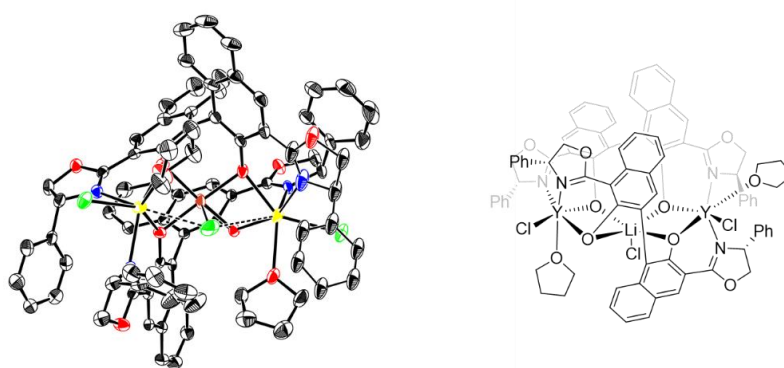


Figure S 3: XRD-Structure of $5(\text{S})(\text{R})^{\text{Ph}}$.

Sample Details

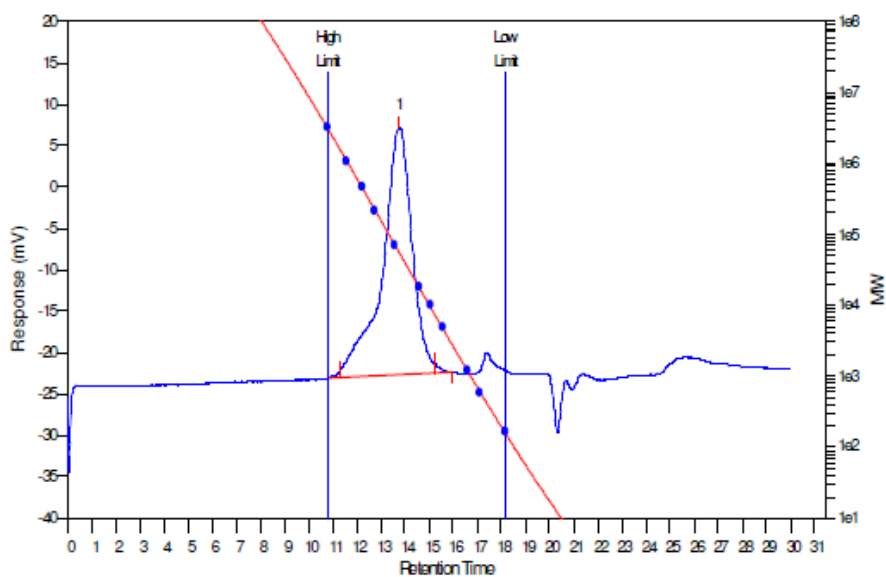
Sample Name: AAR_455	Batch Name: 2018-01-13-AAR
Filename: C:\Cirrus Workbooks\Chloroform_RI-only_2017\2018-01-13-aar-0005.cgrm	
Acquired: 15.01.2018 09:04:28	Eluent: Chloroform
Injection Volume: 100.0 ul	Flow Rate: 1.000000 ml/min
Concentration: mg/ml	Temperature: 25
Column Set:	Column Set Length: 0.000000 mm

Analysis Using Method: Relative_Auswertung

Results File: C:\Cirrus Workbooks\Chloroform_RI-only_2017\2018-01-13-aar-0005.rst

Calibration Used: 30.06.2017 15:40:33

Calibration Type: Narrow Standard Curve Fit Used: 3
 Calibration Curve: $y = 10.814856 - 0.129997x^1 - 0.034082x^2 + 0.000832x^3$



MW Averages

Peak No	Mp	Mn	Mw	Mz	Mz+1	Mv	PD
1	55938	48906	131815	436286	814496	108573	2.69527

Figure S 4: GPC trace of PHB measured in chloroform (Chapter 9.3, Table 4, Entry 3).

Sample Details

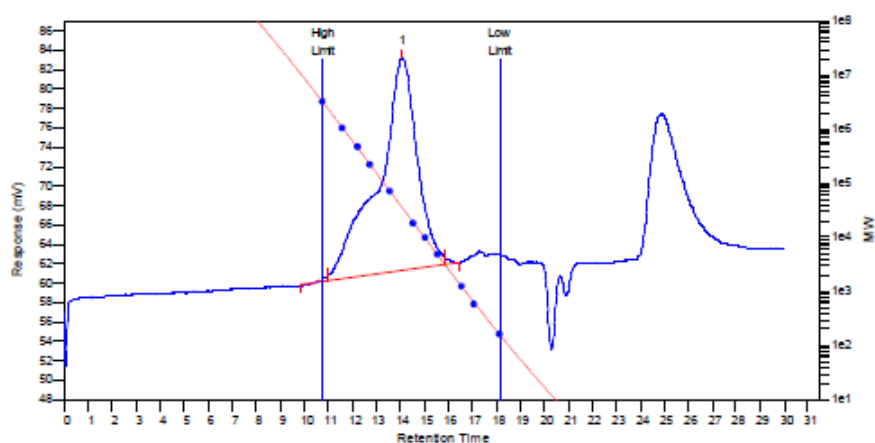
Sample Name: AAR_448 Batch Name: 2017-11-02
 Filename: C:\Cirrus Workbooks\Chloroform_RI-only_2017\2017-11-02-0001.ogrn
 Acquired: 02.11.2017 15:41:44 Eluent: Chloroform
 Injection Volume: 100.0 ul Flow Rate: 1.000000 ml/min
 Concentration: mg/ml Temperature: 25
 Column Set: Column Set Length: 0.000000 mm

Analysis Using Method: Relative_Auswertung

Results File: C:\Cirrus Workbooks\Chloroform_RI-only_2017\2017-11-02-0001.rst

Calibration Used: 30.06.2017 15:40:33

Calibration Type: Narrow Standard Curve Fit Used: 3
 Calibration Curve: $y = 10.814856 - 0.129997x^1 - 0.034082x^2 + 0.000832x^3$



MW Averages

Peak No	Mp	Mn	Mw	Mz	Mz+1	Mv	PD
1	38249	30689	156551	643133	1117054	118290	5.10121

Figure S 5: GPC trace of PHB measured in chloroform (Chapter 9.3, Table 6, Entry 1).

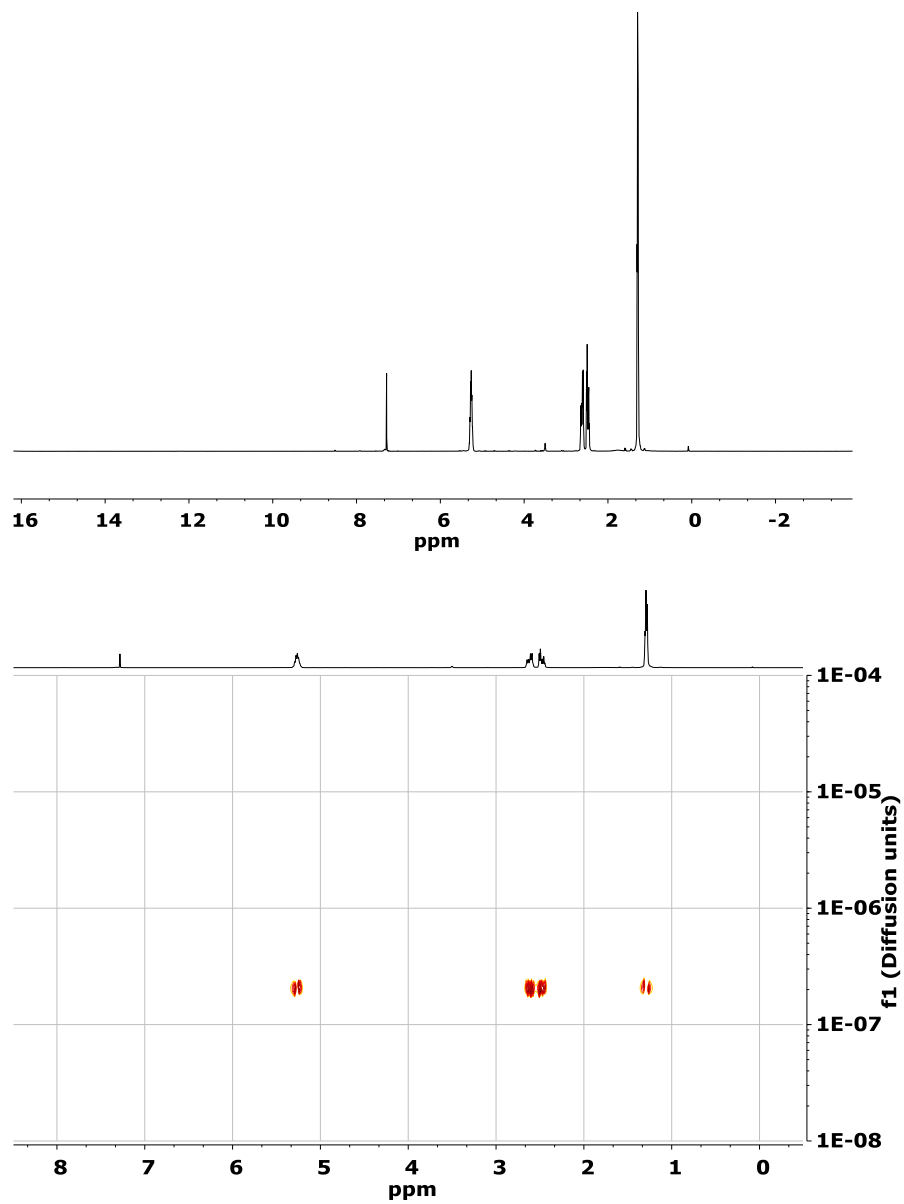


Figure S 6: ^1H and DOSY-NMR of PHB ($P_r = 0.67$) in CDCl_3 .

14.6 Supporting Information: “(Co)polymerization of (-)-Menthide and β -Butyrolactone catalyzed by Heteroaromatic Yttrium-bis(phenolates): Tuning Material Properties of Sustainable Polyesters”

Supporting Information for the Manuscript Entitled

(Co)polymerization of (-)-Menthide and β -Butyrolactone catalyzed by Heteroaromatic Yttrium-bis(phenolates): Tuning Material Properties of Sustainable Polyesters

Friederike Adams, Thomas M. Pehl, Moritz Kränzlein, Sebastian A. Kernbichl, and Bernhard Rieger*

WACKER-Chair of Macromolecular Chemistry
Catalysis Research Center
Department of Chemistry
Technical University Munich
Lichtenbergstr. 4, 85748 Garching bei München (Germany)
E-mail: rieger@tum.de

Table of Contents

1) Experimental section.....	2
2) Characterization of monomers.....	4
3) NMR spectra of polymers.....	7
4) ESI-MS analysis.....	15
5) GPC-traces.....	16
6) Kinetic measurements of <i>rac</i> -BBL with catalyst 4.....	23
7) Kinetic measurements of (-)-menthide with catalyst 1.....	24
8) Thermogravimetric analysis.....	25
9) Differential scanning calorimetry.....	26
10) Powder-XRD.....	30
11) References.....	30

1) Experimental section

Materials, Methods and Characterization of Polymer-Samples:

All reactions were carried out under argon atmosphere using standard Schlenk or glovebox techniques. All glassware was heat dried under vacuum prior to use. Unless otherwise stated, all chemicals were purchased from Sigma-Aldrich, Acros Organics, or ABCR and used as received. Toluene, thf, diethyl ether, dichloromethane and pentane were dried using a MBraun SPS-800 solvent purification system. *Racemic* β -butyrolactone was purchased from Sigma-Aldrich and stirred with BaO (1.5 equivalents per amount of butyric, hydroxybutyric and crotonic acids; determined *via* ^1H -nmr spectroscopy) for 2 days. After centrifugation, the butyrolactone was dried over calcium hydride and distilled prior to use. (-)-Menthide was synthesized according to literature^[1-2] and further purified *via* double sublimation.

The precursor complexes $\text{Y}(\text{CH}_2\text{TMS})_3(\text{thf})_2$ and $\text{Y}(\text{bdsa})_3(\text{thf})_2$,^[3] the 2-methoxyethylamino-bis(phenolate) ligand^[4], $[(\text{ONOO})^{\text{tBu}}\text{Y}(\text{CH}_2\text{TMS})(\text{thf})]^{[5]}$ and complexes **1**^[6], **2**^[7], **3**^[8] and **4**^[9] are prepared according to literature procedure.

Nmr spectra were recorded on a Bruker AVIII-300, AVIII-400 and AVIII-500 Cryo spectrometer. Unless otherwise stated, ^1H - and ^{13}C -nmr spectroscopic chemical shifts δ are reported in ppm. δ (^1H) is calibrated to the residual proton signal, δ (^{13}C) to the carbon signal of the solvent. Deuterated solvents were obtained from Sigma-Aldrich and dried over 3 Å molecular sieves.

Elemental analysis was measured at the Laboratory for Microanalysis at the Institute of Inorganic Chemistry at the Technische Universität München.

GC-MS analysis was performed using a 7890B GC System from Agilent Technologies equipped with a 30 m HP-5MS UI column (ID = 0.25mm, film = 0.25 μm) and a 5977A mass selective detector from Agilent Technologies. He (5.0) was used as carrier gas.

Molecular weights and polydispersities of PHB and polydispersities of all copolymers were measured *via* gel permeation chromatography (GPC) with samples of 2-3 mg/ml concentration on an PL-GPC 50 Plus from Polymer Laboratories using a refractive index detector (RI detector) with chloroform as eluent relative to polystyrene standards. Absolute molecular weights and polydispersities of PM and the first block of the copolymers were determined by triple detection using two angle light scattering, a refractive index detector and a viscometer in tetrahydrofuran with 0.22 g/L 2,6-di-tert-butyl-4-methylphenol as eluent. The dn/dc was determined *via* GPC measurement of three samples with different concentrations of polymers with various molar masses. It was determined as 0.067 mL/g.

The tacticity determination of PHB was performed by ^{13}C -nmr-spectroscopy at room temperature in CDCl_3 on a AVIII 500 Cryo spectrometer with 1000 scans and analyzed according to literature.^[10]

DSC measurements were performed on a DSC Q2000 from TA Instruments. It was measured in exo down mode with a heating rate of 10 K/min in a temperature range of $-50\text{ }^\circ\text{C}$ – $170\text{ }^\circ\text{C}$ with samples of 6-9 mg. Three cycles were run per measurement (heating, cooling, heating). The first run is omitted in the graphics.

TGA was measured on a TGA Q5000 from TA Instrument. A high-resolution method was used with a sensitivity of 2.0 and a resolution of 4.0. The sample was heated with a ramp of 10 °C/min to 500.00 °C under argon.

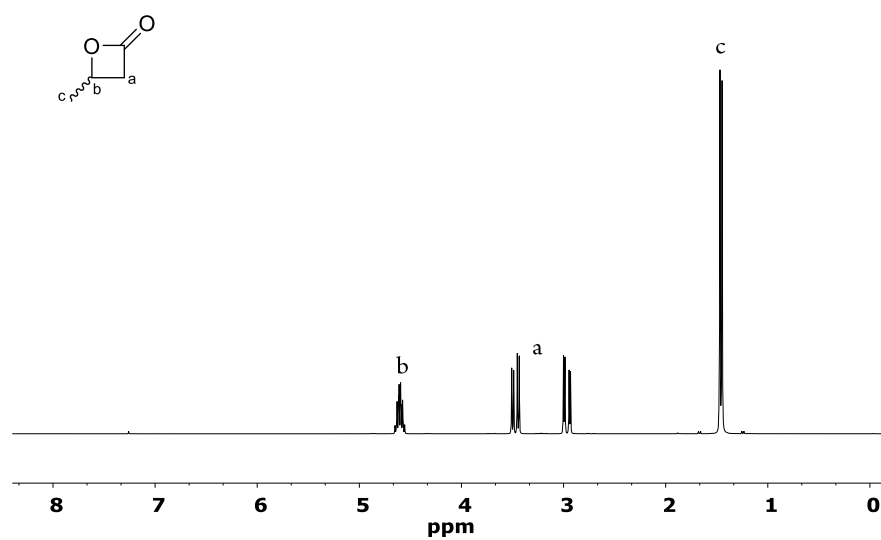
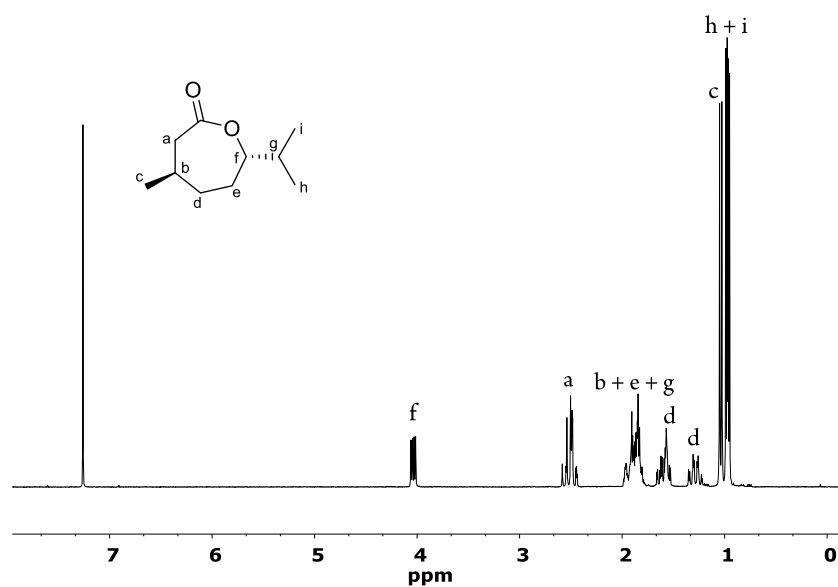
ESI-MS analytical measurements were performed with acetonitrile solutions on a Varian 500-MS spectrometer in positive ionization mode.

Powder X-ray diffraction measurements were performed using *Bragg-Brentano* geometry in a *PANalytical* Empyrean diffractometer equipped with a *PANalytical* PIXcel 1D detector. X-ray Cu K α radiation ($\lambda_1 = 1.5406 \text{ \AA}$, $\lambda_2 = 1.5444 \text{ \AA}$, $I_2/I_1 = 0.5$) was used for the measurements. K β radiation is removed with a Ni-filter. Voltage and intensity were 45 kV and 40 mA, respectively. The measurement range was from 5.0° to 40.0° (2θ) with a step size of 0.01313° (2θ) and an acquisition time of 313.65 seconds per step. The obtained diffractograms were Cu-K α stripped using *Rachingers* method and the background was determined after *Sonneveld* and *Visser* with a bending factor of 8 and a granularity of 82. For comparison reasons, the highest reflex of all diffractograms is normalized to 1.

In situ IR measurements were performed under argon atmosphere using an ATR IR *MettlerToledo* system.

Stress-strain measurements were performed on a *ZwickRoell* machine with a strain rate of 5 mm/min and analyzed with testXpert II software. Dog-bone shaped specimens were prepared *via* hot molding at 117 °C under vacuum. Young's modulus was determined as the slope between a strain of 0.05% and 0.5%.

2) Characterization of monomers

Figure S 1: ¹H-nmr spectrum of *rac*-BBL after distillation (CDCl₃, 300 MHz).Figure S 2: ¹H-nmr spectrum of (-)-menthede after sublimation (CDCl₃, 300 MHz). Assignment according to Hillmyer and Tolman.^[1]

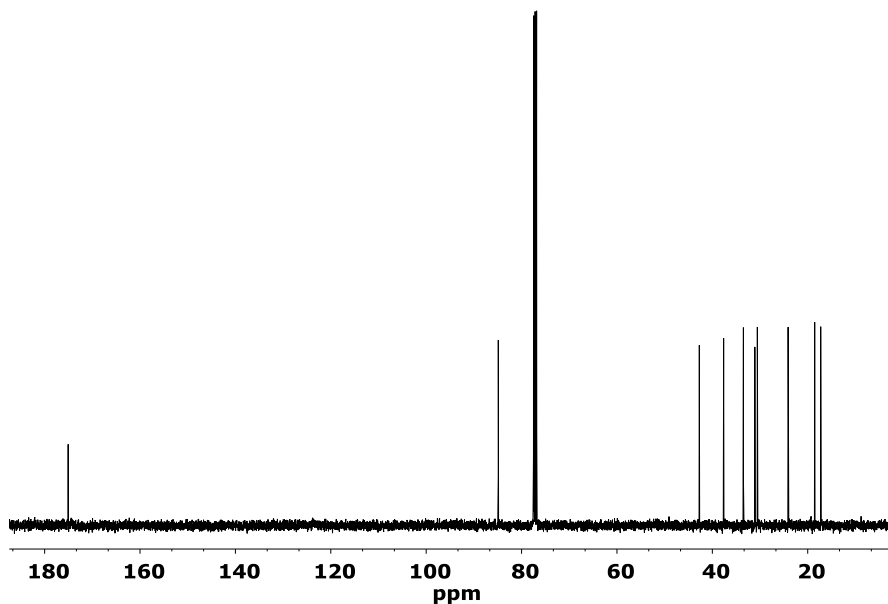
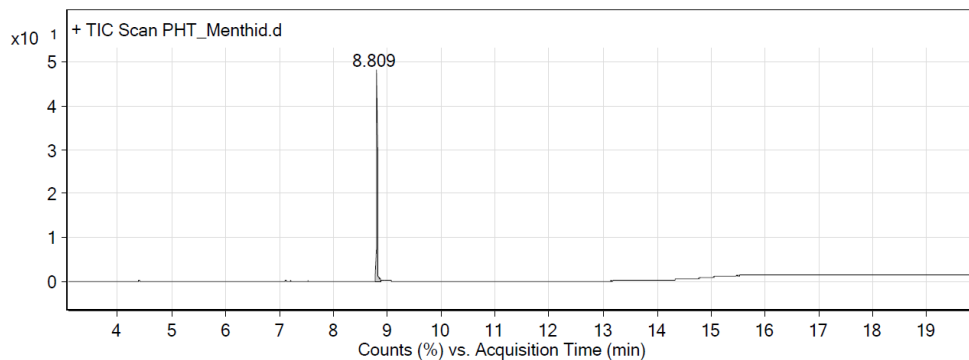


Figure S 3: ¹³C-nmr spectrum of (-)-menthine (101 MHz, CDCl₃).

Elemental analysis of (-)-menthine:

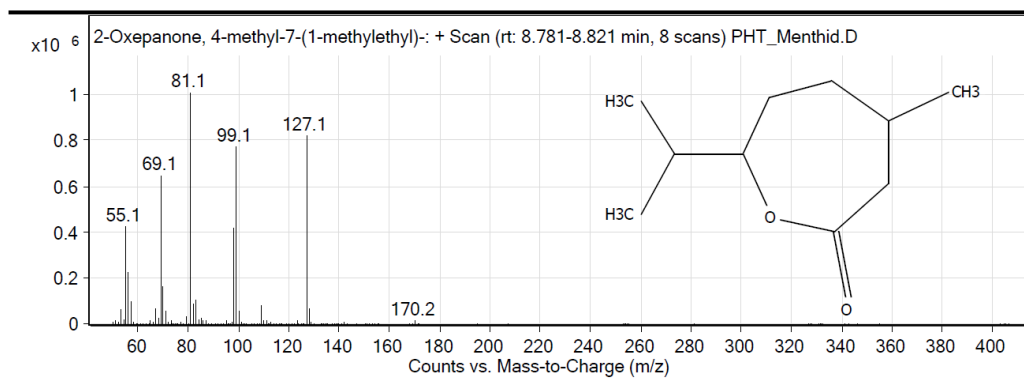
calculated: C 70.55 H 10.66
 found: C 70.52 H 10.78

GC-MS:

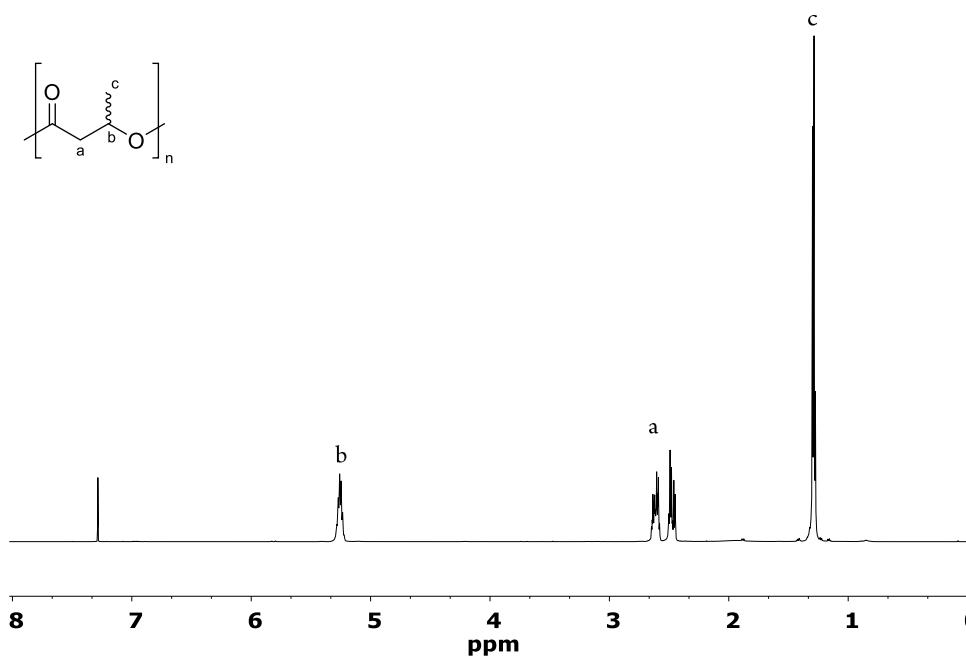
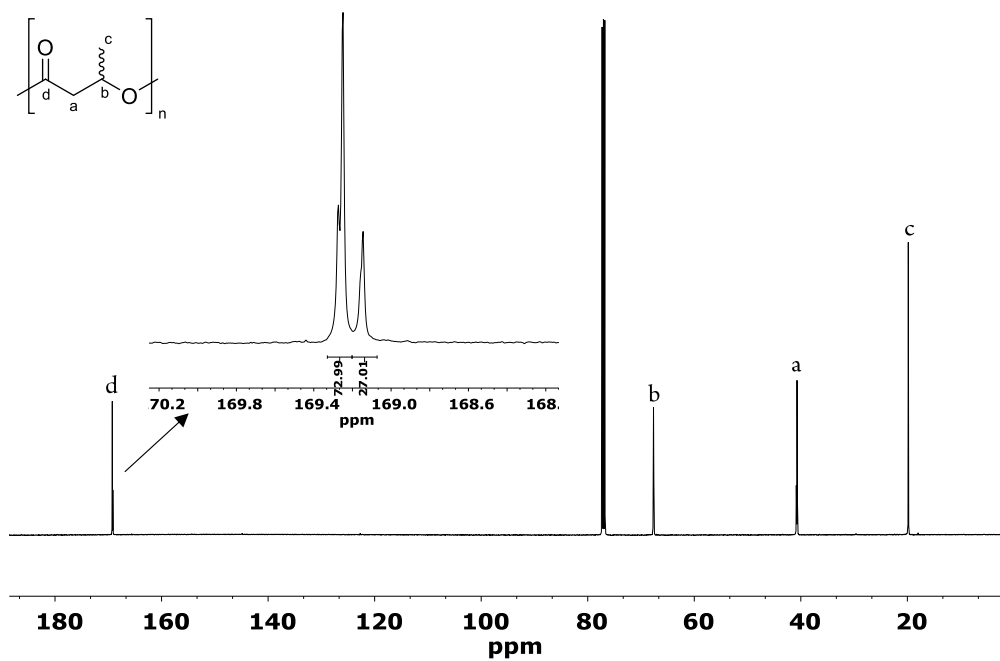


Integration Peak List						
Peak	Start	RT	End	Height	Area	Area %
1	8.765	8.809	8.884	11761657.79	15740309.77	100

Qualitative Analysis Report



3) NMR spectra of polymers

Figure S 4: $^1\text{H-NMR}$ spectrum of syndio-PHB (Table 2, Entry 9, 500 MHz, CDCl_3).Figure S 5: $^{13}\text{C-NMR}$ spectrum of PHB with $P_r = 0.73$ (126 MHz, 1000 scans, CDCl_3 , Table 2, Entry 9).

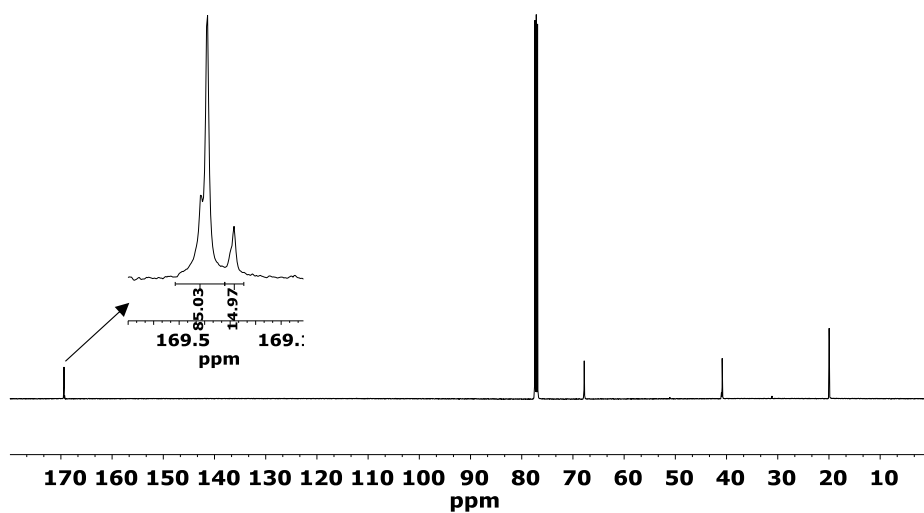


Figure S 6: ^{13}C -nmr spectrum of PHB with $P_r = 0.85$ (126 MHz, 1000 scans, CDCl_3 , Table 1, Entry 4).

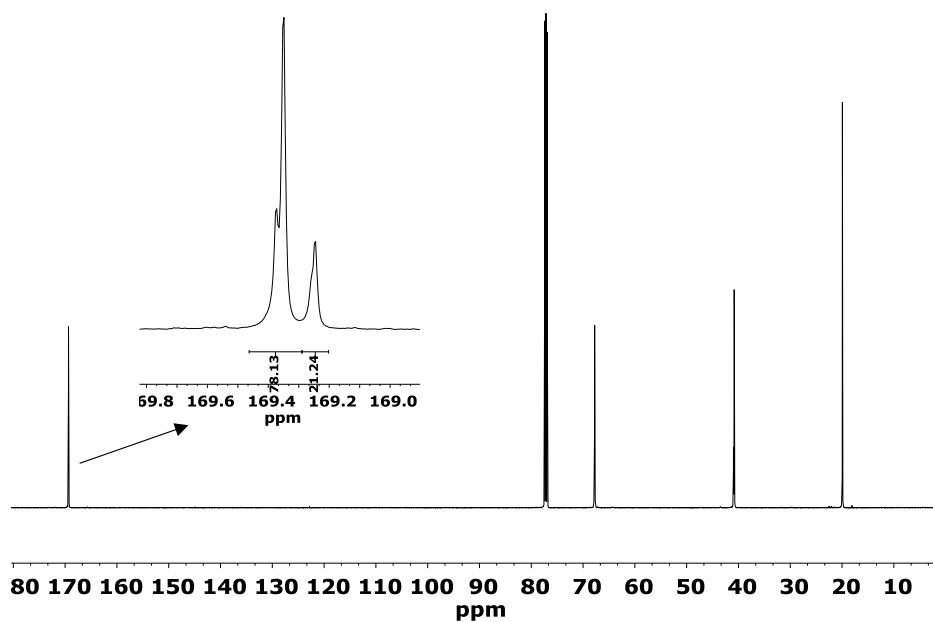


Figure S 7: ^{13}C -nmr spectrum of PHB with $P_r = 0.78$ (126 MHz, 1000 scans, CDCl_3 , Table 2, Entry 7).

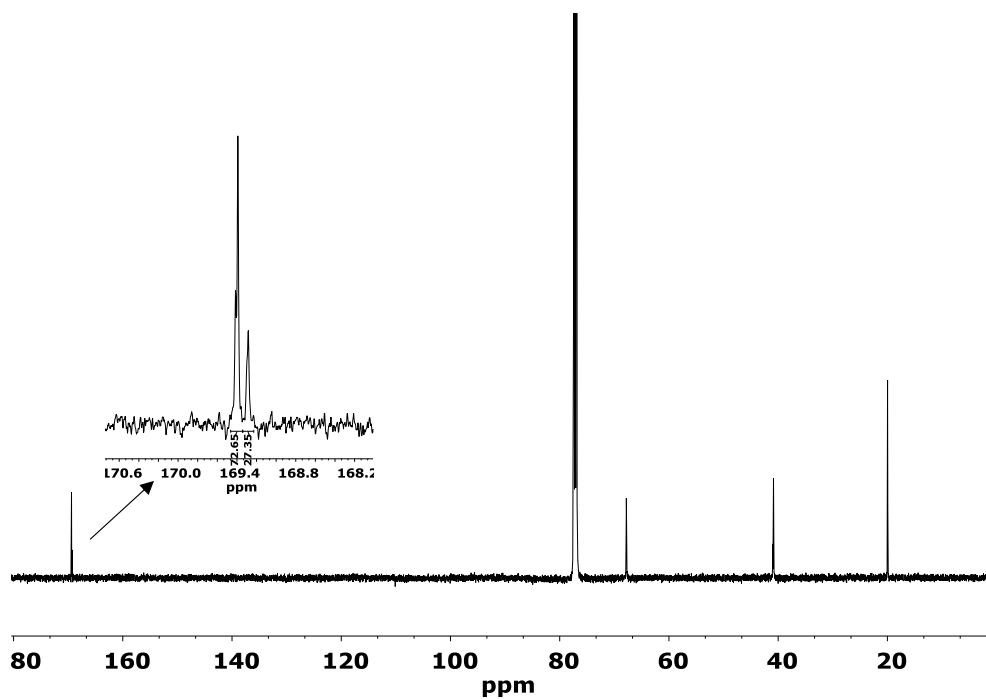


Figure S 8: ^{13}C -nmr spectrum of PHB with $P_r = 0.73$ (126 MHz, 1000 scans, CDCl_3 , Table 2, Entry 2).

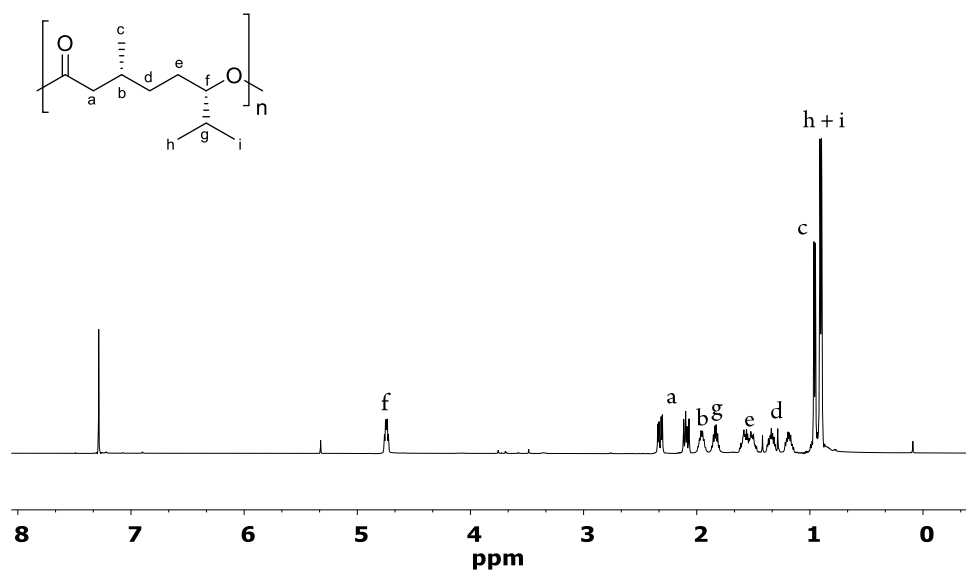


Figure S 9: ^1H -nmr spectrum of PM (Table 3, Entry 1, 500 MHz, CDCl_3). Assignment according to Hillymer and Tolman.^[1]

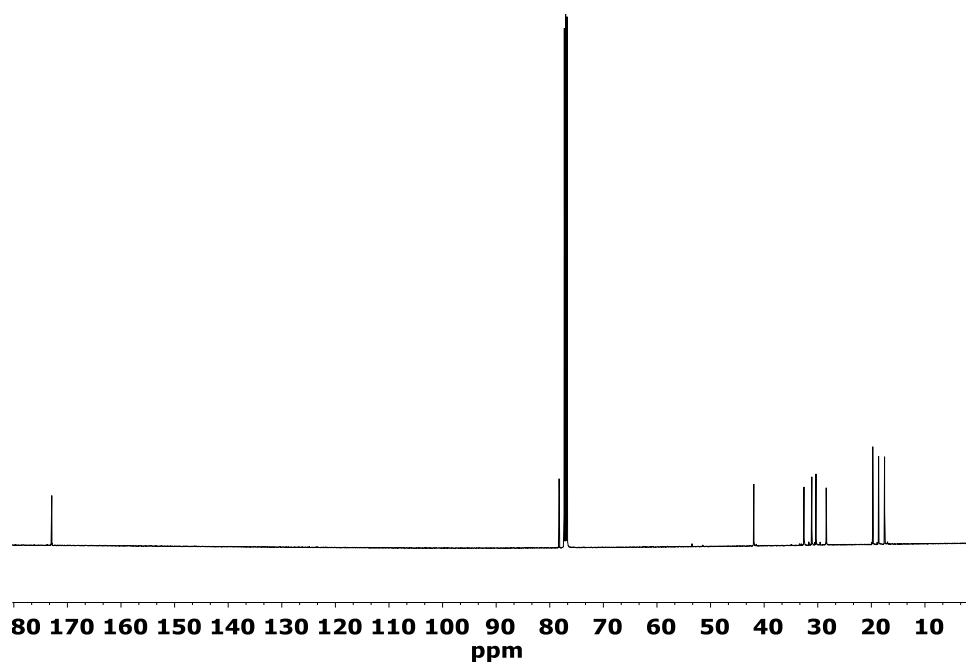


Figure S 10: ^{13}C -nmr spectrum of PM (126 MHz, 1000 scans, CDCl_3 , Table 3, Entry 2).

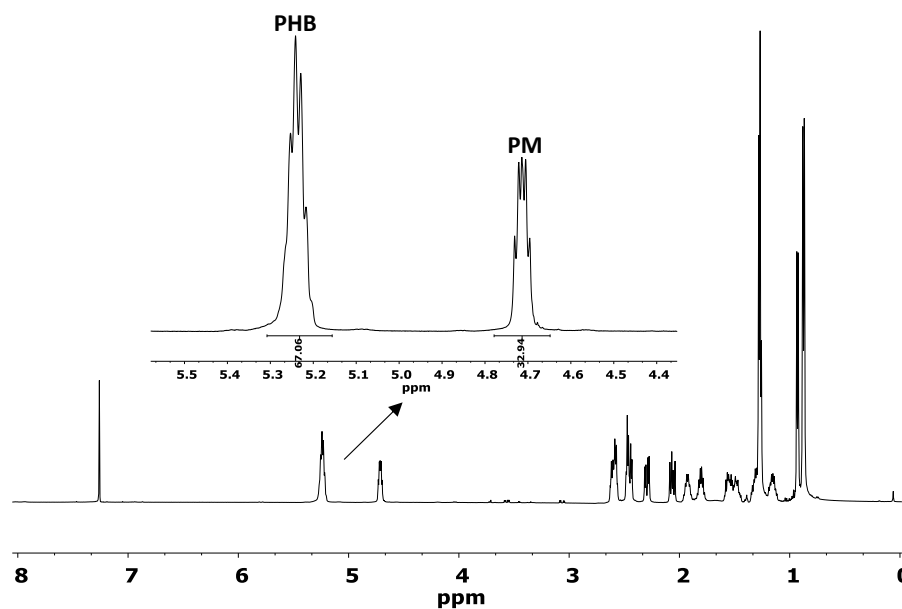


Figure S 11: ^1H -nmr spectrum of AB^1 (Table 4, Entry 1, 500 MHz, CDCl_3).

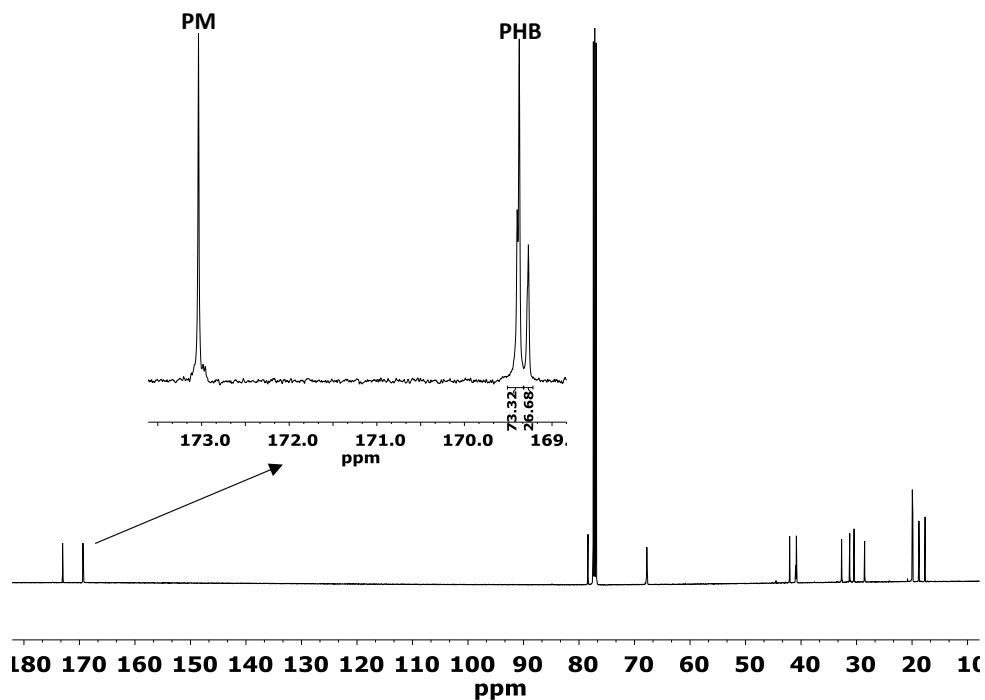


Figure S 12: ^{13}C -nmr spectrum of AB¹ (Table 4, Entry 1, 126 MHz, 1000 scans, CDCl_3).

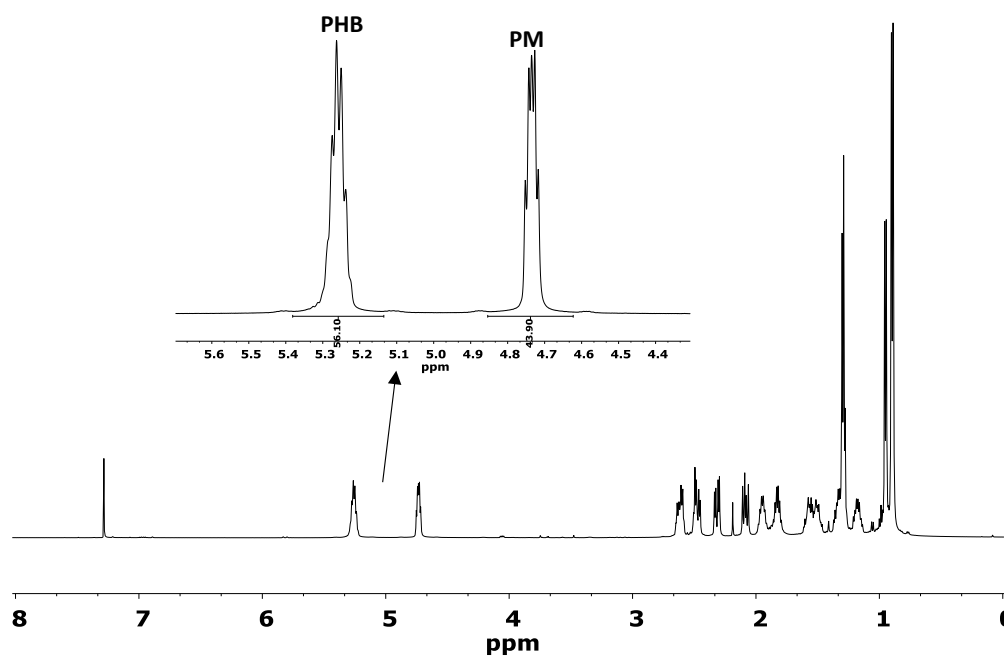


Figure S 13: ^1H -nmr spectrum of BAB³ (Table 4, Entry 5, 500 MHz, CDCl_3).

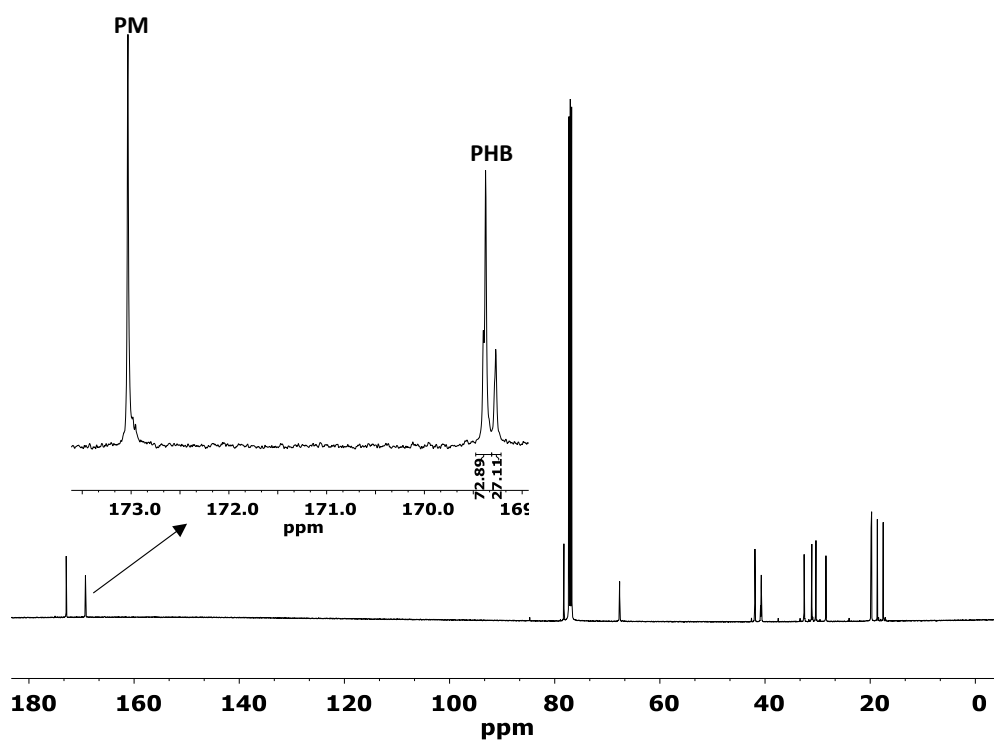


Figure S 14: ^{13}C -nmr spectrum of BAB^3 (Table 4, Entry 5, 126 MHz, 1000 scans, CDCl_3).

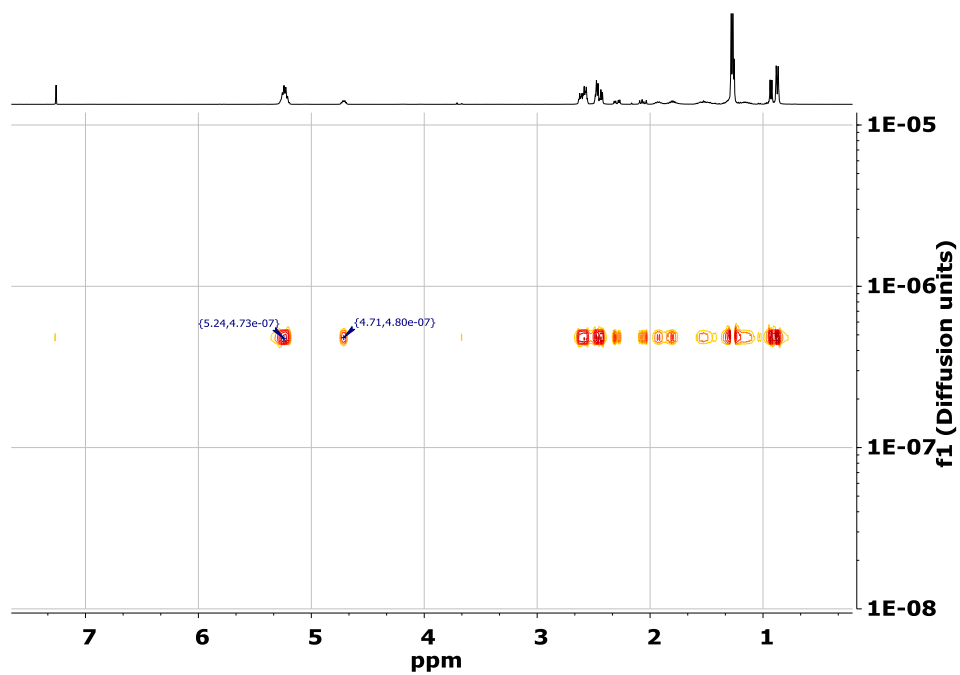


Figure S 15: DOSY-nmr of BAB^1 (Table 4, Entry 3, 400 MHz, 32 scans, CDCl_3 , resolution factor: 1, repetitions: 1, points in diffusion dimension: 128).

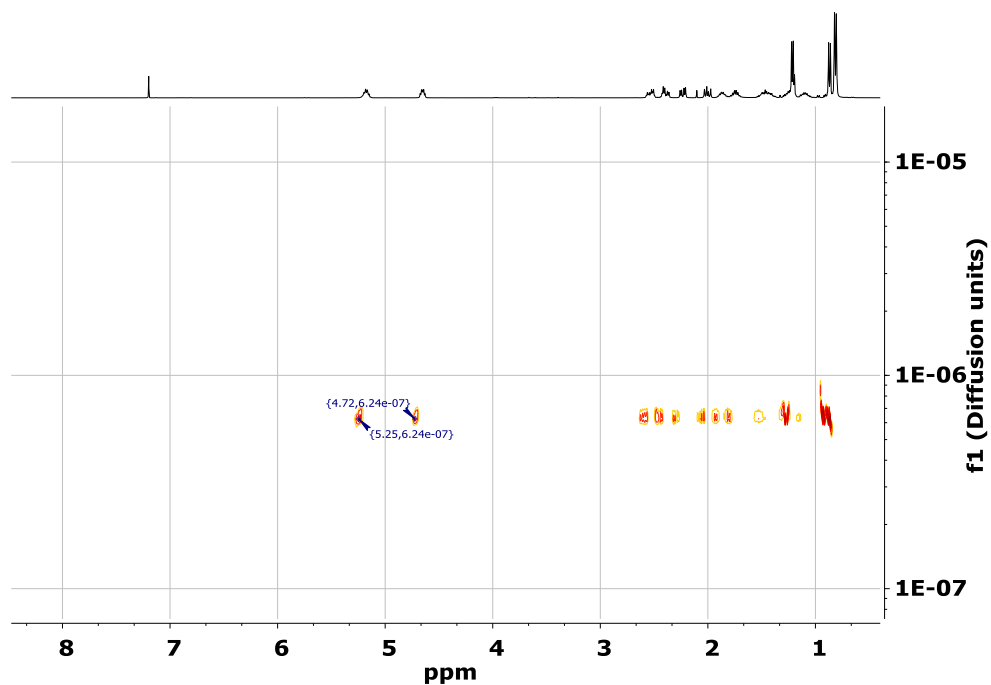


Figure S 16: DOSY-nmr of BAB³ (Table 4, Entry 5, 400 MHz, 32 scans, CDCl₃, resolution factor: 1, repetitions: 1, points in diffusion dimension: 128).

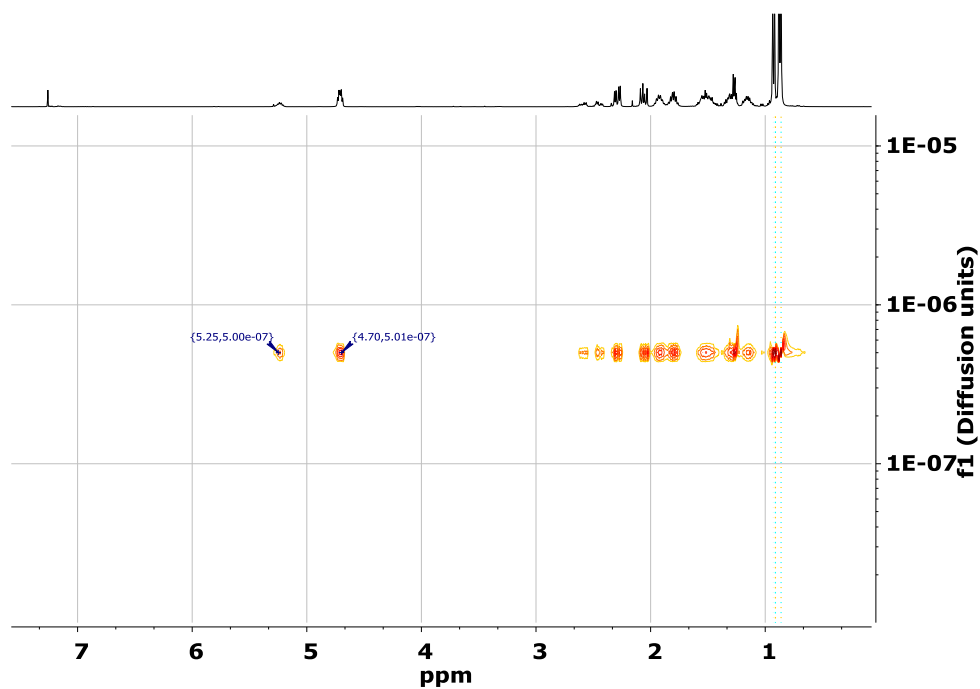


Figure S 17: DOSY-nmr of BAB⁴ (Table 4, Entry 6, 400 MHz, 32 scans, CDCl₃, resolution factor: 1, repetitions: 1, points in diffusion dimension: 128).

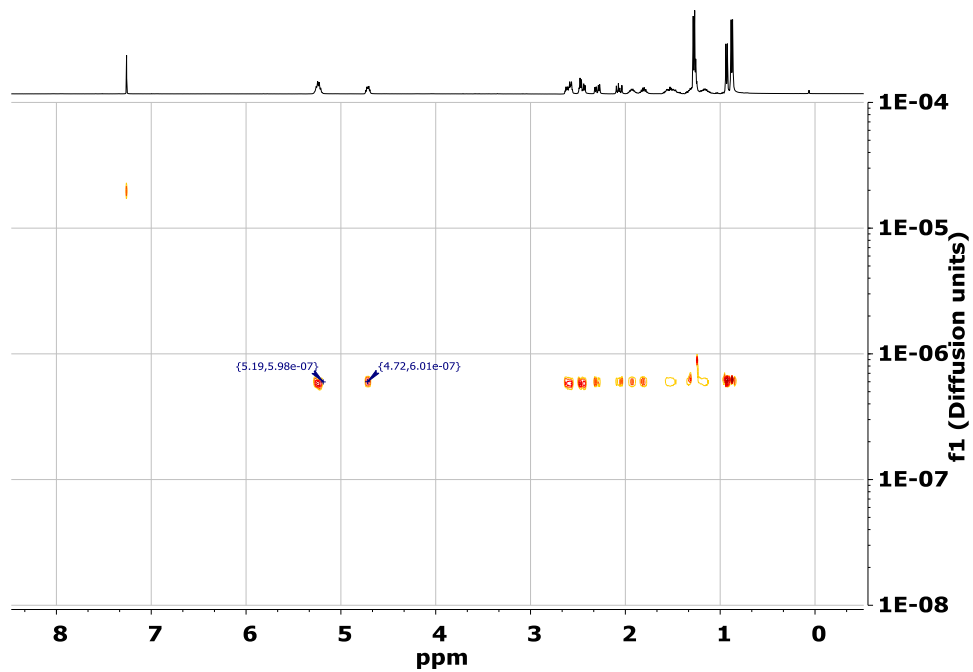


Figure S 18: DOSY-nmr of AB¹ (Table 4, Entry 1, 400 MHz, 32 scans, CDCl₃, resolution factor: 1, repetitions: 1, points in diffusion dimension: 128).

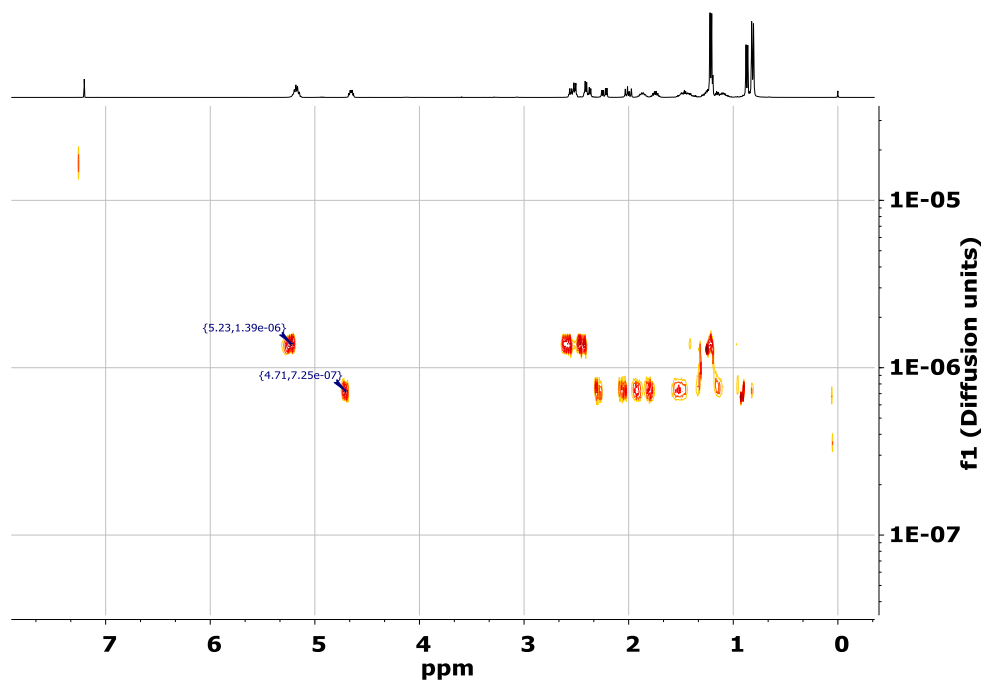


Figure S 19: DOSY-nmr of a blend from PM and PHB with the same composition (PM/PHB = 67:33; PM = 16800 g/mol) as AB¹ (400 MHz, 32 scans, CDCl₃, resolution factor: 1, repetitions: 1, points in diffusion dimension: 128).

4) ESI-MS analysis

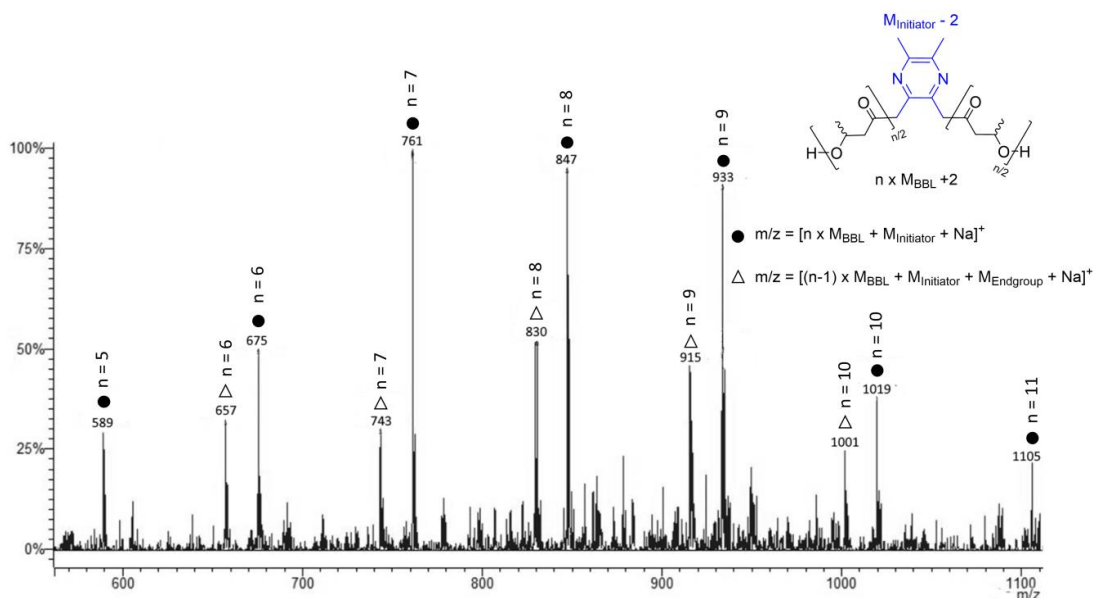


Figure S 20: End-group analysis by ESI-MS measured in acetonitrile with catalyst 4 and *rac*-BBL (7 μmol of catalyst, 93 μmol *rac*-BBL, 1 ml toluene, 20 $^{\circ}\text{C}$).

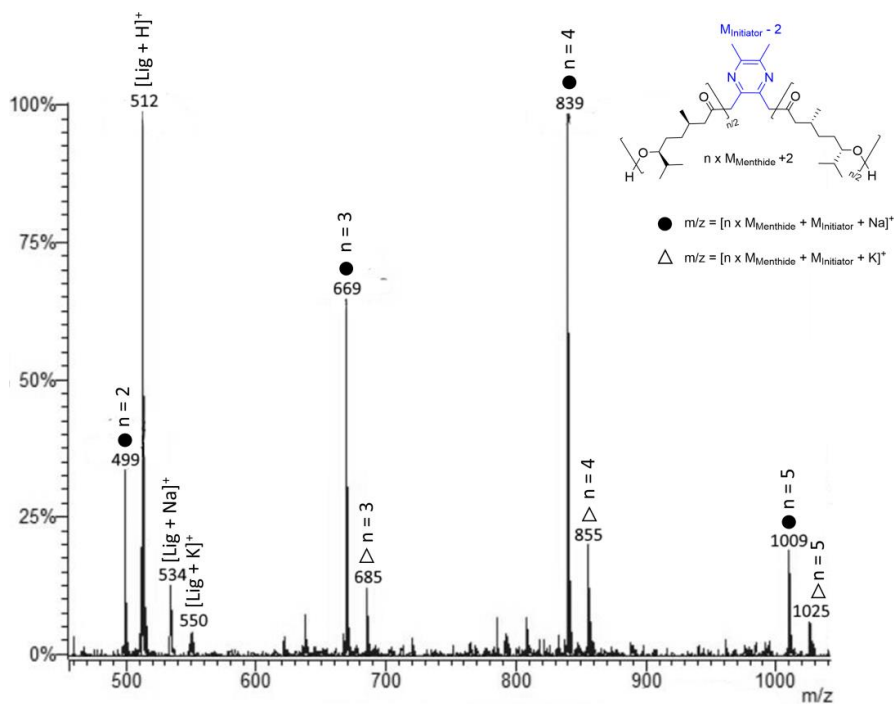


Figure S 21: End-group analysis by ESI-MS measured in acetonitrile with catalyst 4 and (-)-menthide (7 μmol of catalyst, 117 μmol (-)-menthide, 1 ml toluene, 20 $^{\circ}\text{C}$).

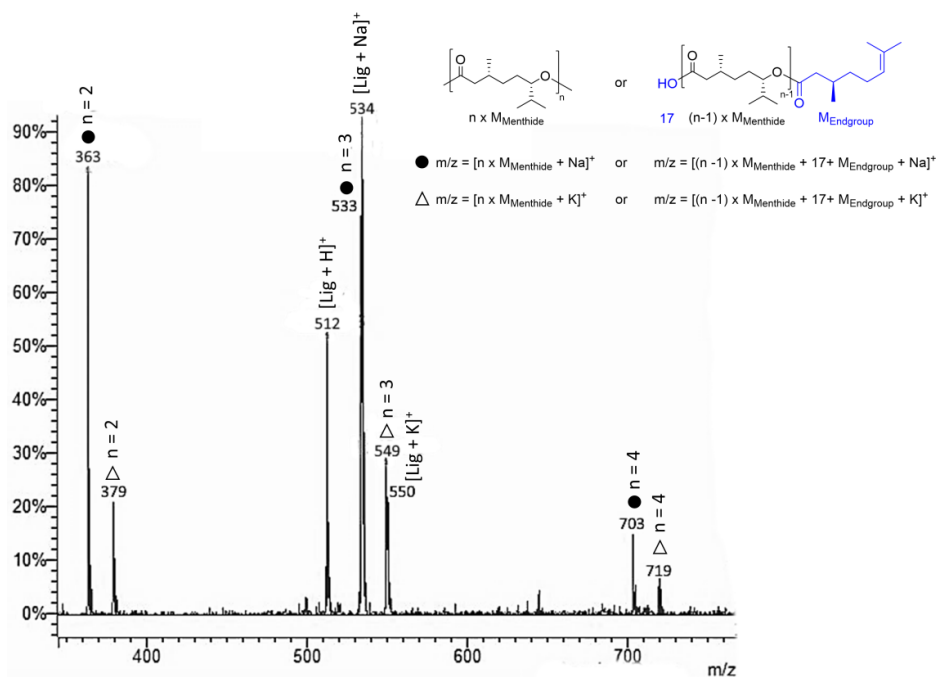
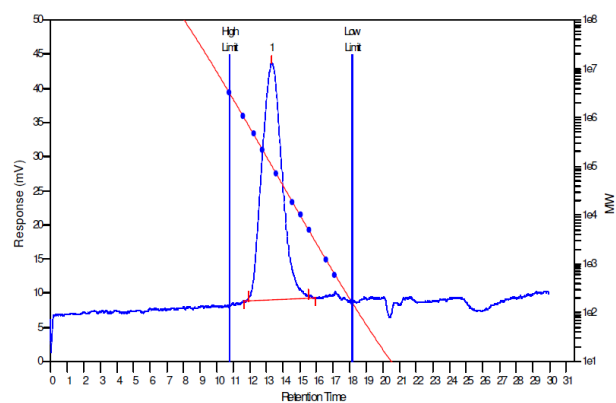


Figure S 22: End-group analysis by ESI-MS measured in acetonitrile with catalyst 1 and (-)-menthite (16 μmol of catalyst, 73 μmol (-)-menthite, 1 ml toluene, 20 $^{\circ}\text{C}$).

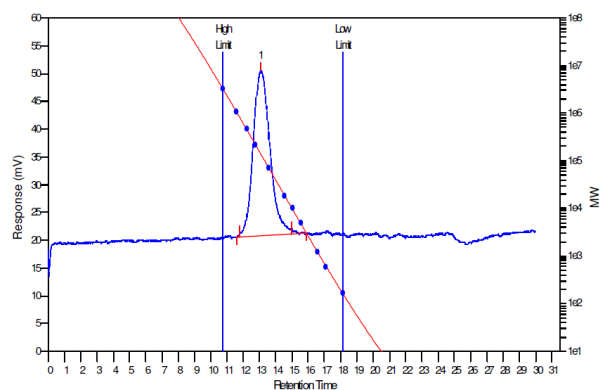
5) GPC-traces



MW Averages

Peak No	Mp	Mn	Mw	Mz	Mz+1	Mv	PD
1	101292	66076	122933	192509	265667	113845	1.86048

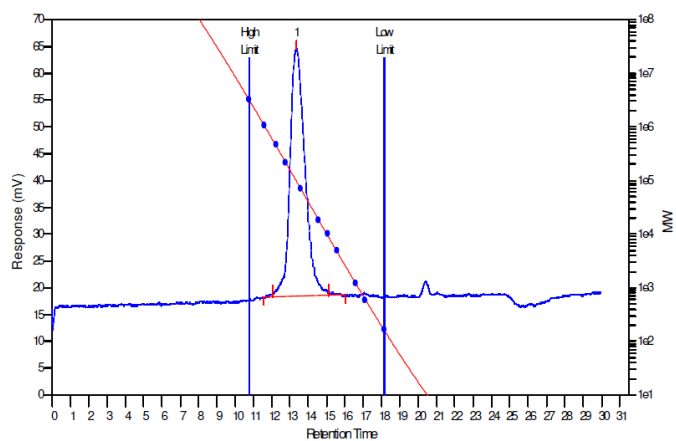
Figure S 23: GPC trace in chloroform of PHB produced with catalyst 1 (Table 1, Entry 1).



MW Averages

Peak No	Mp	Mn	Mw	Mz	Mz+1	Mv	PD
1	139420	91903	150558	220023	301920	141478	1.63823

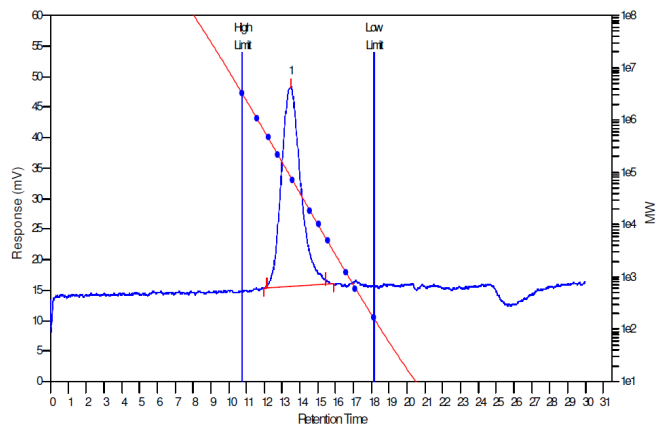
Figure S 24: GPC trace in chloroform of PHB produced with catalyst 2 (Table 1, Entry 2).



MW Averages

Peak No	Mp	Mn	Mw	Mz	Mz+1	Mv	PD
1	94587	68886	97668	134805	192075	93136	1.41782

Figure S 25: GPC trace in chloroform of PHB produced with catalyst 3 (Table 1, Entry 3).



MW Averages

Peak No	Mp	Mn	Mw	Mz	Mz+1	Mv	PD
1	80614	52753	92064	137601	188215	86029	1.74519

Figure S 26: GPC trace in chloroform of PHB produced with catalyst 4 (Table 1, Entry 4).

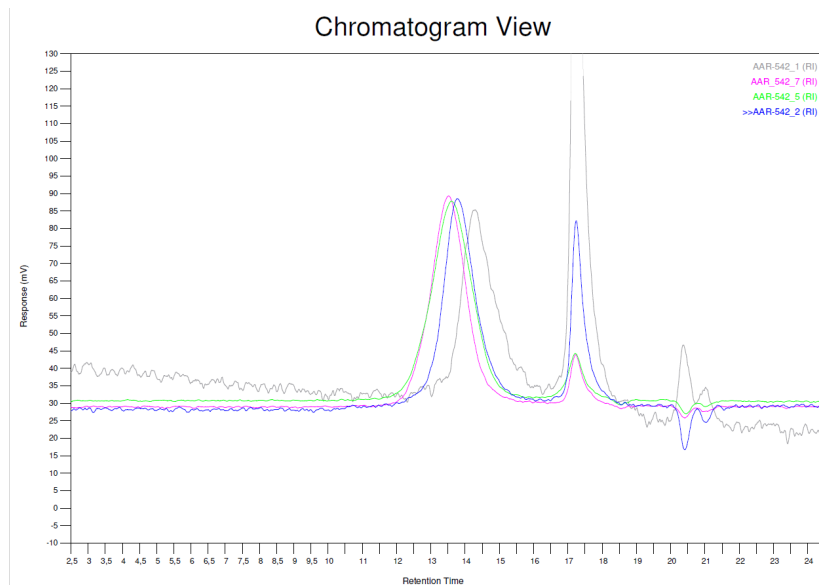


Figure S 27: Shift of molar masses during BBL-polymerization with catalyst 4 (Figure 3) measured via aliquot method (Aliquot 1 (grey), 2 (blue), 5 (green), and 7 (pink) are depicted). All samples are measured on a GPC in chloroform.

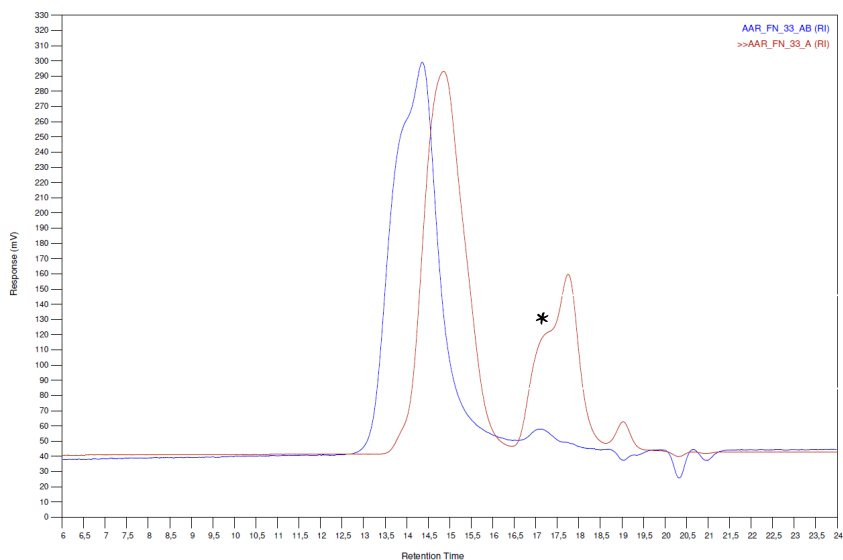


Figure S 28: Shift from Block A (red) to AB¹ (blue, Table 4, Entry 1). Both samples are measured on a GPC in chloroform (* = residual menthide in aliquot sample).

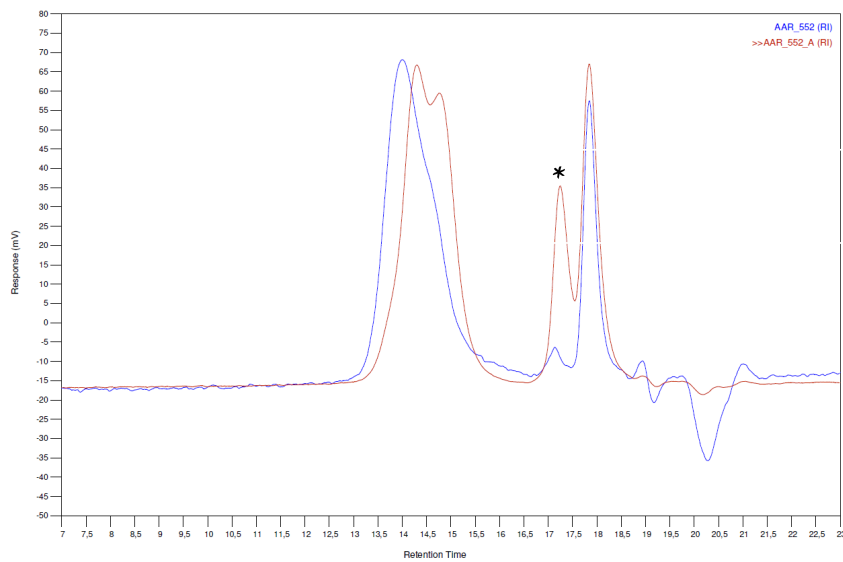


Figure S 29: Shift from Block A (red) to BAB³ (blue, Table 4, Entry 5). Both samples are measured on a GPC in chloroform (* = residual menthide in aliquot sample).

Analysis Using Method: Triple

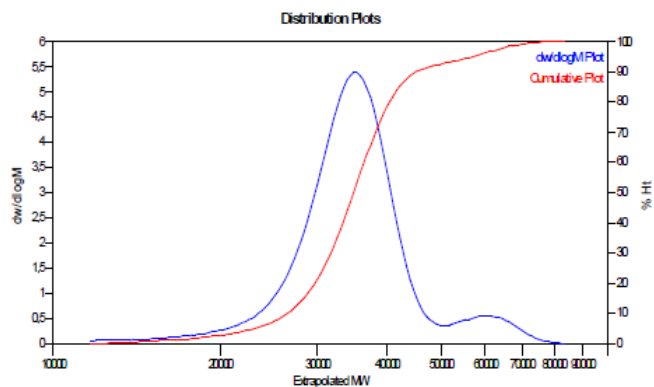
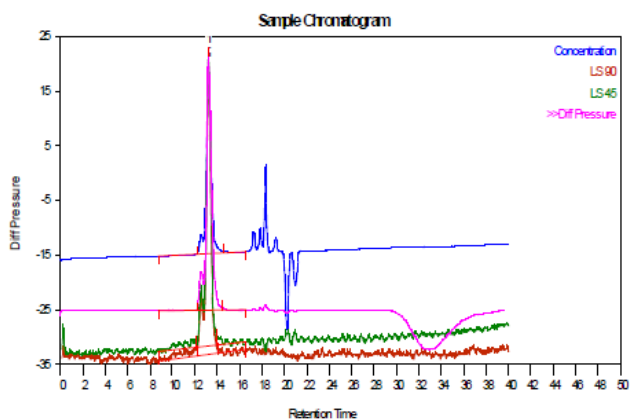
Results File: C:\Cirrus Workbooks\THF-2017-multi\30.05.2018-0002-Repeat (01).rst
 Calculated dn/dc 0.067000; dn/dc used 0.067000

Ligt Scattering Results:

LS 15° Mw: 33577

Bulk IV 0.314186

LS 90° Mw: 34209



MW Averages

Peak No	Mp	Mn	Mw	Mz	Mz+1	Mv	PD
1	35300	33366	35635	38104	41028	34505	1.068

Figure S 30: GPC trace in tetrahydrofuran of PM produced with catalyst 1 (Table 3, Entry 1).

Analysis Using Method: Triple

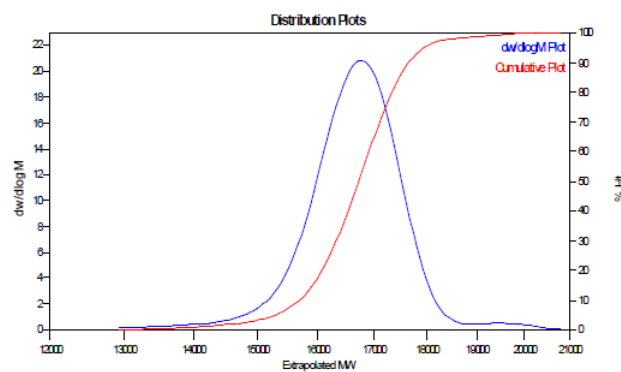
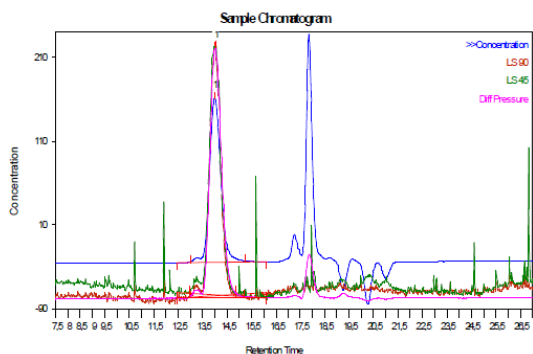
Results File: C:\Cirrus Workbooks\THF-2017-multi\2018-10-14_kem-0003-Repeat (01).rst
 Calculated dn/dc 0.067000; dn/dc used 0.067000

Ligt Scattering Results:

LS 15° Mw: 15693

Bulk IV 0.175695

LS 90° Mw: 14554

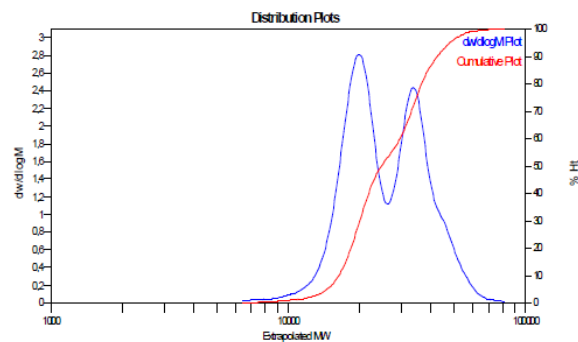
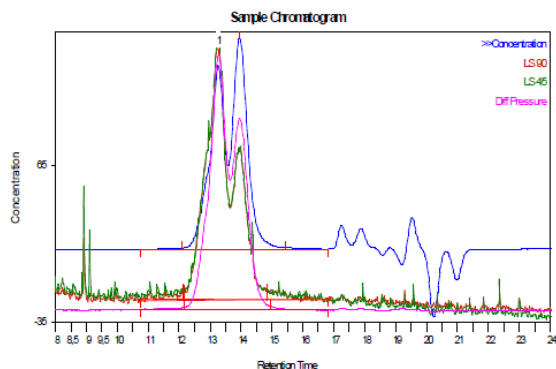


MW Averages

Peak No	Mp	Mn	Mw	Mz	Mz+1	Mv	PD
1	16790	16627	16674	16721	16767	16567	1.00283

Figure S 31: GPC trace in tetrahydrofuran of PM produced with catalyst 2 (Table 3, Entry 5).

Analysis Using Method: Triple
 Results File: C:\Cirus Workbooks\THF-2017-multi\2018-09-25-kem-0002-Repeat (02).rst
 Calculated dn/dc: 0.067000; dn/dc used: 0.067000
 Light Scattering Results: Bulk IV: 0.235222
 LS 15° Mw: 25981 LS 90° Mw: 26480

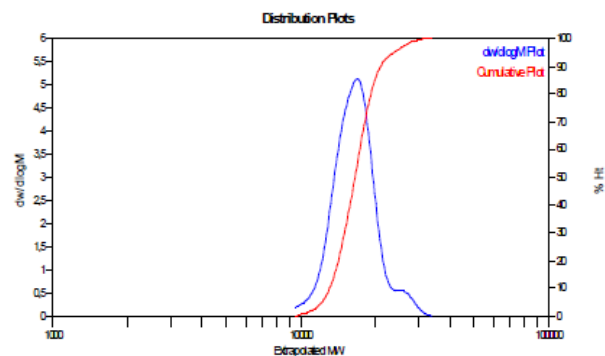
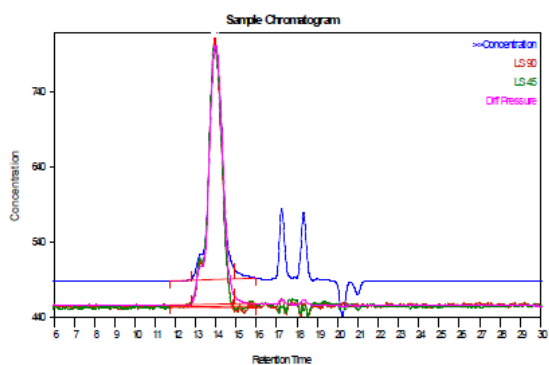


MW Averages

Peak No	Mp	Mn	Mw	Mz	Mz+1	Mv	PD
1	19976	23715	27496	31720	36095	25993	1.15943

Figure S 32: GPC trace in tetrahydrofuran of PM produced with catalyst 4 (Table 3, Entry 6).

Analysis Using Method: Triple
 Results File: C:\Cirus Workbooks\THF-2017-multi\2018_01_06_aar-0005-Repeat (01).rst
 Calculated dn/dc: 0.067000; dn/dc used: 0.067000
 Light Scattering Results: Bulk IV: 0.200289
 LS 15° Mw: 16255 LS 90° Mw: 16839



MW Averages

Peak No	Mp	Mn	Mw	Mz	Mz+1	Mv	PD
1	16847	16210	16851	17560	18355	16581	1.0395

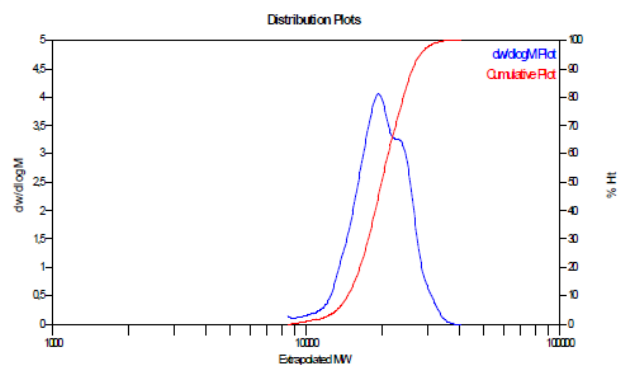
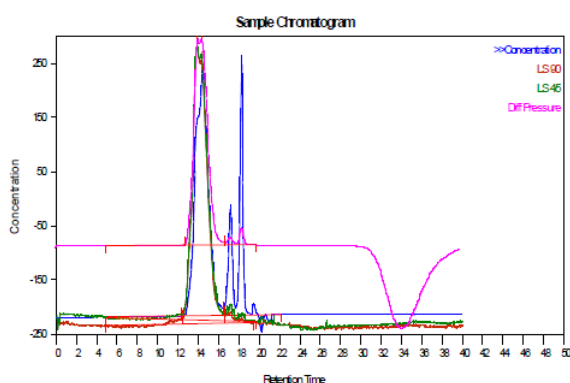
Figure S 33: GPC trace in tetrahydrofuran of Block A of AB¹ produced with catalyst 4 (Table 4, Entry 1).

Analysis Using Method: Triple

Results File: C:\Cirrus Workbooks\THF-2017-multi\2018_04_06_aar-0002-Repeat (01).rst
 Calculated dn/dc: 0.067000; dn/dc used 0.067000

Light Scattering Results:
 LS 15° Mw: 18461

Bulk IV 0.177029
 LS 90° Mw: 18835



MW Averages

Peak No	Mp	Mn	Mw	Mz	Mz+1	Mv	PD
1	19228	19036	20129	21187	22214	19893	1.05739

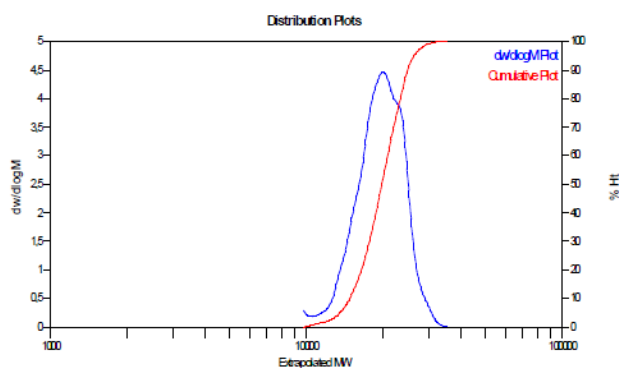
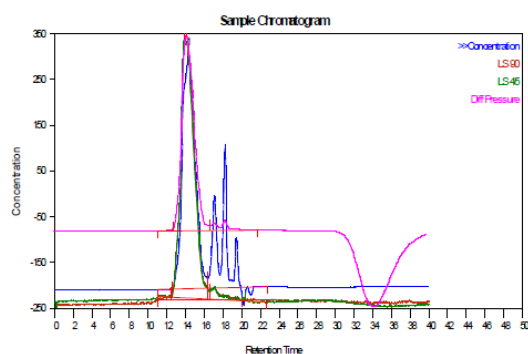
Figure S 34: GPC trace in tetrahydrofuran of Block A of BAB² produced with catalyst 4 (Table 4, Entry 4).

Analysis Using Method: Triple

Results File: C:\Cirrus Workbooks\THF-2017-multi\2018_04_06_aar-0003-Repeat (02).rst
 Calculated dn/dc: 0.067000; dn/dc used 0.067000

Light Scattering Results:
 LS 15° Mw: 18299

Bulk IV 0.185203
 LS 90° Mw: 19427



MW Averages

Peak No	Mp	Mn	Mw	Mz	Mz+1	Mv	PD
1	19973	18950	19785	20581	21342	19589	1.04402

Figure S 35: GPC trace in tetrahydrofuran of Block A of BAB⁴ produced with catalyst 4 (Table 4, Entry 6).

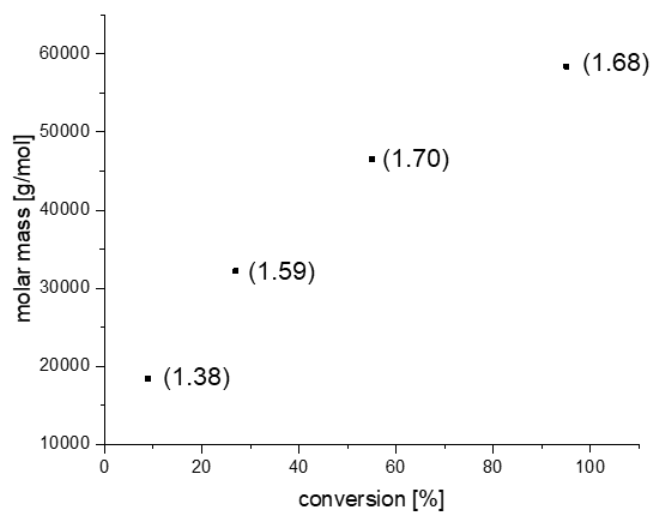
6) Kinetic measurements of *rac*-BBL with catalyst 4

Figure S 36: Growth of the molar mass M_n [g/mol] (measured *via* GPC in chloroform) as a function of monomer conversion (determined *via* ^1H nmr spectroscopy) during BBL-polymerization with catalyst 4 (\bar{D} in brackets).

7) Kinetic measurements of (-)-menthide with catalyst 1

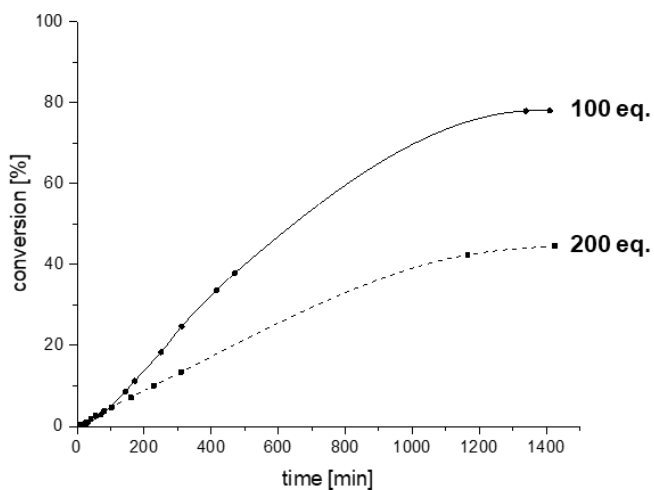


Figure S 37: Catalytic activity of catalyst 1 with 100 and 200 eq. of (-)-menthide ([cat.] = 74.7 μmol , toluene = 1.5 ml, T = 25 $^{\circ}\text{C}$) measured via aliquot method. Conversion determined via ^1H -nmr spectroscopy.

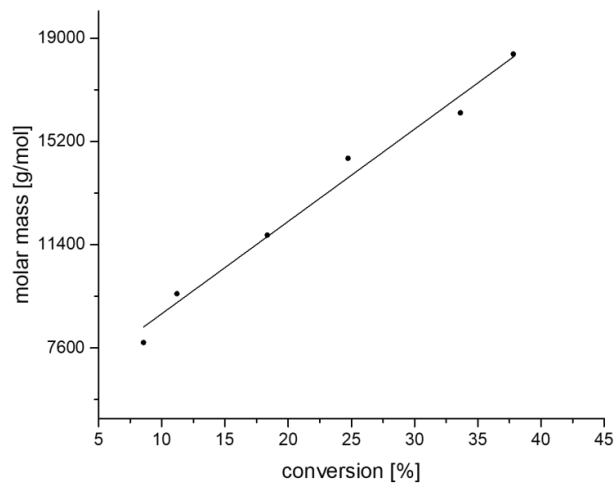


Figure S 38: Linear growth of the molar mass M_n [g/mol] (measured via GPC in chloroform) as a function of monomer conversion (determined via ^1H nmr spectroscopy) during (-)-menthide-polymerization (100 eq.) with catalyst 1.

8) Thermogravimetric analysis

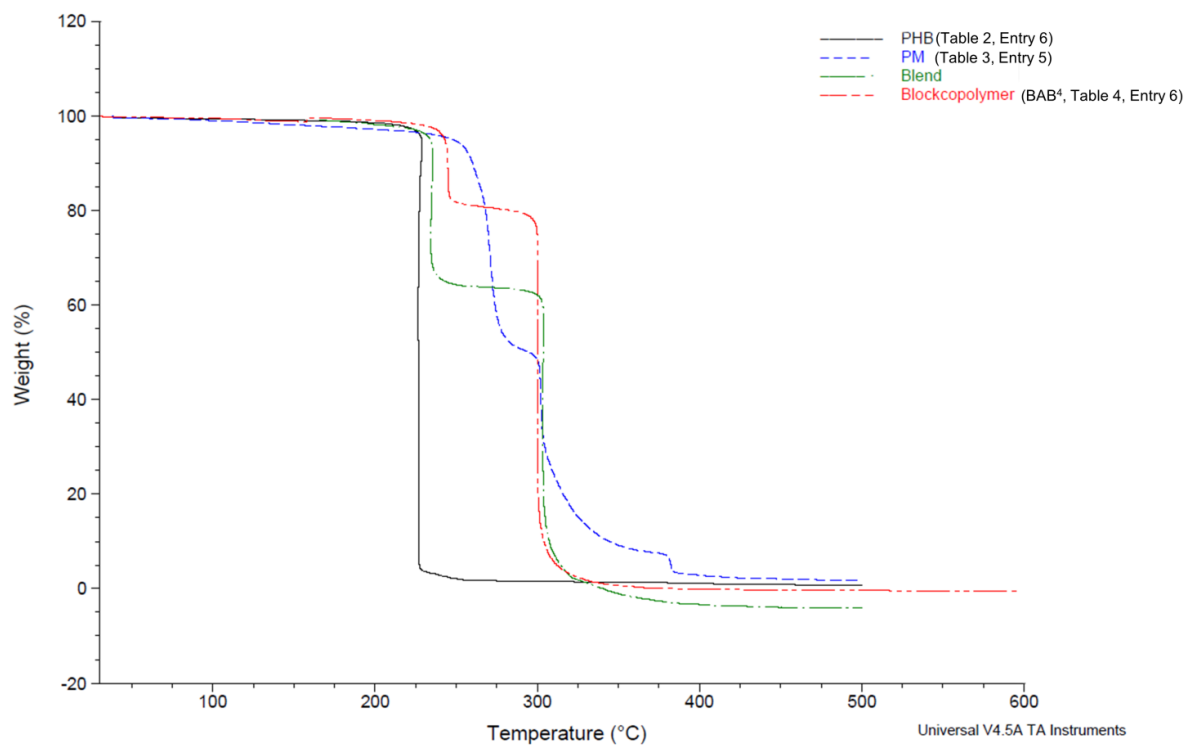


Figure S 39: High-resolution TGA of PHB (black), PM (blue), a blend of these two samples (green) and BAB⁴ (red).

9) Differential scanning calorimetry

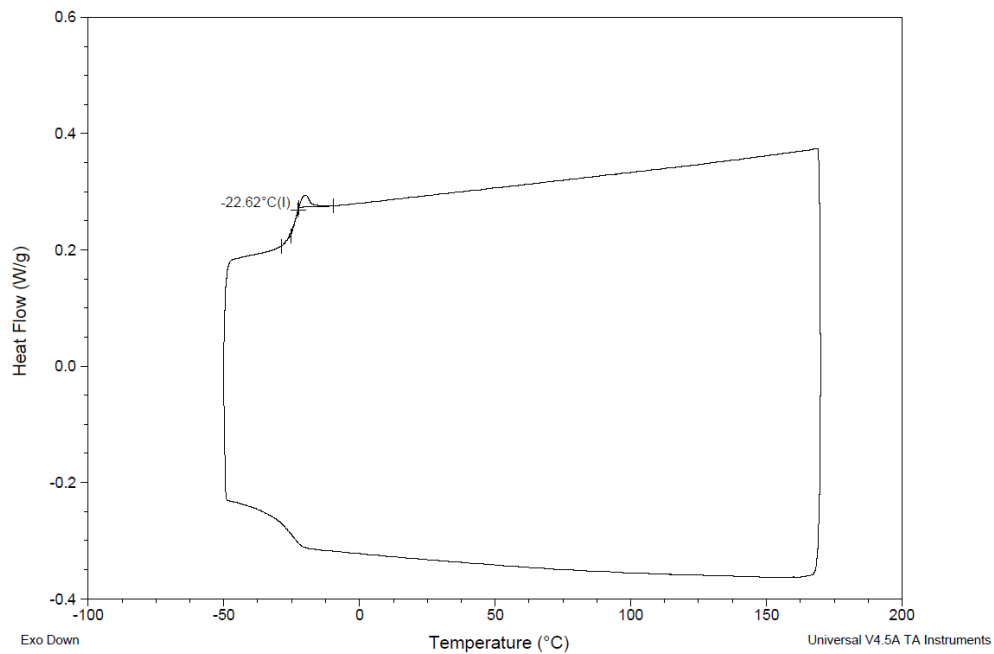


Figure S 40: DSC analysis of PM (Table 3, Entry 5).

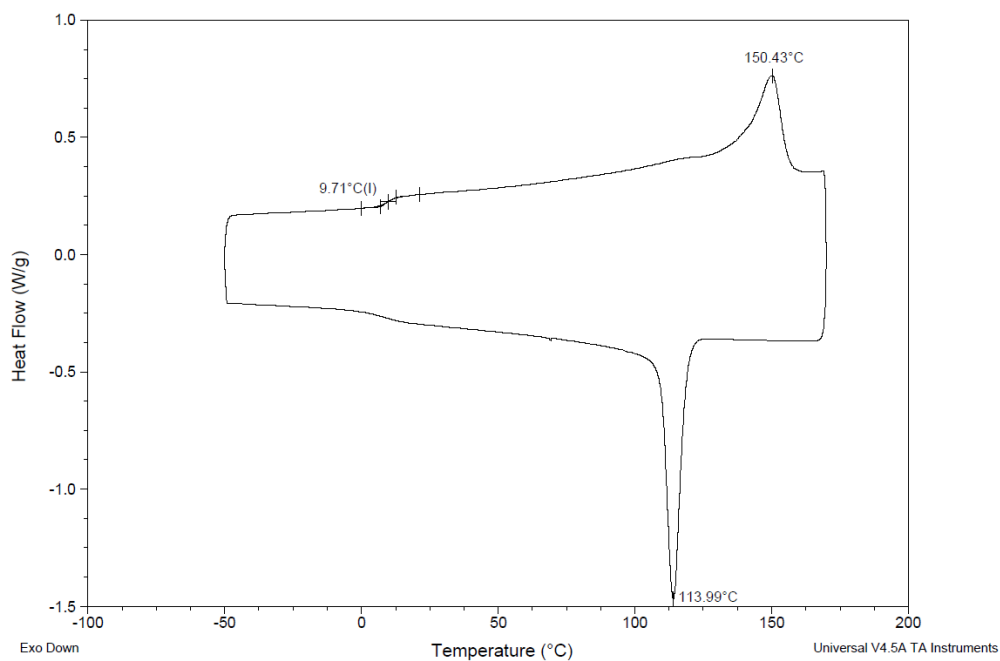


Figure S 41: DSC analysis of PHB ($P_r = 0.85$; Table 1, Entry 4).

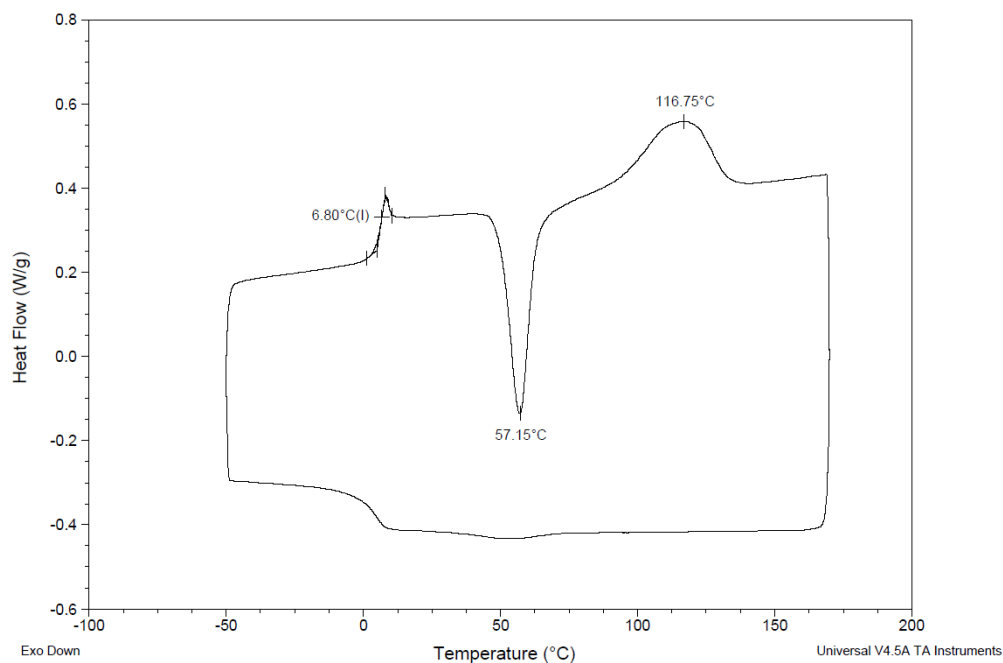


Figure S 42: DSC analysis of PHB ($P_r = 0.74$; Table 2, Entry 3).

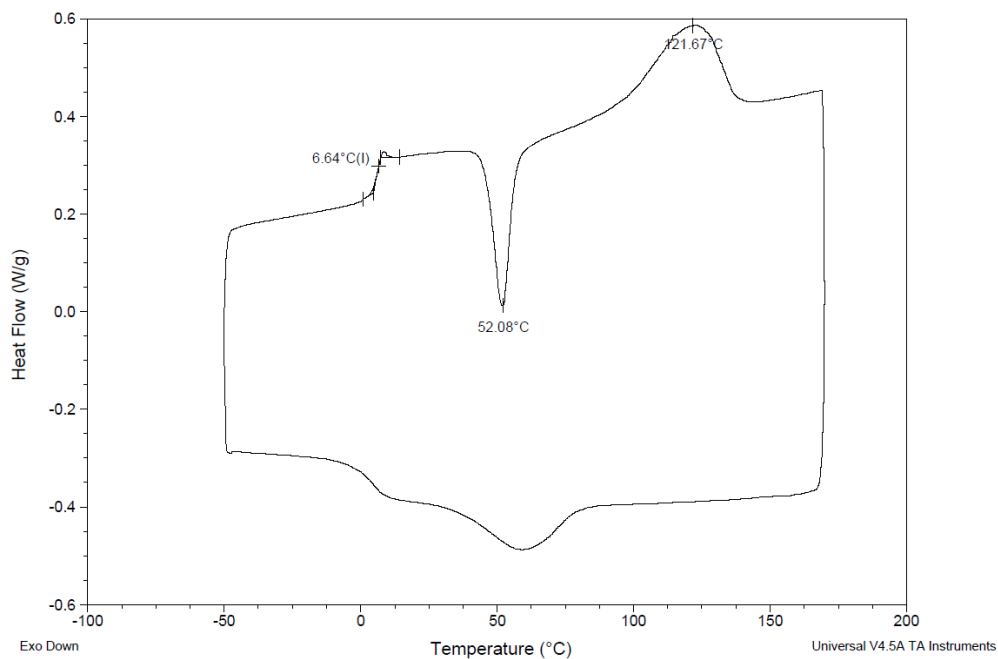


Figure S 43: DSC analysis of PHB ($P_r = 0.73$; Table 2, Entry 9).

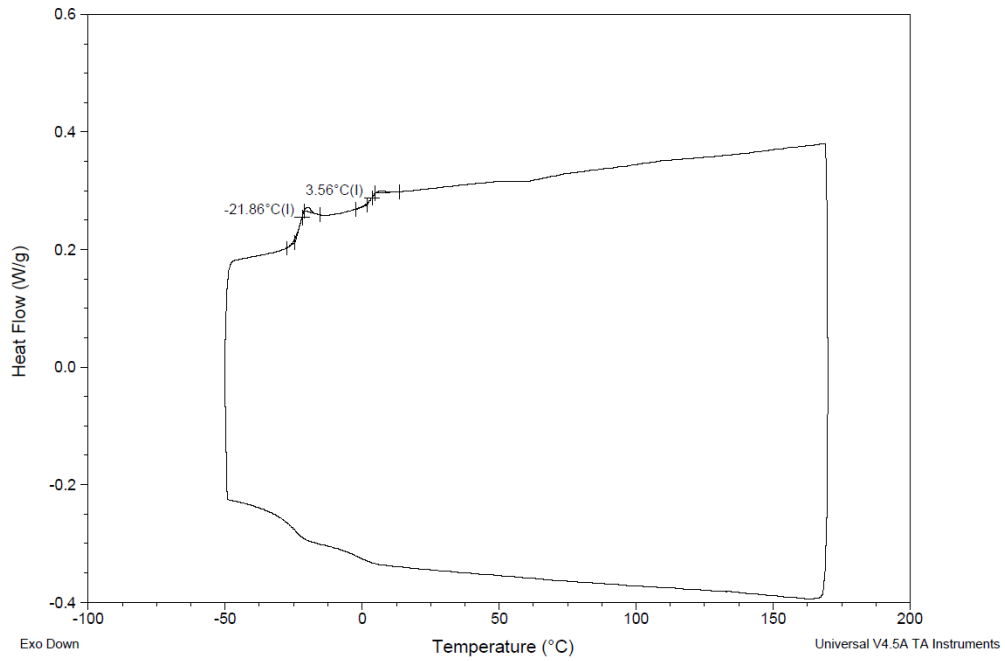


Figure S 44: DSC analysis of AB² (PM/PHB = 54/46; Table 4, Entry 2).

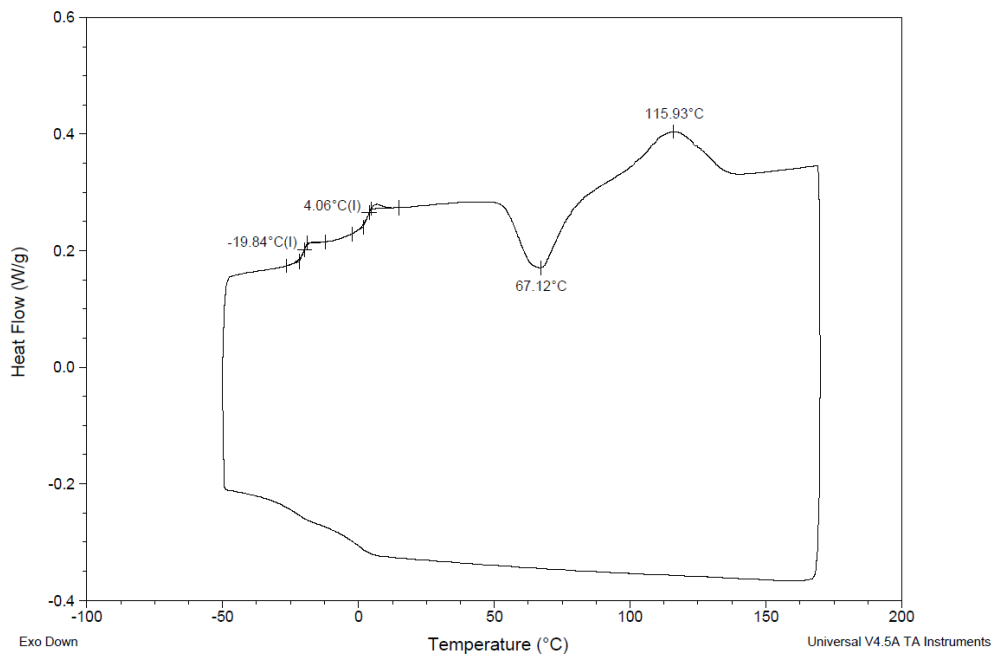


Figure S 45: DSC analysis of BAB² (PM/PHB = 30/70; Table 4, Entry 4).

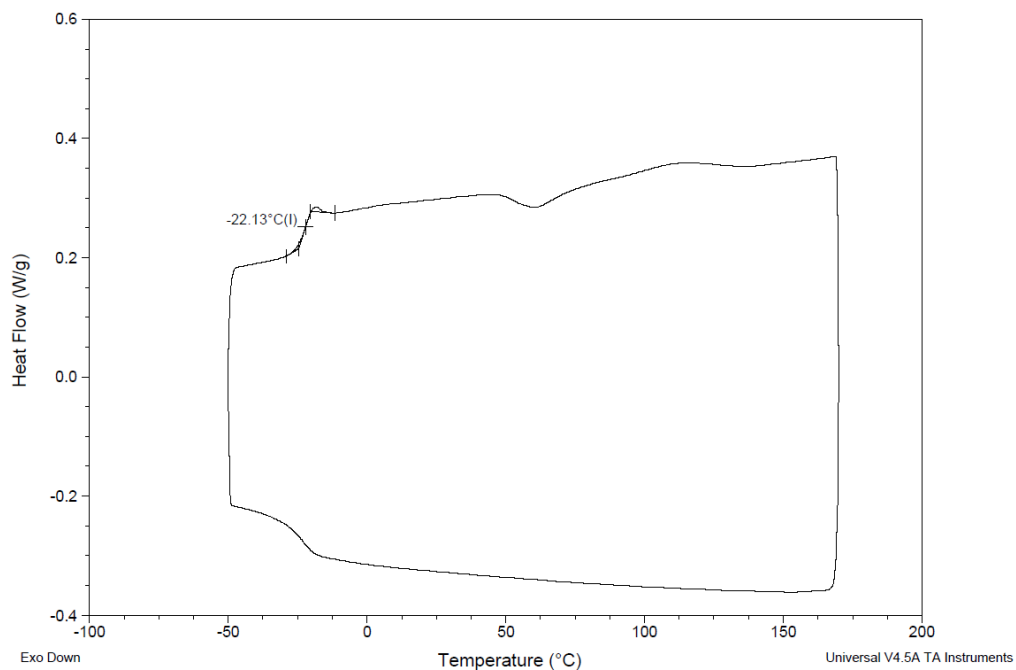


Figure S 46: DSC analysis of BAB⁵ (PM/PHB = 77/23; Table 4, Entry 6).

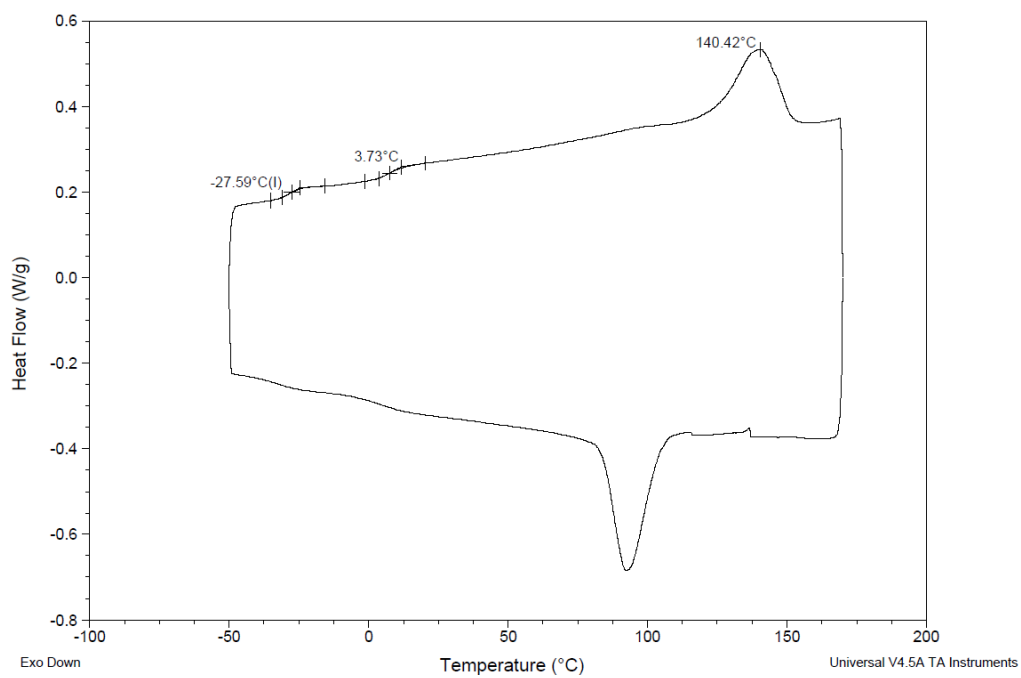


Figure S 47: DSC analysis of a blend from PM (16000 g/mol) and PHB ($P_r = 0.85$ and $M_n = 18000$ g/mol).

10) Powder-XRD

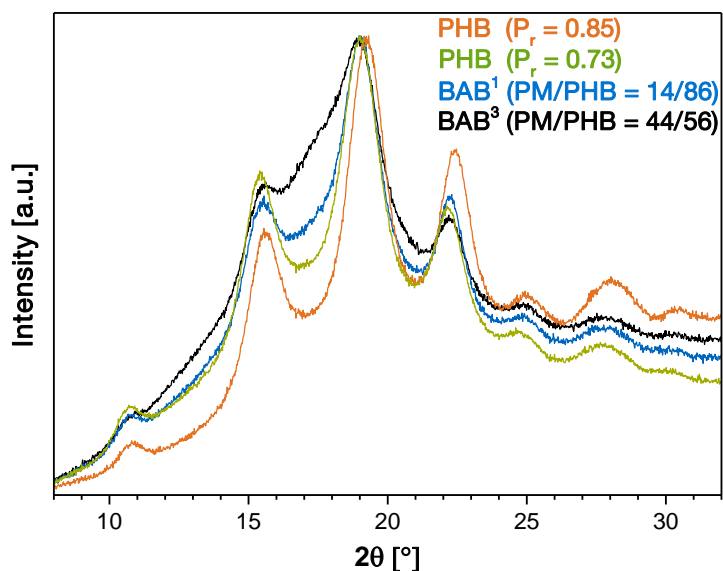


Figure S 48: Powder XRD measurements without background correction of PHB (orange, $P_r = 0.85$; Table 1, Entry 4), PHB (green, $P_r = 0.73$; Table 2, Entry 9), BAB¹ (blue, $P_r = 0.73$; Table 4, Entry 3) and BAB³ (black, $P_r = 0.73$; Table 4, Entry 5).

11) References

- [1] D. Zhang, M. A. Hillmyer, W. B. Tolman, *Biomacromolecules* **2005**, *6*, 2091-2095.
- [2] J. Shin, M. T. Martello, M. Shrestha, J. E. Wissinger, W. B. Tolman, M. A. Hillmyer, *Macromolecules* **2011**, *44*, 87-94.
- [3] K. C. Hultsch, P. Voth, K. Beckerle, T. P. Spaniol, J. Okuda, *Organometallics* **2000**, *19*, 228-243.
- [4] E. Y. Tshuva, S. Groysman, I. Goldberg, M. Kol, Z. Goldschmidt, *Organometallics* **2002**, *21*, 662-670.
- [5] P. T. Altenbuchner, B. S. Soller, S. Kissling, T. Bachmann, A. Kronast, S. I. Vagin, B. Rieger, *Macromolecules* **2014**, *47*, 7742-7749.
- [6] C.-X. Cai, L. Toupet, C. W. Lehmann, J.-F. Carpentier, *J. Organomet. Chem.* **2003**, *683*, 131-136.
- [7] F. Adams, M. R. Machat, P. T. Altenbuchner, J. Ehrmaier, A. Pothig, T. N. V. Karsili, B. Rieger, *Inorg. Chem.* **2017**, *56*, 9754-9764.
- [8] F. Adams, M. Pschenitza, B. Rieger, *ChemCatChem* **2018**, *0*.
- [9] P. T. Altenbuchner, P. D. Werz, P. Schöppner, F. Adams, A. Kronast, C. Schwarzenböck, A. Pöthig, C. Jandl, M. Haslbeck, B. Rieger, *Chem. Eur. J.* **2016**, *22*, 14576-14584.
- [10] N. Ajellal, M. Bouyahyi, A. Amgoune, C. M. Thomas, A. Bondon, I. Pillin, Y. Grohens, J.-F. Carpentier, *Macromolecules* **2009**, *42*, 987-993.

15 Statutory declaration

I declare that I have authored this thesis independently, that I have not used other than the declared sources and that I have explicitly marked all material, which has been quoted either literally or by content from the used sources.

Munich, 14.11.2018

Friederike Adams